Mémoire présenté pour obtenir

l'Habilitation à Diriger des Recherches

Camille Risi

Laboratoire de Météorologie Dynamique

Institut Pierre-Simon Laplace

Camille.Risi@lmd.jussieu.fr

Les isotopes stables de l'eau : application pour évaluer et améliorer les modèles de climat

Water stable stable isotopes: application to evaluate and improve climate models

soutenance prévue le 17 janvier 2016 devant le jury composé de:

Présidente	Hélène Chepfer
Rapporteurs	Rémy Roca Bjorn Stevens Florence Sylvestre
Examinateurs	Peter Blosser Sandrine Bony

Remerciements

Je remercie les membres du jury d'avoir accepté d'évaluer ce travail, en relisant attentivement ce manuscrit (Rémy Roca, Bjorn Stevens, Florence Sylvestre) ou en participant à ma soutenance (Hélène Chepfer, Sandrine Bony, Peter Blossey).

Ce travail est une étape importante dans ma carrière de chargée de recherche au CNRS, que je suis très heureuse d'avoir pu rejoindre en 2011. Etre chargée de recherche au CNRS me permet une grande liberté dans mon travail, et je mesure chaque jour la chance que j'ai d'avoir cette situation. Je remercie tous ceux qui ont contribué à faire de ma candidature au CNRS un succès. Je remercie Vincent Cassé de m'avoir accueillie dans son laboratoire.

Je dois beaucoup à Sandrine Bony, qui m'a encadrée lors de mon stage de M2 (2006) puis ma thèse (2006-2009). C'est elle qui m'a fait découvrir la convection, le climat tropical et les isotopes de l'eau. Elle m'a tellement appris, aussi bien sur le plan scientifique que du point de vue du fonctionnement de la recherche! Elle m'a permis de voyager dans de nombreuses conférences. C'est grâce à elle que j'ai eu envie de devenir chercheuse. Sandrine reste encore aujourd'hui un modèle pour moi.

Tout au cours de mon parcours, j'ai été influencée par de nombreux autres chercheurs que j'ai rencontré et avec qui j'ai collaboré. Sans être exhaustive, je citerai quelques un de ces chercheurs pour qui je garde une grande admiration: Frédéric Hourdin, qui m'a encadré lors de mon 1er stage en laboratoire en 2003, Kerry Emmanuel, qui m'a encadré lors de mon stage de maitrise en 2004, Françoise Vimeux, avec qui j'ai beaucoup travaillé en M2 et pendant ma thèse, Jean-Philippe Lafore, qui m'a beaucoup appris sur les lignes de grain et le climat Sahélien, David Noone, qui m'a encadré pendant mon post-doc (2009-2011), John Worden, avec qui j'ai étroitement collaboré depuis mon post-doc.

Le Laboratoire de Météorologie Dynamique est un endroit très agréable à vivre. Quand j'ai fini ma thèse et que je suis partie en post-doc aux Etats-Unis, je n'avais qu'une idée en tête: y revenir. J'ai toujours eu du mal à imaginer travailler un jour dans un autre laboratoire que le LMD. De nombreuses personnes ont contribué à faire que je me sente bien au LMD, et je ne pourrai pas tous les citer. Je regrette bien sur Martine Maherou, si maternelle. Je garde un souvenir ému de mes anciens collègues de bureau pendant ma thèse (Jing Mei Yu, Florent Brient, Nicolas Rochetin), puis depuis ma prise de fonction en 2011 (Christine Nam, Laura Kerber, Sandrine Guerlet).

Enfin, je ne pourrai terminer ces remerciements sans évoquer ma famille: mes parents, pour qui les études avaient tant d'importance, mon mari, et mon bébé adoré, à qui j'ai pensé en écrivant chacune des lignes de ce manuscrit.

Résumé

Les projections de changement climatique diffèrent selon les modèles de climat utilisés, notamment concernant l'amplitude du réchauffement à venir et les changements de précipitation associés. La représentation des processus convectifs et nuageux est une source majeure d'incertitude. L'enjeu de mes recherches est donc de mieux évaluer la représentation de ces processus dans les modèles de climat et la crédibilité de leurs projections.

Dans ce cadre, j'essaye d'exploiter les mesures de composition isotopique de l'eau. L'eau se présente en effet sous différentes formes isotopiques ($H_2^{16}O$, $H_2^{18}O$, HDO ou $H_2^{17}O$) dont l'abondance est affectée par les changements de phase au cours du cycle de l'eau. Si l'apport des mesures isotopiques en paléo-climatologie est indéniable, leur apport pour mieux comprendre les processus atmosphériques dans le climat présent, et mieux les représenter dans les modèles de climat, est plus difficile à démontrer. Depuis plusieurs années, une révolution technologique a eu lieu permettant de mesurer la composition isotopique de la vapeur d'eau au sol et par satellite avec une fréquence, une couverture spatio-temporelle et une résolution verticale sans précédent. Dans le même temps, la modélisation isotopique s'est développée et diversifiée. Mes travaux reposent sur ces nouvelles opportunités.

Je discute d'abord des processus contrôlant la composition isotopique de la vapeur d'eau dans la troposphère tropicale. Les processus convectifs et nuageux jouent un rôle crucial. En particulier, les descentes convectives et la ré-évaporation de la pluie appauvrissent la vapeur d'eau dans la basse troposphère, tandis que le détrainement convectif enrichit la vapeur dans la haute troposphère. Dans la moyenne troposphère, l'un ou l'autre de ces effets domine selon la profondeur de la convection. Enfin, sur les continents, le recyclage de la pluie par évapo-transpiration joue un rôle significatif, mais il est difficile à démêler du rôle de la convection.

Forte de cette compréhension, je propose ensuite quelques exemples d'utilisation des mesures isotopiques dans la vapeur d'eau pour évaluer et améliorer la représentation des processus atmosphériques dans les modèles de climat. En étudiant la saisonnalité de la composition isotopique de la vapeur d'eau dans la troposphère subtropicale, je montre que dans la plupart des modèles de climat, le biais humide dans la haute troposphère tropicale et subtropicale est causé par une advection verticale trop diffusive. Je montre aussi que les modèles sont incapables de reproduire la distribution latitudinale de la composition isotopique de la vapeur d'eau dans la haute troposphère, à moins de considérer que l'efficacité de précipitation dépend de l'intensité de la convection. Enfin, les mesures isotopiques dans la vapeur d'eau pourraient permettre de mieux contraindre les profils verticaux de mélange convectif.

Enfin, je discute l'utilisation des archives paléo-climatiques d'isotopes de l'eau dans les tropiques pour évaluer la capacité des modèles à simuler les changements de précipitation en réponse aux variations climatiques. Je montre qu'on peut contraindre les changements de précipitation futurs en connaissant les changements de précipitations passé, par exemple en Amérique du Sud. Dans les tropiques, l'interprétation des archives isotopiques est débattue. Mes simulations confirment la difficulté du débat, montrant que le signal isotopique reflète la température ou les précipitations selon les régions, la période paléo-climatique et la version du modèle.

Summary

Climate change projections depend on climate models, in particular regarding the magnitude of future warming and associated precipitation changes. The representation of convective and cloud processes is a major source of uncertainty. The overall goal of my research is to better evaluate climate models and the credibility of their projections.

In this context, I try to exploit water isotopic composition measurements. The water molecule has several isotopic forms ($H_2^{16}O$, $H_2^{18}O$, HDO or $H_2^{17}O$) whose concentrations are affected by phase changes along the water cycle. While the contribution of isotopic measurements to paleo-climatology has been crucial, it is more difficult to demonstrate the added value of water isotopes their to better understand atmospheric processes in the present climate, and better evaluate their representation in climate models. For several years, a technological revolution has led to isotopic measurements in water vapor from the ground and by satellite with unprecedented frequency, spatio-temporal coverage and vertical resolution. In the meanwhile, isotopic modeling has considerably grown. My work is based on these new opportunities.

First, I will discuss the processes controlling the isotopic composition of water vapor in the tropical troposphere. Convective cloud processes and play a crucial role. In particular, convective descents and rain re-evaporation deplete the water vapor in the lower troposphere, while convective detrainment enriches water vapor in the upper troposphere. In the middle troposphere, one of these effects dominate depending on the convective depth. Finally, over land, rain recycling by evapotranspiration plays a significant role, but it is difficult to disentangle it from the role of convection.

With this understanding, I present some examples in which water vapor isotopic measurements are used to evaluate the representation of atmospheric processes in climate models. Studying the seasonality of water vapor isotopic composition in the subtropical troposphere, I show that in most climate models, the wet bias in the tropical and subtropical upper troposphere is caused by an excessively diffusive vertical advection. I also show that models are unable to reproduce the latitudinal distribution of the water vapor isotopic composition in the upper troposphere, unless they consider that precipitation efficiency depends on convective intensity. Finally, isotopic measurements may help better constrain the profiles of convective mixing.

Finally, I discuss using paleo-climatic water isotope records in the tropics to assess the ability of models to simulate rainfall changes in response to climate variations. I show that past precipitation changes could help constrain future precipitation changes, for example in South America. In the tropics, the intepretation isotopic records is debated. My simulations confirm the difficulty of the debate, showing that the isotopic signal reflects temperature or precipitation depending on the region, paleo-climatic period and model version.

Foreword: justification of some choices on the subject of this document

To write a coherent and concise document, I have deliberately chosen to focus on the heart of my current activities. In particular, I leave aside many pieces of work that I have done through collaborations.

First, I chose to focus exclusively **in the tropics**. The cloud response in the tropics is at the heart of the inter-model spread for climate sensitivity ([Bony and Dufresne, 2005]). In addition, the models spread in terms of precipitation change projections is largest in the tropics ([Oueslati et al., 2016]). Besides, I have extensively studied the role of **convective processes** on the water isotopic composition ([Risi et al., 2008a], section 2.1). In the tropics, convective processes, whose representation in models remains a challenge, play a crucial role. Finally, the tropics are where the interpretation of isotopic paleo-climatic archives is the more debated (sections 1.2.2, 4.2).

Second, I chose to focus on **water isotopes in the vapor phase**. I leave aside a significant piece of my PhD work that was devoted to understanding the isotopic composition in the precipitation. I do not want this document to be a repetition of my PhD thesis. Furthermore, in the past few years, the emergence of water vapor isotopic measurements from ground and space (section 1.3.1) have dramatically modified the context of isotopic research. Since my post-doc, I have focused almost exclusively on these new measurements, and I will continue to focus on these in the future. I will discuss the interpretation of precipitation paleo-climatic archives (section 4.2), evidencing the importance of better understanding isotopic controls in the vapor phase.

Third, I decided to focus on the **evaluation and improvement of climate models**, rather than on the understanding of processes in nature. Evaluation and improvement of climate models is an important issue in itself, given the persistent spread in climate change projections in terms of climate sensitivity and precipitation changes (section 1.1). In addition, using water isotopic measurements to understand of processes in nature is very promising but challenging. On the road to achieve this challenging goal, I think that the evaluation and improvement of climate models is a necessary step (section 1.2.3).

Fourth, I chose to write mainly about my **recent work**. I do not feel like repeating once again what I have already written in my thesis or in articles and what I have explained many times in conferences. Rather, I want this document to be a springboard for my future work. This is why several sections of this document are based on unpublished work (sections 2.1.5, 2.1.6, 3.3 and 4.2). In appendix A, I give some ideas of subjects for future students, post-docs or myself.

Contents

Chapter 1

Introduction

1.1 Motivation: inter-model spread in climate change projections

For several decades, there has been a persistent spread in climate change projections simulated by climate models, in particular for the magnitude of future global warming and for the patterns of precipitation changes ([Meehl et al., 2007, Knutti and Sedláček, 2013], figure 1.1). So the overall goal of my research is to **better assess climate models and the credibility of their projections**. In this document, I summarize how I try to contribute to this goal using water stable isotopic measurements.

The representation of atmospheric convection and cloud processes is a major source of uncertainty. In particular, the magnitude of future global warming is strongly impacted by cloud feedbacks in tropical regions ([Bony et al., 2004, Bony and Dufresne, 2005, Sherwood et al., 2014]). Changes in precipitation are very sensitive to the representation of deep convection cloud processes ([Frierson, 2007, Kang et al., 2008, Frierson and Hwang, 2012, Hwang and Frierson, 2013]). Since the isotopic composition of water vapor is very sensitive to convective and cloud processes (chapter 2), I try to **use water stable isotopic measurements to evaluate the representation of convective and cloud processes by climate models** (chapter 3).

The climate response of a model to a given forcing could be evaluated using past climate changes ([Schmidt, 2010, Schmidt et al., 2013, Hargreaves et al., 2013, Hargreaves et al., 2012]). Water isotopic proxies are potentially useful proxies for past precipitation changes ([Pausata et al., 2011]), especially over tropical land regions where the projection spread is the largest ([Knutti and Sedláček, 2013, Oueslati et al., 2016]). Therefore, I try to understand **how precipitation changes are imprinted into isotopic archives and how these records could be used to assess our confidence in precipitation projections** (chapter 4).

1.2 Why use water isotopes?

1.2.1 What are water isotopes?

Water molecules exhibit different isotopic species ($H_2^{16}O$, $H_2^{18}O$, HDO or $H_2^{17}O$) that undergo fractionation during phase changes. In particular, the lightest water molecules ($H_2^{16}O$) preferentially evaporate, while the heaviest molecules preferentially concentrate in the most condensed phase (liquid or solid) ([Dansgaard, 1964]). As a consequence, the isotopic composition of water vapor or precipitation is affected by the history of phase changes throughout the water cycle (figure 1.2).

The relative isotopic abundance in a sample is quantified as an anomaly compared to a reference ocean water using the δ notation and expressed in ‰. For example, the relative abundance in HDO is quantified by δD:

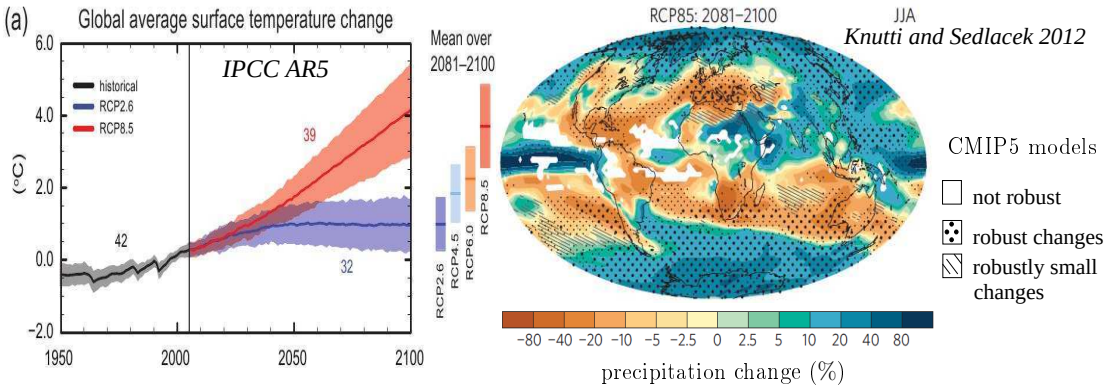

Figure 1.1: a) Global average surface temperature change for two different emission scenarios. The solid line shows the multi-model mean, whereas the envelope shows the range of individual model results. b) Precipitation change from present-day to the last two decade of the 21st century. Colors show the multi-model average, whereas stippling and Hatching illustrates the robustness of model results.

$$\delta D = \left(\left(\frac{HDO}{H_2O} \right)_{sample} / \left(\frac{HDO}{H_2O} \right)_{reference} - 1 \right) \cdot 1000$$

When δD is high, we say that the sample is enriched. Conversely, when δD is low, we say that the sample is depleted.

$\delta^{18}O$ is defined in the same way. To first order, $\delta^{18}O$ exhibit similar variations as δD, but 8 times smaller. The second order parameter d-excess, defined as $d = \delta D - 8 \cdot \delta^{18}O$, reflects the effect of non-equilibrium fractionation.

1.2.2 An important contribution to paleoclimate reconstructions

Water stable isotopes in precipitation can be stored in a variety of paleo-climatic archives. Since the isotopic composition of precipitation reflects the numerous phase change processes that occurred along the air mass trajectory, isotopic archives yield information on past climates. The contribution of water isotopic research to paleo-climatology is impressive. In polar regions, isotopic variations recorded in ice cores can be used as a proxy for temperature ([Jouzel et al., 2000]). They have allowed to document the glacial-interglacial cycles ([Dansgaard et al., 1969, Johnsen et al., 1972, Lorius et al., 1979, Jouzel et al., 1987a]) and to discover abrupt climate variations ([Dansgaard et al., 1989, Dansgaard et al., 1993]). In other regions, isotopic variations observed in speleothems ([Wang et al., 2001, Fleitmann et al., 2007]) or mountain ice cores ([Thompson et al., 1995, Thompson et al., 1998, Thompson et al., 2000]) have evidenced worldwide responses to these modes of variability.

Even though the precision of the isotopic thermometer in polar regions can be discussed ([Jouzel and Alley, 1997, Krinner and Werner, 2003, Sime et al., 2009]) and the interpretation of isotopic records in tropical regions remains debated ([Vuille et al., 2003], section 4.2), the value of water stable isotopes for paleoclimate reconstructions is well established.

1.2.3 More challenging applications to study present-day processes

A wide range of potential applications

More recently, water stable isotopic observations have been used in an attempt to better understand present-day hydrological and atmospheric processes. Since water isotopic composition is affected by so many processes, it has been used for many different applications (figure 1.3). Near the surface, the isotopic enrichment in water vapor has been used to try to estimate continental recycling ([Salati

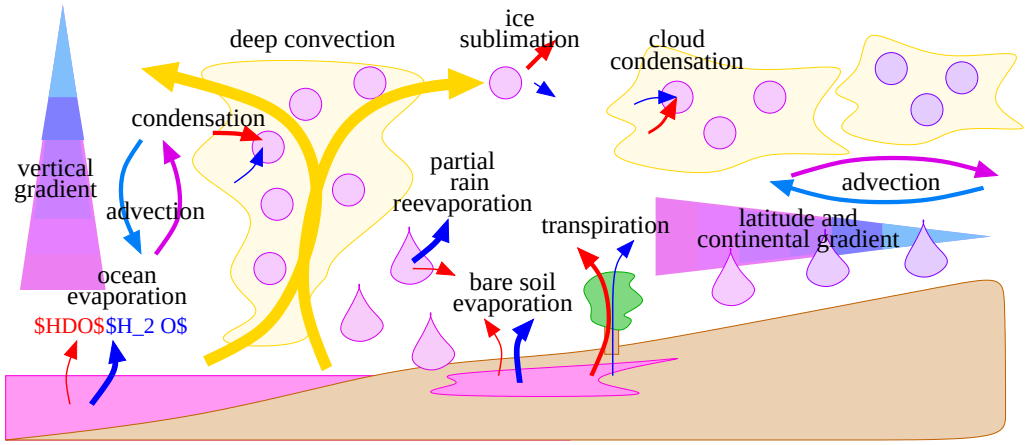

Figure 1.2: Overview of atmospheric processes affecting the isotopic composition of water vapor. Red and blue arrows illustrate the HDO and H_2O fluxes respectively during phase changes. Red-ish and blue-ish colors indicate more enriched and depleted colors respectively. HDO preferentially stays in the liquid phase during evaporation from ocean and bare soil. Transpiration does not fractionate. HDO preferentially condenses in clouds. This results in vertical, latitudinal and continental gradients. Advection downstream these gradients has a depleting effect, while advection against these gradients has an enriching effect. Sublimation of ice crystals does not fractionate and imprints the enriched signature of the condensate.

et al., 1979, Risi et al., 2013], section 2.2). A second order parameter called d-excess had been used to try to estimate the proportion of evapo-transpiration that occurs as evaporation or transpiration ([Gat and Matsui, 1991, Aemisegger et al., 2014]). In addition, the surface water vapor is impacted by convective processes, such as unsaturated downdrafts ([Risi et al., 2008a, Risi et al., 2010a], section 2.1.3), rain re-evaporation ([Worden et al., 2007]), or the degree of organization ([Lawrence et al., 2004]). In the middle troposphere, the water isotopic composition reflects the proportion of precipitation that occurs as convective or large-scale precipitation ([Lee et al., 2009, Kurita, 2013], section 2.1.6). In the sub-tropics, the water isotopic composition reflects vertical mixing ([Risi et al., 2012b], section 3.1.2). In the upper troposphere, the isotopic composition has been used to try to quantify convective detrainment ([Moyer et al., 1996, Webster and Heymsfield, 2003], section 2.1.2) and study ice microphysics ([Bolot et al., 2013]).

Water isotopic composition are affected by many processes allowing for many potential applications, but the flip side is that it is difficult to attribute isotopic variations to only one cause. Isotopic signals are very complex to interpret. In spite of many attempts to make quantitative estimates of the above-mentioned processes, most papers remain at a stage where they argue that water isotopes are *promising* or *have the potential* to solve problems. Going beyond this stage is a challenge.

Two examples of attempts to use water isotope measurements to quantify processes in nature, and their limitations

For example, clouds associated with deep convective detrainment and cirrus clouds associated with in-situ condensation have very distinct isotopic signature ([Webster and Heymsfield, 2003], figure 1.4, physical explanation in section 2.1.2). Based on the enriched signature of the isotopic composition observed in the tropical tropopause layer, [Kuang et al., 2003] concluded that convective detrainment contributes to the water budget at this altitude. But this conclusion was already known from non-isotopic measurements, such as cloud observations ([Gettelman et al., 2002, Gettelman et al., 2002]). The remaining question is: what is the quantitative contribution of convective detrainment to water budget? Water isotope measurements have not been able to provide any quantitative answer so far.

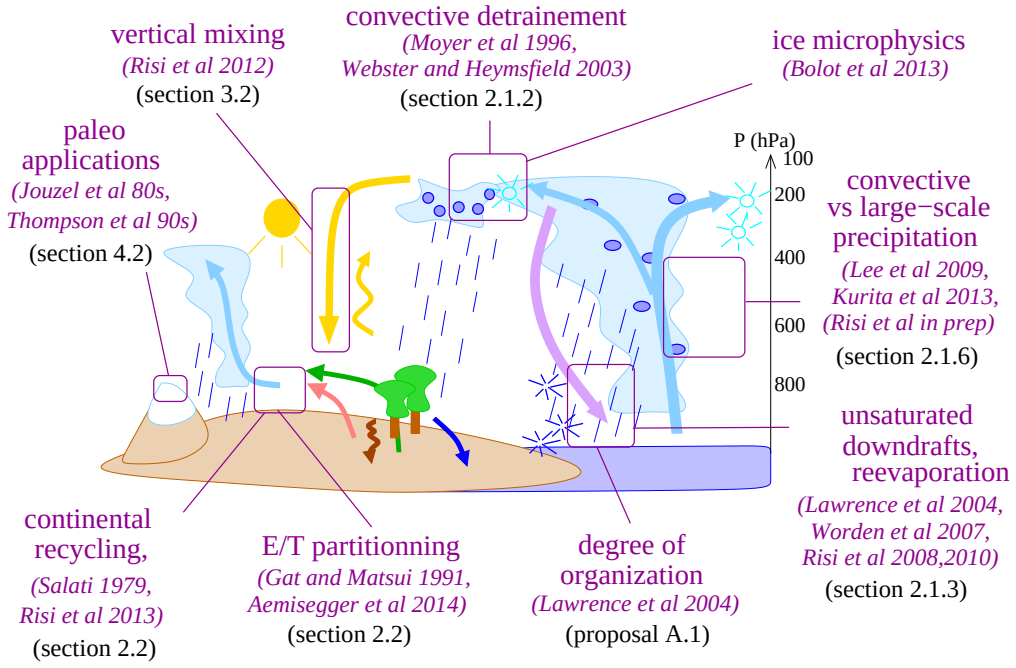

Figure 1.3: Different applications of water isotopic measurements. References and sections of this manuscript where these applications are discussed are indicated.

As another example, [Worden et al., 2007] proposed to use water vapor δD observations to quantify the proportion of tropospheric water vapor that orginates from rain-reevaporation. They developped a simple model for the effect of rain reevaporation on water vapor δD. Fitting their measurements with their model (figure 1.5), they endded up with values ranging from 0 to 50%. But what is the accuracy of these estimates, given the strong approximations in their model for rain reevaporation (proposal A.3), the numerous other atmospheric processes that were ignored (section 1.3.3) and the isotopic measurement uncertainties (section 1.3.1)? It is likely that the uncertainty range of such estimates is much larger than what we can obtain by other methods, such as water and energy budget considerations ([Folkins and Martin, 2005]) or model simulation of intensive field campaign cases ([Sud and Walker, 1993]).

1.2.4 Use water isotopes to evaluate and improve models: a necessary first step and a goal in itself

A major difficulty in trying to use water vapor isotopes to understand and quantify processes in nature is that they are sensitive to so many processes that comprehensive and complex models need to be used, such as climate models. For example, if a relationship can be found between the isotopic composition and some processes of interest among model simulations, then isotopic observations can discriminate the most realistic simulation, and processes can be analyzed and quantified in this simulation (figure 1.6). In this perspective, **evaluating and improving climate models using water isotopic measurements is a necessary step before we can actually use water isotopic measurements to understand and quantify processes in nature**.

In addition, evaluating and improving climate models is an important goal in itself (section 1.1) to which water isotopes can contribute.

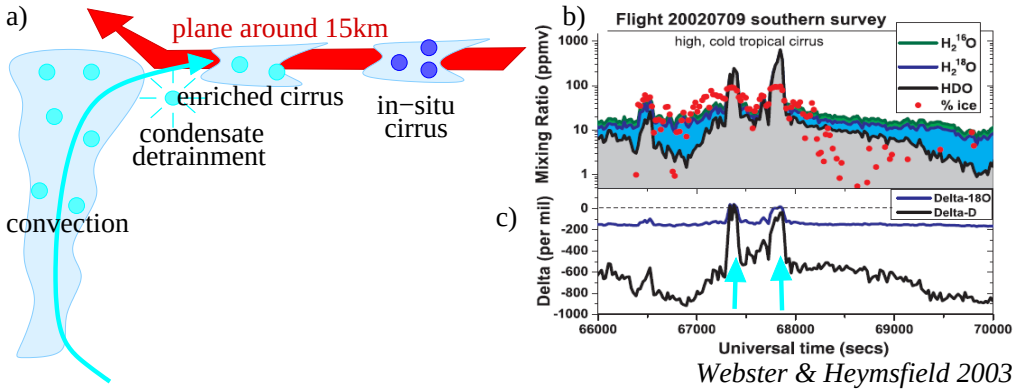

Figure 1.4: a) Measurements by plane in the upper troposphere. The plane crossed different kinds of cirrus clouds, some associated with convective detrainment and some associated with in-situ condensation. b) Humidity mixing ratio (green) along the plave path. c) Total-water δD (black) along the path. The two peaks in humidity and δD correspond to cirrus clouds originating from deep convection (light blue arrows).

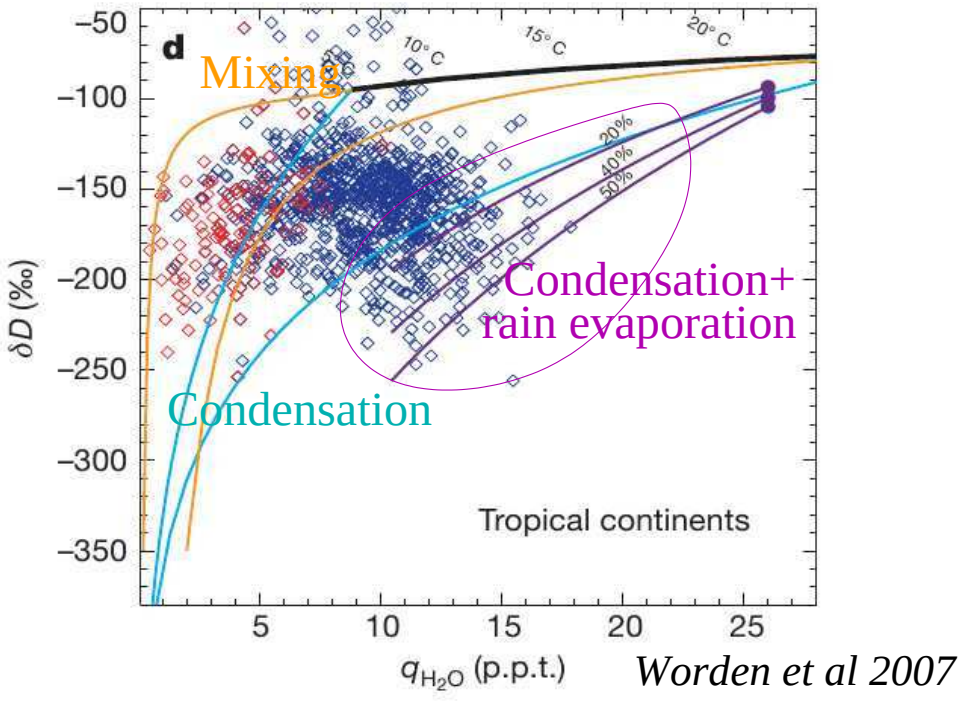

Figure 1.5: q-δD diagram (water vapor δD as a function of specific humidity q), as popularized by [Worden et al., 2007]. According to their simple model, the orange lines show the ensemble of q-δD values that can be explained by mixing processes, the blue lines show the ensemble of q-δD values that can be explained by condensation processes, and the purple lines show the ensemble of q-δD values that can be explained by condensation plus different contributions of rain reevaporation (from 20 to 50%). Markers illustrate the TES satellite observations in the lower middle troposphere over tropical continents for clear-sky (red) and cloudy (blue) scenes. This diagram was used to attempt to estimate the contribution of rain reevaporation to tropospheric humidity. Several cloudy scenes are consistent with the purple lines indicating between 20% and 50% of the vapor originating from rain reevaporation.

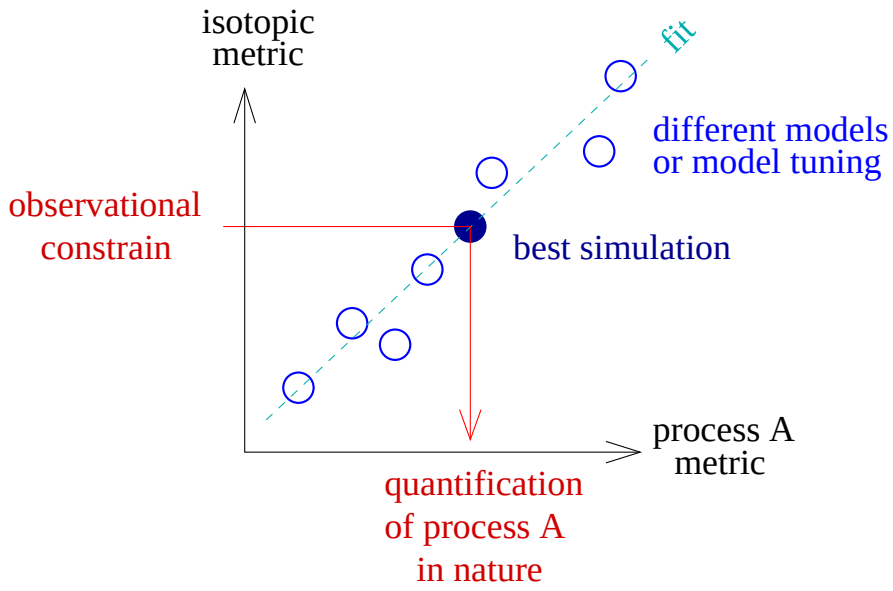

Figure 1.6: Schematic showing how combining isotopic measurements and models could help us quantify processes in nature. First, there should be a relationship among different models (or different model tuning) between a metric for process A and an isotopic metric. Isotopic observations can discriminate the most realistic simulation. Then process A can be estimated in this simulation, and we assume that this estimate is representative of what goes on in nature.

1.2.5 Personal opinion on trying to make isotopes useful

Sometimes I wonder why isotope scientists try so hard to make water isotopes useful. Ideally, research should **start with science questions** (figure 1.7, orange): for example, what is the contribution of different processes to the observed distribution of a meteorological variable? Do models represent it properly? What is the cause of a model bias for a given meteorological variable? Then, scientists wonder which observations are the most adequate to discriminate between different hypotheses. In most cases, non-isotopic observations (e.g. observations of conventional meteorological variables, cloud properties, flux tower measurements...) are the most suited to address the science questions. In some (rare) cases, the isotopic observations, combined with other observations, are the most suited. In this case, this motivates the implementation of field campaigns or satellite missions to perform isotopic measurements.

But in practice, research is often conducted the other way round (figure 1.7, pink). Isotopic measurements are performed first, motivated mainly by curiosity. Then we wonder: what can these measurements be useful for? To address this question, first we need to understand what processes control the isotopic composition displayed by the measurements. Once the main process is identified, we look for science questions associated with this process, and we try to answer it using the isotopic measurements. Although this approach looks like conducted the wrong way, accumulating understanding on processes controlling the isotopic composition is useful. It allows us to know whether a science question can be best answered using water isotopic composition or not.

Therefore, I think that at this stage of isotopic research, pretending to use water isotopes to better "evaluate and improve climate models", which I often do myself, is a bit premature. I think more and more that studies whose goal is **"simply" to understand isotopic controls**, without pretending to make any use of it, should receive more credit. This is why in this document I devote chapter 2 to "simply" understanding isotopic controls, before trying to use isotopic measurements to evaluate and improve models (chapter 3). In appendix I suggest several ideas to deepen our understanding isotopic controls (proposals A.2, A.3, A.4, A.5).

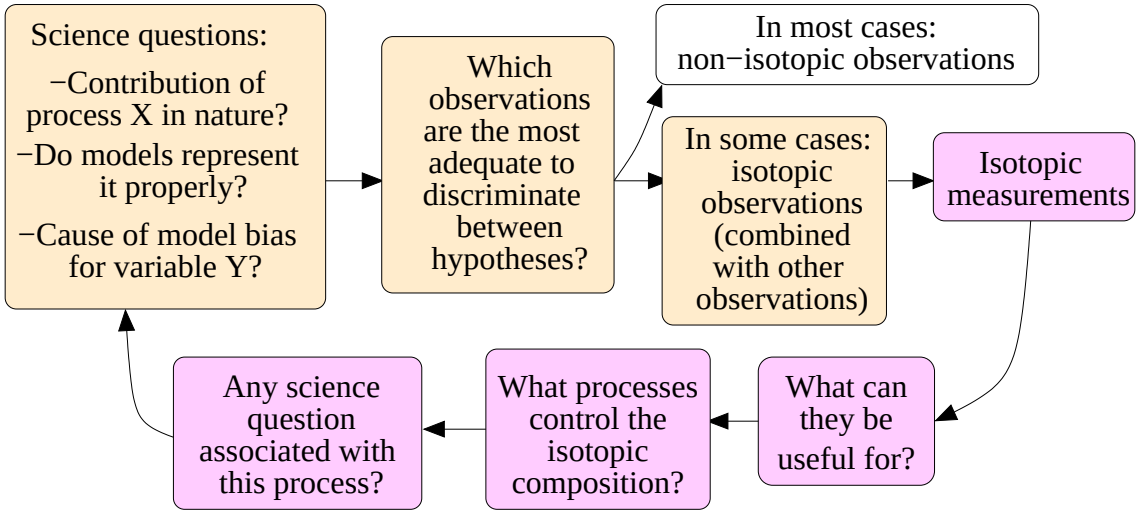

Figure 1.7: Schematics illustrating the scientific approach from science questions to isotopic measurements, and vice versa.

1.3 New opportunities and challenges in current water isotopic research

Nowadays is a good time to study isotopic controls and exploring the use of isotopic measurements to evaluate and improve models. The recent development of new measurement techniques (section 1.3.1) and new modelling tools (section 1.3.2) offers unprecedented opportunities.

1.3.1 Measurements

Why should we measure water isotopes is the water vapor phase?

Water stable isotopes are measured in various water reservoirs and fluxes of the Earth system, such as precipitation ([Dansgaard, 1964]), water vapor (next sections), rivers ([Kendall and Coplen, 2001]), lakes ([Gibson et al., 2005]), underground waters ([Fontes, 1980]), soil water ([Brunel et al., 1997]), stem water and leaf water ([Lai et al., 2006, Twining et al., 2006]), surface evaporation flux ([Griffis et al., 2010]), paleo-climatic proxies (section 4.2)... In this document, we focus mainly on **water vapor measurements**:

- We focus on atmospheric processes, which are most directly imprinted in water vapor Isotopic composition in land water reservoirs are affected by additional fractionation processes.
- The isotopic composition of water vapor is the only atmospheric *prognostic* variable, i.e. the isotopic composition in water vapor and all water reservoirs at time t depends on the isotopic composition of water vapor at time $t - dt$. In contrast, the isotopic composition of precipitation is purely *diagnostic*, i.e. at each time t it can be deduced from the that of water vapor. Understanding isotopic variations in water vapor is thus the first step before understanding those in all water reservoirs, including precipitation and derived paleo-climatic proxies.
- The isotopic composition of water vapor is defined continuously in time and in the three spatial dimensions every where in the atmosphere. In contrast, the isotopic composition of the precipitation, for example, is defined only during precipitation events.
- Studying the isotopic composition of water vapor has bloomed over the past decade, due to an instrumental revolution of water vapor isotopic measurements.

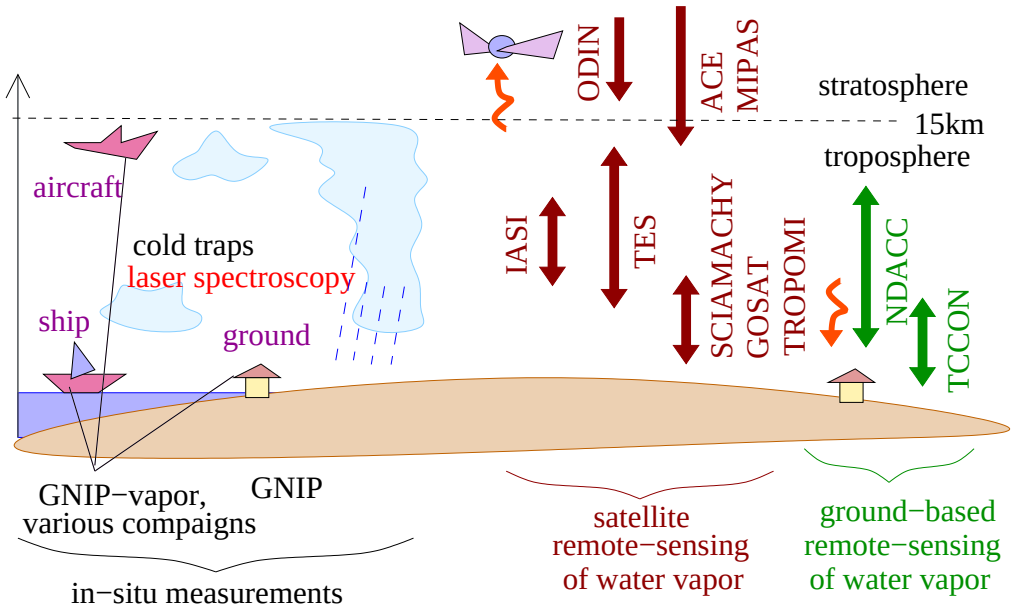

Figure 1.8: Overview of available isotopic measurements in water vapor and the altitude they sample.

Instrumental revolution of water vapor isotopic measurements

First isotopic measurements in water vapor were performed in-situ by cryogenic sampling followed by mass spectrometer analysis ([Ehhalt, 1974, Moreira et al., 1997, Lawrence et al., 2004, Uemura et al., 2008]). However, this method was long and tedious, so that temporal resolution and spatio-temporal coverage was weak. Therefore, most isotopic studies have long been limited to measurements in precipitation ([Dansgaard, 1964, Rozanski et al., 1993]).

In the past decade, an instrumental revolution has led to the development of two kinds of water vapor measurements: by in-situ laser instruments and by remote-sensing instruments.

Laser instruments

Laser instruments have been developed to perform in-situ isotopic measurements continuously and at a high frequency ([Gupta et al., 2009]), possibly during several years ([Tremoy et al., 2014, Steen-Larsen et al., 2014]). This allows to study isotopic variations in the near-surface vapor

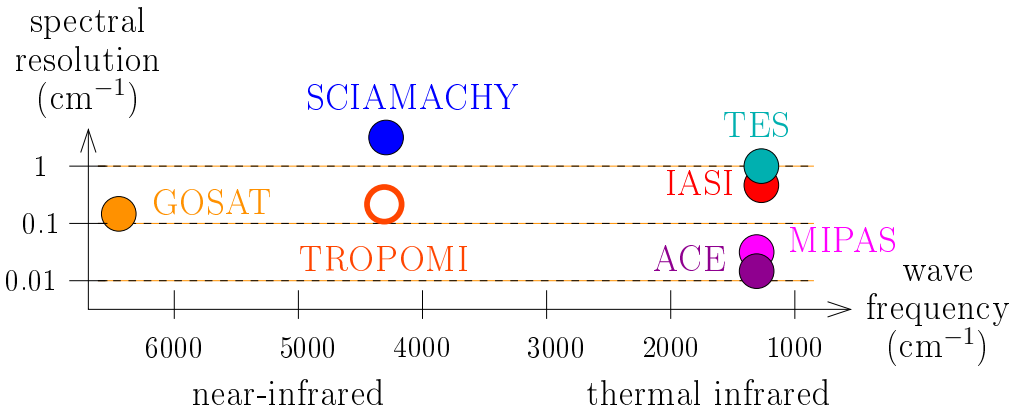

Figure 1.9: Overview of the spectral domain and resolution used for the water vapor isotopic satellite measurements.

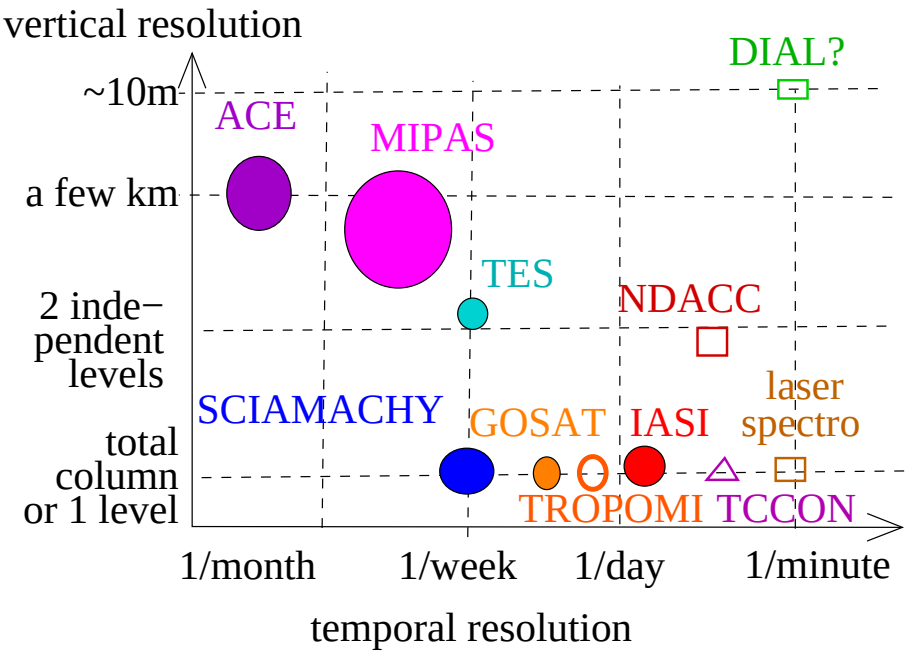

Figure 1.10: Overview of the vertical and temporal resolutions of the different measurements of water vapor δD. The temporal resolution for satellite measurements considers the return time for a measurement in a typical GCM grid box. The size of markers indicate the precision: the bigger the marker, the less precise, for the corresponding temporal resolution.

over a wide range of time scales, from the intra-rain event scale ([Tremoy et al., 2014]) to the diurnal ([Bailey et al., 2013]), synoptic and intra-seasonal ([Bonne et al., 015 , Galewsky and Samuels-Crow, 2014, Tremoy et al., 2012]), seasonal ([Tremoy et al., 2012, Steen-Larsen et al., 2014]) and inter-annual time scales. The measurement precision is as good as with older spectrometer techniques, i.e. $\simeq$0.5 ‰ for δD and $\simeq$5-10 ‰ for d-excess ([Tremoy et al., 2011]).

Remote-sensing instruments

Remote-sensing instruments have been developed for both ground-based and satellited measurements. They are passive sensors that used near-infrared radiance (in this case, they measure the vertically integrated δD) or thermal infrared radiance (in this case, they may have some profiling capacities) (figures 1.8, 1.9).

1. **Ground-based** instruments can measure the isotopic composition in the total-column (e.g. TCCON network, [Wunch et al., 2011]) or at different tropospheric levels (e.g. NDACC network, [Schneider et al., 2010a, Schneider et al., 2015]). Compared to in-situ measurements, they observe higher altitudes, and have the longest data records so far ([Schneider et al., 2010b]). The drawbacks are to record only δD ($\delta^{18}O$ is not precise enough to be useful), to be less precise ($\simeq$5 to 50 ‰ for δD depending on conditions and instruments) and to be limited to clear-sky conditions. Averaging measurements over some period of time refine the precision, but decrease the temporal resolution of the record.

2. **Satellite** measurements can measure the isotopic composition in the total-column (e.g. SCIAMACHY: [Frankenberg et al., 2009, Scheepmaker et al., 2012], GOSAT: [Frankenberg et al., 2013], soon TROPOMI: [Scheepmaker et al., 2016]) , at different tropospheric levels (e.g. TES: [Worden et al., 2006, Worden et al., 2007, Worden et al., 2012], IASI: [Schneider, 2011, Lacour et al., 2012]), or at different levels through the upper troposphere, stratosphere and higher (ACE: [Nassar et al., 2007], MIPAS: [Payne et al., 2007, Steinwagner et al., 2010], ODIN: [Urban et al., 2007]). The major advantage is that they allow us to visualize the global δD distribution. All these instruments retrieve only δD and only in clear-sky con-

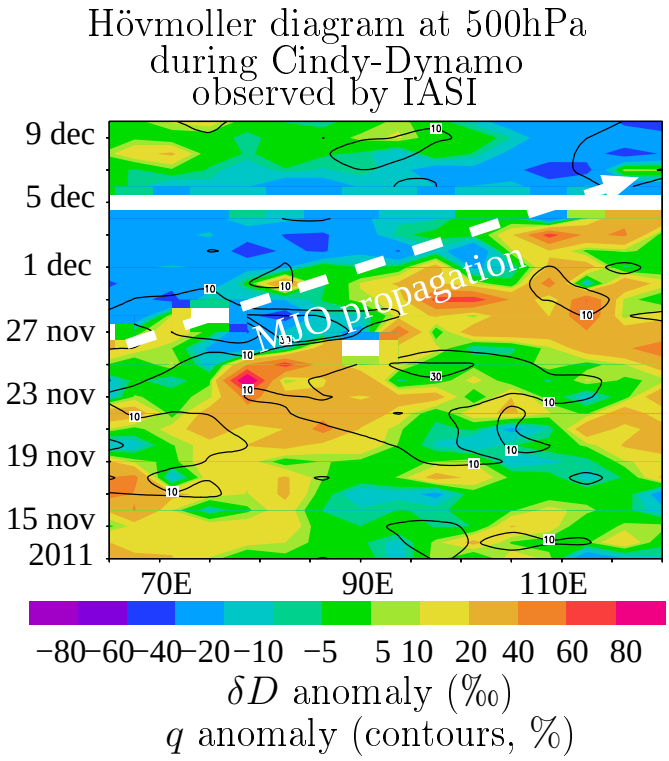

Figure 1.11: Time-longitude diagram for specific humidity (contours) and water vapor δD (shaded) at 500hPa as observed by IASI during the November 2011 Cindy-Dynamo field campaign case. This illustrates the unprecedented spatio-temporal coverage of IASI.

ditions, but they have various spatio-temporal coverage, vertical resolutions and precision properties (figure 1.10).

Figures 1.8, 1.9 and 1.10 compare the vertical resolutions and coverage, temporal resolution, spectral domains and resolutions of these different datasets. Most of the above-mentioned datasets are detailed and compared in [Risi et al., 2012a]. Table 1.1 summarizes the main advantages and drawbacks of the different insrument techniques.

Among satellite measurements, the **IASI** instrument on-board MetOp has the **best spatio-temporal coverage**: it retrieves δD globally twice a day! This allows to study for the first time the isotopic evolution in time and space during individual synoptic or intra-seasonal events ([Bonne et al., 015 , Tuinenburg et al., 2015], for example during an Madden-Julian Oscillation (MJO) event (figure 1.11). The future TROPOMI instrument should have a similar coverage.

The **TES** instrument has the **best vertical resolution**. It retrieves vertical profiles of δD with several independent levels of information through the troposphere. This is a unique opportunity to study the effect of some meteorological conditions or some convective processes as a function of altitude (figure 1.12).

In the future, the **DIAL** (differential absorption lidar) remote-sensing instrument, operated from the ground or from an aircraft, is very promising ([Bruneau et al., 2001]). Contrary to all instrument listed earlier, the DIAL is based on active remote-sensing technology. Preliminary studies suggest a vertical resolution of 10-100m, a temporal resolution of a few minutes and a precision arounf 10‰ (project by Cyrille Flamant).

measurement technique	advantages	drawbacks
cryogenic sampling and mass spectrometry	very precise small horizontal footprint	tedious very scarce
in-situ laser spectrometry	very precise continuous high frequency (< 1 minute) small horizontal footprint	local measurements
TCCON	continuous small horizontal footprint	local measurements clear-sky only
NDACC	continuous long time series information on vertical profiles small horizontal footprint	local measurements clear-sky only
DIAL	continuous precise good vertical resolution (100m) high frequency (a few minutes) small horizontal footprint	not available yet: under development local clear-sky only
TES	spatial distribution information on vertical profiles (3 independant levels)	relatively weak spatio-temporal coverage clear-sky only
IASI	spatial distribution very good spatio-temporal coverage (global twice daily) plans for long time series	clear-sky only very costly retrievals, available only on demand.
SCIAMACHY	spatial distribution	relatively weak spatio-temporal coverage clear-sky only
GOSAT	spatial distribution good spatio-temporal coverage over land	clear-sky only
TROPOMI	spatial distribution very good spatio-temporal coverage (global twice daily)	not available yet clear-sky only
ACE	spatial distribution good vertical resolution in upper-troposphere-stratosphere	weak spatio-temporal coverage clear-sky only
MIPAS	spatial distribution good vertical resolution in upper-troposphere-stratosphere	clear-sky only

Table 1.1: Table summarizing the main advantages and drawbacks of the different instruments measuring water vapor isotopes.

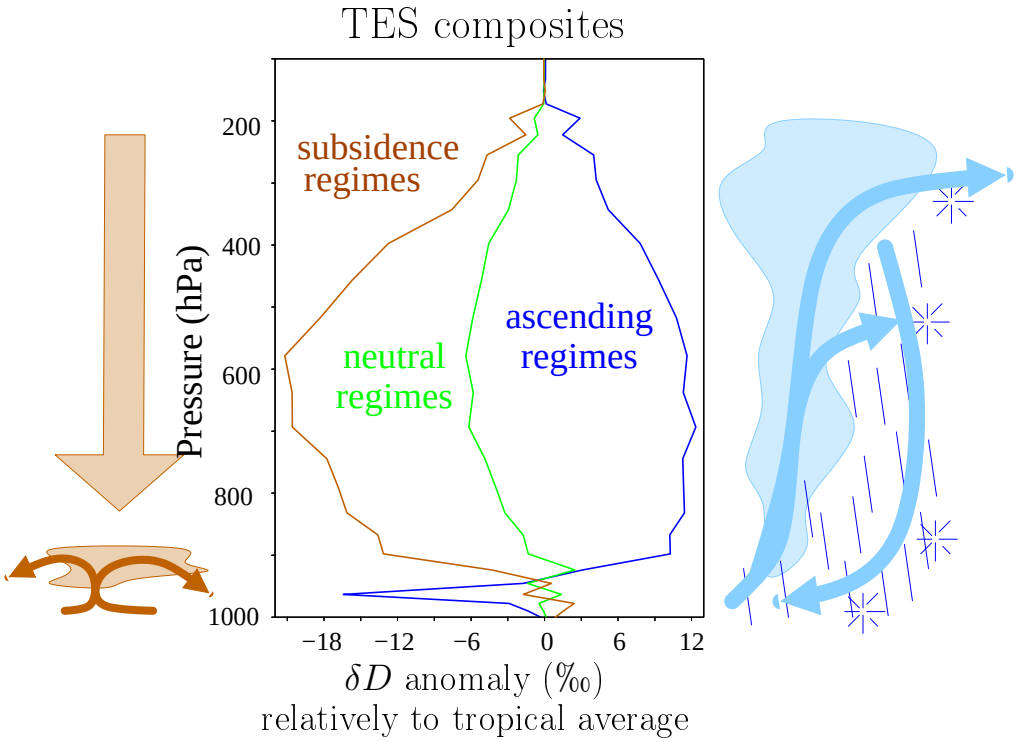

Figure 1.12: Vertical profiles of water vapor δD as measured by TES in the tropics, on average for dynamical regimes based on NCEP monthly large-scale vertical velocity: ascending regimes ($\omega < -20hPa/d$, blue), neutral regimes ($-20hPa/d \leqslant \omega \leqslant 20hPa/d$, green) and subsidence regimes ($\omega > 20hPa/d$, brown). This illustrates the vertical resolution of TES, with up to 3 independent levels of information.

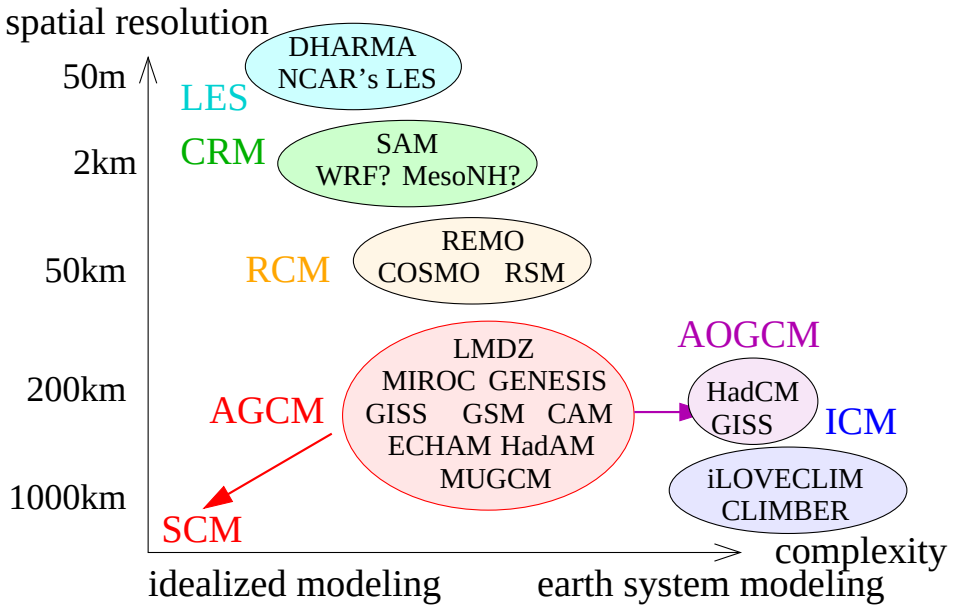

Figure 1.13: Overview of available isotopic models, as a function of spatial resolution and complexity in terms of the diversity in modeled processes.

1.3.2 Modeling

Many modeling tools simulating water isotopes have became available in the past few years (figure 1.13).

General circulation models

General circulation models (GCMs) are the best tool to try and understand the complexity of the controls on the isotopic composition of water vapor and precipitation, because they represent all physical processes involved in these controls (figure 1.2), albeit in a parameterized way. In addition, they are global, so that the only necessary boundary condition for water isotopes is the ocean water composition. Their limitation is their relatively coarse resolution ($\geqslant$100 km).

Since the pioneering work of [Joussaume et al., 1984], water isotopes have been implemented in at least a semi-dozen GCMs: GISS ([Jouzel et al., 1987b, Schmidt et al., 2007]), ECHAM ([Hoffmann et al., 1998]), MUGCM ([Noone and Simmonds, 2002]), GENESIS ([Mathieu et al., 2002]), CAM ([Lee et al., 2007]), GSM ([Yoshimura et al., 2008]), Hadley GCM ([Tindall et al., 2009]), LMDZ ([Risi et al., 2010b]); MIROC ([Kurita et al., 2011]). These models have been used for a wide range of applications, from paleo-climates ([Jouzel et al., 2000, Vuille et al., 2003, Pausata et al., 2011]) to isotopic data assimilation ([Yoshimura et al., 2014]). Some of these models can be coupled to isotope-enabled land surface models, to investigate land-atmosphere interactions ([Yoshimura et al., 2006, Risi et al., 2013]), or to isotope-enabled ocean GCMs, to investigate the feedback of ocean isotopic composition on atmospheric isotopic composition ([LeGrande and Schmidt, 2008]).

The number of isotopic GCMs allows us to perform **model inter-comparison studies**. The SWING (Stable Water Inter-comparison Group) inter-comparison project, phases 1 and 2, provide monthly outputs for AMIP simulations (i.e. with prescribed sea surface conditions) ([Noone and Sturm, 2010, Xi, 2014]). Using the SWING2 archive, inter-comparison studies have been useful to:

- check the robustness between simulated results ([Yao et al., 2013, Conroy et al., 2013, Gryazin et al., 2014]),
- understand the cause of model biases ([Risi et al., 2012b], section 3.2).

In the future possible extensions of SWING2 could include:

- Daily outputs from the existing AMIP simulations, to investigate synoptic and intra-seasonal variability, or even higher-frequency outputs, to investigate the isotopic response to the diurnal cycle.
- Simulations for paleo-climate conditions, i.e. an isotopic version of the Paleo-climate Model Inter-comparison Project (PMIP, [Braconnot et al., 2007, Braconnot et al., 2012]), to investigate how climate variations are imprinted in isotopic archives.
- Simulations using Single Column Model (SCM) versions of GCMs. Outside the isotopic community, studies with SCM are very useful to compare GCMs with data gathered during field campaigns ([Randall et al., 1996, Randall et al., 2003]), to develop and test parameterizations ([Rio and Hourdin, 2007, Hourdin et al., 2012]) or to study processes in an idealized framework ([Sobel and Bretherton, 2000]). This tool could be useful for the isotopic community as well. Vertical isotopic profiles simulated in convective-radiative equilibrium could provide an isotopic "ID" for each GCM.

Higher resolution models

As in GCMs, water isotopes have been implemented in regional models (RCMs): REMO ([Sturm et al., 2005]); isoRSM ([Yoshimura et al., 2010]), COSMO ([Pfahl et al., 2012]). With its zoom functionality, the LMDZ GCM also falls into this category. These models can be use for the same applications as GCMs, but their resolution ($\simeq$10-50km) allows to investigate processes at a much finer scale, e.g. during specific weather events ([Yoshimura et al., 2010, Pfahl et al., 2012]). High-resolution simulations are especially necessary in regions of high and complex topography ([Gao et al., 2013]) and can be used to for paleo-climate applications in such regions ([Eagle et al., 2013]).

Like GCMs, RCMs rely on parameterizations to represent sub-grid scale processes such as atmospheric shallow and deep convection. To represent explicitly these processes, Cloud Resolving Models (CRMs) or Large Eddy Simulations (LES) are necessary. Isotopes have been implemented in a few of such models: SAM ([Blossey et al., 2010]), DHARMA ([Smith et al., 2006]), NCAR's LES ([Lee et al., 2012]). There are on-going projects for WRF and Meso-NH. Such simulations are very useful to study the isotopic response to convective processes without relying on approximations and uncertainties inherent to parameterizations ([Smith et al., 2006, Moore et al., 2014], proposal A.4).

CRMs or LES simulations are very promising tools for the isotopic community and remain to be exploited:

- Idealized simulations could be directly compared to SCMs ([Rio et al., 2009, Couvreux et al., 2010, Hourdin et al., 2012]);
- CRMs or LES applied for case studies derived from observational campaigns could help to understand processes and evaluate GCMs. The lack of isotopic measurements that can provide initial and boundary conditions is a challenge for this application.

Earth system modeling

For paleo-climate applications, water isotopes have been implemented in Intermediate Complexity Models (ICM) (CLIMBER: [Roche et al., 2004], iLOVECLIM: [Roche, 2013]). Compared to GCMs, the advantage of these models is that they are more time efficient, allowing them to run several thousands of years, and they represent more components of the Earth system, including ice sheets. The drawback is that the atmospheric component is less detailed, with much coarser horizontal and vertical resolution and much simpler physical parameterizations.

Model-data synergy

Following the recent increase in data and model availability, tools have been developed in the past few years to rigorously compare models with observations.

Observations must be **co-located** in time and space with the available measurements. GCM simulations in which winds are **nudged** towards reanalyses are useful to ensure that the simulated

meteorological conditions are realistic on a day-to-day basis ([Yoshimura et al., 2008, Risi et al., 2010b]). In the case of remote-sensing observations, the instrument sensitivity is taken into account by applying **averaging kernels** to the model outputs ([Rodgers and Connor, 2003]). These kernels may come directly from retrieval analysis ([Risi et al., 2012a]) or from a "observation simulator" ([Field et al., 2012]).

For paleo-climate applications, forward-proxy models of isotopic archives can be plugged to GCMs or ICMs (e.g. [Caley and Roche, 2013] for marine carbonates).

To summarize, **many observational and modeling tools are now available to study water isotopes.** I think that **the limiting factor now is how to make use of these tools to improve our understanding** of isotopic controls. In the next section we argue that we need to develop new interpretative frameworks.

1.3.3 Interpretative frameworks

Isotopic fractionation

Isotopic fractionation occurs due to the difference in molecule mass (equilibrium fractionation) and diffusivity (kinetic fractionation). Equilibrium fractionation coefficients are well know ([Merlivat and Nief, 1967, Majoube, 1971a, Majoube, 1971b]), except for ice-vapor fractionation at very low temperature ([Ellehoej, 2011]). Kinetic fractionation, which occurs during evaporation from liquid water in unsaturated conditions ([Merlivat and Jouzel, 1979]) or during condensation of ice crystal in supersaturated conditions ([Jouzel and Merlivat, 1984]) is more uncertain. Key uncertainties are the estimation of molecular diffusivities ([Merlivat and Jouzel, 1979, Cappa et al., 2003]), of the supersaturation in cold conditions ([Ciais and Jouzel, 1994, Casado et al., 2016]), of the effective relative humidity around re-evaporating rain drops ([Stewart, 1975, Bony et al., 2008]) or of a coefficient involved in the evaporation of bare soil that depends on the flow regime (turbulent, laminar and stagnant) ([Mathieu and Bariac, 1996, Braud et al., 2009b, Braud et al., 2009a]).

These uncertainties affect mainly second-order parameters such as d-excess, but to a lesser extent δD or $\delta^{18}O$. **Outside very low temperatures (polar regions, near the tropopause) and areas of strong rain re-evaporation in dry environments, the effect of individual phase changes on the water vapor δD are relatively well known.**

q-δD diagrams

The effect of individual phase changes on the water vapor δD can be visualized in q-δD diagrams popularized by [Worden et al., 2007] (figure 1.5), where q stands for specific humidity.

In these diagrams, **Rayleigh distillation** represents the dehydration of an air parcel through condensation. In a case where the condensate precipitates immediately, the remaining water vapor becomes more and more depleted following a logarithmic curve (blue on figure 1.5). In a case where the precipitation re-evaporates partially, the remaining water vapor becomes more and more depleted following a line that lie below Rayleigh (purple curves on figure 1.5). As an air parcel is dehydrated by mixing with a very dry (distilled) air parcel, the remaining water vapor becomes more and more depleted following a hyperbolic curve (orange on figure 1.5) that lies above Rayleigh.

Therefore, the advantage of these diagrams is to visualize the added value of δD compared to q only: different dehydrating processes may have the same effect on q but different effects on δD. Similarly, different moistening processes may have the same effect on q but different effects on δD. The joint q-δD distribution allows us to **discriminate between different moistening and dehydrating processes** ([Noone, 2009, Galewsky and Hurley, 2010, Noone, 2012, Galewsky and Samuels-Crow, 2014]). For example, these diagrams have been used to try and quantify the contribution of rain re-evaporation to tropical humidity ([Worden et al., 2007]), to try and understand moistening processes during the Madden-Julian Oscillation ([Berkelhammer et al., 2012, Tuinenburg et al., 2015], section 2.1.7) or to discriminate between different hypothesis explaining the dryness of the air during a stratospheric intrusion event ([Galewsky and Samuels-Crow, 2014]).

Beyond q-δD diagrams?

We know how each individual phase change and mixing event impacts water vapor δD. The difficulty is how to combine a large number of individual events to reproduce the complex reality. How much of the each air mass condenses, is mixed, is re-moistened with surface evaporation, rain re-evaporation, condensate detrainment? In addition, mixing usually involves more than two air parcels. In fact, air parcels involved are many, since air parcels at each level undergo mixing with air parcels at levels below and/or above and/or to the South, North, West and East, where the condensation, mixing and re-moistening history is different. How could we account for this complexity? q-δD diagrams cannot increase indefinitely in complexity. A better understanding requires to bridge the gap between this simple framework and more complex numerical modeling such as GCM modeling. I think that our progress is currently limited by the lack of an intermediate framework or model. This document will not provide any answer but I plan to work on it in the future (proposal A.4).

1.4 Document outline

In chapter 2, I will review processes controlling the water vapor isotopic composition, with a focus on those for which I have contributed to the understanding. In chapter 3, I try to apply this understanding to better evaluate the representation of convective and cloud processes in GCMs. In chapter 4, I try to apply this understanding to better evaluate the simulated climate response to past climate variations.

Chapter 2

Understanding controls on the water vapor isotopic composition

This chapter is devoted to the understanding of processes controlling the water vapor isotopic composition in the tropical troposphere, both in nature and in models. This is not a comprehensive review: rather, I focus on processes for which I have contributed to the understanding, i.e. convective and cloud processes (section 2.1) and continental recycling (section 2.2).

Process understanding was gained using the **simple** $q - \delta D$ **framework** (section 1.3.3), a single-column model ([Bony et al., 2008, Risi et al., 2008a]), the **LMDZ** GCM ([Hourdin et al., 2006]) in which I have implemented water isotopes ([Risi et al., 2010b]) or the LMDZ GCM coupled to the ORCHIDEE land surface model ([Krinner et al., 2005]) in which I have also implemented water isotopes ([Risi et al.,]).

2.1 Impact of convective and cloud processes

2.1.1 Distillation in convective ascents

The impact of convective and cloud processes on water vapor δD can be understood using the $q - \delta D$ diagram (figure 2.1). Boundary-layer water vapor (point 1 on figure 2.1) lifted by convective updrafts up to the upper troposphere (point 5) undergoes Rayleigh distillation (blue). To first order, vertical profiles of water vapor δD in the tropical environment are set by convective detrainment. Since water vapor δD decreases as air rises in convective updrafts, δD decreases with altitude in the environment.

2.1.2 In the upper troposphere: impact of convective condensate detrainment

In the upper troposphere, convective detrainment is a mixture of the distilled water vapor with condensate. Condensate is enriched: in the upper troposphere, nearly all the initial water vapor has been converted into condensate, so mass conservation implies that averaged over the vertical, condensate has a δD similar to that in the boundary layer vapor. Therefore, when distilled water vapor in the upper troposphere (e.g. point 3) mixes with condensate, δD increases following a mixing line connected with point 1 (cyan curve on figure 2.1). Consequently, even for a small moistening effect, condensate detrainment has a strongly enriched signature.

The strong enriched signature of convective condensate detrainment had been demonstrated by many studies based on satellite observations ([Moyer et al., 1996, Kuang et al., 2003, Nassar et al., 2007]), in-situ observations ([Webster and Heymsfield, 2003, Hanisco et al., 2007, Sayres et al., 2010]) and modeling ([Smith et al., 2006, Bony et al., 2008, Blossey et al., 2010]). The role of the shape of the mixing curve was pointed out by [Dessler and Sherwood, 2003] to explain the strong impact of of detrainment on δD even for a very small moistening (cyan on figure 2.1).

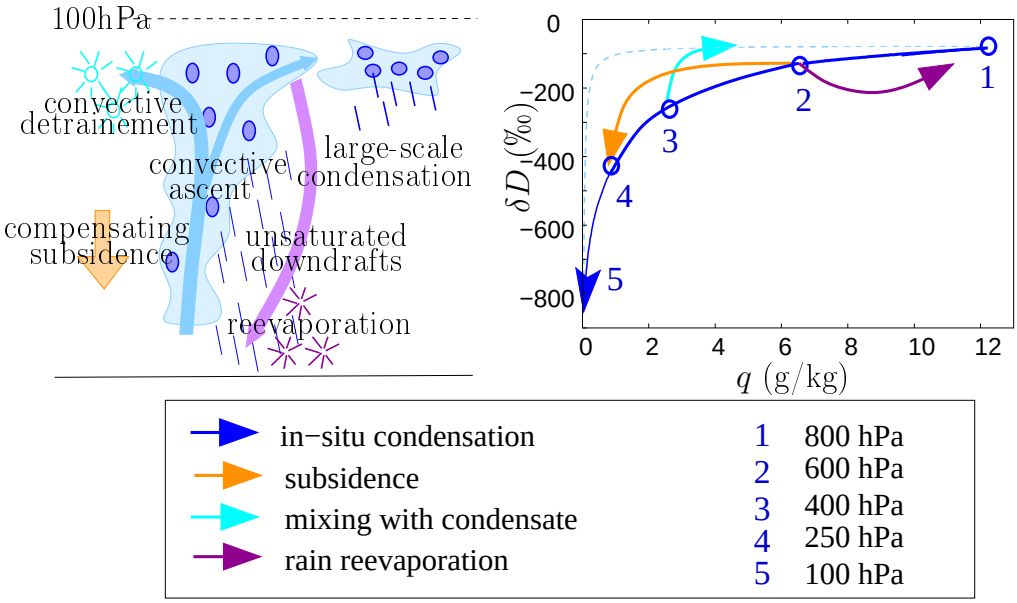

Figure 2.1: Effect of moistening and dehydrating processes associated with tropical deep convection, as illustrated in a q-δD diagram. Point 1 represents the boundary layer vapor. Points 2, 3, 4 and 5 represent distilled boundary layer vapor at different tropospheric levels, following a Rayleigh line.

In the upper troposphere, some in-situ condensation may also occur in anvils or in cirrus clouds. In this case, δD decreases following the same Rayleigh line (blue). All in all, the impact of detrainment on δD dominates over that of in-situ condensation since TES and MIPAS observations suggest that convective regions are associated with more enriched upper-tropospheric δD values (figure 2.2a).

Factors controlling the transport of water vapor from the upper troposphere to the lower stratosphere have been debated. In particular, the low humidity of stratospheric water vapor may be explained either by the low temperature in convective overshoots or by in-situ condensation during slow ascent through the tropical tropopause layer (TTL, $\simeq$14-19 km) [Sherwood and Dessler, 2000, Holton and Gettelman, 2001]). The relative contributions of these two processes is difficult to quantify. The large-scale contribution of the direct injection of ice crystals into the TTL by convective detrainment is unknown ([Folkins et al., 1999, Gettelman et al., 2002, Khaykin et al., 2009]). Water isotope measurement are consistent with some convective injection of ice water through the tropopause layer. Could we use water isotopes to quantify the contribution of direct convective ice detrainment to the moistening of the tropical tropopause layer and lower stratosphere? So far, quantitative estimations have remained a challenge (section 1.2.3).

2.1.3 In the lower troposphere, impact of downdrafts and rain re-evaporation

In the middle or lower troposphere, air can be dehydrated by subsidence in meso-scale descents, convective downdrafts or, in models, by the compensating subsidence. Subsidence at a given level (e.g. point 2) acts as mixing with air at a higher level (e.g. point 4). Therefore, δD decreases following a mixing line connected with point 4.

Rain re-evaporation has a complex effect on water vapor. When rain re-evaporation is partial, light isotopes evaporate first so δD decreases in the water vapor. However, if rain re-evaporation is total, it plays a role similar to mixing with condensate, so δD increases in the water vapor. Therefore, **rain re-evaporation can have either a depleting or an enriching effect**, depending on the fraction of rain drops that re-evaporate (purple curve on figure2.1). At the scale of the tropics, [Worden et al., 2007, Field et al., 2010], using observations and model simulations respectively, argue for a depleting effect. In the Sahel, an arid region, [Risi et al., 2010a] argues for an enriching effect.

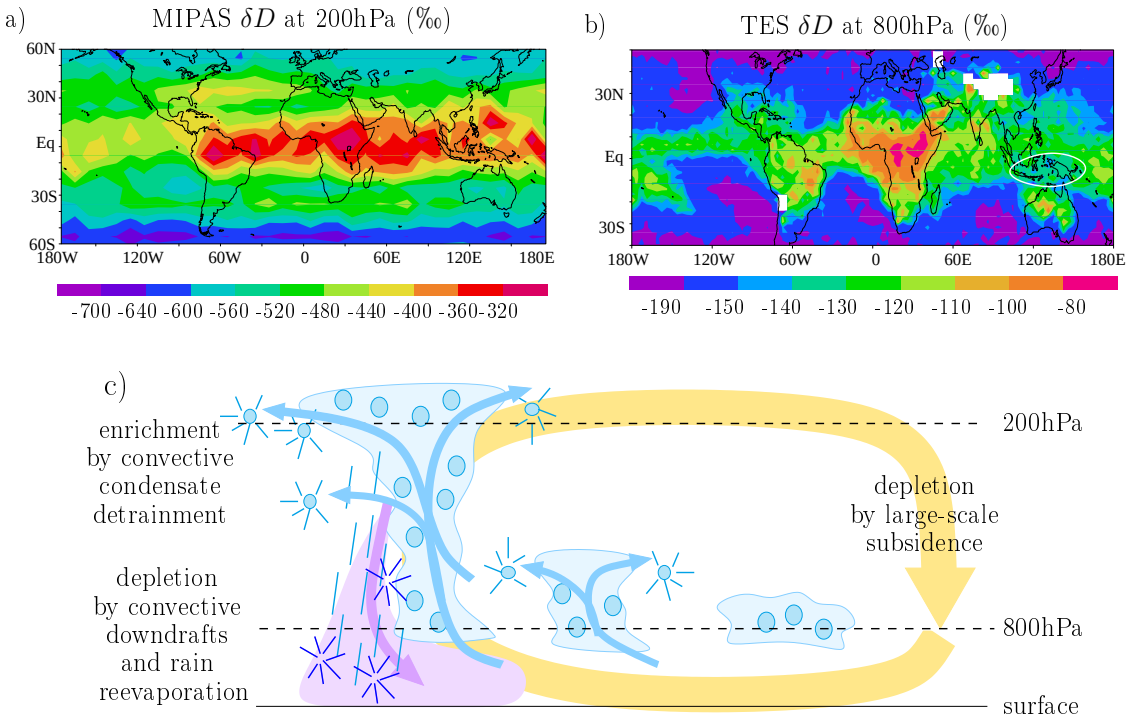

Figure 2.2: Annual mean maps of water vapor δD measured at 200hPa by MIPAS (a) and at 800hPa by TES (b). The white circle shows the Maritime Continent where the amount effect (section 2.1.3) can be observed the most clearly. c) Schematics explaining to first order the distribution of δD at these two levels, with deep convection enriching the water vapor by convective detrainment in the upper troposphere and depleting it by unsaturated downdrafts and rain re-evaporation in the lower troposphere.

In the case where the air is saturated, rain cannot re-evaporate but diffusive exchanges between the rain and the ambient vapor may occur. Since the rain falls from higher altitudes, it is more depleted than if it was in isotopic equilibrium with the ambient vapor. Therefore, diffusive exchanges act to deplete the vapor ([Lawrence et al., 2004, Lee and Fung, 2008]).

In the lower troposphere, deep convective regions are associated with more depleted δD values (figure 2.2b, mainly over the Maritime Continent). It has long been observed that regions and seasons with greater precipitation amount have more depleted precipitation ([Dansgaard, 1964]): this is called the "**amount effect**". The lower-tropospheric water vapor behaves in a similar way. The depletion is explained by a combination of subsidence in unsaturated downdrafts, meso-scale descents and compensating subsidence, of rain re-evaporation and of diffusive exchanges ([Risi et al., 2008a, Field et al., 2010, Kurita, 2013]), in proportions that remain to be quantified.

Note that some studies have explained the amount effect by the vertically-integrated water vapor budget ([Lee et al., 2007, Moore et al., 2014]). Deep convection is associated with convergence of air masses. As convergence increases, more of the vapor originates from the surrounding boundary layer vapor and less originates from fresh surface evaporation. The former being more depleted, as convergence increases, the column-integrated water vapor becomes more depleted. This explanation does not contradict the effect of subsidence, rain re-evaporation and of diffusive exchanges, which are necessary to explain why the surrounding boundary layer vapor is more depleted than fresh surface evaporation. It is just an another angle of view of the same processes.

2.1.4 In the middle troposphere

In the mid-troposphere, the impact of convection is probably a mixture of the effects occurring in the lower and in the upper troposphere, in proportions that depend on the depth of the convective mixing and on the height of convective detrainment ([Lacour, 2015], section 2.1.5).

2.1.5 Impact of convective depth

While precipitation amount is high in many areas of the inter-tropical convergence zone (ITCZ), the expected decrease in lower-tropospheric water vapor δD associated with the increase in precipitation amount (i.e. amount effect) can be seen very clearly only over the Maritime Continent (figure 2.2b,). Does the amount effect depend on the character of deep convection? Several studies suggest that the contributions of deep and shallow convection to precipitation could play a role ([Lee et al., 2015, Sutanto et al., 2015]). Here we test the hypothesis that the amount effect depends on the depth of deep convection.

As a proxy for precipitation amount, or convective intensity, we use the monthly large-scale vertical velocity (ω) at 500 hPa (ω_{500}) ([Bony et al., 2004]). We refer to the amount effect as "strong" if δD steeply decreases with increased ascent (i.e. negative ω_{500}). Conversely, we refer to the amount effect as "weak" if δD weakly decreases with increased ascent, or even increases. As a proxy for the convective depth, we use the pressure level at which the ω profile exhibits the maximum ascent. For example, ω peaking in the upper troposphere is consistent with deep convection, whereas ω peaking in the lower troposphere is consistent with shallow convection.

In LMDZ, locations and months where ω peaks in the upper troposphere, the amount effect is the strongest (figure 2.1.5a, blue). In contrast, in locations and months where ω peaks in the lower troposphere, the amount effect is the weakest (figure 2.1.5a, green). We can explain this behavior as follows (figure 2.1.5b): as deep convection increases, condensation, downdrafts and rain re-evaporation deplete the lower mid-troposphere efficiently. In contrast, as shallow convection increases, more HDO-enriched condensate is detrained into the lower mid-troposphere.

This property simulated by LMDZ is consistent with TES (figure 2.1.5c) and with IASI observations ([Lacour et al., 2016]). This explains why in the lower troposphere, strong convection is associated with depleted water vapor over the Maritime Continent, where convection is the deepest, whereas it is associated with enriched water vapor over equatorial Africa, where shallow convection is very active (figure 2.2b).

This work hs not been published yet.

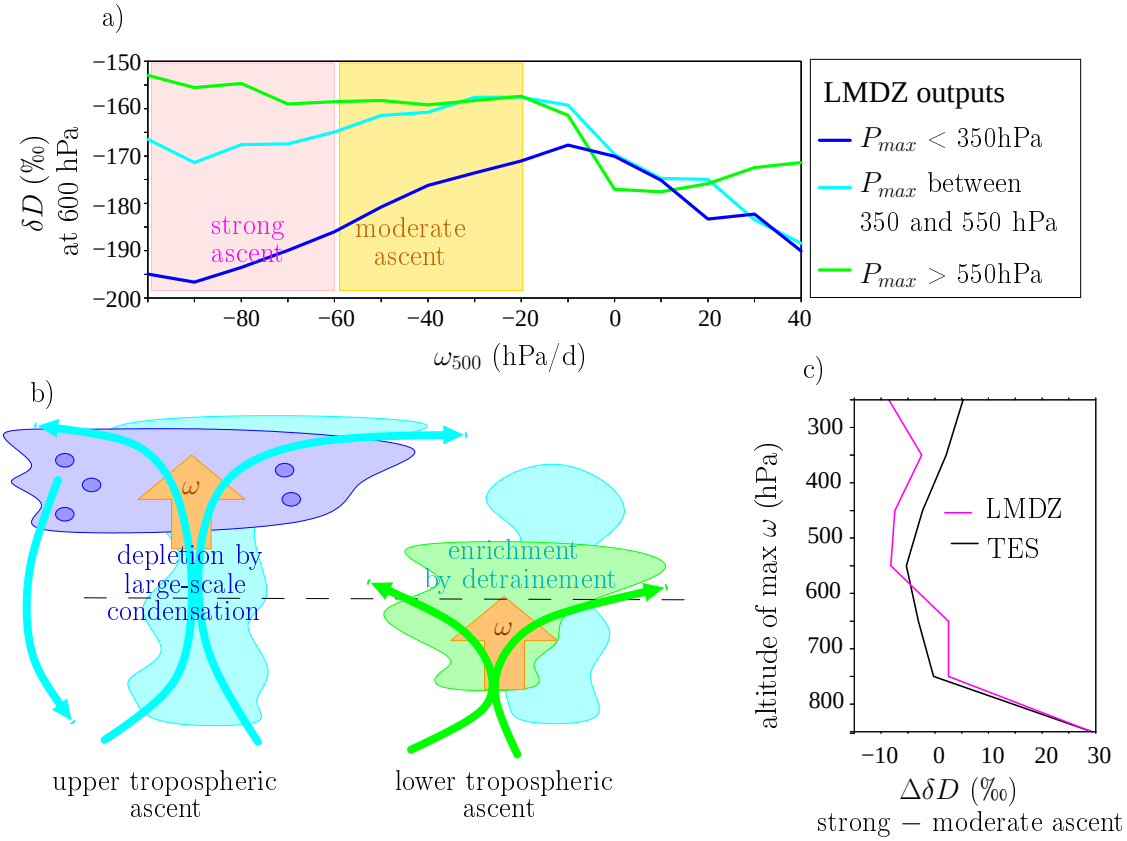

Figure 2.3: a) Monthly water vapor δD simulated by LMDZ at 600hPa as a function of the monthly large-scale vertical velocity at 500 hPa (ω), over tropical oceans. Results are classified into 3 categories depending on the shape of the vertical profile of ω: maximum ascent above 350 hPa (blue), between 350 and 550 hPa (cyan) or below 550 hPa (green). We see that δD decreases more strongly with increased ascent when the ascent peaks in the upper troposphere. b) Processes explaining this effect. c) Difference of δD at 600 hPa between the "strong" and "moderate" ascent regimes (as defined on panel a), for LMDZ and for the TES data.

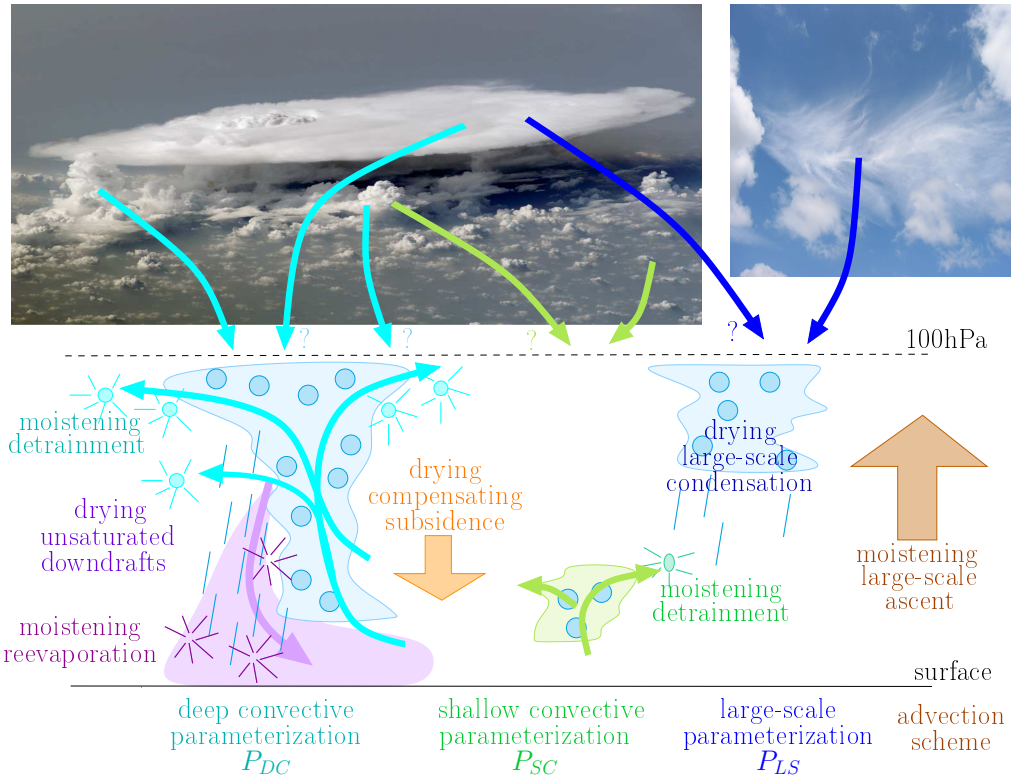

Figure 2.4: Partitioning of precipitation between deep convection (P_{DC}), shallow convection (P_{SC}) and large-scale precipitation (P_{LS}).

2.1.6 In models, impact of convective vs large-scale precipitation partitioning

In GCMs, precipitation is produced mainly by two kinds of parameterizations (Figure 2.4). First, **deep convection** represents the precipitation occurring in convective updrafts at the sub-grid scale. Second, the **large-scale condensation** scheme represents the precipitation produced at the grid scale, when the relative humidity at a given level exceeds a threshold. Partitioning between these two schemes is arbitrary ([Lawrence and Salzmann, 2008]). Its is model and resolution-specific. For example, some convective updrafts could be resolved at the grid-scale and therefore be dealt by the large-scale condensation parameterization. In contrast, some anvils could be represented by convective mixtures in the convection scheme (e.g. with the Emanuel scheme, [Emanuel, 1991]). Nevertheless, the partitioning between deep convection and large-scale condensation has an important impact on the simulated transport of water vapor and chemical species ([Rasch et al., 1997]), on the cloud vertical distribution and on the intra-seasonal variability of precipitation ([Kim et al., 2012]). Therefore, for a given model in a given configuration, this partitioning must be evaluated.

The isotopic composition of water vapor in the middle to upper troposphere is particularly sensitive to this partitioning (figure 2.5). We compare four versions of LMDZ (described in [Risi et al., 2012b]) in which parameters involved in the convective parameterization, in the large-scale condensation scheme or in the large-scale advection scheme were perturbed (figure 2.5). The proportion of the precipitation occurring as deep convection varies from 18% in the cyan version to 85% in the blue version. To investigate the strength of the "amount effect" in the upper troposphere, we plot water vapor δD at 400 hPa as a function of monthly large-scale vertical velocity at 500 hPa (ω_{500}) over all tropical oceans (figure 2.5a). Some LMDZ versions have a weak amount effect, i.e. δD decreases weakly from moderate to strong ascent regimes (red and blue versions). These versions

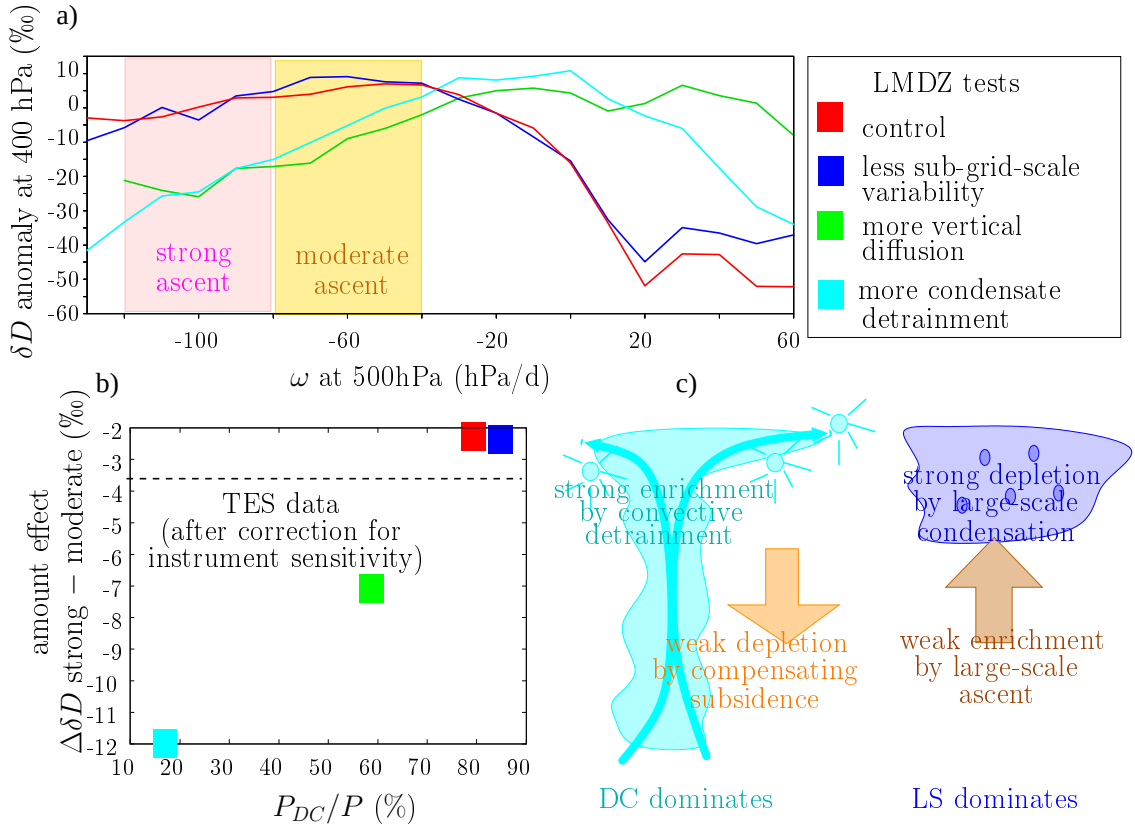

Figure 2.5: a) Monthly water vapor δD at 400 hPa (anomaly with respect to its tropical average) as a function of monthly vertical velocity of large-scale 500 hPa (ω_{500}) over tropical oceans, for four LMDZ versions. Whatever the version of the model, the water vapor is more depleted in subsidence regimes and in regimes of strong ascent characterized by intense convection. The depletion observed when the convection is more intense is called the "amount effect". The magnitude of the amount effect depends on the model version. b) The magnitude of the amount effect (quantified by the δD difference between regimes of strong and moderate ascent) as a function of the proportion of the precipitation (P) produced by deep convection (P_{DC}) to the expense of large-scale condensation. The amount effect is stronger as more precipitation is produced by large scale condensation. c) Schematic to explain this effect.

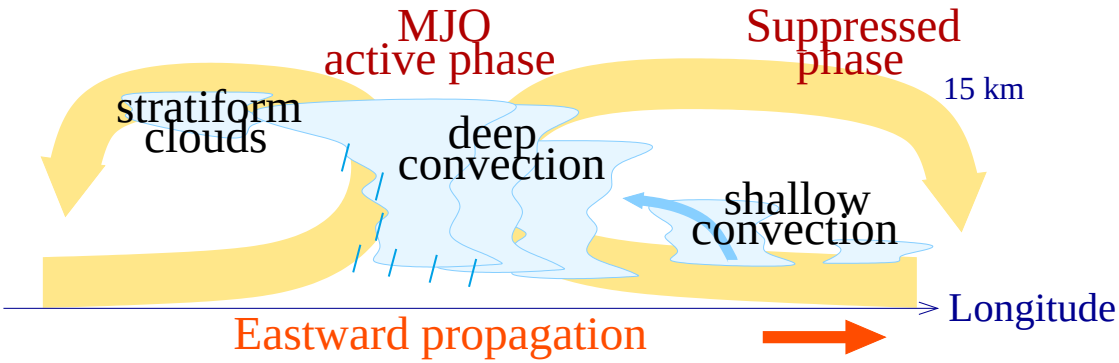

Figure 2.6: Sequence of cloud types associated with the propagation of an MJO event.

happen to be those with the strongest proportion of precipitation occurring as deep convection (figure 2.5b). In contrast, the other versions have a strong amount effect, i.e. δD decreases steeply from moderate to strong ascent regimes (green and cyan versions). These versions happen to be those with a lower proportion of precipitation occurring as deep convection. In fact, there is a very good relationship between the strength of the amount effect and the proportion of precipitation occurring as deep convection (figure 2.5b): **precipitation depletes the upper-tropospheric water vapor all the more as it occurs as large-scale precipitation at the expense of deep convective precipitation**.

When deep convection dominates, the largest terms in the water budget are the moistening by deep convective detrainment compensated by the dehydration by the compensation subsidence (figure 2.5c). In contrast, when large-scale precipitation dominates, the largest terms in the water budget are the moistening by large-scale vertical advection of water vapor compensated by the dehydration by large-scale condensation. According to the $q-\delta D$ framework (section 1.3.3), condensate detrainment has a strong enriching effect. For a given moistening, convective detrainment enriches the water vapor more than vertical advection. Therefore, when the detrainment-subsidence balance dominates over the advection-condensation balance, the source of water vapor is much more enriched. This contributes to the more enriched δD when deep convection dominates. In addition, according to the $q-\delta D$ framework, for a given dehydrating effect, subsidence depletes the water vapor less than condensation. This also contributes to the more enriched δD when deep convection dominates.

This property could open the door to the use of isotopic observations to constrain the partitioning between deep convection and large-scale condensation parameterizations. This work has not been published yet.

2.1.7 Convective processes during the Madden-Julian Oscillation

What is the MJO? Why is it so difficult to simulate by GCMs?

The Madden-Julian Oscillation (MJO, [Madden and Julian, 1971, Madden and Julian, 1972]) is the largest mode of intra-seasonal variability in the tropical atmosphere ([Zhang, 2005]). With a periodicity of 30-90 days, it exhibits a large area of strong convection that initiates over the Western Indian Ocean and propagate westwards until it fades away in the central Pacific (figure 2.6). It involves a tight coupling between large-scale circulation, convective, cloud and radiative processes, and air-sea interactions. For example, the large-scale dynamical response of the atmosphere to convective heating leads to large-scale convergences that feeds back positively onto convection ([Ghil and Mo, 1991]). The greenhouse effect of anvil clouds associated with convection can also contribute to the heating ([Kim et al., 2015]). Shallow and mid-level convective moistening play a key role to pre-condition the atmosphere to the active phase of the MJO ([Inness et al., 2001, Benedict and Randall, 2007, Cai et al., 2013]). Moisture-convection feedbacks may contribute to slowing down the MJO propagation ([Bony and Emanuel, 2005]). A recharge-discharge mechanism, in which shallow convection progressively moistens the free troposphere until a threshold is reached

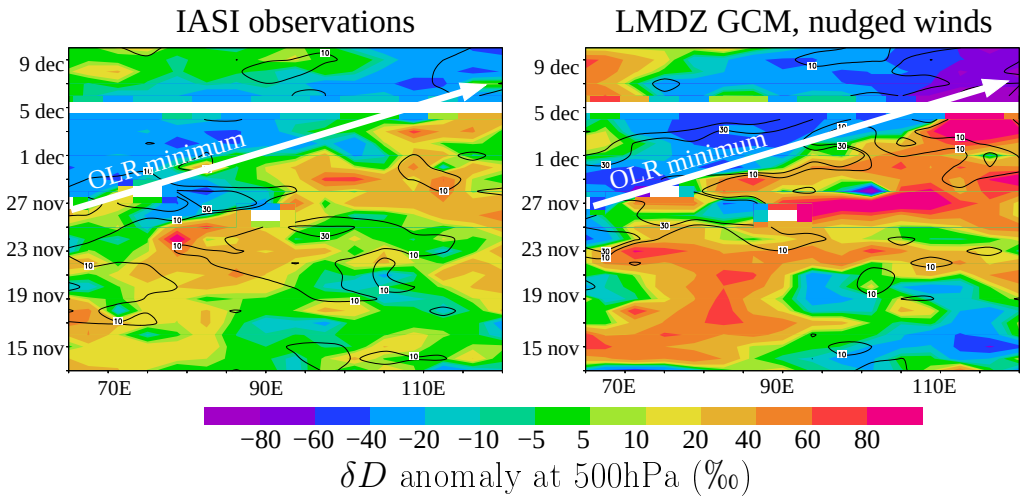

Figure 2.7: Propagation of the November 2011 MJO event as observed by the IASI satellite instrument (a) and as simulated by the LMDZ model when nudged by reanalysis winds (b). Water vapor δD and q at 500 hPa are plotted as colors and contours respectively, as a function of longitude and time. The white arrow illustrate the propagation of the minimum in OLR (Out-going Long-wave Radiation) which tracks the convective maximum.

that allows for the maintenance of deep convection, may explain the slow periodicity ([Maloney, 2009]). Air-sea coupling may also play a role ([Waliser et al., 1999, DeMott et al., 2014]).

To reproduce the MJO, a GCM must therefore have a set of physical parameterizations that can simulate all these feedbacks. It is therefore not surprising that for decades, GCMs have had difficulties to simulate the MJO ([Slingo et al., 1996, Lin and Coauthors, 2006, Kim et al., 2009, Hung et al., 2013]).

Joint $q - \delta D$ evolution during observed MJO events

Since these feedbacks at play during the MJO involve convective and cloud processes that are known to impact water stable isotopes, could isotopic measurement help to understand the reason for the model difficulties? This was the motivation of my CONVISO project (2013-2017, funded by the French National Research Agency), in collaboration with my post-doc Obbe Tuinenburg. As a first step, the impact of convective and cloud processes on water vapor δD during MJO events needs to be understood, both in nature and in models.

Using TES observations, q and δD during composites of MJO events can be analyzed ([Berkelhammer et al., 2012]). With the unprecedented spatio-temporal coverage offered by IASI, q and δD during individual MJO events can be also documented. For example, figure 2.7a shows q and δD observed at 500 hPa during the November 2011 MJO event that took place during the CINDY-DYNAMO campaign ([Yoneyama et al., 2013]). Observed q is maximum 0 to 1 day before the convective maximum, whereas observed δD is minimum 3 days after after the convective maximum.

For more representative statistics, we plot the joint $q - \delta D$ evolution for 7 MJO events in the central Indian Ocean, including the November 2011 event (figure 2.8). In observations, on average, the $q - \delta D$ evolution follows a circular clockwise shape: a moistening before the active phase, a depletion during the active phase, then a drying and finally a re-enrichment (figure 2.8a).

Joint $q - \delta D$ evolution during MJO events simulated by LMDZ

LMDZ captures the observed $q - \delta D$ cycle for the CINDY-DYNAMO case, notably the δD minimum lagging the convective maximum by several days (figure 2.7b). LMDZ captures the circular clockwise shape to some extent for about one third of MJO events (figure 2.8b). But for many other events, the shape is simply a “return trip” following a diagonal: simultaneous moistening and depletion up to the convective maximum, followed by a drying and re-enrichment after the

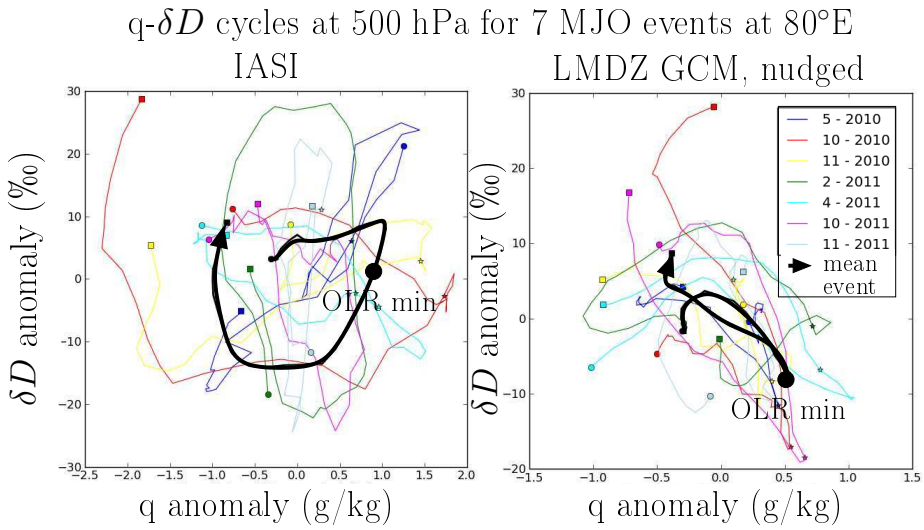

Figure 2.8: δD anomaly as a function of q anomaly at 500 hPa as observed by IASI (a) and simulated by LMDZ (b) for 7 MJO events at 80°E (in the central Indian Ocean) during the period 2010-2011. The black line shows the average over the different events. Stars represent values on the day of maximum precipitation, circles represent values 17 days before this maximum, and squares represent values 17 days after this maximum. The date (month and year) of the start of each event is listed in the legend.

convective maximum (figure 2.8b). This suggests that LMDZ does not reproduce the sequence of moistening and drying processes properly during these MJO events.

What determines the $q - \delta D$ shape in LMDZ? To address this question, dq/dt and $d\delta D/dt$ tendencies from the different parameterizations were analyzed in detail ([Tuinenburg et al., 2015]).

What determines the q-δD shape in LMDZ for well-simulated events and in nature?

For events showing the circular clockwise shape, there is first a moistening by large-scale convergence that occurs without affecting δD. Then, during the few days surrounding the convective maximum, both convection and large-scale condensation deplete the water vapor (consistent with the amount effect), while strong large-scale ascent supplies enough water vapor for q to remain constant. Then, the large-scale ascent weakens and becomes to weak to compensate for the drying by convection and large-scale condensation, so q decreases. Finally, large-scale convergence recycles the air with fresh and enriched vapor, so δD increases back to its initial value.

Since LMDZ captures the observed $q - \delta D$ evolution well for these events, we propose that a similar sequence of processes occurs in nature. The $q - \delta D$ evolution suggests that before the active phase, **humidity builds up mainly due to large-scale convergence**. If the humidity build-up was due to shallow convection ([Benedict and Randall, 2007, Maloney, 2009]), we would expect a simultaneous increase in δD, which is not the case here. More analysis is needed to check that the observed $q - \delta D$ evolution reflects a dominant role of large-scale convergence over shallow convection in the moisture build-up.

What determines the q-δD shape in LMDZ for poorly-simulated events? Implications to understand model difficulties in simulating the MJO

For events showing the diagonal return-trip shape, the processes at play are the same but the time sequence is different. In particular, convection triggers sooner, as soon as q increases, leading the δD to decrease in concert with the q increase. Then, convection and large-scale condensation weaken sooner while the large-scale convergence recycles the air sooner, leading the δD to increase in concert with the q decrease.

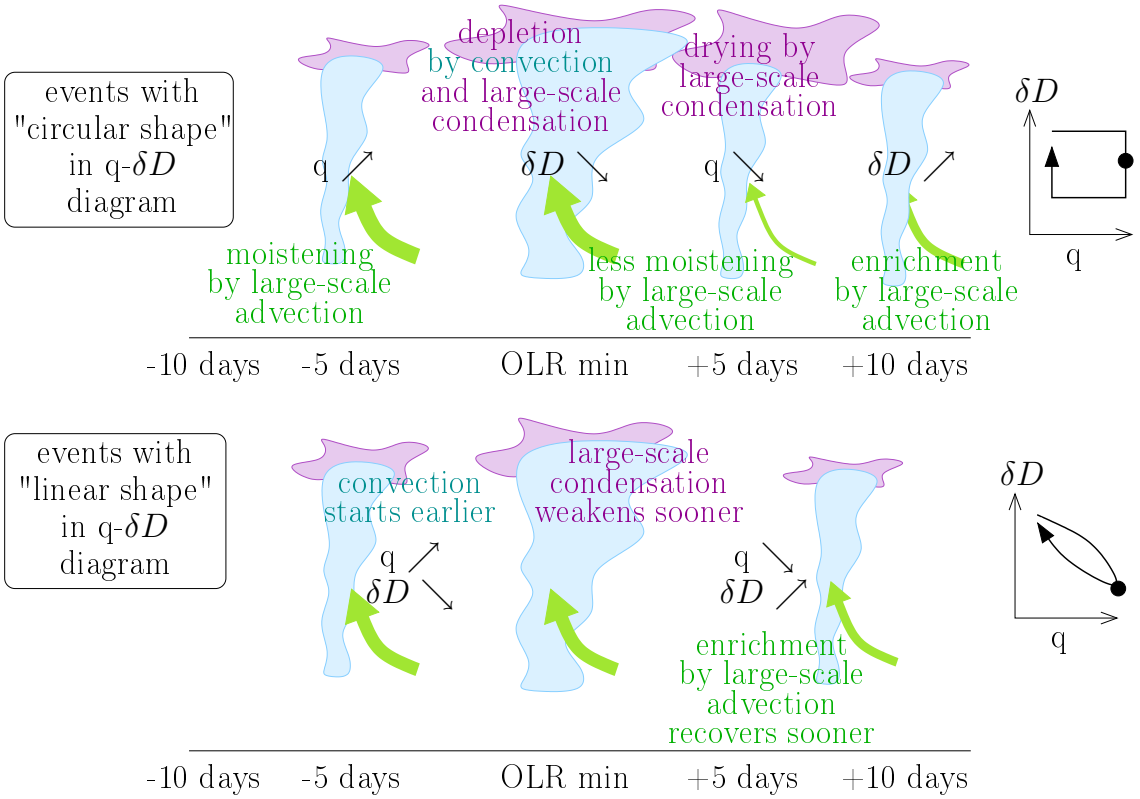

Figure 2.9: Schematic showing the sequence of moistening and dehydrating process simulated by LMDZ during two kinds of MJO events: events showing the circular, clockwise shape (a) and those showing the diagonal return-trip shape (b) in the $q-\delta D$ diagram. Blue and purple clouds represent deep convective clouds and large-scale condensation clouds respectively. Green arrows represent large-scale advection.

Since LMDZ does not capture the observed $q - \delta D$ evolution for these events, we hypothesize that the simulated sequence of events reflects LMDZ faults. These faults might be responsible for the poor MJO simulation when LMDZ is run in a free mode. In particular, the fact that **convection triggers too soon**, before the moisture has the time to build up, is a possible cause for the poor MJO simulation by models ([Kim et al., 2012, Kim et al., 2014]). This could be due to the underestimated sensitivity of convection to tropospheric humidity of most convective parameterizations ([Derbyshire et al., 2004]).

These results suggest that the joint $q - \delta D$ evolution during MJO events is useful for model evaluation. Work is in progress to test this hypothesis by comparing sensitivity tests with LMDZ (proposal A.7).

2.2 Impact of continental recycling

2.2.1 Impact of continental recycling on water vapor δD and d-excess

Water vapor δD is all the more enriched as recycling of precipitation through evapo-transpiration is high. This property may contribute to the maximum enrichment that is observed by satellites over tropical land masses ([Worden et al., 2007, Brown et al., 2008, Frankenberg et al., 2009]). This property is also the basis for studies trying to quantify continental recycling ([Salati et al., 1979, Risi et al., 2013]). Water vapor from vegetation transpiration is much more enriched than oceanic evaporation. This is because lighter isotopes evaporate more easily from free liquid surfaces. In contrast, transpiration is not associated with fractionation relatively to soil water, because there is no fractionation during root extraction ([Washburn and Smith, 1934, Barnes and Allison, 1988, Flanagan and Ehleringer, 1991]) and all water extracted by the root needs to be transpired shortly after. Soil water originates from precipitation, which is to first order at equilibrium with the ambient vapor ([Field et al., 2010]), and thus more enriched than the ambient vapor (figure 2.10).

Evaporation from bare soil is characterized by a strong signature in the second-order parameter d-excess ($d = \delta D - 8 \cdot \delta^{18}O$, section 1.2.1) (figure 2.10). This is because kinetic fractionation during the evaporation of soil water is very strong ([Mathieu and Bariac, 1996, Braud et al., 2009b, Braud et al., 2009a]). As kinetic fractionation increases, the diffusivity coefficients become important and the evaporation of HDO is favored by its high diffusivity. This property is the basis of studies trying to partition continental recycling into its transpiration and evaporation components ([Gat and Matsui, 1991]).

2.2.2 Implications to quantify continental recycling

These two properties could in theory be exploited to quantify both the continental recycling (with $\delta^{18}O$ or δD) and its components (with d-excess). In practice, it is difficult. First, d-excess cannot presently be measured by satellite, and in-situ measurements with sufficient precision remain scarce ([Noone et al., 2012, Tremoy et al., 2012]). Satellites can measure δD from space with reasonable precision and spatio-temporal coverage, but lack absolute calibration. Placing satellite measurements on figure 2.10 in an attempt to quantify continental recycling is thus not applicable.

In [Risi et al., 2013], I rather tried to focus on temporal variations of water vapor δD. I explored the potential of satellite isotope measurements to quantify the contribution of continental recycling to the intra-seasonal variability in water vapor in different regions. I compared estimates of this contribution by directly tracking water in LMDZ-ORCHIDEE or by isotopic methods. I showed that unfortunately, it is difficult to get quantiative estimates of the recycling contribution from isotopic methods, for two reasons. First, uncertainties associated with isotopic satellite observations lead to contradictory results between the TES and GOSAT datasets. Second, and more fundamentally, the isotopic composition of water vapor is sensitive to other processes than continental recycling, such as the intensity and depth of the turbulent and convective mixing (section 2.1). It is **very difficult to disentangle the different processes and extract the continental recycling component only**.

With the growing deployment of in-situ instruments that measure surface water vapor d-excess (section 1.3.1), will we be able to use this parameter? Even if the case, the same limitation

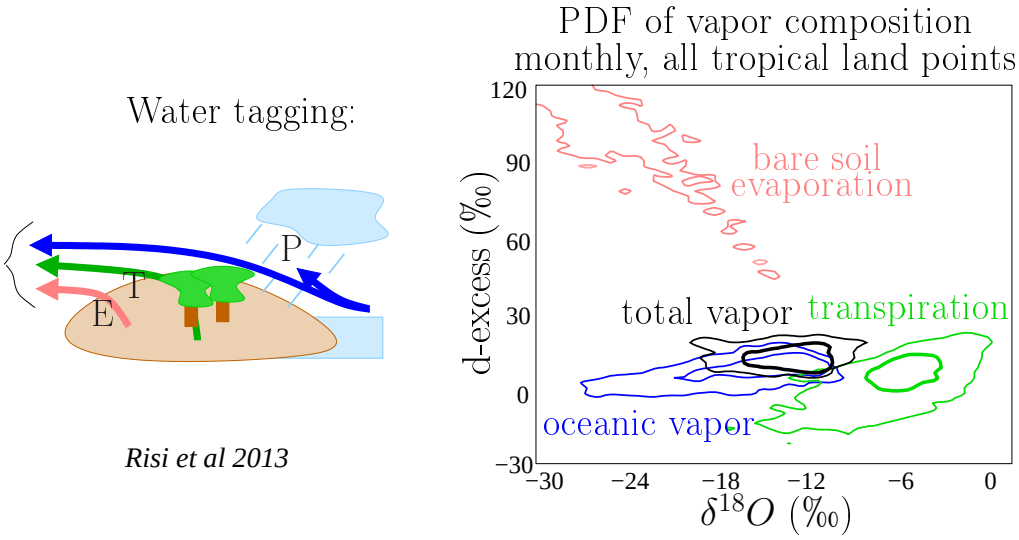

Figure 2.10: Probability density function of near-surface water vapor δD and d-excess (black) simulated by LMDZ for all tropical land locations. Using water tagging, water vapor was decomposed into three components depending on their evaporative origins: vapor originating from ocean evaporation (blue), vapor originating from land surface transpiration (green) and vapor originating from bare soil evaporation (pink).

associated with our incomplete understanding will remain. In the case of d-excess, uncertainties reside in atmospheric processes but also in land surface hydrological processes. In particular, a multi-layer soil model is necessary to simulate the d-excess of the evapo-transpiration flux ([Risi et al.,]).

Chapter 3

Using water stable isotope measurements to evaluate and improve physical parameterizations

In this chapter, I try to use the understanding reviewed in chapter 2 to better evaluate and improve the representation of convective and cloud processes in GCMs, trying to go beyond the usual suggestion that water isotope measurement *have the potential* to help evaluate and improve models.

3.1 Overview

3.1.1 A necessary condition: the representation of isotopic processes is less uncertain than that of physical processes

Using isotopes for improving the representation of physical processes by models is possible only if the representation of isotopic processes is less uncertain than the representation of physical processes. In section 1.3.3, we argue that isotopic fractionation during individual phase changes is well known, at least for δD in the tropical troposphere. The major uncertainty in the simulation of δD is thus how to combine all phase changes of the water cycle and all advection and mixing events between air parcels to reproduce the complex reality.

3.1.2 Water isotopes to understand the cause of model biases

When there is a well-known model bias in the simulation of a meteorological variable M, water isotope measurements can help discriminate between different hypotheses to explain this bias. To do so, we can plot the bias for an isotopic variable I as a function of the bias for M, for different sensitivity tests or for different models (figure 3.1, squares). Using some theory, we can predict how the bias in I should relate to the bias in M depending on the reason for the bias M (figure 3.1, arrows). If the different model simulations plot along one of these theoretical lines, this suggests the most likely reason for the bias in M. I will illustrate this method by my study on the middle-upper tropospheric subtropical bias in relative humidity ([Risi et al., 2012b], section 3.2).

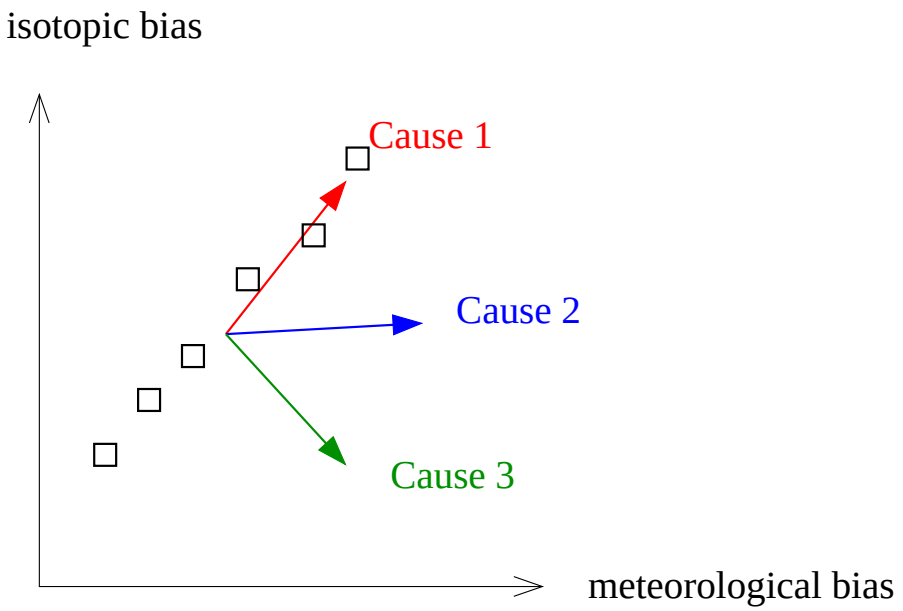

Figure 3.1: Method to discriminate between different hypotheses for processes causing a meteorological bias in a GCM. Arrows represent the expected relationship between the meteorological bias and an isotopic bias depending on the reason for these biases. Squares represent different models or sensitivity tests.

3.1.3 "Isotopic mysteries": water isotopes to detect shortcomings in the representation of physical processes

GCMs exhibit some common model biases for water isotopes. For example, all isotopic GCMs underestimate the latitudinal gradient in upper tropospheric water vapor δD ([Risi et al., 2012a]). They all underestimate the variability in water vapor and precipitation d-excess at the daily scale in polar regions ([Steen-Larsen et al., 2013]). They all underestimate the isotopic depletion recorded at LGM in tropical archives ([Jouzel et al., 2000, Werner et al., 2001, Risi et al., 2010b, Jasechko et al., 2015]). Do these biases reveal a common problem of GCMs to represent some physical processes? Does it mean some key processes are missing?

If a climate simulation seems correct when compared to classical climate variables, it could be at the price of compensating errors. Such errors may compoensate for q and other hydrological variables, but not always for water isotopes. Therefore, water isotopes are helpful to detect shortcomings in the representation of physical processes. This opportunity has remained largely unexplored so far. I present a possible explanation for underestimated latitudinal gradient in upper tropospheric δD (section 3.3).

3.1.4 Water isotopes to tune physical parameters

GCMs rely on physical parameterizations, in which empirical model parameters are tuned to optimize the global simulation ([Mauritsen et al., 2012, Hourdin et al., 2012]). Several studies have shown the sensitivity of simulated water isotopic composition of vapor or precipitation to model parameters in cloud or convective parameterizations ([Schmidt et al., 2005], [Bony et al., 2008], [Lee et al., 2009], [Field et al., 2014]). This suggests that water isotopic measurements could help constrain some tunable model parameters.

However, processes controlling water isotopes are complex. Several model parameters can impact the water isotopic composition in the same way, so the model tuning is an under-constrained problem. Ideally, it is recommended to combine several variables, and not only isotopic variables, in the tuning procedure. It is also important to understand exactly to which physical process water isotopes are sensitive, beyond individual model parameters.

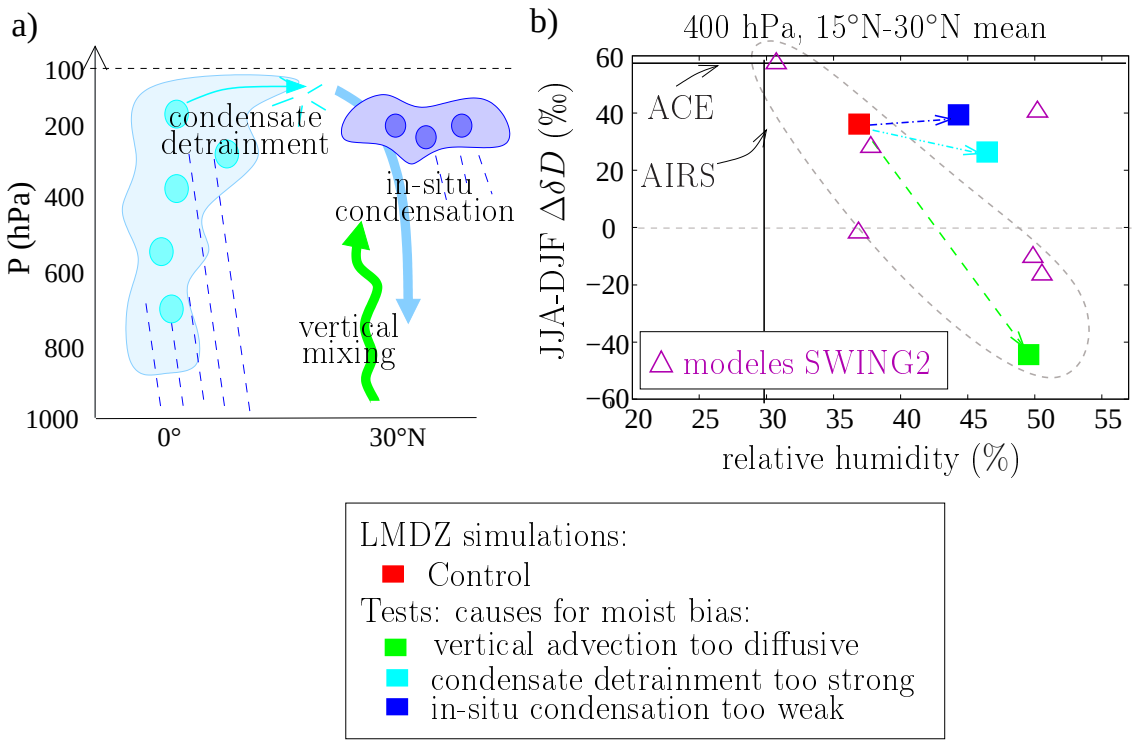

Figure 3.2: a) Hypotheses for processes that could explain the moist bias in the subtropical middle and upper troposphere shared by all GCMs: insufficient condensation (blue), excessive convective detrainement (cyan), or excessive vertical diffusion (green). b) Seasonality ofδD as a function of relative humidity in the subtropical mid-troposphere, for observations (black), sensitivity tests with the LMDZ GCM (full colored squares) and for SWING2 models (purple empty squares) ([Risi et al., 2012b]). Relative humidity and isotopic observations from AIRS and ACE respectively are also shown.

In section 3.4, I present a preliminary study using water vapor δD measurements to evaluate the convective depth (section 3.4).

3.2 Understanding the bias in middle and upper-tropospheric subtropical humidity

This is an example of how water isotope measurements could be used to understand a well-known meteorological bias, using the methodology explained in section 3.1.2.

For decades, climate models have suffered from a wet bias in the middle and upper tropical and subtropical troposphere ([Soden and Bretherton, 1994, Salathe and D, 1995, Chen et al., 1996, Roca et al., 1997, Chen et al., 1998, Allan et al., 2003, Brogniez et al., 2005, Pierce et al., 2006, John and Soden, 2007, Sherwood et al., 2010, Chung et al., 2011]). The bias can be explained by many different hypotheses, such as insufficient condensation, excessive convective detrainement, or excessive vertical diffusion ([Risi et al., 2012b], figure 3.2a). To test whether these different hypotheses are associated with specific isotopic signatures, 3 sensitivity tests with LMDZ were performed:

1. one with a modified parameter in the large-scale condensation scheme leading to reduced large-scale condensation (blue),
2. another with reduced precipitation efficiency in the convective scheme leading to enhanced convective detrainment (cyan),
3. another with a modified advection scheme leading to enhanced vertical diffusion (green).

In each of these tests, the moist bias is enhanced in the same way, so humidity measurements alone cannot discriminate what is the cause of the moist bias. In contrast, the effect on δD depends on the test, especially the effect on the seasonality of subtropical mid-tropospheric δD (figure 3.2b). The δD seasonality is not affected much when large-scale condensation is reduced or when detrainment is enhanced, but it is strongly reduced, or even reversed, when the vertical diffusion is increased (figure 3.2b, green).

Relative humidity observations by AIRS show that the control LMDZ simulation (red) is already too moist (figure 3.2b), consistent with the common moist bias shared by all GCMs. In addition, ACE observations show that the δD seasonality simulated by the control version of LMDZ is lower than observed. More precisely, the control LMDZ simulation plots along the line linking the observations and the excessive diffusion simulation. This suggests that in the control LMDZ simulation, the cause of the moist bias is a vertical advection that is already too diffusive.

To identify the reason of the moist bias in GCMs, the available SWING2 models were plotted on figure 3.2b (purple triangles). Most models plot along a line linking the control and the excessive diffusion simulation. Models exhibiting the largest moist bias have the lowest (or most reversed) seasonality. This suggests that **the most frequent reason for the moist bias in most of these models is excessive vertical diffusion**. For example, this could be due to insufficient vertical resolution.

3.3 Identifying a missing process controlling upper-tropospheric convective detrainment

All GCMs from the SWING2 archive systematically underestimate the zonal gradient in upper tropospheric water vapor δD ([Risi et al., 2012a]). Does this indicate that a process in the upper troposphere is missing in all those GCMs? This study has not been published yet.

A systematic bias in the simulated upper tropospheric δD

In MIPAS observations, annual-mean upper-tropospheric water vapor δD at 200 hPa is maximum in deep convective regions, i.e. in the inter-tropical convergence zone (ITCZ), especially above equatorial land masses (equatorial South America and Africa) (figure 3.3a). This probably reflect the enriching effect of condensate detrainment by deep convection (section 2.1.2). Subtropical regions are comparatively more depleted, especially the regions undergoing strong subsidence at the East of oceanic basins (off the coast of California, Peru and Angola). We can quantify this pattern by calculating the difference $\Delta\delta D$ between annual zonal-mean δD in the equatorial region (15°S-15°N) and annual zonal-mean δD in the tropical region as a whole (30°S-30°N). In MIPAS observations, δD is 50‰ more enriched in the equatorial region than in the tropical region as a whole ($\Delta\delta D = 50$‰). ACE observations are qualitatively consistent ($\Delta\delta D$=30‰.

LMDZ cannot capture this pattern (figure 3.3b). It does capture a local maximum of upper-tropospheric water vapor δD above equatorial land masses, but it is much weaker. Over ocean, LMDZ does not capture the observed enrichment above the inter-tropical convergence zone. In LMDZ, $\Delta\delta D$ is only 13‰.

All other GCMs from the SWING2 database share the same difficulties as LMDZ (figure 3.3c), with $\Delta\delta D$ ranging from -14‰ to 18‰.

Upper tropospheric δD reflects the moistening impact of convective detrainment

To try and understand the reason for the disagreement, we compared different sensitivity tests (the same as in section 3.2, [Risi et al., 2012b]). We notice that simulated $\Delta\delta D$ is very sensitive to the contribution of upper tropospheric convective detrainment to the water budget (figure 3.3c). In sensitivity tests where convective detrainment moistens the upper troposphere the most, $\Delta\delta D$ is the largest. This is consistent with the hypothesis that the equatorial maximum in δD is associated with a maximum in convective detrainement. The absence of any relationship between Δq (defined

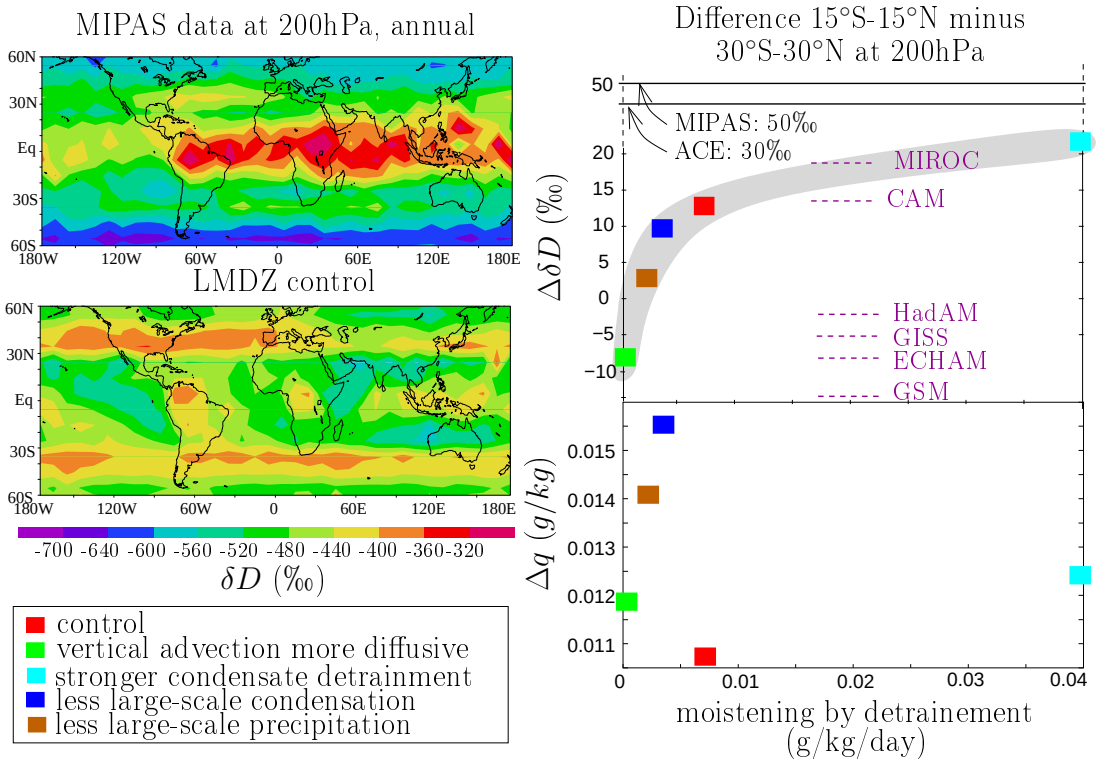

Figure 3.3: a) Annual-mean distribution of water vapor δD observed at 200 hPa by MIPAS. b) Same as (a) but simulated by LMDZ. The model outputs were co-located and averaging kernels were applied. c) Difference of δD ($\Delta\delta D$) between the tropical average (30°S-30°N) and the equatorial average (15°S-15°N) as a function of moistening by convective detrainment at 200 hPa simulated by LMDZ, for 5 sensitivity tests. $\Delta\delta D$ is a proxy for the contrast between the equatorial, deep convective region, where observed δD is enriched, and the subtropical regions, where observed δD is depleted. $\Delta\delta D$ observed by MIPAS and ACE and simulated by other GCMs from the SWING2 database are also shown. The moistening by detrainment is not available as a diagnostic in the SWING2 archive, so only the $\Delta\delta D$ values are shown. d) Same as (c) but for q instead of δD.

similarly as $\Delta\delta D$) and moistening by detrainement supports the advantage of δD to quantify the effect of convective detrainment (figure 3.3d).

In spite of the link between δD and the moistening by detrainement, none of the sensitivity tests is able to simulate a $\Delta\delta D$ as strong as observed. The relationship with moistening by detrainment seems to saturate. In one of the tests (cyan on figure 3.3c), the convective precipitation efficiency (i.e. the proportion of the condensate that falls as precipitation, ϵ_p, prescribed as horizontally constant in LMDZ) was divided by 2, leading the moistening by detrainment being multiplied by a factor of 5 compared to the control version. Even in this extreme test, $\Delta\delta D$ remains limited to 20‰ only. This suggests that simply tuning parameters is not sufficient to capture the observed δD distribution.

We note that the range of $\Delta\delta D$ values for the 6 other GCMs coincides with the range of $\Delta\delta D$ values simulated by the different model versions of LMDZ (figure 3.3c), suggesting that our sensitivity tests allow us to sample the diversity of behaviors in GCMs. A common process may be missing in all models.

The missing effect of updraft velocity on precipitation efficiency

To increase $\Delta\delta D$, we would need to decrease ϵ_p in the most convective regions only. To do so, the convective precipitation efficiency ϵ_p, prescribed as horizontally constant in GCMs, should vary with convective intensity. We expect that when updrafts are more vigorous, the fall speed of ice

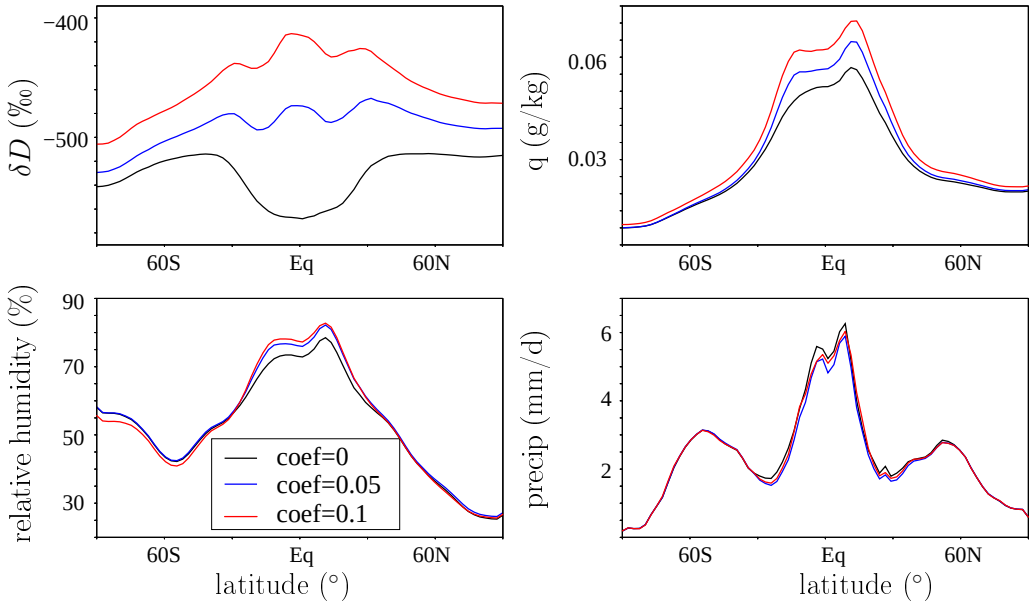

Figure 3.4: a) Annual, zonal mean δD at 200 hPa simulated by LMDZ for 3 values of $coef$. b) Same for q.

crystals is smaller, so a larger proportion of condensate should detrain rather than precipitate. So ϵ_p should be smaller. We hypothesize that neglecting this effect in GCMs is responsible for the difficulties to simulate upper-tropospheric δD.

To test this hypothesis, we implemented this effect in LMDZ. In LMDZ ϵ_p varies linearly with height from 0 at cloud base to ϵ_p^{max} at cloud top, where ϵ_p^{max} is a global constant. To simulate the effect of updraft velocity on ϵ_p, we replace ϵ_p^{max} by $\epsilon_p^{max,eff}$ calculated as:

$$\epsilon_p^{max,eff} = \epsilon_p^{max} - coef \cdot \sqrt{CAPE}$$

where $CAPE$ is the convective available potential energy. $\sqrt{CAPE}$ is an approximation for updraft velocity ([Williams and Renno, 1993]). $coef$ is a tunable parameter: when set to 0, $\epsilon_p^{max,eff} = \epsilon_p^{max}$ as in the control version. As $coef$ increases, the impact of updraft velocity on ϵ_p increases.

Although the impact of this modification on simulated upper-tropospheric q is small, the impact on upper-tropospheric δD is very large (figure 3.4). With $coef$ set to 0.1, $\Delta\delta D$ reaches 30‰, consistent with observations.

Therefore, upper tropospheric water vapor δD measurements suggest that in all models, the sensitivity of precipitation efficiency to updraft velocity is missing. Adding this process is the only way to capture the observed δD distribution. The global impact of this modification remains to be studied.

3.4 Evaluating the convective mixing depth

[Sherwood et al., 2014] has shown that the relative proportion of shallow to deep convective mixing in the tropical atmosphere simulated by climate models was a key factor to determine the cloud response to sea surface temperature changes, and thus the climate sensitivity. Models with the strongest proportion of shallow convective mixing are the most sensitive. They split this proportion into a sub-grid scale component, directly associated with convective parameterizations, and a large-scale component, representing the depth of the large-scale tropical overturning circulation. They estimate the large-scale component using vertical profiles of large-scale vertical velocity, $\omega(z)$, from reanalyses. Although reanalyses are constrained by a variety of observations, $\omega(z)$ remains a

model product, since it has to balance the latent heating generated by shallow and deep convective parameterizations.

Here we attempt to provide an independent, observation-based constrain for the depth of the large-scale component of tropical mixing using water vapor isotope measurements. Indeed, both observations and model results show that the water vapor δD in the lower middle troposphere is sensitive to the depth of deep convection (section 2.1.5, [Lacour et al., 2016]). Since to first order in cloudy regions latent heat release by condensation balances the adiabatic cooling by large-scale ascent ([Emanuel et al., 1994]), the convective depth is tied to the $\omega(z)$ profile. The amount effect, defined here as the decrease of lower-tropospheric water vapor δD when the regime is more ascending, is weak when $\omega(z)$ peaks in the lower troposphere, whereas it is strong when $\omega(z)$ peaks in the upper troposphere.

Does this property linking the shape of $\omega(z)$ to the magnitude of the amount effect also holds when inter-comparing SWING2 models? SWING2 models show a wide spread in their simulation of the amount effect (figure 3.5a). In some models, such as LMDZ-free, the amount effect is weak, i.e. simulated δD at 600 hPa decreases weakly when the large-scale velocity is more ascending (figure 3.5a, black). In average over the regimes of strong ascent, these models happen to simulate $\omega(z)$ profiles peaking in the lower troposphere (figure 3.5b). In other models, such as GSM, the amount effect is strong (figure 3.5a, purple). These models happen to simulate $\omega(z)$ profiles peaking in the upper troposphere. There is a significant relationship between the magnitude of the amount effect and bottom-heaviness the of $\omega(z)$ profiles (figure 3.5c), consistent with the expected effect of convective depth on the magnitude of the amount effect. Therefore, we propose that the magnitude of the amount effect, observed by IASI and TES, provides an independent observational constrain for the depth of the tropical mixing.

This study has not been published yet.

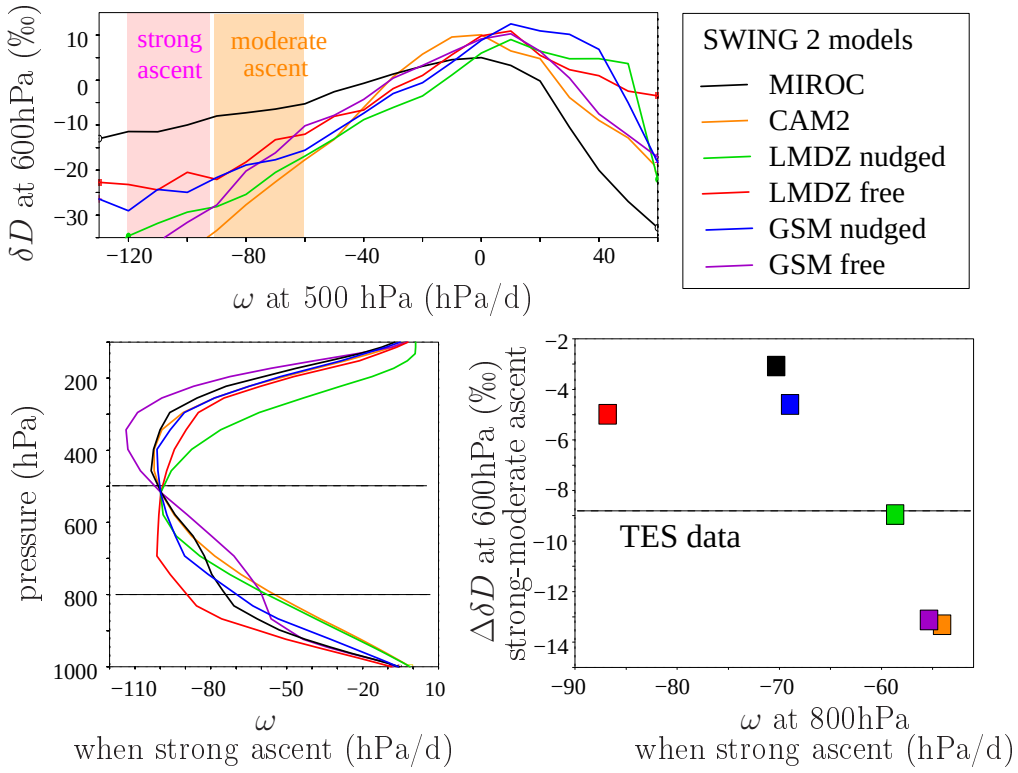

Figure 3.5: a) Monthly water vapor δD at 600 hPa as a function of monthly large-scale vertical velocity at 500 hPa, over the tropical oceans, for 6 SWING2 simulations. b) Shape of $\omega(z)$ profiles in average over the regimes of strong ascent, for the same SWING2 models. c) Proxy for the magnitude of the amount effect (difference of water vapor δD at 600 hPa between regimes of strong and moderate ascent, as defined on panel a) and a proxy for the bottom-heaviness of $\omega(z)$ profiles (ω at 800 hPa in average over regimes of strong ascent) for the same SWING2 models. The magnitude of the amount effect observed by TES is also shown.

Chapter 4

Using water isotope measurements to evaluate the capacity of climate models to simulate climate variations

To assess our credibility in climate change projections, observational tests of the models are necessary ([Hall and Qu, 2006, Boé et al., 2009, Brient and Bony,]). Testing the capacity of climate models to represent climate change in response to an external forcing in the context of past climates is a possible solution ([Braconnot et al., 2007, Schmidt, 2010, Schmittner et al., 2011, Braconnot et al., 2012, Hargreaves et al., 2012, Schmidt et al., 2013]). If a model is better for the past, is it more credible for the future? To address this question, we investigate links between the model behavior for past climates and for global warming projections. For example, links between tropical-mean temperature change during the last glacial maximum (LGM) and the future climate sensitivity ([Hargreaves et al., 2012]) have been evidenced. In section 4.1, I report my contribution to this topic by showing a link between precipitation changes in the future and during the Mid-Holocene.

Even if the similarity between physical processes involved in past and future climate changes remain to be verified ([Yoshimori et al., 2009, Yoshimori et al., 2011]), the effective use of paleo-climates to constrain future climate changes relies on the existence of precise and well dated paleo-climatic archives ([Hargreaves et al., 2013]). Traditional paleo-climatic information, such as pollen data, is sparse over most tropical continental regions ([Farrera et al., 1999, MARGO project members, 2008, Bartlein et al., 2010]). Could we use paleo archives of precipitation isotopic composition for this purpose? In section 4.2, I discuss the paleo-climatic interpretation of paleo-climatic isotopic archives in tropical regions.

4.1 Using paleo-climate archives to evaluate the credibility of future projections

4.1.1 Necessary conditions

To use paleo-climate archives to evaluate the credibility of future projections, 3 conditions are necessary:

1. there should be an inter-model statistical link between the behavior for past climates and for future projections,
2. this statistical link should be explained by robust physical processes,
3. paleo-climate data should be available to constrain the model behavior for past climates.

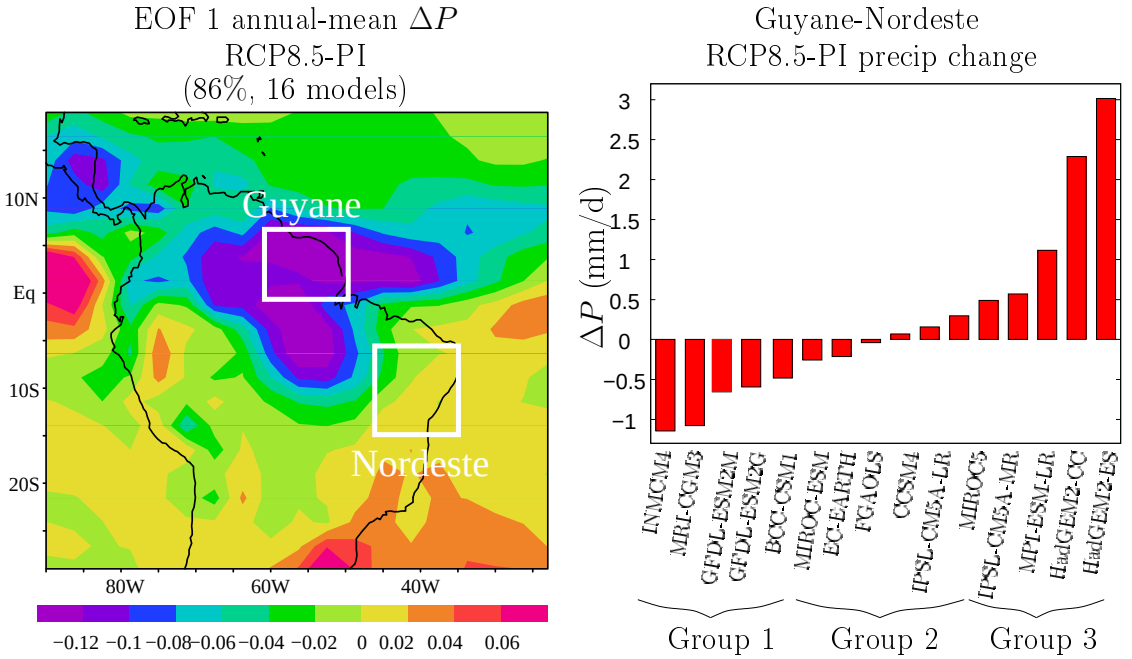

Figure 4.1: a) EOF analysis of the multi-annual-mean precipitation change ΔP between the RCP8.5 scenario and pre-industrial simulations, for 16 CMIP5 models. The number of models is used instead of the traditional time dimension of the EOF. The map of the 1st EOF shows a dipole pattern between the Northern and the Eastern parts of South America. We define the "Guyana" region and the "Nordeste" regions as highlighted with white boxes. b) RCP8.5 minus pre-industrial ΔP difference between the Guyana and Nordeste region, for the difference models. Positive values indicate that in RCP8.5, precipitation increases in Guyana and decrease in Nordeste, reflecting a Northward shift in the ITCZ. Conversely, negative values indicate that in RCP8.5, precipitation increases in Nordeste or decreases in Guyana, reflecting a Southward shift in the ITCZ. Models are classified into 4 groups based on these values.

The CMIP5 (Coupled Model Intercomparison Project version 5, [Taylor et al., 2012]) offers a unique opportunity to check the first two conditions: for the first time, the same models are used for present, past and future simulations.

4.1.2 Pilot study on precipitation changes in tropical South America

I present here my contribution to checking the first condition, focusing on precipitation changes in tropical South America. Results were reported in [Schmidt et al., 2013].

We use CMIP5 simulations for pre-industrial (PI), the most pessimistic climate change scenario (RCP8.5) and Mid-Holocene (MH) simulations.

To extract the most common patterns of future precipitation change, we performed an EOF (empirical orthogonal function) analysis over the different models for multi-annual mean of precipitation change (ΔP) from pre-industrial to RCP8.5. The first EOF shows a dipole pattern between Northern and Eastern South America (figure 4.2a), indicating that some models project an increase in precipitation in the Northern part and a decrease in precipitation in the Eastern part whereas other models simulate the opposite. Hereafter we refer to the Northern and Eastern part as "Guyana" and "Nordeste".

The precipitation change difference between "Guyana" and "Nordeste", ΔP_{G-N}, exhibits a very large spread across models, from -1 mm/d to +3 mm/d (figure 4.2b). We classify models into 3 groups based on ΔP_{G-N}. Group 1 models project a precipitation decrease in Guyana and a precipitation increase in Nordeste (figure 4.2a), consistent with a Northward shift of the ITCZ (Inter-tropical Convergence Zone). In contrast, group 3 models project a precipitation increase in

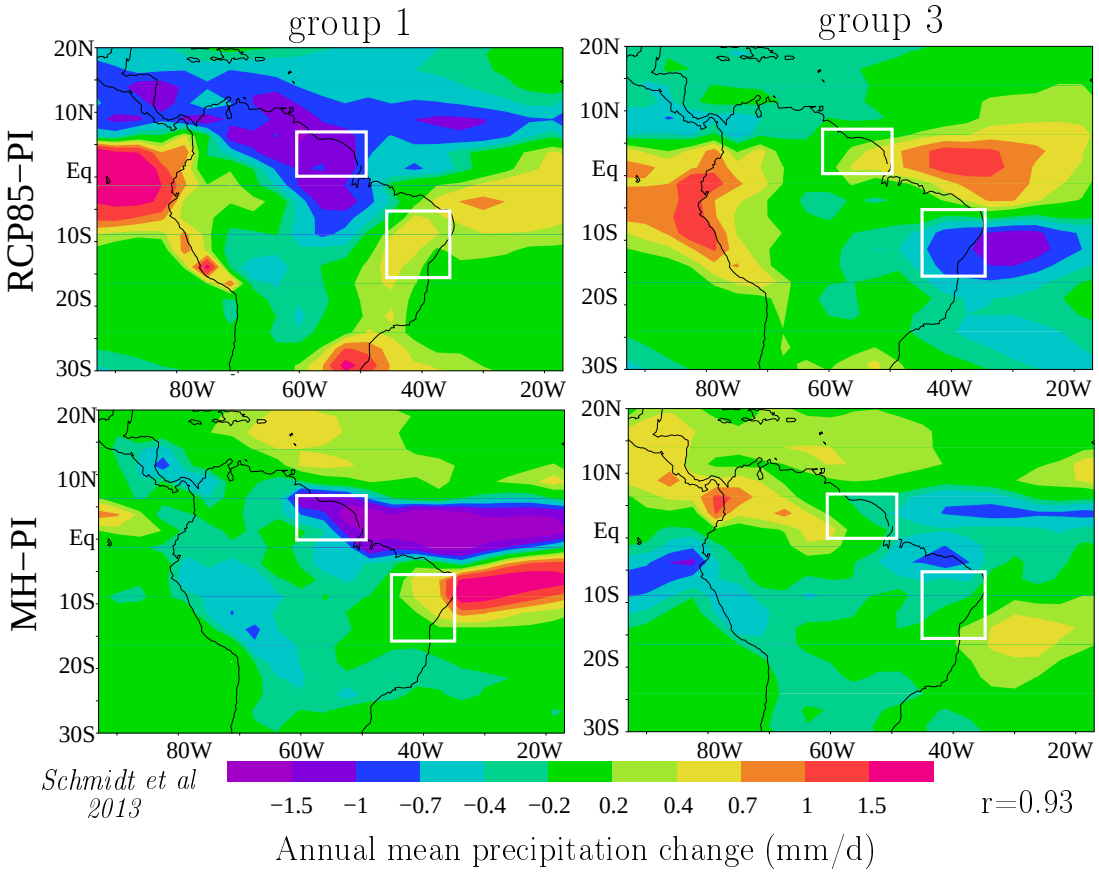

Figure 4.2: (a-b) Multi-annual-mean precipitation change ΔP between the RCP8.5 scenario and pre-industrial simulations, for models classified as group 1 (a) and group 3 (b). The classification is explained in figure 4.1. (c-d): as a-b but for ΔP between the Mid-Holocene and pre-industrial.

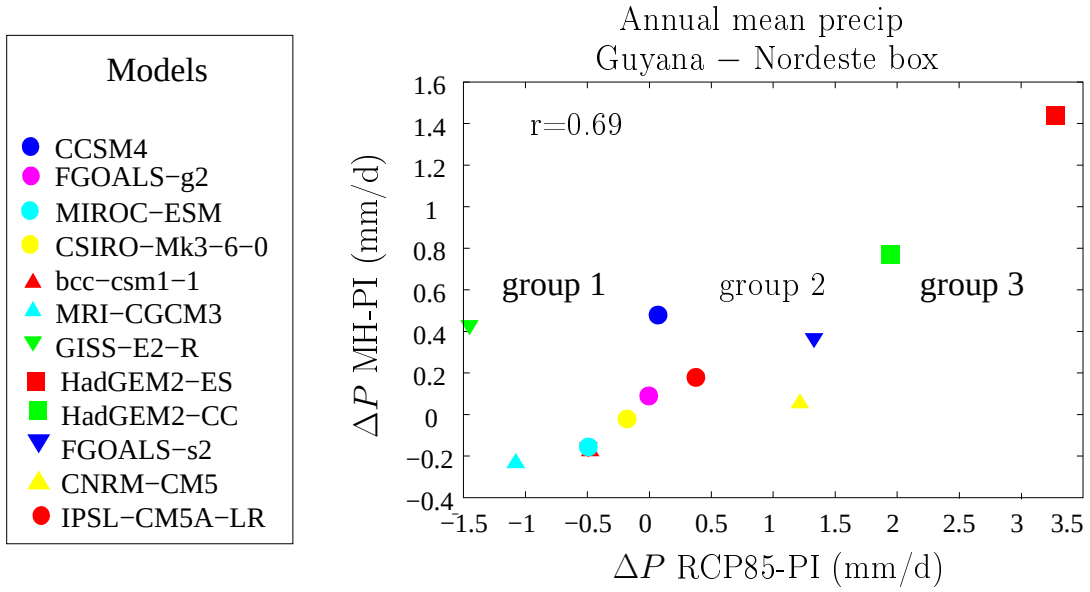

Figure 4.3: e) "Guyana" −"Nordeste" difference of ΔP from pre-industrial to Mid-Holocene as a function of the "Guyana" −"Nordeste" difference of ΔP from pre-industrial to RCP8.5.

Guyana and a precipitation decrease in Nordeste (figure 4.2b), consistent with a Southward shift of the ITCZ.

For the MH, group 1 models simulate a precipitation increase in Nordeste and a precipitation decrease in Guyana (figure 4.2c), similar to the precipitation change projected for the future climate. In contrast, group 3 models simulate a tripole pattern that reflects a widening of the ITCZ (figure 4.2d). Therefore, the behavior of a model for the MH determines its behavior for the future climate. Tob be more quantitative, we plot ΔP_{G-N} for the MH as a function of ΔP_{G-N} for the future climate (figure 4.2). We find a significant correlation (r=0.69), suggesting that paleo archives of ΔP_{G-N} for the MH could constrain ΔP_{G-N} for the future climate.

Physical processes explaining this common behavior between MH and future climate still need to be understood. To this aim, the decomposition methodology into dynamical and physical components ([Bony and Bellon, 2013]) and a moist static energy budget ([Oueslati et al., 2016]) could be applied (proposal A.9).

Are group 1 or group 3 models more realistic? Group 3 models more frequently show the double ITCZ problem for present-day simulations. However, the mechanisms linking the double-ITCZ problem for present-day and the behavior for past future changes still need to be understood.

This "pilot study" is encouraging about the potential of paleo precipitation archives to provide constrains on future precipitation changes. In the future, we plan to extend this to all tropical regions and to deepen our understanding of physical processes (proposal A.9).

4.2 Interpretation of paleo-climatic isotopic archives in the tropics

4.2.1 Introduction

The isotopic composition of precipitation can be archived in many archives such as ice cores ([Thompson et al., 2000]) in speleothems ([McDermott, 2004]), shelly fossils ([Eagle et al., 2013]), cellulose ([McCarroll and Loader, 2004]) or ground waters ([Gasse, 2000]), leaf waxes ([Tierney et al., 2008, Collins et al., 2013]). In the tropics however, the interpretation of water isotopic records has been debated. They were first interpreted in terms of **temperature** ([Thompson et al., 1989, Thompson et al., 1998]), as was the case for polar ice cores ([Jouzel, 2003]). This interpretation is supported by the fact that all tropical ice core records show a common depletion at LGM ([Thompson et al., 2000], figure 4.4a), suggesting that a global-scale feature is recorded and supporting this interpretation. In addition, the amplification of temperature changes with altitude may explain the strongest signals in high altitude records ([Poulsen and Jeffery, 2011]).

In contrast, most recent studies have interpreted tropical isotopic records as **precipitation** proxies ([Vuille et al., 2003]), consistent with the effect of convection on water vapor and precipitation ("amount effect", section 2.1). This effect has been observed in present-day precipitation at the spatial ([Dansgaard, 1964, Rozanski et al., 1993]), seasonal ([Dansgaard, 1964, Rozanski et al., 1993, Vimeux et al., 2005]), intra-seasonal ([Vimeux et al., 2011, Risi et al., 2008b, Gao et al., 2011]) and inter-annual time ([Hoffmann, 2003]) scales. Convection may therefore also play a role at the paleo-climatic scale. Finally, some authors point out the importance of the large-scale circulation and origin of air masses ([LeGrande and Schmidt, 2009]).

The goal of this study is to try and understand what controls isotopic variations recorded in tropical archives: temperature, precipitation, a bit of both, or none of them?

4.2.2 LMDZ paleo simulations

To this purpose, a series of LMDZ simulations were performed for 11 different "climates". Each climate is characterized by sea surface temperatures (SSTs), sea ice cover, ice sheets, orbital parameters and various greenhouse gas concentrations. The 11 climates include Last Glacial Maximum (LGM), Mid-Holocene (MH), CO_2 doubling with SSTs projected by different CMIP5 models, last inter-glacial... In addition, some of these climates were simulated with 4 different model physics (the same sensitivity tests as described in section 3.2), and some climates were also simulated with the zoom functionality to refine the resolution over South America or over the Tibetan Plateau.

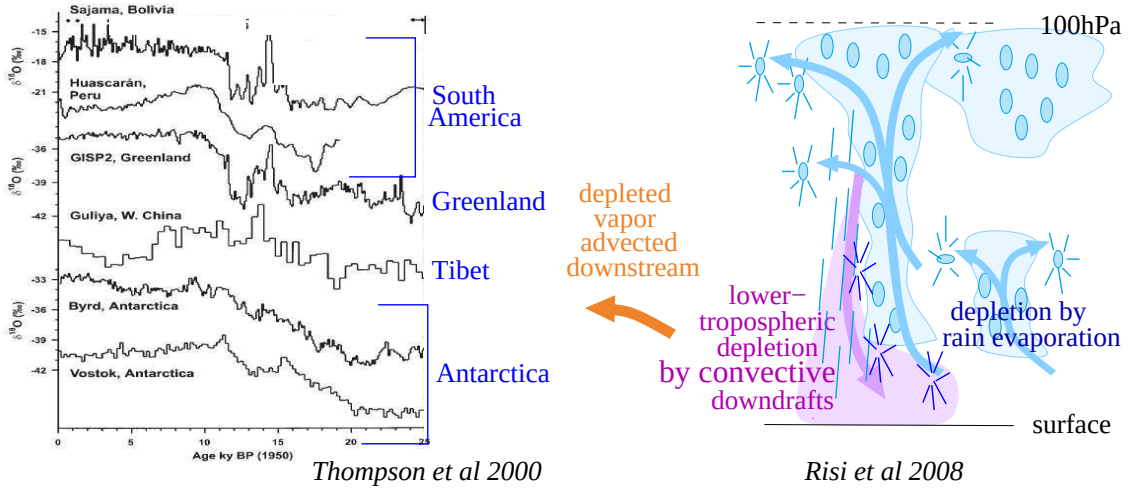

Figure 4.4: a) Ice core isotopic records on different continents, from 25 000 years to today. All records show the LGM depletion. b) Processes by which convection impacts the isotopic composition recorded in tropical archives. Convective downdrafts and rain re-evaporation deplete the lower-tropospheric water vapor. This depleted water vapor is advected downstream, imprinting a depleted signature into the subsequent precipitation.

These two regions concentrate most of tropical ice core records and the mountainous conditions require high resolution ([Yao et al., 2013, Eagle et al., 2013]).

As an example, we evaluate the LGM simulations using available paleo-climatic archives of precipitation $\delta^{18}O$ ($\delta^{18}O_p$). LMDZ simulates more depleted $\delta^{18}O_p$ during the LGM, and the depletion is all the largest as the elevation is high, consistent with the altitude amplification effect described by [Poulsen and Jeffery, 2011]. However, the depletion observed in Andean ice cores is strongly underestimated, even in the high-resolution simulation. The difficulty to simulate the LGM depletion as large as observed in the tropics is common to all GCMs ([Jouzel et al., 2000, Werner et al., 2001, Jasechko et al., 2015]) and the cause remains a mystery.

4.2.3 Interpreting $\delta^{18}O_p$ changes using a simple Rayleigh distillation model

To interpret $\delta^{18}O_p$ changes observed in paleo-climatic archives, the simulated $\delta^{18}O_p$ changes at some sites is decomposed into different components using a simple Rayleigh distillation model. This method is described in [Botsyun et al., 2016, Gao et al., 2016]:

$$R_p = (R_p - R_v) + R_v$$

and

$$R_v = R_{v0} \cdot \left(\frac{h \cdot q_s(T)}{h_0 \cdot q_s(T_0)} \right)^{\alpha - 1} + r$$

where R_p and R_v are the water isotopic ratio in precipitation and in water vapor; h_0, T_0 and R_0 are arbitrary initial conditions (whose choice has little impact on the final results) for relative humidity, temperature and water vapor isotopic ratio; h and T are relative humidity and temperature at the site of interest, q_s is the saturation specific humidity as a function of temperature, r is a residual term.

Variations in R_p are decomposed into 4 terms:

1. a term representing variations in the precipitation-vapor difference, $R_p - R_v$, which reflects condensation and post-condensation processes,

2. a term representing variations in local temperature T,

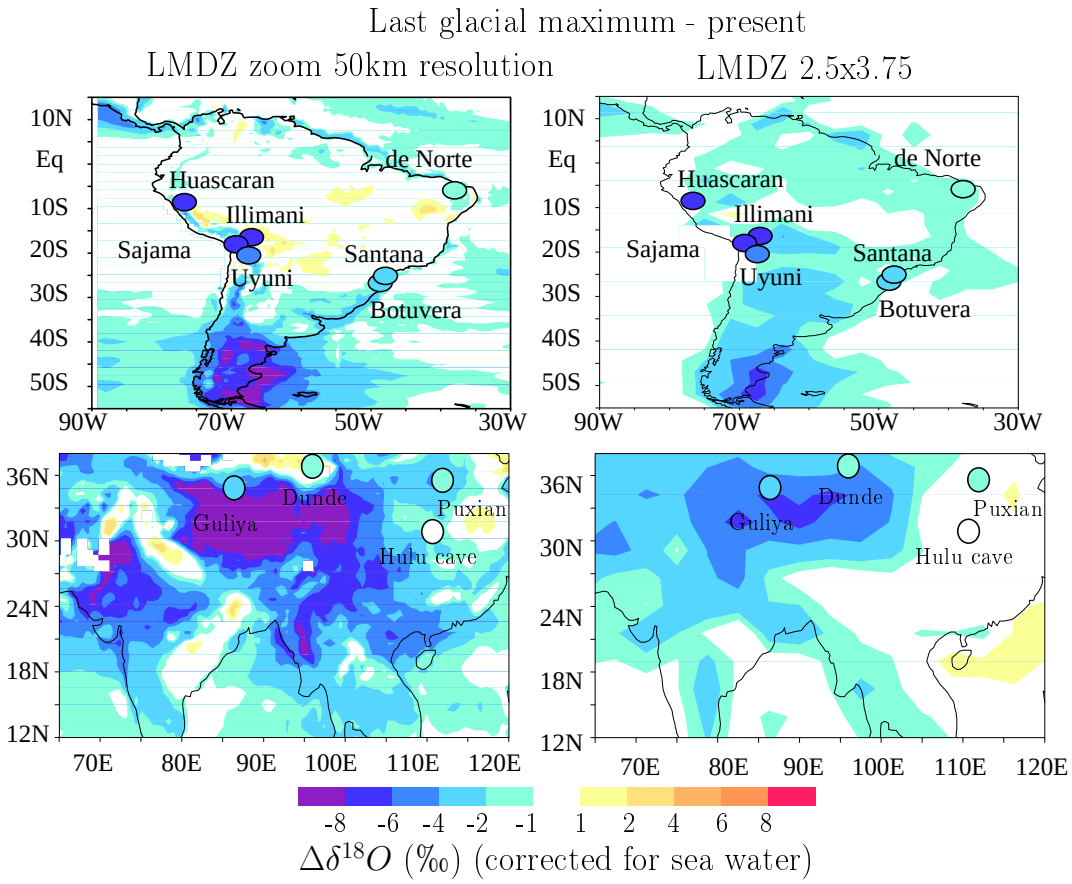

Figure 4.5: Evaluation of the simulated precipitation $\delta^{18}O$ changes from present-day to LGM in South America (a-b) and over the Tibetan Plateau (c-d) for the standard resolution simulation (a,c) and for the high-resolution simulations (b-d). Some available paleo-climatic archives are indicated for comparison.

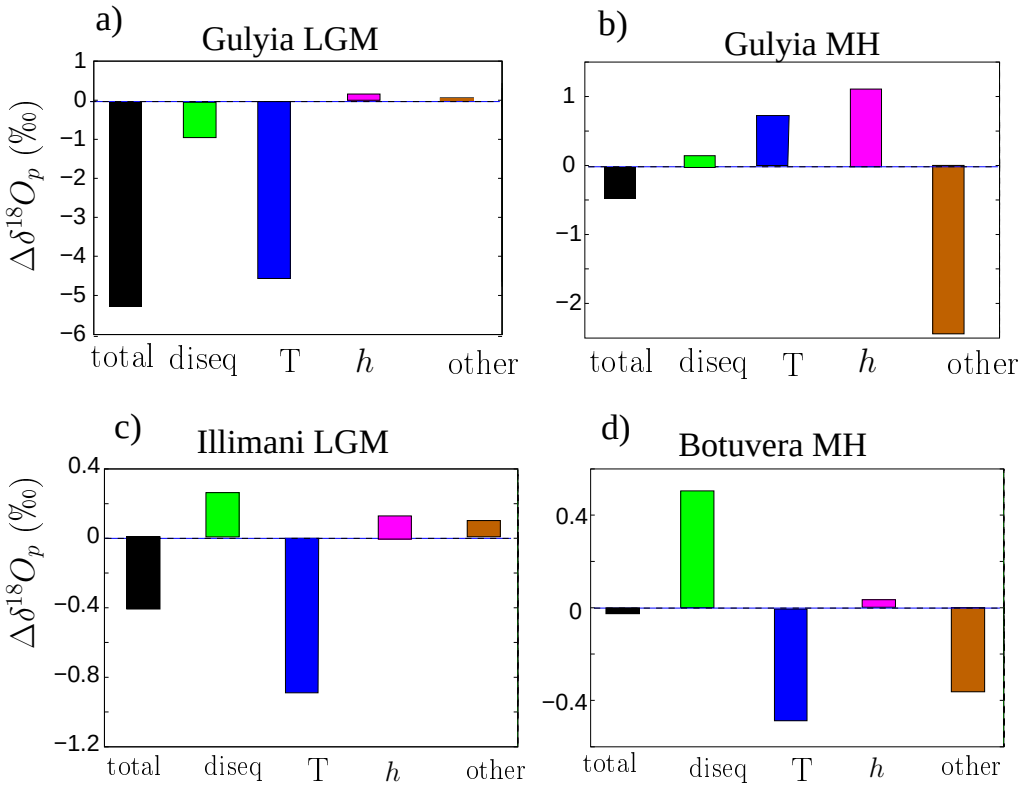

Figure 4.6: Decomposition of the total simulated $\delta^{18}O_p$ change (black) into 4 contributions: condensation and post-condensation effects (green), local temperature (blue), local relative humidity (pink) and a residual that includes the effect of deep convection along air mass trajectories (brown). The decomposition is shown for the Guliya ice core during the LGM (a) and the MH (b), for Illimani for the LGM (c) or for the Botivera cave for the MH (d).

3. a term representing variations in local relative humidity h,

4. a term representing variations in the residual term, r , encompassing changes in moisture source properties, deep convection and continental recycling along back-trajectories.

During the LGM, at most sites, the simulated $\delta^{18}O_p$ changes are dominated by the effect of local temperature changes (figure 4.6a,c). This supports the interpretation of $\delta^{18}O_p$ in terms of temperature ([Thompson et al., 2000]). In contrast, during the MH, the simulated $\delta^{18}O_p$ changes are dominated by local temperature, condensation and post-condensation processes, or by the residual term, depending on the sites (figure 4.6b,d). For example, for the Guliya ice core, the dominance of the residual term, which probably represents the impact of deep convective activity along monsoon flow trajectories, is consistent with several studies arguing for interpreting Asia ice cores in terms of past monsoon intensity ([Pausata et al., 2011]).

To conclude, what controls $\delta^{18}O_p$ changes may depend on the past climatic epoch of interest. **For epochs with large temperature changes, the temperature effect may dominate, but for epochs with smaller temperature changes, the convective effect may dominate**.

4.2.4 Inter-climate correlations with sea surface temperature and deep convection

Correlation between $\delta^{18}O_p$ in tropical ice cores and sea surface temperature

To check whether large-scale temperature changes impact the $\delta^{18}O_p$ in tropical ice cores at the paleo-climatic time scales, we calculated correlations between tropical-mean sea surface temperature (SST) changes and $\delta^{18}O_p$ changes, across the 11 climates. For the standard version of LMDZ,

the correlation is significant in most regions of South America and Asia, even at low elevations (figure 4.7a,c). This supports the interpretation of tropical records in terms of temperature.

How robust is it with respect to model physics?

To check whether this results is robust with respect to the model physics, we compared different perturbed-physics versions of LMDZ. At the Guliya ice core for example, all perturbed-physics versions of LMDZ show a significant correlation with SST (figure 4.7b). The dominance of the temperature control is thus robust to the model physics in this region. In contrast, the Illimani ice core is in a "pocket" where the standard version of LMDZ simulates no correlation with SST. At Illimani, only one of the LMDZ versions simulates a correlation with temperature (figure 4.7d). This suggests that at some sites, **the effect of temperature is sensitive to the model physics**. For example, a possible impact of convective entrainment on simulated isotopic lapse rates has been eveidenced ([Tripati et al., 2014]).

Correlation between $\delta^{18}O_p$ in tropical ice cores and upstream precipitation

To check whether deep convection impacts the $\delta^{18}O_p$ in tropical ice cores at the paleo-climatic time scales, we calculated correlations between regional precipitation changes and $\delta^{18}O_p$ changes at a site of interest across the 11 climates. For the standard version of LMDZ, at Guliya ice core, there is a strong anti-correlation with precipitation in North Western India, up to -0.9 (figure 4.8a). This region is on the way of monsoon flow trajectories. The importance of deep convection upstream air mass trajectories is consistent with paleo-climatic interpretation of $\delta^{18}O_p$ in terms of precipitation and with the isotopic controls observed at the daily time scale at Lhasa ([Gao et al., 2013]). For the Illimani ice core, there is a very strong anti-correlation with precipitation in Eastern Brazil (figure 4.8c), below -0.9 in some places. This region is also on the way of monsoon flow trajectories. The importance of deep convection upstream air mass trajectories is also consistent with the isotopic controls observed at the daily time scale in Bolivia ([Vimeux et al., 2005]).

How robust is it with respect to model physics?

To check whether this results is robust with respect to the model physics, we plotted $\delta^{18}O_p$ changes as a function of precipitation averaged over the upstream region for different perturbed-physics versions of LMDZ (figure 4.8b,c). For both Guliya and Illimani, the correlation is very good for the standard version of LMDZ, but breaks down for other versions. Therefore, **the importance of upstream convection in controlling $\delta^{18}O_p$ changes is sensitive to the model physics**.

Summary

To summarize, depending on model versions, LMDZ can simulate either a dominance of temperature or of upstream convection in controlling $\delta^{18}O_p$ changes in paleo-climatic archives. What model version is the most credible? Could daily water vapor observations help us to discriminate between different model versions? This is what we propose to do in the future (proposal A.6).

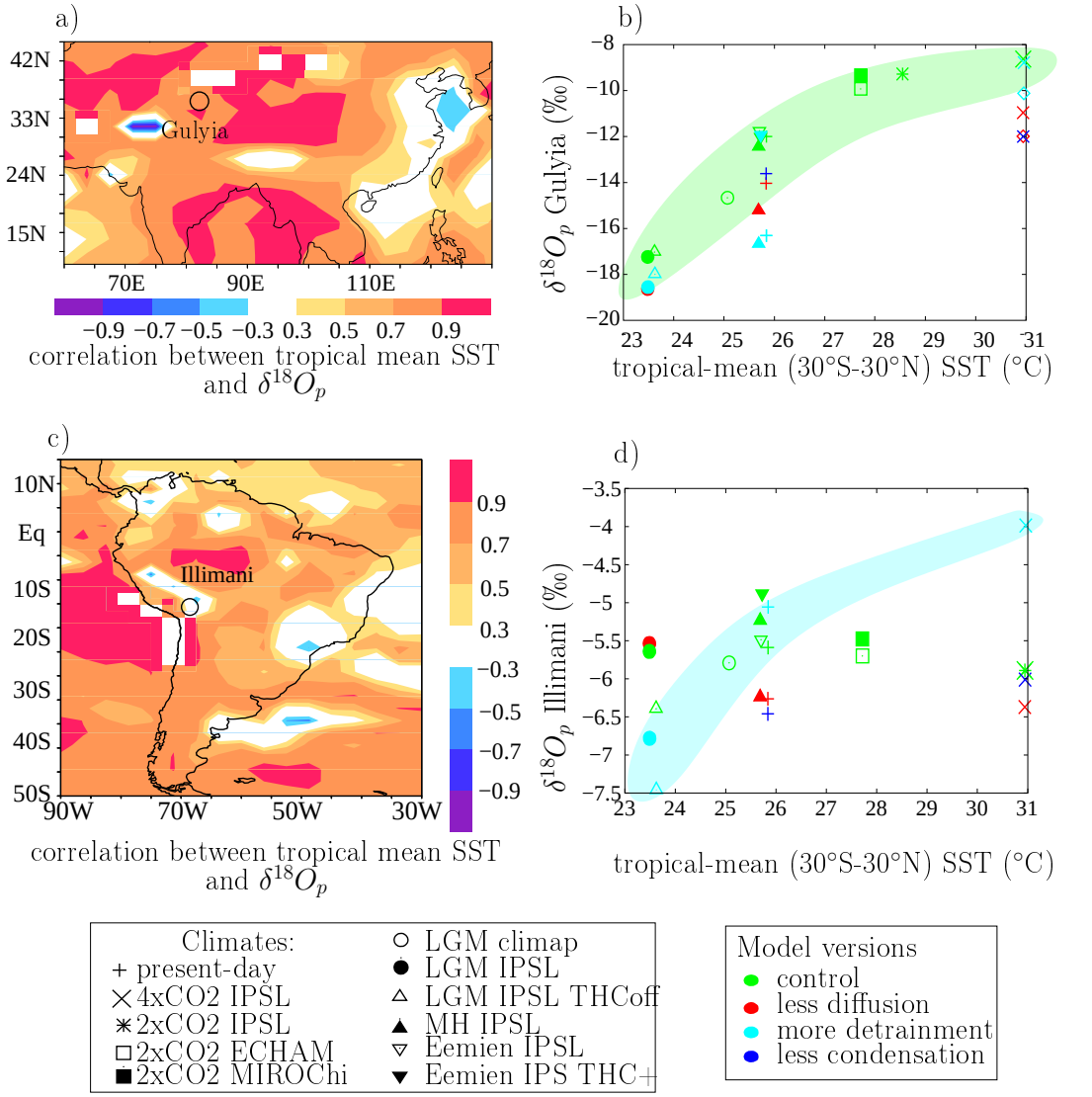

Figure 4.7: a) Correlation between tropical-mean sea surface temperature (SST) changes and simulated $\delta^{18}O_p$ in each grid box across the 11 climates for the standard version of LMDZ, over Asia. b) Simulated $\delta^{18}O_p$ change at Guliya ice core as a function of tropical-mean SST, for the 11 different climates (markers) and the 4 LMDZ versions (colors). c) Same as a but over South America. d) Same as b but at the Illimani ice core.

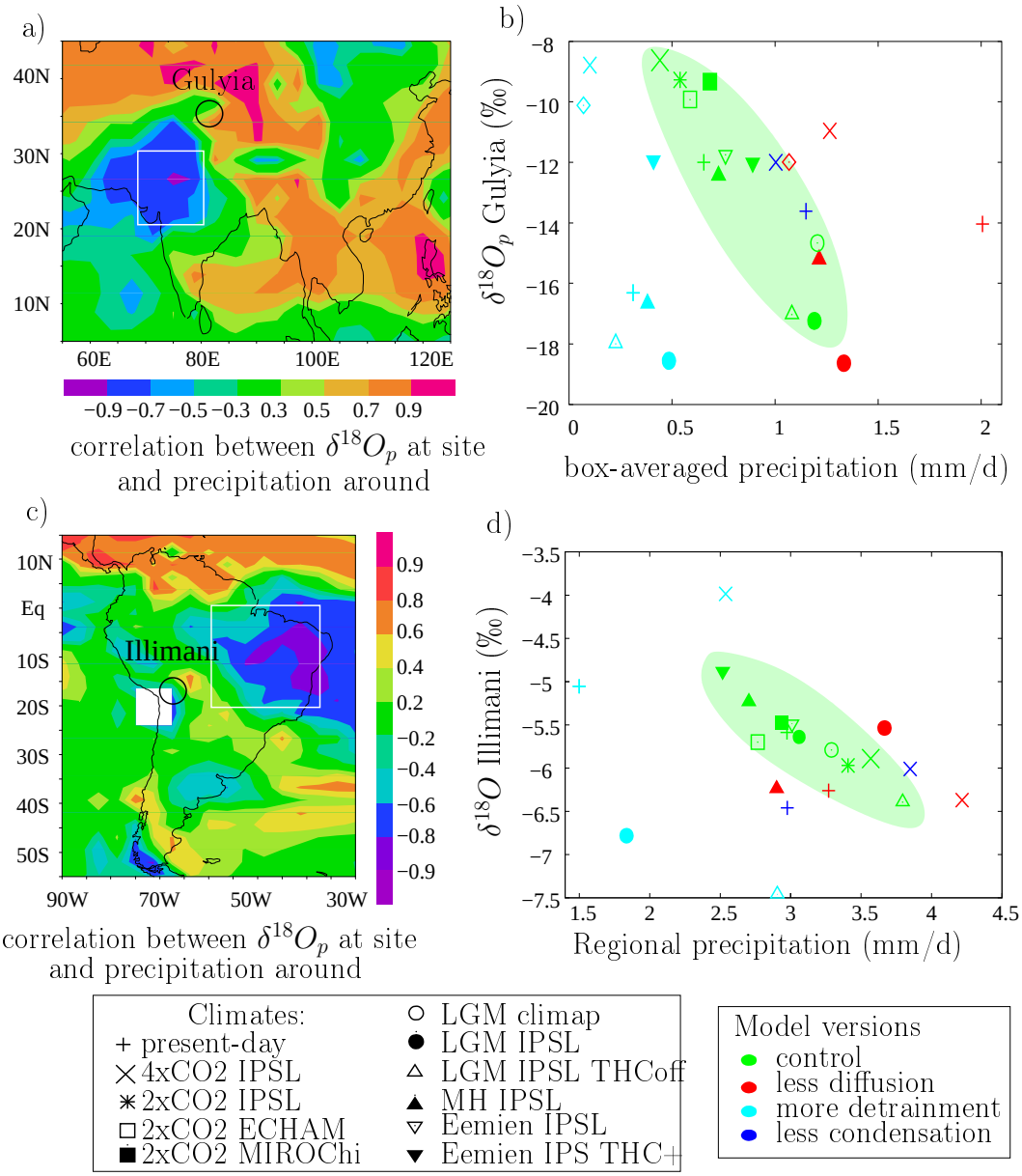

Figure 4.8: a) Correlation between the simulated $\delta^{18}O_p$ at the Guliya ice core site and the precipitation rate in each grid box across the 11 climates for the standard version of LMDZ. b) Simulated $\delta^{18}O_p$ change at Guliya ice core as a function of precipitation change averaged over the white box, for the 11 different climates (markers) and the 4 LMDZ versions (colors). c) Same as a but for the Illimani ice core site. d) Same as b but at the Illimani ice core.

Chapter 5

Conclusion and perspectives

5.1 Conclusion

Water isotope measurements are potentially useful to quantify the relative importance of moistening and dehydrating processes (e.g. mixing, convective processes, continental recycling), to detect and understand biases in models, and to evaluate and improve models.

The main difficulty is to go beyond the demonstration that water isotopes are "potentially useful", and actually use water isotope measurements quantitatively. Studies actually proposing model improvement based on water isotopes (chapter 3) are few, and even among those, none have lead to effective changes in climate models. We still have a long way to go before water isotopes become part of the model development process; I think that this is because we, as isotopists, still have a lot of work to do to demonstrate the real added value of water isotopes.

A major limiting factor in doing so is that **what controls the water isotopic composition is not fully understood yet**. I think that more efforts should be put into understanding what controls water vapor isotopes, before we pretend to use them.

When trying to gain better understanding of isotopic controls, another limiting factor is the big **gap between complex numerical modeling and the simple $q-\delta D$ theoretical framework** (section 1.3.3). Intermediate models would be necessary.

A great amount of measurements and modeling tools are now available, which gives hope that there will be a lot of progress in isotopic research in the years to come. Unfortunately, many of these measurements and modeling tools have been under-exploited so far. A limiting factor is that we are missing human work force to analyze all the already-available measurements and simulations.

Finally, consolidating the link between isotopists and model developers is crucial. It ensures that isotopic research addresses questions that are relevant to model developers and that isotopic constraints translate into model parameterization improvement. My position at LMD, near the LMDZ development team, is ideal for this purpose, although I would like to make a better job in the future collaborating with the development team.

5.2 Perspectives

Here are some suggestions to try to overcome the limiting factors described above, together with my plans to contribute to this effort. I give a series of 9 proposals for master's students, PhD students, post-docs or myself, to make my plans more concrete.

5.2.1 Better understand the isotopic response to convective and cloud processes

First, I plan to consolidate the understanding of the isotopic response to convective and cloud processes (section 2.1). To understand how these processes impact isotopic spatio-temporal variations with time and space (section 2.1), I plan to document isotopic variations associated with different

phases of the convective life and with different degrees of convective aggregation, by co-locating various satellite datasets (proposals A.1 and A.2). One possible application is to identify what are the moistening and drying processes responsible for the observed effect of convective aggregation on tropospheric humidity ([Tobin et al., 2012]).

The impact of rain re-evaporation on water vapor isotopic composition remains uncertain (section 2.1.3). I would like to combine the surface meteorological data, satellite observations and continuous isotopic measurements available at Niamey in the Sahel ([Tremoy et al., 2012]) to quantify the effect of rain re-evaporation on both q, water vapor δD and d-excess in cold pools of squall lines (proposal A.3). One possible application is to quantify the contribution of rain re-evaporation to intra-seasonal variations in Sahelian humidity ([Poan et al., 2013]).

To evaluate the isotopic response to convective and cloud processes simulated by GCMs, I'd like to use high-resolution (CRM or LES) simulations, where convection is explicitly represented (proposal A.4). Such simulations are ideal for a detailed process study, and could be compared with GCM or SCM simulations using the conditional sampling methodology ([Couvreux et al., 2010]). Inter-comparing SCM from different GCMs, by including isotopes into some GEWEX case studies or by extending the SWING initiative to SCM simulations, would be very interesting.

5.2.2 Better understand what controls the isotopic composition at the large-scale

From a more fundamental point of view, to better understand what controls the isotopic composition at the large-scale, bridging the gap between complex numerical modeling by GCMs and the simple $q - \delta D$ framework would be useful. In an attempt to do so, I'd like to investigate processes along air mass trajectories in the LMDZ GCM. The Lagrangian framework would allow for a easier comparison with the theoretical lines in the $q - \delta D$ framework. Based on this study, a new set of lines, representing better the diversity and complexity of atmospheric processes, will be develop (proposal A.5).

With paleo-climatic applications in mind, to check to what extent our understanding of isotopic controls at the daily scale helps us understanding the isotopic controls at the paleo time scale, processes at play at the two time scales will be compared in LMDZ simulations (proposal A.6). Inter-comparing different GCMs, by including isotopes into CMIP6 or by extending the SWING initiative to paleo simulations, would be very useful for this purpose.

5.2.3 Work more closely with model evaluation and improvement issues

The goal of the CONVISO project was to help evaluate and improve the simulation of the MJO by GCMs. Most of the time of this project has been used so far in understanding processes controlling the isotopic composition (section 2.1.7), which is a necessary first step. Now, to what extent could water isotope measurements provide process-oriented diagnostics that can predict the realism of the MJO simulation? I'd like to address this issue by comparing different sensitivity tests with LMDZ (proposal A.7), and, ideally, comparing different isotopic GCMs as well. Extending the SWING initiative to provide daily outputs would be useful for this purpose.

When trying to apply water isotope measurements to evaluate models, we need to keep in mind that for many processes, water isotopes may not be the best tools. Combining different isotopic and chemical tracers, such as CO, O_3, ^{10}Be (proposal A.8), would be maximize the probability to develop useful constraints on parameterizations ([Folkins et al., 2006, Liu et al., 2009]).

Finally, I think comparing simulated and observed paleo-climatic variations is a very powerful test the model capacity to respond to climate forcing, in a way that integrates the effect of all parameterizations. I'd like to continue to investigate the link between past and future precipitation variations and develop pertinent diagnostics, possibly based on water isotopes (proposal A.9).

Appendix A

Some proposals for future students, post-docs or myself

A.1 Moistening and dehydrating processes as a function of convective aggregation

Context and science questions

A significant part of the spread in future precipitation projections can be attributed to the representation by climate models of atmospheric convection. It is thus important to understand the role of convection on its environment. This role may depend on the degree of aggregation. Convective systems can be either aggregated as large meso-scale systems (figure A.1a) or isolated (figure A.1b). [Tobin et al., 2012] developed a diagnostic to quantify the degree of aggregation of convection, and showed that more aggregated systems are associated with lower tropospheric relative humidity. Why? Do convective processes depend on the degree of aggregation of convection? Does convection moistens its environment more when it is less aggregated, and if so, by what mechanism? By stronger convective detrainment? Or more efficient re-evaporation of the raindrops?

What impact does this effect has on the climate and its variability? The degree of aggregation of convection is not considered in current climate models ([Tobin et al., 2013]). To what extent does this lead models to ignore some important moisture-convection feedbacks?

The isotopic composition of water vapor, observed by satellite, can give some information about moistening and dehydrating process. For example, convective detrainment enriches vapor water while moderate re-evaporation of raindrops depletes it. The goal of this study is to document the impact of convective aggregation on the tropospheric specific humidity (q) and water vapor δD in the environment and to link it with processes by which aggregation impacts tropospheric humidity.

Where we stand

Tropospheric profiles of q and water vapor δD observed by TES were co-located with the degree of aggregation at the $10° \times 10°$ scale diagnosed by [Tobin et al., 2012] and with precipitation observed by TRMM. For a given precipitation rate, more aggregated convection is associated with drier free troposphere (consistent with previous studies, [Tobin et al., 2012]), with more enriched lower troposphere (suggesting less rain evaporation) and with more depleted middle and upper troposphere (suggesting less condensate detrainment or more subsidence) (internship by Natacha Legrix).

Although LMDZ does not explicitly represents convective aggregation, when nudged to reanalyses winds, it captures most of these features to some extent. This suggests that at least some of the observed q and δD signal is not a direct consequence of convective aggregation. Convective aggregation may be associated with some meteorological situations that impact q and δD.

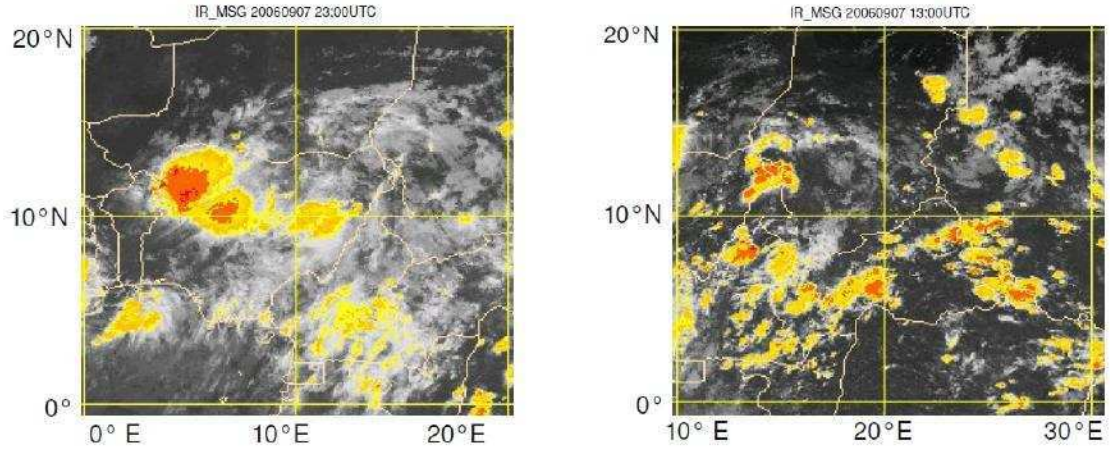

Figure A.1: Satellite images illustrating different states of convective aggregation: aggregated (a) and scattered (b).

Road map

- To isolate the direct impact of convective aggregation on observed q and δD, we will investigate the influence of other factors, such as large-scale vertical velocity profiles, sea surface temperature, proximity with land or moisture origin.
- To assess whether convective aggregation impacts its environment or whether meteorological situation favors some states of convective aggregation, we will look at temporal evolution of convective aggregation, q and δD.
- To check the robustness of q and δD signals and to document full tropospheric profiles, we will extend the analysis to the IASI, GOSAT and MIPAS datasets.
- Once the real impact of convective aggregation on tropospheric q and δD profiles is documented, we will investigate the convective processes at play and conclude on the mechanisms linking convective aggregation to tropospheric humidity.
- Finally, we will discuss the consequence for climate models to neglect the effect of convective aggregation.

A.2 Moistening and dehydrating processes as a function of the convective life cycle

Context and science questions

A significant part of the spread in future precipitation projections can be attributed to the representation by climate models of atmospheric convection. It is thus important to understand the role of convection on its environment. Meso-scale convective systems (MCS) often follow a typical life cycle, in which they initiate as small isolated cumulonimbus, organize into larger convective clusters that may propagate (figure A.1b), and then dissipate. Convective and cloud processes depend on the phase of the life cycle ([Sherwood and Wahrlich, 1999, Bouniol et al., 2016]). How do moistening and dehydrating processes vary with the phase of the life cycle? Can climate model capture these different processes?

Since the isotopic composition of water vapor can give some information about moistening and dehydrating process, the goal of this study is to document the tropospheric specific humidity (q) and water vapor δD along the convective life cycle and to link it with convective processes at play in the different phases.

Where we stand

In collaboration with R. Roca, we used MCS properties (duration, track, size and brightness temperature along their track) derived from geostationary satellites and coputed using a tracking algorithm ([Fiolleau and Roca, 2013a]) to build composite life cycles ([Fiolleau and Roca, 2013b]). TES, GOSAT and IASI q and δD observations in the vicinity of MCSs were selected and composited for different phases of the life cycle and for different precipitation rates as measured by TRMM. A preliminary analysis with a few months of data over Western Africa suggests that results are noisy, not robust across datasets and inconsistent with expectations, maybe due to insufficient data sampling (internship by Florentin Breton).

Road map

- To increase the data sampling, the analysis should be extended to several years and over a larger spatial domain. Since q and δD observations are clear-sky only, the co-location algorithm to select observations in the vicinity of MCSs may have to be refined.
- To isolate the direct impact of local convective processes, we must quantify and subtract the effect of the fact that some phases are preferentially sampled in some regions, in some seasons or during some hours of the day. We must also remove the effect of instrument sensitivity, by comparing LMDZ results with or without account for this effect.
- For a given precipitation rate, how do q and δD tropospheric profiles vary along the convective life cycle? What can we deduce about the convective processes at play?
- Can LMDZ, when nudged to reanalyses winds, capture the observed q and δD evolution? If not, what processes are missing, and what is the impact on the model capacity to simulate some meteorological conditions?

A.3 Role of rain re-evaporation: case study in the Sahel

Context and science questions

Rain re-evaporation is among the micro-physical processes whose parameterization rely on several empirical and unknown parameters. How much of the rain drops re-evaporate? How does this depend on the type (e.g. size, propagation, organization, life cycle) of convective systems and on environmental conditions (e.g. relative humidity profile)? Do climate models represent this process well? What is the role of rain re-evaporation on tropospheric humidity? Studies have suggested that rain re-evaporation could contribute to intra-seasonal variations of tropospheric humidity in the Sahel ([Poan et al., 2013]): could we quantify this contribution?

Tropospheric water vapor δD observed by TES has been used to attempt to quantify the proportion of water vapor that originates from rain re-evaporation ([Worden et al., 2007]). However, this study relied on the approximation that the fraction of the rain that re-evaporates is very small, which is often not valid. In the general case, the δD of the vapor evaporating from rain drops may have either an enriching or a depleting effect ([Risi et al., 2010a]) depending on the fraction of the drop that re-evaporates. Tropospheric water vapor δD observations are thus more difficult to interpret.

The goal of this study is to develop a model for predicting tropospheric water vapor δD, or d-excess, as a function of rain re-evaporation. Then, could this model be used to address the above-mentioned science questions?

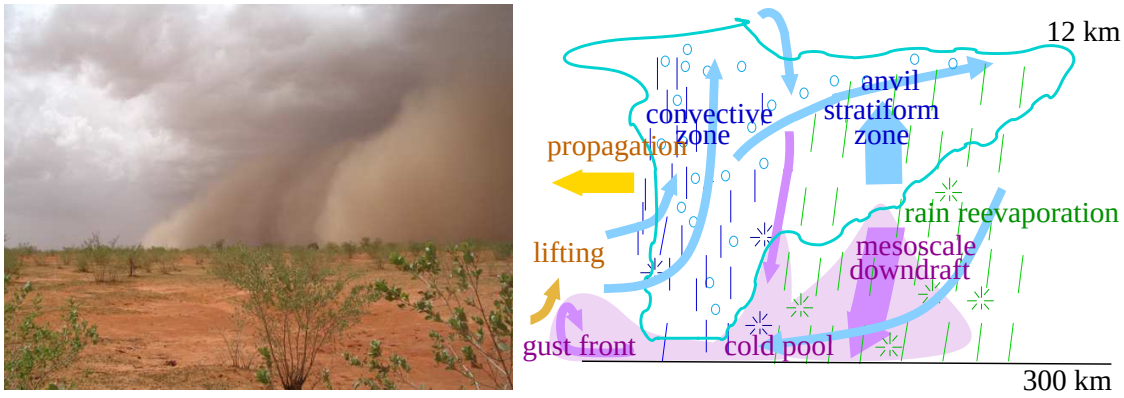

Figure A.2: a) Picture of the gust front of a squall line in Mali. The gust front materializes the border of the cold pool. b) Processes leading to the cold pool in a typical squall line.

Where we stand

As a case study, we investigated cold pools of convective systems in the Sahel (internship of Yannick Lamarre in collaboration with F. Vimeux). These cold pools are driven by rain re-evaporation that cools the air (figure A.2). We used 3 years of continuous in-situ measurements of surface water vapor δD and d-excess in Niamey (Niger), in the Sahel ([Tremoy et al., 2012, Tremoy et al., 2014]), combined with meteorological data. All convective systems during these 3 years were identified based on field notes. Convective system properties, including size, propagation, organization and life cycle, were examined based on Meteosat images every 15 minutes. Cold pools were identified based on observed temperature drops characteristic of cold pools. Temperature, humidity (q), δD and d-excess variations associated with each cold pool were estimated. Based on a moist static energy budget and on twice-daily radio-soundings, the fraction of the water vapor originating from rain re-evaporation, q_{ev}, was calculated.

Road map

- What controls q_{ev}? Among possible factors, cloud system properties based on Meteosat images and tropospheric relative humidity profiles based on radio-soundings will be investigated.

- How do surface water vapor δD and d-excess vary with q_{ev}? What are the other factors controlling δD and d-excess? A model for predicting tropospheric water vapor δD and d-excess as a function of rain re-evaporation will be developped.
- Using this model, we will revisit the interpretation of the TES data in terms of rain re-evaporation. We will also use the IASI data. What is the contribution of rain re-evaporation to tropospheric moisture? How does it depend on convective and environmental properties?
- Using this model, we will also try and quantify the contribution of rain re-evaporation to intra-seasonal variations of tropospheric humidity in the Sahel.
- Finally, we will use δD measurements to evaluate the representation of rain re-evaporation in the LMDZ model.

A.4 Understanding the isotopic signature of convective processes using Cloud Resolving Model simulations

Context and science questions

Our understanding of how convection impact the isotopic composition of water vapor is still incomplete. Relying on convective parameterizations may contribute to the gap between understanding based on GCMs and reality. The goal of this study is to use Cloud Resolving Models (CRMs) or Large-Eddy Simulations (LES) (figure A.3) to understand the isotopic response to convection and evaluate its simulation in GCMs.

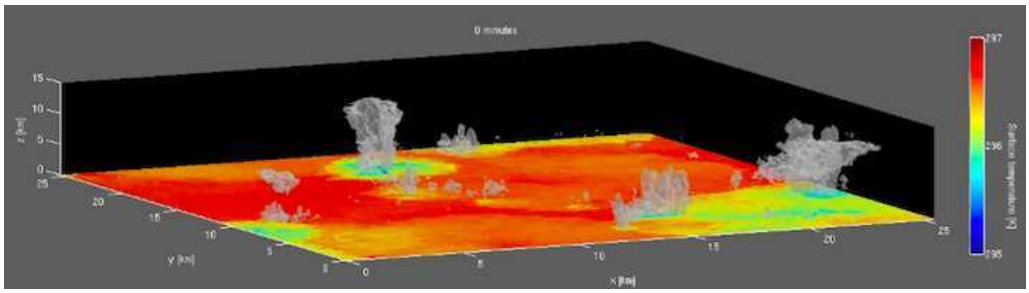

Figure A.3: Illustration of convective clouds simulated by a Large-Eddy Simulation (LES) ([Muller and Held, 2012]).

Where we stand

Using the SAM CRM, [Moore et al., 2014] performed a series of CRM simulations in Radiative-Convective Equilibrium (RCE) spanning different precipitation rates. Although they studied the amount effect, processes were not examined in detail and the specific advantages of a CRM simulation were not exploited. I would like to analyze these simulations in more details, in collaboration with Peter Blossey.

Road map

- Single Column Model (SCM) simulations equivalent to the CRM simulations will be performed with LMDZ. How do the simulated δD profiles compare with those from the CRM simulations?
- Criteria for identifying unsaturated downdrafts, saturated downdrafts and updrafts in CRM simulations will be developed. The isotopic composition of the water vapor and condensate in each of these drafts will be diagnosed, following the conditional sampling methodology ([Couvreux et al., 2010]).
- How does the isotopic composition in the different drafts in CRM simulations compare with the isotopic composition computed as internal variables by the different components of the convective parameterization in the SCM?
- To understand what controls the isotopic composition of tropospheric water vapor, water and isotopic budget will be performed at different levels, in both the CRM and SCM. Where CRM and SCM show different results, are physical parameterizations or isotopic parameterizations responsible for the difference?

A.5 Bridging the gap between theoretical Lagrangian models and reality

Context and science questions

Much of the understanding on what controls the isotopic composition of precipitation has been gained thank to the use of theoretical curves in the $q - \delta D$ framework ([Worden et al., 2007, Noone, 2012]). However, the simplicity of this framework makes it difficult to connect with GCM simulations and with reality, where processes are much more complex, diverse and inter-mingled (figure A.4). The goal of this study is to try to bridge the gap between the $q - \delta D$ framework and GCM simulations.

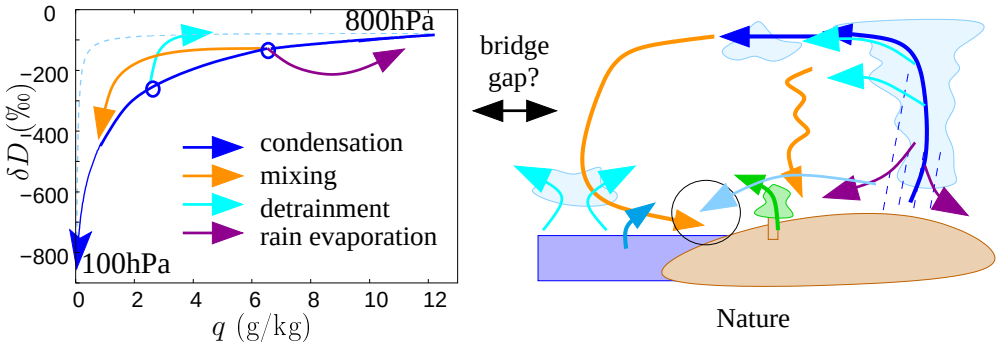

Figure A.4: a) Idealized $q - \delta D$ framework. b) Diversity and complexity of processes in a GCM and in reality.

Where we stand

During his post-doc, Obbe Tuinenburg connected the $q - \delta D$ evolution simulated by LMDZ during MJO events to the simulated tendencies (i.e. the effect of each physical parameterization on q and δD) ([Tuinenburg et al., 2015]). During his PhD thesis, You He looked at tendencies simulated by LMDZ along back-trajectories to interpret the simulated isotopic variability observed at Lhasa (Tibet) ([He et al., 2015]). These studies showed that looking at LMDZ tendencies is useful to interpret $q - \delta D$ variations at the daily scale.

Road map

- Identify a few sites of interest and calculate back-trajectories
- Look at physical tendencies simulated by LMDZ along back-trajectories and plot them in the $q - \delta D$ diagram. How does this relate to theoretical curves? Should we create new ones?
- Can we develop a new framework that relates the $q - \delta D$ at the site of interest with the sum of all tendencies that affected q and δD along the trajectories?

A.6 Temperature or precipitation: how should we interpret paleo-climate archives of precipitation isotopes?

Context and science questions

In polar regions, paleo-climate archive of precipitation isotopic composition ($\delta^{18}O$) have long been interpreted in terms of changes in temperature. In the tropics, the interpretation of such archives (Andean glaciers and Tibetan, speleothems...) is more controversial. Inspired by studies in polar regions, the tropical $\delta^{18}O$ signal was first interpreted in terms of the temperature change ([Thompson et al., 1989, Thompson et al., 1998, Thompson et al., 2000]). This interpretation is supported by the fact that all tropical ice cores exhibit similar $\delta^{18}O$ variations over last 25 000 years, with depleted values during the last glacial maximum as in polar cores (figure 4.4a). However, at inter-annual to daily scales in present-day observations, precipitation $\delta^{18}O$ anti-correlates with local ([Dansgaard, 1964]) or upstream ([Vimeux et al., 2005, Gao et al., 2013]) precipitation amount. This is because atmospheric convection depletes the lower-tropospheric water vapor (figure 4.4b). Thus many authors now interpret the isotopic variations in tropical paleo-climatic records in terms of regional precipitation variations ([Vuille and Werner, 2005, Pausata et al., 2011]).

The aim of this study is to understand what controls the isotopic variations in tropical rainfall at the paleo-climatic scale (thousands of years): temperature, precipitation, both?

Where we stand

A series of simulations were performed with LMDZ for different climates and for different versions of the model physical package (section 4.2). In some model versions, the temperature is the dominant control, while in other versions, the regional precipitation is the dominant control. Which version is more credible?

During his PhD thesis, You He used daily in-situ and satellite data to investigate how convective processes impact the isotopic composition of water vapor along back-trajectories and controls the isotopic signal recorded in the precipitation at Lhasa ([He et al., 2015]). How can this improved understanding at the daily scale be used for paleo-climatic interpretations?

Road map

- It is likely that results will depend on the region of interest. If the case, the same road map will be repeated for each region.
- Two model versions will be identified: one that produces a dominant temperature control, and another that produces a dominant precipitation controls, at the paleo-climatic time scale.
- How do these model versions simulate the control of precipitation $\delta^{18}O$ at the daily time scale? Could daily observations be used to discriminate which one is the most realistic?
- If precipitation is more depleted for a given paleo-climatic epoch, is it because it is systematically more depleted, or because there is a higher frequency of depleted events, or because depleted events are more intense? The daily probability distribution of precipitation $\delta^{18}O$ will be compared for different epochs. Based on the results, can we interpret some paleo-climatic variations in the light of our increased knowledge of daily processes at present-day?
- To better understand processes controlling the precipitation $\delta^{18}O$, processes along back trajectories will be analyzed and compared between different model versions and model epochs. Are there processes that are common to all time scales?

A.7 Does the simulation of moistening and dehydrating processes associated with convection determines the quality of MJO simulation?

Context and science questions

The Madden-Julian Oscillation (MJO) is the main mode of intra-seasonal variability in the tropical troposphere. GCMs have persistent difficulties to simulate this mode of variability ([Slingo et al., 1996, Lin and Coauthors, 2006, Kim et al., 2009, Hung et al., 2013]). What determines the capacity of GCMs to simulate well or not the MJO?

The MJO results from feedbacks between convective processes and the large-scale circulation (figure A.5). In models, convective processes respond to the large-scale dynamical forcing. In turn, convective processes affect temperature and humidity profiles, which can feedback on convective processes or on the large-scale circulation. Therefore, the capacity of a model to simulate the MJO may depend on several factors:

1. the response of convective and cloud parameterizations to the dynamical forcing in terms of moistening and dehydrating processes (green on figure A.5),
2. the response of convective and cloud parameterizations to the dynamical forcing in terms of heating and cooling profiles (orange),
3. the dynamical response to heating and cooling profiles (purple).

In the case of hypothesis (1), water vapor isotope measurements could help evaluate the moistening and dehydrating processes at play. This hypothesis would be consistent with the suggested importance of shallow convection to moisten the free troposphere and pre-condition the atmosphere to deep convection ([Maloney, 2009]).

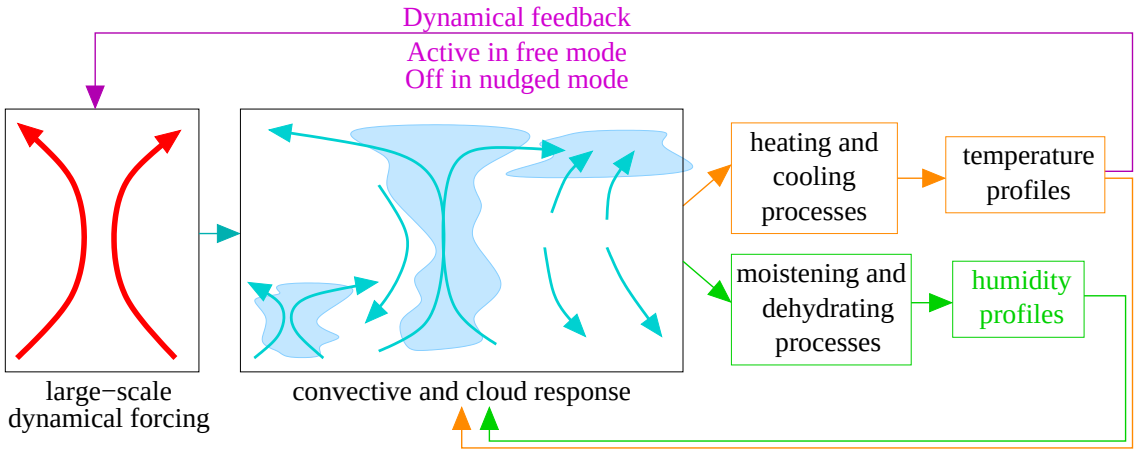

Figure A.5: Feedback between the large-scale dynamics and convective and cloud processes: the large-scale dynamics acts as a forcing to convective and cloud processes simulated by physical parameterizations. These parameterizations represent heating and cooling processes that impact large-scale temperature profiles, and moistening and dehydrating processes that impact large-scale q profiles. These profiles can feedback onto convective and cloud processes. In free-running simulations, temperature profiles also feed-back onto the large-scale dynamics. In nudged simulations, the large-scale dynamics is imposed, cutting the feedback loop.

Where we stand

To test hypothesis (1) (i.e. that a good simulation of moistening and dehydrating processes is crucial for a good simulation of the MJO), we compared different versions of LMDZ with perturbed physical parameters. The simulation of moistening and dehydrating processes as a response to the

dynamical forcing is diagnosed using $q - \delta D$ cycles simulated when winds are nudged towards reanalyses ([Tuinenburg et al., 2015]). The simulation of the MJO is diagnosed in free-running simulations using published diagnostics ([Kim et al., 2009, Waliser et al., 2008]).

During her internship, Ella Tribes compared two versions of LMDZ: the standard version with a poor MJO simulation, and a version with modified entrainment in which the MJO is improved. This improvement is associated with a moister middle troposphere, which is due to a smaller contribution of the deep convective scheme to precipitation.

Road map

- After identifying other perturbed-physics versions of LMDZ in which the MJO is improved, Ella Tribes's analysis will be redone: are improvements in the MJO simulation determined by the convective response to dynamical forcing in terms of moistening and dehydrating processes?

- To better understand how precipitation anomalies are amplified more or less strongly by convective-dynamical feedbacks depending on simulations, **hindcasts** of different MJO events and with different model versiosn of LMDZ will be performed

- To extend the perturbed-physics experiments accounting for model architecture, several isotopic GCMs will be compared in nudged and free modes. An **isotopic GCM intercomparison study** has started involving the GISS, GSM and ECHAM models, in collaboration with R. Field (GISS), K. Yoshimura (U. Tokyo), and M. Werner (AWI Germany) respectively. Ella Tribes's analysis will be redone.

- If in some models or model versions MJO simulation improvements result from improvements in the convective response to dynamical forcing in terms of moistening and dehydrating processes, then we will try to develop process-oriented diagnostics for the MJO simulation based on water isotope measurements. In contrast, if MJO simulation improvements always result from improvements in the convective response to dynamical forcing in terms of heating and cooling processes, then we will communicate on this result and my research on isotopes during the MJO will stop there.

A.8 Multi-tracer signature of convection

Context and science questions

Water vapor isotope measurements are potentially useful to evaluate the representation of some convective or cloud processes in atmospheric models, but they cannot solve everything. The problem is often under-constrained. For example, δD in the upper troposphere increases when the detrainment of condensate increases (section 2.1.2). But δD cannot make the difference between an increase in condensate detrainment associated with an increase in the condensate load of the detraining air, or an increase in the detrainment flux. A low-tropospheric air tracer, such as carbon monoxide (CO), would be useful to estimate the detrainment flux.

How could we combine different isotopic and chemical tracers (CO, ozone O_3, Beryllium Be...) to optimally constrain the different components of convective schemes?

Where we stand

To my knowledge, the only study combining water isotope measurements with other chemical measurements is [Liu et al., 2009], who investigate ozone variability and use water isotopes are used to infer the origin of air masses.

I find the study by [Folkins et al., 2006] very inspiring: he simulates simultaneously H_2O , CO, O_3 and nitric acid (HNO_3) profiles in single-column and 3D versions of GCMs. He investigates the sensitivity of these profiles to convective parameterizations and discusses how these combined chemical tracers could provide constrains on convective parameterizations.

Road map

- To simulate both humidity, water isotopes and chemical tracer profiles, a single-column model simulation with LMDZ equipped with both isotopes and the **chemical module INCA** (Interaction with Chemistry and Aerosols , [Hauglustaine et al., 2004]) will be set up. Simulations will be evaluated to first order using averaged climatologies.

- A simple, theoretical framework will be developed to interpret simultaneously the humidity, water isotopes and chemical tracer profiles. Ideally, for n tracers, we would end up with a model with n parameters quantifying key processes in convective and cloud parameterizations (e.g. precipitation efficiency, rain reevaporation fraction...). The advantages of combining different tracers will be discussed.

- Sensitivity tests to model parameters will help develop and validate the theoretical framework.

- For more realistic simulation and rigorous model-data comparisons, 3D LMDZ simulations equipped with both isotopes and the chemical module INCA will be performed. Outputs will be compared with TES or IASI data, which simultaneously retrieve water vapor, water isotopes and a variety of chemical tracers.

A.9 Link between past and future behavior of climate models for tropical precipitation changes

Context and science questions

Climate models show persistent spread in their simulation of future tropical precipitation changes. Could we use paleo-climatic archives of precipitation changes to assess which model simulates the most credible future precipitation changes?

The goal of this study is to establish links between the behavior of climate model for past climate changes and that for future climate changes, and to use these links to develop paleo-climatic constrains for future precipitation changes.

Where we stand

As a pilot study, CMIP5 simulations for pre-industrial, Mid-Holocene and RCP8.5 scenario were compared over tropical South America. We showed that models that shift the ITCZ to the North in Mid-Holocene also do so in future climate projections (section 4.1, [Schmidt et al., 2013]).

During his internship, Benedikt Rakotonirina-Hess tried to extend this study to Last Glacial Maximum (LGM) simulations and to the entire globe. The main conclusion was that tropical precipitation changes are usually not zonally consistent, so such studies should remain at the regional scale. He also examined the physical and dynamical components of precipitation changes, following the decomposition by [Bony and Bellon, 2013]. He found that when there is a link between past and future changes, this link is explained mainly by the dynamical component of precipitation changes.

Road map

- CMIP5 simulations for pre-industrial, Mid-Holocene and $4 \times CO_2$ scenario will be inter-compared over different tropical land regions. To search for statistical links between past and future behavior, EOF analysis will be used to identify the main patterns of precipitation changes depending on models.
- When statistical links are identified, we will try to explain it in terms of physical processes, using the decomposition into dynamical and physical components ([Bony and Bellon, 2013]). The dynamical component will be further decomposed based on the moist static energy budget ([Oueslati et al., 2016]).
- To check our interpretation of physical processes, we may run sensitivity tests with LMDZ simulations. For example, if the impact of cloud radiative effects on ITCZ shifts ([Hwang and Frierson, 2013]) is confirmed, simulations with and without cloud radiative effects can be performed.
- When a statistical link is identified for a given region, a given precipitation pattern and a given paleo-climatic epoch, and if the underlying physical processes are understood, we will check whether paleo-climatic archives for past precipitation changes (isotopic or non-isotopic) are available. If the case, we will propose a paleo-climatic constrain on that specific regional past precipitation change pattern and discuss its implications for future climate change.

Appendix B

Curriculum Vitae

Last update: October 20th, 2016

B.1 Contact information

Adress : LMD
case postale 99,
4, place Jussieu
75252 Paris Cedex 05
Phone: 01-44-27-52-62
Fax: 01-44-27-62-72
Email : Camille.Risi@lmd.jussieu.fr
Web : http://www.lmd.jussieu.fr/~crlmd

B.2 Education

2005-2006: Master "Ocea , Atmosphere, Climate and Remote Sensing" at the Université Pierre and Marie Curie (UPMC) (mention ■Très Bien■).

2004-2005: Preparation of the "Agrégation" (national competitive exam for posts in the teaching staff of french high schools and Universities) in Biology-Geology; accepted 4 th

2002-2004: "Licence" and ■Maîtrise" of Earth Sciences at the Ecole Normale Supérieure (ENS) of Paris.

2000-200: "Classes préparatoires" of Biology, Geology, Physics and Chemistry in Paris: preparation of national competitive exams to enter the ENS and engineering schools; accepted at the ENS of Paris.

2000: "Baccalauréat" in Sciences, Mathematics speciality (mention ■Très Bien■).

B.3 Reaseach

B.3.1 Research experience

2011-: Research Scientist at the Laboratoire de Météorologie Dynamique (LMD) , Paris

2010-2011: post-doc at the University of Colorado at Boulder (USA) at the Cooperative Institute for Research in Environmental Science, advised by David Noone

2006-2009: PhD at LMD, Paris, co-advised by Sandrine Bony and Jean Jouzel, untitled "Water stable isotopes: applications to study the water cycle and climate variations"

2006: 5-month Master internship at LMD advised by Sandrine Bony, on the relationship between atmospheric convection and the isotopic composition of tropical water.

2004: 6-month "Maîtrise" internship at the Massachusetts Institute of Technology, advised by Kerry Emanuel, on the simulation of tropical cyclones tracks using a statistical model

	Articles in international journals (accepted or published)	including article written as a first author	Articles in national journals (accepted or published)
total	69	10	5
2016	10	0	1
2015	13	0	1
2014	9	0	2
2013	13	2	0
2012	8	2	0
2011	7	0	1
2010	5	4	0
2009	0	0	0
2008	3	2	0
2007	0	0	0
2006	1	0	0

Table B.1: Summary table of publications for different years.

2003: 5-week "Licence" internship at LMD, advised by Frédéric Hourdin, on boundary layer parametrization.

B.3.2 Publications

- 69 publications in international journals with review comitees (tables B.1 and B.2, list in appendix C)
- 5 publications in national journals with review comitees (list in appendix D)

B.3.3 Funded projects

- **2013-2018**: Principal Investigator of the "ANR jeune chercheur-jeune chercheuse" project CONVISO

B.4 Advised students and post-docs

So far, I have advised 1 post-doc, co-advised 3 other post-docs, co-advised a PhD student and 1 Masters' student, advised 12 bachelor students and advised one "mission doctorale".

1. Florentin Breton, **2016**, "M1" internship, on the isotopic signature of the convective life cycle
2. Natacha Legrix, **2016**, "L3" internship, on the isotopic signature of the convective aggregation
3. Ella Tribes, **2016**, "M1" internship, on the impact of the representation of convective processes on the simulation of the MJO
4. Rongrong Zhang, **2016**, "M1" internship, on what controls the isotopic variations simulated during the last glacial maximum
5. Benedikt Rakotonirina-Hess, **2014**, "M1" internship, on past and future tropical precipitation changes in CMIP5 models
6. Yannick Lamarre, **2014**, "M1" internship, on cold pools in Niamey
7. Anis Bouchelit, **2014**, "M1" internship, on diabatic heating profiles simulated by LMDZ-1D
8. Obbe Tuinenburg, **2013-2015**: post-doc on water isotopes during MJO events

Journal	Number of articles
J. Geophys. Res.	20
Clim. Past	13
Atmos. Chem. Phys.	7
Earth Planet. Sci. Lett.	5
Atmos. Meas. Tech.	4
The Cryosphere	4
Clim. Dyn.	3
P. Natl. Acad. Sci. USA	2
Geophys. Res. Lett.	2
Rev. Geophysics	2
Water Ressources Res.	2
Nature Comm.	1
Quat. J. R. Meteorol. Soc.	1
Quat. Sci. Rev.	1
Tellus	1
Hydrology: Current Research	1
La Météorologie	5

Table B.2: Summary table of publications in different journals.

9. Alexandre Cauquoin, **2013-2015**: post-doc co-advised with Amaelle Landais on tritium modeling in LMDZ

10. Marion Saint-Lu, **2012-2013**: "Mission Doctorale" (PhD student) on the educational software SimClimat

11. Francesca Guglielmo, **2012-2013**: post-doc co-advised with Catherine Ottlé on the modeling of soil water isotopes in Siberia using the ORCHIDEE land surface model

12. Victor Gryazin, **2012-2013**: post-doc co-advised with Jean Jouzel on model-data comparison in Siberia

13. You He, **2012-2014**: PhD student co-advised with Valérie Masson-Delmotte and Gao Jing, on the interpretation of daily isotopic variability observed at Lhasa.

14. Tiana Jacquemart and Julie Meyer, **2012**, tandem "L3" internship, on daily isotopic variability observed at Darwin during the TWPice campaign and simulated by LMDZ in a single-column

15. Gaelle Benoit, **2012**, "L3" internship, on isotopic modeling using single-column LMDZ radiative-convective equilibrium

16. Lorraine Desbordes, **2012**, "M1" internship, on the influence of irrigation on precipitation distribution

17. Magali Hug, **2012**, "M1" internship, on water vapor isotopic variations observed by TES during El-Nino events

18. Guillaume Tremoy, **2009**, "M2" internship co-advised with Françoise Vimeux, on the interpretation of Andean ice core records

19. Marie Vicompte, **2007**, "L3" internship co-advised with Sandrine Bony, on Sahelian squall lines

B.5 Awards

- **2010**: "Prix André Prud'homme" of the "Société Météorologique de France" for my PhD thesis
- **2010**: "Prix Le Monde de la recherche universitaire" for my PhD thesis
- **2010**: "Prix de la meilleure thèse" of the EADS fundation for my PhD thesis.
- **2016**: "Médaille de bronze" of CNRS.

B.6 Teaching

- **2015**, **2016**: Course on climate modeling for Masters' students in "Sciences et Génie de l'Environnement" of Paris 7.
- **2014**: Advised students in the "Science diffusion" section of UPMC.
- **2013**: Course on Climate at Ecole Polytechnique Féminine.
- **2011-2012**: Training students who prepare the competitive exam to become Biology-Geology teachers at UPMC.
- July **2012**: Teaching a workshop on Climate during the Summer school of "KIC-Climat" in Polytechnique.
- **2006-2009**: Teaching at Université Pierre et Marie Curie (UPMC) in Physics and Geology.

B.7 Outreach activities

B.7.1 Educational software on climate: SimClimat

http://www.lmd.jussieu.fr/~crlmd/simclimat

This educational software simulates climate given user-chosen parameters. Through a friendly interface, the user chooses the length of the simulation (from 100 years to a few billions years) and the initial conditions, and tests the influence of various parameters involved in climate: astronomic forcing, atmospheric composition, carbone cycle, climatic feedbacks (ice albedo, vegetation, ocean, water vapor). Simulation results (such as temperature, sea level and ice cover), calculated by a physical climate model, appear on the interface, through curves and images (figure).

Work on this software included:

- 2006-2008: software development
- tests in high schools in the Paris region
- advised "mission doctorale" of Marion Saint-Lu to improve the software
- contribution to a "hackaton" as part of the "train du climat" (october 2015).

B.7.2 Contribution to the "La Météorologie" outreach journal

La Météorologie is a journal on meteorology and climate targeting students, teachers and enthusiasts.

- **2012-**: member of the editorial comitee
- wrote 5 articles (list in chapter D)
- wrote 3 short articles and 1 editorial

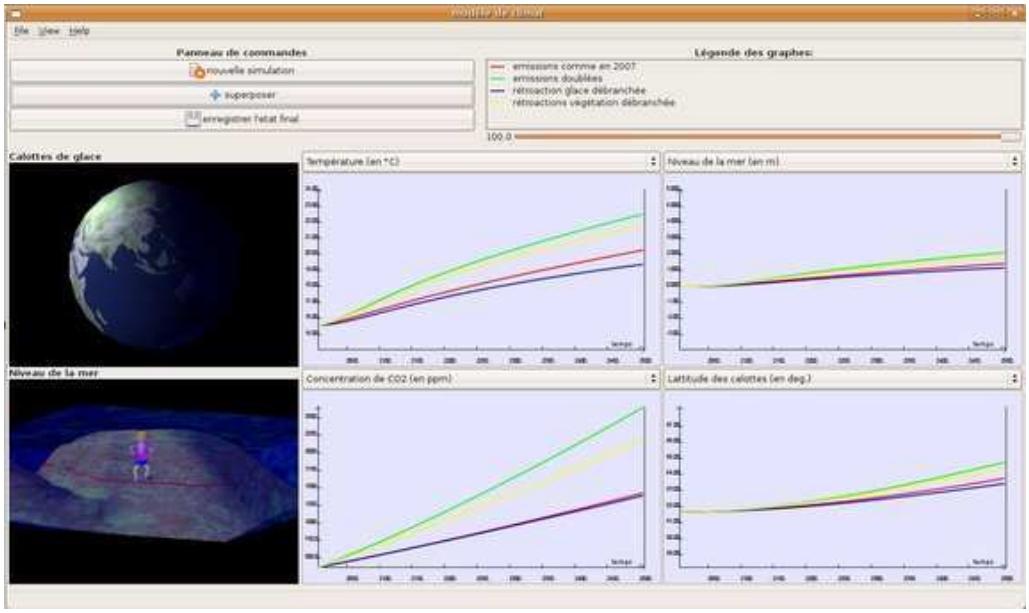

Figure B.1: Snapshot of the SimClimat graphical interface.

B.7.3 Round tables and outreach workshops

- April **2015**: Invited to a round table on multi-disciplinarity in climate sciences at the "disciplines sans frontières" workshop in Paris
- March **2015**: Invited to a round table at the workshop "Educate and train on climate change" on "How to conduct a debate in an educational context?" at the "Conseil Economique, Social et Environnemental de Paris".
- January **2015**: Participation in the workstop "Climatologie, météorologie et enseignement(s)" at the "Forum des ressources pour l'éducation au développement durable", Amiens

B.7.4 Presenting experiments in science festivals

During science festivals, I usually present educational experiments on clouds and atmospheric physics, play with the SimClimat software or discuss about climate.

- October **2016**: Participation in the IPSL tent during the the Fête de la Science, UPMC.
- March **2015**: Participation in the IPSL tent at the Forum de la Météorologie, Paris
- October **2014**: Participation in the INSU tent at the "cité de sciences de la Vilette" during the Fête de la science
- October **2014**: Participation in the Fête de la Science at LMD
- April **2014**: Participation in the IPSL tent at the Forum de la Météorologie, Paris
- October **2013**: Participation in the Fête de la Science at LMD, UPMC
- May-June **2013**: Participation in the CNRS and UPMC tents at "salon des Jeux et de la culture mathématiques" at the "cité des sciences de la Villette".
- March **2013**: Participation in the "Bar des sciences" "Météo, mode d'emploi" at the Chamarande castle.
- November **2013**: Participation in the "forum Climat du Grand Troyes" in Troyes

- October **2013**: Participation in the INSU tent during the "Forum de la Météorologie", Paris.
- October **2012**: Participation in the Fête de la Science at LMD
- December **2012**: organisation of the visit of a secondary school class at LMD
- Novembre **2012**: Participation in the "forum Climat du Grand Troyes" in Troyes
- October **2011**: Participation in the Fête de la Science at LMD
- October **2011**: Participation in the INSU tent during the "Forum de la Météorologie", Paris.
- October 2**009**: Participation in the Fête de la Science at LMD
- October **2009**: Participation in the INSU tent during the "Forum de la Météorologie", Paris.
- October **2008**: Participation in the Fête de la Science at LMD
- October **2008**: Participation in the INSU tent during the "Forum de la Météorologie", Brussels.
- October **2008**: Participation in a tent on climate change at the Fête de l'Essone.
- March **2008**: Presentation of educational experiments at the "commission Education Formation" of the "Conseil Supérieur de la Météorologie", Ecole Polytechnique.
- October **2007**: Participation in the Fête de la Science at LMD
- October **2007**: Participation in the INSU tent during the "Forum de la Météorologie", Paris.
- Summer **2007**: Participation in a tent on volcanoes at the Paris-Montagne festival
- October **2006**: Participation in the Fête de la Science at LMD
- Summer **2006**: Participation in a tent on climate change at the Paris-Montagne festival

B.7.5 Conferences in Universities

- September **2016**: Conference on climate change during the inauguration of the new campus of Jussieu

B.7.6 Conferences in primary and secondary schools

- December **2014**: Organizing the visit of LMD by a secondary school class of Lycée Voltaire.
- December **2014**: Conference in a secondary school, Confolens.
- November **2014**: Conference at lycée Voltaire in Paris
- September **2014**: Debate with Roland Schlisch at lycée Louis Le Grand following the projection of the moovie "Entérrés volontaires"
- April **2014**: Climate activities for secondary school pupils as part of the "Sciences Ouvertes" association.
- March **2014**: Conference in a secondary school, La Ferté-sous-Jouarre
- March **2014**: Conference in a primary school, Nogent-sur-Seine, as part of the "festival des Sciences et Techniques de l'Aube" and the "Terre Avenir" association.
- April **2012**: Conference to a network of primary schools, Nogent-sur Oise.
- February **2012**: Conference in a secondary school, Argenteuil.
- March **2009**: Conference in a secondary school as part of "1000 ambassadrices pour les Sciences à Paris"
- Décembre **2007**: Conference in a secondary school, lycée Soeur Rosalie-Louise de Marillace, Paris

B.7.7 Conference in jails

- February **2016**: Conference on climate change at the “Maison d’Arrêt des Hauts de Seine”, Nanterre.

B.7.8 Radio and TV

- May **2016**: “E=M6” show on M6 channel on super-cell thunderstorms
- December **2015**: Discussion on climate change on “Radio Grenouille” as part of the COP21.
- April **2015**: Interview for an audio podcast on a blog for scientific information “indesciences”
- March **2015**: Video on ”climate modeling and pedagogy” as a resource for the education for sustainable development of the “Education Nationale”.
- October **2014**: Show ”3 minutes for the planet” on “Radio Classique”.
- October **2014**: Debate on the science diffusion on the ”Aligre FM” radio

B.7.9 Teacher training

- February **2016**: Training animators for the association ”Pionniers de France” to take part at the ”Planète mômes” festival
- October **2015**: Course on climate modeling as part of the training “Formaterre” for secondary school teachers.
- May **2015**: course on climate as part of a training for secondary school teachers.
- January **2015**: Round table on ”Climatology, meteorology and teaching(s)” at the “forum sur l’éducation au développement durable” for secondary school teachers.
- August **2012**: workshop on climate change in the Summer school of mathematics (for teachers) at Sourdun, for secondary school teachers

B.7.10 Miscellaneous

- Hosted 5 secondary school pupils at LMD
- Helped many secondary school pupils and students for their science projects (“TPEs” and “TIPEs”)

B.8 Administrative and miscelaneuous activities

B.8.1 Member of PhD committees

1. Maximilien Bolot, Approche théorique de la distribution des isotopologues stables de l’eau dans l’atmosphère tropicale, de l’échelle convective aux grandes échelles. ENS Paris, **2013**
2. J-L Lacour, Estimations du profil du rapport isotopique δD de la vapeur d’eau dans la troposphère à partir des spectres mesurés par le sondeur satellitaire IASI dans l’infrarouge thermique : Méthodologie d’inversion et analyses des premières distributions spatiales. ULB (Belgium), **2014**

B.8.2 Expertise of research articles and proposals

- expertise of research articles: $>$ 40 articles including Nature, JGR, GRL, Clim Dyn...
- expertise of proposals: 5: ECOS-Sud, NSF, ANR, LEFE (x2).

B.8.3 Miscellaneous

- 2011-: Responsible for GENCI project 0292 for HPC resources: managing accounts, writing proposals for computational time and reports on computational activities
- 2013-: Member of the "MJO Task Force"
- 2015: Member of the working group on Water vapor for a "Phase-0" study at CNES.

Appendix C

List of international publications

Last update: October 20th, 2016

1. Galewsky, J, Steen-Larsen, H C, Field, R, Worden, J, Risi, C. Stable isotopes in atmospheric water vapor and applications to the hydrologic cycle. **Accepted** by Reviews of Geophysics.

2. Cauquoin, A., Jean-Baptiste, P., Risi, C., Fourré, E., Stenni, B., and Landais, A. Modeling the global bomb-tritium transient signal with an Atmospheric General Circulation Model: a promising method to evaluate the dynamics of the hydrological cycle in the models and its link with stratospheric air intrusions. **Accepted** by J.Geophys. Res.,

3. C. Risi S. Bony, J. Ogée, T. Bariac, Naama Raz-Yaseef and Lisa Wingate, Welker, J, Knohl, A, Kurz-Besson, C, Leclerc, M, Zhang, G, Buchmann, N, Santrucek, J, Hronkova, M, David, T, Peylin, P, Guglielmo, F. The water isotopic version of the land-surface model ORCHIDEE: implementation, evaluation, sensitivity to hydrological parameters. **Accepted** by Hydrology: Current Research.

4. Stenni, B, Scarchilli, C, Masson-Delmotte, V, Schlosser, E, Ciardini, V, Dreossi, G, Grigioni, P, Bonazza, M, Cagnati, A, Karlicek, D, Risi, C, Udisti, R, Valt, M. Three-year monitoring of stable isotopes of precipitation at Concordia Station, East Antarctica, **accepted**, The Cryosphere.

5. Bolliet, T., Brockmann, P., Masson-Delmotte, V., Bassinot, F., Daux, V., Genty, D., ... and Risi, C. (**2016**). Water and carbon stable isotope records from natural archives: a new database and interactive online platform for data browsing, visualizing and downloading. Climate of the Past, 12(8), 1693-1719., doi:10.5194/cp-12-1693-2016

6. Scheepmaker, R., aan de Brugh, J., Hu, H., Borsdorff, T., Frankenberg, C., Risi, C., Hasekamp, O., Aben, O., Landgraf, J. (**2016**). HDO and H2O total column retrievals from TROPOMI shortwave infrared measurements, Atmos. Meas. Tech., 9, 3921-3937, 2016, doi:10.5194/amt-9-3921-2016

7. Ritter, F, Steen-Larsen, H C, Werner, M, Masson-Delmotte, V, Orsi, Anais, Behrens, M, Birnbaum, G, Freitag, J, Risi, C, and Kipfstuhl, S (**2016**). Isotopic exchange on the diurnal scale between near-surface snow and lower atmospheric water vapor at Kohnen station, East Antarctica, The Cryosphere, 10, 1647-1663, 2016 doi:10.5194/tc-10-1647-2016

8. Touzeau, A, A. Landais, B. Stenni, R. Uemura, K. Fukui, S. Fujita, S. Guilbaud, A. Ekaykin, M. Casado, E. Barkan, B. Luz, O. Magand, G. Teste, E. Le Meur, M. Baroni, J. Savarino, I. Bourgeois, and C. Risi (**2016**). Acquisition of isotopic composition for surface snow in East Antarctica and the links to climatic parameters. The Cryosphere, 10, 837-852, 2016, doi:10.5194/tc-10-837-2016

9. Oueslati, B, Bony, S, Risi, C, Dufresne, J-L (**2016**). Interpreting the inter-model spread in regional precipitation projections in the tropics: Role of surface evaporation and cloud radiative effects. *Clim. Dyn.* 47: 2801-2815. doi:10.1007/s00382-016-2998-6

10. Botsyun, S, Sepulchre, P, C. Risi, and Y. Donnadieu (**2016**). Impacts of Tibetan Plateau uplift on atmospheric dynamics and associated precipitation d18O . Clim. Past, 12, 1401-1420, 2016. doi:10.5194/cp-12-1401-2016

11. Retanauer C, A. Landais, T. Blunier, C. Bréant, M. Kageyama, M.-N. Woillez, C. Risi, V. Mariotti, and P. Braconnot (**2015**), Quantifying molecular oxygen isotope variations during a Heinrich Stadial. *Clim. Past* 11, 1527– 1551

12. Jasechko, S, Lechler, A, Pausata, F S R, Fawcett, P J, Gleeson, T, Cendron, D I, Galewsky, J, LeGrande, A N, Risi, C, Sharp, Z D, Welker, J M, Werner, M, Yoshimura, K (**2015**). Late-glacial to late-Holocene shifts in global precipitation delta18O. *Clim. Past* , 11, 1375-1393

13. Cauquoin, A., Jean-Baptiste, P., Risi, C., Fourré, E., Stenni, B., and Landais, A. (**2015**). The global distribution of natural tritium in precipitation simulated with an Atmospheric General Circulation Model and comparison with observations. *Earth Planet. Sci. Lett.*, 427, 160-170. doi:10.1016/j.epsl. 2015.06.043

14. Tuinenburg, O, C. Risi, J.-L. Lacour, M. Schneider, A. Wiegele, J. Worden, N. Kurita, J.P. Duvel, N. Deutscher, S. Bony, P.F. Coheur, C. Clerbaux (**2015**). Moist processes during MJO events as diagnosed from water isotopic measurements from the IASI satellite. *J. Geophys. Res.* 120(20):10,619.10,636.

15. V. Masson-Delmotte, H.C. Steen-Larsen, P. Ortega, D. Swingedouw, T. Popp, B.M. Vinther, H. Oerter, A.E. Sveinbjornsdottir, J.E. Box, S. Falourd, X. Fettweis, H. Gallée, E. Garnier, J. Jouzel, A. Landais, B. Minster, N. Paradis, A. Orsi, C. Risi, M. Werner, H. Gudlaugsdottir, and J.W.C. White. Recent changes in North West Greenland climate documented by NEEM shallow ice core data and simulations, and implications for past temperature reconstructions. by *The Cryosphere*, 9, 1481-1504

16. S S.P. Shen, T. Yao, C. Risi, N. Tafolla, Y He. (**2015**) Reconstruction of precipitation delta18O over the Tibetan Plateau since 1910. *J. Geophys. Res., 120, 10, 4878-4888*

17. He, Y, C. Risi, J. Gao, V. Masson-Delmotte, T. Yao, J. Worden, C. Frankenberg, and G. Cesana (**2015**). Impact of atmospheric convection on the isotopic composition of Tibetan precipitation using a combination of satellite data and atmospheric general circulation modeling. *J. Geophys. Res.* 120(9):3852–3871

18. Gao, J, et al. (**2015**) Southern Tibetan Plateau ice core $\delta^{18}O$ reflects abrupt shifts in atmospheric circulation in the late 1970s. *Clim Dyn.* 46(1):291-302

19. Benetti, M, Aloisi, G, Reverdin, G and Risi, C., Sèze, G. (**2015**), Importance of boundary layer mixing for the isotopic composition of surface vapor over the subtropical North Atlantic Ocean. *J. Geophys. Res.* 120(6):2190-2209, doi:10.1002/2014JD021947

20. Bonne, J-L, Steen-Larsen, H C, Risi, C, Werner, M, Sodemann, H, Lacour, J-L, Fettweis, X, Cesana, G, Delmotte, M, Cattani, O, Vallelonga, P, Kjaer, H A, Clerbaux, C, Sveinbjörnsdottir, A E and Masson-Delmotte, V. (**2015**). The summer 2012 Greenland heat wave: in-situ a,d remote sensing observations of water vapor isotopic composition during an atmospheric river event. *J. Geophys. Res.*, 120(7): 2970-2989

21. J.-L. Lacour, L. Clarisse, J. Worden, M. Schneider, S. Barthlott, C. Risi, C. Clerbaux, D. Hurtmans, and P.-F. Coheur (**2015**). Cross-validation of IASI/MetOp derived tropospheric deltaD with TES and ground-based FTIR observations. *Atmos. Meas. Tech.*, 8, 1447-1466, doi:10.5194/amt-8-1447-2015

22. Day, J, Fung, I and Risi, C. (**2015**). Weak Coupling of Juillet-Aout Precipitation between India and East Asia. *J. Climate*, 28, 4330-4356doi: http://dx.doi.org/10.1175/JCLI-D-14-00393.1

23. Pang, H, Hou, S, Landais, A et al. (**2015**). Spatial distribution of 17O-excess in surface snow along a traverse from Zhongshan station to Dome A, East Antarctica. *Earth Planet. Sci. Lett.*, 414:126-133 doi:10.1016/j.epsl.2015.01.014

24. Gryazin V, Risi C, Jouzel J, Kurita N, Worden J, Frankenberg C, Bastrikov V, Gribanov K, Stukova O (**2014**) . The added value of water isotopic measurements for understanding model biases in simulating the water cycle over Western Siberia. *Atmos. Chem. Phys.*, 2014. doi:10.5194/acp-14-9807-2014

25. J-L Bonne, V Masson-Delmotte, O Cattani, M Delmotte, C Risi, H Sodemann, HC Steen-Larsen (**201**4). The isotopic composition of water vapour and precipitation in Ivittuut, southern Greenland. *Atmos. Chem. Phys.*, 14, 4419-4439, 2014. doi:10.5194/acp-14-4419-2014

26. Pommier, M., Lacour, J. L., Risi, C., Bréon, F. M., Clerbaux, C., Coheur, P.-F., Gribanov, K., Hurtmans, D., Jouzel, J., and Zakharov, V. (**2014**). Observation of tropospheric deltaD by IASI over the Western Siberia: Comparison with a GCM. Accepted in *Atmospheric Measurement Techniques*. DOI: 10.5194/amtd-6-11055-2013

27. Liu, Z., Yoshimura, K., Bowen, G. J., Buenning, N. H., Risi, C., Welker, J. M., and Yuan, F. (**2014**). Paired oxygen isotope records reveal modern North American atmospheric dynamics during the Holocene. *Nature communications*, 5. doi:10.1038/ncomms4701

28. P. Ortega, D. Swingedouw, V. Masson-Delmotte, C. Risi, B. Vinther, P. Yiou, R. Vautard, K. Yoshimura (**2014**). Characterizing atmospheric circulation signals in Greenland ice cores: insights from a weather regime approach. *Clim. Dyn.,* 1-21. doi:10.1007/s00382-014-2074-z

29. M. Benetti, G. Reverdin, C. Pierre, L. Merlivat, C. Risi, F. Vimeux (**2014**). Deuterium excess in marine water vapor: Dependency on relative humidity and surface wind speed during evaporation. *J. Geophys. Res*, 119, 584-593, DOI: 10.1002/2013JD020535

30. M. Butzin, M. Werner, C. Frankenberg, J. Jouzel, V. Masson-Delmotte, C. Risi, and V. I. Zakharov (**2014**). Variations of oxygen-18 in West Siberian precipitation during the last 50 years. *Atmos. Chem. Phys.* 14, 5853-5869, doi:10.5194/acp-14-5853-2014

31. G Tremoy, F Vimeux, S Soumana, I Souley, C Risi, O Cattani, G Favreau, M Oi (**2014**). Clustering mesoscale convective systems with laser-based water vapor delta18O monitoring in Niamey (Niger). *J. Geophys. Res.*, DOI: 10.1002/2013JD020968

32. Steen-Larsen, H. C., Masson-Delmotte, V., Hirabayashi, M., Winkler, R., Satow, K., Prié, F., Bayou, N., Brun, E., Cuffey, K. M., Dahl-Jensen, D., Dumont, M., Guillevic, M., Kipfstuhl, S., Landais, A., Popp, T., Risi, C., Steffen, K., Stenni, B., and Sveinbjörnsdottír, A. E. (**2014**) What controls the isotopic composition of Greenland surface snow? *Clim. Past,* 10, 377-392, 2014, doi:10.5194/cp-10-377-2014

33. Jouzel, J, Delaygue, G, Landais, A, Masson-Delmotte, V, Risi, C, Vimeux, F (**2013**). Water isotopes as tools to document oceanic sources of continental precipitation. *Water Ressources Res.*, 49, 7469-7486, DOI: 10.1002/2013WR013508

34. G. A. Schmidt, J. D. Annan, P. J. Bartlein, B. I. Cook, E. Guilyardi, J. C. Hargreaves, S. P. Harrison, M. Kageyama, A. N. LeGrande, B. Konecky, S. Lovejoy, M. E. Mann, V. Masson-Delmotte, C. Risi, D. Thompson, A. Timmerman, L.-B. Tremblay, P. Yiou (**2013**). Using paleo-climate comparisons to constrain future projections in CMIP5. *Clim. Past* doi:10.5194/cp-10-221-2014

35. Gao, J., V. Masson-Delmotte, C. Risi, Y. He, T. Yao (**2013**). What controls southern Tibetan Plateau precipitation deltaO18 at seasonal and intra-seasonal scales? A case study at Lhasa and Nyalam. *Tellus*, http://dx.doi.org/10.3402/tellusb.v65i0.21043

36. T. Yao, V. Masson-Delmotte, J. Gao, L. Tian, W. Yu, X. Yang, C. Risi, C. Sturm, N. Kurita, Y. He, C Shi and S. Hou (**2013**). A Review of Stable Isotope Studies in precipitation from observation stations and Ice Cores in Tibetan Plateau and surrounding regions. *Rev. Geophysics* DOI: 10.1002/rog.20023

37. R. Winkler, A Landais, C Risi, M Baroni, A Ekaykin, J Jouzel, J-R Petit, F Prie, B Minster, S Falourd. (**2013**). Interannual variation of water isotopologues at Vostok indicates a contribution from stratospheric water vapor, *P. Natl. Acad. Sci. USA*.. doi: 10.1073/pnas.1215209110

38. Risi, C, Noone, D, Frankenberg, C, Worden, J. (**2013**). The role of continental recycling in intra-seasonal variations of continental moisture as deduced from model simulations and water vapor isotopic measurements. *Water Ressources Res.* DOI:10.1002/wrcr.20312

39. R. Eagle, C. Risi, J. Mitchell, J. Eiler, U. Seibt, D. Neelin, G. Li, A. Tripati (**2013**). High regional climate sensitivity over continental China inferred from glacial-recent changes in temperature and the hydrologic cycle, *P. Natl. Acad. Sci. USA*. doi: 10.1073/pnas.1213366110

40. L. C. Sime, C. Risi, J. C. Tindall, J. Sjolte, E. W. Wolff, V. Masson-Delmotte, E. Capron (**2013**). Warm climate isotopic simulations: What do we learn about interglacial signals in Greenland ice cores?. *Quaternary Science Reviews* doi:10.1016/j.quascirev.2013.01.009

41. H. C. Steen-Larsen, et al. (**2013**) Continuous monitoring of summer surface water vapour isotopic composition above the Greenland Ice Sheet. *Atmos. Chem. Phys.*, 13, 4815-4828, doi:10.5194/acp-13-4815-2013

42. M. Casado, P. Ortega, V. Masson-Delmotte, C. Risi, D. Swingedouw, V. Daux, D. Genty, F. Maignan, N. Viovy, O. Solomina, B. Vinther, P. Yiou (**2013**). Impact of precipitation intermittency on NAO-temperature signal in proxy records. *Clim. Past,* 9, 871-886, 2013 doi:10.5194/cp-9-871-2013

43. Frankenberg, C, Wunch, D, Toon, G, Risi, C, Scheepmaker, R, Lee, J-E, and Worden, J. (**2013**) Water vapor isotopologues retrievals from high resolution GOSAT short-wave infrared spectra, *Atmos. Meas. Tech.* 6, 263-274, 2013. doi:10.5194/amt-6-263-2013

44. D. Noone, C. Risi, A. Bailey, M. Berkelhammer, D.P. Brown, N. Buenning, S. Gregory, J. Nusbaumer, D. Schneider, J. Sykes, B. Vanderwende, J. Wong, Y. Meillier, and D. Wolfe (**2013**). Determining water sources in the boundary layer from tall tower profiles of water vapor and surface water isotope ratios after a snowstorm in Colorado. *Atmos. Chem. Phys.* 13, 1607-1623, 2013. doi:10.5194/acp-13-1607-2013

45. Risi, C, Landais, A, Winkler, R, Vimeux, F. (**2013**) Can we determine what controls the spatio-temporal distribution of d-excess and 17O-excess in precipitation using the LMDZ general circulation model? *Clim. Past.* 9, 2173-2193, 2013. doi:10.5194/cp-9-2173-2013

46. R. D. Field, C. Risi, G. A. Schmidt, J. Worden, A. Voulgarakis, A. N. LeGrande, A. H. Sobel, and R. J. Healy. (**2012**) A Tropospheric Emission Spectrometer HDO/H2O retrieval simulator for climate models, *Atmos. Chem. Phys.* doi:10.5194/acp-12-10485-2012

47. Lacour, J-L, Risi, C, Clarisse, L, Bony, S, Hurtmans, D, Clerbaux, C, Coheur, P-F. (**2012**). Mid-troposheric deltaD observations from IASI/MetOp at high spatial and temporal resolution, *Atmos. Chem. Phys.* doi:10.5194/acp-12-10817-2012

48. S. Sherwood and C. Risi (**2012**). The HDO/H2O relationship in tropospheric water vapor in an idealized "last-saturation" model, *J. Geophys. Res.* doi:10.1029/2012JD018068

49. J-E. Lee, I. Fung, C. Risi, J. Worden, R. Scheepmaker, C. Frankenberg (**2012**). Asian monsoon hydrology from LMDZ GCM and two satellite measurements (TES and SCIAMACHY) of water vapor isotopes: implications for speleothem data interpretation, *J. Geophys. Res.*, doi:10.1029/2011JD017133

50. Tremoy, T., Vimeux, F., Mayaki, S., Souley, I., Cattani, O., Risi, C. Favreau, G. Oi, M (**2012**). A 1-year long delta18O record of water vapor in Niamey (Niger) reveals insightful atmospheric processes at different timescales, *Geophys. Res. Lett.* doi:10.1029/2012GL051298

51. Risi, C., D. C. Noone, J. Worden, C. Frankenberg, G. P. Stiller, M. Kiefer, B. Funke, K. A. Walker, P. F. Bernath, M. Schneider, D. Wunch, V. J. Sherlock, N. Deutscher, D. W.T Griffith, P. O. Wennberg, K. Strong, D. Smale, E. Mahieu, S. Barthlott, F. Hase, O. García, J. Notholt, T. Warneke, G. C. Toon, D. S. Sayres, S. Bony, J. Lee, D. P. Brown, R. Uemura, and C. Sturm (**2012**). Process-evaluation of tropospheric humidity simulated by general circulation models using water vapor isotopologues. Part 1: Comparison between models and observations, *J. Geophys. Res.*, doi:10.1029/2011JD016621

52. Risi, C., D. C. Noone, J. Worden, C. Frankenberg, G. P. Stiller, M. Kiefer, B. Funke, K. A. Walker, P. F. Bernath, M. Schneider, S. Bony, J. Lee, D. P. Brown, and C. Sturm (**2012**). Process-evaluation of tropospheric humidity simulated by general circulation models using water vapor isotopic observations. Part 2: Using isotopic diagnostics to understand the mid and upper tropospheric moist bias in the tropics and subtropics, *J. Geophys. Res.*, doi:10.1029/2011JD016623

53. Berkelhammer, M., C. Risi, N. Kurita, and D. C. Noone (**2012**). The moisture source sequence for the Madden-Julian Oscillation as derived from satellite retrievals of HDO and H2O, *J. Geophys. Res.*, doi:10.1029/2011JD016803.

54. Kurita, N., D. Noone, C. Risi, G. A. Schmidt, H. Yamada, and K. Yoneyama (**2011**), Intraseasonal isotopic variation associated with the Madden-Julian Oscillation, *J. Geophys. Res.*, doi:10.1029/2010JD015209

55. V. Masson-Delmotte, P. Braconnot, G. Hoffmann, J. Jouzel, M. Kageyama, A. Landais, Q. Lejeune, C. Risi, L. Sime, J. Sjolte, D. Swingedouw, and B. Vinther (**2011**). Sensitivity of interglacial Greenland temperature and delta18O to orbital and CO2 forcing: climate simulations and ice core data. *Clim. Past.* 7, 1041-1059, doi:10.5194/cp-7-1041-2011.

56. C. Shi, V. Daux, C. Risi, S.-G. Hou, M. Stievenard, M. Pierre, Z. Li, and V. Masson-Delmotte (**2011**). Reconstruction of southeast Tibetan Plateau summer cloud cover over the past two centuries using tree ring delta18O. *Clim. Past* doi:10.5194/cp-8-205-2012

57. F. Vimeux, G. Tremoy, C. Risi, R. Gallaire (**2011**). A strong control of the South American SeeSaw on the intraseasonal variability of the isotopic composition of precipitation in the Bolivian Andes. *Earth. Planet. Sci. Lett.* doi:10.1016/j.epsl.2011.04.031

58. C. Shi, V. Masson-Delmotte, C. Risi, T. Eglin, M. Stievenard, M. Pierre, X. Wang, J. Gao, F-M. Bréon, Q-B. Zhang, V. Daux (**2011**). Sampling strategy and climatic implications of tree-ring stable isotopes in Southeast Tibetan Plateau, *Earth. Planet. Sci. Lett.* doi:10.1016/j.epsl.2010.11.014

59. J. Gao, V. Masson-Delmotte, T. Yao, L. Tian, C. Risi et G. Hoffmann (**2011**). Precipitation water isotopes in the South Tibetan Plateau: observations and modeling, *J. Clim* .doi:10.1175/2010JCLI3736.1

60. H-C. Steen-Larsen, V. Masson-Delmotte, J. Sjolte, S. Johnsen, B. Vinther, F-M. Breon, H. Clausen, D. Dahl-Jensen, S. Falourd, X. Fettweis, H. Gallee, J. Jouzel, M. Kageyama, H. Lerche, B. Minster, G. Pichard, H. Punge, C. Risi, D. Salas-Mélia, J. Schwander, K. Steffen, A. Sveinbjornsdottir, A. Svensson, J. White. (**2011**) Understanding the climatic signal in the water stable isotope records from the NEEM cores in North-West Greenland, *J. Geophys. Res.* doi:10.1029/2010JD014690

61. C. Risi, S. Bony, F. Vimeux and J. Jouzel (**2010**), Water stable isotopes in the LMDZ4 General Circulation Model: model evaluation for present day and past climates and applications to climatic interpretation of tropical isotopic records, *J. Geophys. Res.* doi:10.1029/2009JD013255

62. C. Risi, A. Landais, S. Bony, V. Masson-Delmotte, J. Jouzel and F. Vimeux (**2010**), Understanding the 17O-excess glacial-interglacial variations in Vostok precipitation, *J. Geophys. Res.* doi:10.1029/2008JD011535

63. C. Risi, S. Bony, F. Vimeux, M. Chong and L. Descroix (**2010**), Evolution of the water stable isotopic composition of the rain sampled along Sahelian squall lines, *Quat. J. Roy. Met. Soc.* doi:10.1002/qj.485

64. A. Landais, C. Risi, S. Bony, F. Vimeux et L. Descroix (**2010**). Combined measurements of 17Oexcess and d-excess in African monsoon precipitation: Implications for evaluating convective parameterizations, *Earth. Planet. Sci. Lett.* doi:10.1016/j.epsl.2010.07.033

65. C. Risi, Sandrine Bony, Françoise Vimeux, Christian Frankenberg, David Noone and John Worden (**2010**). Understanding the Sahelian water budget through the isotopic composition of water vapor and precipitation, *J. Geophys. Res.* doi:10.1029/2010JD014690

66. C. Risi, S. Bony, F. Vimeux, L. Descroix, B. Ibrahim, E. Lebreton, I. Mamadou, B. Sultan (**2008**), What controls the isotopic composition of the African monsoon precipitation? Insights from event-based precipitation collected during the 2006 AMMA field campaign, *Geophys. Res. Lett.* doi:10.1029/2008GL035920

67. S. Bony, C. Risi and F. Vimeux, (**2008**), Influence of convective processes on the isotopic composition (d18O and dD) of precipitation and water vapor in the tropics: 1. Radiative-convective equilibrium and Tropical Ocean-Global Atmosphere-Coupled Ocean-Atmosphere Response Experiment (TOGA-COARE) simulations, *J. Geophys. Res.* doi: 10.1029/2008JD009942

68. C. Risi, S. Bony and F. Vimeux, (**2008**), Influence of convective processes on the isotopic composition (d18O and dD) of precipitation and water vapor in the tropics: 2. Physical interpretation of the amount effect, *J. Geophys. Res.*, doi: 10.1029/2008JD009943

69. K. Emanuel, S. Ravela, E. Vivant, and C. Risi (**2006**): A Statistical Deterministic Approach to Hurricane Risk Assessment. *Bull. Amer. Meteor. Soc.*, 87, 299-314, doi:10.1175/BAMS-87-3-299

Appendix D

List of national publications

Last update: October 20th, 2016

1. C. Risi, V Journé, J-L Dufresne, J-Y Grandpeix, A Spiga, **2016**. Mise en évidence de la chaleur latente liée à l'évaporation et à la condensation de l'eau: Applications au fonctionnement des orages. *La Météorologie*, n°94

2. C. Risi, **2015**. SimClimat, un logiciel pédagogique de simulation du climat. *La Météorologie*, n°88

3. C. Risi, J-L Dufresne, J-Y Grandpeix, S Labetoulle, G Sèze, A Spiga, **2014**, Comment se forment les nuages? L'expérience du nuage dans une bouteille. *La Météorologie*, n°86

4. C. Risi and J-P Duvel, **2014**. L'oscillation de Madden Julian. *La Météorologie*. n°86

5. C. Risi and S. Bony, **2011**. Évaluer les modèles de climat et leurs projections: la valeur ajoutée de la composition isotopique de l'eau. *La Météorologie*, n°74

Appendix E

Articles attached at the end of this document

1. C. Risi, S. Bony and F. Vimeux, (**2008**), Influence of convective processes on the isotopic composition (d18O and dD) of precipitation and water vapor in the tropics: 2. Physical interpretation of the amount effect, *J. Geophys. Res.*

2. C. Risi, S. Bony, F. Vimeux, M. Chong and L. Descroix (**2010**), Evolution of the water stable isotopic composition of the rain sampled along Sahelian squall lines, *Quat. J. Roy. Met. Soc.*

3. C. Risi, S. Bony, F. Vimeux and J. Jouzel (**2010**), Water stable isotopes in the LMDZ4 General Circulation Model: model evaluation for present day and past climates and applications to climatic interpretation of tropical isotopic records, *J. Geophys. Res.*

4. Risi, C., D. C. Noone, J. Worden, C. Frankenberg, G. P. Stiller, M. Kiefer, B. Funke, K. A. Walker, P. F. Bernath, M. Schneider, S. Bony, J. Lee, D. P. Brown, and C. Sturm (**2012**). Process-evaluation of tropospheric humidity simulated by general circulation models using water vapor isotopic observations. Part 2: Using isotopic diagnostics to understand the mid and upper tropospheric moist bias in the tropics and subtropics, *J. Geophys. Res.*

5. Risi, C, Noone, D, Frankenberg, C, Worden, J. (**2013**). The role of continental recycling in intra-seasonal variations of continental moisture as deduced from model simulations and water vapor isotopic measurements. *Water Ressources Res.*

Bibliographie

[Aemisegger et al., 2014] Aemisegger, F., Pfahl, S., Sodemann, H., Lehner, I., Seneviratne, S. I., and Wernli, H. (2014). Deuterium excess as a proxy for continental moisture recycling and plant transpiration. *Atmospheric Chemistry and Physics*, 14(8) :4029–4054.

[Allan et al., 2003] Allan, R., Ringer, M. A., and Slingo, A. (2003). Evaluation of moisture in the Hadley Centre climate model using simulations of HIRS water-vapour channel radiances. *Quat. J. Roy. Met. Soc.*, 129 (595) :3371–3389.

[Bailey et al., 2013] Bailey, A., Toohey, D., and Noone, D. (2013). Characterizing moisture exchange between the hawaiian convective boundary layer and free troposphere using stable isotopes in water. *Journal of Geophysical Research : Atmospheres*, 118(15) :8208–8221.

[Barnes and Allison, 1988] Barnes, C. and Allison, G. (1988). Tracing of water movement in the unsaturated zone using stable isotopes of hydrogen and oxygen. *J. Hydrol*, 100 :143–176.

[Bartlein et al., 2010] Bartlein, P. J., Harrison, S. P., Brewer, S., Connor, S., Davis, B. A. S., Gajewski, K., Guiot, J., Harrison-Prentice, T. I., Henderson, A., and et al., O. P. (2010). Pollen-based continental climate reconstructions at 6 and 21 ka : a global synthesis. *Clim. Dyn*, 37 (3-4) :775–802, DOI : 10.1007/s00382–010–0904–1.

[Benedict and Randall, 2007] Benedict, J. J. and Randall, D. A. (2007). Observed characteristics of the mjo relative to maximum rainfall. *Journal of the atmospheric sciences*, 64(7) :2332–2354.

[Berkelhammer et al., 2012] Berkelhammer, M., Risi, C., Kurita, N., and Noone., D. (2012). The moisture source sequence for the Madden-Julian Oscillation as derived from satellite retrievals of HDO and H2O. *J. Geophys. Res.*, 117 :D03106, doi :10.1029/2011JD016803.

[Blossey et al., 2010] Blossey, P. N., Kuang, Z., and Romps, D. M. (2010). Isotopic composition of water in the tropical tropopause layer in cloud-resolving simulations of an idealized tropical circulation. *J. Geophys. Res.*, 115 :D24309, doi :10.1029/2010JD014554.

[Bolot et al., 2013] Bolot, M., Legras, B., and Moyer, E. J. (2013). Modelling and interpreting the isotopic composition of water vapour in convective updrafts. *Atmospheric Chemistry and Physics*, 13(16) :7903–7935.

[Bonne et al., 015] Bonne, J.-L., Steen-Larsen, H. C., Risi, C., Werner, M., Sodemann, H., Lacour, J.-L., Fettweis, X., Cesana, G., Delmotte, M., Cattani, O., Vallelonga, P., Kjaer, H. A., Clerbaux, C., Sveinbjörnsdottir, A. E., and Masson-Delmotte, V. (2015). The summer 2012 greenland heat wave : in-situ a,d remote sensing observations of water vapor isotopic composition during an atmospheric river event. *J. Geophy. Res.*

[Bony and Bellon, 2013] Bony, S. and Bellon, Gand Klocke, D. S. S. F. S. D. S. (2013). Robust direct effect of carbon dioxide on tropical circulation and regional precipitation. *Nature Geoscience*, 6(6) :447–451.

[Bony and Dufresne, 2005] Bony, S. and Dufresne, J. (2005). Marine boundary layer clouds at the heart of tropical cloud feedback uncertainties in climate models. *Geophys. Res. Lett*, 32 :L20806, doi :10.1029/2005GL023851.

[Bony et al., 2004] Bony, S., Dufresne, J.-L., Le Treut, H., Morcrette, J.-J., and Senior, C. (2004). On dynamic and thermodynamic components of cloud changes. *Climate Dynamics*, 22 :71–86.

[Bony and Emanuel, 2005] Bony, S. and Emanuel, K. (2005). On the role of moist processes in tropical intraseasonal variability : Cloud-radiation and moisture-convection feedbacks. *J. Atmos. Sci.*, 62 :2770–2789.

[Bony et al., 2008] Bony, S., Risi, C., and Vimeux, F. (2008). Influence of convective processes on the isotopic composition (deltaO18 and deltaD) of precipitation and water vapor in the Tropics. Part 1 : Radiative-convective equilibrium and TOGA-COARE simulations. *J. Geophys. Res.*, 113 :D19305, doi :10.1029/2008JD009942.

[Botsyun et al., 2016] Botsyun, S., Sepulchre, P., Risi, C., and Donnadieu, Y. (2016). Impacts of tibetan plateau uplift on atmospheric dynamics and associated precipitation δ 18 o. *Climate of the Past*, 12(6) :1401–1420.

[Bouniol et al., 2016] Bouniol, D., Roca, R., Fiolleau, T., and Poan, D. E. (2016). Macrophysical, microphysical, and radiative properties of tropical mesoscale convective systems over their life cycle. *Journal of Climate*, 29(9) :3353–3371.

[Boé et al., 2009] Boé, J., Hall, A., and Qu, X. (2009). September sea-ice cover in the arctic ocean projected to vanish by 2100. *Nature Geoscience*, 2 :341–343, doi :10.1038/ngeo467.

[Braconnot et al., 2012] Braconnot, P., Harrison, S. P., Kageyama, M., Bartlein, P. J., Masson-Delmotte, V., Abe-Ouchi, A., Otto-Bliesner, B., and Zhao, Y. (2012). Evaluation of climate models using palaeoclimatic data. *Nature Climate Change*, 2 :417 ?424, doi :10.1038/nclimate1456.

[Braconnot et al., 2007] Braconnot, P., Otto-Bliesner, B., Harrison, S., Joussaume, S., Peterschmitt, J.-Y., Abe-Ouchi, A., Crucifix, M. ansd Driesschaert, E., Fichefet, T., Hewitt, C. D., Kageyama, M., Kitoh, A. aand Laîné, A., Loutre, M.-F., Marti, O., Merkel, U., Ramstein, G., Valdes, P., Weber, S. L., Yu, Y., , and Zhao, Y. (2007). Results of PMIP2 coupled simulations of the Mid-Holocene and Last Glacial Maximum - Part 1 : experiments and large-scale features. *Climate of the Past*, 3 :261–277.

[Braud et al., 2009a] Braud, I., Bariac, T., Biron, P., and Vauclin, M. (2009a). Isotopic composition of bare soil evaporated water vapor. Part II : Modeling of RUBIC IV experimental results. *J. Hydrol.*, 369 :17–29.

[Braud et al., 2009b] Braud, I., Biron, P., Bariac, T., Richard, P., Canale, L., Gaudet, J., and Vauclin, M. (2009b). Isotopic composition of bare soil evaporated water vapor. Part I : RUBIC IV experimental setup and results. *J. Hydrol.*, 369 :1–16.

[Brient and Bony,] Brient, F. and Bony, S. On the robustness of the positive low-cloud feedback in a climate model. *Geophy. Res. Lett.*, in preparation.

[Brogniez et al., 2005] Brogniez, C., Roca, R., and Picon, L. (2005). Evaluation of the distribution of subtropical free tropospheric humidity in AMIP-2 simulations using METEOSAT water vapor channel data. *Geophy. Res. Lett.*, 32 (19) :L19708–L19708.

[Brown et al., 2008] Brown, D., Worden, J., and Noone, D. (2008). Comparison of atmospheric hydrology over convective contnental regions using water vapor isotope measurements from space. *J. Geophys. Res.*, 113.

[Bruneau et al., 2001] Bruneau, D., Quaglia, P., Flamant, C., Meissonnier, M., and Pelon, J. (2001). Airborne lidar leandre ii for water-vapor profiling in the troposphere. i. system description. *Applied optics*, 40(21) :3450–3461.

[Brunel et al., 1997] Brunel, J., Walker, G., Dighton, J., and Montenya, B. (1997). Use of stable isotopes of water to determine the origin of water used by the vegetation and to partition evapotranspiration. A case study from HAPEX-Sahel. *J. Hydrol*, 188-189 :466–481.

[Cai et al., 2013] Cai, Q., Zhang, G. J., and Zhou, T. (2013). Impacts of shallow convection on mjo simulation : A moist static energy and moisture budget analysis. *Journal of Climate*, 26(8) :2417–2431.

[Caley and Roche, 2013] Caley, T. and Roche, D. (2013). δ 18 o water isotope in the iloveclim model (version 1.0)–part 3 : A palaeo-perspective based on present-day data–model comparison for oxygen stable isotopes in carbonates. *Geoscientific Model Development*, 6(5) :1505–1516.

[Cappa et al., 2003] Cappa, C., Hendricks, M., DePaolo, D., and Cohen, R. (2003). Isotopic fractionation of water during reevaporation. *Journal of Geophysical Research*, 108 :4525–4542.

[Casado et al., 2016] Casado, M., Cauquoin, A., Landais, A., Israel, D., Orsi, A., Pangui, E., Landsberg, J., Kerstel, E., Prie, F., and Doussin, J.-F. (2016). Experimental determination and theoretical framework of kinetic fractionation at the water vapour–ice interface at low temperature. *Geochimica et Cosmochimica Acta*, 174 :54–69.

[Chen et al., 1996] Chen, C., Roeckner, E., and Soden, B. J. (1996). A comparison of satellite observations and model simulations of column-integrated moisture and upper-tropospheric humidity. *J. Clim*, 9 :1561–1585.

[Chen et al., 1998] Chen, M., Rood, R. B., and Read, W. G. (1998). Upper tropospheric water vapor from GEOS reanalysis and UARS MLS observation. *, J. Geophys. Res*, 103(D16) :19, 587 ?19, 594.

[Chung et al., 2011] Chung, E.-S., Soden, B. J., Sohn, B.-J., and Schmetz, J. (2011). Model-simulated humidity bias in the upper troposphere and its relation to the large-scale circulation. *J. Geophy. Res.*, 116 (D10110) :doi :10.1029/2011JD015609.

[Ciais and Jouzel, 1994] Ciais, P. and Jouzel, J. (1994). Deuterium and oxygen 18 in precipitation : isotopic model, including cloud processes. *J. Geophys. Res.*, 99 :16,793–16,803.

[Collins et al., 2013] Collins, J. A., Schefuß, E., Mulitza, S., Prange, M., Werner, M., Tharammal, T., Paul, A., and Wefer, G. (2013). Estimating the hydrogen isotopic composition of past precipitation using leaf-waxes from western africa. *Quaternary Science Reviews*, 65 :88–101.

[Conroy et al., 2013] Conroy, J. L., Cobb, K. M., and Noone, D. (2013). Comparison of precipitation isotope variability across the tropical Pacific in observations and SWING2 model simulations. *J. Geophys. Res. Atmos.*, 118 :5867–5892, doi :10.1002/jgrd.50412.

[Couvreux et al., 2010] Couvreux, F., Hourdin, F., and Rio, C. (2010). Resolved versus parametrized boundary-layer plumes. Part I : A parametrization-oriented conditional sampling in large-eddy simulations. *Boundary-layer meteorology*, 134(3) :441–458.

[Dansgaard, 1964] Dansgaard (1964). Stable isotopes in precipitation. *Tellus*, 16 :436–468.

[Dansgaard et al., 1993] Dansgaard, W., Johnsen, S., Clausen, H., Dahl-Jensen, D., Gundestrup, N., Hammer, C., Hvidberg, C., Steffensen, J., Sveinbjörnsdottir, A., Jouzel, J., et al. (1993). Evidence for general instability of past climate from a 250-kyr ice-core record. *Nature*, 364(6434) :218–220.

[Dansgaard et al., 1969] Dansgaard, W., Johnsen, S. J., Møller, J., and Langway, C. C. (1969). One thousand centuries of climatic record from camp century on the greenland ice sheet. *Science*, 166(3903) :377–380.

[Dansgaard et al., 1989] Dansgaard, W., White, J., and Johnsen, S. (1989). The abrupt termination of the younger dryas climate event. *Nature*, 339 :532–534.

[DeMott et al., 2014] DeMott, C. A., Stan, C., Randall, D. A., and Branson, M. D. (2014). Intraseasonal variability in coupled gcms : The roles of ocean feedbacks and model physics. *Journal of Climate*, 27(13) :4970–4995.

[Derbyshire et al., 2004] Derbyshire, S. H., Beau, I., Bechtold, P., Grandpeix, J.-Y., Piriou, J.-M., Redelsperger, J.-L., and Soares, P. M. M. (2004). Sensitivity of moist convection to environmental humidity. *Quat. J. Roy. Met. Soc.*, 130 (604) :3055 – 3079.

[Dessler and Sherwood, 2003] Dessler, A. E. and Sherwood, S. C. (2003). A model of HDO in the tropical tropopause layer. *Atmos. Chem. Phys.*, 3 :2173–2181.

[Eagle et al., 2013] Eagle, R., Risi, C., Eiler, J. M., Seibt, U., Li, G., and Tripati, A. K. (2013). High regional climate sensitivity over continental China inferred from glacial-recent changes in temperature and the hydrologic cycle. *Proc Natl Acad Sci*, 110(22) :8813–8818.

[Ehhalt, 1974] Ehhalt, D. H. (1974). Vertical profiles of hto, hdo, and h2o in the troposphere. *NCAR technical note*, NCAR-TN-STR-100.

[Ellehoej, 2011] Ellehoej, M. (2011). *Ice-vapor equilibrium fractionation factor experimental investigations and possible impacts on the understanding of the hydrological cycles on Earth and Mars*. PhD thesis, University of Copenhagen.

[Emanuel et al., 1994] Emanuel, K., Neelin, D., and Bretherton, C. (1994). On large-scale circulations in convecting atmospheres. *Quaterly Journal of the Royal Meteorological Society*, 120 :1111–1143.

[Emanuel, 1991] Emanuel, K. A. (1991). A Scheme for Representing Cumulus Convection in Large-Scale Models. *J. Atmos. Sci.*, 48 :2313–2329.

[Farrera et al., 1999] Farrera, I., Harrison, S. P., Prentice, I. C., Ramstein, G., Guiot, J., Bartlein, P. J., Bonnefille, R., Bush, M., Cramer, W., von Grafenstein, U., Holmgren, K., Hoohiemstra, H., Hope, G., Jolly, D., Lauritzen, S.-E., Ono, Y., Pinot, S., Stute, M., and Yu, G. (1999). Tropical climates at the Last Glacial Maximum : a new synthesis of terrestrial palaeoclimate data. I. Vegetation, lake-levels and geochemistry. *Clim. Dyn.*, 15 :823–856.

[Field et al., 2010] Field, R. D., Jones, D. B. A., and Brown, D. P. (2010). The effects of post-condensation exchange on the isotopic composition of water in the atmosphere. *J. Geophy. Res.*, 115, D24305 :doi :10.1029/2010JD014334.

[Field et al., 2014] Field, R. D., Kim, D., LeGrande, A. N., Worden, J., Kelley, M., and Schmidt, G. A. (2014). Evaluating climate model performance in the tropics with retrievals of water isotopic composition from Aura TES. *Geophy. Res. Lett.*, page DOI : 10.1002/2014GL060572.

[Field et al., 2012] Field, R. D., Risi, C., Schmidt, G. A., Worden, J., Voulgarakis, A., LeGrande, A. N., Sobel, A., and Healy, R. J. (2012). A tropospheric emission spectrometer hdo/h2o retrieval simulator for climate models. *Atmospheric Chemistry and Physics*, 12(21) :10485–10504.

[Fiolleau and Roca, 2013a] Fiolleau, T. and Roca, R. (2013a). An algorithm for the detection and tracking of tropical mesoscale convective systems using infrared images from geostationary satellite. *IEEE transactions on Geoscience and Remote Sensing*, 51(7) :4302–4315.

[Fiolleau and Roca, 2013b] Fiolleau, T. and Roca, R. (2013b). Composite life cycle of tropical mesoscale convective systems from geostationary and low earth orbit satellite observations : method and sampling considerations. *Quarterly Journal of the Royal Meteorological Society*, 139(673) :941–953.

[Flanagan and Ehleringer, 1991] Flanagan, L. B. and Ehleringer, J. R. (1991). Stable isotope composition of stem and leaf water : applications to the study of plant use. *Functional Ecology*, 5 (2) :270–277.

[Fleitmann et al., 2007] Fleitmann, D., Burns, S., Mangini, A., Mudelsee, M., Kramers, J., Villa, I., Neff, U., Al-Subbary, A. A., Buettner, A., Hppler, D., and Matter, A. (2007). Holocene ITCZ and Indian monsoon dynamics recorded in stalagmites from Oman and Yemen (Socotra). *Quat. Sci. Rev.*, 16 :170–188.

[Folkins et al., 2006] Folkins, I., Bernath, P., Boone, C., Donner, L. J., Eldering, A., Lesins, G., Martin, R. V., Sinnhuber, B.-M., and Walker, K. (2006). Testing convective parameterizations with tropical measurements of hno3, co, h2o, and o3 : Implications for the water vapor budget. *J. Geophys. Res.*, 111 (D23304) :doi :10.1029/2006JD007325.

[Folkins et al., 1999] Folkins, I., Loewenstein, M., Podolske, J., Oltmans, S. J., and Proffitt, M. (1999). A barrier to vertical mixing at 14 km in the tropics : Evidence from ozonesondes and aircraft measurements. *J. Geophys. Res.*, 104(18) :22095–22102.

[Folkins and Martin, 2005] Folkins, I. and Martin, R. (2005). The vertical structure of tropical convection and its impact on the budgets of water vapor and ozone. *J. Atmos. Sci.*, 62 :560–1573.

[Fontes, 1980] Fontes, J. C. (1980). Environmental isotopes in groundwater hydrology. In *Handbook of environmental isotope geochemistry. Vol. 1.*

[Frankenberg et al., 2009] Frankenberg, C., Yoshimura, K., Warneke, T., Aben, I., Butz, A., Deutscher, N., Griffith, D., Hase, F., Notholt, J., Schneider, M., Schrijver, H., and Röckmann, T. (2009). Dynamic processes governing lower-tropospheric HDO/H2O ratios as observed from space and ground. *Science*, 325 :1374–1377.

[Frankenberg et al., 2013] Frankenberg, C., W. D., Toon, G., Risi, C., Scheepmaker, R., Lee, J.-E., and Worden, J. (2013). Water vapor isotopologues retrievals from high resolution GOSAT short-wave infrared spectra. *Atm. Chem. Phys.*, 6 :263–274, doi :10.5194/amt–6–263–2013.

[Frierson, 2007] Frierson, D. M. (2007). The dynamics of idealized convection schemes and their effect on the zonally averaged tropical circulation. *Journal of the atmospheric sciences*, 64(6) :1959–1976.

[Frierson and Hwang, 2012] Frierson, D. M. and Hwang, Y.-T. (2012). Extratropical influence on itcz shifts in slab ocean simulations of global warming. *Journal of Climate*, 25(2) :720–733.

[Galewsky and Hurley, 2010] Galewsky, J. and Hurley, J. V. (2010). An advection-condensation model for subtropical water vapor isotopic ratios. *J. Geophys. Res.*, 115 (D16) :D16115 , doi :10.1029/2009JD013651.

[Galewsky and Samuels-Crow, 2014] Galewsky, J. and Samuels-Crow, K. (2014). Water vapor isotopic composition of a stratospheric air intrusion : Measurements from the chajnantor plateau, chile. *Journal of Geophysical Research : Atmospheres*, 119(16) :9679–9691.

[Gao et al., 2013] Gao, J., Masson-Delmotte, V., Risi, C., He, Y., and Yao, T. (2013). What controls southern Tibetan Plateau precipitation deltaO18 at seasonal and intra-seasonal scales ? A case study at Lhasa and Nyalam. *Tellus*.

[Gao et al., 2011] Gao, J., Masson-Delmotte, V., Yao, T., Risi, C., Hoffmann, G., and Tian, L. (2011). Precipitation water stable isotopes in the south Tibetan Plateau : observations and modelling. *J. Clim.*, 24 :3161–3178.

[Gao et al., 2016] Gao, J., Risi, C., Masson-Delmotte V, He, Y., and Xu, B. (2016). Southern tibetan plateau ice core delta18o reflects abrupt shifts in atmospheric circulation in the late 1970s. *Clim. Dyn*, 46 :291, doi :10.1007/s00382–015–2584–3.

[Gasse, 2000] Gasse, F. (2000). Hydrological changes in the African tropics since the Last Glacial Maximum. *Quat. Sci. Rev.*, 19 :189–211.

[Gat and Matsui, 1991] Gat, J. R. and Matsui, E. (1991). Atmospheric water balance in the Amazon basin : An isotopic evapotranspiration model. *J. Geophys. Res.*, 96 :13179–13188.

[Gettelman et al., 2002] Gettelman, A., Randel, W. J., Wu, F., and Massie, S. T. (2002). Transport of water vapor in the tropical tropopause layer. *Geophysical Research Letters*, 29 :9–1.

[Gettelman et al., 2002] Gettelman, A., Salby, M. L., and Sassi, F. (2002). Distribution and influence of convection in the tropical tropopause region. *J. Geophys. Res.*, 107.

[Ghil and Mo, 1991] Ghil, M. and Mo, K. (1991). Intraseasonal oscillations in the global atmosphere. part i : Northern hemisphere and tropics. *Journal of the Atmospheric Sciences*, 48(5) :752–779.

[Gibson et al., 2005] Gibson, J. J., Edwards, T. W. D., Birks, S. J., Amour, N. A. S., Buhay, W. M., McEachern, P., Wolfe, B. B., and Peters1, D. L. (2005). Progress in isotope tracer hydrology in Canada. *Hydrol. Processes*, 19 :303–327.

[Griffis et al., 2010] Griffis, T., Sargent, S., Lee, X., Baker, J., Greene, J., Erickson, M., Zhang, X., Billmark, K., Schultz, N., Xiao, W., et al. (2010). Determining the oxygen isotope composition of evapotranspiration using eddy covariance. *Boundary-layer meteorology*, 137(2) :307–326.

[Gryazin et al., 2014] Gryazin, V., Risi, C., Jouzel, J., Kurita, N., Worden, J., Frankenberg, C., Bastrikov, V., Gribanov, K. G., and Stukova, O. (2014). To what extent could water isotopic measurements help us understand model biases in the water cycle over Western Siberia. *Atmos. Chem. Phys.*, 14 :9807–9830, doi :10.5194/acp–14–9807–2014.

[Gupta et al., 2009] Gupta, P., Noone, D., Galewsky, J., Sweeney, C., , and Vaughn, B. H. (2009). Demonstration of high-precision continuous measurements of water vapor isotopologues in laboratory and remote field deployments using wavelength-scanned cavity ring-down spectroscopy (WS-CRDS) technology. *Rapid Commun. Mass Spectrom.*, 23 :2534–2542.

[Hall and Qu, 2006] Hall, A. and Qu, X. (2006). Using the current seasonal cycle to constrain snow albedo feedback in future climate change. *Geophys. Res. Lett.*, 33 :L03502, doi :10.1029/2005GL025127.

[Hanisco et al., 2007] Hanisco, T., Moyer, E., Weinstock, E., St Claire, J. M., Sayres, D. S., Smith, J. B., Lockwood, R., Anderson, J. G., Dessler, A. E., Keutsh, F. N., Spackman, J. R., Read, W. G., and Bui, T. P. (2007). Observations of deep convective influence on stratospheric water vapor and its isotopic composition. *Geophysical research letters*, 34.

[Hargreaves et al., 2013] Hargreaves, J., Annan, J., Ohgaito, R., Paul, A., and Abe-Ouchi., A. (2013). Skill and reliability of climate model ensembles at the last glacial maximum and mid-holocene. *Clim. Past*, 9 :811 ?823, doi :10.5194/cp–9–811–2013.

[Hargreaves et al., 2012] Hargreaves, J., Annan, J., Yoshimori, M., and Abe-Ouchi, A. (2012). Can the last glacial maximum constrain climate sensitivity ? *Geophy. Res. Lett.*, 39 :L24702, doi :10.1029/2012GL053872.

[Hauglustaine et al., 2004] Hauglustaine, D. A., Hourdin, F., Jourdain, L., Filiberti, M.-A., Walters, S., Lamarque, J.-F., and Holland, E. A. (2004). Interactive chemistry in the Laboratoire de Météorologie Dynamique general circulation model : Description and background tropospheric chemistry evaluation. *J. Geophy. Res.*, 109 :D04314, doi :10.1029/2003JD003957.

[He et al., 2015] He, Y., Risi, C., Gao, J., Masson-Delmotte, V., Yao, T., Worden, J., Frankenberg, C., and Cesana., G. (2015). Impact of atmospheric convection on the isotopic composition of tibetan precipitation using a combination of satellite data and atmospheric general circulation modeling. *J. Geophy. Res.*, 120 (9) :3852–3871, DOI : 10.1002/2014JD02218.

[Hoffmann, 2003] Hoffmann, G. (2003). Taking the pulse of the tropical water cycle. *Science*, 301 :776–777.

[Hoffmann et al., 1998] Hoffmann, G., Werner, M., and Heimann, M. (1998). Water isotope module of the ECHAM atmospheric general circulation model : A study on timescales from days to several years. *J. Geophys. Res.*, 103 :16871–16896.

[Holton and Gettelman, 2001] Holton, J. R. and Gettelman, A. (2001). Horizontal transport and the dehydration of the stratosphere. *Geophys. Res. Lett.*, 28(14) :2799–2802.

[Hourdin et al., 2012] Hourdin, F., Grandpeix, J.-Y., Rio, C., Bony, S., Jam, A., Cheruy, F., Rochetin, N., Fairhead, L., Idelkadi, A., Musat, I., Dufresne, J.-L., Lahellec, A., Lefebvre, M.-P., and Roehrig, R. (2012). LMDZ5B : the atmospheric component of the IPSL climate model with revisited parameterizations for clouds and convection. *Clim. Dyn*, pages DOI 10.1007/s00382–012–1343–y.

[Hourdin et al., 2006] Hourdin, F., Musat, I., Bony, S., Braconnot, P., Codron, F., Dufresne, J.-L., Fairhead, L., Filiberti, M.-A., Friedlingstein, P., Grandpeix, J.-Y., Krinner, G., Levan, P., Li, Z.-X., and Lott, F. (2006). The LMDZ4 general circulation model : climate performance and sensitivity to parametrized physics with emphasis on tropical convection. *Clim. Dyn.*, 27 :787–813.

[Hung et al., 2013] Hung, M.-P., Lin, J.-L., Wang, W., Kim, D., Shinoda, T., and Weaver, S. J. (2013). MJO and convectively coupled equatorial waves simulated by CMIP5 climate models. *Journal of Climate*, 26(17) :6185–6214.

[Hwang and Frierson, 2013] Hwang, Y.-T. and Frierson, D. M. (2013). Link between the double-intertropical convergence zone problem and cloud biases over the southern ocean. *Proceedings of the National Academy of Sciences*, 110(13) :4935–4940.

[Inness et al., 2001] Inness, P. M., Slingo, J. M., Woolnough, R. B., Neale, R. B., and Pope, V. D. (2001). Organization of tropical convection in a gcm with varying vertical resolution ; implications for the simulation of the madden-julian oscillation. *Clim. Dyn.*, 17 (10) :777–793, DOI : 10.1007/s003820000148.

[Jasechko et al., 2015] Jasechko, S., Lechler, A., Pausata, F. S. R., Fawcett, P. J., Gleeson, T., Cendón, D. I., Galewsky, J., LeGrande, A. N., Risi, C., Sharp, Z. D., Welker, J. M., Werner, M., and Yoshimura, K. (2015). Glacial-interglacial shifts in global and regional precipitation deltaO18. *Climate of the Past*, 11(2) :1375–1393.

[John and Soden, 2007] John, V. O. and Soden, B. J. (2007). Temperature and humidity biases in global climate models and their impact on climate feedbacks. *Geophys. Res. Lett.*, 34 :L18704, doi :10.1029/2007GL030429.

[Johnsen et al., 1972] Johnsen, S., Dansgaard, W., Clausen, H., and Langway, J. C. (1972). Oxygen isotope profiles through the Antarctic and Greenland ice sheets. *Nature*, 235 :429–434.

[Joussaume et al., 1984] Joussaume, S., Jouzel, J., and Sadourny, R. (1984). A general circulation model of water isotope cycles in the atmosphere. *Nature*, 311 :24–29.

[Jouzel, 2003] Jouzel, J. (2003). Water Stable Isotopes : Atmospheric Composition and Applications in Polar Ice Core Studies. *Treatise on Geochemistry*, 4 :213–243.

[Jouzel and Alley, 1997] Jouzel, J. and Alley, R. (1997). Validity of the temperature reconstruction from ice cores. *J. Geophys. Res.*, 102 :26471–26487.

[Jouzel et al., 1987a] Jouzel, J., Genthon, C., Lorius, C., Petit, J., and Barkov, N. (1987a). Vostok ice core-a continuous isotope temperature record over the last climatic cycle (160,000 years). *Nature*, 329 :403–408.

[Jouzel et al., 2000] Jouzel, J., Hoffmann, G., Koster, R. D., and Masson, V. (2000). Water isotopes in precipitation : data/model comparison for present-day and past climates. *Quat. Sci. Rev.*, 19 :363–379.

[Jouzel et al., 1987b] Jouzel, J., Koster, R. D., Suozzo, R. J., Russel, G. L., White, J. W. C., and Broecker, W. S. (1987b). Simulations of the HDO and H2O18 atmospheric cycles using the NASA GISS General Circulation Model : The seaosnal cycle for present day conditions. *J. Geophys. Res.*, 92 :14,739–14,760.

[Jouzel and Merlivat, 1984] Jouzel, J. and Merlivat, L. (1984). Deuterium and oxygen 18 in precipitation : modeling of the isotopic effects during snow formation. *J. Geophys. Res.*, 89 :11 :749.

[Kang et al., 2008] Kang, S., Held, I., Frierson, D., and Zhao, M. (2008). The response of the ITCZ to extratropical thermal forcings : idealized slab ocean experiments with a GCM. *J. Clim.*, 21 :3521–3532.

[Kendall and Coplen, 2001] Kendall, C. and Coplen, T. B. (2001). Distribution of oxygen-18 and deuterium in river waters across the United States. *Hydrol. Processes*, 15 :1363–1393.

[Khaykin et al., 2009] Khaykin, S., Pommereau, J.-P., Korshunov, L., , V. Yushkov and, J. N., , N. L. T. C., Garnier, A., Lukyanovand, A., and E.Williams (2009). Hydration of the lower stratosphere by ice crystal geysers over land convective systems. *Atmos. Chem. Phys.*, 9 :2275 ?2287.

[Kim et al., 2015] Kim, D., Ahn, M.-S., Kang, I.-S., and Del Genio, A. D. (2015). Role of longwave cloud–radiation feedback in the simulation of the madden–julian oscillation. *Journal of Climate*, 28(17) :6979–6994.

[Kim et al., 2012] Kim, D., Sobel, A. H., Genio, A. D. D., Chen, Y., Camargo, S. J., Yao, M.-S., Kelley, M., and Nazarenko, L. (2012). The tropical subseasonal variability simulated in the nasa giss general circulation model. *J. Clim.*, 25.

[Kim et al., 2009] Kim, D., Sperber, K., Stern, W., Waliser, D., Kang, I.-S., Maloney, E., Wang, W., Weickmann, K., Benedict, J., Khairoutdinov, M., et al. (2009). Application of mjo simulation diagnostics to climate models. *Journal of Climate*, 22(23) :6413–6436.

[Kim et al., 2014] Kim, D., Xavier, P., Maloney, E., Wheeler, M., Waliser, D., Sperber, K., Hendon, H., Zhang, C., Neale, R., Hwang, Y.-T., et al. (2014). Process-oriented mjo simulation diagnostic : Moisture sensitivity of simulated convection. *Journal of Climate*, 27(14) :5379–5395.

[Knutti and Sedláček, 2013] Knutti, R. and Sedláček, J. (2013). Robustness and uncertainties in the new CMIP5 climate model projections. *Nature Climate Change*, 3(4) :369–373.

[Krinner et al., 2005] Krinner, G., Viovy, N., de Noblet-Ducoudre, N., Ogee, J., Polcher, J., Friedlingstein, P., Ciais, P., Sitch, S., and Prentice, I. C. (2005). A dynamic global vegetation model for studies of the coupled atmosphere-biosphere system. *Glob. Biogeochem. Cycles*, 19.

[Krinner and Werner, 2003] Krinner, G. and Werner, M. (2003). Impact of precipitation seasonality changes on isotopic signals in polar ice cores : a multi-model analysis. *Earth Planet. Sci. Lett.*, 216 :525–538.

[Kuang et al., 2003] Kuang, Z., Toon, G., Wennberg, P., and Yung, Y. L. (2003). Measured HDO/H2O ratios across the tropical tropopause. *Geophysical Research Letters*, 30 :25–1.

[Kurita, 2013] Kurita, N. (2013). Water isotopic variability in response to mesoscale convective system over the tropical ocean. *Journal of Geophysical Research*, 118(18) :10–376.

[Kurita et al., 2011] Kurita, N., Noone, D., Risi, C., Schmidt, G. A., Yamada, H., , and Yoneyama, K. (2011). Intraseasonal isotopic variation associated with the Madden-Julian Oscillation. *J. Geophy. Res.*, 116 :D24, D24101, doi :10.1029/2010JD015209.

[Lacour, 2015] Lacour, J.-L. (2015). *Estimations du profil du rapport isotopique deltaD de la vapeur d ?eau dans la troposphère à partir de spectres mesurés dans l ?infrarouge thermique par le sondeur IASI : Méthodologie d ?inversion et analyses des premières distributions spatiales.* . PhD thesis, Université Libre de Bruxelles.

[Lacour et al., 2012] Lacour, J.-L., Risi, C., Clarisse, L., Bony, S., Hurtmans, D., Clerbaux, C., and Coheur, P.-F. (2012). Mid-tropospheric deltaD observations from IASI/MetOp at high spatial and temporal resolution. *Atmos. Chem. Phys.*, 12 :10817–10832, doi :10.5194/acp–12–10817–2012.

[Lacour et al., 2016] Lacour, J.-L., Risi, C., Worden, J., Clerbaux, C., and Coheur, P.-F. (2016). Isotopic signature of convection's depth in water vapor as seen from iasi and tes d observations. *Geophys. Res. Lett*, submitted :submitted.

[Lai et al., 2006] Lai, C.-T., Ehleringer, J., Bond, B., and U, K. P. (2006). Contributions of evaporation, isotopic non-steady state transpiration, and atmospheric mixing on the deltaO18 of water vapor in Pacific Northwest coniferous forests. *Plant, Cell and Environment*, 29(1) :77–94.

[Lawrence et al., 2004] Lawrence, J. R., Gedzelman, S. D., Dexheimer, D., Cho, H.-K., Carrie, G. D., Gasparini, R., Anderson, C. R., Bowman, K. P., and Biggerstaff, M. I. (2004). Stable isotopic composition of water vapor in the tropics. *J. Geophys. Res.*, 109 :D06115, doi :10.1029/2003JD004046.

[Lawrence and Salzmann, 2008] Lawrence, M. G. and Salzmann, M. (2008). On interpreting studies of tracer transport by deep cumulus convection and its effects on atmospheric chemistry. *Atm. Chem. Phys.*, 8 (20) :6037–6050.

[Lee et al., 2015] Lee, J., Worden, J., Noone, D., Chae, J. H., and Frankenberg, C. (2015). Isotopic changes due to convective moistening of the lower troposphere associated with variations in the enso and iod from 2005 to 2006. *Tellus B*, 67.

[Lee and Fung, 2008] Lee, J.-E. and Fung, I. (2008). "Amount effect" of water isotopes and quantitative analysis of post-condensation processes. *Hydrological Processes*, 22 (1) :1–8.

[Lee et al., 2007] Lee, J.-E., Fung, I., DePaolo, D., and Fennig, C. C. (2007). Analysis of the global distribution of water isotopes using the NCAR atmospheric general circulation model. *J. Geophys. Res.*, 112 :D16306, doi :10.1029/2006JD007657.

[Lee et al., 2009] Lee, J.-E., Pierrehumbert, R., Swann, A., and Lintner, B. R. (2009). Sensitivity of stable water isotopic values to convective parameterization schemes. *Geophy. Res. Lett.*, 36 :doi :10.1029/2009GL040880.

[Lee et al., 2012] Lee, X., Huang, J., and Patton, E. G. (2012). A large-eddy simulation study of water vapour and carbon dioxide isotopes in the atmospheric boundary layer. *Boundary-layer meteorology*, 145(1) :229–248.

[LeGrande and Schmidt, 2008] LeGrande, A. N. and Schmidt, G. A. (2008). Ensemble, Water-Isotope Enabled, Coupled General Circulation Modeling Insights into the 8.2-kyr Event. *Paleoceanography*, 23.

[LeGrande and Schmidt, 2009] LeGrande, A. N. and Schmidt, G. A. (2009). Sources of Holocene variability of oxygen isotopes in paleoclimate archives. *Clim. Past*, 5 :441455.

[Lin and Coauthors, 2006] Lin, J.-L. and Coauthors (2006). Tropical Intraseasonal Variability in 14 IPCC AR4 Climate Models. Part I : Convective Signals. *J. Climate*, 19 :26652690. doi : http ://dx.doi.org/10.1175/JCLI3735.1.

[Liu et al., 2009] Liu, J. J., Jones, D. B. A., Worden, J. R., Noone, D., Noone, D., Parrington, M., and Kar, J. (2009). Analysis of the summertime buildup of tropospheric ozone abundances over the middle east and north africa as observed by the tropospheric emission spectrometer instrument. *J. Geophys. Res*, 114 :D05304, doi :10.1029/2008JD010993.

[Lorius et al., 1979] Lorius, C., Merlivat, L., Jouzel, J., and Pourchet, M. (1979). A 30,000 yr isotope climatic record from Antarctic ice. *Nature*, 280 :644–648.

[Madden and Julian, 1971] Madden, R. A. and Julian, P. R. (1971). Detection of a 40-50 day oscillation in the zonal wind in the tropical pacific. *J. Atmos. Sci.*, 28 :702–708.

[Madden and Julian, 1972] Madden, R. A. and Julian, P. R. (1972). Description of global-scale circulation cells in the tropics with a 40-50 day period,. *J. Atmos. Sci.*, 29 :1109–1123.

[Majoube, 1971a] Majoube, M. (1971a). Fractionnement en O18 entre la glace et la vapeur d'eau. *Journal de Chimie Physique*, 68 :625–636.

[Majoube, 1971b] Majoube, M. (1971b). Fractionnement en Oxygène 18 et en Deutérium entre l'eau et sa vapeur. *Journal de Chimie Physique*, 10 :1423–1436.

[Maloney, 2009] Maloney, E. D. (2009). The moist static energy budget of a composite tropical intraseasonal oscillation in a climate model. *Journal of Climate*, 22(3) :711–729.

[MARGO project members, 2008] MARGO project members (2008). Constraints on the magnitude and patterns of ocean cooling at the Last Glacial Maximum. *Nature Geoscience*, 2 :127–132.

[Mathieu and Bariac, 1996] Mathieu, R. and Bariac, T. (1996). A numerical model for the simulation of stable isotope profiles in drying soils. *J. Geophys. Res.*, 101 (D7) :12685–12696.

[Mathieu et al., 2002] Mathieu, R., Pollard, D., Cole, J., White, J. W. C., Webb, R. S., and Thompson, S. L. (2002). Simulation of stable water isotope variations by the GENESIS GCM for modern conditions. *J. Geophys. Res.*, 107 (D4) :doi :10.1029/2001JD900255.

[Mauritsen et al., 2012] Mauritsen, T., Stevens, B., Roeckner, E., Crueger, T., Esch, M., Giorgetta, M., Haak, H., Jungclaus, J., Klocke, D., Matei, D., et al. (2012). Tuning the climate of a global model. *Journal of Advances in Modeling Earth Systems*, 4(3).

[McCarroll and Loader, 2004] McCarroll, D. and Loader, N. (2004). Stable isotopes in tree rings. *Quat. Sci. Rev.*, 23 :771–801.

[McDermott, 2004] McDermott, F. (2004). Palaeo-climate reconstruction from stable isotope variations in speleothems : a review. *Quaternary Science Reviews*, 23 (7-8) :901–918.

[Meehl et al., 2007] Meehl, G. A., Covey, K., Delworth, T., Latif, M., McAvaney, B., Mitchell, J. F. B., Stouffer, R. J., and Taylor, K. (2007). The WCRP CMIP3 multimodel dataset : A new era in climate change research. *Bull. Am. Meteor. Soc.*, 7 :1383–1394.

[Merlivat and Jouzel, 1979] Merlivat, L. and Jouzel, J. (1979). Global climatic interpretation of the Deuterium-Oxygen 18 relationship for precipitation. *J. Geophys. Res.*, 84 :5029–5332.

[Merlivat and Nief, 1967] Merlivat, L. and Nief, G. (1967). Fractionnement isotopique lors des changements d'états solide-vapeur et liquide-vapeur de l'eau à des températures inférieures à 0C. *Tellus*, 19 :122–127.

[Moore et al., 2014] Moore, M., Kuang, Z., and Blossey, P. N. (2014). A moisture budget perspective of the amount effect. *Geophys. Res. Lett.*, 41 :1329–1335, doi :10.1002/2013GL058302.

[Moreira et al., 1997] Moreira, M., Sternberg, L., Martinelli, L., Victoria, R., Barbosa, E., Bonates, C., and Nepstad, D. (1997). Contribution of transpiration to forest ambient vapor based on isotopic measurements. *Global Change Biol.*, 3 :439–450.

[Moyer et al., 1996] Moyer, E. J., Irion, F. W., Yung, Y. L., and Gunson, M. R. (1996). ATMOS stratospheric deuterated water and implications for troposphere-stratosphere transport. *Geophys. Res. Lett.*, 23 :2385–2388.

[Muller and Held, 2012] Muller, C. J. and Held, I. M. (2012). Detailed investigation of the self-aggregation of convection in cloud-resolving simulations. *J. Atmos. Sci.*, 69 :2551–2565, doi : http ://dx.doi.org/10.1175/JAS–D–11–0257.1.

[Nassar et al., 2007] Nassar, R., Bernath, P. F., Boone, C. D., Gettelman, A., McLeod, S. D., and Rinsland, C. P. (2007). Variability in HDO/H2O abundance ratio in the Tropical Tropopause Layer. *J. Geophys. Res.*, 112 (D21) :doi :10.1029/2007JD008417.

[Noone, 2009] Noone, D. (2009). An isotopic evaluation of the factors controlling low humidity air in the troposphere. *J. Clim.*, submitted.

[Noone, 2012] Noone, D. (2012). Pairing measurements of the water vapor isotope ratio with humidity to deduce atmospheric moistening and dehydration in the tropical mid-troposphere. *Journal of Climate*, 25(13) :4476–4494.

[Noone et al., 2012] Noone, D., Risi, C., Bailey, A., Brown, D., Buenning, N., Gregory, S., Nusbaumer, J., Sykes, J., Schneider, D., Vanderwende, B., Wong, J., Meillier, Y., and Wolf, D. (2012). Factors controlling moisture in the boundary layer derived from tall tower profiles of water vapor isotopic composition following a snowstorm in colorado. *Atmos. Chem. Phys. Discuss.*, 12 :16327–16375, doi :10.5194/acpd–12–16327–2012.

[Noone and Simmonds, 2002] Noone, D. and Simmonds, I. (2002). Associations between delta18O of Water and Climate Parameters in a Simulation of Atmospheric Circulation for 1979-95. *J. Climate*, 15 :3150–3169.

[Noone and Sturm, 2010] Noone, D. and Sturm, C. (2010). *Comprehensive Dynamical Models of Global and Regional Water Isotope Distributions, in Isoscapes : Understanding movement, pattern, and process on Earth through isotope mapping.* Springer Netherlands.

[Oueslati et al., 2016] Oueslati, B., Bony, S., Risi, C., and Dufresne, J.-L. (2016). Interpreting the inter-model spread in regional precipitation projections in the tropics : role of surface evaporation and cloud radiative effects. *Climate Dynamics*, pages 1–15.

[Pausata et al., 2011] Pausata, F. S., Battisti, D. S., Nisancioglu, K. H., and Bitz, C. M. (2011). Chinese stalagmite delta18o controlled by changes in the indian monsoon during a simulated heinrich event. *Nature Geoscience*, 4(7) :474–480.

[Payne et al., 2007] Payne, V. H., Noone, D., Dudhia, A., Piccolo, C., and Grainger, R. G. (2007). Global satellite measurements of HDO and implications for understanding the transport of water vapour into the stratosphere. *Quart. J. R. Meteor. soc.*, 133 :1459–1741.

[Pfahl et al., 2012] Pfahl, S., Wernli, H., Yoshimura, K., and Dubey, M. (2012). The isotopic composition of precipitation from a winter storm–a case study with the limited-area model cosmo iso. *Atmospheric Chemistry & Physics*, 12(3).

[Pierce et al., 2006] Pierce, D. W., Barnett, T. P., Fetzer, E. J., , and Gleckler, P. J. (2006). Three-dimensional tropospheric water vapor in coupled climate models compared with observations from the AIRS satellite system. *Geophys. Res. Lett.*, 33 :L21701, doi :10.1029/2006GL027060.

[Poan et al., 2013] Poan, D. E., Roehrig, R., Couvreux, F., and Lafore, J.-P. (2013). West african monsoon intraseasonal variability : a precipitable water perspective. *Journal of the Atmospheric Sciences*, 70(4) :1035–1052.

[Poulsen and Jeffery, 2011] Poulsen, C. J. and Jeffery, M. L. (2011). Climate change imprinting on stable isotopic compositions of high-elevation meteoric water cloaks past surface elevations of major orogens. *Geology*, 39 :595 ?598, doi :10.1130/G32052.1.

[Randall et al., 2003] Randall, D., Krueger, S., Bretherton, C., Curry, J., Duynkerke, P., Moncrieff, M., Ryan, B., Starr, D., Miller, M., Rossow, W., et al. (2003). Confronting models with data : The gewex cloud systems study. *Bulletin of the American Meteorological Society*, 84(4) :455–469.

[Randall et al., 1996] Randall, D. A., Xu, K.-M., Somerville, R. J., and Iacobellis, S. (1996). Single-column models and cloud ensemble models as links between observations and climate models. *Journal of Climate*, 9(8) :1683–1697.

[Rasch et al., 1997] Rasch, P., Mahowald, N., and Eaton, B. (1997). Representations of transport, convection, and the hydrologic cycle in chemical transport models : Implications for the modeling of short-lived and soluble species. *Journal of Geophysical Research : Atmospheres*, 102(D23) :28127–28138.

[Rio and Hourdin, 2007] Rio, C. and Hourdin, F. (2007). A thermal plume model for the convective boundary layer : representation of cumulus clouds. *J. Atm. Sci.*, 65 :407–425.

[Rio et al., 2009] Rio, C., Hourdin, F., Grandpeix, J.-Y., and Lafore, J.-P. (2009). Shifting the diurnal cycle of parameterized deep convection over land. *Geophy. Res. Lett.*, 36 :L07809, doi :10.1029/2008GL036779.

[Risi et al.,] Risi, C., Bony, S., Ogée, J., Bariac, T., Raz-Yaseed, N., Wingate, L., Welker, J., Knohl, A., Kurz-Besson, C., Leclerc, M., Zhang, G., N, B., Santrucek, J., Hronkova, M., David, T., Peylin, P., and Guglielmo, F. The water isotopic version of the land-surface model ORCHIDEE : implementation, evaluation, sensitivity to hydrological parameters. *Hydrology : Current Research*, submitted.

[Risi et al., 2008a] Risi, C., Bony, S., and Vimeux, F. (2008a). Influence of convective processes on the isotopic composition (O18 and D) of precipitation and water vapor in the Tropics : Part 2 : Physical interpretation of the amount effect. *J. Geophys. Res.*, 113 :D19306, doi :10.1029/2008JD009943.

[Risi et al., 2010a] Risi, C., Bony, S., Vimeux, F., Chong, M., and Descroix, L. (2010a). Evolution of the water stable isotopic composition of the rain sampled along Sahelian squall lines. *Quart. J. Roy. Meteor. Soc.*, 136 (S1) :227 – 242.

[Risi et al., 2008b] Risi, C., Bony, S., Vimeux, F., Descroix, L., Ibrahim, B., Lebreton, E., Mamadou, I., and Sultan, B. (2008b). What controls the isotopic composition of the African monsoon precipitation ? Insights from event-based precipitation collected during the 2006 AMMA campaign. *Geophys. Res. Lett.*, 35 :doi :10.1029/2008GL035920.

[Risi et al., 2010b] Risi, C., Bony, S., Vimeux, F., and Jouzel, J. (2010b). Water stable isotopes in the LMDZ4 General Circulation Model : model evaluation for present day and past climates and applications to climatic interpretation of tropical isotopic records. *J. Geophys. Res.*, 115, D12118 :doi :10.1029/2009JD013255.

[Risi et al., 2013] Risi, C., Noone, D., Frankenberg, C., and Worden, J. (2013). Role of continental recycling in intraseasonal variations of continental moisture as deduced from model simulations and water vapor isotopic measurements. *Water Resour. Res.*, 49 :4136–4156, doi : 10.1002/wrcr.20312.

[Risi et al., 2012a] Risi, C., Noone, D., Worden, J., Frankenberg, C., Stiller, G., Kiefer, M., Funke, B., Walker, K., Bernath, P., Schneider, M., Wunch, D., Sherlock, V., Deutscher, N., Griffith, D., Wernberg, P., Bony, S., Jeonghoon Lee, D. B., Uemura, R., and Sturm, C. (2012a). Process-evaluation of tropical and subtropical tropospheric humidity simulated by general circulation models using water vapor isotopic observations. Part 1 : model-data intercomparison. *J. Geophy. Res.*, 117 :D05303.

[Risi et al., 2012b] Risi, C., Noone, D., Worden, J., Frankenberg, C., Stiller, G., Kiefer, M., Funke, B., Walker, K., Bernath, P., Schneider, M., Wunch, D., Sherlock, V., Deutscher, N., Griffith, D., Wernberg, P., Bony, S., Lee, J., Brown, D., Uemura, R., and Sturm, C. (2012b). Process-evaluation of tropical and subtropical tropospheric humidity simulated by general circulation models using water vapor isotopic observations. Part 2 : an isotopic diagnostic of the mid and upper tropospheric moist bias. *J. Geophy. Res.*, 117 :D05304.

[Roca et al., 1997] Roca, R., Picon, L., Desbois, M., Le Treut, H., and Morcrette, J.-J. (1997). Direct comparison of Meteosat water vapor channel data and general circulation model results. *Geophy. Res. Lett.*, 24 (2) :147–150.

[Roche, 2013] Roche, D. (2013). δ 18 o water isotope in the iloveclim model (version 1.0)–part 1 : Implementation and verification. *Geoscientific Model Development*, 6(5) :1481–1491.

[Roche et al., 2004] Roche, D., Paillard, D., and Cortijo, E. (2004). Constraints on the duration and freshwater release of Heinrich event 4 through isotope modelling. *Nature*, 432 :379–382.

[Rodgers and Connor, 2003] Rodgers, C. D. and Connor, B. J. (2003). Intercomparison of remote sounding instruments. *J. Geophys. Res.*, 108 :4116, doi :10.1029/2002JD002299.

[Rozanski et al., 1993] Rozanski, K., Araguas-Araguas, L., and Gonfiantini, R. (1993). Isotopic patterns in modern global precipitation. *Geophys. Monogr. Seri., AGU*, Climate Change in Continental Isotopic records.

[Salathe and D, 1995] Salathe, E. J. and D, C. (1995). Variability of moisture in the upper troposphere as inferred from TOVS satellite observations in the ECMWF model analyses in 1989. *J. Clim*, 8 :120–132.

[Salati et al., 1979] Salati, E., Dall'Olio, A., Matsui, E., and Gat, J. (1979). Recycling of water in the Amazon basin : An isotopic study. *Water Resources Research*, 15 :1250–1258.

[Sayres et al., 2010] Sayres, D. S., Pfister, L., Hanisco, T. F., Moyer, E. J., Smith, J. B., Clair, J. M. S., O'Brien, A. S., Witinski, M. F., Legg, M., and Anderson, J. G. (2010). Influence of convection on the water isotopic composition of the tropical tropopause layer and tropical stratosphere,. *J. Geophys. Res.*, 11 :D00J20, doi :10.1029/2009JD013100.

[Scheepmaker et al., 2016] Scheepmaker, R., aan de Brugh, J., Hu, H., Borsdorff, T., Frankenberg, C., Risi, C., Hasekamp, O., Aben, I., and Landgraf, J. (2016). Hdo and h2o total column retrievals from tropomi shortwave infrared measurements. *Atmospheric Measurement Techniques Discussions*, 2016 :1–35.

[Scheepmaker et al., 2012] Scheepmaker, R. A., Frankenberg, C., Galli, A., Butz, A., Schrijver, H., Deutscher, N. M., Wunch, D., Warneke, T., Fally, S., , and Aben, I. (2012). Improved water vapour spectroscopy in the 4174-4300cm-1 region and its impact on sciamachy hdo/h2o measurements. *Atmos. Meas. Tech. Discuss.*, 5 :8539–8578, doi :10.5194/amtd–5–8539–2012.

[Schmidt, 2010] Schmidt, G. (2010). Enhancing the relevance of palaeoclimate model/data comparisons for assessments of future climate change. *J. Quaternary Sci.*, 25 :79–87, DOI : 10.1002/jqs.1314.

[Schmidt et al., 2005] Schmidt, G., Hoffmann, G., Shindell, D., and Hu, Y. (2005). Modelling atmospheric stable water isotopes and the potential for constraining cloud processes and stratosphere-troposphere water exchange. *J. Geophys. Res.*, 110 :D21314, doi :10.1029/2005JD005790.

[Schmidt et al., 2007] Schmidt, G., LeGrande, A., and Hoffmann, G. (2007). Water isotope expressions of intrinsic and forced variability in a coupled ocean-atmosphere model. *J. Geophys. Res.*, 112.

[Schmidt et al., 2013] Schmidt, G. A., Annan, J. D., Bartlein, P. J., Cook, B. I., Guilyardi, E., Hargreaves, J. C., Harrison, S., Kageyama, M., LeGrande, A., Konecky, B., Lovejoy, S., Mann, M. E., Masson-Delmotte, V., Risi, C., Thompson, D., Timmermann, A., , Tremblay, L.-B., and Yiou, P. (2013). Using paleo-climate comparisons to constrain future projections in cmip5. *Climate of the Past Discussions*, 9(1) :775–835.

[Schmittner et al., 2011] Schmittner, A., Urban, N. M., Shakun, J. D., Mahowald, N. M., Clark, P. U., Bartlein, P. J., Mix, A. C., and Rosell-Melé, A. (2011). Climate sensitivity estimated from temperature reconstructions of the last glacial maximum. *Science*, 334 :1385–1388,DOI : 10.1126/science.1203513.

[Schneider, 2011] Schneider, M abd Hase, F. (2011). Optimal estimation of tropospheric H2O and deltaD with IASI/METOP. *Atmos. Chem. Phys.*, 11 :11207–11220, doi :10.5194/acp–11–11207–2011.

[Schneider et al., 2015] Schneider, M., González, Y., Dyroff, C., Christner, E., Wiegele, A., Barthlott, S., García, O. E., Sepúlveda, E., Hase, F., Andrey, J., Blumenstock, T., Guirado, C., Ramos, R., and Rodríguez, S. (2015). Empirical validation and proof of added value of MUSICA's tropospheric deltaD remote sensing products. *Atmospheric Measurement Techniques*, 8(1) :483–503.

[Schneider et al., 2010a] Schneider, M., Toon, G., Blavier, J.-F., Hase, F., and Leblanc, T. (2010a). H2O and deltaD profiles remotely-sensed from ground in different spectral infrared regions. *Atmos. Meas. Tech.*, 3 :1599–1613.

[Schneider et al., 2010b] Schneider, M., Yoshimura, K., Hase, F., and Blumenstock, T. (2010b). The ground-based FTIR network's potential for investigating the atmospheric water cycle. *Atm. Chem. Phys.*, 10 :3427–3442.

[Sherwood et al., 2014] Sherwood, S., Bony, S., and Dufresne, J.-L. (2014). Spread in model climate sensitivity traced to atmospheric convective mixing. *Nature*, 505 :37–42, doi :10.1038/nature12829.

[Sherwood and Dessler, 2000] Sherwood, S. C. and Dessler, A. E. (2000). On the control of stratospheric humidity. *Geophys. Res. Lett.*, 27 :2513–2516.

[Sherwood et al., 2010] Sherwood, S. C., Ingram, W., Tsushima, Y., Satoh, M., M. Roberts, P. L. V., and O'Gorman, P. A. (2010). Relative humidity changes in a warmer climate. *J. Geophys. Res., 115*, 115 :D09104, doi :10.1029/2009JD012585.

[Sherwood and Wahrlich, 1999] Sherwood, S. C. and Wahrlich, R. (1999). Observed evolution of tropical deep convective events and their environment. *Mon. Wea. Rev.*, 127 :1777–1795.

[Sime et al., 2009] Sime, L. C., Wolff, E. W., Oliver2, K. I. C., and Tindall, J. C. (2009). Evidence for warmer interglacials in East Antarctic ice cores. *Nature*, 462 :doi :10.1038/nature08564.

[Slingo et al., 1996] Slingo, J. M., Sperber, K. R., Boyle, J. S., Ceron, J.-P., Dix, M., Dugas, B., Ebisuzaki, W., Fyfe, J., Gregory, D., Gueremy, J.-F., and co authors (1996). Intraseasonal oscillations in 15 atmospheric general circulation models : results from an AMIP diagnostic subproject . *Clim. Dyn*, 12 (5) :325–357, DOI : 10.1007/BF00231106.

[Smith et al., 2006] Smith, J. A., Ackerman, A. S., Jensen, E. J., and Toon, O. B. (2006). Role of deep convection in establishing the isotopic composition of water vapor in the tropical transition layer. *Geophys. Res. Lett.*, 33 :6812.

[Sobel and Bretherton, 2000] Sobel, A. H. and Bretherton, C. S. (2000). Modeling tropical precipitation in a single column. *J. Climate*, 13 :4378–43–92.

[Soden and Bretherton, 1994] Soden, B. J. and Bretherton, C. (1994). Evaluation of water vapor distribution in general circulation models using satellite observations. *J. Geophy. Res.*, 99 (D1) :1187–1210, doi :10.1029/93JD02912.

[Steen-Larsen et al., 2013] Steen-Larsen, H.-C., Johnsen, S., Masson-Delmotte, V., Stenni, B., Risi, C., Sodemann, H., Balslev-Clausen, D., Blunier, T., Dahl-Jensen, D., Ellehoej, M., Falourd, S., Gkinis, V., Grindsted, A., Jouzel, J., Popp, T., Sheldon, S., Simonsen, S., Sjolte, J., Steffensen, J., Sperlich, P., Sveinbjornsdottir, A., Vinther, B., and White, J. (2013). Continuous monitoring of summer surface water vapour isotopic composition above the greenland ice sheet. *Atmos. Chem. Phys*, 13 :4815–4828, doi :10.5194/acp–13–4815–2013.

[Steen-Larsen et al., 2014] Steen-Larsen, H. C., Masson-Delmotte, V., Hirabayashi, M., Winkler, R., Satow, K., Prié, F., Bayou, N., Brun, E., Cuffey, K. M., Dahl-Jensen, D., Dumont, M., Guillevic, M., Kipfstuhl, S., Landais, A., Popp, T., Risi, C., Steffen, K., Stenni, B., and Sveinbjörnsdottír, A. E. (2014). What controls the isotopic composition of greenland surface snow ? *Clim. Past*, 10 :377–392.

[Steinwagner et al., 2010] Steinwagner, J., Fueglistaler, S., Stiller, G., von Clarmann, T., Kiefer, M., Borsboom, P.-P., van Delden, A., and Röckmann, T. (2010). Tropical dehydration processes constrained by the seasonality of stratospheric deuterated water. *Nature Geoscience*, 3 :262–266, DOI : 10.1038/NGEO822.

[Stewart, 1975] Stewart, M. K. (1975). Stable isotope fractionation due to evaporation and isotopic exchange of falling waterdrops : Applications to atmospheric processes and evaporation of lakes. *J. Geophys. Res.*, 80 :1133–1146.

[Sturm et al., 2005] Sturm, K., Hoffmann, G., Langmann, B., and Stichler, W. (2005). Simulation of 18O in precipitation by the regional circulation model REMOiso. *Hydrological Processes*, 19 :3425–3444.

[Sud and Walker, 1993] Sud, Y. and Walker, G. (1993). A rain evaporation and downdraft parameterization to complement a cumulus updraft scheme and its evaluation using gate data. *Monthly weather review*, 121(11) :3019–3039.

[Sutanto et al., 2015] Sutanto, S., Hoffmann, G., Worden, J., Scheepmaker, R., Aben, I., and Roeckmann, T. (2015). Atmospheric processes governing the changes in water isotopologues during enso events from model and satellite measurements. *Journal of Geophysical Research : Atmospheres*, 120(13) :6712–6729.

[Taylor et al., 2012] Taylor, K. E., Stouffer, R. J., and Meehl, G. A. (2012). An overview of CMIP5 and the experiment design. *Bulletin of the American Meteorological Society*, 93(4) :485–498.

[Thompson et al., 1989] Thompson, L., Mosley-Thompson, L., Davis, M., Bolzan, J., Yao, T., Gundestrup, N., Wu, X., Klein, L., and Xie, Z. (1989). Holocene-late Pleistocene climatic ice core records from Quinghai-Tibetan Plateau. *Science*, 246 :474–477.

[Thompson et al., 1998] Thompson, L. G., Davis, M. E., Mosley-Thompson, E., Sowers, T. A., Henderson, K. A., Zagorodnov, V. S., Lin, P.-N., Mikhalenko, V. N., Campen, R. K., Bolzan, J. F., Cole-Dai, J., and Francou, B. (1998). A 25,000-year tropical climate history from Bolivian ice cores. *Science*, 282 :1858–1864.

[Thompson et al., 1995] Thompson, L. G., Mosley-Thompson, E., Davis, M. E., Lin, P.-N., Henderson, K. A., Cole-Dai, J., Bolzan, J. F., and b. Liu, K. (1995). Late Glacial Stage and Holocene Tropical Ice Core Records from Huascarán, Peru. *Science*, 269 :46 – 50, DOI : 10.1126/science.269.5220.46.

[Thompson et al., 2000] Thompson, L. G., Mosley-Thompson, E., and Henderson, K. A. (2000). Ice-core paleoclimate records in Tropical South America since the Last Glacial Maximum. *J. Quat. Sci.*, 15 :1579–1600.

[Tierney et al., 2008] Tierney, J., Russel, J. M., Huang, Y., Sinninghe Damsté, J. S., Hopmans, E. C., and Cohen, A. S. (2008). Northern hemisphere controls on tropical southeast african climate during the past 60,000 years. *Science*, 322 :252–255 , DOI : 10.1126/science.1160485.

[Tindall et al., 2009] Tindall, J. C., Valdes, P., and Sime, L. C. (2009). Stable water isotopes in HadCM3 : Isotopic signature of El Nino-Southern Oscillation and the tropical amount effect. *J. Geopys. Res.*, 114 :D04111, doi :04110.01029/02008JD010825.

[Tobin et al., 2013] Tobin, I., Bony, S., Holloway, C. E., Grandpeix, J.-Y., Seze, G., Coppin, D., Woolnough, S. J., and Roca, R. (2013). Does convective aggregation need to be represented in cumulus parameterizations ? *Journal of Advances in Modeling Earth Systems*, 5(4) :692–703.

[Tobin et al., 2012] Tobin, I., Bony, S., and Roca, R. (2012). Observational evidence for relationships between the degree of aggregation of deep convection, water vapor, surface fluxes and radiation. *Journal of Climate*.

[Tremoy et al., 2011] Tremoy, G., Vimeux, F., Cattani, O., Mayaki, S., Souley, I., and Favreau, G. (2011). Measurements of water vapor isotope ratios with wavelength-scanned cavity ring-down spectroscopy technology : new insights and important caveats for deuterium excess measurements in tropical areas in comparison with isotope-ratio mass spectrometry. *Rapid Communications in Mass Spectrometry*, 25(23) :3469–3480.

[Tremoy et al., 2012] Tremoy, G., Vimeux, F., Mayaki, S., Souley, I., Cattani, O., Favreau, G., and Oi, M. (2012). A 1-year long delta18O record of water vapor in Niamey (Niger) reveals insightful atmospheric processes at different timescales. *Geophys. Res. Let.*

[Tremoy et al., 2014] Tremoy, G., Vimeux, F., Soumana, S., Souley, I., Risi, C., Cattani, O., Favreau, G., and Oi, M. (2014). Clustering mesoscale convective systems with laser-based water vapor delta18O monitoring in Niamey (Niger). *J. Geophys. Res.*, 119(9) :5079–5103, DOI : 10.1002/2013JD020968.

[Tripati et al., 2014] Tripati, A. K., Sahany, S., Pittman, D., Eagle, R. A., Neelin, J. D., Mitchell, J. L., and Beaufort, L. (2014). Modern and glacial tropical snowlines controlled by sea surface temperature and atmospheric mixing. *Nature Geoscience*, 7(3) :205–209.

[Tuinenburg et al., 2015] Tuinenburg, O. A., Risi, C., Lacour, J., Schneider, M., Worden, J., Kurita, N., Deutscher, N., Duvel, J.-P., Coheur, P.-F., Clerbeaux, C., Wiegele, A., and Bony, S. (2015). Moist processes during mjo events as diagnosed from water isotopic measurements from the iasi satellite. *J. Geophy. Res.*, submitted.

[Twining et al., 2006] Twining, J., Stone, D., Tadros, C., Henderson-Sellers, A., and A, W. (2006). Moisture Isotopes in the Biosphere and Atmosphere (MIBA) in Australia : A priori estimates and preliminary observations of stable water isotopes in soil, plant and vapour for the Tumbarumba Field Campaign. *Global and Planetary Change*, 51 :59–72.

[Uemura et al., 2008] Uemura, R., Matsui, Y., Yoshimura, K., Motoyama, H., and Yoshida, N. (2008). Evidence of deuterium-excess in water vapour as an indicator of ocean surface conditions. *J. Geophys. Res.*, 113 :doi :10.1029/2008JD010209.

[Urban et al., 2007] Urban, J., Lautié, N., Murtagh, D., Erikson, P., Kasai, Y., Loßow, Dupuy, E., de la Noë, J., Frisk, U., Oldberg, M., Le Flochmoën, E., and Ricuaud, P. (2007). Global observations of middle atmospheric water vapour by the Odin satellite : An overview . *Planet. Space Sci.*, 55 (9) :1093–1102.

[Vimeux et al., 2005] Vimeux, F., Gallaire, R., Bony, S., Hoffmann, G., and Chiang, J. C. H. (2005). What are the climate controls on deltaD in precipitation in the Zongo Valley (Bolivia) ? Implications for the Illimani ice core interpretation. *Earth Planet. Sci. Lett.*, 240 :205–220.

[Vimeux et al., 2011] Vimeux, F., Tremoy, G., Risi, C., and Gallaire, R. (2011). A strong control of the South American SeeSaw on the intraseasonal variability of the isotopic composition of precipitation in the Bolivian Andes. *Earth. Planet. Sci. Lett.*, 307 (1-2) :47–58.

[Vuille et al., 2003] Vuille, M., Bradley, R. S., Werner, M., Healy, R., and Keimig, F. (2003). Modeling delta18O in precipitation over the tropical Americas : 1. Interannual variability and climatic controls. *J. Geophys. Res.*, 108 :1–1.

[Vuille and Werner, 2005] Vuille, M. and Werner, M. (2005). Stable isotopes in precipitation recording South American summer monsoon and ENSO variability : observations and model results. *Climate Dynamics*, 25 :401–413.

[Waliser et al., 2008] Waliser, D., Sperber, K., Hendon, H., Kim, D., Maloney, E., Wheeler, M., Weickmann, K., Zhang, C., Donner, L., Gottschalk, J., Higgins, W., Kang, I. S., Legler, D., Moncrieff, J., Schubert, S., Stern, W., F, V., Wang, B., Wang, W., and Woolnough, S. (2008). Mjo simulation diagnostics. *J Clim.*, 22(11) :http ://dx.doi.org/10.1175/2008JCLI2731.1.

[Waliser et al., 1999] Waliser, D. E., Lau, K., and Kim, J.-H. (1999). The influence of coupled sea surface temperatures on the madden-julian oscillation : A model perturbation experiment. *Journal of the Atmospheric Sciences*, 56(3) :333–358.

[Wang et al., 2001] Wang, Y. J., Cheng, H., Edwards, R. L., An, Z. S., Wu, J. Y., Shen, C. C., and Dorale, J. A. (2001). A high-resolution absolute-dated late Pleistocene Monsoon record from Hulu Cave, China. *Science*, 294(5550) :2345–8.

[Washburn and Smith, 1934] Washburn, E. and Smith, E. (1934). The isotopie fractionation of water by physiological processes. *Science*, 79 :188–189.

[Webster and Heymsfield, 2003] Webster, C. R. and Heymsfield, A. J. (2003). Water Isotope Ratios D/H, 18O/16O, 17O/16O in and out of Clouds Map Dehydration Pathways. *Science*, 302 :1742–1746.

[Werner et al., 2001] Werner, M., Heimann, M., and Hoffmann, G. (2001). Isotopic composition and origin of polar precipitation in present and glacial climate simulations. *Tellus*, 53B :53–71.

[Williams and Renno, 1993] Williams, E. and Renno, N. (1993). An analysis of the conditional instability of the tropical atmosphere. *Monthly Weather Review*, 121(1) :21–36.

[Worden et al., 2006] Worden, J., Bowman, K., Noone, D., Beer, R., Clough, S., Eldering, A., Fisher, B., Goldman, A., Gunson, M., Herman, R., Kulawik, S. S., Lampel, M., Luo, M., Osterman, G., Rinsland, C., Rodgers, C., Sander, S., Shephard, M., and Worden, H. (2006). Tropospheric Emission Spectrometer observations of the tropospheric HDO/H2O ratio : Estimation approach and characterization. *J. Geophy. Res.*, 111 :D16309, doi :10.1029/2005JD006606.

[Worden et al., 2007] Worden, J., Noone, D., and Bowman, K. (2007). Importance of rain evaporation and continental convection in the tropical water cycle. *Nature*, 445 :528–532.

[Worden et al., 2012] Worden, J., Wecht, K., Frankenberg, C., Alvarado, M., Bowman, K., Kort, E., Kulawik, S., Lee, M., Payne, V., and Worden, H. (2012). CH4 and CO distributions over tropical fires as observed by the Aura TES satellite instrument and modeled by GEOS-Chem. *Atmos. Chem. Phys.*, 13 :3679–3692.

[Wunch et al., 2011] Wunch, D., Toon, G. C., Blavier, J.-F. L., Washenfelder, R. A., Notholt, J., Connor, B. J., Griffith, D. W. T., Sherlock, V., and Wennberg, P. O. (2011). The Total Carbon Column Observing Network. *Phil. Trans. R. Soc. A*, 369 (1943) :2087–2112, doi : 10.1098/rsta.2010.0240.

[Xi, 2014] Xi, X. (2014). A Review of Water Isotopes in Atmospheric General Circulation Models : Recent Advances and Future Prospects. *International Journal of Atmospheric Sciences*, 250920 :doi :10.1155/2014/250920.

[Yao et al., 2013] Yao, T., Masson-Delmotte, V., Gao, J., Yu, W., Yang, X., Risi, C., Sturm, C., Werner, M., Zhao, H., He, Y., et al. (2013). A review of climatic controls on δ18o in precipitation over the tibetan plateau : Observations and simulations. *Reviews of Geophysics*, 51(4) :525–548.

[Yoneyama et al., 2013] Yoneyama, K., Zhang, C., and Long, C. N. (2013). Tracking pulses of the maddenjulian oscillation. *Bull. Amer. Meteor. Soc.*, 94 :18711891. doi : http ://dx.doi.org/10.1175/BAMS–D–12–00157.1.

[Yoshimori et al., 2011] Yoshimori, M., Hargreaves, J. C., Annan, J. D., Yokohata, T., and Abe-Ouchi, A. (2011). Dependency of feedbacks on forcing and climate state in physics parameter ensembles. *Journal of Climate*, 24(24) :6440–6455.

[Yoshimori et al., 2009] Yoshimori, M., Yokohata, T., and Abe-Ouchi, A. (2009). A comparison of climate feedback strength between co2 doubling and lgm experiments. *J. Climate*, 22 :3374 ?3395, doi : http ://dx.doi.org/10.1175/2009JCLI2801.1.

[Yoshimura et al., 2010] Yoshimura, K., Kanamitsu, M., and Dettinger, M. (2010). Regional downscaling for stable water isotopes : A case study of an atmospheric river event. *J. Geophy. Res.*, in press :doi :10.1029/2010JD014032.

[Yoshimura et al., 2008] Yoshimura, K., Kanamitsu, M., Noone, D., and Oki, T. (2008). Historical isotope simulation using reanalysis atmospheric data. *J. Geophys. Res.*, 113 :D19108, doi :10.1029/2008JD010074.

[Yoshimura et al., 2006] Yoshimura, K., Miyazaki, S., Kanae, S., and Oki, T. (2006). IsoMATSIRO, a land surface model that incorporates stable water isotopes. *Glob. Planet. Change*, 51 :90–107.

[Yoshimura et al., 2014] Yoshimura, K., Miyoshi, T., and Kanamitsu, M. (2014). Observation system simulation experiments using water vapor isotope information. *Journal of Geophysical Research : Atmospheres*, 119(13) :7842–7862.

[Zhang, 2005] Zhang, C. (2005). Madden-julian oscillation. *Rev. Geophys.*, 43 :RG2003, doi :10.1029/2004RG000158.

JOURNAL OF GEOPHYSICAL RESEARCH, VOL. 113, D19306, doi:10.1029/2008JD009943, 2008

Influence of convective processes on the isotopic composition (δ^{18}O and δD) of precipitation and water vapor in the tropics: 2. Physical interpretation of the amount effect

Camille Risi,[1] Sandrine Bony,[1] and Françoise Vimeux[2]

Received 8 February 2008; revised 18 May 2008; accepted 23 June 2008; published 11 October 2008.

[1] In the tropics, the proportion of heavier water isotopes in precipitation is anticorrelated with the precipitation amount. The physical processes underlying this so-called amount effect are still poorly understood and quantified. In the present study, stable water isotopes ($H_2^{18}O$ and HDO) have been introduced in a single column model including the Emanuel convection parameterization. We investigate the physical processes underlying the amount effect and propose a methodology to quantify their relative contributions. We focus on convective processes, since the idealized framework of the single column models does not allow us to consider the effects of large-scale horizontal advections of air masses of different isotopic signatures. We show that two kinds of processes predominantly explain the amount effect: first, the reevaporation of the falling rain and the diffusive exchanges with the surrounding vapor; and second, the recycling of the subcloud layer vapor feeding the convective system by convective fluxes. This highlights the importance of a detailed representation of rain evaporation processes to simulate accurately the isotopic composition of precipitation in the tropics. The variability of the isotopic composition on different timescales (from days to months) is also studied using a unidimensional simulation of the Tropical Ocean–Global Atmosphere–Coupled Ocean-Atmosphere Response Experiment (TOGA-COARE) campaign. The amount effect is best observable at intraseasonal or longer timescales. The period of time over which convective activity significantly affects the isotopic composition of precipitation is related to the residence time of water within atmospheric reservoirs.

Citation: Risi, C., S. Bony, and F. Vimeux (2008), Influence of convective processes on the isotopic composition (δ^{18}O and δD) of precipitation and water vapor in the tropics: 2. Physical interpretation of the amount effect, *J. Geophys. Res.*, *113*, D19306, doi:10.1029/2008JD009943.

1. Introduction

1.1. Context

[2] The isotopic composition of Andean ice cores is a promising means to constrain past climate variations [*Thompson et al.*, 2000; *Hoffmann et al.*, 2003]. This requires knowing how climate controls the isotopic composition of precipitation. In the Tropics, a major feature of the isotopic composition of precipitation is the observed anticorrelation at the surface between the amount of precipitation and the proportion of heavier isotopes in the precipitation, called the "amount effect" [*Dansgaard*, 1964]. This robust effect is observed at monthly and annual scales, especially on oceanic conditions such as on tropical islands [*Dansgaard*, 1964; *Rozanski et al.*, 1993].

[3] While work as been done to calibrate the relationship between precipitation amount and the isotopic composition of the precipitation [*Vimeux et al.*, 2005] and to interpret the Andean ice cores as informing about past precipitation amounts [*Hoffmann et al.*, 2003; *Ramirez et al.*, 2003], the physical processes explaining this observed "amount effect" are still poorly understood and quantified. This is partly because most of the precipitation in the tropics is related to convective processes, whose influence on the isotopic composition is complex. As stated by *Dansgaard* [1964], "When looking for reasons for the amount effect we are confronted with difficulties, mainly because of the extreme complexity of the isotopic turnover in the processes forming the convective rain." Little has been done since then to better understand physically and quantitatively how convective processes contribute to the amount effect. The amount effect is often interpreted by the depletion of air parcels by condensation and precipitation. For example,

[1] Laboratoire de Météorologie Dynamique, IPSL, UPMC, CNRS, Paris, France.
[2] IRD-UR Great Ice, LSCE, IPSL, CEA, UVSQ, CNRS, Gif-sur-Yvette, France.

0148-0227/08/2008JD009943$09.00

Vuille et al. [2003] explains: "As condensation proceeds, the isotopically enriched molecules are preferentially removed, leaving the isotopic composition of the remaining vapor increasingly lighter. The stronger the convective nature of a particular rainfall event, the higher the total amount of precipitation and thus the more depleted the isotopic composition of this rainwater." However, *Dansgaard* [1964] cited several other possible reasons for the amount effect: the falling rain gets less reenriched as rainfall gets stronger, through either a lowest reevaporation rate or more efficient diffusive exchanges with the water vapor.

1.2. Goal and Approach

[4] The goal of this article is to better understand the physical processes underlying the amount effect, and to quantify their relative importance. Since most precipitation in the tropics is related to atmospheric convection, we will examine convective processes in particular.

[5] For this purpose, isotopes were introduced in the Emanuel convective parameterization [*Emanuel*, 1991; *Emanuel and Zivkovic-Rothman*, 1999] and in a single column model of radiative-convective equilibrium including this parameterization as well as parameterizations of clouds [*Bony and Emanuel*, 2001], radiation and surface fluxes. The model was optimized and carefully evaluated for tropical conditions associated with a strong convective activity during the TOGA-COARE (Tropical Ocean–Global Atmosphere–Coupled Ocean-Atmosphere Response Experiment) campaign [*Emanuel and Zivkovic-Rothman*, 1999; *Bony and Emanuel*, 2001]. The physical package of the single column model and the convection scheme, as well as the implementation of water stable isotopes, are described in a companion paper [*Bony et al.*, 2008] (hereafter named P1).

[6] The idealized framework of radiative-convective equilibrium allows one to study, to first order, the dependence on boundary conditions of temperature and humidity profiles in the tropics [*Xu and Emanuel*, 1989]. Likewise, we assume that this framework can be used to study the isotopic composition of water and its sensitivity to boundary conditions. Radiative-convective equilibrium simulations are run over ocean, so as to better isolate the role of convective processes (rather than land surface processes for example). Moreover, we neglect horizontal gradients of isotopic composition in this idealized framework, and we will thus not consider the effect of horizontal advection of air masses. Consequently, while the goal of our study is a better understanding of the amount effect, taking into account horizontal advections or land surface processes will be necessary in the future to draw paleoclimatic conclusions over locations such as in the Andes.

[7] The Emanuel convective parameterization represents the effect of microphysical and turbulent processes. This makes this parameterization ideal for process studies. In particular, it explicitly represents an unsaturated downdraft (downdraft generated by the cooling of air due to the reevaporation of the falling precipitation), in which precipitation reevaporates partially or totally when it falls through unsaturated atmospheric layers. Simulating rain fall processes is all the more important as precipitation reevaporation and diffusive exchanges between raindrops and the surrounding vapor during the rain fall have both been cited as having a strong impact on the precipitation composition [*Dansgaard*, 1964; *Liebminger et al.*, 2006; *Lawrence and Gedzelman*, 1996]. Fractionation during reevaporation and diffusive exchanges are both taken into account in our model following Stewart's theory [*Stewart*, 1975]. The implementation of water stable isotopes in the unsaturated downdraft is described in detail by P1.

[8] In section 2, the amount effect simulated by the model is compared to the observed amount effect and the main features of the amount effect are introduced. In section 3, the methodology used to analyze and quantify the physical processes controlling the amount effect is presented. Section 4 discusses the results of this analysis and proposes a new interpretation of the amount effect. In section 5, we examine the characteristic timescales of the amount effect, using a simulation of the TOGA-COARE campaign. A summary and conclusion are given in section 6.

2. Comparison of the Observed and Simulated Amount Effect in Tropical Marine Stations

[9] The goal in this section is to ensure that the amount effect simulated by the model agrees sufficiently well with data to be used to investigate the physical processes controlling the isotopic composition of precipitation. However, we insist that a more realistic 3-D framework would be necessary for a careful evaluation (an implementation of water isotopes into an atmospheric general circulation model using the same convective parameterization is ongoing).

[10] The methodology used for the model-data comparison was described by P1 and is briefly summarized here. The unidimensional model was run on nine selected tropical maritime GNIP (Global Network for Isotopes in Precipitation) stations. Boundary conditions for the model are monthly observed sea surface temperature (SST) [*Reynolds et al.*, 2002], a constant background surface wind speed and a 6-hourly large-scale vertical velocity derived from ERA40 reanalysis data [*Uppala et al.*, 2005]. We advect temperature, moisture and isotopes consistently with the vertical velocity profile with the assumption that there are no horizontal gradients. For each station, the SST and large-scale circulation forcings are averaged over a grid box including the station. To ensure the consistency between the local precipitation collected by the GNIP station and the large-scale forcing, only stations whose GNIP seasonal cycle of precipitation amount was representative of that at larger scale were selected.

[11] An extensive comparison of simulated and observed δD, δ^{18}O and the deuterium excess ($d = \delta\mathrm{D} - 8 \cdot \delta^{18}\mathrm{O}$ [*Dansgaard*, 1964]) in precipitation is given by P1. In this paper, to avoid repetition, only the main results concerning δD will be reported. Results for δ^{18}O are qualitatively similar.

[12] The model systematically underestimates δD in precipitation (Figure 1a), possibly owing to the single column model framework (as discussed by P1). However, the amount effect, which is the subject of this paper and is measured by the slope $\frac{d\,\delta\mathrm{D}_p}{d\,P}$ (i.e., the rate of change of δD in precipitation, $\delta\mathrm{D}_p$, with precipitation rate P), is well simulated by the model (Figure 1b). The simulated slopes for

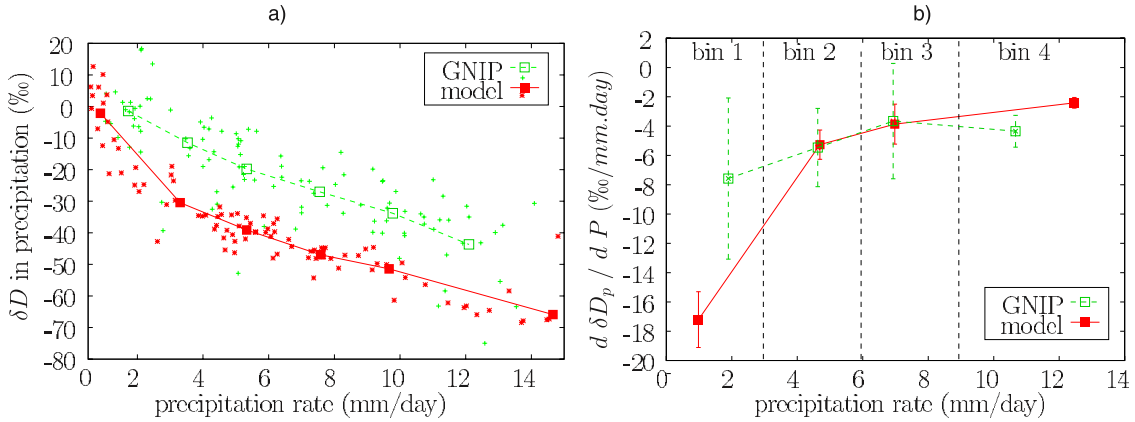

Figure 1. (a) Relationship between δD in precipitation and precipitation rate on nine tropical maritime IAEA stations the GNIP database (green dashed line) and for the single column model (red solid line). Dots represent raw data or results, while the lines represent an average relationship calculated by averaging these data or results within each of six bins. (b) Slope in the δD in precipitation versus precipitation rate diagram, $\frac{d\,\delta D_{precip}}{d\,precip}$, as a function of precipitation amount, for model results (red solid line) and GNIP data (green dashed line) from nine tropical islands. The slope is calculated for each bin of 3 mm d^{-1}, by performing a linear regression on the points within each bin. The error bars represent the standard deviation of the slope.

precipitation rates higher than 4 mm d^{-1} are between -6‰ mm^{-1} d and -4‰ mm^{-1} d, in good agreement with the data. The model also captures the observed nonlinearity of the amount effect. The observed δD_p is more sensitive to precipitation rates in regimes of low precipitation than in regimes of strong precipitation (-7.5‰ mm^{-1} d around precipitation rates of 2 mm d^{-1} and -4‰ mm^{-1} d around precipitation rates of 10 mm d^{-1}). Similarly, simulated slopes are greater (in absolute value) for low precipitation rates. However, the nonlinearity is exaggerated in the model: the simulated slopes are slightly overestimated for low precipitation rates (below 3–4 mm d^{-1}). Here are some possible explanations for this overestimation. (1) We assume that all raindrops have the same size. At low precipitation rates, however, rain drops are expected to be smaller and some may reevaporate totally without fractionation. In an idealized example, totally evaporating half of the droplets for P = 0.8 mm d^{-1} leads to a decrease of δD_p by about 10‰. If no drops reevaporate totally for $P > 4$ mm d^{-1}, then the amount effect below 4 mm d^{-1} is reduced by about 2.5‰ mm^{-1} d. Neglecting the spectrum of droplets' size is thus a plausible contributor to our overestimation of the amount effect. (2) In the Emanuel scheme, the fractional area of the unsaturated downdraft σ_d is assumed constant at $\sigma_d = 0.05$. As another idealized example, if σ_d increased with convective intensity through $\sigma_d = 0.01\,P$, then the amount effect would be reduced by about 1‰ mm^{-1} d for $P < 4$ mm d^{-1}. The representation of the unsaturated downdraft is thus another plausible contributor to the bias. (3) Finally, as explained by P1, the overestimation of the amount effect for low precipitation rates might also result from the single column framework and neglecting horizontal advections of water isotopes from the surrounding vapor.

[13] The amount effect simulated by the model being a robust feature of the model and in good agreement with observations for precipitation rates higher than 4 mm d^{-1}, we now explore how convective processes contribute to the amount effect.

3. Analysis Method

3.1. Equilibrium Simulations

[14] To better understand the physical processes that control the amount effect, we perform different radiative-convective equilibrium simulations, differing by their precipitation rates at equilibrium. The precipitation rates are varied between the different simulations by changing the large-scale dynamical forcing. For example, convection is more active and the precipitation rate is higher when a large-scale ascent is prescribed in the model. The large-scale dynamical forcing is represented as a vertical profile of large-scale vertical velocity, with an extremum ω at 500 hPa and canceling out at the surface and at the top of the atmosphere. We vary ω between -60 hPa d^{-1} (strong convection) and 30 hPa d^{-1} (weak convection), which are typical variation ranges in the Tropics. We neglect horizontal gradients in the isotopic composition when advecting moisture by the large-scale circulation.

[15] P1 showed that variations of the large-scale dynamical forcing only, with SST variations neglected, lead to an amount effect that is close (within 15%) to the one simulated when both the large-scale dynamical forcing and SST variations are considered. For this reason, and for the sake of simplicity of the analysis, we vary the precipitation rate through variations of the large-scale dynamical forcing only. Similarly, we did not consider variations of the background surface wind speed Vs_0. The effect of Vs_0 on δD_p is smaller than that of convection, notably because for surface wind speed below 7 m s^{-1} (which is the case), kinetic fractionation during evaporation remain constant [*Merlivat and Jouzel*, 1979]. The effect of convection on surface wind speed is taken into account through a gust velocity factor associated with unsaturated downdrafts, which is added to Vs_0.

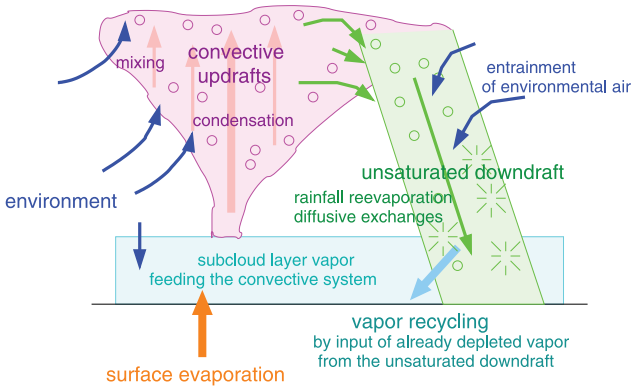

Figure 2. Scheme illustrating how the amount effect is decomposed into a sum of different contributions, each corresponding to one or to an ensemble of physical processes. Each color in the scheme represents a contribution.

[16] The amount effect simulated in these idealized simulations (red curve on Figure 3 in section 4) is close to the amount effect observed in the GNIP data (green curve on Figure 1), with an amount effect of -9‰ mm^{-1} d and -4‰ mm^{-1} d for precipitation rates around 2 mm d^{-1} and 7 mm d^{-1}, respectively.

3.2. Quantification of the Different Physical Processes Contributing to the Amount Effect

[17] The isotopic composition of the precipitation depends first on the composition of the subcloud layer (hereafter named SL), from which ascending drafts of the convective system originate. The SL represents the first 50 hPa (roughly the first 400 m) of the model. The composition of the SL depends on the composition of its sources (surface evaporation, vapor from the unsaturated downdraft injected into the SL, subsiding environment, rain reevaporation), and on the relative proportion of these different sources. Then, the composition of the rain depends on the composition of the environment entrained into the convective system, on the fractionation during the condensation in updrafts, and on the fractionation as the rain falls, partially reevaporates and reequilibrates with the surrounding vapor through diffusive exchanges.

[18] To explain the amount effect, we thus quantify the contributions from these different processes. For this purpose, using a methodology detailed in the appendices, we split the amount effect (ie the sensitivity of the δD in precipitation to precipitation rate, $\frac{d\,\delta \mathrm{D}_p}{d\,P}$) into a sum of contribution from five different types of processes, whose physical meanings are illustrated on Figure 2 and detailed below:

$$\frac{d\,\delta \mathrm{D}_p}{d\,P} = \frac{d\,\delta \mathrm{D}_{surf}}{d\,P} + c_{ascend} + c_{unsat} + c_{recycling} + c_{env}.$$

The different terms are defined below.

[19] 1. The term $\frac{d\,\delta \mathrm{D}_{surf}}{d\,P}$ (orange on Figure 2) represents the effect of the composition of the evaporated water from the ocean surface. This composition directly affects the composition of the SL vapor feeding the convective system and therefore the whole system.

[20] 2. The c_{ascend} (pink on Figure 2) represents the effect of processes in convective updrafts affecting the composition of the condensate relatively to the composition of the SL vapor. This depends on the altitude at which the precipitating condensate has formed.

[21] 3. The term c_{unsat} (green on Figure 2) represents the effect of processes in the unsaturated downdraft. This includes on the one hand a direct effect on the falling precipitation by reevaporation and diffusive exchange with the surrounding vapor. It also includes a more indirect effect on the composition of the SL vapor, through the composition of the unsaturated downdraft vapor that is injected into the SL.

[22] 4. The term $c_{recycling}$ (cyan on Figure 2) represents the effect of the origin of the SL vapor. More specifically, it represents the effect of the relative fraction of the SL vapor coming from surface evaporation or from already depleted vapor recycled into the SL through the unsaturated downdraft or through environmental subsidence.

[23] 5. The term c_{env} (dark blue on Figure 2) represents the effect of the composition of the environment entrained into the convective system (into convective updrafts, into unsaturated downdrafts or into the SL by environmental subsidence). The composition of the environment is taken relatively to the composition of the SL vapor. Therefore, this contribution represents the effect of the vertical gradient of isotopic composition in the atmosphere.

4. Results: Interpretation of the Amount Effect

[24] Figure 3 shows $\frac{d\,\delta \mathrm{D}_p}{d\,P}$ and its five contributions as a function of the precipitation rate.

[25] 1. The contribution of condensation and precipitation processes in updrafts (pink on Figure 3) is approximately constant for all precipitation amounts and contribute for an amount effect of -1 to -2‰ mm^{-1} d. They explain no more than 30% of the amount effect (maximum for highly convective regimes). When convective activity is stronger, the condensate that precipitate forms on average at slightly higher altitude, and is thus more depleted.

[26] 2. The origin of the SL vapor (cyan on Figure 3) represents an important component of the amount effect, especially for large precipitation rates (-4‰ mm^{-1} d). Indeed, when convection is more intense, the convective mass fluxes are larger, and unsaturated downdrafts are stronger. Therefore, the contribution of the downdraft mass flux to the balance of the SL vapor increases. As illustrated on Figure 4, the proportion of the SL vapor originating from the unsaturated downdraft is 45% for the strongly convective regime, but only 34% for the light precipitation regime, despite a more efficient reevaporation in the weakly convective regime case. Since the composition of the unsaturated downdraft vapor is always more depleted than the SL vapor (as shown also on Figure 4), the stronger the downdraft mass flux, the more depleted the SL vapor feeding the system. This process is summarized on the left part of Figure 5. We call this contribution "downdraft recycling" because the downdraft recycles already depleted water into the subcloud layer and therefore into the whole system. The more efficient this recycling, the more depleted the SL vapor and therefore the rain, as pointed by *Lawrence and Gedzelman* [1996] and *Lawrence et al.* [2004] to explain highly depleted rains and vapor in organized convective systems.

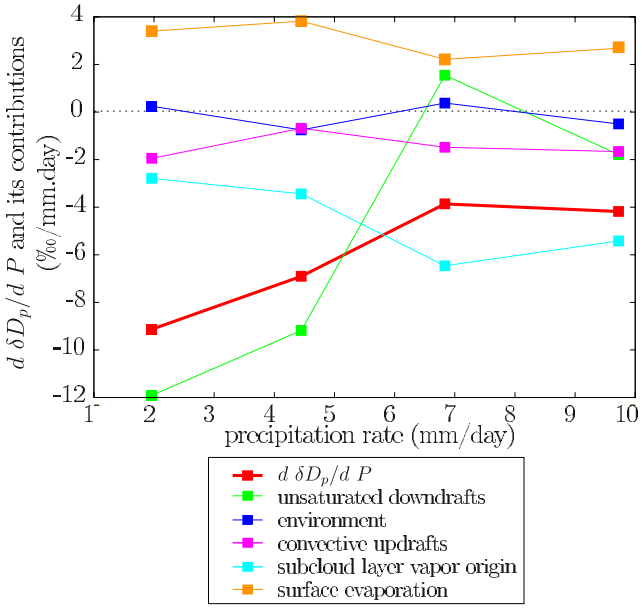

Figure 3. Sensitivity of the δD in precipitation to precipitation rate ($\frac{d\,\delta D_p}{dP}$) and its contributions from different processes as a function of precipitation rate. The contributions are the processes in unsaturated downdrafts (green), the isotopic composition of the environment (blue), processes in ascending drafts (magenta), origin of the low-level vapor (cyan), and composition of the surface evaporation flux (orange). The meanings of these contributions are illustrated on Figure 2 using the same color code and explained in the text.

[27] 3. Processes in unsaturated downdrafts (green on Figure 3) provide a major contribution to the amount effect in regimes of low precipitation rates (Figure 3). Furthermore, they explain the nonlinearity of the amount effect. The contribution of the unsaturated downdraft is explained by two effects (Figure 5), each accounting for about one half of the downdraft contribution: (1) First, a direct effect on precipitation. If the precipitation rate increases, the fraction of reevaporated rain (ie the ratio of the precipitation rate on the ground surface to the vertically integrated flux of condensate that precipitates) is decreased, both owing to a stronger precipitation rate and a higher relative humidity: the reevaporated fraction is 38% for a rain rate of 9.7 mm d^{-1} and 73% for a rain rate of 2 mm d^{-1}. Consequently, the falling precipitation gets less enriched by reevaporation. This evaporative effect was already cited by *Dansgaard* [1964] as a possible reason for the amount effect. The evaporative enrichment is further reduced at higher precipitation rates by the fact that the fractionation during reevaporation is less efficient for high relative humidity: as explained in the appendices of P1, reevaporation acts as a reverse distillation process (highly fractionating) for low relative humidity and as a diffusive reequilibration for high relative humidity (less fractionating). Note that diffusive exchanges tend to reequilibrate the falling rain with the vapor, so that they enrich the precipitation and deplete the vapor. In regimes of very high precipitation rates, diffusive exchanges dominate. When precipitation rate increases, relative humidity increases, and diffusive exchanges are more effective to reenrich the rain. This explains the slightly positive contribution of the unsaturated downdrafts at high precipitation rates. (2) Second, an indirect effect on the SL vapor. When the precipitation rate increases, the fraction of the reevaporated rain f_{revap} decreases, because the relative humidity increases. Because f_{revap} decreases, the composition of the vapor evaporating from the rain is more depleted (indeed, the composition of the vapor evaporating from the rain is generally more depleted than the rain, but tends toward that of the rain as f_{revap} tends toward 1; the evaporating vapor is thus richer when f_{revap} increases, and more depleted when f_{revap} decreases). The vapor in the unsaturated downdraft, which originates partly from the rain reevaporation, is thus more depleted for higher precipitation rates (Figure 4). Besides, as the relative humidity increases, diffusive exchanges become more efficient. As already pointed by *Dansgaard* [1964] and *Lawrence and Gedzelman* [1996] and explained above, diffusive exchanges deplete the vapor. The vapor thus gets more depleted when the relative humidity is higher. This diffusive effect was already cited by *Dansgaard* [1964] as another possible reason for the amount effect. Note that for precipitation rates lower than 4 mm d^{-1}, the model overestimates the amount effect (as was shown in section 2). Downdrafts processes in the model might be responsible for this overestimation, so that their contribution for very low precipitation rates might be overestimated and should be taken with caution.

[28] 4. the contribution of the isotopic vertical gradient in the environment (dark blue on Figure 3) is small. This is because in equilibrium simulations, variations in the large-scale dynamical forcing do not modify much the isotopic gradient in the environment.

[29] 5. The contribution of ocean evaporation (orange on Figure 3) has a sign opposite to the amount effect: the larger the precipitation amount, the more depleted the vapor at low levels, and the more enriched the evaporation flux. For example, as shown on Figure 4, for a strongly convective regime (precipitation rate of about 9.7 mm d^{-1}), δD_{surf} is 5‰ while for a light rain regime (2 mm d^{-1}), δD_{surf} is of −53‰. Ocean evaporation thus acts to reduce the amount effect.

[30] To summarize, this quantitative analysis of the amount effect shows that the amount effect is not a simple effect interpretable only by the depletion of an air mass as condensation proceeds. It is rather a sum of contributions from different processes. The two main processes are (1) the recycling of the SL vapor by injection of depleted vapor through convective fluxes into the SL, and (2) the reevaporation and diffusive processes affecting the rain and its surrounding vapor as the rain falls. The first process contributes the most to the amount effect in regimes of weak precipitation, while the second is predominant in regimes of strong precipitation. The importance of the reevaporative processes highlights the importance of a detailed representation of such convective processes for an accurate simulation of the precipitation isotopic composition.

[31] The robustness of the observed amount effect at monthly scale might be explained by the fact that the main processes involved (SL recycling and reevaporative processes) all act together to contribute to the amount effect.

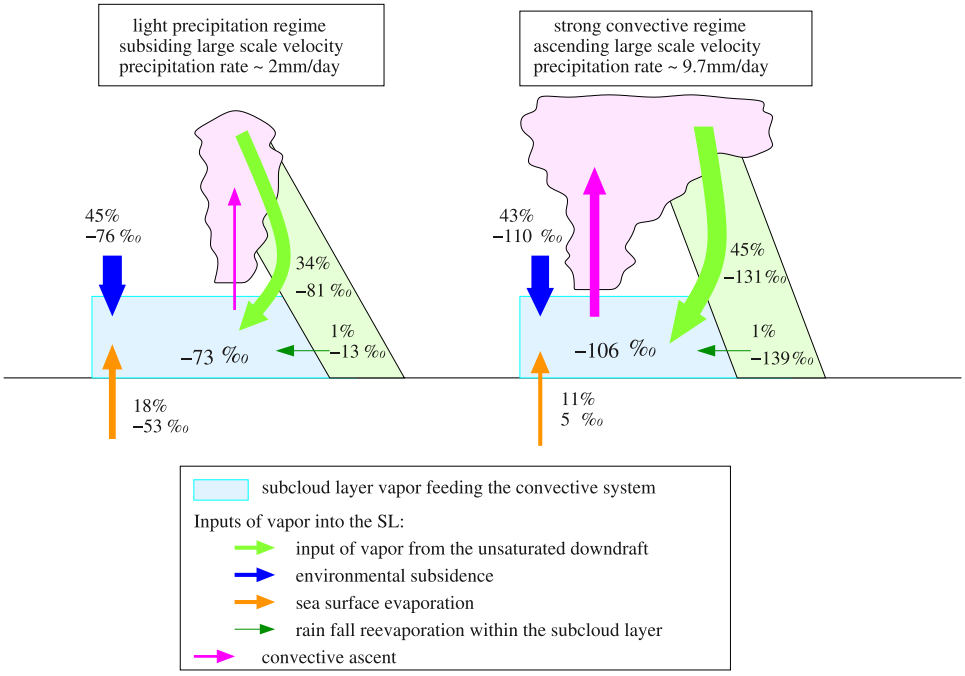

Figure 4. Illustration of what controls the isotopic composition of the water vapor in the subcloud layer. The water mass fluxes from different sources are illustrated as colored arrows: sea surface evaporation (orange), unsaturated downdraft (light green), subsiding environment (dark blue), and reevaporation of rain (dark green). The proportion of the total water input from each flux into the subcloud layer (in %), as well as the δD composition of the incoming vapor (in ‰), are indicated as numbers next to each arrows, for two different regimes: (left) a subsiding regime with light precipitation (simulated with $\omega = 20$ hPa d^{-1}) and (right) a convective regime with strong precipitation (simulated with $\omega = -60$ hPa d^{-1}). We omit the input of vapor from large-scale ascent because it does not change the isotopic composition of the SL vapor since we neglect horizontal isotopic gradients.

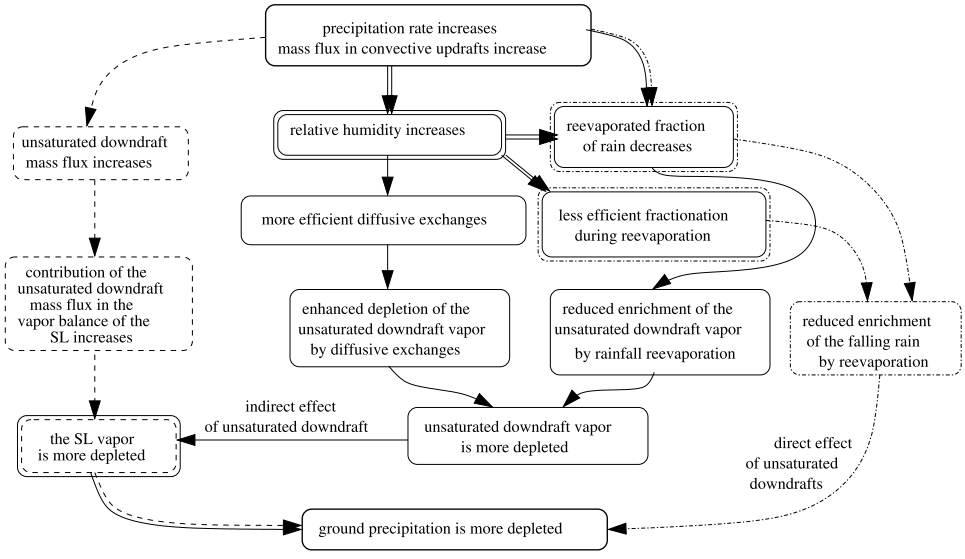

Figure 5. Summary of the main processes that explain the amount effect: subcloud layer vapor recycling (dashed line, left side) and processes during the reevaporation of the rain: (1) direct effect on the precipitation composition (dash-dotted line, right side), and (2) effect on the composition of the vapor in the unsaturated downdraft (solid line, middle).

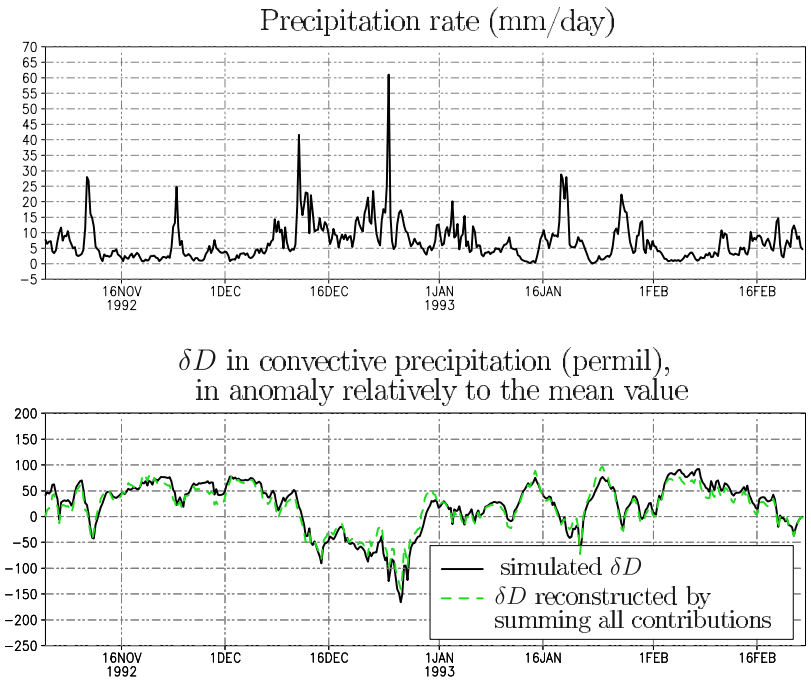

Figure 6. Temporal evolution of the precipitation rate and the δD in the convective precipitation during the TOGA-COARE simulation (black solid curves). The δD values are given relatively to the mean δD values. The dashed green line is the evolution of δD in precipitation as reconstructed by summing up all the contributions from the different processes.

[32] Surprisingly, condensation processes, often believed to be the main reason for the amount effect, have a relatively small contribution. Such a little impact might be dependent on the representation of convective updrafts in the parameterization. In the model, precipitation comes mainly from adiabatic updrafts that originate from the SL and ascend sufficiently rapidly to conserve all the condensate during their ascent. The condensation in adiabatic updrafts thus occur as in a closed system. Therefore, the composition of the condensate is strongly constrained between (1) at the upper bound, the composition of a condensate in equilibrium with the SL vapor, and (2) at the lower bound, the composition of the SL vapor. Besides, the altitude of the cloud top in the Emanuel scheme does not vary much with convective activity, hence small variations in the altitude of condensation. Although the quantitative value of the condensation contribution is linked to the representation of convective updrafts in the Emanuel scheme, our results suggest that such processes are not required to explain the largest part of the amount effect.

[33] The recycling of the SL vapor, which is one of the main contributions, includes the proportion of vapor originating from surface evaporation, environmental subsidence or unsaturated downdrafts. In our single column framework, this does not include horizontal advection of air masses of different origins, which could also modulate the isotopic composition. *Yoshimura et al.* [2003], *Cole et al.* [1999] and *Vuille et al.* [2003] underlined the importance of the advection of moisture of different isotopic signatures in controlling the isotopic composition of the rain. Neglecting large-scale horizontal advections in our model might explain why we predict overdepleted precipitation compared to observations in regimes of strong precipitation. However, our study suggests that the horizontal advection of air masses of different isotopic compositions is not required to explain the amount effect, which appears as a robust feature of convective atmospheres.

5. Timescales of the Amount Effect

5.1. Goals and Approach

[34] So far, we have studied the amount effect through equilibrium simulations. This represents large spatial (the scale of a GCM grid) and temporal scales (monthly scales or longer). Although the amount effect seems to be a robust feature of the tropical atmosphere at these scales, some studies showed no amount effect at the event scale [*Vimeux et al.*, 2005]. The question thus arises as to what are the characteristic timescales of the amount effect, and to what extent the above interpretation of the amount effect applies to shorter timescales.

[35] To answer these questions, we performed a simulation of the TOGA-COARE campaign, forced by observed 6-hourly large-scale advections of heat and moisture (described in more detail by P1). This simulation is chosen because (1) the single column model and its physical package have been carefully evaluated and optimized on their water vapor prediction for this simulation [*Emanuel and Zivkovic-Rothman*, 1999; *Bony and Emanuel*, 2001], and (2) convective activity during this campaign featured a pronounced intraseasonal variability (P1).

5.2. Factors Controlling Precipitation δD Depending on Timescale

[36] The evolution of the precipitation rate and the δD in precipitation (hereafter δD_p) are shown in Figure 6. The

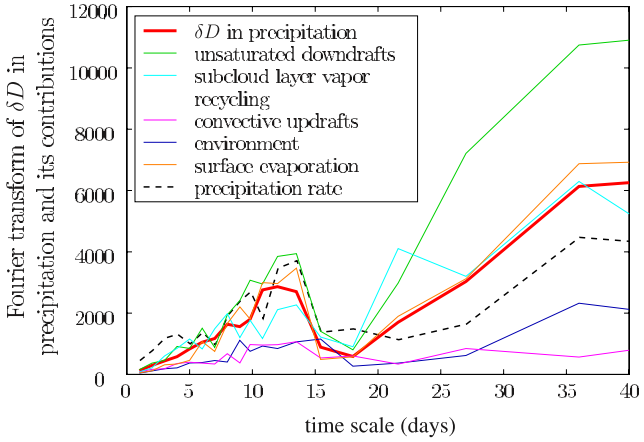

Figure 7. Spectral analysis of the δD signal in precipitation during the TOGA-COARE simulation (red), and of its different contribution (colors defined on Figure 2). The spectral analysis of the precipitation rate is also shown (black dashed line; its Fourier transform was multiplied by a factor of 8 to facilitate comparison with the Fourier transform of the δD in precipitation).

precipitation rate exhibits two prominent timescales of variability (Figure 7, black dashed lines): 10–15 days (related to Kelvin waves) and 30–40 days (related to tropical intraseasonal oscillations). The δD_p exhibits similar timescales of variability, except that variability at scales smaller than a few days is reduced (Figure 7, red lines).

[37] To analyze what explains the amount effect at different timescales, the decomposition of δD_p presented in section 4 is applied at each time step to the TOGA-COARE simulation (as detailed in Appendix A4). We check that the sum of all our contributions closely matches the original δD_p signal (Figure 6): the mean difference between the sum of all our contributions (green curve on Figure 6) and the simulated δD (black curve on Figure 6) is approximately 1.5‰, which is small compared to the standard deviation of the δD signal of more than 100‰. The spectral analysis of the different contributions to δD_p is shown by colored lines on Figure 7. The relative importance of the different processes to δD_p variations at different timescales are quite similar to the one predicted at equilibrium. At all timescales, the δD_p variations are largely due to reevaporation processes, and, to a lesser extent, to surface evaporation and SL recycling. The contribution of processes in ascending drafts is small. The effect of the composition of the environment is small, but higher than predicted at steady state. This might be because the composition of the free troposphere in this simulation shows larger and less vertically uniform variations than at equilibrium, as shown by P1.

[38] In brief, over tropical ocean at timescales ranging from a few days to a month, the modulation of δD_p with time is likely to reveal mostly the effect of the modulation of rain reevaporation and of the unsaturated downdraft mass flux. The effect the advection of air masses with different isotopic composition could also be significant [*Yoshimura et al.*, 2003] and would reduce the amplitude of δD_p variations.

5.3. At Which Timescale is the Amount Effect Observable?

[39] At which periodicity of isotopic sampling is the amount effect observable? Figure 8a shows the correlation between the average of precipitation $\bar{P}$ over the τ_m previous days ($\bar{P} = \int_{t-\tau_m}^{t} P(t) \cdot dt$) and the precipitation-weighted average of δD_p over the τ_m previous days

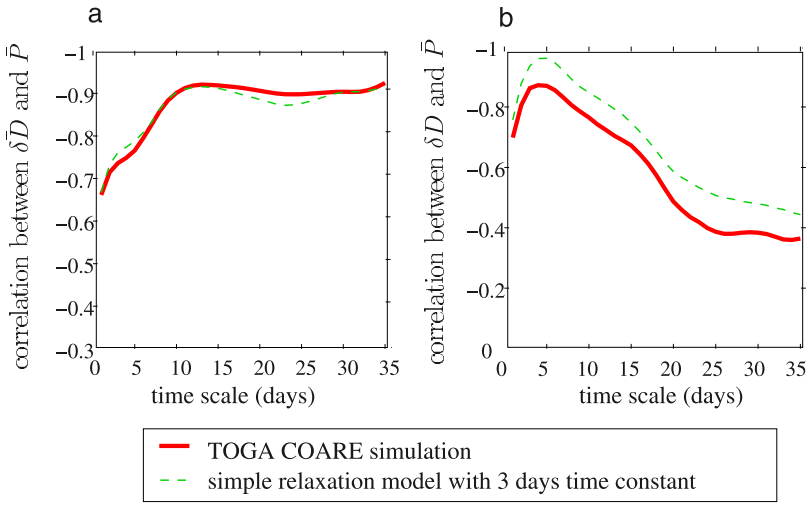

Figure 8. Sprectral-analysis-of (a) Temporal correlation between the precipitation-weighted average of δD_p over the τ_m previous days ($\delta\bar{D}_p(t) = \frac{\int_{t-\tau_m}^{t} \delta D_p(t) \cdot P(t) \cdot dt}{\bar{P}}$) and the precipitation rate averaged over the τ_m previous days ($\bar{P}(t) = \int_{t-\tau_m}^{t} P(t) \cdot dt$), as a function of time constant τ_m. The red solid curve corresponds to TOGA-COARE simulation results. The green dashed curve corresponds to what predicts the simple equation $\frac{d\delta D_p}{dt}(t) = S \cdot P(t) - \frac{\delta D_p}{T}$ with $T = 3$ days (the precipitation rate is taken from the TOGA-COARE simulation). (b) Same as Figure 8a, but correlations are between the instantaneous $\delta D_p(t)$ and the average precipitation ($\bar{P}$) over the time constant τ_m.

($\delta\bar{\mathrm{D}}_p = \frac{\int_{t-\tau_m}^{t} \delta\mathrm{D}_p(t)\cdot P(t)\cdot dt}{\int_{t-\tau_m}^{t} P(t)\cdot dt}$), as a function of the sampling period τ_m. The amount effect becomes optimally observable at timescales higher than about 10 days. At the daily scale, the precipitation amount explains less than half of the isotopic variance ($r < 0.7$). This is consistent with studies observing the amount effect at interannual [*Rozanski et al.*, 1993], monthly [*Dansgaard*, 1964; *Rozanski et al.*, 1993] and intraseasonal [*Sturm et al.*, 2007] timescales, but seldom at the event timescale [*Vimeux et al.*, 2005]. The $\delta\bar{\mathrm{D}}_p$ is therefore an indicator of low-frequency variations in convective activity.

5.4. Characteristic Timescale of the Amount Effect

[40] To investigate the timescales of the amount effect, we calculate the correlation between $\delta\mathrm{D}_p(t)$ (each time t corresponds to a 6-hourly average) and the average of the precipitation over the τ_m previous days ($\bar{P}$). The anticorrelation is maximum at a timescale of $\tau_m^{\max} = 4$ days (red curve on Figure 8b). This means that event-scale $\delta\mathrm{D}_p$ (which is roughly represented by the 6-hourly averages) does not depend on the event precipitation rate, in agreement with event-scale isotopic observations [*Vimeux et al.*, 2005]. Event-scale $\delta\mathrm{D}_p$ appears more related to the convective activity (here measured by precipitation rate P) that occurred during the $\tau_m^{\max}$ previous days (here 4 days) than to the instantaneous convective activity. The isotopic composition of precipitation is thus an integrator of past convective activity. One reason for this is that $\delta\mathrm{D}_p$ strongly depends on the isotopic composition of the SL vapor, whose reaction to convection is slower than convective activity owing to its dependence on large scale subsidence and surface evaporation.

[41] The "memory" in the response of $\delta\mathrm{D}_p$ to convective activity can be understood through a simple relaxation equation of the form

$$\frac{d\delta D_p}{dt}(t) = S\cdot P(t) - \frac{\delta D_p}{T}, \qquad (1)$$

where the first term represents the cumulative effect of convection on $\delta\mathrm{D}_p$ and the second term is a relaxation with a time constant T. Note that this equation is unchanged if several (n) timescales of relaxation (T_i) are involved (for example, in nature, reevaporation in convective downdrafts varies very quickly at the convective timescale, whereas the isotopic composition of the SL evolves more slowly): in this case, $\frac{1}{T} = \sum_{i=1}^{n} \frac{1}{T_i}$. The maximum anticorrelation in the TOGA-COARE simulation, $\tau_m^{\max}$, is best predicted for $T =$ 3 days (green curve on Figure 8b). The time constant $\tau_m^{\max}$ depends not only on T, but also on the timescales of convective variability. As an idealized example, for sinusoidal variations of precipitation rate of period τ_p, the anticorrelation between $\delta\mathrm{D}_p$ and the average precipitation would be maximum for $\tau_m^{\max} = \frac{\tau_p}{\pi}\cdot atan(\frac{2\pi T}{\tau_p})$ (Appendix B). Therefore, $\delta\mathrm{D}_p$ integrates temporally past convective activity all the more as convection varies at lower frequency.

[42] T represents the residence time of the water reservoir whose composition affects the composition of the precipitation. In the model, T is a combination of the residence time of water in the subcloud layer (<1 day) and that of the whole troposphere (of the order of 10 days), both reservoirs influencing the isotopic composition of the precipitation. Over the continents, T could in addition be related to the residence time in continental reservoirs such as soil moisture. The time constant T, which could be inferred from event-scale isotopic measurements (by optimizing the prediction of $\tau_m^{\max}$ through equation (1) for example), could thus yield some information about the time constant of the water recycling within atmospheric or continental water reservoirs.

[43] Note that in this study, we considered the local correlation between the isotopic composition of precipitation and the precipitation rate. Cases in which the isotopic composition is sensitive to convection upstream of air mass trajectories (e.g., in the Andes [*Vimeux et al.*, 2005]) are beyond the scope of this paper. However, we anticipate that the property of the isotopic composition to integrate convective activity over the previous days still hold in these cases [*Sturm et al.*, 2007].

6. Summary, Discussion, and Conclusion

[44] Water stable isotopes have been implemented in the Emanuel convection scheme. This scheme was included in a single column model optimized in its prediction of humidity in convective oceanic cases. Radiative-convective equilibrium simulations have been performed to better understand the influence of convective processes on the isotopic composition of the atmospheric vapor and precipitation in the Tropics.

[45] Precipitation amount was shown by *Bony et al.* [2008] to strongly control the composition of precipitation over tropical oceans. In this paper, the observed relationship between precipitation amount and δD in precipitation, called the amount effect, is analyzed quantitatively and interpreted in terms of physical processes. The fractionation occurring during the rain fall (associated with rain reevaporation and diffusive exchanges with the surrounding vapor) and the injection of vapor from the unsaturated downdraft (driven by rain reevaporation) into the subcloud layer constitute the two main contributions of the amount effect. The first process contributes the most to the amount effect in regimes of weak precipitation, while the second is predominant in regimes of strong precipitation. While these processes were already hypothesized by *Dansgaard* [1964] to possibly contribute to the amount effect, this study rigourously and explicitly quantifies these contributions.

[46] The results yields a new interpretation of the amount effect. The amount effect is often interpreted in terms of depletion of an air mass through rainout (e.g., *Vuille et al.* [2003]: the more intense the convection, the more intense the condensation during the ascent of the air parcels, and the more depleted the following vapor and precipitation). On the contrary, we show that the predominant processes are related to the fall and reevaporation of the precipitation, rather than processes occurring during the ascent of air parcels. More generally, we show that the amount effect is associated with an ensemble of physical and microphysical processes in the convective system, whose sum yields an observable and robust signal on the ground between precipitation amount and precipitation composition.

[47] Does the quantification of the contributions to the amount effect depend on the convective parameterization used? Particular features of the Emanuel parameterization

that might affect the relative contributions are for instance: (1) the assumption that condensate is lofted up to the cloud top altitude before precipitation processes start to operate, and (2) the small sensitivity of the cloud top altitude to convective regime. Besides, since the explicit representation of an unsaturated downdraft is a particularity of the Emanuel scheme, the rain reevaporation and the recycling of the low-level vapor by convective fluxes might affect the isotopic composition of the precipitation differently in other models. However, an explicit representation of an unsaturated downdraft might not be necessary to represent at least qualitatively the two major effects, which are likely to be robust features: (1) reduced reevaporation of the rain and (2) stronger vertical mixing (here taking the form of unsaturated downdrafts) when convective activity is stronger.

[48] Our analysis method provides a general framework to quantify the relative importance of different convective processes in the control of the isotopic composition of precipitation. This method could be applied to other models to test the sensitivity of our results to the representation of microphysical processes in different convective parameterizations.

[49] Because of a delay in the response of the atmospheric water vapor to convection, the amount effect is best observable at intraseasonal or longer timescales. The period of time over which convective activity significantly affects the isotopic composition of precipitation might give some additional information about the residence time of water.

[50] Our results underline the importance of some microphysical processes, in particular those occurring during the fall of the rain. Besides, *Bony et al.* [2008] showed that the simulated amount effect was sensitive to some model parameters related to rain reevaporation. This highlights the importance of a detailed representation of such processes to accurately simulate the isotopic composition of precipitation. In turn, the isotopic composition of the precipitation may be used to evaluate the representation of rain reevaporation in convective parameterization, as was pointed by *Bony et al.* [2008].

[51] Our physical interpretation of the amount effect underlines the importance of the origin of the low-level vapor feeding the convective system. Although not required to explain the amount effect, low-level horizontal advection of air masses of various isotopic compositions, neglected in this single column approach, might affect the amount effect. Besides, our study was restricted to maritime conditions. In order to more rigourously evaluate our model and better understand what controls the isotopic composition of precipitation in a broader range of conditions, including in tropical ice cores, taking into account horizontal advection of air masses and land surface processes would be necessary. For this purpose, we are currently implementing water isotopes in the general circulation model LMDZ4 developed at the LMD [*Hourdin et al.*, 2006], which uses the Emanuel scheme as the convective parameterization. Three-dimensional simulations will allow us to make a more rigorous model evaluation with comparison with GNIP data. Results and analyses of LMDZ isotopic simulations will be reported in a future paper.

Appendix A: Decomposition of the Amount Effect

[52] The analysis method described here provides a general framework for quantifying the effect of different processes on the control of the isotopic composition of precipitation.

[53] To unravel the different processes responsible for the amount effect, $\frac{d\,\delta D_p}{d\,P}$ is split into a sum of contributions from different processes.

A1. Chasles's Relationship

[54] First, we use Chasles's relationship to split the isotopic composition of the precipitation δD_p into that of the SL feeding the convective system, the effect of processes converting this vapor into condensate that precipitates, and the effect of processes converting this condensate into precipitation,

$$\delta D_p = \delta D_{SL} + (\delta D_{dtr} - \delta D_{SL}) + \left(\delta D_p - \delta D_{dtr}\right), \qquad \text{(A1)}$$

where δD_{SL} is the composition of the environment in the subcloud layer (the lowest 50 hPa in which the adiabatic updraft originates, hereafter named SL); δD_{dtr} is the average composition of the condensate that precipitates at all altitudes. Therefore, the first term represents the composition of low-level vapor feeding the convective system. The second term represents the modifications of the isotopic composition of water during the ascent, from low-level vapor to precipitating condensate. These modifications are related to processes such as fractionation during condensation or entrainment of environmental air. The last term represents the modification of the isotopic composition of the precipitating water during its fall down to the surface.

[55] To isolate the different contributions from different processes on the amount effect, that is, on $\frac{d\,\delta D_p}{d\,P}$, equation (A1) is differentiated,

$$d\,\delta D_p = d\,\delta D_{SL} + d\,(\delta D_{dtr} - \delta D_{SL}) + d\left(\delta D_p - \delta D_{dtr}\right). \qquad \text{(A2)}$$

A2. Decomposition of the Subcloud-Layer Vapor

[56] At steady state, the isotopic composition of the SL vapor is determined by the composition of the different sources of vapor into the SL. We thus decompose the $d\,\delta D_{SL}$ component by calculating the water budget in the subcloud layer. Water inputs are as follows (Figure 2).

[57] 1. Evaporation from the ocean surface. The water input flux is referred to as F^q_{surf} and its composition as δD_{surf}.

[58] 2. Input of already depleted water vapor from the unsaturated downdraft. The water input flux is referred to as F^q_{vp} and its composition as δD_{vp}.

[59] 3. Input of environmental moisture from above through the environmental subsidence. This environmental subsidence is due on the one hand to the compensation of convective ascending fluxes, and on the other hand to large-scale subsidence when the large-scale vertical motion is subsident. The water input flux is referred to as F^q_{subs} and its composition as δD_{subs}.

[60] 4. Input from rain reevaporation within the subcloud layer. The water input flux is referred to as F^q_{revap} and its composition as δD_{revap}.

[61] 5. Input of low-level moisture through horizontal advection. The water input flux is referred to as F^q_{LS} and its composition as δD_{LS}.

[62] The only output of SL vapor is the ascent in convective updrafts. Since there is no fractionation associ-

ated with this output (i.e., no condensation below cloud base, homogeneous composition in the SL), at steady state, the composition of the vapor in the subcloud layer is the weighted mean of the composition of all these inputs,

$$\delta \mathrm{D}_{SL}^{eq} = r_{surf} \cdot \delta \mathrm{D}_{surf} + r_{vp} \cdot \delta \mathrm{D}_{vp} + r_{subs} \cdot \delta \mathrm{D}_{subs} + r_{revap} \cdot \delta \mathrm{D}_{revap} + r_{LS} \cdot \delta \mathrm{D}_{LS} \tag{A3}$$

where r_{surf}, r_{vp}, r_{subs}, r_{revap} and r_{LS} are the proportions of vapor in the subcloud layer originating from each process, at steady state ($r_{surf} + r_{vp} + r_{subs} + r_{revap} + r_{LS} = 1$). For example,

$$r_{surf} = \frac{F_{surf}^{q}}{F_{surf}^{q} + F_{vp}^{q} + F_{subs}^{q} + F_{revap}^{q} + F_{LS}^{q}}.$$

[63] Since the compositions of water in convective drafts and in the environment all depends on the composition of the SL vapor (a shift in the SL composition would be propagated in all convective drafts), we write all the compositions in reference to $\delta \mathrm{D}_{SL}^{eq}$, to better isolate the influence of the different convective processes. Equation (A3) therefore yields

$$\delta \mathrm{D}_{SL}^{eq} = \delta \mathrm{D}_{surf} + r'_{vp} \cdot \left(\delta \mathrm{D}_{vp} - \delta \mathrm{D}_{SL}^{eq}\right) + r'_{subs} \cdot \left(\delta \mathrm{D}_{subs} - \delta \mathrm{D}_{SL}^{eq}\right) + r'_{revap} \cdot \left(\delta \mathrm{D}_{revap} - \delta \mathrm{D}_{SL}^{eq}\right) + r'_{LS} \cdot \left(\delta \mathrm{D}_{LS} - \delta \mathrm{D}_{SL}^{eq}\right), \tag{A4}$$

where $r'_{vp} = \frac{r_{vp}}{r_{surf}}$, and other r' coefficients are defined similarly.

[64] It appears now more clearly that $\delta \mathrm{D}_{SL}^{eq}$ is equal to the composition of the surface evaporation, plus modifications by other water fluxes. Equation (A4) can be compared with the traditional closure assumption [*Merlivat and Jouzel*, 1979], in which water fluxes other than surface evaporation are neglected and thus $\delta \mathrm{D}_{SL}^{eq} = \delta \mathrm{D}_{surf}$.

[65] Finally, equation (A4) is differentiated to yield the contributions from different processes,

$$\begin{aligned} d\delta \mathrm{D}_{SL}^{eq} = {} & d\delta \mathrm{D}_{surf} + r'_{vp} \cdot d\left(\delta \mathrm{D}_{vp} - \delta \mathrm{D}_{SL}^{eq}\right) \\ & + r'_{revap} \cdot d\left(\delta \mathrm{D}_{revap} - \delta \mathrm{D}_{SL}^{eq}\right) \\ & + r'_{subs} \cdot d\left(\delta \mathrm{D}_{subs} - \delta \mathrm{D}_{SL}^{eq}\right) + r'_{LS} \cdot d\left(\delta \mathrm{D}_{LS} - \delta \mathrm{D}_{SL}^{eq}\right) \\ & + dr'_{vp} \cdot \left(\delta \mathrm{D}_{vp} - \delta \mathrm{D}_{SL}^{eq}\right) + dr'_{subs} \cdot \left(\delta \mathrm{D}_{subs} - \delta \mathrm{D}_{SL}^{eq}\right) \\ & + dr'_{revap} \cdot \left(\delta \mathrm{D}_{revap} - \delta \mathrm{D}_{SL}^{eq}\right) + dr'_{LS} \cdot \left(\delta \mathrm{D}_{LS} - \delta \mathrm{D}_{SL}^{eq}\right). \end{aligned} \tag{A5}$$

A3. Summary of This Decomposition

[66] To summarize, the $d\ \delta \mathrm{D}_p$ signal is decomposed into five contributions,

$$\frac{d\ \delta \mathrm{D}_p}{d\ P} = \frac{d\ \delta \mathrm{D}_{surf}}{d\ P} + c_{ascend} + c_{unsat} + c_{recycling} + c_{env}. \tag{A6}$$

[67] The term $\frac{d\ \delta \mathrm{D}_{surf}}{d\ P}$ is the contribution due to the composition of the evaporative flux from the ocean: $d\delta \mathrm{D}_{surf}$. It is represented in orange on Figures 3 and 7.

[68] The term c_{ascend} is the contribution due to condensation and precipitation processes in the ascending drafts: $\delta \mathrm{D}_{dtr} - \delta \mathrm{D}_{SL}$, with the effect of the composition of the entrained environment subtracted. It is represented in pink on Figures 3 and 7.

[69] The term c_{unsat} is the contribution due to all processes during the fall of the rain, including the direct effect of reevaporation and diffusive exchange on the falling precipitation composition ($\delta \mathrm{D}_{precip} - \delta \mathrm{D}_{dtr}$), and the effect of the composition of the vapor in the unsaturated downdraft on the composition of the SL vapor ($r'_{vp} \cdot d(\delta \mathrm{D}_{vp} - \delta \mathrm{D}_{SL}^{eq}) + r'_{revap} \cdot d(\delta \mathrm{D}_{revap} - \delta \mathrm{D}_{SL}^{eq})$), with the effect of the composition of the entrained environment substracted. This is represented in green on Figures 3 and 7.

[70] The term $c_{recycling}$ is the contribution due to the origin of the SL vapor: $dr'_{vp} \cdot (\delta \mathrm{D}_{vp} - \delta \mathrm{D}_{SL}^{eq}) + dr'_{subs} \cdot (\delta \mathrm{D}_{subs} - \delta \mathrm{D}_{SL}^{eq}) + dr'_{revap} \cdot (\delta \mathrm{D}_{revap} - \delta \mathrm{D}_{SL}^{eq}) + dr'_{LS} \cdot (\delta \mathrm{D}_{LS} - \delta \mathrm{D}_{SL}^{eq})$. This depends on the proportion of vapor originating from the surface evaporation or from the convective fluxes, but not directly on their isotopic composition. It is represented in cyan on Figures 3 and 7.

[71] The c_{env} is the contribution due to the composition of the environment relatively to that of the subcloud layer vapor: $r'_{subs} \cdot d(\delta \mathrm{D}_{subs} - \delta \mathrm{D}_{SL}^{eq}) + r'_{LS} \cdot d(\delta \mathrm{D}_{LS} - \delta \mathrm{D}_{SL}^{eq})$. We also add the effect of the composition of the environment entrained into convective drafts. This contribution thus gathers the effects of the composition of the environment through entrainment into ascending drafts and unsaturated downdrafts, and through environmental subsidence. It mainly represents the effect of the vertical gradient of the isotopic composition in the environment. It is represented in dark blue on Figures 3 and 7.

A4. Diagnostic of These Contributions

[72] Each contributing term in equations (A2) and (A5) is diagnosed from the model.

[73] In section 4, the amount effect and its contributions are calculated by comparing two equilibrium simulations simulating different precipitation rates. For example, if simulations (1) and (2) simulate different precipitations rates around P, we calculate:

$$\frac{d\ \delta \mathrm{D}_p}{dP}(P) = \frac{\delta \mathrm{D}_p(2) - \delta \mathrm{D}_p(1)}{P(2) - P(1)}$$

[74] The amount effect and its contributions are shown as a function of precipitation rate on Figure 3.

[75] In section 5, the variability of $\delta \mathrm{D}_p$ and its contributions are calculated as a function of time t every 6 hours by comparing variables at time t to the mean values over the simulation. For example, at each time t,

$$d\ \delta \mathrm{D}_p(t) = \delta \mathrm{D}_p(t) - \delta \bar{\mathrm{D}}_p.$$

[76] The evolution of $d\ \delta \mathrm{D}_p(t)$ simulated by the model as well as $d\ \delta \mathrm{D}_p(t)$ reconstructed by summing all the different contributions are shown on Figure 6. The spectral analysis of each contribution is performed on Figure 7.

Appendix B: Timescale of Maximum Correlation Between $\delta \mathrm{D}_p$ and Averaged Precipitation

[77] The goal here is to calculate the timescale of maximum correlation, $\tau_m^{\max}$, between $\delta \mathrm{D}_p(t)$ and the average of

the precipitation rate over the τ_m previous days: $\bar{P}(t) = \int_{t-\tau_m}^{t} P(t)dt$. As an idealized example, we assume that precipitation $P(t)$ is a sinusoid of period τ_p: $P(t) = P_0 \cdot \cos(\frac{2\pi}{\tau_p})$ (in nature, precipitation signals are more complex). We further assume that the response of δD_p to $P(t)$ is given by the following differential equation:

$$\frac{d\delta D_p}{dt} = S \cdot P(t) - \frac{\delta D_p}{T}. \tag{B1}$$

[78] The correlation is maximal when δD_p and $\bar{P}$ are in phase.

B1. Phase of $\bar{P}(t)$

[79]

$$\bar{P}(t) = \int_{t-\tau_m}^{t} P(t)dt = \frac{P_0 \cdot \tau_p}{\pi} \cdot \sin\left(\frac{\pi\tau_m}{\tau_p}\right) \cdot \cos\left(\frac{2\pi}{\tau_p}\left(t - \frac{\tau_m}{2}\right)\right). \tag{B2}$$

[80] $\bar{P}$ is thus delayed by $\frac{\tau_m}{2}$ compared to P.

B2. Phase of δD_p

[81] The differential equation is solved in the frequency domain, with $P(t) = \Re(P_0 \cdot e^{i\omega t})$ and $\delta D_p(t) = \Re(\delta\hat{D}_p \cdot e^{i\omega t})$, where $\omega = \frac{2\pi}{\tau_p}$ is the frequency of both P and δD_p:

$$i\omega\delta\hat{D}_p = S \cdot P_0 - \frac{\delta\hat{D}_p}{T} \tag{B3}$$

[82] Thus

$$\delta\hat{D}_p = S \cdot P_0 \frac{1}{\frac{1}{T} + i\omega} = S \cdot P_0 \frac{1}{\sqrt{\frac{1}{T^2} + \omega^2}} e^{i \cdot \arctan(\omega \cdot T)} \tag{B4}$$

[83] Thus δD_p is shifted by $\frac{1}{\omega} \cdot \arctan(\omega \cdot T)$ compared to $P(t)$.

[84] Therefore, δD_p and $\bar{P}$ are in phase when

$$\tau_m = \frac{\tau_P}{\pi} \cdot \arctan\left(\frac{2\pi T}{\tau_P}\right) \tag{B5}$$

[85] Note that in nature, the relationship between T and τ_m is complexified by the continuous spectrum of variability frequencies.

[86] **Acknowledgments.** The authors acknowledge Jean-Yves Grandpeix, Georg Hoffmann, and Jean Jouzel for useful discussions about the physics of water stable isotopes or atmospheric convection. We thank Kerry Emanuel and two anonymous reviewers for their interesting comments and suggestions. This work was funded by CNRS, by IPSL, and by the French national programs for climate studies (PNEDC-LEFE) Amancay and MISSTERRE.

References

Bony, S., and K. A. Emanuel (2001), A parameterization of the cloudiness associated with cumulus convection: Evaluation using TOGA COARE data, *J. Atmos. Sci.*, *58*, 3158–3183.

Bony, S., C. Risi, and F. Vimeux (2008), Influence of convective processes on the isotopic composition ($\delta^{18}O$ and δD) of precipitation and water vapor in the tropics: 1. Model description, vertical profiles and isotopic composition of precipitation, *J. Geophys. Res.*, *113*, D19305, doi:10.1029/2008JD009942.

Cole, J. E., D. Rind, R. S. Webb, J. Jouzel, and R. Healy (1999), Climatic controls on interannual variability of precipitation $\delta^{18}O$: Simulated influence of temperature, precipitation amount, and vapor source region, *J. Geophys. Res.*, *104*, 14,223–14,236.

Dansgaard, W. (1964), Stable isotope in precipitation, *Tellus*, *16*, 436–468.

Emanuel, K. A. (1991), A scheme for representing cumulus convection in large-scale models, *J. Atmos. Sci.*, *48*, 2313–2329.

Emanuel, K. A., and M. Zivkovic-Rothman (1999), Development and evaluation of a convection scheme for use in climate models, *J. Atmos. Sci.*, *56*, 1766–1782.

Hoffmann, G., et al. (2003), Coherent isotope history of andean ice cores over the last century, *Geophys. Res. Lett.*, *30*(4), 1179, doi:10.1029/2002GL014870.

Hourdin, F., et al. (2006), The LMDZ general circulation model: Climate performance and sensitivity to parameterized physics with emphasis on tropical convection, *Clim. Dyn.*, *19*(15), 3445–3482.

Lawrence, J. R., and S. D. Gedzelman (1996), Low stable isotope ratios of tropical cyclone rains, *Geophys. Res. Lett.*, *23*, 527–530.

Lawrence, J. R., S. D. Gedzelman, D. Dexheimer, H.-K. Cho, G. D. Carrie, R. Gasparini, C. R. Anderson, K. P. Bowman, and M. I. Biggerstaff (2004), Stable isotopic composition of water vapor in the tropics, *J. Geophys. Res.*, *109*, D06115, doi:10.1029/2003JD004046.

Liebminger, A., G. Haberhauer, W. Papesch, and G. Heiss (2006), Correlation of the isotopic composition in precipitation with local conditions in alpine regions, *J. Geophys. Res.*, *111*, D05104, doi:10.1029/2005JD006258.

Merlivat, L., and J. Jouzel (1979), Global climatic interpretation of the deuterium-oxygen 18 relationship for precipitation, *J. Geophys. Res.*, *84*, 5029–5032.

Ramirez, E., et al. (2003), A new Andean deep ice core from Nevado Illimani (6350 m), Bolivia, *Earth Planet. Sci. Lett.*, *212*, 337–350.

Reynolds, R. W., N. A. Rayner, T. M. Smith, D. C. Stokes, and W. Wang (2002), An improved in situ and satellite SST analysis for climate, *J. Clim.*, *15*, 1609–1625.

Rozanski, K., L. Araguás-Araguás, and R. Gonfiantini (1993), Isotopic patterns in modern global precipitation, in *Climate Change in Continental Isotopic Records*, *Geophys. Monogr. Ser.*, vol. 78, edited by P. K. Swart et al., pp. 1–36, AGU, Washington, D. C.

Stewart, M. K. (1975), Stable isotope fractionation due to evaporation and isotopic exchange of falling waterdrops: Applications to atmospheric processes and evaporation of lakes, *J. Geophys. Res.*, *80*, 1133–1146.

Sturm, C., F. Vimeux, and H. Krinner (2007), Intraseasonnal variability in South America recorded in stable water isotopes, *J. Geophys. Res.*, *112*, D20118, doi:10.1029/2006JD008298.

Thompson, L. G., E. Mosley-Thompson, and K. A. Henderson (2000), Ice-core paleoclimate records in tropical south america since the last glacial maximum, *J. Quat. Sci.*, *15*, 1579–1600.

Uppala, S., et al. (2005), The ERA-40 re-analysis, *Q. J. R. Meteorol. Soc.*, *131*, 2961–3012.

Vimeux, F., R. Gallaire, S. Bony, G. Hoffmann, and J. C. H. Chiang (2005), What are the climate controls on δD in precipitation in the Zongo Valley (Bolivia)? Implications for the Illimani ice core interpretation, *Earth Planet. Sci. Lett.*, *240*, 205–220.

Vuille, M., R. S. Bradley, M. Werner, R. Healy, and F. Keimig (2003), Modeling $\delta^{18}O$ in precipitation over the tropical Americas: 1. Interannual variability and climatic controls, *J. Geophys. Res.*, *108*(D6), 4174, doi:10.1029/2001JD002038.

Xu, K.-M., and K. Emanuel (1989), Is the tropical atmosphere conditionally unstable?, *Mon. Weather Rev.*, *117*, 1471–1479.

Yoshimura, K., T. Oki, N. Ohte, and S. Kanae (2003), A quantitative analysis of short-term 18O variability with a Rayleigh-type isotope circulation model, *J. Geophys. Res.*, *108*(D20), 4647, doi:10.1029/2003JD003477.

S. Bony and C. Risi, Laboratoire de Météorologie Dynamique, IPSL, UPMC, CNRS, case courrier 99, 4 Place Jussieu, F-75252 Paris CEDEX 05, France. (camille.risi@lmd.jussieu.fr)

F. Vimeux, IRD-UR Great Ice, LSCE, IPSL, CEA, UVSQ, CNRS, CE Saclay, Orme des Merisiers, Bât 701, F-91191 Gif-sur-Yvette CEDEX, France.

QUARTERLY JOURNAL OF THE ROYAL METEOROLOGICAL SOCIETY
Q. J. R. Meteorol. Soc. **136(s1)**: 227–242 (2010)
Published online 28 September 2009 in Wiley InterScience
(www.interscience.wiley.com) DOI: 10.1002/qj.485

Evolution of the stable water isotopic composition of the rain sampled along Sahelian squall lines†

Camille Risi,[a]* Sandrine Bony,[a] Francoise Vimeux,[b,c] Michel Chong[d] and Luc Descroix[e]

[a]*LMD/IPSL, CNRS, UPMC, Paris, France*
[b]*Institut de Recherche pour le Développement – Laboratoire HydroSciences Montpellier, France*
[c]*IPSL – Laboratoire des Sciences du Climat et de l'Environnement (UMR CEA, CNRS, UVSQ), Gif-sur-Yvette, France*
[d]*Laboratoire d'Aérologie, Université de Toulouse and CNRS, Toulouse, France*
[e]*Laboratoire d'étude des Transferts en Hydrologie et Environnement, CNRS, Grenoble, France*

ABSTRACT: In the Tropics, the stable isotopic composition (HDO, $H_2^{18}O$) of precipitation is strongly modulated by convective activity. To better understand how convective processes impact the precipitation isotopic composition, we analyze the isotopic composition of rain collected during the passage of four squall lines over the Sahel (Niamey, Niger) in August 2006 during the African Monsoon Multidisciplinary Analysis (AMMA) campaign. The high-frequency sampling (5−10 min) of the precipitation allows us to investigate the evolution of the precipitation isotopic composition in different phases of the squall lines. Despite a large variability among the different squall lines, some robust isotopic features appear: the W shape of the $\delta^{18}O$ evolution and the deuterium excess decrease in the first part of the stratiform zone. To understand more quantitatively how convective processes impact the precipitation isotopic composition, a simple stationary two-dimensional transport model including a representation of cloud microphysics and isotopic fractionation is developed and forced by three-dimensional winds retrieved from the Massachusetts Institute of Technology (MIT) radar on 11 August 2006. The model reproduces the robust observed features and a large sensitivity to the squall-line dynamics. This model suggests that the main controlling factors of the isotopic evolution are (1) squall-line dynamics, especially the downward advection of air at the rear of the squall lines, affecting the vapour composition and, by isotopic equilibration, the subsequent precipitation composition and (2) rain re-evaporation. This suggests that water isotopes have the potential to better constrain squall-line dynamics and rain re-evaporation, and to evaluate the representation of convective processes in numerical models. Copyright © 2009 Royal Meteorological Society

KEY WORDS rain evaporation; AMMA; convection

Received 2 December 2008; Revised 26 May 2009; Accepted 6 July 2009

1. Introduction

Owing to mass and symmetry differences, stable water isotopes ($H_2^{16}O$, HDO, $H_2^{18}O$) are sensitive to phase changes and diffusive processes. Stable water isotopes have long been used in polar studies as proxies for climate and especially temperature changes. In the Tropics, however, the primary control of the isotopic composition of the precipitation is not temperature but precipitation amount (Dansgaard, 1964). A recent analysis using a single-column model including the Emanuel convective parametrization (Emanuel, 1991) suggests that the relationship between the enrichment in heavier isotopes and the precipitation rate, known at the monthly scale as the 'amount effect', is primarily controlled by rain re-evaporation (raindrops get more enriched as they re-evaporate), diffusive exchanges and the recycling of the boundary-layer vapour by depleted vapour from convective downdraughts generated by the rain re-evaporation (Risi *et al.*, 2008a).

The intensity of convection and rain re-evaporation are known to exhibit a systematic evolution along the life cycle of individual convective systems (Houze, 1977; Zipser, 1977; Sherwood and Wahrlich, 1999). The temporal evolution of the rain isotopic composition in well-organized convective systems is therefore likely to reveal the effect of these processes on the precipitation isotopic composition. To test this hypothesis, measuring the rain isotopic composition along squall lines in the Sahel is appealing: the Sahel is associated with both intense convective systems and strong re-evaporation (Chong and Hauser, 1990; Zahiri, 2007), because of the dryness of the air in the vicinity of the Sahara. Taupin and Gallaire (1998) noted a systematic evolution of the isotopic composition along squall lines in Niamey, Niger. A systematic evolution was also observed along convective systems in other regions (Celle-Jeanton *et al.*, 2004; Barras and Simmonds, 2009) or along radial transects in tropical cyclones (Gedzelman *et al.*, 2003; Fudeyasu *et al.*, 2008). These studies identified a variety of processes controlling the observed isotopic evolution of the precipitation, such

*Correspondence to: Camille Risi, LMD/IPSL, CNRS, UPMC, Paris, France. E-mail: camille.risi@lmd.jussieu.fr
†This article was published online on 28 September, 2009. An error was subsequently identified. This notice is included in the online and print versions to indicate that both have been corrected 18 January 2010.

as (1) the origin of air masses (Taupin and Gallaire, 1998), (2) rain re-evaporation (Taupin and Gallaire, 1998; Barras and Simmonds, 2009), (3) condensation altitude (at higher condensation altitude, the vapour is more depleted due to previous condensation, and thus the condensate forming the precipitation is more depleted: Celle-Jeanton *et al.*, 2004) and (4) diffusive exchanges between the low-level vapour and the raindrops that deplete the vapour (particularly efficient when the relative humidity is high: Gedzelman *et al.*, 2003; Fudeyasu *et al.*, 2008). However, the large number of processes potentially involved makes the details of the observed evolution difficult to interpret.

In this study, we take advantage of the second special observation period (15 July–15 September: SOP-2) of the African Monsoon Multidisciplinary Analysis (AMMA) campaign (Redelsperger *et al.*, 2006; Janicot *et al.*, 2008) to analyze the evolution of the isotopic composition of precipitation sampled along four squall lines in Niamey, Niger, in August 2006. The campaign offers a huge quantity of data documenting each system (radars, mobile facility from the Atmospheric Radiation Measurement (ARM) programme, *in situ* measurements, satellites), allowing a more detailed interpretation of isotopic data. In addition, three-dimensional (3D) winds have been retrieved from the Massachusetts Institute of Technology (MIT) radar data (Chong, 2009, this issue) for one of the squall lines sampled, on 11 August 2006.

The main goal of this study is thus to better understand the role of convective processes in controlling the precipitation isotopic composition, and more generally to explore what information may be learned from water isotopes regarding cumulus convection and atmospheric processes.

In section 2, we present and compare the evolution of the isotopic composition of the precipitation along four squall lines and suggest some processes to explain the isotopic evolution. In section 3, we focus on the 11 August squall line, on which a simple two-dimensional (2D) model of transport and microphysics is run: we first describe this model, and then use it to investigate what controls the isotopic composition along squall lines. A discussion and concluding remarks are given in section 4.

2. Data

2.1. Rainwater collection and isotopic analysis

Rain from squall-line systems on 6, 11, 18 and 22 August 2006 was sampled on the roof of the Institut de Recherche pour le Développement (IRD) building in Niamey (13.53°N, 2.1°E), at about 3 m above the ground and with no nearby obstacles or vegetation. Rain re-evaporation in the pluviometer is strongly limited: the pluviometer is devised with this aim, the relative humidity of the surface air is always above 90% during rainfall and the precipitation never spends more than 30 min in the pluviometer. Every five minutes, we read the precipitation amount and collect precipitation samples from the pluviometer into 15 ml bottles. When precipitation was weak, we waited until there was enough precipitation in the pluviometer to fill the bottle, increasing the time step up to 30 min at maximum.

The isotopic composition is expressed as an enrichment in heavier isotopes HDO or $H_2^{18}O$ relative to the Standard Mean Ocean Water (SMOW), denoted respectively by δD and δ^{18}O:

$$\delta = \left(\frac{R_{\text{sample}}}{R_{\text{SMOW}}} - 1 \right) \times 1000.$$

The R notation denotes the ratio of the HDO or $H_2^{18}O$ mixing ratio over that of $H_2^{16}O$; R_{sample} and R_{SMOW} are the ratio in the sample and the SMOW respectively. At first order, variations in δD are eight times those of δ^{18}O. The deviation from this behaviour is measured by the deuterium excess: $d = \delta\text{D} - 8\delta^{18}\text{O}$ (Dansgaard, 1964). Hereafter, we denote the δ^{18}O and d of the precipitation by $\delta^{18}O_p$ and d_p.

All δ^{18}O and δD measurements are performed with an accuracy of ± 0.05‰ and ± 0.5‰ respectively, leading to an accuracy of about ± 0.7‰ for d.

2.2. Variability and robust features among squall lines

Snapshots of radar reflectivity from the MIT (Williams *et al.*, 1992) and ARM mobile facility radars at Niamey airport (about 10 km from IRD), thermodynamical profiles from radio-soundings and the corresponding evolution of the observed precipitation rate, $\delta^{18}O_p$ and d_p, for the four squall lines are plotted in Figures 1 and 2. West African squall lines are convective systems aligned roughly in the north–south direction (Figure 1(a)) and propagating westwards. Therefore, assuming that the squall line is stationary, the temporal evolution at the sampling site corresponds to the spatial evolution along an east–west transect of the squall line. In agreement with previous squall-line studies (Houze, 1977), the precipitation rate features two maxima corresponding to the convective zone at the front and the stratiform zone at the rear, with a transition zone between these two maxima (Figure 2). Only for 22 August are the convective and stratiform zone not clearly defined.

The amplitude of isotopic variations along each squall line is of the order of 2–4‰ for $\delta^{18}O_p$ and 10–30‰ for d_p, demonstrating the strong influence of the different phases of convection on the isotopic composition. At first sight, the isotopic composition exhibits a large variability from one line to another, which is not surprising given the differences in the squall-line structures and dynamics, as illustrated by the radar reflectivity patterns (Figure 1(b)). However, squall lines show some consistent features, confirming the robust effect of some convective processes on the isotopic composition. In particular, $\delta^{18}O_p$ exhibits a 'W' shape: $\delta^{18}O_p$ decreases at the beginning of the squall line (the range of this decrease is 0.8–3.5‰ depending on the squall line), reaching a local minimum at the core of the convective zone. It increases then (0.2–1.5‰) to reach a local maximum during the transition zone (or just after for 18 August). $\delta^{18}O_p$ decreases along the stratiform

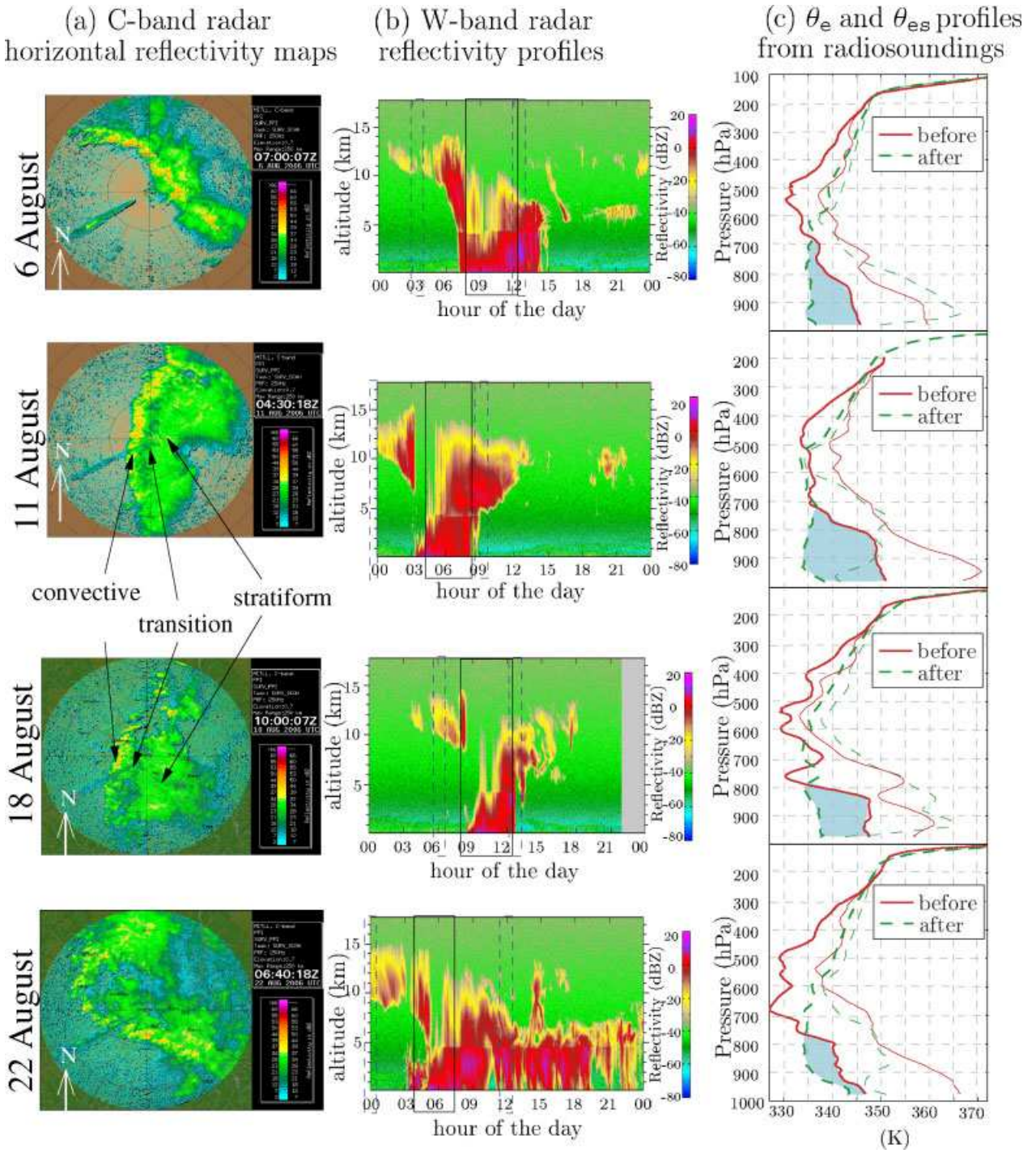

Figure 1. (a) Snapshots of C-band radar reflectivity maps for the four squall lines sampled, obtained by the MIT radar. (b) W-band reflectivity profiles obtained by the ARM radar. (c) Profiles of equivalent potential temperature (θ_e, thick) and equivalent potential temperature at saturation (θ_{es}, thin) from available radio-soundings before (solid/red) and after (dashed/green) the systems, giving information about the stabilization of the atmosphere by the system, notably through unsaturated downdraughts and mesoscale subsidence. The time of the radio-soundings is indicated in (b) by dashed/blue rectangles. A 20 hPa smoothing filter was applied for an easier visualization. Radio-soundings performed with RS80-A sondes (6 August 0300 UTC and 11 August 0900 UTC) were corrected following Nuret *et al.* (2008). In (b), the time period over which the rain was sampled is indicated by black solid rectangles. This figure is available in colour online at www.interscience.wiley.com/journal/qj

zone (0.5–1.5‰), before increasing again at the end of the squall line (0.2–1‰). Such a 'W' shape was also observed by Rindsberger *et al.* (1990) and by Taupin and Gallaire (1998) in a Niamey squall line.

The d_p value shows different evolutions in the convective zones (an increase for 6 and 18 August, a decrease for 22 August and stable for 11 August), but some robust features appear in the stratiform zone. It follows a similar pattern to $\delta^{18}O_p$, especially for 11 and 22 August: it decreases in the first portion of the transition zone (by 7–23‰ depending on the squall line), and then increases at the end of the squall line (by 5–15‰, except

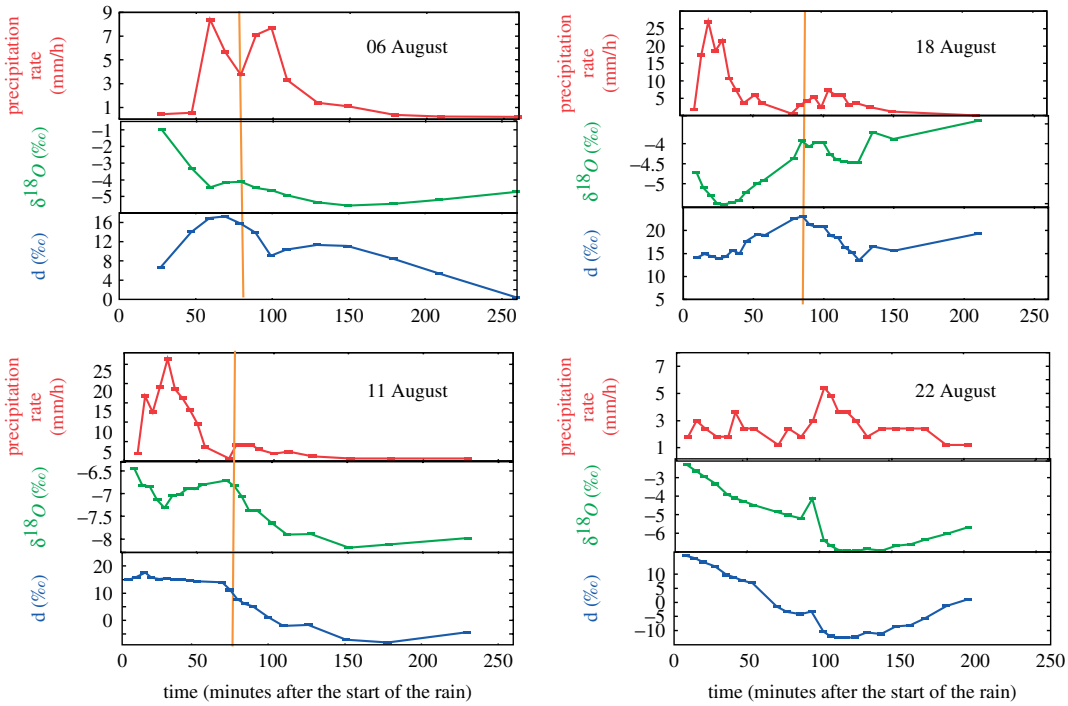

Figure 2. Evolution of precipitation rate, δ^{18}O and d-excess along the four squall lines. The vertical/orange line indicates the transition zone (defined as the local precipitation minimum between the convective and stratiform precipitation maxima), except for the 22 August squall line for which the transition zone is not obvious. This figure is available in colour online at www.interscience.wiley.com/journal/qj

for the 6 August squall line). These features were also observed by Taupin and Gallaire (1998).

2.3. Preliminary hypotheses

In this section, we present different preliminary hypotheses that may explain the observed evolution of $\delta^{18}O_p$ and d_p along squall lines (Figure 4).

2.3.1. Rain re-evaporation

In previous studies, the evolution of $\delta^{18}O_p$ and d_p during storms has often been interpreted as the signature of rain re-evaporation (Taupin and Gallaire, 1998): as rain re-evaporates, $\delta^{18}O_p$ increases (since the heavier isotopes concentrate in the condensed phase) and d_p decreases (since HDO diffuses faster than $H_2^{18}O$ out of the drop boundary layer). Re-evaporation is stronger where rainfall is weaker and relative humidity (RH) is lower: at the start, in the transition zone and at the end of the rainfall. This could explain the W shape of $\delta^{18}O_p$. Re-evaporation is also higher in the stratiform than in the convective zone (Zahiri, 2007), which could explain the decrease of d in the stratiform zone. At the start and at the end of the 6 August squall line, the opposite evolution of $\delta^{18}O_p$ and d_p further supports the role of rain re-evaporation. However, re-evaporation alone would make $\delta^{18}O_p$ and d_p vary in opposite directions all along the squall line, in contradiction with the common evolution of $\delta^{18}O_p$ and d_p observed on 11, 18 and 22 August (Figure 2). Moreover, the evolution of δD_p and $\delta^{18}O_p$ in the δD versus δ^{18}O diagram (Figure 3) does not follow the classical evaporation line with slope

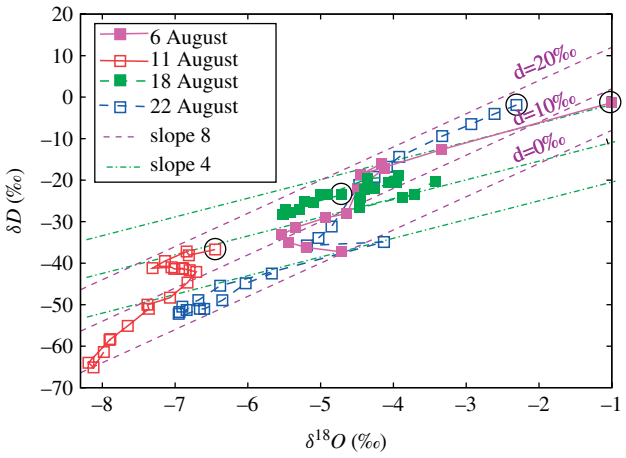

Figure 3. Evolution of δD versus δ^{18}O of the precipitation for the four squall lines sampled. The first sample is highlighted with a black circle. Lines of slope 8 and 4 are also shown. Traditionally, condensation processes at equilibrium are assumed to follow a line of slope 8 and evaporation processes with kinetic fractionation a line of slope about 4 (Dansgaard, 1964). This figure is available in colour online at www.interscience.wiley.com/journal/qj

of the order of 4 or 5 expected from the effect of evaporation (Dansgaard, 1964). Therefore, this suggests that in addition to rain re-evaporation other processes are likely to be involved. We hypothesize in the following a series of processes that might explain the observed evolution (Figure 4).

2.3.2. Condensation height

The evolution of the precipitation composition might be related to that of the condensate that forms the

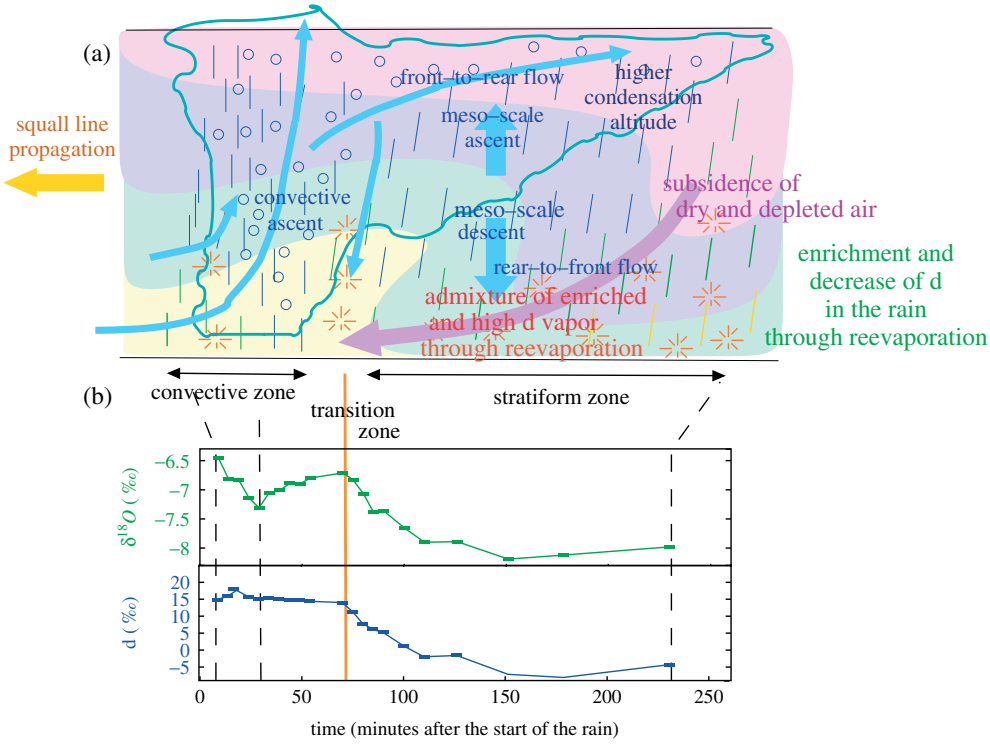

Figure 4. (a) Conceptual scheme illustrating the different mechanisms controlling the isotopic evolution along squall lines: condensation altitude, modification of the rain and low-level vapour by rain re-evaporation and diffusive exchanges and subsidence of depleted air. See section 2.3 for more details. (b) Evolution of δ^{18}O and d-excess for the 11 August squall line. This figure is available in colour online at www.interscience.wiley.com/journal/qj

precipitation. The condensate is all the more depleted as it condenses higher in altitude, since the vapour is more strongly depleted by previous condensation at higher altitude due to the lower temperature (Celle-Janton *et al.*, 2004; Gonfiantini *et al.*, 2001). We expect the condensate to form higher in altitude in the stratiform zone than in the convective zone, since the mesoscale updraught in the stratiform zone is restricted to above the 0°C isotherm approximately (Houze, 1977; Caniaux *et al.*, 1994), whereas the convective updraughts extend throughout the troposphere. This could explain why $\delta^{18}O_p$ is usually lower in the stratiform zone than in the convective zone.

2.3.3. *Re-equilibration of raindrops with vapour*

As rain falls, it partially re-equilibrates isotopically with the surrounding vapour through diffusive exchange. This process is all the more efficient as RH is high (Stewart, 1975). Through this process, variations in the composition of the low-level vapour can be transmitted to the precipitation. The following two points are possible reasons for such variations in the low-level vapour composition.

2.3.4. *Mesoscale subsidence*

Owing to fractionation during condensation, vapour is more depleted as altitude increases. Therefore, a subsiding vapour is all the more depleted as it originates from higher in altitude. In squall lines, the mesoscale downdraught, combined with the rear-to-front flow, advects depleted vapour down to low levels under the stratiform zone. Re-equilibration of the rain with more depleted vapour might explain the lower $\delta^{18}O_p$ in the stratiform zone observed in most squall lines.

Through this process, the $\delta^{18}O_p$ should decrease more strongly after the transition zone in squall lines for which the mesoscale subsidence at the rear is strongest. To verify this hypothesis, we estimate qualitatively the strength of the subsidence by analyzing profiles of equivalent potential temperature (θ_e) before and after the systems (Figure 1(c)): since θ_e is minimum in the mid-troposphere before the arrival of the systems, a strong decrease of θ_e in the lower troposphere suggests a strong subsidence (Zipser, 1977; Chalon *et al.*, 1988). The 11 August squall line, which features a strong $\delta^{18}O_p$ decrease by 1.5‰ from the transition zone to the minimum in the stratiform zone, also exhibits a strong θ_e decrease extending up to 700 hPa. Conversely, the 18 August squall line, featuring a weak $\delta^{18}O_p$ decrease of only 0.4‰, exhibits a weaker θ_e decrease restricted to below 800 hPa. The 6 August squall line is intermediate, with a $\delta^{18}O_p$ decrease by 1.4‰ and a θ_e decrease extending up to 700 hPa but weaker than that for 11 August. This comparison between the squall lines suggests that the subsidence effect on $\delta^{18}O_p$ could be substantial.

In addition, low RH at low levels associated with subsidence leads to lower d_p through rain re-evaporation. This could explain the parallel decrease of $\delta^{18}O_p$ and d_p observed after the transition zones.

2.3.5. Vapour modification through interaction with rain

As raindrops re-evaporate or re-equilibrate isotopically with the vapour, the composition of the latter is modified. In squall lines, as low-level air flows from the rear to the front, it is exposed to rain re-evaporation and becomes more and more affected by diffusive exchanges and rain re-evaporation.

For strong rates of rain re-evaporation, the vapour resulting from rain re-evaporation is richer than the vapour at low levels, since its composition tends towards that of the rain when the re-evaporation is close to total. As an idealized example, using the module of isotopic fractionation during rain re-evaporation of Bony *et al.* (2008), we calculate that at 70% relative humidity the re-evaporation of a droplet of $\delta^{18}O = -15‰$ into a vapour of $\delta^{18}O = -20‰$ (respectively $-25‰$) enriches the vapour if the re-evaporated fraction exceeds 70% (respectively 40%). The re-evaporated fraction above which the vapour becomes enriched by evaporation is all the lower when the relative humidity is high and as the vapour becomes more depleted compared with the rain.

For low evaporation rates, in contrast, diffusive exchanges dominate over rain re-evaporation. In these conditions, the vapour might become more and more depleted by interaction with the rain (Gedzelman *et al.*, 2003; Lee and Fung, 2008).

Zahiri (2007) calculated re-evaporation rates of 40–70% in the stratiform regions of Sahelian squall lines, suggesting that rain re-evaporation rather enriches the vapour in squall lines, in particular in stratiform zones.

In addition, the vapour from the rain re-evaporation has a higher d, since HDO diffuses faster than $H_2^{18}O$. Therefore, $\delta^{18}O$ and d in the vapour both increase as the air moves frontwards and is humidified by rain re-evaporation. In turn, the composition of the vapour affects the composition of the subsequent rain by isotopic equilibration (section 2.3.3). This would explain the simultaneous decrease of $\delta^{18}O_p$ and d_p rearwards along the stratiform zone after the transition zone, which is particularly visible on 11 and 22 August.

In the next section, we evaluate the relative contributions of these different processes in 2D simulations of the 11 August squall line.

3. Detailed analysis of the 11 August 2006 squall line using a 2D model

The restitution of the 3D wind field by Chong (2009) for the 11 August 2006 squall line, combined with a simple 2D model, offers a unique opportunity to evaluate the contribution of the aforementioned hypotheses. The 2D model allows us to simulate both microphysical and isotopic properties of the squall line. Although this model does not accurately simulate the observed isotopic evolution, given its simplicity (incorporating isotopes in a Cloud-Resolving Model (CRM) might be necessary for a more accurate prediction), we use it to investigate the processes controlling the isotopic composition of precipitation.

3.1. Model description

3.1.1. Model physics, boundary conditions and numerical solution

The model represents the transport and microphysics in a 2D (altitude–longitude) framework and we assume that the squall line is stationary. The model is inspired by the microphysical retrieval technique of Hauser *et al.* (1988), though simplified. The water vapour, cloud water and rain are advected in the 2D domain by 2D winds using an upstream advection scheme. Vapour condenses as soon as it reaches saturation. Microphysical processes are parametrized by the Kessler scheme (Kessler, 1969) using the same parameters as Hauser *et al.* (1988). The model also includes a representation of diffusion to ensure numerical stability.

West and east boundary conditions for RH are the 30 min averaged ARM profiles before and after the squall line (0100 UTC and 0900 UTC respectively) below 10 km and National Centers for Environmental Prediction (NCEP) profiles at 0600 UTC above this altitude. Temperature and pressure are assumed to be horizontally homogeneous and are taken from the ARM profiles at 0100 UTC below 10 km and from the reanalyses at 0600 UTC above 10 km. Our results are not significantly sensitive to the representation of horizontal temperature perturbations (section 3.4). We neglect air and water fluxes throughout the bottom and top boundaries, but a sensitivity test to the addition of surface evaporation is presented in section 3.4.

In contrast to Hauser *et al.* (1988), we here calculate the stationary solution by temporal integration, because it facilitates the subsequent implementation of water isotopes. The advection, diffusion and microphysical processes are evaluated every 30 s until reaching a steady state, after about 15 h. The model is initialized with the profiles of the west boundary conditions.

3.1.2. Wind fields

The 3D winds were retrieved following the procedure described in Chong (2009), using a squall-line propagation speed of 13.7 m/s. The wind field is highly variable in the along-line dimension, consistently with the high spatial and temporal variability pointed out by Lafore *et al.* (1988). We force the advection scheme with 2D winds obtained by averaging the 3D winds in the along-line (south–north) direction over different domains (Figure 5). Missing values are filled using a Cressman interpolation scheme as in Hauser *et al.* (1988). Winds are slightly modified so that they respect the conservation of air mass given the 2D framework and the prescribed temperature and pressure profiles. The along-line wind component is neglected. Such 2D winds are represented in Figure 6(a) and (b). Note that the domain is 122 km in the across-line direction and does not capture completely the rear of the squall line. However, extending the domain

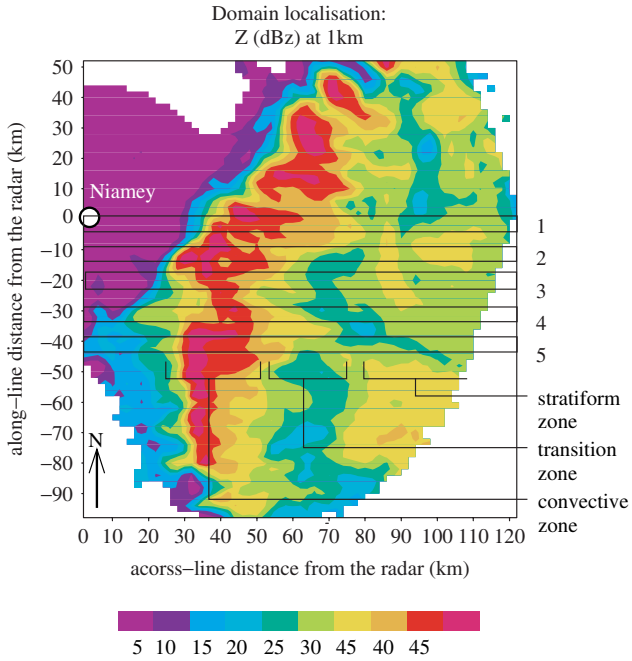

Figure 5. Horizontal reflectivity map from the MIT radar at 1 km on 11 August 2006 between 0241 and 0311 UTC, in the domain of the 3D wind retrieval extending over 120 and 150 km in the west–east and south–north directions, respectively. The five domains selected for our analysis in Figures 6 and 7 are indicated. The position of Niamey ($x = 0$ km, $y = 0$ km) is indicated by a white dot. This figure is available in colour online at www.interscience.wiley.com/journal/qj [Correction made here after initial online publication.]

by 100 km using additional wind profiles in the rear of the squall line has no influence on our results.

3.1.3. *Representation of isotopic processes*

Isotopic species are transported passively by advection and diffusion, but fractionation is introduced at each phase change. The implementation of fractionation during condensation, evaporation and diffusive exchanges is detailed in Bony *et al.* (2008). It is similar to that used in most isotopic general circulation models (Jouzel *et al.*, 1991; Hoffmann *et al.*, 1998; Noone and Simmonds, 2002b; Lee *et al.*, 2007; Tindall *et al.*, 2009) except for rain re-evaporation: we calculate explicitly the degree of equilibration between rain and vapour and take into account the concomitant evolution of both rain and vapour composition throughout the evaporation process (appendix A of Bony *et al.*, 2008).

The isotopic boundary and initial conditions are Rayleigh distillation profiles, which represent the effect of previous condensation and precipitation:

$$R_{\mathrm{v}}(z) \sim R_{\mathrm{v0}} \left(\frac{q_{\mathrm{sat}}(z)}{q_{\mathrm{v0}}} \right)^{\alpha - 1},$$

where $R_{\mathrm{v}}(z)$ is the profile of the isotopic ratio in the vapour, R_{v0} and q_{v0} are the isotopic ratio and the specific humidity at the lowest level (0–500 m), $q_{\mathrm{sat}}(z)$ is the saturation specific humidity at the temperature of level z and α is the effective fractionation (including kinetic fractionation) at the same temperature. We take $\delta^{18}\mathrm{O}_{\mathrm{v0}} = -15‰$ and $d_{\mathrm{v0}} = 10‰$ to yield $\delta^{18}\mathrm{O}_{\mathrm{p}}$ and d_{p} of the same order of magnitude as those observed (the evolution of $\delta^{18}\mathrm{O}_{\mathrm{p}}$ and d_{p} is insensitive to these values). Sensitivity to the Rayleigh assumption will be discussed in section 3.4.

3.2. Model results

Given the strong along-line variability in the wind field, we consider various cross-line transects of the squall line (Figure 5). Rather than trying to reproduce exactly the observed isotopic evolution, we explore the different dynamics based on a single squall line, as a 'proxy' for different squall lines. Figure 6 shows five of these simulations, representative of the variability range of the results. The goal is to extract the robust and consistent features among the different simulations, as well as exploring the along-line variability.

The simulated precipitation (Figure 6(e)) is of the same order of magnitude as in the observations (Figure 2), and with similar evolution: the model simulates a maximum corresponding to the convective zone and a secondary maximum corresponding to the stratiform zones. The simulated 2D fields of relative humidity (Figure 6(c)), cloud water content (Figure 6(d)), condensation, precipitation and evaporation rates (not shown) are consistent with fields retrieved by the unidimensional method of Chong (2009) for this same squall line. More generally, these fields are consistent in patterns and in magnitude with fields for other squall lines retrieved by the more sophisticated method of Hauser *et al.* (1988) or simulated by 3D models (Lafore *et al.*, 1988; Caniaux *et al.*, 1994). The physics of the squall line is thus reasonably well captured by the 2D model, and can be used to investigate isotopic controls.

The isotopic evolution of the precipitation is very sensitive to the squall-line dynamics: for the same microphysical model and the same squall line, along-line wind variations induce a strong variability in the shape of

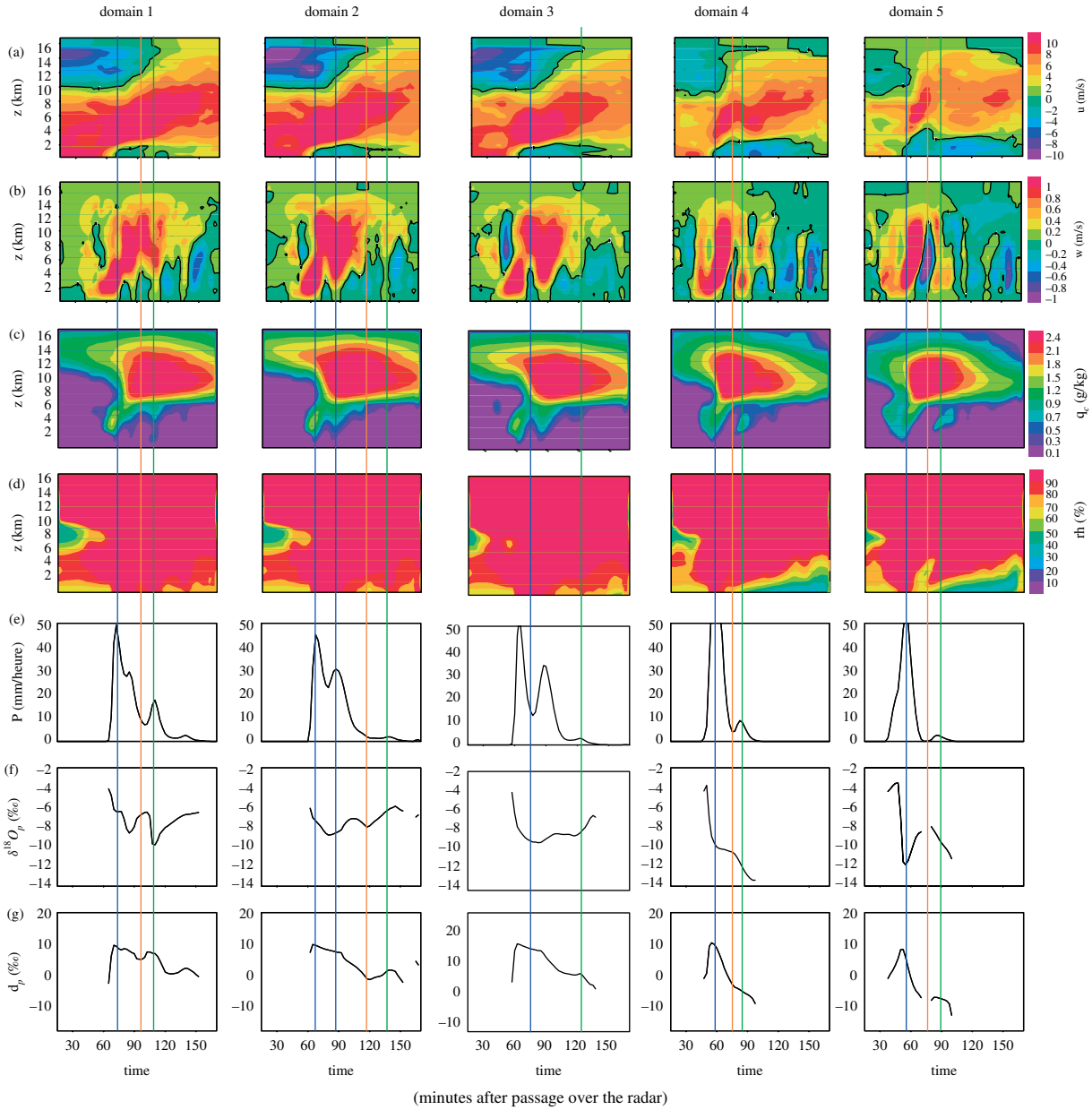

Figure 6. Five examples of simulations along different across-line transects of the 11 August 2006 squall line. (a) and (b) Across-line and vertical wind components of the 2D wind field used to force the model; the zero isoline is highlighted. (c) Simulated condensate water content (both liquid and ice). (d) Simulated relative humidity. (e), (f) and (g) Simulated evolution of the precipitation rate, δ^{18}O and d-excess. The different domains are shown in Figure 5. The vertical lines indicate the position of the convective cores (dashed/blue), transition zones (solid/orange) and stratiform precipitation maxima (dotted/green). This figure is available in colour online at www.interscience.wiley.com/journal/qj

the isotopic evolution, especially in $\delta^{18}O_p$ (Figure 6(f)). However, all simulations share the same robust features observed for the different squall lines (section 2.2), i.e. the W shape of the $\delta^{18}O_p$ evolution and the decrease of d_p.

The different simulations also span the variability observed for the different squall-line samples: domain 2, for example, features in addition to the W shape an increasing trend of δ^{18}O of about 1‰ from the convective precipitation maximum to the stratiform precipitation maximum, as observed for the 18 August squall line. On the other hand, the other domains feature decreasing trends spanning from 1–4‰, in the range of the other observed squall lines. The d_p decrease in the first part of the stratiform zone is well reproduced in all simulations (Figure 6(g)). However, the re-increase of d_p at the end of the squall line is never simulated. Also, none of the simulations was able to reproduce the particular d_p pattern of August 18, suggesting that the dynamics or microphysics of this line were unique.

3.3. Processes controlling the isotopic composition in the model

Although the exact isotopic evolution of the 11 August squall line was not reproduced, the simulated isotopic features are consistent with the observations, and the simulated along-line isotopic variability is comparable with the variability observed among squall lines. We now

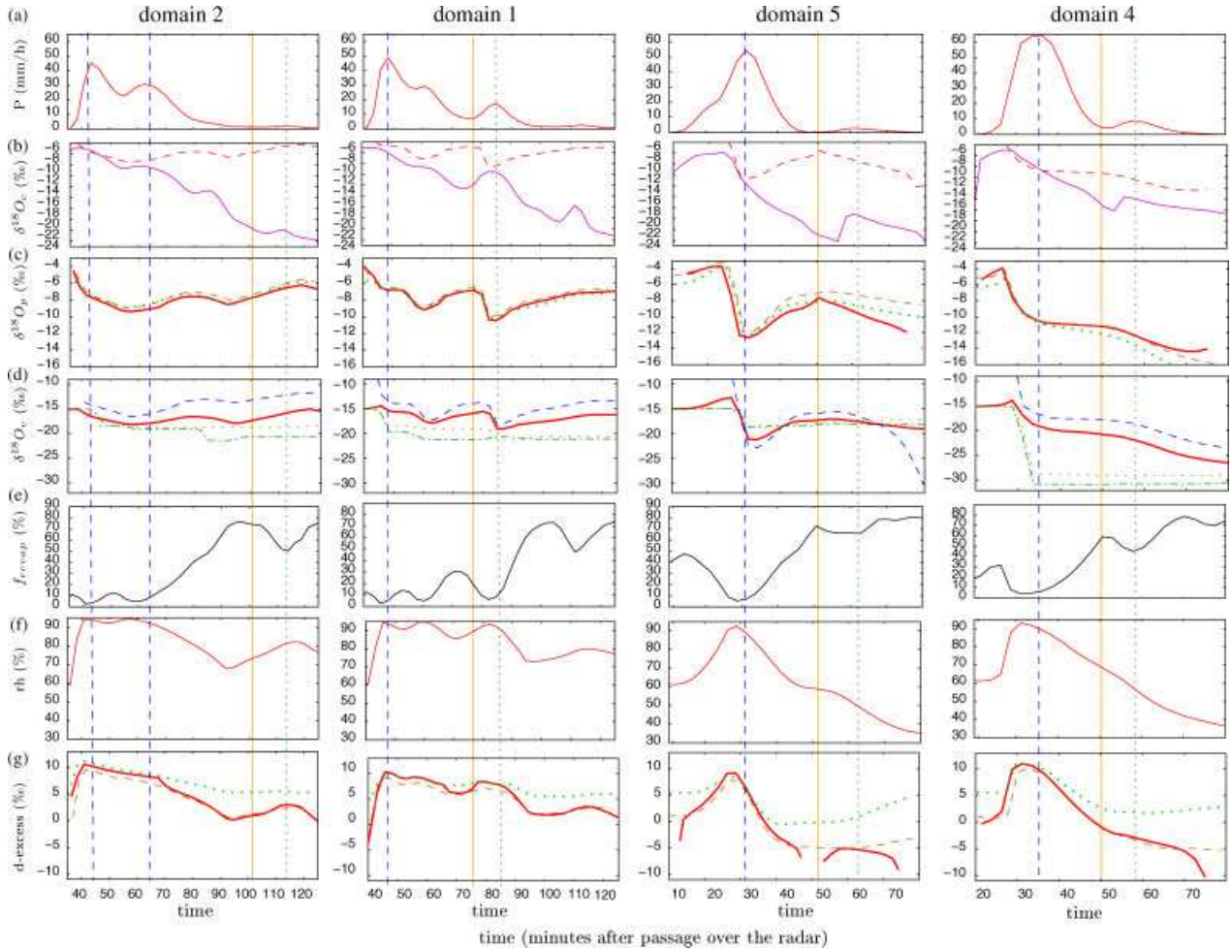

Figure 7. Evolution of some simulated characteristics illustrating what controls the isotopic evolution along the squall line in the model. (a) Precipitation rate. (b) δ^{18}O of the condensate forming the precipitation (solid/purple). The δ^{18}O of the precipitation is shown in dashed/red for comparison. (c) δ^{18}O of the precipitation simulated by the 2D model (solid/red) and predicted by the simple re-evaporation equation (1) (dashed/brown). The liquid in equilibrium with the lowest-level vapour is shown in dotted/green. (d) δ^{18}O of the vapour at the lowest level of the model: total vapour simulated by the model (thick solid/red), vapour originating from rain re-evaporation in the model (dashed/blue) and vapour advected from the different levels (dash–dotted/green). The vapour predicted by a Rayleigh distillation using the maximum altitude undergone, $\overline{z_{\max}}$, is shown in dotted/brown. (e) Fraction of the rain re-evaporated. (f) Relative humidity at the lowest level. (g) *d*-excess of the precipitation simulated by the 2D model (solid/red) and predicted by the simple re-evaporation equation (1) (dashed/brown). The liquid in equilibrium with the lowest-level vapour is shown in dotted/green. As in Figure 6, the vertical lines indicate the position of the convective cores (dashed/blue), transition zones (solid/orange) and stratiform precipitation maxima (dotted/green). This figure is available in colour online at www.interscience.wiley.com/journal/qj

use the model to explore what processes, among the ones described in section 2.3, control this isotopic evolution.

3.3.1. *Control of precipitation $\delta^{18}O$*

The evolution of $\delta^{18}O_p$ (Figure 7(c)) has no similarities with the evolution of the δ^{18}O of the condensate from which the precipitation originates ($\delta^{18}O_c$, i.e. vertically averaged δ^{18}O of the condensate weighted by the rate of conversion to precipitation, Figure 7(b)). Variations in $\delta^{18}O_c$ thus do not yield any visible variations in $\delta^{18}O_p$, suggesting that processes controlling $\delta^{18}O_c$ (such as condensation height) have little influence on $\delta^{18}O_p$. On the contrary, $\delta^{18}O_p$ tightly follows the δ^{18}O of the low-level vapour (between 0 and 500 m, hereafter $\delta^{18}O_v$, Firue 7(d)), suggesting that the precipitation re-equilibrates isotopically as it falls, 'forgetting' its condensation history.

To check this hypothesis and to interpret the isotopic ratio in the precipitation, R_p, simulated by the 2D model, we use a deliberately simple equation (Stewart, 1975):

$$R_p = R_{l0} f_r^{\beta} + \gamma R_v (1 - f_r^{\beta}), \qquad (1)$$

where R_v is the simulated isotopic ratio in the lowest-level vapour, f_r the simulated vertically integrated fraction of the rain that remains after re-evaporation (Figure 7(e)), R_{l0} the composition of the condensate that forms the precipitation and β and γ coefficients depending on low-level RH (defined by Stewart (1975) and recalled in appendix A of Bony *et al.* (2008)). This Equation (1) is a strong simplification of processes represented in the 2D model: the goal here is to reproduce the modelled results with as simple an equation as possible, to identify the dominant processes. Firstly, we assume that R_v varies little as evaporation proceeds, neglecting the

feedback of re-evaporation on R_v (Stewart, 1975). Secondly, we assume that the composition of the condensate forming the precipitation is constant ($\delta^{18}O_c = -15‰$, corresponding to the average values in the simulations), so as to check that variations in $\delta^{18}O_c$ are not a dominant control on $\delta^{18}O_p$. Thirdly, we consider only the vertically integrated f_r and take R_v and RH at the lowest level only, whereas re-evaporation is treated at all vertical levels in the 2D model.

This equation is able to reproduce well the $\delta^{18}O_p$ evolution simulated by the 2D model (Figure 7(c)), showing that variations in the condensate composition have little influence on $\delta^{18}O_p$. Rather, rain re-evaporation and isotopic equilibration with the vapour are key controls of $\delta^{18}O_p$. $\delta^{18}O_p$ is actually very close to isotopic equilibrium with the vapour (Figure 7(c)), in agreement with Lee and Fung (2008), who simulated a degree of rain–vapour equilibration above 70% over the Tropics. Therefore, understanding of $\delta^{18}O_p$ requires an understanding of what controls $\delta^{18}O_v$. This is discussed below.

3.3.2. *Control of vapour $\delta^{18}O$*

The vapour at low levels in the 2D model is a mixture of vapour originating from rain re-evaporation and vapour advected from different levels. In section 2.3, we hypothesized that rain re-evaporation and subsidence could influence the low-level vapour composition. To evaluate these two hypotheses, we implemented a method to track the vapour origin in the 2D model, as detailed in appendix A. This method allows us to estimate (1) the fraction of the vapour that originates from rain re-evaporation or advection from different levels, and (2) the isotopic composition of air parcels originating from rain re-evaporation ($\delta^{18}O_e$) or advection by the dynamics ($\delta^{18}O_{dyn}$).

Since the two sources of vapour are rain evaporation and advection by the dynamics (and more particularly by subsidence), the evolution of $\delta^{18}O_v$ is intermediate between the evolution of $\delta^{18}O_e$ and $\delta^{18}O_{dyn}$ (Figure 7(d)). For domain 4, the 11‰ decrease in $\delta^{18}O_v$ along the line is driven by the 16‰ decrease of $\delta^{18}O_{dyn}$. Since any departure of $\delta^{18}O_{dyn}$ from the boundary value of $-15‰$ is entirely due to the subsidence, this demonstrates the impact of subsidence on $\delta^{18}O_v$. More generally, the role of the dynamics is dominant in all the domains in which $\delta^{18}O_p$ features a strong depletion (more than 5‰) from the convective to the stratiform zone (not shown). For the other domains, the evolution of $\delta^{18}O_v$ follows more closely the evolution of $\delta^{18}O_e$ and is thus primarily affected by rain re-evaporation. For example, in domain 1 the 2‰ variations in $\delta^{18}O_v$ around the transition zone are due to the 3‰ variation in $\delta^{18}O_e$.

In the following paragraphs, we detail what controls the evolution of $\delta^{18}O_{dyn}$ and $\delta^{18}O_e$.

The method to track the vapour origin in the 2D model allows us to estimate the average maximum altitude reached by low-level parcels during their transport through the squall line (appendix A). The maximum altitude $\overline{z_{max}}$ that parcels have undergone is equivalent to the minimum temperature encountered (since we neglect horizontal temperature perturbations) and thus represents the maximum depletion undergone by the parcels as they condense during their ascent. The $\overline{z_{max}}$ altitude thus controls, at first order, the composition of the subsiding vapour, in an analogous way to the minimum saturation temperature encountered controlling the relative humidity of subsiding vapour (Pierrehumbert and Roca, 1998). Indeed, as shown in Figure 7(d) (dashed), a simple Rayleigh distillation predicts well the composition of the vapour advected by the dynamics $\delta^{18}O_{dyn}$:

$$R_{dyn} \sim R_{v0} \left(\frac{q_{sat}(\overline{z_{max}})}{q_{v0}} \right)^{\alpha - 1},$$

where R_{v0} and q_{v0} are the composition and specific humidity of the boundary vapour at low levels, and α the effective isotopic fractionation. Note that this equation neglects the effect of cloud and rain re-evaporation on the vertical isotopic profiles.

Due to the squall-line dynamics (mesoscale downdraught and rear-to-front flow), $\overline{z_{max}}$ increases from the convective to the stratiform zone. For domain 4, $\overline{z_{max}}$ increases from 0 km at the beginning of the line (no subsidence) to 2.5 km in the stratiform zone, leading to the strong decrease of $\delta^{18}O_{dyn}$ (from -15 to $-31‰$) and thus that of $\delta^{18}O_v$ (-15 to $-22‰$) and $\delta^{18}O_p$ (-4 to $-12‰$). This confirms the importance of mesoscale subsidence in the control of isotopic composition of the vapour and precipitation along squall lines.

On the other hand, the composition of the re-evaporated vapour ($\delta^{18}O_e$) follows the evolution of the re-evaporated fraction f_{revap}. Indeed, the higher f_{revap}, the more enriched the vapour from rain re-evaporation. As expected from section 2.3.5, the rain re-evaporation is generally more enriched than the vapour, by 1–4‰. In addition to the effect of f_{revap}, the evolution of $\delta^{18}O_e$ is modulated by how the squall-line dynamics transports the re-evaporated vapour.

To conclude regarding the control of $\delta^{18}O_p$ in the 2D model, $\delta^{18}O$ in vapour and thus in precipitation is controlled by two processes: (1) mesoscale subsidence of depleted air and (2) admixture of vapour arising from the re-evaporation of the falling rain and transported by the squall-line dynamics. Note that the controls on low-level RH are very similar: subsidence brings dry air downwards, while evaporation moistens this air as it moves frontwards under the stratiform region.

3.3.3. *Control of precipitation deuterium excess*

The evolution of deuterium excess in precipitation (d_p) follows very tightly that of low-level (0–500 m) RH (Figure 7(f) and (g)). d_p thus seems to be mainly controlled by RH during rain re-evaporation: the lower the RH, the more dominant kinetic fractionation is relative to equilibrium fractionation, and thus the lower d_p. The good prediction of the d_p evolution by Equation (1) (Figure 7(g); dashed), which includes the effect of

low-level RH, confirms that re-evaporation is the key control on d_p.

The linear correlation coefficient between the evolution of d_p and low-level RH (where the precipitation is significant: > 0.5 mm/h) varies from 0.90–0.97 for the different domains (not shown). The relationship d_p–RH is robust, with a slope ranging from 0.30–0.37‰/%. In our model, d_p is thus an excellent indicator of the RH. However, this d_p–RH relationship cannot be checked with observations, because although we do have RH measurements at the surface along the squall line sampled, the RH at the surface does not accurately reflect the low-level RH that affects the isotopic composition of the rain.

3.4. Sensitivity tests to dynamics, microphysics and isotopes

We discuss below the sensitivity of our results to different assumptions made in our model.

3.4.1. Horizontal temperature perturbations

We neglect horizontal perturbations in the 2D model, whereas Hauser *et al.* (1988) evaluated temperature perturbations of the order of −4 K in the rear-to-front flow. Decreasing the temperature by about 4 K in the rear-to-front flow slightly increases the relative humidity by 10% locally, increases $\delta^{18}O_p$ by 2‰ and d_p by about 5‰. However, it does not qualitatively change the isotopic evolution.

3.4.2. Rayleigh assumption

In nature, isotopic profiles in the upper troposphere are usually more enriched than predicted by a Rayleigh distillation, due to convective detrainment (Moyer *et al.*, 1996; Dessler and Sherwood, 2003; Webster and Heymsfield, 2003; Bony *et al.*, 2008). Here we consider Rayleigh distillation as west and east boundary conditions. However, modifying the isotopic profile at upper levels does not affect our results much: when assuming that 50% of the condensate formed during the Rayleigh distillation is detrained rather than instantaneously precipitated (leading to an enrichment of up to 70‰ at 16 km), $\delta^{18}O$ only increases by 1–2‰ in the stratiform zone.

3.4.3. Microphysics

We also performed sensitivity tests to microphysics (not shown). Little isotopic sensitivity was found to Kessler parameter variations, even though the precipitation evolution was sometimes deeply distorted. This confirms that the dynamic control dominates. The isotopic parameter ϕ (controlling the intensity of kinetic effects during evaporation, see appendix A of Bony *et al.*, 2008) was the only isotopic parameter to have a significant sensitivity. When $\phi = 0$ (strong kinetic effects), $\delta^{18}O_p$ is increased by 3‰ and d_p is decreased by 10‰ at the start and the rear of the squall line, where evaporation is the strongest and the atmosphere the driest. This confirms that the details of the parametrization of the isotopic behaviour during re-evaporation are crucial in dry conditions. However, this parameter had little influence on the evolution in the convective and stratiform zones.

The drop-size distribution has been shown to influence the isotopic evolution of the rain as it re-evaporates (Lee and Fung, 2008). However, explicitly taking into account the effect of the drop-size distribution, rather than assuming homogeneous drop sizes, has little influence on our 2D model results. In our model, the rain drop-size distribution influences the re-evaporated fraction f_{revap}, since the smallest drops would re-evaporate totally whereas the largest drops conserve most of their mass. In a sensitivity experiment, the drop-size distribution was determined by the Kessler microphysics scheme (Kessler, 1969) and isotopic calculations were performed in each of 40 size bins. The results were virtually unchanged, except in extremely dry re-evaporation conditions. For example, for $f_{revap} = 80\%$ and $h = 50\%$, $\delta^{18}O_p$ in the squall-line precipitation was decreased by 2‰ and d_p was increased by 1‰ when taking into account the drop-size distribution.

3.4.4. Surface evaporation

None of our simulations is able to reproduce the d_p increase observed at the end of most squall lines. A possible interpretation might be the re-evaporation of the water accumulated on the soil, neglected in our model, which would increase d_v and thus d_p by re-equilibration of raindrops with the vapour. To check this hypothesis, we performed simulations in which we added surface evaporation, calculated by a simple Penman-like equation (appendix B). A large uncertainty in this calculation is the net radiation minus soil heat flux, $R_n - G$, under the heavy cloud cover of a squall line. Therefore, we performed tests with different values for $R_n - G$. As justified in appendix B, we take $R_n - G = 150$ W/m^2 as an upper bound for a midday squall line, and $R_n - G = 0$ W/m^2 for a night-time squall line.

For $R_n - G = 150$ W/m^2 (midday), the resulting evaporation reaches maxima of 6 mm/day in the stratiform zone for domains with very dry air in the stratiform zone (domains 4, 5) and 3 mm/day for domains with wetter air (domains 1, 2). For $R_n - G = 0$ W/m^2 (night), the evaporation peaks at 2 mm/day. The moistening effect of surface evaporation is very small. It is maximum for squall lines with dry stratiform regions (domains 4 and 5) at midday, but the relative humidity is increased by only 4–6%. This is because the surface evaporation flux under the squall line is much smaller than the vapour flux from advection, due to the small spatial scale of the squall line.

The effect on $\delta^{18}O_p$ is negligible (always lower than 1‰). The d of the evaporation flux, d_{sfc}, is highly sensitive to the kinetic fractionation formulation. Taking Mathieu and Bariac (1996)'s formulation for a saturated soil, d_{sfc} is 140‰ higher than d_v. The d_v is increased by 7‰ at midday in dry stratiform zones, but only by 2–3‰ in wetter stratiform zones at midday and by less than 1‰ during the night. This effect of surface evaporation on

d_v is almost totally transmitted to d_p. The transmission of the d_v anomaly to d_p is by rain re-equilibration with the vapour, since the vapour from surface evaporation is only confined to low levels due to the subsidence in the stratiform zone.

Therefore, the effect of surface evaporation on d_p may be significant for dry stratiform zones at midday. However, the increase of d_p at the end of the 22 August stratiform zone by 15‰ presumably does not result from surface evaporation only. Since the 11 August squall line occurred mainly during night-time, the 5‰ increase in d_p is also not attributable to surface evaporation only.

4. Summary and conclusions

4.1. Summary

This paper presents the evolution of precipitation $\delta^{18}O$ and d along different squall lines observed in the Sahel during the AMMA campaign. Despite a large variability in the isotopic evolution among the different squall lines, some robust features appear, such as the W shape of $\delta^{18}O_p$ and the decrease of d_p in the stratiform region. Several processes may a priori contribute to such evolution, such as the condensation altitude, modifications of the rain composition as it re-evaporates during its fall and variations of the composition of the vapour with which the rain re-equilibrates, due either to subsidence or to interaction with the falling rain.

To test these hypotheses and explore the relative contributions of the dynamics and the microphysics of the squall line to the evolution of the isotopic composition of the rain, a simple 2D model of transport and microphysics forced by observed wind fields was developed. The 2D model run on various along-line transects is able to simulate isotopic evolutions consistent with observations and with a comparable amplitude of variability. In the model, $\delta^{18}O_p$ is mainly controlled by (1) the squall-line dynamics: mesoscale subsidence in the stratiform portion of the system advects depleted water vapour downward and the horizontal flows redistribute this vapour in the low levels, and (2) the re-evaporation of the rain, which moistens the low-level vapour and affects its composition.

4.2. What can we learn from water isotopes about squall lines?

The robust features of the evolution of $\delta^{18}O_p$ and d_p along squall lines demonstrate the strong influence of convective processes on the isotopic composition. $\delta^{18}O_p$ is particularly sensitive to both the squall-line dynamics and rain re-evaporation processes, and could thus provide some integrated information about the dynamics within the squall line (e.g., the vertical Lagrangian excursions of the air parcels). On the other hand, d_p is a more direct tracer of rain re-evaporation, and the 2D model suggests a very robust relationship between d_p and relative humidity of the air at low levels. If incorporated into a CRM, stable water isotopes could thus serve as a tool to validate the squall-line dynamics or the recycling of water through rain re-evaporation.

4.3. Implication for the control of the composition of tropical precipitation on larger scales

One of the goals of this study was to better understand the effect of convective processes on the composition of tropical precipitation. Risi *et al.* (2008a), in very different conditions (a single-column model over the ocean), suggested that the effect of condensation processes was relatively small compared with the effect of two other processes, namely (1) rain re-evaporation, enriching the raindrops as they fall and (2) mesoscale subsidence of higher altitude vapour, depleting the low-level vapour. The minimal effect of condensation processes is confirmed in this study: as the raindrops re-equilibrate with the low-level vapour, they totally 'forget' the effect of condensation processes, in agreement with Lee and Fung (2008). This study also confirms the strong effects of rain re-evaporation (especially on d_p) and mesoscale subsidence (particularly on $\delta^{18}O_p$). The primary control of the isotopic composition of tropical precipitation by rain re-evaporation and mesoscale subsidence or convective-scale downdraughts thus seems to occur over a wide range of conditions and time and space scales.

In addition, the 2D model suggests that rain re-evaporation has a significant role on the vapour $\delta^{18}O$. Using global satellite data, Worden *et al.* (2007) had already cited rain re-evaporation as a control for vapour $\delta^{18}O$. However, they hypothesized that rain re-evaporation depletes the vapour, whereas our study suggests that rain re-evaporation tends to enrich the low-level vapour. The difference is due to (1) the strong re-evaporation of the rain in our case, which invalidates the approximation made in Worden *et al.* (2007) that the composition of the evaporation does not depend on the re-evaporated fraction of the rain, and (2) the strong depletion of the low-level vapour by mesoscale subsidence in our case (neglected in Worden *et al.*, 2007). Based on our results, we would therefore suggest that the strong depletion of water vapour observed by Worden *et al.* (2007) is related to unsaturated downdraughts and mesoscale subsidence associated with convection (Zipser, 1977).

The large temporal $\delta^{18}O_p$ variations along squall lines (up to 5‰ in the 6 and 22 August squall lines) are almost the same order of magnitude as the intraseasonal variations of the event-averaged isotopic composition after the onset, with $\delta^{18}O_p$ ranging from -1.5‰ to -7.5‰ (Risi *et al.*, 2008b). This raises the question of the role of individual squall-line dynamics in controlling the $\delta^{18}O_p$ at the intraseasonal scale. However, no correlation was found between $\delta^{18}O_p$ and the rainfall amount or type of system at the scale of individual events: $\delta^{18}O_p$ instead seems to record a large-scale, low-frequency signal of intraseasonal variability. Using the 2D model, we investigated the effect of $\delta^{18}O_p$ perturbations of the vapour at different levels on the event-averaged precipitation. A

$\delta^{18}O$ perturbation in the monsoon flow layer (0–3 km) is almost totally (85%) imprinted in the averaged $\delta^{18}O_p$. In contrast, perturbations at the level of the African Easterly Jet (3–6 km), which are potentially larger (Bony *et al.*, 2008), are only partially (15%) imprinted in the averaged $\delta^{18}O$. This is because $\delta^{18}O_p$ is mainly controlled by the $\delta^{18}O$ of low level vapour, and the stratiform zone, affected by $\delta^{18}O$ perturbations at higher levels through subsidence, contributes little to the total precipitation. We hypothesize that $\delta^{18}O_p$ temporally integrates the convective activity because convection strongly affects the $\delta^{18}O$ of the boundary-layer vapour, which in turn then controls the $\delta^{18}O_p$ of the following rain event. More work is needed to understand the relative impact on the isotopic composition of tropical precipitation of (1) the dynamics and convective processes in individual convective systems and (2) the impact of larger-scale processes imprinted in the large-scale vapour feeding the systems at different levels.

4.4. Perspectives

We are aware of the limits of the 2D model, due to the simple microphysics parametrization, assuming that the squall line is stationary and neglecting the along-line wind component. In particular, Lafore *et al.* (1988) and Redelsprger and Lafore, 1987) have shown that along-line variability in the 3D wind field and transient flows substantially contributes to the moisture transport. We are not able to simulate the observed evolution accurately, although all observed evolution is in the range of the various simulations performed. Incorporating stable water isotopes into a CRM could be a next step. The coupling of such a model with a detailed soil model would also enable a more quantitative estimate of the effect of surface evaporation on the isotopic composition at the end of squall lines.

In addition, measuring the isotopic composition simultaneously in the precipitation and in the vapour would yield invaluable information about what controls $\delta^{18}O_p$ and d_p: it would allow us to evaluate the degree of re-equilibration of raindrops with the low-level vapour, which might depend on drop size (Lee and Fung, 2008). Similar evolution in the precipitation and vapour would confirm good re-equilibration between the rain and vapour and would support the idea that the dynamics and the modification of the vapour by re-evaporation are the main controls of $\delta^{18}O_p$. On the other hand, the converse would indicate that, contrary to our model, the precipitation does not re-equilibrate well with the vapour, and the conditions of rain re-evaporation as well as the condensation altitude would contribute more significantly to the observed $\delta^{18}O_p$ variations. More systematic measurements of stable water isotopes in vapour and in precipitation during field experiments focused on tropical convection, or in instrumented sites, would thus be very valuable to discriminate between these two hypotheses, and more generally to better document the evolution of rain re-evaporation and mesoscale subsidence in convective systems.

Appendix

Appendix A: Tagging water and isotopic species in the 2D transport and microphysics model

Tracking the origin of water and isotopes has been implemented in several isotopic general circulation models (Cole *et al.*, 1999; Delaygue *et al.*, 2000); Werner *et al.*, 2001; Noone and Simmonds, 2002a) to determine the geographic origin of water vapour. Here, we use the same tracking concept, but for tracking altitude and re-evaporation. We define n altitude layers, and refer to the summit and middle of the layer $j \in [1, n]$ as z_s^j and z_m^j. We consider $n = 4$ layers: 0–2 km, 2–4 km, 4–6 km, $>$ 6 km. We also define $n + 1$ 2D fields X_v^j corresponding to vapour tracers: n fields for tracking the n altitude layers, and one field to track re-evaporation. At each time and in each grid box, the sum of these tracers is equal to that of the total vapour content q_v:

$$\sum_{j=1}^{n+1} X_v^j = q_v,$$

so that the vapour can be exactly decomposed into the $n + 1$ origins. Similarly, additional tracer fields are defined for the condensate and the precipitation, q_c and q_p, as well as for all the isotopic species in vapour, condensate and precipitation.

In the initial state, we assume that all the vapour originates from the lowest layer: $X_v^j = 0$ for $j \in [2, n + 1]$ and $X_v^1 = q_v$. Then, during the simulation, all tracers are advected passively like 'normal' water and isotopes, and behave similarly during phase changes. However, after advection, the following operation is performed so that tracers trace the maximum altitude encountered: at each grid point (let z be the altitude of the grid point), for each of the tracer layers $j \in [1, n - 1]$, if both $X_v^j > 0$ and $z > z_s^j$ then the content of X_v^j is transferred to X_v^{j+1}. In addition, to track the water originating from rain re-evaporation, all the rain that re-evaporates, whatever its origin, is transferred to X_v^{n+1}. One can thus estimate, at each grid point, the fraction of the vapour that has originated from rain re-evaporation, r_e:

$$r_e = \frac{X_v^{n+1}}{q_v}.$$

Approximating the average altitude of the tracers in each layer by the altitude of the middle of the layer, z_m^j, we can also estimate the maximum altitude encountered by the vapour on average, $\overline{z_{max}}$:

$$\overline{z_{max}} = \frac{\sum_{j=1}^{n} (X_v^j z_m^j)}{\sum_{j=1}^{n} X_v^j}.$$

Note that the estimate of $\overline{z_{max}}$ bears uncertainties due to the heterogeneous distribution of the tracers in each altitude layer. The uncertainty is half the thickness of the layers, i.e. 1 km.

Appendix B: Surface evaporation

To estimate the effect of surface evaporation on the rain isotopic composition, we calculate the surface evaporation E as

$$E = \lambda(EP),$$

with EP the potential evaporation and λ a parameter depending on the soil water q_{soil}. We assume that the soil becomes quickly saturated as rain falls: $\lambda = 1$ when $q_{\mathrm{soil}} > 10$ mm and $\lambda = q_{\mathrm{soil}}/10$ otherwise, with q_{soil} in mm. The soil water at grid point i is calculated using the precipitation and evaporation rates between the beginning of the line and point i:

$$q_{\mathrm{soil}}(i) = \sum_{j=1}^{i} \{P(j) - E(j)\} \frac{\Delta x}{u_{\mathrm{SL}}}, \tag{B1}$$

with P the precipitation rate, u_{SL} the advection speed of the squall line and Δx the horizontal resolution of the model.

We calculate the potential evaporation using a Penman-like equation (Penman (1948), used for Niger by Wallace and Holwill (1997)):

$$EP = \frac{R_{\mathrm{n}} - G}{L_{\mathrm{v}}} \frac{\Delta}{\Delta + \gamma} + \rho \frac{1}{r} \{q_{\mathrm{s}}(T_{\mathrm{a}}) - q_{\mathrm{a}}\} \frac{\gamma}{\Delta + \gamma},$$

with $\Delta = [L_{\mathrm{v}} q_{\mathrm{s}}(T_{\mathrm{a}})]/(R_{\mathrm{d}} T_{\mathrm{a}}^2)$, $\gamma = c_{\mathrm{p}}/L_{\mathrm{v}}$, $1/r = C_{\mathrm{d}} u$, L_{v} the latent heat of vaporization, q_{s} the specific humidity at saturation, R_{d} the perfect gas constant, T_{a} and q_{a} the air temperature and specific humidity in the lowest layer (0–500 m), c_{p} and ρ the heat capacity and volumetric mass of air, u the wind speed, c_{d} a drag coefficient set to 1.2×10^{-3}, R_{n} the net radiation and G the heat flux to the soil. We neglect the presence of vegetation, which is very sparse in Niamey.

We then add this evaporated water directly into the lowest layer of the model, neglecting the effect of turbulence on vapour transport. This approximation is justified because most of the evaporation occurs in the stratiform zone associated with subsidence.

There is a large uncertainty in the calculation of the net radiation term $R_{\mathrm{n}} - G$. We thus tested two extreme values, for night-time and for midday. During the night, R_{n} is close to 0 W/m^2 or slightly negative in the Sahel (Wallace and Holwill, 1997; Guichard *et al.*, 2008). At midday in August, R_{n} under clear sky is of the order of 700 W/m^2 (Guichard *et al.*, 2008). During the passage of a non-precipitating cloud system, data show a reduction of R_{n} by half (F. Guichard, personal communication). Assuming $G \simeq 0.4 R_{\mathrm{n}}$ (Wallace and Holwill, 1997), an upper bound for $R_{\mathrm{n}} - G$ at midday is thus about 150 W/m^2. We test $R_{\mathrm{n}} - G$ values between 0 and 150 W/m^2.

For isotopes, we calculate that the soil composition R_{soil} at point i using the precipitation and evaporation rates P and E and their compositions R_{p} and R_{e} between the beginning of the line and point i, in a similar way to Equation (B1). The simulated soil composition is close to the composition of the convective rain, because it is more abundant than the stratiform rain and because evaporation is negligible compared to precipitation on the scale of a squall line.

We use the Craig and Gordon (1965) equation to calculate the composition of the surface evaporation:

$$R_{\mathrm{e}} = \frac{1}{\alpha_{\mathrm{K}}} \frac{\frac{R_{\mathrm{soil}}}{\alpha_{\mathrm{eq}}} - h R_{\mathrm{v}}}{1 - h},$$

with h the relative humidity in the lowest layer, R_{v} the isotopic composition of the vapour and α_{eq} and α_{K} the equilibrium and kinetic fractionation coefficients. We use the kinetic fractionation formulation from Mathieu and Bariac (1996):

$$\alpha_{\mathrm{K}} = \left(\frac{D}{D'}\right)^{n'_k},$$

with n'_k an exponent taking into account the ratio of molecular versus turbulent diffusivities of vapour and varying from 0.67 for saturated soil conditions to 1 in dry soils (Mathieu and Bariac, 1996). We take $n'_k = 0.67$, by assuming saturated soil conditions. The resulting kinetic fractionations are $\alpha_{\mathrm{K}} - 1 = 19.0‰$ for $H_2^{18}O$ and 16.8‰ for HDO.

The d-excess of the evaporation flux is highly sensitive to the formulation of the kinetic fractionation. If taking the kinetic fractionation values from Merlivat and Jouzel (1979), for example, the d-excess of the evaporative flux would be four times smaller.

Acknowledgements

We thank J.-P. Lafore, Aaron Boone, Françoise Guichard and J.-Y. Grandpeix for useful discussions and suggestions, M. Nuret for providing corrected RS80-A radiosoundings, S. Falourd and B. Minster for helping with the isotopic measurements, E. Williams for providing the MIT radar data, the AMMA database for providing snapshots of the MIT radar and ARM data, and two anonymous reviewers for their interesting comments and suggestions.

Based on a French initiative, AMMA was built by an international scientific group and is currently funded by a large number of agencies, especially from France, the United Kingdom, the United States and Africa. It has been the beneficiary of a major financial contribution from the European Community's Sixth Framework Research Programme. Detailed information on scientific coordination and funding is available on the AMMA International web site http://www.amma-international.org.

This work was funded by the IPSL project, AMMA API and MISTERRE programme.

References

Barras V, Simmonds I. 2009. Observation and modelling of stable water isotopes as diagnostics of rainfall dynamics over southeastern Australia. *J. Geophys. Res.* In press.

Bony S, Risi C, Vimeux F. 2008. Influence of convective processes on the isotopic composition (deltaO18 and deltaD) of precipitation and water vapour in the Tropics. Part 1: Radiative–convective equilibrium and TOGA–COARE simulations. *J. Geophys. Res.* **113**: D19 305–. DOI:10.1029/2008JD009 942

Caniaux G, Redelsperger JL, Lafore JP. 1994. A numerical study of the stratiform region of a fast moving squall line. Part 1: General description and water and heat budgets. *J. Atm. Sci* **51**: 2046–2074.

Celle-Jeanton H, Gonfiantini R, Travia Y, Solc B. 2004. Oxygen-18 variations of rainwater during precipitation: Application of the Rayleigh model to selected rainfalls in Southern France. *J. Hydrol.* **289**: 165–177.

Chalon JP, Jaubert G, Lafore JP, Roux F. 1988. The West African squall line observed on 23 June 1981 during COPT 81: Mesoscale structure and transports. *J. Atmos. Sci.* **45**: 2744–2763.

Chong M. 2009. The 11 August 2006 squall-line system as observed from MIT Doppler radar during the AMMA SOP. *Q. J. R. Meteorol. Soc.* **136**(s1): 210–227

Chong M, Hauser D. 1990. A tropical squall line observed during the COPT81 experiment in West Africa: Part III: heat and moisture budgets. *Mon. Weather Rev.* **118**: 1696–1706.

Cole JE, Rind D, Webb RS, Jouzel J, Healy R. 1999. Climatic controls on interannual variability of precipitation delta18O: Simulated influence of temperature, precipitation amount, and vapour source region. *J. Geophys. Res.* **104**: 14 223–14 236. DOI 10.1029/1999JD900182

Craig H, Gordon LI. 1965. Deuterium and oxygen-18 variations in the ocean and marine atmosphere. *Stable Isotope in Oceanographic Studies and Paleotemperatures*.

Dansgaard W. 1964. Stable isotopes in precipitation. *Tellus* **16**: 436–468.

Delaygue G, Masson V, Jouzel J, Koster RD, Healy RJ. 2000. The origin of Antarctic precipitation: A modelling approach. *Tellus* **52B**: 19–36.

Dessler AE, Sherwood SC. 2003. A model of HDO in the tropical tropopause layer. *Atmos. Chem. Phys.* **3**: 2173–2181.

Emanuel KA. 1991. A scheme for representing cumulus convection in large-scale models. *J. Atmos. Sci.* **48**: 2313–2329.

Fudeyasu H, Ichiyanagi K, Sugimoto A, Yoshimura K, Ueta A, Yamanaka MD, Ozawa K. 2008. Isotope ratios of precipitation and water vapour observed in Typhoon Shanshan. *J. Geophys. Res.* **113**: D12 113–. DOI:10.1029/2007JD009 313

Gedzelman S, Lawrence J, Gamache J, Black M, Hindman E, Black R, Dunion J, Willoughby H, Zhang X. 2003. Probing hurricanes with stable isotopes of rain and water vapour. *Mon. Weather Rev.* **131**: 112–1127.

Gonfiantini R, Roche MA, Olivry JC, Fontes JC, Zuppi GM. 2001. The altitude effect on the isotopic composition of tropical rains. *Chem. Geol.* **181**: 147–167.

Guichard F, Kergoat L, Mougin E, Timouk F, Baup F, Hiernaux P, Lavenu F. 2008. Surface thermodynamics and radiative budget in the Sahelian Gourma: Seasonal and diurnal cycles. *J. Hydrol.* DOI:10.1016/j.jhydrol.2008.09.007

Hauser D, Roux F, Amayenc P. 1988. Comparison of two methods for the retrieval of thermodynamic and microphysical variables from Doppler radar measurements: application to the case of a tropical squall line. *J. Atmos. Sci.* **45**: 1285–1303.

Hoffmann G, Werner M, Heimann M. 1998. Water isotope module of the ECHAM atmospheric general circulation model: A study on timescales from days to several years. *J. Geophys. Res.* **103**: 16 871–16 896. DOI: 10.1029/98JD00423

Houze RA. 1977. Structure and dynamics of a tropical squall line system. *Mon. Weather Rev.* **105**: 1540–1567.

Janicot S, Thorncroft D, Ali A, Asencio N, coauthors. 2008. Large-scale overview of the summer monsoon over West and Central Africa during the AMMA field experiment in 2006. *Ann. Geophys.* **26**: 2569–2595.

Jouzel J, Koster R, Suozzo R, Russell G, White J, Broecker W. 1991. Simulations of the HDO and H2O-18 atmospheric cycles using the NASA GISS general circulation model: Sensitivity experiments for present-day conditions. *J. Geophys. Res.* **96**: 7495–7507.

Kessler E. 1969. On the distribution and continuity of water substance in atmospheric circulation. *Meteorol. Monographs* **32**: 84.

Lafore JP, Redelsperger JL, Jaubert G. 1988. Comparison between a three-dimensional simulation and Doppler radar data of a tropical squall line: Transports of mass, momentum, heat and moisture. *J. Atmos. Sci.* **45**: 3483–3500.

Lee JE, Fung I. 2008. 'Amount effect' of water isotopes and quantitative analysis of post-condensation processes. *Hydrol. Processes* **22**: 1–8.

Lee JE, Fung I, DePaolo D, Fennig CC. 2007. Analysis of the global distribution of water isotopes using the NCAR atmospheric general circulation model. *J. Geophys. Res.* **112**: D16 306. DOI:10.1029/2006JD007 657

Mathieu R, Bariac T. 1996. A numerical model for the simulation of stable isotope profiles in drying soils. *J. Geophys. Res.* **101**: 12 685–12 696.

Merlivat L, Jouzel J. 1979. Global climatic interpretation of the Deuterium–Oxygen 18 relationship for precipitation. *J. Geophys. Res.* **84**: 5029–5332.

Moyer EJ, Irion FW, Yung YL, Gunson MR. 1996. ATMOS stratospheric deuterated water and implications for troposphere–stratosphere transport. *Geophys. Res. Lett.* **23**: 2385–2388. DOI: 10.1029/96GL01489

Noone D, Simmonds I. 2002a. Annular variations in moisture transport mechanisms and the abundance of deltaO18 in Antarctic snow. *J. Geophys. Res.* **107**: 4742. DOI:4710.1029/2002JD002 262

Noone D, Simmonds I. 2002b. Associations between delta18O of water and climate parameters in a simulation of atmospheric circulation for 1979–95. *J. Climate* **15**: 3150–3169.

Nuret M, Lafore JP, Guichard F, Redelsperger JL, Bock O, Augusti-Panareda A, N'Gamini JB. 2008. Correction of humidity bias for Vaisala RS80-A sondes during the AMMA 2006 observing period. *J. Atmos. Oceanic Technol.* **25**: 2152–2158.

Penman HL. 1948. Natural evaporation from open water, bare soil and grass. *Proc. R. Soc. London Ser. A* **193**: 120–145.

Pierrhumbert RT, Roca R. 1998. Evidence for control of Atlantic subtropical humidity by large scale advection. *Geophys. Res. Lett.* **25**: 4537–4540.

Redelsperger JL, Lafore JP. 1987. A three dimensional simulation of a tropical squall line: Convective organisation and thermodynamic vertical transport. *J. Atmos. Sci.* **47**: 1334–1356.

Redelsperger JL, Thorncroft C, Arona D, Lebel T, Parker D, Polcher J. 2006. African Monsoon Multidisciplinary Analysis: An international research project and field campaign. *Bull. Am. Meteorol. Soc.* **87**: 1739–1746.

Rindsberger M, Jaffe S, Rahamim S, Gat R. 1990. Patterns of the isotopic composition of precipitation in time and space: Data from the Israeli storm water collection program. *Tellus* **42**: 263–271.

Risi C, Bony S, Vimeux F. 2008a. Influence of convective processes on the isotopic composition (O18 and D) of precipitation and water vapour in the Tropics: Part 2: Physical interpretation of the amount effect. *J. Geophys. Res.* **113**.

Risi C, Bony S, Vimeux F, Descroix L, Ibrahim B, Lebreton E, Mamadou I, Sultan B. 2008b. What controls the isotopic composition of the African monsoon precipitation? Insights from event-based precipitation collected during the 2006 AMMA campaign. *Geophys. Res. Lett.* **35**: DOI:10.1029/2008GL035 920

Sherwood SC, Wahrlich R. 1999. Observed evolution of tropical deep convective events and their environment. *Mon. Weather Rev.* **127**: 1777–1795.

Stewart MK. 1975. Stable isotope fractionation due to evaporation and isotopic exchange of falling waterdrops: Applications to atmospheric processes and evaporation of lakes. *J. Geophys. Res.* **80**: 1133–1146.

Taupin JD, Gallaire R. 1998. Variabilité isotopique à l'échelle infra-événement de quelques épisodes pluvieux dans la région de Niamey, Niger. *C.R.A.S.* **326**: 493–498.

Tindall JC, Valdes P, Sime LC. 2009. Stable water isotopes in HadCM3: Isotopic signature of El Nino–Southern Oscillation and the tropical amount effect. *J. Geophys. Res.* **114**: D04 111–. DOI:04 110.01 029/02 008JD010 825

Wallace J, Holwill C. 1997. Soil evaporation from Tiger-bush in south-west Niger. *J. Hydrol.* **188–189**: 426–442.

Webster CR, Heymsfield AJ. 2003. Water isotope ratios D/H, 18O/16O, 17O/16O in and out of clouds map dehydration pathways. *Science* **302**: 1742–1746. DOI: 10.1126/science.1089496

Werner M, Heimann M, Hoffmann G. 2001. Isotopic composition and origin of polar precipitation in present and glacial climate simulations. *Tellus* **53B**: 53–71. DOI: 10.1034/j.1600-0889.2001.01154.x

Williams E, Rutledge SA, Geotis SG, Renno N, Rsmussen E, Rickenbach T. 1992. A radar and electrical study of Tropical 'hot towers'. *J. Atmos. Sci.* **49**: 1386–1395.

Worden J, Noone D, Bowman K. 2007. Importance of rain evaporation and continental convection in the tropical water cycle. *Nature* **445**: 528–532.

Zahiri EP. 2007. '*Cycle de l'eau des systèmes convectifs ouest-africains: preparation à l'exploitation des mesures radar xport dans amma par simulations*'. PhD thesis. Université Paul Sabatier – Toulouse III: Toulouse.

Zipser E. 1977. Mesoscale and convective scale downdrafts as distinct components of squall-line structure. *Mon. Weather Rev.* **105**: 1568–1589.

JOURNAL OF GEOPHYSICAL RESEARCH, VOL. 115, D12118, doi:10.1029/2009JD013255, 2010

Water-stable isotopes in the LMDZ4 general circulation model: Model evaluation for present-day and past climates and applications to climatic interpretations of tropical isotopic records

Camille Risi,[1] Sandrine Bony,[1] Françoise Vimeux,[2] and Jean Jouzel[3]

Received 27 September 2009; revised 18 December 2009; accepted 13 January 2010; published 23 June 2010.

[1] We present simulations of water-stable isotopes from the LMDZ general circulation model (the LMDZ-iso GCM) and evaluate them at different time scales (synoptic to interannual). LMDZ-iso reproduces reasonably well the spatial and seasonal variations of both $\delta^{18}O$ and deuterium excess. When nudged with reanalyses, LMDZ-iso is able to capture the synoptic variability of isotopes in winter at a midlatitude station, and the interannual variability in mid and high latitudes is strongly improved. The degree of equilibration between the vapor and the precipitation is strongly sensitive to kinetic effects during rain reevaporation, calling for more synchronous vapor and precipitation measurements. We then evaluate the simulations of two past climates: Last Glacial Maximum (21 ka) and Mid-Holocene (6 ka). A particularity of LMDZ-iso compared to other isotopic GCMs is that it simulates a lower d excess during the LGM over most high-latitude regions, consistent with observations. Finally, we use LMDZ-iso to explore the relationship between precipitation and $\delta^{18}O$ in the tropics, and we discuss its paleoclimatic implications. We show that the imprint of uniform temperature changes on tropical $\delta^{18}O$ is weak. Large regional changes in $\delta^{18}O$ can, however, be associated with dynamical changes of precipitation. Using LMDZ as a test bed for reconstructing past precipitation changes through local $\delta^{18}O$ records, we show that past tropical precipitation changes can be well reconstructed qualitatively but not quantitatively. Over continents, nonlocal effects make the local reconstruction even less accurate.

Citation: Risi, C., S. Bony, F. Vimeux, and J. Jouzel (2010), Water-stable isotopes in the LMDZ4 general circulation model: Model evaluation for present-day and past climates and applications to climatic interpretations of tropical isotopic records, *J. Geophys. Res.*, *115*, D12118, doi:10.1029/2009JD013255.

1. Introduction

[2] Because of differences in mass and symmetry of the main isotopic forms of the water molecule ($H_2^{16}O$, HDO, $H_2^{18}O$), an isotopic fractionation occurs during phase changes depending on atmospheric conditions. As a consequence, water-stable isotopes are widely used as a tracer of past climate variations and of the present-day water cycle. In particular, the isotopic composition recorded in polar ice cores have long been used to reconstruct past temperatures [*Dansgaard*, 1953; *Jouzel*, 2003]. More recently, the isotopic composition recorded in low-latitude ice cores [*Thompson et al.*, 2000; *Ramirez et al.*, 2003] or speleothems [*Wang et al.*, 2008; *Cruz et al.*, 2005a] have also been used to infer past temperatures [*Thompson et al.*, 2000] or precipitation rates [*Hoffmann et al.*, 2003].

[3] However, processes that control the water isotopic composition are numerous and complex. For the Greenland ice cores, for example, using the spatial slope as a surrogate for the temporal slope to evaluate past local temperature changes leads to a large uncertainty of a factor of 2 [*Jouzel*, 1999; *Jouzel*, 2003]. This could be due to a change in air mass origins [*Werner et al.*, 2001] or in precipitation seasonality [*Krinner et al.*, 1997b; *Krinner and Werner*, 2003], or to a dampening of isotopic changes by ocean evaporation [*Lee et al.*, 2008]. At low latitudes, the paleoclimatic interpretation of isotopic records is even less quantitative. Most of the tropical precipitation arises from convective processes, which strongly affect the isotopic composition of both vapor and precipitation [*Lawrence et al.*, 2004; *Bony et al.*, 2008; *Risi et al.*, 2008a, 2008b]. While the earliest interpretation of Andean ice cores had linked isotopes to temperatures [*Thompson et al.*, 2000], more recent studies have stressed the importance of the precipitation intensity upstream the air mass trajectories [*Hoffmann*, 2003; *Vimeux et al.*, 2005] and the role of tropical Pacific sea surface temperatures (SSTs) on the isotopic variability in Andean ice core records [*Bradley et al.*, 2003]. As a consequence, while Rayleigh distillation models (representing the loss of

[1] LMD, IPSL, UPMC, CNRS, Paris, France.
[2] UR Great Ice, IRD, LSCE, IPSL, (CEA, CNRS, UVSQ), Gif-sur-Yvette, France.
[3] LSCE, IPSL (CEA, CNRS, UVSQ), Gif-sur-Yvette, France.

0148-0227/10/2009JD013255

heavier isotopes during condensation and precipitation) are useful to study at first order the evolution of air masses as they are transported from a moisture source region to higher latitudes [*Ciais and Jouzel*, 1994], more complex models are necessary to take into account the numerous processes affecting the isotopic composition of precipitation.

[4] Atmospheric general circulation models (GCM) are now frequently used for isotopic studies. They represent the three-dimensional transport of air masses and isotopes as well as large-scale condensation and atmospheric convection, albeit in a parameterized way. Since the pioneering work of *Joussaume et al.* [1984], water isotopes have been implemented in at least a half-dozen GCMs: GISS [*Jouzel et al.*, 1987; *Schmidt et al.*, 2007], ECHAM [*Hoffmann et al.*, 1998], MUGCM [*Noone and Simmonds*, 2002a], GENESIS [*Mathieu et al.*, 2002], CAM [*Lee et al.*, 2007], GSM [*Yoshimura et al.*, 2008], Hadley GCM [*Tindall et al.*, 2009] as well as in regional models (REMO [*Sturm et al.*, 2005]). They have been used, for example, to better understand how the climatic signal is recorded by isotopes in ice cores, at the interannual to decadal time scales [*Vuille et al.*, 2003; *Vuille and Werner*, 2005] and at paleoclimatic time scales [*Werner et al.*, 2001].

[5] In this paper, we present the implementation of water-stable isotopes in the LMDZ4 model (whose isotopic version is hereafter named LMDZ-iso). The LMDZ4 model is the GCM developed at the Laboratoire de Mtorologie Dynamique (LMD) [*Hourdin et al.*, 2006]. It is the atmospheric component of the Institut Pierre Simon Laplace (IPSL) ocean-land-atmosphere coupled model [*Marti et al.*, 2005] that participated in CMIP3 [*Meehl et al.*, 2007]. Its dynamical and physical packages have completely changed since the pioneering work of *Joussaume et al.* [1984]. An interesting particularity of this GCM now is the possibility of using stretched grids [*Hourdin et al.*, 2006], allowing studies at both global and regional scales [e.g., *Krinner et al.*, 1997a].

[6] The first goal of this paper is to evaluate the simulation of water-stable isotopes by LMDZ-iso at different time scales. We evaluate the present-day isotopic spatial and seasonal distribution and the isotopic variability at time scales ranging from synoptic to interannual. For this purpose, we have performed an Atmospheric Model Intercomparison Project (AMIP) [*Gates*, 1992] simulation forced by monthly observed SSTs from 1979 to 2007. To evaluate the isotopic simulation in a more rigorous way, we have also performed an AMIP simulation over the same period with the large-scale atmospheric dynamics nudged by meteorological reanalyses. Since a particular effort has been invested in the representation of the droplet reevaporation in the model [*Bony et al.*, 2008], we pay particular attention to evaluating the equilibrium between droplets and water vapor using simultaneous vapor and precipitation data available at some stations. We also pay a lot of attention to evaluating the d excess, which is sensitive to kinetic fractionation notably during rain reevaporation. Finally, we evaluate the isotopic distribution for two past climates for which isotopic data are available: Last Glacial Maximum (21,000 years ago, 21 ka) and Mid-Holocene (6 ka).

[7] The second goal is to use LMDZ-iso to investigate the controls of the isotopic composition of precipitation in the tropics, where the paleoclimatic interpretation is the most uncertain. In particular, what are the relative influences of temperature and precipitation changes on the isotopic composition of tropical precipitation? How useful may $\delta^{18}O$ records be for reconstructing past local precipitation changes in the tropics?

[8] In section 2, we describe the LMDZ4 model, the implementation of water-stable isotopes and the various simulations performed. In section 3, we evaluate the simulation of the isotopic composition for the present-day climatology, synoptic variability, interannual variability and past climates. In section 4, we use LMDZ-iso to explore what paleoclimatic information is recorded in tropical isotopic records. We conclude and give perspectives in section 5.

2. Model and Simulations Description

[9] In this section we briefly describe the LMDZ4 GCM, the implementation of water-stable isotopes and the different simulations performed.

2.1. LMDZ4 GCM

[10] The dynamical equations are discretized in a latitude-longitude grid, with a standard resolution of 2.5° × 3.75° and 19 vertical levels. Water in its vapor and condensed forms is advected by the Van Leer advection scheme [*Van Leer*, 1977], which is a monotonic second-order finite volume scheme. The physical package is described in detail by *Hourdin et al.* [2006]. It includes in particular the Emanuel convective parameterization [*Emanuel*, 1991; *Grandpeix et al.*, 2004] coupled to the *Bony and Emanuel* [2001] cloud scheme. Each grid cell is divided into four subsurfaces: ocean, land, ice sheet and sea ice. In the stand-alone version of LMDZ4 used here, the land surface is represented as a simple bucket model, and land surface evaporation is calculated as a single flux: no distinction is made between transpiration, bare soil evaporation, or evaporation of intercepted water by the canopy.

2.2. Isotopic Processes

[11] Water isotopic species ($H_2^{16}O$, $H_2^{18}O$ and HDO) are transported and mixed passively by the large-scale advection and various air mass fluxes. In the Van Leer advection scheme, it is assumed that the water content advected from one box to the next is a linear combination of the water contents in the two grid boxes involved. For numerical reasons, we assume similarly that the isotopic ratio of the water advected from one box to the next (rather than the isotopic content) is a linear combination of the isotopic ratios in the two grid boxes involved (Appendix A).

[12] Equilibrium fractionation coefficients between vapor and liquid water or ice are calculated after *Merlivat and Nief* [1967] and *Majoube* [1971a, 1971b]. We take into account kinetic effects during the evaporation from the sea surface following *Merlivat and Jouzel* [1979] and during snow formation following *Jouzel and Merlivat* [1984], with the supersaturation parameter λ set to 0.004 to optimize the simulation of d excess over Antarctica (section 3.1.1).

[13] Given the simplicity of the land surface parameterization in LMDZ4, no information is available about the fraction of the evapo,transpiration flux arising from fractionating evaporation (e.g., evaporation of bare soil [*Barnes and Allison*, 1988]). We thus assume no fractionation during

the evapotranspiration over land, as done in most other GCMs [e.g., *Hoffmann et al.*, 1998; *Lee et al.*, 2007]. The coupling with the more detailed land surface scheme ORCHIDEE [*Ducoudré et al.*, 1993; *Rosnay and Polcher*, 1998; *Krinner et al.*, 2005] will be reported in a subsequent paper.

[14] The implementation of water-stable isotopes in the convective scheme has been extensively described by *Bony et al.* [2008]. We pay particular attention to the representation of the reevaporation and diffusive exchanges as the rain falls, which is significantly different compared to other GCMs. While the proportion of the drop that reequilibrates isotopically is prescribed in many GCMs [e.g., *Hoffmann et al.*, 1998], here the relative proportion of evaporative enrichment and diffusive equilibration is calculated depending on relative humidity following *Stewart* [1975]. In addition, the model takes into account the evolution of the compositions of both the rain and the surrounding vapor as the rain drops reevaporate [*Bony et al.*, 2008]. However, when the relative humidity is 100% we simply assume total reequilibration between raindrops and vapor, contrary to *Stewart* [1975] and *Lee and Fung* [2008], who take into account the raindrop size distribution in this particular case.

2.3. Simulations

2.3.1. AMIP Simulations

[15] A first 1979–2007 simulation has been performed following the AMIP protocol [*Gates*, 1992], using prescribed monthly and interannually varying SST and sea ice and a constant CO_2 value of 348 ppm. We allowed a spin-up time of 17 months before January 1979. This simulation is named "free." Another simulation, named "nudged," uses the same protocol but was nudged by the three-dimensional horizontal winds from ERA-40 reanalyses [*Uppala et al.*, 2005] until 2002 and operational analyses thereafter. We did not notice any discontinuity associated with this change in the nudging data set. The simulated wind fields are relaxed toward the reanalyzed winds with a time constant τ = 1 h, so that each component of the horizontal wind field u verifies the following differential equation:

$$\frac{\partial u}{\partial t} = \sum_{i=1}^{n} U_i + \frac{u_{obs} - u}{\tau}$$

where u_{obs} is the reanalysis wind and U_i are the temporal tendencies of each of the n dynamical and physical packages in the model.

[16] The 17 month spin-up time seems to be enough to reach an equilibrium: for example, in the nudged simulation, the globally and annually average $\delta^{18}O$ in precipitation for 1979 is −7.56‰, very close to the average value over 1979–2007 of −7.55‰ compared to the range of interannual variability of 0.06‰ over 1979–2007.

2.3.2. Sensitivity Tests

[17] Sensitivity tests to tunable parameters in the physical or isotopic parameterization have been performed on 3 year simulations with climatological SST, with a spin-up of 17 months. The sensitivities to parameters discussed in this paper are much larger than the interannual variability, justifying shorter simulations that are computationally less expensive than the AMIP 1979–2007 simulations.

[18] Additional 6 year simulations have been performed using the same protocol, but with uniform SST perturbations (as suggested by *Cess and Potter* [1988]): −4 K, −2 K, and +2 K. The sea ice distribution is not modified consistently with the SST in these simulations, but we restrict their analysis to tropical regions in this paper.

2.3.3. Past Climate Simulations

[19] As suggested by the Paleoclimate Model Intercomparison Project (PMIP) project [*Joussaume and Taylor*, 1995; *Braconnot et al.*, 2007] and as in other isotopic modeling studies [e.g., *Jouzel et al.*, 2000], we perform past climate simulations for two periods: the Last Glacial Maximum (LGM, 21 ka) and the Mid-Holocene (MH, 6 ka). For both these periods, a large amount of data is available for model evaluation. These simulations are 5 years long, with a spin-up of 17 months.

[20] A first LGM simulation was performed following a protocol similar to PMIP1 [*Joussaume and Taylor*, 1995], using the Climate: Long-Range Investigation, Mapping, and Prediction (CLIMAP) [*CLIMAP Project Members*, 1981] SST and sea ice, a CO_2 concentration of 180 ppm, orbital parameters following *Berger* [1978]. We set the sea surface $\delta^{18}O$ to 1.2‰ [*Labeyrie et al.*, 1987] and d to 0‰. Contrary to the PMIP1 protocol, we use the *Peltier* [1994] ICE-5G ice sheet reconstruction (as in the work by *Lee et al.* [2008] and PMIP2 [*Braconnot et al.*, 2007]), which differs from the ICE-4G reconstruction (from *Peltier* [1994], used by *Joussaume and Jouzel* [1993] and *Jouzel et al.* [2000]) in the spatial extent and height of Northern Hemisphere ice sheets. Except for the different ice sheet topography, our simulation is similar to that performed by *Joussaume and Jouzel* [1993], *Jouzel et al.* [2000], and *Werner et al.* [2001].

[21] The MH simulations were performed following the PMIP1 protocol, as in work by *Jouzel et al.* [2000]. The only changes compared to present day are the orbital configuration [*Berger*, 1978] and atmospheric gas concentrations (CO_2 concentration of 280 ppm).

[22] The LGM and MH simulations are compared to the free AMIP simulation, considered as a reference for present day (PD).

[23] The warm tropical SSTs and the extensive sea ice of the CLIMAP reconstruction have been questioned [e.g., *MARGO Project Members*, 2009]. Therefore, as in work by *Lee et al.* [2008], we perform an additional simulation using the SST and sea ice simulated by a coupled model (here the IPSL model [*Marti et al.*, 2005] for LGM conditions. We use here the climatological SST from an LGM simulation performed under the PMIP2 protocol (*Braconnot et al.* [2007], with LGM orbital configuration and a CO_2 concentration of 185 ppm), averaged over 50 years. However, significant SST biases in the IPSL model are common to all climate conditions, including LGM and PD. Therefore the direct comparison between SSTs simulated for LGM by the IPSL model ($T_{LGM/IPSL}$) and SSTs observed at PD (T_{PD}) is misleading: SST biases in the IPSL model could be confused with LGM-PD signals. To circumvent this problem, we use the SSTs from an IPSL model pre-industrial simulation (PI) simulation, performed following the PMIP2 protocol (with present-day orbital configuration and a CO_2 concentration of 280 ppm). We force our additional LGM simulation with $T'_{LGM/IPSL} = T_{LGM/IPSL} - T_{PI} + T_{PD}$. This way, the biases in the IPSL model common to both the

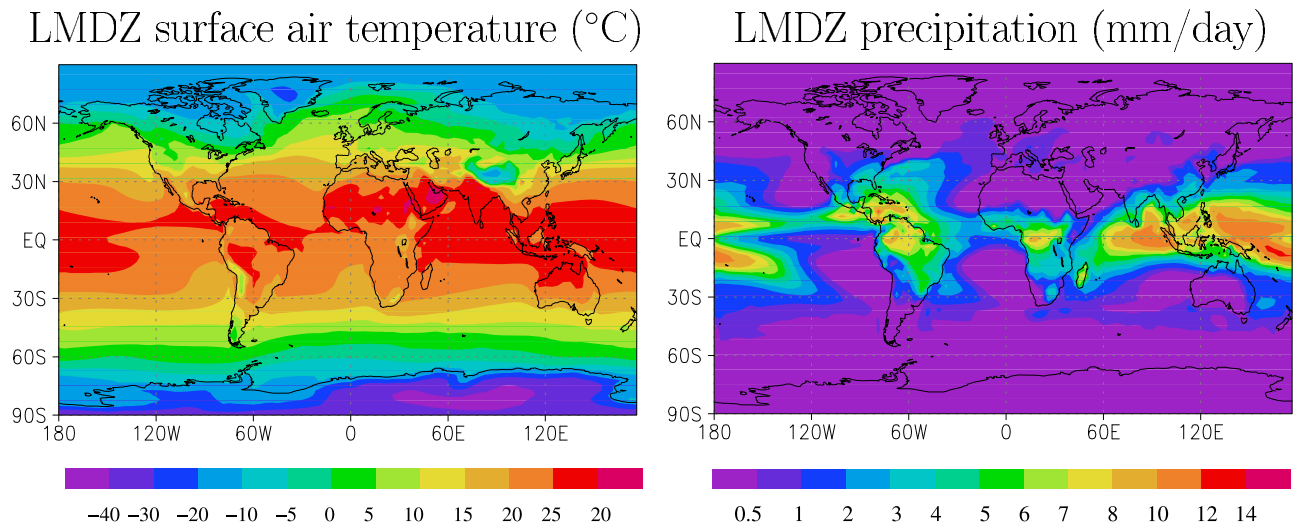

Figure 1. Annual mean (left) temperature and (right) precipitation in the LMDZ-iso nudged simulation.

LGM and PI simulations are canceled out. We can thus compare our LGM isotopic simulations from both CLIMAP and IPSL SSTs in a consistent way.

3. Evaluation and Sensitivity Tests

[24] The present-day climate simulated by LMDZ4 has been extensively evaluated by *Hourdin et al.* [2006]. The mean annual temperature and precipitation maps in the nudged simulation are given in Figure 1 for reference. We focus here on the isotopic simulation. First, we examine the isotopic spatial and seasonal distribution, then its variability at synoptic to interannual time scales in the present-day climate, and finally we evaluate isotopic variations associated with past climates.

[25] We present an evaluation of $\delta^{18}O$, expressed in permil, defined as

$$\delta = \left(\frac{R_{\text{sample}}}{R_{\text{SMOW}}} - 1\right) \cdot 1000,$$

where R_{sample} and R_{SMOW} are the ratio of HDO or $H_2^{18}O$ over $H_2^{16}O$ in the sample and the Standard Mean Ocean Water (SMOW) reference, respectively. At first order, variations in δD follow the same patterns as $\delta^{18}O$ but are 8 times larger. The deviation to this behavior is quantified by the deuterium excess: $d = \delta D - 8 \cdot \delta^{18}O$ [*Dansgaard*, 1964]. This second-order parameter is known to be more difficult to simulate by GCMs [*Lee et al.*, 2007; *Mathieu et al.*, 2002]. We thus present an evaluation of this parameter as well, which is expected to provide stronger constraints on the simulated hydrological and isotopic processes.

3.1. Evaluation of the Spatial and Seasonal Distributions

[26] We use in this section the whole AMIP simulations averaged over the period 1979–2007 to produce average seasonal cycles. We compare the spatial distribution and seasonal cycle with the Global Network of Isotopes in Precipitation (GNIP) data [*Rozanski et al.*, 1993], to which we add data from Antarctica (compiled by *Masson-Delmotte et al.* [2008]) and Greenland (compiled by *Masson-Delmotte et al.* [2005b]). Note that since we compare point data with simulated values averaged over a GCM grid box, the scale mismatch may contribute to the model data difference.

3.1.1. Annual Mean Spatial Distribution of Isotopes in Precipitation

[27] The spatial distribution of annual mean $\delta^{18}O$ in precipitation ($\delta^{18}O_p$) is well simulated in the model, featuring the well-known "effects" [*Rozanski et al.*, 1993]: enhanced depletion with decreasing temperature ("temperature effect"), increasing altitude ("altitude effect") or continentality ("continental effect"), or precipitation intensity ("amount effect") (Figure 2). The $\delta^{18}O_p$ over central Greenland and Antarctica is however overestimated, owing to an overestimated temperature over Antarctica (minimum annual temperature over Antarctica of −42°C in nudged LMDZ-iso and −60°C in the work by *Masson-Delmotte et al.* [2008]). This warm bias is frequent in GCMs [*Masson-Delmotte et al.*, 2006] and is worsened when nudging the model with meteorological reanalyses. The temperature effect in Antarctica is, however, relatively well reproduced, with a spatial slope of 0.73‰/K (r = 0.95) in the data and 0.65‰/K in the model (r = 0.97) over the temperature range simulated by LMDZ-iso (Figure 3).

[28] The deuterium excess in precipitation (d_p) is of the right order of magnitude over most regions except on tropical continents (simulated d_p too high by up to 10‰ over equatorial Africa and northern South America). LMDZ-iso reproduces the d minimum over high-latitude oceans [*Uemura et al.*, 2008] and features a relationship with δD consistent with observations over Antarctica (Figures 3 and 4). LMDZ-iso also captures the d_p maximum over the Middle East, as was also the case in other GCMs [*Hoffmann et al.*, 1998; *Schmidt et al.*, 2007]. LMDZ-iso simulates the spatial distribution reasonably well compared to other GCMs: *Yoshimura et al.* [2008] report spatial correlations between 0.39 and 0.52 between observed and simulated annual d_p values in four isotopic GCMs; LMDZ-iso value is 0.45. However, d_p is slightly underestimated by

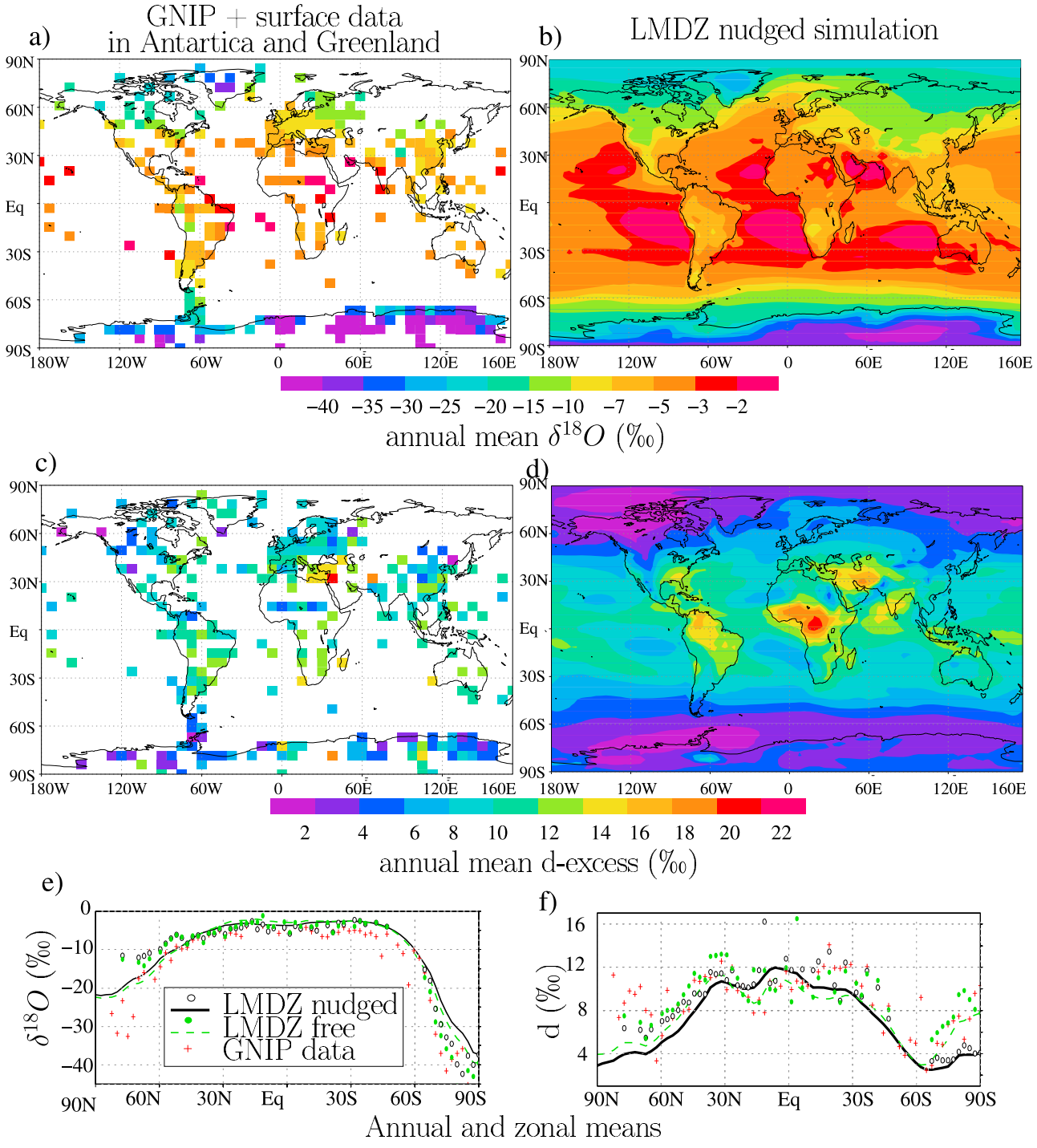

Figure 2. (a, b) Annual mean $\delta^{18}O$ and (c, d) d excess in precipitation, in the data (Figures 2a and 2c) and the LMDZ-iso nudged simulation (Figures 2b and 2d). The data are the GNIP data [*Rozanski et al.*, 1993], the Antarctica data from *Masson-Delmotte et al.* [2008], and Greenland surface data [*Masson-Delmotte et al.*, 2005b]. The data are gridded over a coarse 7.5 × 6.5° grid for visualization purpose. The simulation is the nudged simulation averaged over the 1979–2007 period. Zonal means of the annual averages of (e) δ^{18}O and (f) d excess for the data (red crosses), the nudged simulation (solid black curve), and the free simulation (dashed green curve). The lines are zonal averages for LMDZ-iso simulations, and the points are the values at data stations.

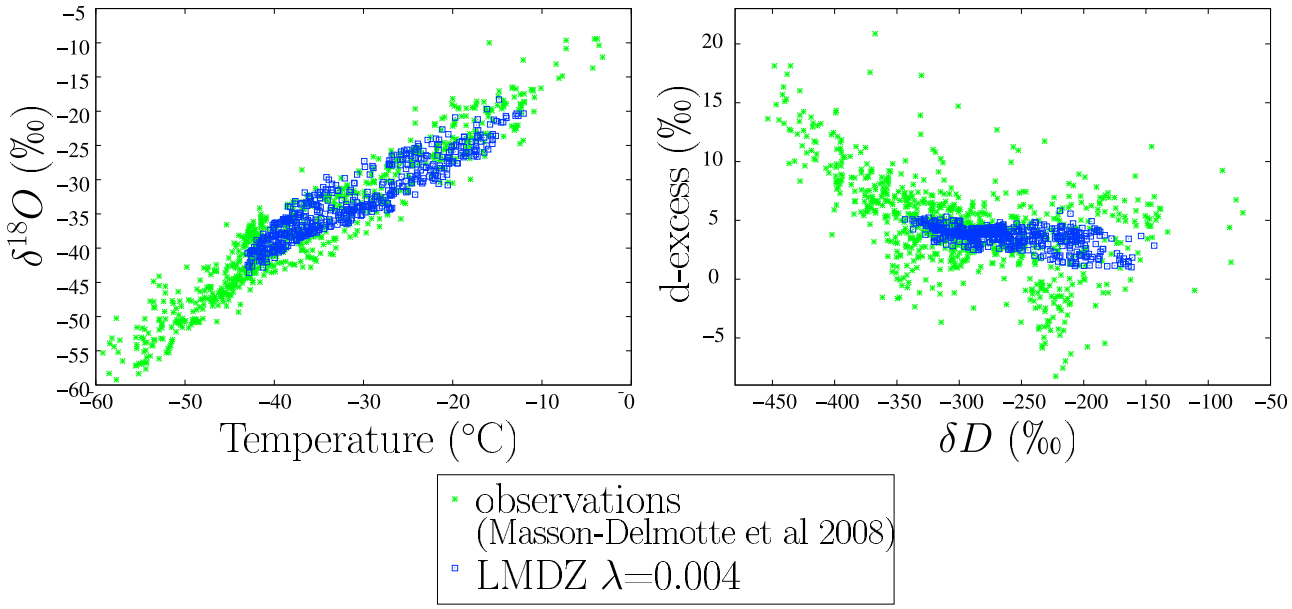

Figure 3. (left) Annual mean δD as a function of annual mean air temperature at first level and (right) annual mean d excess as a function of annual mean δD in precipitation, in the data from *Masson-Delmotte et al.* [2008] (green) and in the LMDZ-iso nudged simulation (blue).

LMDZ-iso at high latitudes, in particular over northwestern America, the Arctic Ocean, and central Antarctica. It is slightly overestimated in convective regions of tropical South America and Africa. Regional patterns in d_p over the tropics differ strongly among the models, in particular over continents. The GISS fully coupled model [*Schmidt et al.*, 2007] and the ECHAM atmospheric GCM [*Hoffmann et al.*, 1998], for example, do not show higher d_p values over South America than over the surrounding oceans, contrary to LMDZ-iso and GNIP. The difference seems unrelated to the representation of fractionating evaporation at the land surface, which is absent in both LMDZ-iso and ECHAM. Instead, it might reveal a different simulated response of d_p to convective activity, which is known to differ between continents and oceans [*Nesbitt and Zipser*, 2003; *Liu and Zipser*, 2005].

[29] The parameter λ, controlling kinetic effects during snow formation, is known to have a strong impact on the d of snowfall in Antarctica [*Jouzel and Merlivat*, 1984; *Schmidt et al.*, 2005]. Typical values for λ are 0.002 [e.g., *Landais et al.*, 2008], 0.003 [e.g., *Hoffmann et al.*, 1998; *Noone and Simmonds*, 2002a] or 0.004 [e.g., *Schmidt et al.*, 2007; *Vimeux et al.*, 2001; *Stenni et al.*, 2001]. In LMDZ-iso, setting λ to 0.002 leads to very strong d_p values over central Antarctica (up to 28‰), whereas setting λ to 0.004 gives results more consistent with the data (Figure 4).

3.1.2. Seasonal Cycles of Isotopes in Precipitation

[30] Figure 5 compares the observed and simulated seasonal cycles of temperature, precipitation, $\delta^{18}O_p$ and d_p over five GNIP stations representative of various climatic conditions (Table 1): Reykjavik (northern Atlantic), Vienna (central Europe), Manaus (Amazon), Apia (western tropical Pacific) and Ankara (Eastern Mediterranean). The seasonal cycles of $\delta^{18}O_p$ are generally well reproduced by LMDZ-iso, especially in the nudged simulation.

[31] On the other hand, the seasonal cycles of d_p are unequally reproduced for the different stations. The performance of LMDZ-iso in simulating the seasonal cycle of d_p is in line with the other GCMs: *Yoshimura et al.* [2008] report a correlation between 0.05 and 0.62 between

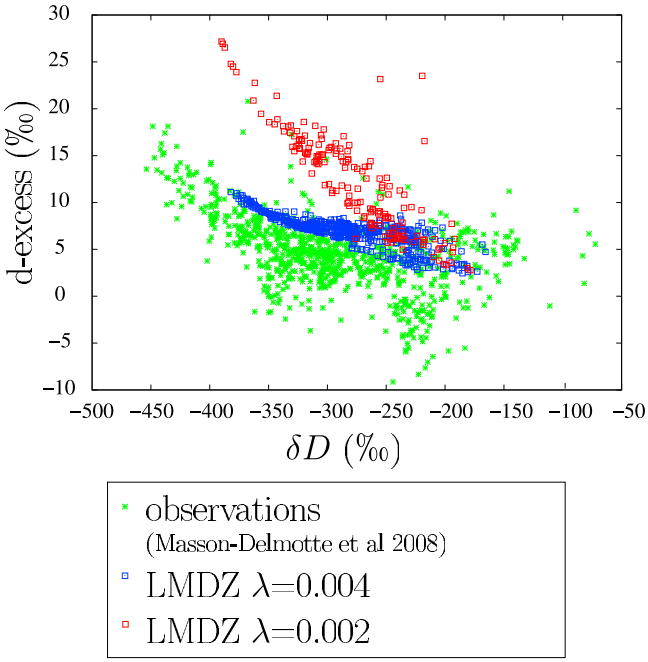

Figure 4. Annual mean d excess as a function of annual mean δD in precipitation in Antarctica, in the data from *Masson-Delmotte et al.* [2008] (green) and in LMDZ-iso free simulations (blue and red). In blue, the supersaturation λ was set to its standard value of 0.004, whereas in red, it was set to 0.002.

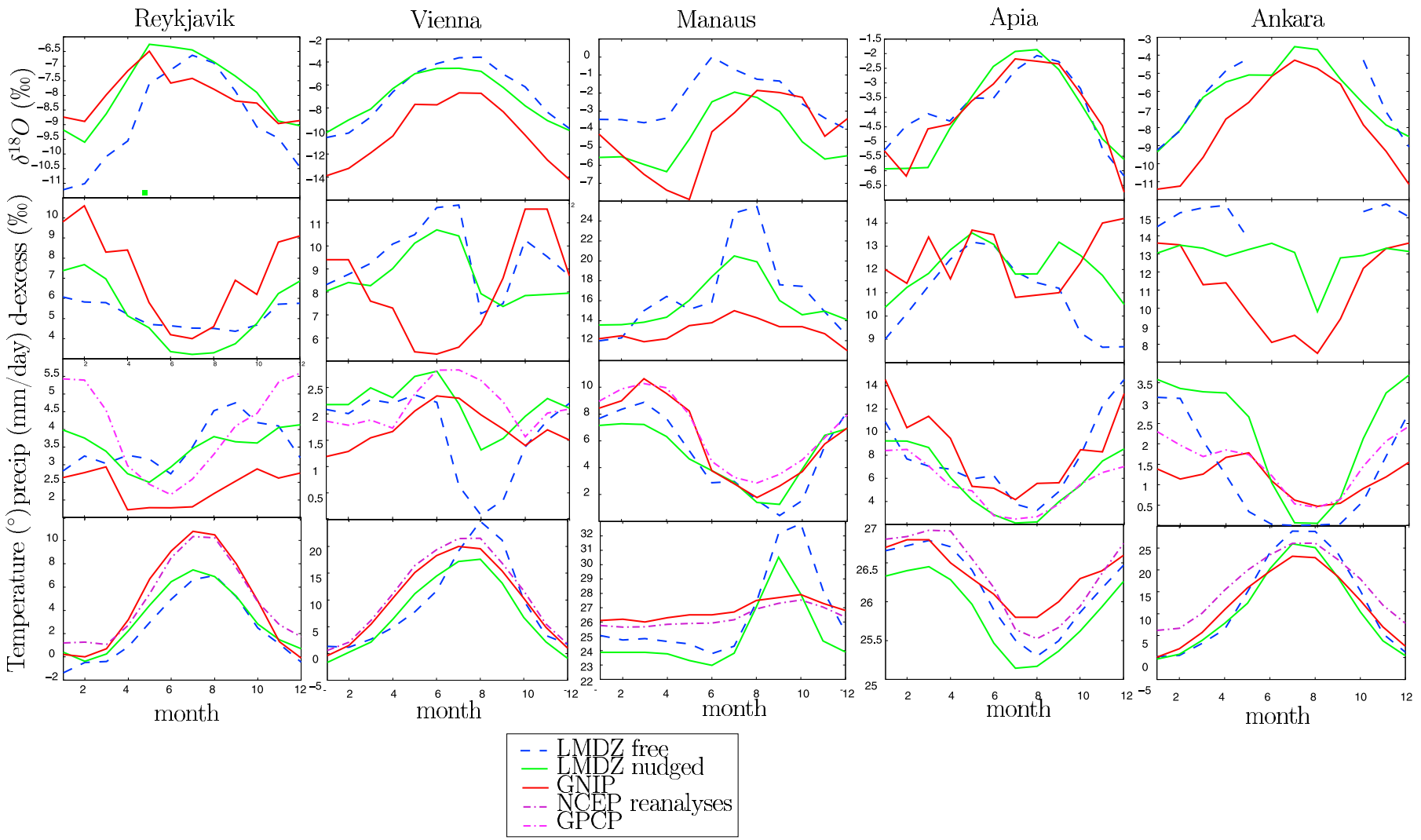

Figure 5. Monthly δ^{18}O and d excess in precipitation, precipitation rate, and temperature over Reykjavik, Vienna, Manaus, Ankara, and Apia for the GNIP data (red) and the LMDZ-iso nudged (green) and free simulations (blue), as well as NCEP [*Kalnay et al.*, 1996] temperatures and GPCP [*Huffman et al.*, 1997] precipitation (pink). Monthly averages are calculated over the 1979–2007 period for LMDZ-iso, NCEP, and GPCP and over the years available for GNIP (Table 1). For LMDZ-iso, we plot the value of the grid box containing the station.

Table 1. Name, Location, and Active Years of the GNIP Stations Chosen to Assess Seasonal Cycles and Interannual Variability of the Isotopic Composition of the Precipitation[a]

Name	Latitude	Longitude	Region	Active Years	Vapor Sampling
Reykjavik	64.13	−21.93	northern Atlantic	1961–2001	-
Vienna	48.25	16.37	central Europe	1961–2001	2001–2003, weekly sampling
Manaus	−3.12	−60.02	central Amazon	1966–1990	1978–1980, monthly sampling
Apia	−13.8	−171.78	western tropical Pacific	1962–1977	-
Ankara	39.95	32.88	eastern Mediterranean	1963–2001	2001–2002, subweekly sampling
Bangkok	13.73	100.50	Southeast Asia	1968–2001	-

[a]"Vapor sampling" gives the frequency and active years of the vapor sampling on some of these stations.

observed and simulated mean June–July–August and December–January–February (JJA-DJF) d_p values in four isotopic GCMs; the LMDZ-iso value is 0.52. At high latitudes, LMDZ-iso simulates everywhere d_p in antiphase with $\delta^{18}O_p$, in agreement with the Reykjavik data (Figure 5) or inland Antarctica [*Fujita and Abe*, 2006] (not shown). But LMDZ-iso is not able to reproduce the phase shift of a few months observed between $\delta^{18}O_p$ and d_p in some stations of coastal Antarctica or Greenland [*Johnsen et al.*, 1989; *Ciais et al.*, 1995; *Delmotte et al.*, 2000]. Over the Mediterranean region, LMDZ-iso simulates an almost flat seasonal cycle of d_p, at odds with the lower d_p observed in summer in Turkey (Ankara, Figure 5) or in Israel [*Angert et al.*, 2008] (not shown). Over the Amazon, LMDZ-iso is able to simulate the maximum of d_p observed during the dry season (e.g., Manaus, Figure 5), though the simulated maximum value is 6‰ too high. During the dry season, simulated d_p values increase with continentality as one goes inland, in agreement with observations [*Salati et al.*, 1979; *Gat and Matsui*, 1991; F. Vimeux et al., manuscript in preparation, 2010]. These features have been interpreted as the effect of fractionating continental recycling (e.g., evaporation from lakes, bare soil [*Salati et al.*, 1979; *Gat and Matsui*, 1991; *Henderson-Sellers et al.*, 2001]). It is thus surprising that LMDZ-iso is able to simulate these features without fractionation during evapotranspiration from land. Processes controlling the seasonal cycle of d_p in South America in LMDZ-iso seem more related to rain-vapor equilibration processes. The reasons for d_p South American cycles in LMDZ-iso, and whether they are the same as in nature, will be investigated in the future.

[32] The amount effect (which refers to the decrease of $\delta^{18}O_p$ with increasing precipitation that is observed in the tropics) is well reproduced by LMDZ-iso (Figure 6): over the nine oceanic tropical stations used by *Bony et al.* [2008], the amount effect is −0.5‰/mm/d in LMDZ-iso compared to −0.7‰/mm/d in the data. The Single Column Model (SCM) of *Bony et al.* [2008], which shares a very similar version of the Emanuel convective parameterization and the same isotopic representation of droplet evaporation, simulates too depleted a precipitation in humid conditions and too strong an amount effect (Figure 6, blue). *Bony et al.* [2008] hypothesized that this bias could be due to the very simple framework of the SCM, in which horizontal isotopic gradients were neglected. Figure 6 confirms this hypothesis: in nature as in LMDZ-iso, the horizontal moisture advections of air masses of different isotopic composition in LMDZ-iso thus act to dampen the amount effect.

3.1.3. Evaluation of the Vapor-Precipitation Equilibrium

[33] A large uncertainty in the representation of water-stable isotopes in GCMs is the representation of isotopic exchanges between vapor and rain droplets as the rain falls and partially reevaporates [*Lee and Fung*, 2008]. The ECHAM GCM, for example, assumes that a constant fraction of the droplet reequilibrates with the vapor, depending on the cloud type [*Hoffmann et al.*, 1998]. Here we calculate explicitly the relative effect of evaporation and equilibration, but we still rely on a tunable parameter ϕ, controlling the relative humidity at the droplet contact, and thus the intensity of kinetic effects: the relative humidity at the droplet contact is parametrized as $\phi + (1 - \phi) \cdot h$, where h is the relative humidity of the vapor reservoir in which droplets reevaporate. Results are very sensitive to this parameter, especially in dry regions where the reevaporation is strong and kinetic effects are crucial: the stronger the kinetic effects, the more the rain gets enriched by evaporation for a given reevaporated fraction [*Bony et al.*, 2008]. This parameter was set to 0.9 by *Bony et al.* [2008]. When setting ϕ to 0 (i.e., reducing the relative humidity at the droplet contact), then the amount effect becomes much stronger and the d_p much lower in dry regions (Figure 7). In LMDZ-iso as in the SCM, the optimal value for ϕ is 0.9.

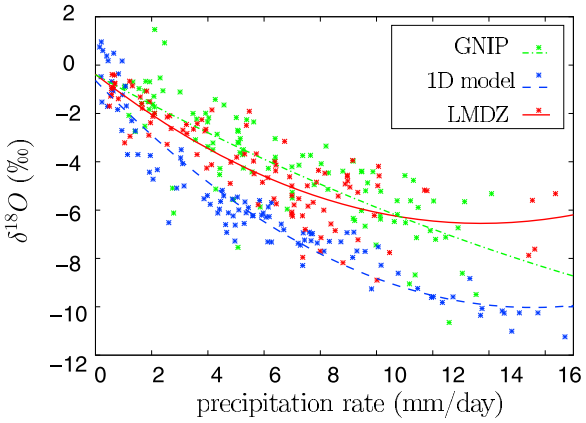

Figure 6. Monthly $\delta^{18}O$ in precipitation as a function of precipitation rate for the nine ocean tropical GNIP stations selected by *Bony et al.* [2008] for the GNIP data (dash-dotted green curve), the LMDZ-iso nudged simulation (solid red curve), and the single-column model of *Bony et al.* [2008] (dashed blue curve). Curves are second-order polynomial fits.

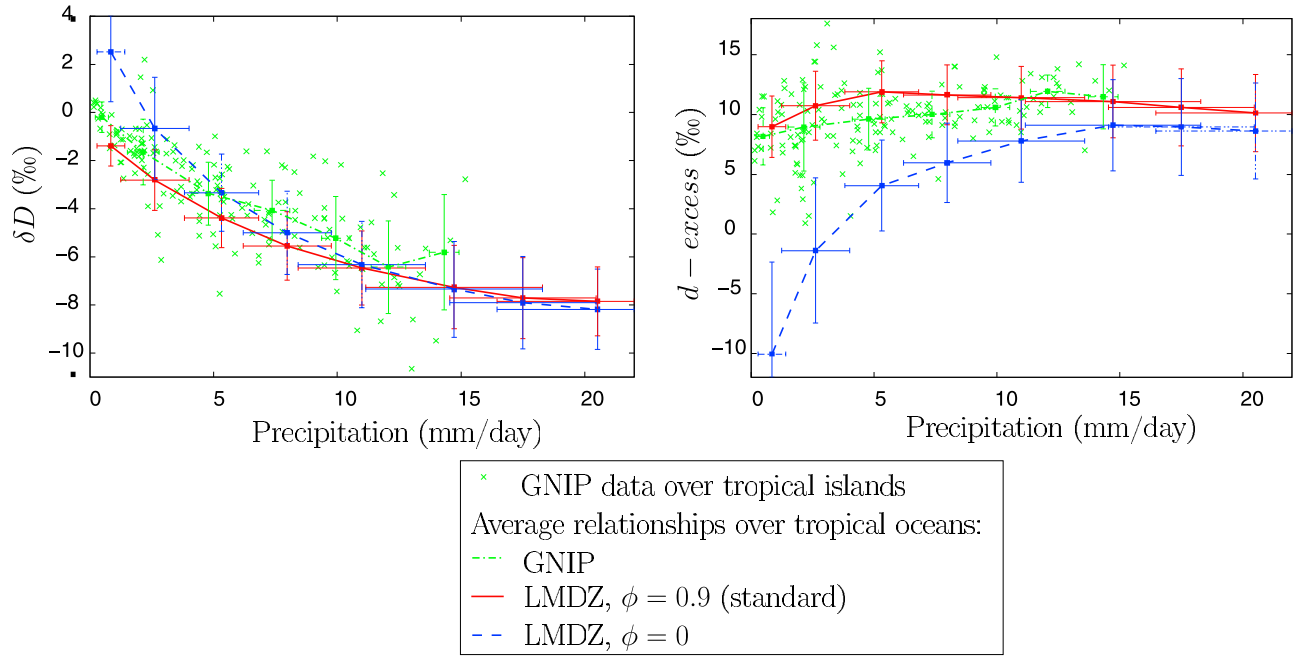

Figure 7. Average relationship between precipitation rate and (left) δ^{18}O and (right) d excess of tropical oceanic precipitation, at the monthly scale, for GNIP data (dash-dotted green curve), and 3 year LMDZ-iso simulations with ϕ set to 0.9 (solid red curve) and to 0 (dashed blue curve). Error bars indicate the standard deviation in each precipitation bin.

[34] As an evaluation of the representation of isotopic processes during evaporation, we compare the degree of equilibration between the vapor and the precipitation at a few stations: Vienna, Manaus, and Ankara, where low-level vapor isotopic compositions are available from the GNIP database at http://nds121.iaea.org/wiser/ (Table 1 and Figure 8). We average both the precipitation and the vapor for all the years available both for the model (1979–2007) and the data (Table 1) to yield monthly averages. Caution is necessary for two sources of uncertainties in the model-data comparison, in addition to possible uncertainties in the data. First, vapor samples were not collected every day and thus may not be representative of monthly averages, given the significant variability observed in the vapor at the daily time scale [e.g., *Angert et al.*, 2008]. However, the relatively smooth seasonal cycles suggest that these data are suitable for a first evaluation of rain-vapor disequilibrium (Figure 8). To estimate this source of uncertainty, we resampled the LMDZ-iso results on the days of observations (Figure 8, dotted green). Second, the precipitation and the vapor samples are not necessarily from the same years. The interannual variability in LMDZ-iso at the three stations is on the order of 1‰ for $\delta^{18}O_v$ and d_v (where $\delta^{18}O_v$ and d_v are the δ^{18}O and d of the vapor), 2‰ for $\delta^{18}O_p$ and up to 3‰ for d_p. We will thus focus on variations in composition exceeding both the standard deviation of measurements within a month for the vapor data (Figure 8) and the typical interannual variability.

[35] In the data over all stations, the rain is more enriched than the low-level vapor ($\delta^{18}O_p - \delta^{18}O_v$ ranges from +7 to +20‰), but over Vienna and Manaus the rain is more depleted (by up to 6‰) than would be expected if the rain was in complete equilibrium with the vapor. This might suggest that the rain, which formed at higher altitude from depleted vapor, reequilibrates only partially. Over Ankara during the dry summer, on the other hand, the rain is more enriched (by about 2‰) than expected from total diffusive equilibration. This suggests some significant evaporative enrichment in dry air. These features are qualitatively well reproduced by LMDZ-iso.

[36] The d_p observed over Vienna and Ankara is lower than in the vapor and lower than would be expected from equilibrium with the vapor (4 up to 19‰ lower). This low d_p could arise from the evaporation of the rain drops as they fall [*Dansgaard*, 1964]. LMDZ-iso strongly underestimates this disequilibrium. It underestimates d in the vapor (d_v), whereas d_p is of the right order of magnitude. This mismatch could arise from (1) a problem in the representation of the kinetic effects during rain evaporation and isotopic exchanges or (2) difficulties in comparing surface vapor samples with an average over a GCM layer (about 20 hPa or 200 m) if some surface processes have an influence restricted to the first few meters above the surface. Over Manaus on the other hand, observed d_p is generally higher than would be expected from equilibrium with the vapor. This could arise from low rain reevaporation in a wet atmosphere. This behavior is qualitatively well captured by LMDZ-iso, but the noisiness of the data limits any deeper analysis.

[37] This calls for more vapor measurements to better constrain and evaluate the representation of isotopic processes during rain fall.

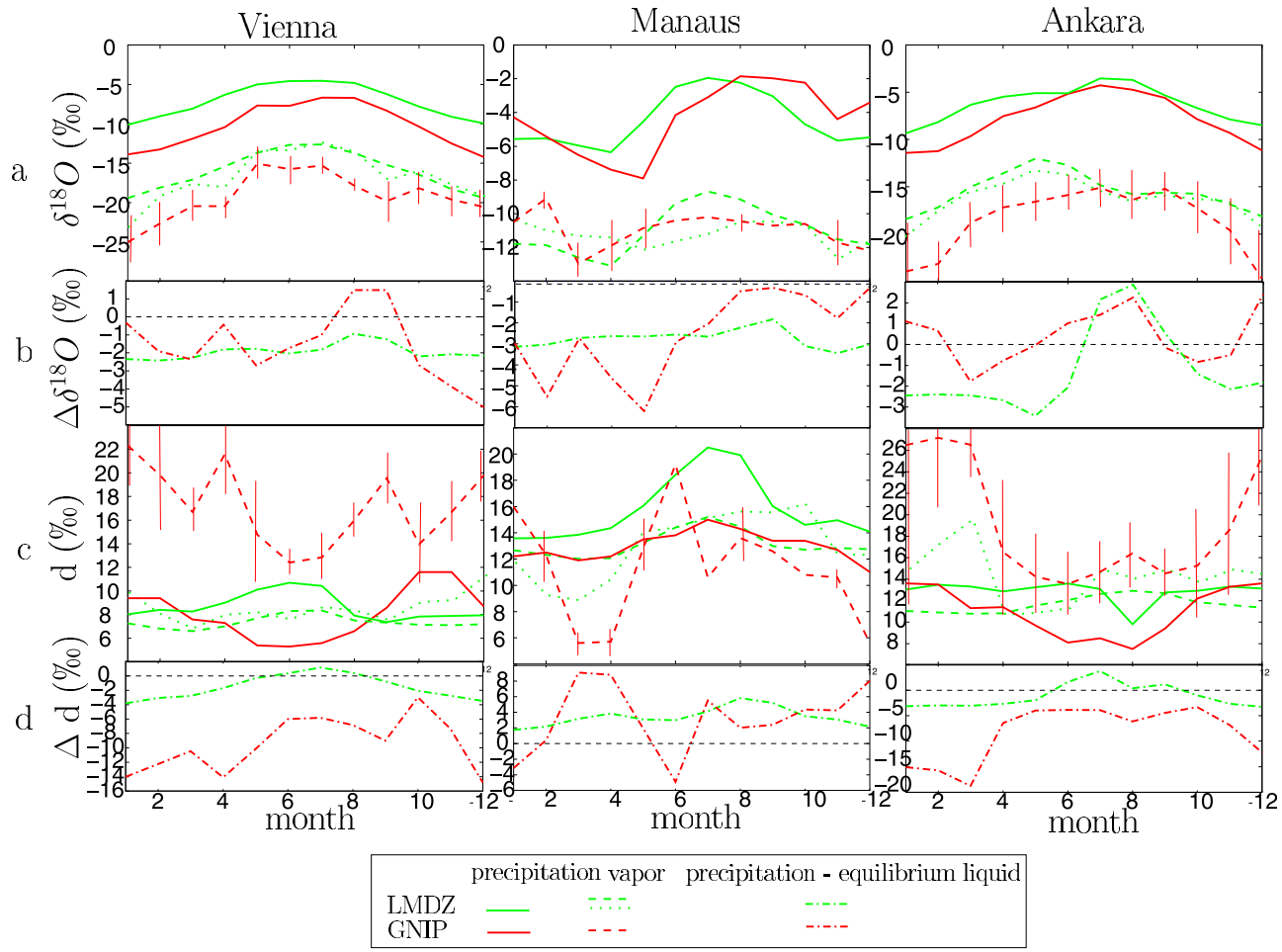

Figure 8. (a) Monthly δ^{18}O in precipitation (solid curves) and vapor at the lowest level (dashed curves) over Vienna, Manaus, and Ankara for the GNIP-vapor data (red curves) and the LMDZ-iso nudged simulation (green curves). For the simulated vapor composition, the dotted green curves show the LMDZ results sampled on the same days as GNIP vapor measurements, whereas the dashed lines show the monthly means. (b) Difference between δ^{18}O in precipitation and the δ^{18}O of a liquid that would be in equilibrium with the vapor, for the GNIP-vapor data (red curve) and the LMDZ-iso nudged simulation (green curve). For LMDZ, the monthly means were used. (c) Same as Figure 8a but for d excess. (d) Same as Figure 8b but for d excess. The error bars for the GNIP vapor data correspond to the standard deviation for the different measurements available for a given month.

3.2. Evaluation of the Isotopic Variability at the Synoptic Scale

[38] In this section, we evaluate the ability of the nudged simulation to simulate the variability at the daily and weekly scale. Unless the model is nudged, the model generates its own weather variability uncorrelated to observations, restricting the evaluation to statistics [*Hoffmann et al.*, 1998; *Noone and Simmonds*, 2002a]. Nudging with reanalyzed winds enables a more rigorous evaluation of the isotopic variability at the synoptic scale [*Yoshimura et al.*, 2008]. Here we present an evaluation using unpublished daily data of both vapor and precipitation collected at the surface at the station of Saclay (near Paris, France, 48.73°N, 2.17°E) from September 1982 to September 1984. Vapor was collected by continuous sampling on a daily basis (except during weekends for which the sampling period covers about 3 days). A cryogenic trap was used, and samples were analyzed for δ^{18}O and δD with an overall accuracy of ±0.15‰ and ±1‰, respectively.

[39] The model reproduces the temperature evolution very well (Figure 9a), especially in winter, when the variability is mainly controlled by large-scale synoptic disturbances. The correlation between observed and modeled daily temperatures is 0.84 in winter and 0.51 in summer. Consistently, the daily variability of $\delta^{18}O_v$ is well captured, especially in winter: the correlation between observed and modeled daily $\delta^{18}O_v$ is 0.65 in winter and 0.46 in summer. However, the temporal slope of $\delta^{18}O_v$ versus temperature at the daily scale in winter is underestimated by the model (0.2‰/K in LMDZ-iso and 0.6‰/K in the data). For example, while LMDZ-iso simulates accurately the strong negative temperature and precipitation anomaly during the first three weeks of February 1983, the corresponding anomaly in $\delta^{18}O_v$ is underestimated by a factor of 2. The mismatch

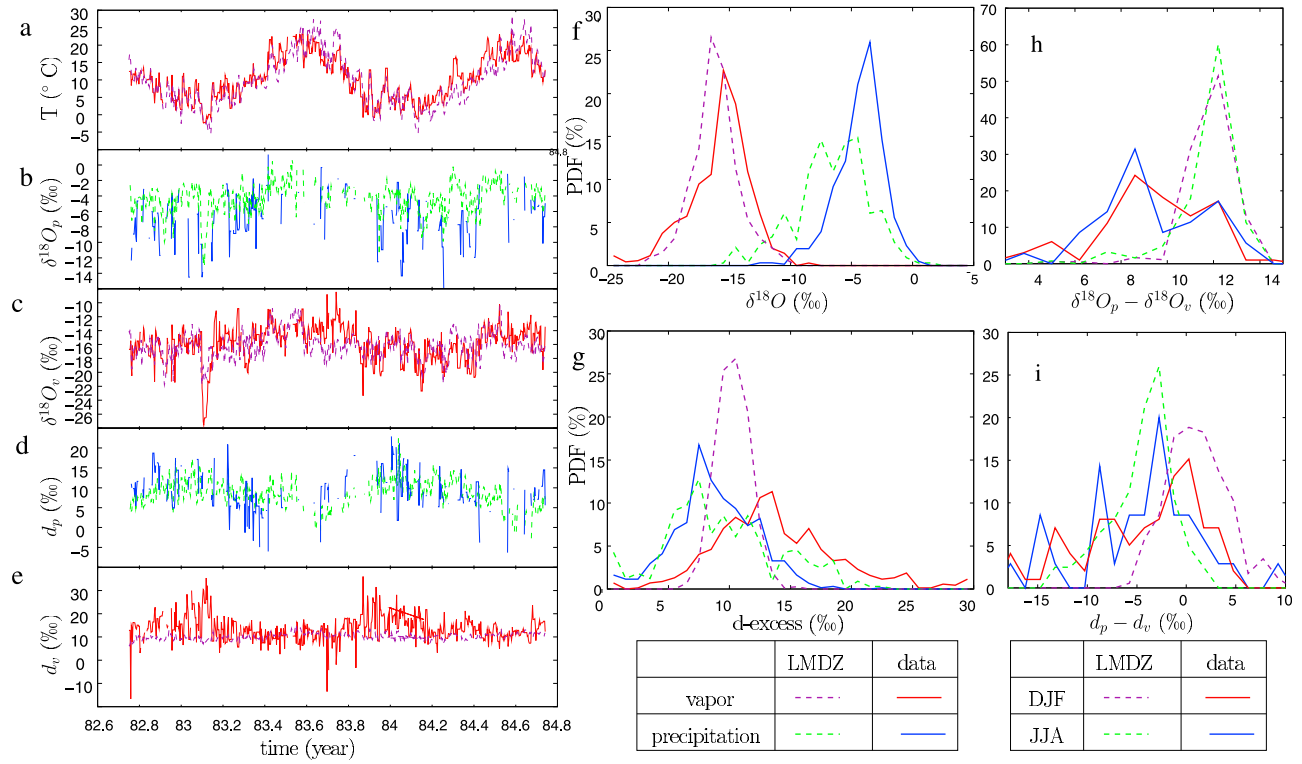

Figure 9. Comparison of the synoptic variability of water isotopes simulated by LMDZ-iso with that observed at the surface in Saclay (near Paris, France, 48.73°N, 2.17°E) from September 1982 to September 1984. Daily evolution of (a) temperature, (b) $\delta^{18}O_p$, (c) $\delta^{18}O_v$, (d) d_p, and (e) d_v. Probability density function of the daily (f) $\delta^{18}O$ and (g) d for all months, in both vapor and precipitation. Probability density function of the daily difference (h) between $\delta^{18}O$ in the precipitation and the vapor and (i) between d in the precipitation and the vapor. Observed temperatures are solid purple curves, measured $\delta^{18}O_v$ and d_v are dashed purple curves, $\delta^{18}O_p$ and d_p are dashed green curves, and LMDZ-iso $\delta^{18}O$ is solid red curve and d is solid blue curve.

could be due to an insufficient distillation of air masses due to a misrepresentation either of the water cycle along the air mass trajectories, or of the trajectories themselves, since LMDZ-iso is not able to simulate the observed 10% decrease in relative humidity during the same period (not shown). This low $\delta^{18}O_v$ event was also underestimated in a nudged simulation by the regional model REMO-iso [*Sturm*, 2005].

[40] The isotopic reequilibration between precipitation and vapor is relatively well reproduced by LMDZ-iso, with the $\delta^{18}O_p$ most frequently 12‰ higher than the vapor in LMDZ-iso and 10‰ in the data.

[41] Although the model satisfactorily simulates the frequency distribution and seasonal variability of d_p, it poorly simulates its synoptic variability (correlation of 0.14 between data and model in winter). The reequilibration between precipitation and vapor for d is well reproduced, with d most frequently 2‰ lower in average in precipitation than in the vapor in LMDZ-iso and about 5‰ lower in the data. This difference between d_p and d_v is strongly sensitive to parameter ϕ controlling kinetic effects during rain re-evaporation: if ϕ is set to 0 (not shown), the simulated d_p is about 8‰ lower than d_v.

[42] The model completely misses the observed variability in d_v, simulating a nearly constant d_v of 10‰ all year round. The correct simulation of d_p is however surprising, suggesting that a good representation of the variability of d_v is not necessary to correctly simulate the variability of d_p. We speculate that some processes near the surface influence d_v in the data, but these processes have no impact on the observed precipitation. The inability of LMDZ-iso to simulate the observed variability in d_v is independent of the vertical resolution: in the standard version of LMDZ-iso (19 levels), the lowest layer is 200 m thick, but there is no improvement in the simulation when using a better vertical resolution (39 levels) with a 35 m thick lowest layer (not shown). This suggests that some processes impacting near-surface d_v are not represented in LMDZ-iso, such as small-scale land surface heterogeneities.

[43] LMDZ-iso, when nudged by reanalyses, can thus satisfactorily simulate the day-to-day variability in temperature that is related to large-scale atmospheric disturbances, and the associated $\delta^{18}O$ variability in vapor and precipitation (at least qualitatively). At the synoptic scale, as is the case at the seasonal scale, the variability in d is more difficult to simulate than that of $\delta^{18}O$. The d_v is even more difficult to simulate than d_p, possibly owing to a mismatch between the scale of in situ measurements and the scale of atmospheric phenomena that can be simulated by a GCM, as was already pointed for the seasonal scale (section 3.1.3).

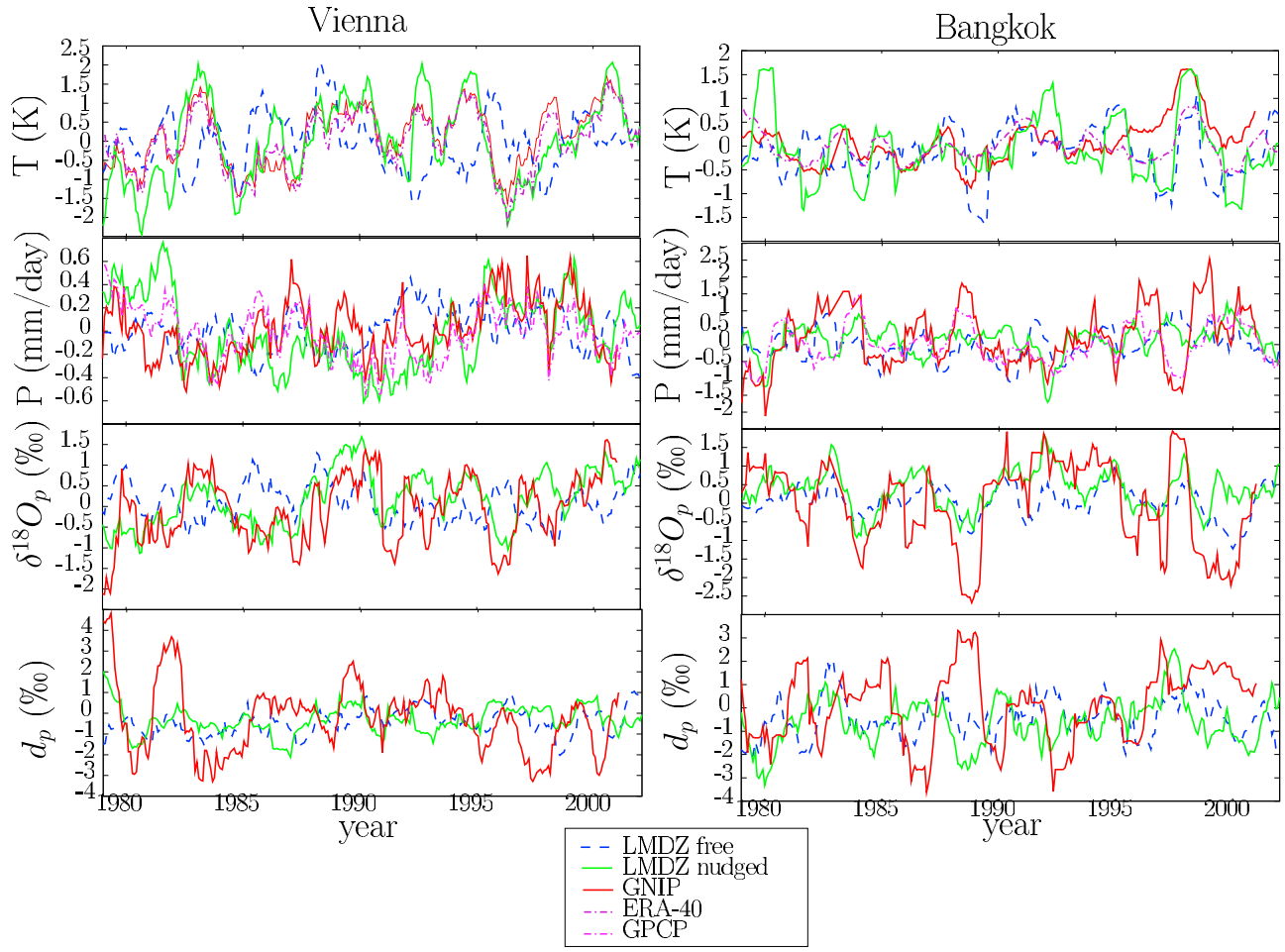

Figure 10. Monthly interannual anomaly of air temperature, precipitation rate, δ^{18}O, and d excess in precipitation over the (left) Vienna and (right) Bangkok GNIP stations, comparing GNIP data and the LMDZ-iso nudged simulation.

Measurements of d_v within the bulk of the boundary layer or at the top of a mat would be more comparable to LMDZ-iso simulations.

3.3. Evaluation of the Isotopic Variability at the Interannual Scale

[44] Water isotopes have been shown to record interannual to decadal variability of the precipitation in the tropics [*Hoffmann*, 2003; *Ramirez et al.*, 2003] and modes of variability in the extratropics such as the North Atlantic Oscillation [*Baldini et al.*, 2008; *Sodemann et al.*, 2008] or the Southern Annular Mode [*Noone and Simmonds*, 2002b]. To evaluate whether LMDZ-iso could be used in the future to study such issues, we evaluate the representation of the isotopic variability at the interannual scale.

[45] The simulation nudged by reanalyzed winds simulates better than the free simulation the interannual variability in temperature, precipitation, and isotopes, as can be shown by time series (Figure 10) over Vienna and Bangkok. These two stations were chosen for their long records and contrasting climate (as in work by *Yoshimura et al.* [2008]) The improvement is particularly strong in midlatitudes. For example, the correlation is 0.80 between model and data monthly anomalies of temperatures (filtered with a 6 month running mean) over Vienna in the nudged simulation compared to 0.05 in the free simulation. Consistently, the variability of $\delta^{18}O_p$ is strongly improved at this station (0.66 compared to 0.26). The simulated variability of precipitation is also improved (0.51 compared to 0.09). On the other hand, in the tropics, the variability in temperature, precipitation, and $\delta^{18}O_p$ is not much improved, consistent with the results of *Yoshimura et al.* [2008]: correlations between model and data $\delta^{18}O_p$ are 0.52 and 0.58 for the nudged and free simulations, respectively. Since tropical SSTs exert a dominant control on the tropical interannual variability, this variability is already well captured by LMDZ-iso just by forcing with observed SST, and the nudging provides little added value. In all simulations, the simulated d_p variability is completely different from the observed variability (correlations of −0.02 and −0.14 over Vienna and Bangkok in the nudged simulations). Also, the interannual variability of d_p is strongly underestimated by LMDZ-iso, as was the case at the synoptic scale.

[46] LMDZ-iso overestimates the correlations of $\delta^{18}O_p$ with both the temperature and the precipitation amount (Figure 11), as pointed out by *Tindall et al.* [2009] for the Hadley model, possibly owing to the different spatial scale of simulations and measurements. LMDZ-iso simulates an

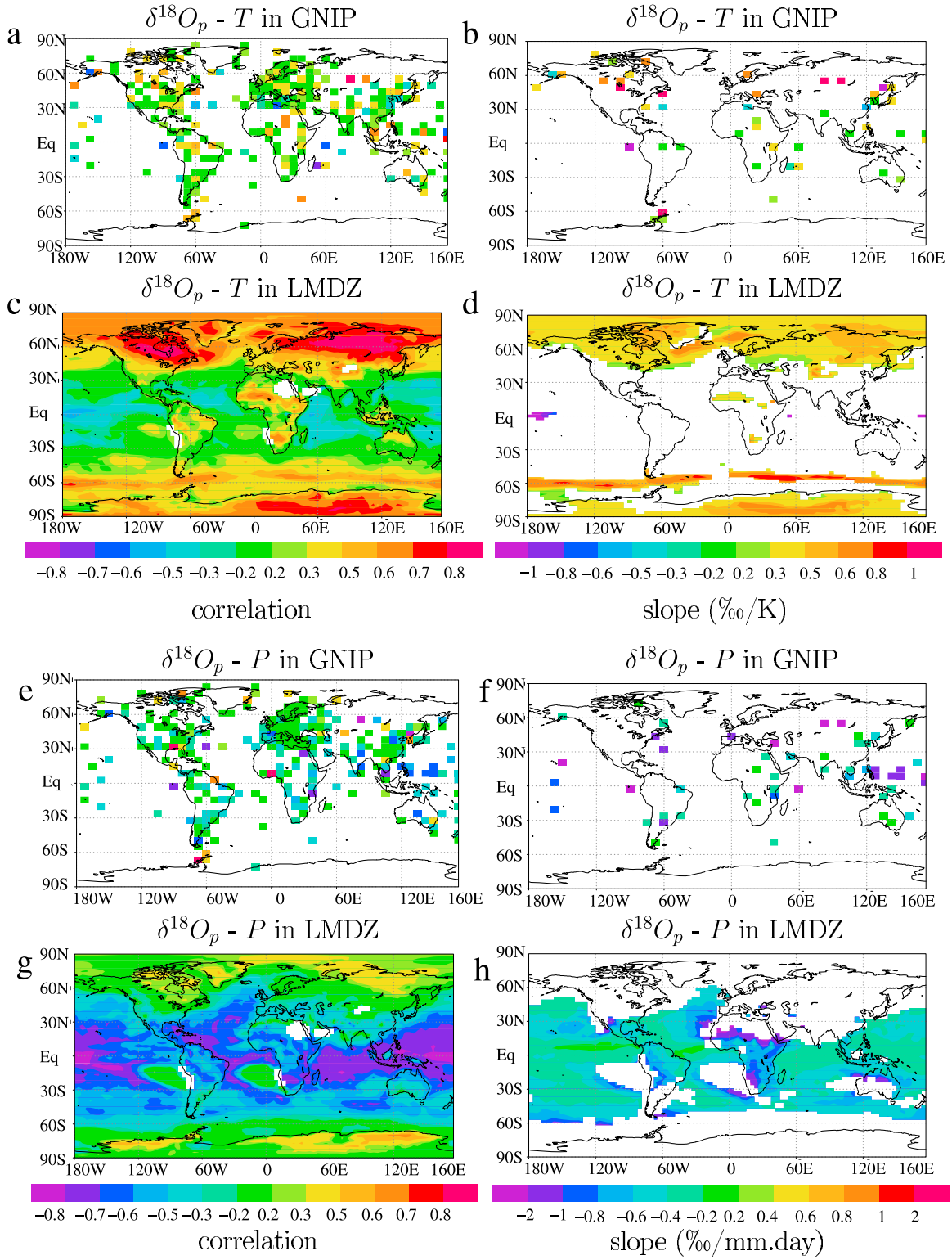

Figure 11. (a, c, e, and g) Correlation coefficients and (b, d, f, and h) slopes of the interannual relationship between monthly anomalies (seasonal cycle subtracted) of $\delta^{18}O$ in precipitation and temperature (Figures 11a–11d) and precipitation rate (Figures 11e–11h). A 6 month running mean was applied to the time series of monthly anomalies before performing the linear regression. The regression is performed for the GNIP data (Figures 11a, 11b, 11e, and 11f) and the nudged 1979–2007 LMDZ-iso simulation (Figures 11c, 11d, 11g, and 11h). White zones correspond to correlations lower than 0.4 in absolute value.

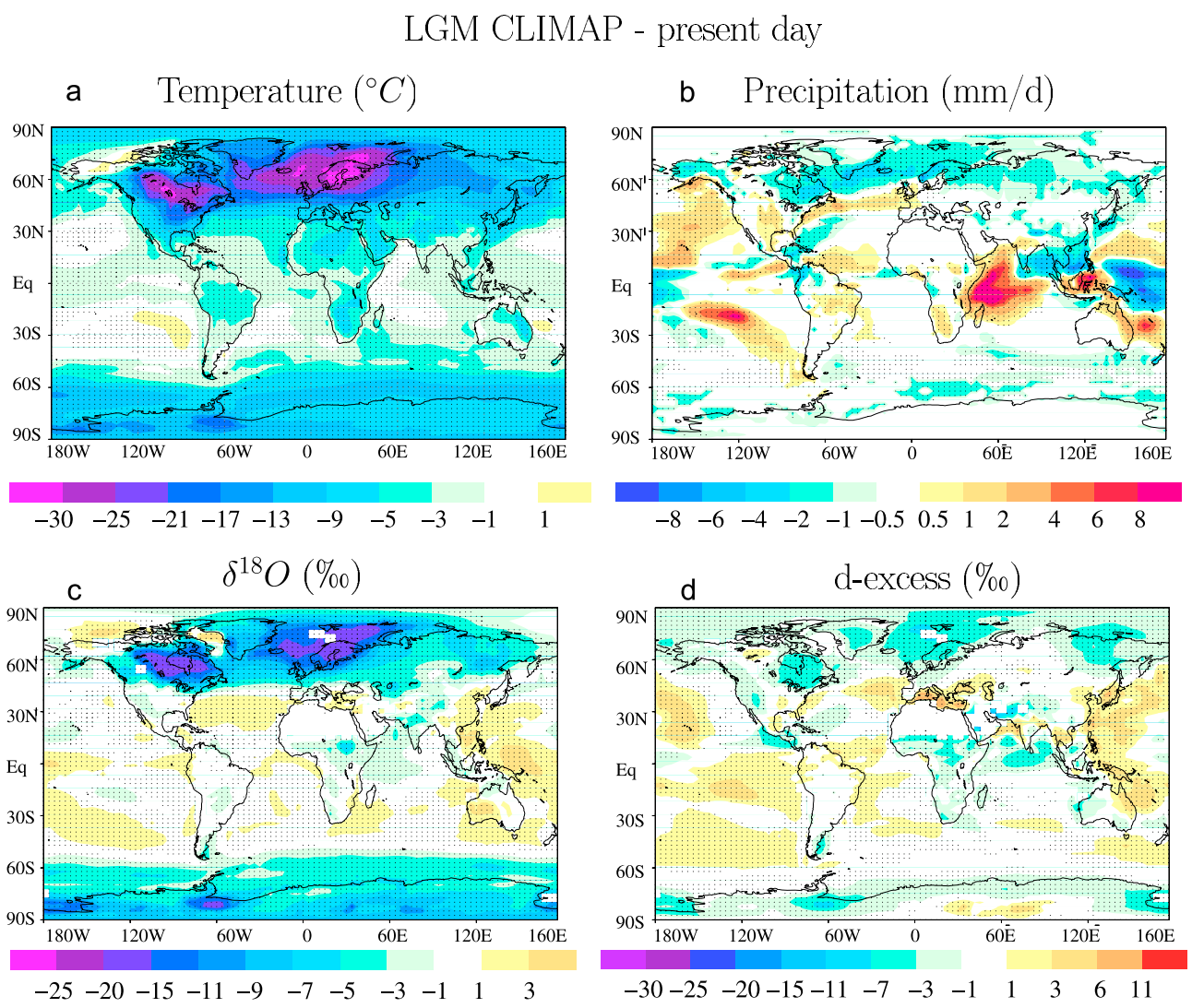

Figure 12. Annual average change between LGM and present day (PD) for (a) temperature, (b) precipitation, (c) $\delta^{18}O$, and (d) d excess. The LGM simulation used the CLIMAP SST [*CLIMAP Project Members*, 1981). Stippling indicates where the LGM-PD difference is stronger than the standard deviation of the interannual variability.

interannual slope of $\delta^{18}O$ versus temperature ranging from 0.3 to 0.8 ‰/K in high latitudes, on the same order of magnitude as those derived from the GNIP data (Figure 11). In the tropics, the simulated amount effect is about −0.5‰/(mm/d), also comparable with GNIP data [*Rozanski et al.*, 1993].

[47] Therefore, LMDZ-iso, when forced by observed SST and nudged by reanalyzed winds, simulates relatively well the interannual variability in $\delta^{18}O_p$, though it has more difficulties in simulating d_p.

3.4. Evaluation of Isotopic Variations at Paleoclimatic Scales

[48] We have seen that LMDZ-iso reproduces reasonably well the present-day climate and its variability from the synoptic, regional scale to the interannual, large scale. In this section, we evaluate the capacity of LMDZ-iso to simulate the isotopic changes associated with two past climates (described in section 2.3.3): the Last Glacial Maximum (LGM) and the Mid-Holocene (MH).

3.4.1. Last Glacial Maximum

[49] Comparing the model results to the data for the LGM is not straightforward. In the case of South American speleothems, for example, the minimum $\delta^{18}O$ values are about −4.5‰ at about 18,000 years before present (18 ka) [*Cruz et al.*, 2006], but values around 21 ka are about −3‰, same as in present day [*Cruz et al.*, 2005b]. Here we consider that the LGM value corresponds to the minimum $\delta^{18}O$ values between 17 and 21 ka, or take the LGM values given by the author. Dating uncertainty could explain the different LGM dates. However, if the minimum $\delta^{18}O$ actually does not occur at the same time at all places (as suggested by some studies [*Smith et al.*, 2005; *Sylvestre*, 2009]), the combination of the LGM data is impossible to simulate with a time slice simulation [*Farrera et al.*, 1999; *Pinot et al.*, 1999], adding an additional source of discrepancy between the model and data.

[50] Figures 12 and 13 show the changes between LGM and PD simulated by LMDZ-iso when forced at LGM by

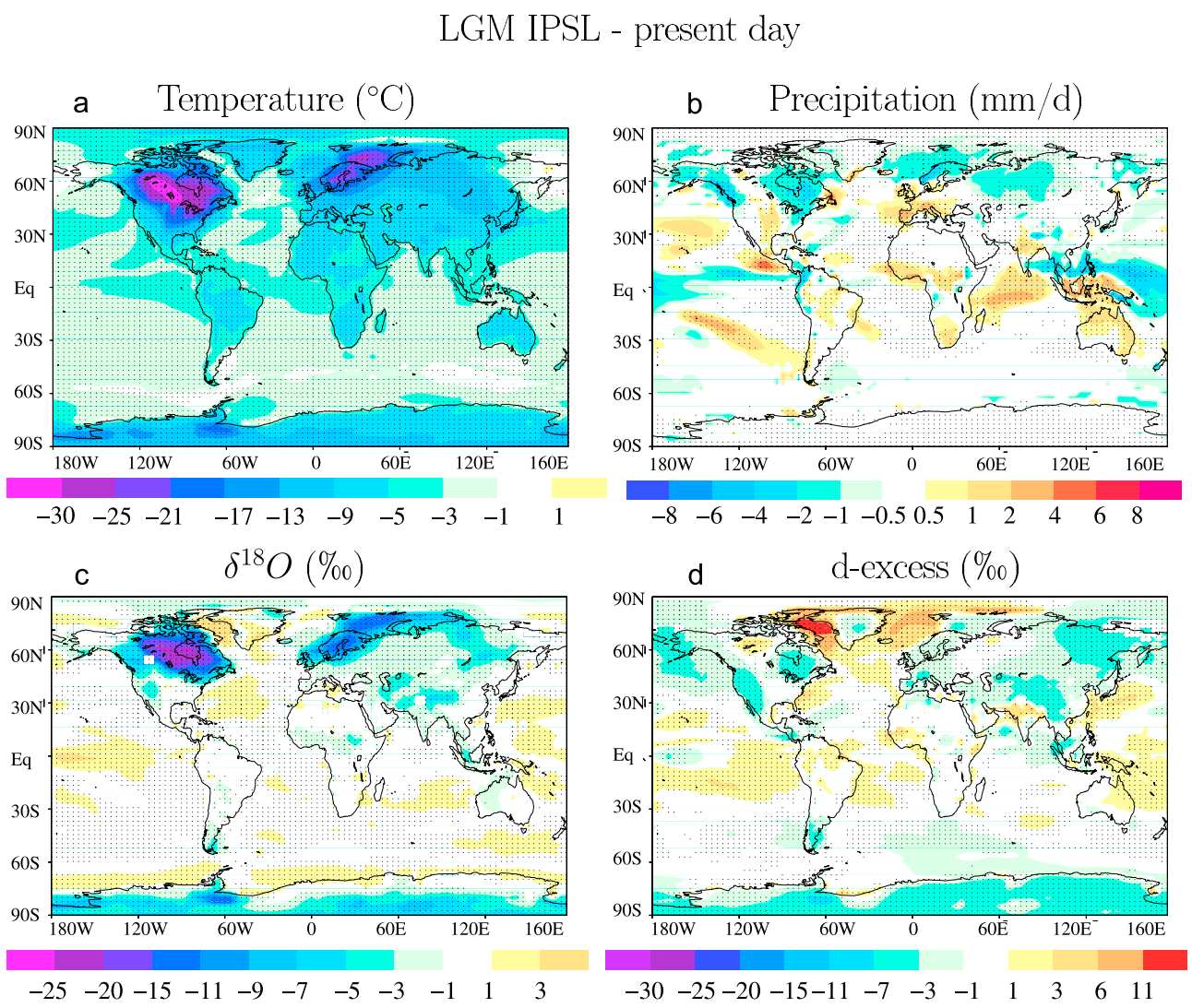

Figure 13. Same as for Figure 12 but for the LGM simulation using the SSTs from an LGM simulation with the coupled IPSL model. The setup of this simulation is detailed in section 2.3.3.

CLIMAP or IPSL SSTs, respectively. Forced by CLIMAP SSTs, LMDZ-iso simulates well the depletion in $\delta^{18}O_p$ over mid and high latitudes during the LGM, except in north-eastern America and over part of the Arctic where a slight enrichment is simulated. Forced by IPSL SSTs, which are up to 10 K warmer than CLIMAP SSTs over high-latitude oceans, LMDZ-iso is able to simulate the depletion observed in ice cores in Antarctica but not in Greenland.

[51] The relevance of spatial slopes for reconstructing paleotemperatures at high latitudes has extensively been discussed [*Jouzel et al.*, 2003; *Lee et al.*, 2008]. In Greenland, the temporal temperature-$\delta^{18}O_p$ slope between LGM and PD (0.3‰/K [*White et al.*, 1997]) has been suggested to be half the spatial slope (0.67‰/K), possibly due to colder source temperatures [*Boyle*, 1997] at LGM or to changes in the seasonality of precipitation [*Krinner and Werner*, 2003; *Werner et al.*, 2000]. This leads to an underestimation by a factor of 2 of temperature changes based on $\delta^{18}O_p$. In Antarctica, on the other hand, studies suggest the temporal and spatial slope are similar with a margin of ±20% [*Jouzel et al.*, 2003; *Krinner and Werner*, 2003], leading to reconstructions of past temperature changes with an error lower than 2°C. This is supported by simulation with the GISS and ECHAM GCMs forced by CLIMAP SSTs: they simulate temporal slopes between LGM and PD in eastern Antarctica on the order of 0.7‰/K and 0.6‰/K, respectively [*Jouzel et al.*, 2003] compared to a spatial slope on the order of 0.75‰/K. On the other hand, the CAM model, when forced by SSTs simulated by a coupled model, simulates temporal slopes half smaller than the spatial slopes in the same region [*Lee et al.*, 2008]. We compare here these results with those from LMDZ-iso forced by the CLIMAP and IPSL LGM SSTs. In Greenland, LMDZ-iso simulates a temporal slope between LGM and PD of about 0.4‰/K over Greenland, half the spatial slope of 0.8‰/K, consistent with earlier studies and all other GCMs [*Jouzel et al.*, 2000]. In Antarctica, LMDZ-iso forced by the CLIMAP SSTs simulates temporal slopes in Vostok of 0.8‰/K, virtually equal to the spatial slope in this region. The simulated temporal slopes are within 20% of the spatial slope over most locations in

Table 2. Data Used for Comparison With the LGM Simulation[a]

Station and Data Type	Latitude	Longitude	Reference	$\Delta\delta^{18}O$ Obs	Δd Obs	$\Delta\delta^{18}O$ LMDZ-iso	Δd LMDZ-iso
GRIP ice core (Greenland)	72.60	−38.5	*GRIP Members* [1993] cited by *Lee et al.* [2008] *Masson-Delmotte et al.* [2005a]	−7	−3	−9.8, +1.9	−3.4, −4
Camp Century ice core (Greenland)	77.17	−61.1	*Johnsen et al.* [1972] cited by *Jouzel et al.* [1994]	−12.9		−4.7, +7.4	−2.3, +8.5
Renland ice core (Greenland)	72	−25	*Johnsen et al.* [1992] cited by *Jouzel et al.* [1994]	−5		−11.9, −2.0	−1.3, −0.4
NGRIP ice core (Greenland)	75.10	−42.32	*NGRIP Members* [2004] cited by *Lee et al.* [2008]	−8		−8.1, +1.5	−3.5, −2.9
England	53	−2	*Bath* [1983] cited by *Joussaume and Jouzel* [1993]	−1.2		−8.1, −3.5	−1.0, −1.2
Vostok ice core (Antarctica)	−78.45	106.85	*Lorius et al.* [1985] cited by *Werner et al.* [2001]	−3 to −5	−2	−6.8, −2.6	−0.2, −4.7
Byrd ice core (Antarctica)	−80.2	−119.5	*Johnsen et al.* [1972] cited by *Lee et al.* [2008]	−8		−6.3, −4.4	−1.4, −2.3
Dome C ice core (Antarctica)	−74.7	124.2	*Lorius et al.* [1979] cited by *Jouzel et al.* [1994] *Stenni et al.* [2001]	−5.4	−4	−6.2, −0.3	−1.3, −5.0
Dome B ice core (Antarctica)	−77.8	94.9	*Vaikmae et al.* [1993] cited by *Jouzel et al.* [1994]	−5		−7.8, −3.3	+0.4, −4.6
Taylor Dome (Antarctica)	−77.8	71.6	*Grootes et al.* [2001] cited by *Lee et al.* [2008]	−3		−6.7, −2.0	+1.6, −4.4
Stampriet aquifer (Namibia)	−25	18	*Stute and Talma* [1998] cited by *Gasse* [2000]	+1.5		−1.5, −0.3	−1.1, −0.5
Huascaran ice core (South America)	−9.11	−77.61	*Thompson et al.* [1995]	−6.3	−4	+1.2, +0.5	+1.2, 0.0
Sajama ice core (South America)	−18.10	−68.97	*Thompson et al.* [1998]	−5.4		−1.1, −1.3	−0.5, −1.0
Illimani ice core (South America)	−16.62	−67.77	*Ramirez et al.* [2003]	−6	−4	−0.4, −0.3	+0.2, +0.2
Botuvera cave (South America)	−27.2	−49.02	*Cruz et al.* [2005b]	−1.5		−1.2, −0.6	+1.0, +1.1
Santana cave (South America)	−24.52	−48.72	*Cruz et al.* [2006]	−1.5		−0.5, 0.1	+0.9, +0.8
Rio Grande do Norte speleothems records (South America)	−5.60	−37.73	*Cruz et al.* [2009]	−0.5		+0.9, −0.3	+0.6, +0.9
Salar de Uyuni (South America)	−20	−68	*Fritz et al.* [2003]	−4		−1.1, −1.3	−0.3, −0.1
Guliya ice core (Tibet)	35.28	81.48	*Thompson et al.* [1997] cited by *Thompson et al.* [2000]	−5.4		−2.2, −5.1	−2.2, −4.9
Dunde ice core (Tibet)	38	96	*Thompson et al.* [1989]	−2		−2.1, −2.3	−0.5, −1.5
Sanbao and Hulu caves (China)	31.67	110.43	*Wang et al.* [2008]	+1.5		−1.6, +0.5	−0.3, −0.8

[a]Name (column 1) and location (columns 2 and 3) of the data stations, reference for the data (column 4), and LGM-PD difference in $\delta^{18}O$ and d excess measured in records (columns 5 and 6) and simulated by LMDZ (columns 7 and 8). We consider as LGM what the author considers as LGM or otherwise take the period of minimum $\delta^{18}O$ in the record between 17 ka and 21 ka. We take an approximate average value over 2 kyr. We take as present day the value averaged over the last 2 kyr. The $\delta^{18}O$ differences in carbonates expressed as PDB were converted in SMOW using $\Delta\delta_{SMOW} \simeq 1.03 \cdot \Delta\delta_{PDB}$ [*Coplen*, 1988]. For LMDZ-iso (columns 7 and 8) the first and second entries in each column are corresponding values for the CLIMAP SST–PD SST and for the IPSL LGM SST–PI, respectively (see section 2.3.3 for simulation setup).

eastern Antarctica, consistently with the GISS and ECHAM simulations reported by *Jouzel et al.* [2003]. On the other hand, when forced by IPSL LGM SSTs, the temporal slopes are most frequently around 0.5‰/K, i.e., 40% lower than the spatial slope. This is in closer agreement with *Lee et al.* [2008], who also used simulated SSTs. This suggests that the controls of $\delta^{18}O_p$ over Antarctica, and thus the accuracy of reconstructions based on present-day spatial slopes, strongly depend on the pattern of SST change. If the change in SST features a strong equator-pole gradient as in CLIMAP, then the spatial slope can be applied to past temperature reconstructions within 20% accuracy. On the other hand, if the SST change has a lower equator to pole gradient, as simulated by the IPSL or CAM coupled models [*Lee et al.*, 2008], then using the spatial slope for temperature reconstruction leads to an underestimation of past temperature changes (by about 40% in the LMDZ-iso simulation forced by IPSL SSTs). At this stage we are more confident in reconstructed than in simulated paleoclimatic SSTs, as large SST pole-equator gradients are confirmed by the recently published MARGO data [*MARGO Project Members*, 2009]. Our results thus rather supports the current use of PD spatial slope to interpret isotopic profiles recovered in central Antarctica.

[52] In the tropics, LMDZ-iso simulates little isotopic change and fails to simulate the depletions ranging from −1.5‰ to −6.3‰ inferred from tropical ice cores and South American speleothems (Table 2). Even when using SSTs from the IPSL coupled model, which are about −2.9 K colder than PD in the tropics, the decrease in $\delta^{18}O_p$ is small (less than 2‰). Temperature does not seem to have any significant effect on tropical $\delta^{18}O_p$ in LMDZ-iso, at any time scale. The failure to simulate lower $\delta^{18}O_p$ in South America is common to other GCMs [*Werner et al.*, 2001; *Jouzel et al.*, 2000]. However, it is not clear whether the depletions measured in available records (Table 2) are representative at the scale of the entire tropics.

[53] Another typical failure of isotopic GCMs for the LGM is their inability to simulate the lower d_p measured in ice cores at high latitudes during LGM [*Werner et al.*,

2001], or more generally to simulate $\delta^{18}O$ and d variations of the same sign on climatic time scales [*Noone*, 2008]. However, LMDZ-iso does simulate a lower d_p over most of Greenland (e.g., Summit: −3.5‰ compared to −3‰ in observations, Table 2), and over most of Antarctica except in central East Antarctica. In the simulation using coupled SSTs, the Antarctic d_p during the LGM is lower than present day by −4‰, in even better agreement with the data. The reason for this behavior of d_p will be the subject of future investigations.

[54] To conclude about the LGM simulations, LMDZ-iso simulates realistic LGM depletions at high latitudes but, like other GCMs, misses the more depleted values measured for LGM at low latitudes. Contrary to other isotopic GCMs [*Werner et al.*, 2001], it simulates a lower d_p in most high-latitude regions, in agreement with the data. However, the CLIMAP LGM simulation still fails to show the lowest glacial d_p over East Antarctica, and the coupled SST LGM simulation generates lower d_p values at the cost of unrealistic high glacial $\delta^{18}O$ values over Greenland.

3.4.2. Mid-Holocene

[55] In agreement with simulations from the GISS and ECHAM models [*Jouzel et al.*, 2000], and in agreement with measurements (Table 3), the isotopic changes between MH and PD are very small in most regions. Exceptions are found, however, over the Sahel, in the Middle East, in central Asia, and in the western United States, where a depletion on the order of 5‰ is simulated (Figure 14).

[56] The monsoon regions are relatively well represented in the LMDZ-iso model, though the precipitation amounts are slightly underestimated in summer [*Hourdin et al.*, 2006]. At orbital time scales, variations in precipitation are antiphased between the hemispheres [*Wang et al.*, 2006; *Kutzbach et al.*, 2008], but this antiphase is not captured by LMDZ. Therefore, LMDZ-iso is not able to reproduce the $\delta^{18}O_p$ changes in monsoon regions that are out of phase between hemispheres [*Cruz et al.*, 2009], but erroneously produces more negative $\delta^{18}O_p$ throughout the entire tropical belt (Figure 14). LMDZ-iso is not able either to reproduce the antiphase observed in $\delta^{18}O_p$ between east and west South America [*Cruz et al.*, 2009].

[57] Still, during the Mid-Holocene, the Indian and African monsoons are enhanced in LMDZ-iso (up to +3 mm/d in annual average), in agreement with other PMIP models [*Joussaume et al.*, 1999]. As a result, the precipitation downstream of these regions of enhanced precipitation is more depleted (up to −8‰ in the Northern Sahel and Tibet), consistent with the amount effect. The corresponding $P - \delta^{18}O_p$ slopes are much higher than at the interannual or seasonal scales. For example, when averaging the western African monsoon precipitation over the 20°W–30°E; 10°N–20°N region [*Joussaume and Taylor*, 1995] and for the July to September months (JJAS), the MH-PD $\delta^{18}O_p$ change ($\Delta\delta^{18}O_p$) is −2.0‰ for a +1.1 mm/d precipitation change (ΔP), leading to a climatic slope ($\Delta\delta^{18}O_p/\Delta P$) for JJAS of −1.7‰/mm/d (much higher than the seasonal or interannual slope of about −0.5‰/mm/d, Figure 11). This climatic slope is even higher when considering annual averages (−5‰/mm/d). This shows that the amount effect may depend on the time scale of variability considered [*Schmidt et al.*, 2007] and that reconstructions of past precipitation based on present-day calibration at the seasonal or interannual scale are to be taken with caution as discussed further in section 4.2.

4. Climatic Information Recorded by Water Isotopes in the Tropics

[58] The precipitation amount dominates the isotopic composition of the tropical precipitation at intraseasonal [*Yoshimura et al.*, 2003; *Sturm et al.*, 2007; *Risi et al.*, 2008b], seasonal [*Dansgaard*, 1964; *Rozanski et al.*, 1993], and interannual scales [*Rozanski et al.*, 1993; *Vuille and Werner*, 2005]. At longer time scales, the interpretation of isotopic records from tropical ice cores has been the subject of debate. *Thompson et al.* [2000] have shown that tropical records from ice cores in South America and Tibet share common $\delta^{18}O$ patterns during the last 25 kyr, with most depleted values during the LGM (by 4 to 6‰) and an increase during the deglaciation. The temporal evolution is also qualitatively similar to higher-latitude records in Greenland and Antarctica [*Thompson et al.*, 2000]. This could suggest a large-scale control of the isotopic signal, which was first interpreted as temperature variations [*Thompson et al.*, 2000]. However, given that the main process controlling low-latitude $\delta^{18}O$ variations at present day is the precipitation amount, these variations have subsequently been interpreted as wetter conditions upstream of ice cores [*Vimeux et al.*, 2009].

[59] Given the ability of LMDZ-iso to reproduce the main features of the observed water isotopic distributions, we now use it to investigate issues related to the interpretation of isotopic records as proxies for past changes in temperature and precipitation. First, we quantify the relative impact of changes in precipitation and large-scale temperature changes on $\delta^{18}O_p$ (section 4.1). We then evaluate the robustness of reconstructions of past precipitation based on water-stable isotopes (section 4.2).

4.1. How Much Do Global Temperature Changes Impact Tropical $\delta^{18}O_p$?

[60] A global temperature change is likely to imprint $\delta^{18}O_p$ over the whole planet. However, if the change in surface temperature is not spatially uniform, the large-scale circulation will also change, which will lead to substantial changes in precipitation. Regional changes in $\delta^{18}O_p$ are thus expected to result both from background temperature and regional circulation changes.

[61] To identify a possible effect of mean temperature on $\delta^{18}O_p$, we perform simulations with uniform changes of SST (−4 K, −2 K, and +2 K). Uniform changes in SST result in uniform shifts in the $\delta^{18}O_p$ probability distribution in the tropics (Figure 15a), by about 0.1 ‰/K. The probability distributions of $\delta^{18}O$ in the vapor and in the evaporation are equally shifted (not shown), suggesting that this small sensitivity to mean SST is mainly due to a change in fractionation during evaporation at the sea surface (a sensitivity of 0.08‰/K is predicted by the *Merlivat and Jouzel* [1979] simple closure assumption). The sensitivity to SST is the same for all uniform SST change experiments (Figure 15b) and consistent with the SCM results of *Bony et al.* [2008]. The LGM simulations are also associated with a decrease in mean $\delta^{18}O_p$. Figure 15c plots $\delta^{18}O_p$ as a function of the

Table 3. Data Used for Comparison With the MH Simulation[a]

Name	Latitude	Longitude	Reference	$\Delta\delta^{18}O$ Obs	Δd Obs	$\Delta\delta^{18}O$ LMDZ-iso	Δd LMDZ-iso
GRIP Ice Core (Greenland)	72.6	−38.5	*GRIP Members* [1993] cited by *Masson-Delmotte et al.* [2005b]	+0.5	−0.2	−1.3	−0.7
North GRIP ice core (Greenland)	75.10	−42.32	*Masson-Delmotte et al.* [2005b]	+0.7	−0.5	−1.3	−0.7
Vostok ice core (Antarctica)	−78.45	106.85	*Lorius et al.* [1985] cited by *Thompson et al.* [2000]	−0.2		+0.4	−0.6
Byrd ice core (Antarctica)	−80.2	−119.5	*Johnsen et al.* [1972] cited by *Thompson et al.* [2000]	+1		−0.4	−0.5
Huascaran ice core (South America)	−9.11	−77.61	*Thompson et al.* [1995]	0		−0.5	0.8
Sajama ice core (South America)	−18.10	−68.97	*Thompson et al.* [1998]	0		−0.4	−0.2
Illimani ice core (South America)	−16.62	−67.77	*Ramirez et al.* [2003]	+0.2		−1.0	0.0
Botuvera cave (South America)	−27.2	−49.02	*Cruz et al.* [2005b]	+0.5		−1.4	+0.5
Santana cave (South America)	−24.52	−48.72	*Cruz et al.* [2005b]	+1		−1.2	+0.1
Rio Grande do Norte speleothems records (South America)	−5.60	−37.73	*Cruz et al.* [2009]	−3.5		−1.5	+1.6
Tigre Perdido (South America)	−5.9	−77.3	*van Breukelen et al.* [2008]	+0.5		+0.1	+1.2
Guliaa ice core (Tibet)	35.28	81.48	*Thompson et al.* [2000]	−2.5		−0.7	−0.4
Sanbao and Hulu caves (China)	31.67	110.43	*Wang et al.* [2008]	−1.8		−0.4	+0.3

[a]Name (column 1) and location (columns 2 and 3) of the data stations, reference for the data (column 4), and MH–present-day difference in $\delta^{18}O$ and d excess measured (columns 5 and 6) and simulated by LMDZ-iso (columns 7 and 8). We take as MH the value at 6 ± 1 ka and for present day the values averaged over the last 2 kyr. The $\delta^{18}O$ differences in carbonates expressed as PDB were converted in SMOW using $\Delta\delta_{SMOW} \simeq 1.03 \cdot \Delta\delta_{PDB}$ [*Coplen*, 1988].

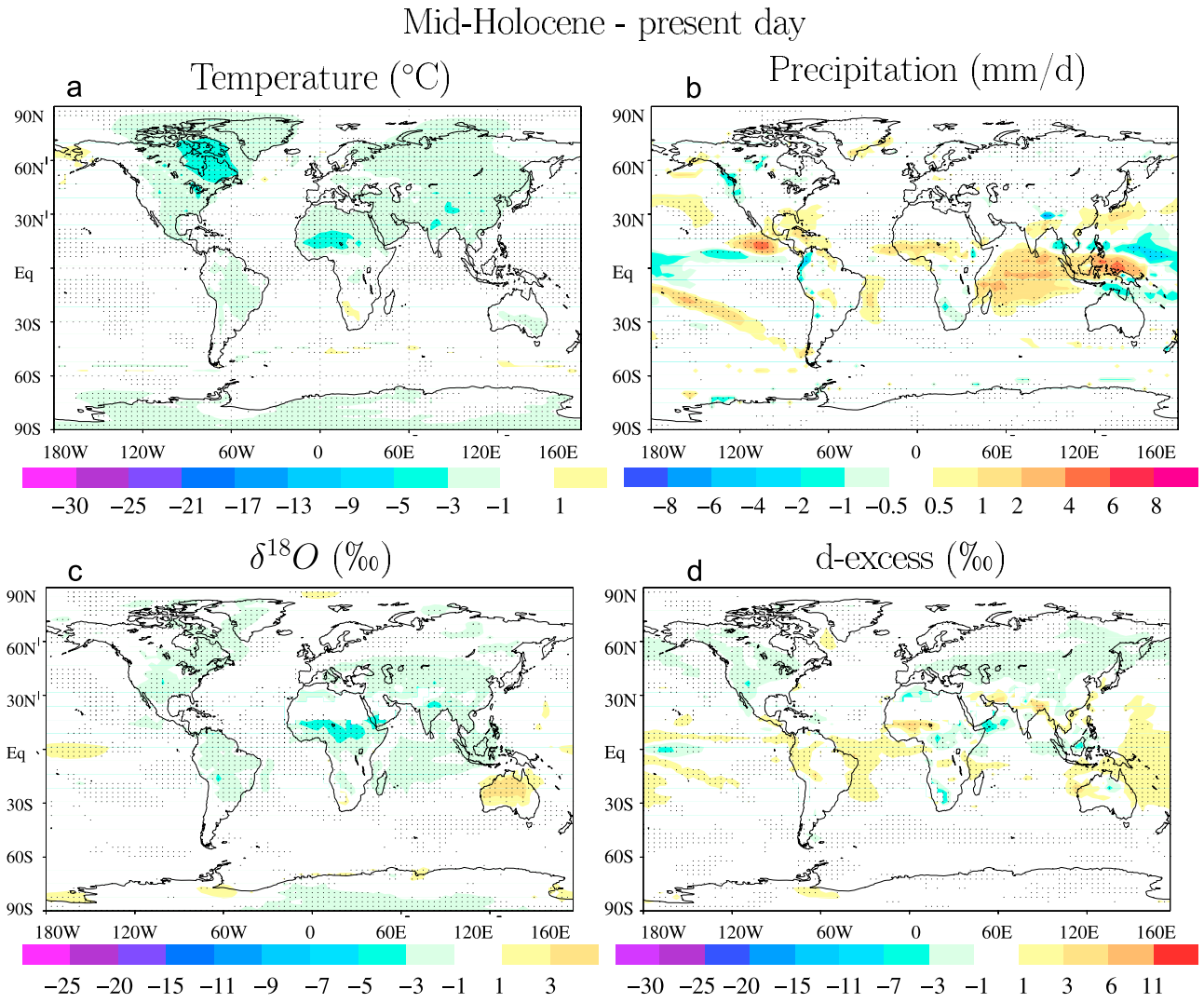

Figure 14. Same as for Figure 12 but for Mid-Holocene minus present day.

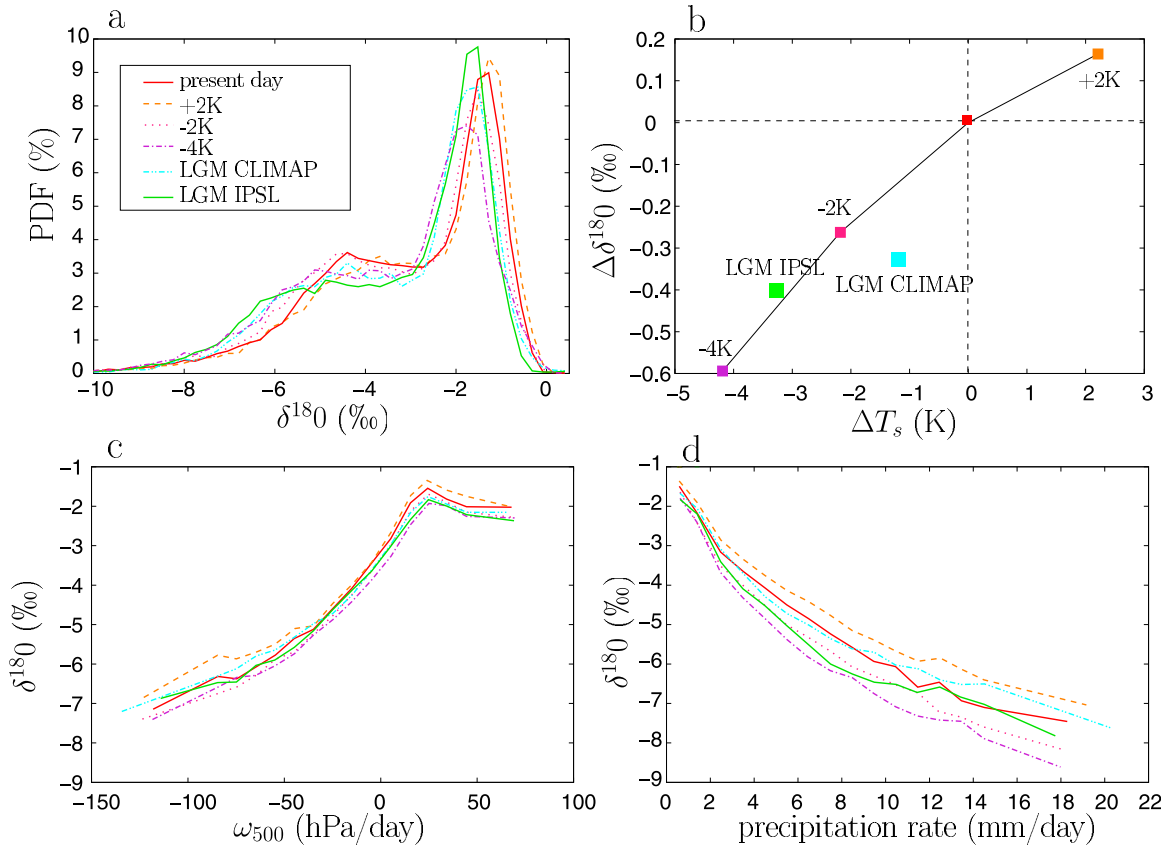

Figure 15. (a) Frequency distribution of the δ^{18}O of precipitation over the tropics (−30°S–30°N) for the different simulations: present day (red), idealized simulation of uniform SST changes, and the two LGM simulations. For each simulation, monthly $\delta^{18}O_p$ values (averaged over the different years of simulation) for all the tropical grid boxes were used. (b) Annually and tropically average change in $\delta^{18}O_p$ (compared to present day) as a function of the annually and tropically averaged change in sea surface temperature. (c) Mean relationship of $\delta^{18}O_p$ over tropical oceans as a function of the large-scale vertical velocity at 500 hPa ω_{500}. For each simulation and in each bin of ω_{500}, we calculate the average $\delta^{18}O_p$ using monthly ω_{500} and $\delta^{18}O_p$ values in all tropical grid boxes. (d) Same as Figure 15c but as a function of the precipitation rate P.

large-scale vertical velocity at 500 hPa, considered as a proxy for dynamical regimes (e.g., large-scale ascent or subsidence [*Bony et al.*, 2004]): the sensitivity to SST is nearly uniform for all dynamical regimes. Therefore, in our GCM, the sensitivity of 0.1‰/K is robust for all types of climate changes and dynamical regimes.

[62] This sensitivity of $\delta^{18}O_p$ to mean SST is smaller than the sensitivity to local temperature measured at high latitudes: temperature-$\delta^{18}O_p$ slopes at high latitudes are about 0.4‰/K at the seasonal scale [*van Ommen and Morgan*, 1997; *Ekaykin and Lipenkov*, 2008] and range from 0.3 to 1‰/K at the interannual scales (Figure 11). Therefore, the sensitivity of $\delta^{18}O_p$ to mean SST in the tropics simulated by LMDZ cannot explain by itself the strong depletion in $\delta^{18}O_p$ measured in the tropics for the LGM. Then, how to interpret the inability of GCMs to reproduce the depletion measured locally in most tropical records? If this is a large-scale mismatch due to an underestimate of the sensitivity of $\delta^{18}O_p$ to mean SST in the tropics, it might reveal a misrepresentation by GCMs of some hydrological or isotopic processes in the tropics. Alternatively, since the largest LGM-PD depletions in the tropics are measured in high-altitude ice cores, the mismatch might be just regional and due to the coarse spatial resolution of GCMs over mountainous regions. However, the coarse resolution may not explain the inability of LMDZ to simulate the 2‰ more depleted precipitation at LGM measured in Brazilian speleothems that are close to the sea level [*Cruz et al.*, 2005a, 2006]. A better spatial coverage of δ^{18}O data at LGM would aid understanding of whether this mismatch is a large-scale or regional feature.

[63] While changes in mean tropical SST have little impact on $\delta^{18}O_p$, the precipitation amount is a dominant control on $\delta^{18}O_p$ in the tropics at the seasonal and spatial scale (Figure 15d). Following the framework of *Bony et al.* [2004], precipitation variations can be decomposed into two components: (1) a dynamical component, due to changes in the large-scale atmospheric circulation associated with changes in the SST distribution, and (2) a thermodynamical component, related to the change in the mean tropical precipitation with mean tropical SST (about 2%/K [*Held and Soden*, 2006]). In LMDZ-iso, a uniform increase in SST leads to both a thermodynamic increase in precipitation and a slight increase in $\delta^{18}O_p$ (Figure 15a), leading to an apparent $P - \delta^{18}O_p$ relationship opposite to the amount

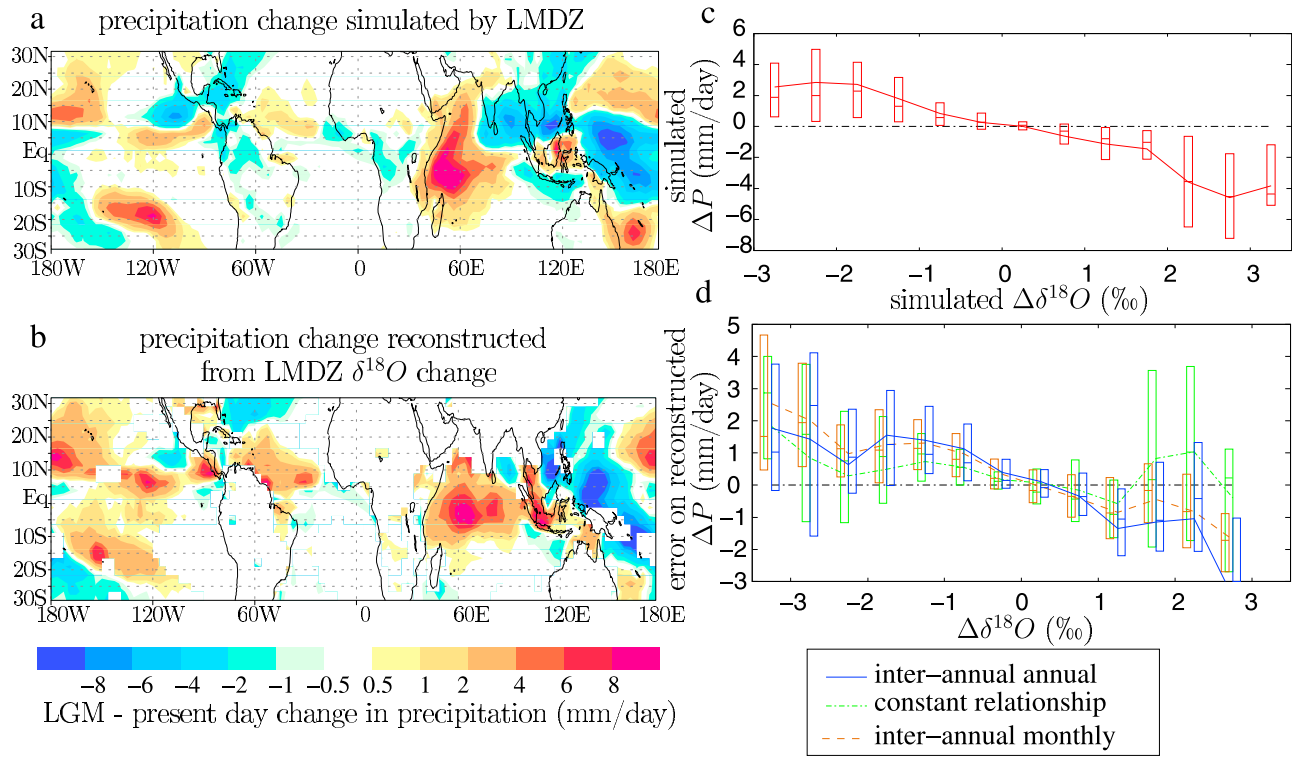

Figure 16. (a) LGM–present-day change in P simulated by LMDZ-iso. (b) LGM–present-day change in P reconstructed from the interannual $\delta^{18}O_p - P$ slope simulated by LMDZ-iso. Areas where the correlation coefficient is higher than −0.25 are white. (c) Annually averaged precipitation change between LGM and PD as a function of the annually averaged change in $\delta^{18}O_p$, simulated by LMDZ-iso, over all tropical locations. The curve shows the average while the bars show the median and quartiles. (d) Error in the reconstructed precipitation change (reconstructed minus simulated by LMDZ-iso) as a function of change in $\delta^{18}O_p$ for different methods: local slope between annual mean precipitation and annual mean $\delta^{18}O$ (dashed blue curve); constant relationship of −0.7‰/(mm/d) (dash-dotted green curve); and local slope between monthly anomalies of $\delta^{18}O_p$ and precipitation, applied on monthly values (dashed brown curve).

effect. The $\delta^{18}O_p$ thus responds only to the dynamical component of the precipitation change, in agreement with a previous SCM study [*Bony et al.*, 2008]. Therefore, the tropical $\delta^{18}O_p$ records mainly regional changes in precipitation related to changes in the large-scale circulation rather than changes in mean temperature or precipitation at the scale of the entire tropics.

4.2. How Much Can We Consider Water Isotopes in Tropical Precipitation as a Good Proxy for Local Precipitation Rate?

[64] In LMDZ-iso, the tropical $\delta^{18}O_p$ records mainly dynamical changes in precipitation. General circulation models simulate precipitation responses to climate change that are very model-dependent, in particular in monsoon regions [e.g., *Held et al.*, 2005]. As the tropical $\delta^{18}O_p$ is closely related to the precipitation amount, the ability of GCMs to reproduce past $\delta^{18}O_p$ changes might help to assess, indirectly, the ability of GCMs to simulate the precipitation response to a global climate change. A prerequisite for this approach, however, is that past local precipitation changes can, indeed, be accurately inferred from water-stable isotopic records. Here, we examine this issue through a "perfect model" experiment, using the CLIMAP LGM and PD simulations: we reconstruct the LGM-PD change in precipitation ($\Delta P_{\text{reconst}}$, Figure 16b) from the LGM-PD $\delta^{18}O_p$ change simulated by LMDZ-iso ($\Delta\delta^{18}O_{sim}$, Figure 12c), and compare this reconstruction with the precipitation change actually simulated by LMDZ-iso (ΔP_{sim}, Figure 16a).

[65] To do so, we first calculate at each grid point the slope of the linear regression (s) of the annual mean $\delta^{18}O_p$ versus annual mean P simulated at the interannual scale by LMDZ-iso. We use annual mean values since the temporal resolution of paleoclimatic records is rarely higher than the year. Then, we reconstruct the precipitation change as $\Delta P_{\text{reconst}} = \frac{1}{s} \cdot \Delta\delta^{18}O_{sim}$, when the coefficient of the linear regression is lower than −0.25, an arbitrary negative cutoff, which ensures that P is indeed a significant control on $\delta^{18}O_p$. Performances of the reconstructions increase as the cutoff decreases, but the relative performances of the different reconstruction methods are insensitive to the choice of the cutoff.

[66] The reconstructed precipitation pattern compares well with the pattern actually simulated by the model (Figures 16a and 16b): the spatial correlation between $\Delta P_{\text{reconst}}$ and ΔP_{sim} is 0.61 (Table 4). The larger the precipitation changes, the better the reconstruction, such as over the Indian Ocean. Where $|\delta^{18}O_p|$ changes are larger than 2‰, 92% of

Table 4. Performance of the Reconstruction of Past Changes in Precipitation Using the Present-Day Interannual Slope of $\delta^{18}O_p$ Versus P in the Perfect Model Experiments[a]

Past Climate	Reconstruction Method	Cutoff	Spatial Correlation	Probability Right Sign $\lvert\Delta\delta^{18}O_p\rvert > 2‰$	Probability Error < 50% $\lvert\Delta\delta^{18}O_p\rvert > 2‰$	Probability Right Sign All Locations	Probability Error < 50% All Locations
LGM CLIMAP	annual	−0.25	0.61	92	29	75	25
LGM CLIMAP	constant	−0.25	0.60	89	34	74	24
LGM CLIMAP	monthly	−0.25	0.74	89	31	71	19
LGM CLIMAP	annual	−0.7	0.68	96	39	81	38
LGM IPSL	annual	−0.25	0.22	72	20	62	14
MH	annual	−0.25	0.62	85	16	72	26
MH	monthly	−0.25	0.59	87	31	73	31

[a]Perfect model experiments are described in section 4.2. We reconstruct changes in precipitation (ΔP) between past climate (column 1) and present day, using different methods (column 2): slope of annual mean $\delta^{18}O_p$ versus annual mean P (annual), constant slope of −0.7‰/(mm/d) (constant), and slope of monthly anomalies of $\delta^{18}O_p$ versus P applied on monthly $\Delta\delta^{18}O_p$ values (monthly). Column 4 gives the spatial correlation between the simulated and reconstructed ΔP. Columns 5 and 7 give the probability that the reconstructed ΔP is of the right sign for locations where $\lvert\Delta\delta^{18}O_p\rvert > 2‰$ and for all locations, respectively. Columns 6 and 8 give the probability that the reconstructed ΔP is within 50% of the simulated ΔP for locations where $\lvert\Delta\delta^{18}O_p\rvert > 2‰$ and for all locations, respectively. All correlations and probabilities are calculated only on locations where the interannual correlation is lower than an arbitrary cutoff (column 3).

the location have $\Delta P_{reconst}$ of the right sign, and 29% of the locations have a reconstructed ΔP relative error (calculated as $(\Delta P_{reconst} - \Delta P_{sim})/\Delta P_{sim}$) smaller than 50% (Table 4). These probabilities decrease to 76% and 25%, respectively, when considering all locations (Table 4). ΔP reconstructions are thus more robust when $\delta^{18}O_p$ variations are larger and thus when the signal to noise ratio is higher. Consistently, reconstructing changes in precipitation is less successful for the Mid-Holocene, for the LGM with IPSL SST, and for uniform SST change experiments, because these simulations show small dynamical changes of precipitation and small $\delta^{18}O_p$ variations. The probability that the relative error in reconstructed ΔP be smaller than 50% at locations where $\lvert\delta^{18}O_p\rvert$ changes are larger than 2‰ is only 20% for the LGM with IPSL SSTs and 17% for the MH (Table 4).

[67] The reconstruction is also the best where the correlation between annual mean $\delta^{18}O_p$ and P is the most negative. For example, the spatial correlation between $\Delta P_{reconst}$ and ΔP_{sim} rises from 0.61 to 0.68 (Table 4) when we choose a cutoff of −0.7 compared to −0.25: where the local P is the main control on $\delta^{18}O_p$ at the interannual scale, it is also the case at the climatic scale. Consequently, changes over land are generally not well captured by the reconstruction, as expected from the lower local correlation there: $\delta^{18}O_p$ in South America, in particular, has been shown to depend more on upstream precipitation [*Vimeux et al.*, 2005].

[68] The reconstruction overestimates the magnitude of precipitation changes (Figure 16d, blue): this means that the $\delta^{18}O_p - P$ slope at the climatic scale is larger in absolute value than the annual slope used in the reconstruction, as was already pointed out for the Mid-Holocene simulation (section 3) and consistent with *Lee et al.* [2009].

[69] To test the importance of a local calibration, we reconstructed the LGM-PD ΔP for the CLIMAP simulation using the same slope at all grid points (Figure 16d, green). The slope yielding, on average, the minimum reconstruction error is −0.7‰/(mm/d), which is significantly stronger than the interannual slope (ranging from −0.3 to −0.6‰/(mm/d)). Using a local calibration compared to a constant slope does not significantly improve the reconstruction (Table 4). Since the climatic slopes are generally higher than the interannual slopes, using a constant slope of −0.7‰/(mm/d) slightly reduces the reconstruction errors (Figure 16d, green).

[70] When taking into account the thermodynamic effect of mean SST on $\delta^{18}O_p$ (0.1‰/K) and on precipitation (2%/K), the reconstructed LGM-PD ΔP is uniformly lower by 0.5 mm/d. Therefore, this thermodynamical effect explains part of the overestimate of the reconstructed LGM precipitation.

[71] So far, we have discussed reconstructions performed at the annual mean scale, i.e., neglecting the seasonal cycle, essentially because monthly $\delta^{18}O_p$ is not available from long-term records. However, the tropical precipitation experiences strong seasonal variations, so that the isotopic records at the annual-scale record preferentially the $\Delta\delta^{18}O_p$, and thus the ΔP, during the wet season. Using annual mean $\delta^{18}O_p$ values to reconstruct the annual mean ΔP thus constitutes a likely source of errors in the reconstruction. We gave an illustrative example of this source of error in section 3.4.2, showing that over West Africa the climatic slope between PD and MH was 3 times larger when calculated with annual averages than with wet season (JJAS) averages, thus leading to an overestimation of $\Delta P_{reconst}$ of a factor of 3 just by neglecting the seasonal variability. To quantify more systematically this source of error, we reconstruct monthly ΔP using simulated monthly $\Delta\delta^{18}O_p$ and the slope calculated on present-day monthly interannual anomalies (Figure 16d, brown). In this case the reconstruction is significantly improved for positive LGM-PD changes. For the LGM CLIMAP simulation, the probability that the reconstructed ΔP relative error is smaller than 50% slightly rises to 31% (compared to 29%) when considering seasonal information (Table 4). The uncertainty in the reconstruction due to the seasonality of the precipitation is the largest for the MH simulation: the probability that the reconstructed ΔP relative error is smaller than 50% rises to 31% (compared to 16%) when considering seasonal information (Table 4). This is consistent with the strong changes in precipitation seasonality for the MH, with the precipitation increase occurring mainly during the wet season in monsoon regions.

[72] To conclude, using the PD interannual $\delta^{18}O_p - P$ slope to reconstruct past precipitation changes yields good results qualitatively: the spatial patterns of ΔP are well reconstructed, especially for past climates involving large circulation changes. Where measured changes of $\delta^{18}O_p$ are high (>2‰), it is very likely that the reconstructed ΔP has the right sign (92%): this means that interannual and climatic controls on $\delta^{18}O_p$ are similar. Quantitatively however, the reconstructed errors are high and most likely above 50%. The magnitude of the reconstructed ΔP is generally overestimated. Considering the seasonal cycle of P and $\delta^{18}O_p$ both for the calibration and reconstruction would improve the reconstructions quantitatively, in particular for past climates associated with strong changes in precipitation seasonality (e.g., MH).

5. Conclusion and Perspectives

5.1. Evaluation of LMDZ-iso

[73] We present the implementation of water-stable isotopes in the LMDZ-iso GCM, and evaluate the present-day isotopic distribution simulated at different time scales: synoptic, seasonal, and interannual, as well as for past climate changes. LMDZ-iso forced by observed SSTs reproduces the annual mean and the seasonal distribution of $\delta^{18}O_p$ reasonably well, as well as its interannual variability in the tropics. Nudging the model winds by atmospheric reanalyses improves the simulation of the interannual and synoptic variability of temperature and $\delta^{18}O$ at middle latitudes.

[74] Deuterium excess is known to be a more difficult parameter to simulate [*Mathieu et al.*, 2002]. Despite some discrepancies over tropical continents, LMDZ-iso is able to correctly simulate the average d excess values as well as the zonal gradient. LMDZ-iso is not able to reproduce the observed variability of d excess in the vapor, neither at synoptic nor at interannual scales, producing near-constant values all year long and for all years in some regions.

[75] Numerous sensitivity tests were performed on both isotopic and nonisotopic parameters of the model. The precipitation composition is most sensitive to two parameters controlling kinetic effects: λ, involved in the parameterization of the supersaturation during snow formation [*Jouzel and Merlivat*, 1984], and ϕ, involved in the parameterization of the relative humidity at the droplet contact [*Bony et al.*, 2008]. These representations of kinetic effects are thus a large source of uncertainties in isotopic modeling. More measurements are certainly needed to better constrain these processes. In particular, the degree of equilibration of the rain drops with the vapor can be parametrized in many ways [e.g., *Stewart*, 1975; *Hoffmann et al.*, 1998; *Mathieu et al.*, 2002; *Lee and Fung*, 2008; *Bony et al.*, 2008] and is difficult to evaluate owing to the scarcity of isotopic measurements in the vapor. It would thus be extremely useful to have simultaneous measurements of precipitation and vapor at the same stations to evaluate the representation of isotopic processes during rain reevaporation in models. New technology [e.g., *Gupta et al.*, 2009] now facilitates measurements in the vapor and will certainly offer new evaluation possibilities.

[76] LMDZ-iso simulates LGM isotopic compositions similar to other GCMs, with relatively realistic depletions at high latitudes, but a near-constant $\delta^{18}O$ in the tropics. Like other GCMs, LMDZ-iso has difficulties simulating the lower measured d excess during the LGM over East Antarctica, though it can simulate it in Greenland and coastal Antarctica.

5.2. Interpretation of Paleoclimatic Proxies

[77] At high latitudes, on the basis of a LGM simulation with LMDZ-iso forced by the CLIMAP SST reconstruction, we show that using the present-day spatial slope to reconstruct past temperatures leads to an underestimation of a factor of 2 in Greenland but is more adequate in Antarctica, in agreement with previous studies [*Jouzel et al.*, 2000, 2003]. However, the accuracy of this reconstruction in Antarctica strongly depends on the equator-pole SST gradients of the reconstructed past climate. If the equator-pole at LGM was weaker than reconstructed by CLIMAP, then past temperature reconstructions in Antarctica would be underestimated, in agreement with *Lee et al.* [2008].

[78] In the tropics changes in $\delta^{18}O_p$ may result from global-scale changes in SSTs, and/or from regional precipitation changes associated with changes in SSTs that are not spatially uniform. We found that changes in mean tropical SSTs have relatively little impact on $\delta^{18}O_p$ (0.1‰/K) and cannot explain the large changes in $\delta^{18}O_p$ recorded in few tropical locations for the LGM. On the other hand, large changes in $\delta^{18}O_p$ are more likely related to precipitation changes associated with a reorganization of SST patterns.

[79] We thus examine the ability of $\delta^{18}O_p$ records to reconstruct past local precipitation changes in the tropics. Our analysis suggests that past local precipitation changes can be reconstructed from $\delta^{18}O_p$ records, but only in cases where the signal to noise ratio for $\delta^{18}O_p$ is the largest. The use of a $\delta^{18}O - P$ slope calibrated locally from present-day annual data seems adequate to reconstruct at least qualitatively the broad pattern and signs of precipitation changes. However, this overestimates the magnitude of precipitation changes. Considering the seasonal cycle of precipitation and $\delta^{18}O_p$ for both the calibration and reconstruction would improve the reconstruction quantitatively. Over continents however, the sensitivity of $\delta^{18}O_p$ to upstream precipitation rather than local precipitation makes reconstructions of past precipitation at the regional scale more adequate [*Vimeux et al.*, 2005]. Besides, changes in continental recycling associated with past vegetation changes, which were not taken into account in this study, may complicate the $\delta^{18}O_p$ signal over continents [*Pierrehumbert*, 1999].

5.3. Perspectives

[80] LMDZ-iso, like other GCMs, does not simulate the large isotopic depletion measured in tropical ice cores, questioning whether all processes affecting $\delta^{18}O_p$ in the tropics are well represented. Tropical ice cores are located in mountainous regions, characterized by a complex topography which can only be resolved with high-resolution modeling [*Sturm et al.*, 2005]. Part of the difficulty in simulating the ice core isotopic data at LGM could be due to the coarse resolution of GCMs (here 2.75 × 3.5°). In the future, we plan to use the stretched grid functionality of LMDZ-iso [e.g., *Krinner et al.*, 1997a] to run zoomed simulations for present day and for LGM over low-latitude mountain regions such as the Andes and Tibet, to better simulate the relationship

between isotopes and climate and explore climatic controls on low-latitude ice core isotopic composition.

[81] Air parcels supplying precipitation to ice core regions usually travel several days over continental regions (the Amazon for the Andes, India for Tibet), over which continental recycling of precipitation occurs. The proportion of precipitation recycled to the atmosphere or lost by runoff has been shown to control continental gradients in $\delta^{18}O$ [*Rozanski et al.*, 1993]. Besides, transpiration does not fractionate relatively to the soil water [*Washburn and Smith*, 1934; *Barnes and Allison*, 1988] whereas bare soil evaporation does and is thus depleted relative to the soil water [*Moreira et al.*, 1997; *Yepez et al.*, 2003; *Williams et al.*, 2004]. A decrease in the ratio of the precipitation evapotranspired back to the atmosphere and of the proportion of the evapotranspiration occurring as transpiration, associated with vegetation changes from forests to grasslands [*Clapperton*, 1993], may contribute to the measured decrease of $\delta^{18}O_p$ in the Andes during the LGM [*Pierrehumbert*, 1999]. Moreover, processes by which precipitation is recycled (transpiration or evaporation from open water or soil) are suggested to strongly affect d excess gradients over the Amazon [*Salati et al.*, 1979; *Gat and Matsui*, 1991; *Henderson-Sellers et al.*, 2004] and thus possibly the Andean ice core d excess. Despite the potentially strong impact of land surface processes on the isotopic distribution, in LMDZ-iso as in most other GCMs, we have assumed no fractionation when recycling precipitation over land, owing to the simplicity of the land surface model. Coupling atmospheric models with more sophisticated land surface models [*Aleinov and Schmidt*, 2006; *Yoshimura et al.*, 2006] would enable a more accurate representation of isotopic fractionation over land and allow us to explore the impact of vegetation changes on continental isotopic records. Water-stable isotopes are being implemented in ORCHIDEE, the land surface component of the IPSL model, and LMDZ-ORCHIDEE-iso coupled simulations will be reported in a future paper.

[82] Finally, further global evaluations of our GCM will be carried out in the future by comparing its simulations with the newly available global isotopic data measured by satellite, in particular the Troposperic Emission Spectrometer (TES) [*Worden et al.*, 2007] and Scanning Imaging Absorption Spectrometer for Atmospheric Cartography (SCIAMACHY) [*Frankenberg et al.*, 2009] data.

Appendix A: Advection of Water-Stable Isotopes

[83] Water isotopes are advected passively during the large-scale water advection. However, for numerical reasons, the advection of water isotopes can be problematic in some schemes [e.g., *Joussaume*, 1989; *Mathieu et al.*, 2002]. We present here the *Van Leer* [1977] advection scheme used in LMDZ-iso and explain the possible problem of isotopic advection and how we handle it. To simplify, we consider in the following a unidimensional advection along the x axis, with a westerly wind.

A1. Van Leer Advection Scheme

[84] The *Van Leer* [1977] scheme used in LMDZ is a finite volume advection scheme, conserving water mass. In the grid box i, m'_i, the total air mass at time $t + \Delta t$ is a function of the total air mass at time t and the air mass fluxes on the left and right border, $U_{i-1/2}$ and $U_{i+1/2}$, respectively:

$$m'_i = m_i + U_{i-1/2} - U_{i+1/2}.$$

[85] Similarly, the averaged specific humidity in grid box i at time $t + \Delta t$, q'_i, is a function of the specific humidity at time t and the water flux on the left and right border, $F_{i-1/2}$ and $F_{i+1/2}$.

$$q_i' = \frac{q_i \cdot m_i + F_{i-1/2} - F_{i+1/2}}{m'_i}.$$

[86] Water fluxes (for example, $F_{i-1/2}$) are calculated as the product of the air mass flux ($U_{i-1/2}$) and the specific humidity of the advected air ($q_{i-1/2}^{\smile}$):

$$F_{i-1/2} = U_{i-1/2} \cdot q_{i-1/2}^{\smile}.$$

[87] In the Van Leer scheme, $q_{i-1/2}^{\smile}$ is interpolated between the averaged specific humidity of the adjacent boxes, so that $q_{i-1/2}^{\smile}$ is a function of (q_i, q_{i+1}, q_{i-1}).

[88] As long as $q_{i-1/2}^{\smile}$ is intermediate between q_i and q_{i-1}, the monotony of the scheme is ensured: q'_i remains intermediate between q_i and q_{i-1} [*Van Leer*, 1977; *Hourdin*, 2005].

A2. Implementation of Water Isotopes in the Van Leer Scheme

[89] As for water, the isotopic equivalent of specific humidity, X, is advected in finite volume

$$X_i' = \frac{X_i \cdot m_i + G_{i-1/2} - G_{i+1/2}}{m'_i},$$

where $G_{i-1/2}$ and $G_{i+1/2}$ are the isotope fluxes at the left and right boundaries. The isotope mass is thus conserved during advection. The isotope flux at the left boundary, $G_{i-1/2}$, is calculated as the product $U_{i-1/2}$ and the isotopic content of the advected air $X_{i-1/2}^{\smile}$,

$$G_{i-1/2} = U_{i-1/2} \cdot X_{i-1/2}^{\smile}.$$

[90] In a purely Lagrangian framework, transport should simultaneously conserve the water, the isotopic content, and the isotopic ratio $R = X/q$: indeed, it can be shown that if X follows the same conservation equation as q of the form $\frac{\partial q}{\partial t} + u \cdot \frac{\partial q}{\partial x} = 0$, then R also follows the same conservation equation.

[91] In the Van Leer scheme, however, owing to the discretization, X and R cannot follow simultaneously the same equation as q. A choice has thus to be made regarding how to handle the transport of water isotopes.

[92] If X were to be treated exactly like water, $X_{i-1/2}^{\smile}$ should be interpolated between the adjacent grid boxes, so that $X_{i-1/2}^{\smile}$ is a function of (X_i, X_{i+1}, X_{i-1}). Then the monotony of the transport would be ensured for q and X. However, the monotony would not be ensured for R, owing to the nonlinearity of R as a function of X and q. In particular, it could happen that the isotopic ratio after advection, R'_i, becomes either larger or smaller than the ratios in

both adjacent grid boxes. Spurious variations of the isotopic ratio could thus appear.

[93] Problems arising from representing the isotopic mixing ratio exactly like the water mixing ratio are justified physically: isotopes are not transported independently from the water but inside the water.

[94] Therefore, to ensure that isotopes are not transported without water, we calculate $X_{i-1/2}^{\smile}$ as the product of the advected water content $q_{i-1/2}^{\smile}$ and the isotopic ratio of this advected water $R_{i-1/2}^{\smile}$,

$$X_{i-1/2}^{\smile} = q_{i-1/2}^{\smile} \cdot R_{i-1/2}^{\smile}.$$

[95] To ensure the monotony of the isotopic ratio, $R_{i-1/2}^{\smile}$ is interpolated between the adjacent boxes, so that $R_{i-1/2}$ is a function of (R_i, R_{i+1}, R_{i-1}).

[96] This representation of the isotopic transport ensures both the conservation of the mass of water isotopes (finite volume scheme) and the monotony of the isotopic ratio.

[97] **Acknowledgments.** We thank Masa Kageyama, Valrie Masson-Delmotte, Gerhard Krinner, and Frédéric Hourdin for useful discussions, Gilles Delaygue and Gavin Schmidt for comments on the manuscript as part of their review of Camille Risi's Ph.D. dissertation, and three anonymous reviewers for their very constructive comments. This work benefited from financial support of the LEFE project MISSTERRE.

References

Aleinov, I., and G. A. Schmidt (2006), Water isotopes in the GISS ModelE land surface scheme, *Global Planet. Change*, *51*, 108–120.

Angert, A., J.-E. Lee, and D. Yakir (2008), Seasonal variations in the isotopic composition of near-surface water vapour in the eastern Mediterranean, *Tellus, Ser. B*, *60*(4), 674–684.

Baldini, L. M., F. McDermott, A. M. Foley, and J. U. L. Baldini (2008), Spatial variability in the European winter precipitation d^{1}8O-NAO relationship: Implications for reconstructing NAO-mode climate variability in the Holocene, *Geophys. Res. Lett.*, *35*, L04709, doi:10.1029/2007GL032027.

Barnes, C., and G. Allison (1988), Tracing of water movement in the unsaturated zone using stable isotopes of hydrogen and oxygen, *J. Hydrol.*, *100*, 143–176.

Bath, A. H. (1983), Stable isotopic evidence for paleo-recharge conditions of groundwater, in *Paleoclimates and Paleowaters: A Collection of Environmental Isotope Studies*, pp. 169–186, Int. At. Energy Agency, Vienna.

Berger, A. (1978), Long-term variations of caloric solar radiation resulting from the Earth's orbital elements, *Quat. Res.*, *9*, 139–167.

Bony, S., and K. A. Emanuel (2001), A parameterization of the cloudiness associated with cumulus convection; Evaluation using TOGA COARE data, *J. Atmos. Sci.*, *58*, 3158–3183.

Bony, S., J.-L. Dufresne, H. Le Treut, J.-J. Morcrette, and C. Senior (2004), On dynamic and thermodynamic components of cloud changes, *Clim. Dyn.*, *22*, 71–86.

Bony, S., C. Risi, and F. Vimeux (2008), Influence of convective processes on the isotopic composition (δO^{18} and δD) of precipitation and water vapor in the tropics: 1. Radiative-convective equilibrium and TOGA-COARE simulations, *J. Geophys. Res.*, *113*, D19305, doi:10.1029/2008JD009942.

Boyle, E. A. (1997), Cool tropical temperatures shift the global $\delta^1$8O-T relationship: An explanation for the ice core $\delta^1$8O–borehole thermometry conflict?, *Geophys. Res. Lett.*, *24*(3), 273–276.

Braconnot, P., et al. (2007), Results of PMIP2 coupled simulations of the Mid-Holocene and Last Glacial Maximum - Part 1: Experiments and large-scale features, *Clim. Past*, *3*, 261–277.

Bradley, R. S., M. Vuille, D. Hardy, and L. G. Thompson (2003), Low latitude ice cores record Pacific sea surface temperatures, *Geophys. Res. Lett.*, *30*(4), 1174, doi:10.1029/2002GL016546.

Cess, R. D., and G. L. Potter (1988), A methodology for understanding and intercomparing atmospheric climate feedback processes in general circulation models, *J. Geophys. Res.*, *93*(D7), 8305–8314.

Ciais, P., and J. Jouzel (1994), Deuterium and oxygen 18 in precipitation: Isotopic model, including cloud processes, *J. Geophys. Res.*, *99*(D8), 16,793–16,803.

Ciais, P., W. White, J. Jouzel, and J. Petit (1995), The origin of present-day Antarctic precipitation from surface snow deuterium excess data, *J. Geophys. Res.*, *100*(D9), 18,917–18,927.

Clapperton, C. M. (1993), Nature of environmental changes in South America at the Last Glacial Maximum, *Palaeogeogr. Palaeoclimatol. Palaeoecol.*, *101*, 189–208.

CLIMAP Project Members (1981), Seasonal reconstructions of the Earth's surface at the Last Glacial Maximum, *Tech. Rep. GM-36*, Geol. Soc. Am., Boulder, Colo.

Coplen, T. (1988), Normalization of oxygen and hydrogen isotope data, *Chem. Geol.*, *72*, 293–297.

Cruz, F. W., S. J. Burns, I. Karmann, W. D. Sharp, M. Vuille, A. O. Cardoso, J. A. Ferrari, P. L. S. Dias, and O. J. Viana (2005a), Insolation-driven changes in atmospheric circulation over the past 116,000 years in subtropical Brazil, *Nature*, *434*, 63–66.

Cruz, F. W., I. Karmann, O. Viana Jr., J. A. Burns, M. Ferrari, M. Vuille, A. N. Sial, and M. Z. Moreira (2005b), Stable isotope study of cave percolation waters in subtropical Brazil: Implications for paleoclimate inferences from speleothems, *Chem. Geol.*, *220*, 245–262.

Cruz, F. W., S. J. Burns, I. Karmann, W. Sharp, and M. Vuille (2006), Reconstruction of regional atmospheric circulation features during the late Pleistocene in subtropical Brazil from oxygen isotope composition of speleothems, *Earth Planet. Sci. Lett.*, *248*(1–2), 495–507, doi:10.1016/j.epsl.2006.06.019.

Cruz, F. W., et al. (2009), Orbitally driven east-west antiphasing of South American precipitation, *Nat. Geosci.*, *2*, 210–214.

Dansgaard, W. (1953), The abundance of ^{1}8O in atmospheric water and water vapour, *Tellus*, *5*, 461–469.

Dansgaard, W. (1964), Stable isotopes in precipitation, *Tellus*, *16*, 436–468.

Delmotte, M., V. Masson, J. Jouzel, and V. Morgan (2000), A seasonal deuterium excess signal at Law Dome, coastal eastern Antarctica: A Southern Ocean signature, *J. Geophys. Res.*, *105*(D6), 7187–7197.

Ducoudré, N., K. Laval, and A. Perrier (1993), SECHIBA, a new set of parametrizations of the hydrological exchanges at the land-atmosphere interface within the LMD atmospheric general circulation model, *J. Clim.*, *6*, 248–273.

Ekaykin, A. A., and V. Y. Lipenkov (2008), Formation of the ice core isotope composition, paper presented at 2nd International Workshop on Physics of Ice Core Records (PICR-2), Hokkaido Univ., Sapporo, Japan.

Emanuel, K. A. (1991), A scheme for representing cumulus convection in large-scale models, *J. Atmos. Sci.*, *48*, 2313–2329.

Farrera, I., et al. (1999), Tropical climates at the Last Glacial Maximum: A new synthesis of terrestrial palaeoclimate data. I. Vegetation, lake-levels and geochemistry, *Clim. Dyn.*, *15*, 823–856.

Frankenberg, C., et al. (2009), Dynamic processes governing lower-tropospheric HDO/H_2O ratios as observed from space and ground, *Science*, *325*, 1374–1377.

Fritz, S., et al. (2003), Hydrologic variation during the last 170,000 years in the Southern Hemisphere tropics of South America, *Quat. Res.*, *61*, 95–104.

Fujita, K., and O. Abe (2006), Stable isotopes in daily precipitation at Dome Fuji, East Antarctica, *Geophys. Res. Lett.*, *33*, L18503, doi:10.1029/2006GL026936.

Gasse, F. (2000), Hydrological changes in the African tropics since the Last Glacial Maximum, *Quat. Sci. Rev.*, *19*, 189–211.

Gat, J. R., and E. Matsui (1991), Atmospheric water balance in the Amazon basin: An isotopic evapotranspiration model, *J. Geophys. Res.*, *96*(D7), 13,179–13,188.

Gates, W. L. (1992), AMIP: The Atmospheric Model Intercomparison Project, *Bull. Am. Meteorol. Soc.*, *73*, 1962–1970.

Grandpeix, J. Y., V. Phillips, and R. Tailleux (2004), Improved mixing representation in Emanuel's convection scheme, *Q. J. R. Meteorol. Soc.*, *130*, 3207–3222.

GRIP Members (1993), Climate instability during the last interglacial period recorded in the GRIP ice core, *Nature*, *364*, 203–207.

Grootes, P. M., E. J. Steig, M. Stuiver, E. D. Waddington, and D. L. Morse (2001), The Taylor Dome Antarctic ^{1}8O record and globally synchronous change in climate, *Quat. Res.*, *56*, 289–298.

Gupta, P., D. Noone, J. Galewsky, C. Sweeney, and B. H. Vaughn (2009), Demonstration of high-precision continuous measurements of water vapor isotopologues in laboratory and remote field deployments using wavelength-scanned cavity ring-down spectroscopy (WS-CRDS) technology, *Rapid Commun. Mass Spectrom.*, *23*, 2534–2542.

Held, I. M., and B. J. Soden (2006), Robust responses of the hydrological cycle to global warming, *J. Clim.*, *19*, 5686–5699.

Held, I. M., T. L. Delworth, K. L. Findell, and T. R. Knutson (2005), Simulation of Sahel drought in the 20th and 21st centuries, *Proc. Natl. Acad. Sci., U. S. A.*, *102*, 17,891–17,896, doi:10.1073/pnas.0509057,102.

Henderson-Sellers, A., K. McGuffie, and H. Zhang (2001), Stable isotopes as validation tools for global climate model predictions of the impact of Amazonian deforestation, *J. Clim*, *15*, 2664–2677.

Henderson-Sellers, A., K. McGuffie, D. Noone, and P. Irannejad (2004), Using stable water isotopes to evaluate basin-scale simulations of surface water budgets, *J. Hydrometeorol.*, *5*, 805–822.

Hoffmann, G. (2003), Taking the pulse of the tropical water cycle, *Science*, *301*, 776–777.

Hoffmann, G., M. Werner, and M. Heimann (1998), Water isotope module of the ECHAM atmospheric general circulation model: A study on timescales from days to several years, *J. Geophys. Res.*, *103*(D14), 16,871–16,896.

Hoffmann, G., et al. (2003), Coherent isotope history of Andean ice cores over the last century, *Geophys. Res. Lett.*, *30*(4), 1179, doi:10.1029/2002GL014870.

Hourdin, F. (2005), Représentation du transport direct et inverse dans les modèles globaux de climat et étude des couplages entre composition et dynamique atmosphérique sur Titan, Habilitation à Diriger des Rech., Orsay, France.

Hourdin, F., et al. (2006), The LMDZ4 general circulation model: Climate performance and sensitivity to parametrized physics with emphasis on tropical convection, *Clim. Dyn.*, *27*, 787–813.

Huffman, G. J., P. Arkin, and J. Janowiak (1997), The Global Precipitation Climatology Project (GPCP) combined precipitation dataset, *Bull. Am. Meteorol. Soc.*, *78*, 5–20.

Johnsen, S., W. Dansgaard, H. Clausen, and J. C. Langway (1972), Oxygen isotope profiles through the Antarctic and Greenland ice sheets, *Nature*, *235*, 429–434.

Johnsen, S., W. Dansgaard, and J. White (1989), Origin of Arctic precipitation under present and glacial conditions, *Tellus, Ser. B*, *41*, 452–458.

Johnsen, S., H. Clausen, W. Dansgaard, N. Gundestrup, M. Hansson, P. Jonsson, J. Steffensen, and A. Sveinbjörnsdottir (1992), A "deep" ice core from East Greenland, *Medd. Groenl. Geosci.*, *29*, 1–22.

Joussaume, S. (1989), Simulations du climat du dernier maximum glaciaire à l'aide d'un modèle de circulation générale de l'atmosphère incluant une modélisation du cycle des isotopes de l'eau et des poussières d'origine désertique, Ph.D. thesis, Univ. Marie et Pierre Curie, Paris.

Joussaume, S., and J. Jouzel (1993), Paleoclimatic tracers: An investigation using an atmospheric general circulation model under ice age conditions: 2. Water isotopes, *J. Geophys. Res.*, *98*(D2), 2807–2830.

Joussaume, S., and K. E. Taylor (1995), Status of the paleoclimate modeling intercomparison project, in *Proceedings of the First International AMIP Scientific Conference*, edited by W. L. Gates, pp. 425–430, World Meteorol. Org., Geneva.

Joussaume, S., J. Jouzel, and R. Sadourny (1984), A general circulation model of water isotope cycles in the atmosphere, *Nature*, *311*, 24–29.

Joussaume, S., et al. (1999), Monsoon changes for 6000 years ago: Results of 18 simulations from the Paleoclimate Modeling Intercomparison Project (PMIP), *Geophys. Res. Lett.*, *26*(7), 859–862.

Jouzel, J. (1999), Calibrating the isotopic paleothermometer, *Science*, *286*, 910–911.

Jouzel, J. (2003), Water stable isotopes: Atmospheric composition and applications in polar ice core studies, *Treatise Geochem.*, *4*, 213–243.

Jouzel, J., and L. Merlivat (1984), Deuterium and oxygen 18 in precipitation: Modeling of the isotopic effects during snow formation, *J. Geophys. Res.*, *89*(D7), 11,749–11,757.

Jouzel, J., R. D. Koster, R. J. Suozzo, G. L. Russel, J. W. C. White, and W. S. Broecker (1987), Simulations of the HDO and $H_2^{18}O$ atmospheric cycles using the NASA GISS General Circulation Model: The seasonal cycle for present-day conditions, *J. Geophys. Res.*, *92*(D12), 14,739–14,760.

Jouzel, J., R. Koster, R. Suozzo, and G. L. Russel (1994), Stable water isotope behavior during the Last Glacial Maximum: A general circulation model analysis, *J. Geophys. Res.*, *99*(D12), 25,791–25,801.

Jouzel, J., G. Hoffmann, R. D. Koster, and V. Masson (2000), Water isotopes in precipitation: Data/model comparison for present-day and past climates, *Quat. Sci. Rev.*, *19*, 363–379.

Jouzel, J., F. Vimeux, N. Caillon, G. Delaygue, G. Hoffmann, V. Masson-Delmotte, and F. Parrenin (2003), Magnitude of isotope/temperature scaling for interpretation of central Antarctic ice cores, *J. Geophys. Res.*, *108*(D12), 4361, doi:10.1029/2002JD002677.

Kalnay, E., et al. (1996), The NCEP/NCAR 40-year reanalysis project, *Bull. Am. Meteorol. Soc.*, *77*, 437–470.

Krinner, G., and M. Werner (2003), Impact of precipitation seasonality changes on isotopic signals in polar ice cores: A multi-model analysis, *Earth Planet. Sci. Lett.*, *216*, 525–538.

Krinner, G., C. Genthon, Z.-X. Li, and P. L. Van (1997a), Studies of the Antarctic climate with a stretched-grid general circulation model, *J. Geophys. Res*, *102*(D12), 13,731–13,745.

Krinner, G., C. Genton, and J. Jouzel (1997b), GCM analysis of local influences on ice core delta signals, *Geophys. Res. Lett*, *24*(22), 2825–2828.

Krinner, G., N. Viovy, N. de Noblet-Ducoudré, J. Ogee, J. Polcher, P. Friedlingstein, P. Ciais, S. Sitch, and I. C. Prentice (2005), A dynamic global vegetation model for studies of the coupled atmosphere-biosphere system, *Global Biogeochem. Cycles*, *19*, GB1015, doi:10.1029/2003GB002199.

Kutzbach, J. E., X. Liu, Z. Liu, and G. Chen (2008), Simulation of the evolutionary response of global summer monsoons to orbital forcing over the past 280,000 years, *Clim. Dyn.*, *30*, 567–579, doi:10.1007/s00382-007-0308-z.

Labeyrie, L. D., J. C. Duplessy, and P. L. Blanc (1987), Variations in mode of formation and temperature of oceanic deep waters over the past 125,000 years, *Nature*, *327*, 477–482.

Landais, A., E. Barkan, and B. Luz (2008), Record of $\delta^{18}O$ and ^{17}O-excess in ice from Vostok Antarctica during the last 150,000 years, *Geophys. Res. Lett.*, *35*, L02709, doi:10.1029/2007GL032096.

Lawrence, J. R., S. D. Gedzelman, D. Dexheimer, H.-K. Cho, G. D. Carrie, R. Gasparini, C. R. Anderson, K. P. Bowman, and M. I. Biggerstaff (2004), Stable isotopic composition of water vapor in the tropics, *J. Geophys. Res.*, *109*, D06115, doi:10.1029/2003JD004046.

Lee, J.-E., and I. Fung (2008), "Amount effect" of water isotopes and quantitative analysis of post-condensation processes, *Hydrol. Processes*, *22*(1), 1–8.

Lee, J.-E., I. Fung, D. DePaolo, and C. C. Fennig (2007), Analysis of the global distribution of water isotopes using the NCAR atmospheric general circulation model, *J. Geophys. Res.*, *112*, D16306, doi:10.1029/2006JD007657.

Lee, J.-E., I. Fung, D. J. DePaolo, and B. Otto-Bliesner (2008), Water isotopes during the Last Glacial Maximum: New general circulation model calculations, *J. Geophys. Res.*, *113*, D19109, doi:10.1029/2008JD009859.

Lee, J.-E., K. Johnson, and I. Fung (2009), Precipitation over South America during the Last Glacial Maximum: An analysis of the "amount effect" with a water isotop-enabled general circulation model, *Geophys. Res. Lett.*, *36*, L19701, doi:10.1029/2009GL039265.

Liu, C., and E. J. Zipser (2005), Global distribution of convection penetrating the tropical tropopause, *J. Geophys. Res.*, *110*, D23104, doi:10.1029/2005JD006063.

Lorius, C., L. Merlivat, J. Jouzel, and M. Pourchet (1979), A 30,000 yr isotope climatic record from Antarctic ice, *Nature*, *280*, 644–648.

Lorius, C., J. Jouzel, C. Ritz, L. Merlivat, N. I. Barkov, Y. S. Korotkevitch, and V. M. Kotlyakov (1985), A 150,000-year climate record from Antarctic ice, *Nature*, *316*, 591–596.

Majoube, M. (1971a), Fractionnement en O^18 entre la glace et la vapeur d'eau, *J. Chim. Phys. Phys. Chim. Biol.*, *68*, 625–636.

Majoube, M. (1971b), Fractionnement en Oxygène 18 et en Deutérium entre l'eau et sa vapeur, *J. Chim. Phys. Phys. Chim. Biol.*, *10*, 1423–1436.

MARGO Project Members (2009), Constraints on the magnitude and patterns of ocean cooling at the Last Glacial Maximum, *Nat. Geosci.*, *2*, 127–132.

Marti, O., et al. (2005), The new IPSL climate system model: IPSL-CM4, *Tech. Rep. 26*, IPSL, Paris.

Masson-Delmotte, V., J. Jouzel, A. Landais, M. Stievenard, S. J. Johnsen, J. W. C. White, M. Werner, A. Sveinbjornsdottir, and K. Fuhrer (2005a), GRIP Deuterium excess reveals rapid and orbital-scale changes in Greenland moisture origin, *Science*, *309*, 118–121.

Masson-Delmotte, V., et al. (2005b), Holocene climatic changes in Greenland: Different deuterium excess signals at Greenland Ice Core Project (GRIP) and NorthGRIP, *J. Geophys. Res.*, *110*, D14102, doi:10.1029/2004JD005575.

Masson-Delmotte, V., et al. (2006), Past and future polar amplification of climate change: Climate model intercomparisons and ice-core constraints, *Clim. Dyn.*, *26*, 513–529.

Masson-Delmotte, V., et al. (2008), A review of Antarctic surface snow isotopic composition: Observations, atmospheric circulation and isotopic modelling, *J. Clim.*, *21*, 3359–3387.

Mathieu, R., D. Pollard, J. Cole, J. W. C. White, R. S. Webb, and S. L. Thompson (2002), Simulation of stable water isotope variations by the GENESIS GCM for modern conditions, *J. Geophys. Res.*, *107*(D4), 4037, doi:10.1029/2001JD900255.

Meehl, G. A., K. Covey, T. Delworth, M. Latif, B. McAvaney, J. F. B. Mitchell, R. J. Stouffer, and K. Taylor (2007), The WCRP CMIP3 multimodel dataset: A new era in climate change research, *Bull. Am. Meteorol. Soc.*, *7*, 1383–1394.

Merlivat, L., and J. Jouzel (1979), Global climatic interpretation of the deuterium-oxygen 18 relationship for precipitation, *J. Geophys. Res.*, *84*(C8), 5029–5332.

Merlivat, L., and G. Nief (1967), Fractionnement isotopique lors des changements d'états solide-vapeur et liquide-vapeur de l'eau à des températures inférieures à 0C, *Tellus*, *19*, 122–127.

Moreira, M., L. Sternberg, L. Martinelli, R. Victoria, E. Barbosa, C. Bonates, and D. Nepstad (1997), Contribution of transpiration to forest ambient vapor based on isotopic measurements, *Global Change Biol.*, *3*, 439–450.

Nesbitt, S. W., and E. J. Zipser (2003), The diurnal cycle of rainfall and convective intensity according to three years of TRMM measurements, *J. Clim.*, *16*, 1456–1475.

NGRIP Members (2004), High-resolution record of Northern Hemisphere climate extending into the last interglacial period, *Nature*, *431*, 147–151.

Noone, D. (2008), The influence of midlatitude and tropical overturning circulation on the isotopic composition of atmospheric water vapor and Antarctic precipitation, *J. Geophys. Res.*, *113*, D04102, doi:10.1029/2007JD008892.

Noone, D., and I. Simmonds (2002a), Associations between δ^{18}O of water and climate parameters in a simulation of atmospheric circulation for 1979–95, *J. Clim.*, *15*, 3150–3169.

Noone, D., and I. Simmonds (2002b), Annular variations in moisture transport mechanisms and the abundance of δ^{18}O in Antarctic snow, *J. Geophys. Res.*, *107*(D24), 4742, doi:10.1029/2002JD002262.

Peltier, W. R. (1994), Ice age paleotopography, *Science*, *265*, 195–201.

Pierrehumbert, R. T. (1999), Huascaran δ^{18}O as an indicator of tropical climate during the Last Glacial Maximum, *Geophys. Res. Lett.*, *26*(9), 1345–1348.

Pinot, S., G. Ramstein, S. P. Harrison, I. C. Prentice, J. Guiot, M. Stute, and S. Joussaume (1999), Tropical paleoclimates at the Last Glacial Maximum: Comparison of Paleoclimate Modeling Intercomparison Project (PMIP) simulations and paleodata, *Clim. Dyn.*, *15*, 857–874.

Ramirez, E., et al. (2003), A new Andean deep ice core from Nevado Illimani (6350 m), Bolivia, *Earth Planet. Sci. Lett.*, *212*, 337–350.

Risi, C., S. Bony, and F. Vimeux (2008a), Influence of convective processes on the isotopic composition (δ^{18}O and δD) of precipitation and water vapor in the tropics: 2. Physical interpretation of the amount effect, *J. Geophys. Res.*, *113*, D19306, doi:10.1029/2008JD009943.

Risi, C., S. Bony, F. Vimeux, L. Descroix, B. Ibrahim, E. Lebreton, I. Mamadou, and B. Sultan (2008b), What controls the isotopic composition of the African monsoon precipitation? Insights from event-based precipitation collected during the 2006 AMMA campaign, *Geophys. Res. Lett.*, *35*, L24808, doi:10.1029/2008GL035920.

Rosnay, P. D., and J. Polcher (1998), Modelling root water uptake in a complex land surface scheme coupled to a GCM, *Hydrol. Earth Sci.*, *2*, 239–255.

Rozanski, K., L. Araguas-Araguas, and R. Gonfiantini (1993), Isotopic patterns in modern global precipitation, in *Climate Change in Continental Isotopic Records*, *Geophys. Monogr. Ser.*, vol. 78, edited by P. K. Swart, pp. 1–36, AGU, Washington, D. C.

Salati, E., A. Dall'Olio, E. Matsui, and J. Gat (1979), Recycling of water in the Amazon basin: An isotopic study, *Water Resour. Res.*, *15*, 1250–1258.

Schmidt, G., G. Hoffmann, D. Shindell, and Y. Hu (2005), Modelling atmospheric stable water isotopes and the potential for constraining cloud processes and stratosphere-troposphere water exchange, *J. Geophys. Res.*, *110*, D21314, doi:10.1029/2005JD005790.

Schmidt, G., A. LeGrande, and G. Hoffmann (2007), Water isotope expressions of intrinsic and forced variability in a coupled ocean-atmosphere model, *J. Geophys. Res.*, *112*, D10103, doi:10.1029/2006JD007781.

Smith, J. A., G. O. Seltzer, D. L. Farber, D. T. Rodbell, and R. C. Finkel (2005), Early local Last Glacial Maximum in the tropical Andes, *Science*, *308*, 678–681.

Sodemann, H., V. Masson-Delmotte, C. Schwierz, B. M. Vinther, and H. Wernli (2008), Interannual variability of Greenland winter precipitation sources: 2. Effects of North Atlantic Oscillation variability on stable isotopes in precipitation, *J. Geophys. Res.*, *113*, D12111, doi:10.1029/2007JD009416.

Stenni, B., V. Masson-Delmotte, S. Johnsen, J. Jouzel, A. Longinelli, E. Monnin, R. Rthlisberger, and E. Selmo (2001), An oceanic cold reversal during the last deglaciation, *Science*, *293*, 2074–2077.

Stewart, M. K. (1975), Stable isotope fractionation due to evaporation and isotopic exchange of falling waterdrops: Applications to atmospheric processes and evaporation of lakes, *J. Geophys. Res.*, *80*(9), 1133–1146.

Sturm, C., F. Vimeux, and H. Krinner (2007), Intraseasonal variability in South America recorded in stable water isotopes, *J. Geophys. Res.*, *112*, D20118, doi:10.1029/2006JD008298.

Sturm, K. (2005), Regional atmospheric modelling of the stable water isotope cycle, Ph.D. thesis, Univ. Joseph Fourier, Grenoble, France.

Sturm, K., G. Hoffmann, B. Langmann, and W. Stichler (2005), Simulation of δ^{18}O in precipitation by the regional circulation model REMO$_{iso}$, *Hydrol. Processes*, *19*, 3425–3444.

Stute, M., and S. Talma (1998), Glacial temperature and moisture transport regimes reconstructed from noble gas and δ^{18}O, Stampriet aquifer, Namibia, in *Isotope Techniques in the Study of Past and Current Environmental Changes in the Hydrosphere and the Atmosphere: Proceedings of Vienna Symposium 1997*, *SM-349/53*, pp. 307–328, IAEA, Vienna.

Sylvestre, F. (2009), Moisture pattern during the Last Glacial Maximum in South America, in *Past Climate Variability in South America and Surrounding Regions*, *Dev. Paleoenviron. Res.*, vol. 14, edited by F. Vimeux et al., pp. 3–27, Springer, New York.

Thompson, L., L. Mosley-Thompson, M. Davis, J. Bolzan, T. Yao, N. Gundestrup, X. Wu, L. Klein, and Z. Xie (1989), Holocene-late Pleistocene climatic ice core records from Quinghai-Tibetan Plateau, *Science*, *246*, 474–477.

Thompson, L. G., E. Mosley-Thompson, M. E. Davis, P.-N. Lin, K. A. Henderson, J. Cole-Dai, J. F. Bolzan, and K. B. Liu (1995), Late glacial stage and Holocene tropical ice core records from Huascaràn, Peru, *Science*, *269*, 46–50, doi:10.1126/science.269.5220.46.

Thompson, L., et al. (1997), Tropical climate instability: The last glacial cycle from a Qinghai-Tibetan ice core, *Science*, *276*, 1821–1825.

Thompson, L. G., et al. (1998), A 25,000-year tropical climate history from Bolivian ice cores, *Science*, *282*, 1858–1864.

Thompson, L. G., E. Mosley-Thompson, and K. A. Henderson (2000), Ice-core paleoclimate records in tropical South America since the Last Glacial Maximum, *J. Quat. Sci.*, *15*, 1579–1600.

Tindall, J. C., P. Valdes, and L. C. Sime (2009), Stable water isotopes in HadCM3: Isotopic signature of El Niño–Southern Oscillation and the tropical amount effect, *J. Geophys. Res.*, *114*, D04111, doi:10.1029/2008JD010825.

Uemura, R., Y. Matsui, K. Yoshimura, H. Motoyama, and N. Yoshida (2008), Evidence of deuterium-excess in water vapour as an indicator of ocean surface conditions, *J. Geophys. Res.*, *113*, D19114, doi:10.1029/2008JD010209.

Uppala, S., et al. (2005), The ERA-40 re-analysis, *Q. J. R. Meteorol. Soc.*, *131*, 2961–3012.

Vaikmae, R., J. Jouzel, J. R. Petit, and M. Stievenard (1993), A new Antarctic climate record from Dome B ice core, paper presented at Isotopic Technique in the Study of Past and Current Environmental Changes in the Hydrosphere and Atmosphere, Int. At. Energy Agency, Vienna.

van Breukelen, M., H. Vonhof, J. Hellstrom, W. Wester, and D. Kroon (2008), Fossil dripwater in stalagmites reveals Holocene temperature and rainfall variation in Amazonia, *Earth Planet. Sci. Lett.*, *275*(1–2), 54–60.

Van Leer, B. (1977), Towards the ultimate conservative difference scheme: IV. A new approach to numerical convection, *J. Comput. Phys.*, *23*, 276–299.

van Ommen, T. D., and T. Morgan (1997), Calibrating the ice core paleothermometer using seasonality, *J. Geophys. Res.*, *102*(D8), 9351–9357.

Vimeux, F., V. Masson, G. Delaygue, J. Jouzel, J. R. Petit, and M. Stievenard (2001), A 420,000 year deuterium excess record from East Antarctica: Information on past changes in the origin of precipitation at Vostok, *J. Geophys. Res.*, *106*(D23), 31,863–31,873.

Vimeux, F., R. Gallaire, S. Bony, G. Hoffmann, and J. C. H. Chiang (2005), What are the climate controls on δD in precipitation in the Zongo Valley (Bolivia)? Implications for the Illimani ice core interpretation, *Earth Planet. Sci. Lett.*, *240*, 205–220.

Vimeux, F., P. Ginot, M. Schwikowski, M. Vuille, G. Hoffmann, L. G. Thompson, and U. Schotterer (2009), Climate variability during the last 1000 years inferred from Andean ice cores: A review of methodology and recent results, *Palaeogeogr. Palaeoclimatol. Palaeoecol.*, *281*, 229–241, doi:10.1016/j.palaeo.2008.03.054.

Vuille, M., and M. Werner (2005), Stable isotopes in precipitation recording South American summer monsoon and ENSO variability: observations and model results, *Clim. Dyn.*, *25*, 401–413.

Vuille, M., R. S. Bradley, M. Werner, R. Healy, and F. Keimig (2003), Modeling δ^{18}O in precipitation over the tropical Americas: 1. Interannual variability and climatic controls, *J. Geophys. Res.*, *108*(D6), 4174, doi:10.1029/2001JD002038.

Wang, X., A. S. Auler, R. L. Edwards, H. Cheng, E. Ito, and M. Solheid (2006), Interhemispheric anti-phasing of rainfall during the last glacial period, *Quat. Sci. Rev.*, *25*, 3391–3403.

Wang, Y., et al. (2008), Millennial- and orbital-scale changes in the East Asian monsoon over the past 224,000 years, *Nature*, *451*, 1090–1093.

Washburn, E., and E. Smith (1934), The isotopie fractionation of water by physiological processes, *Science*, *79*, 188–189.

Werner, M., U. Mikolajewicz, M. Heimann, and G. Hoffmann (2000), Borehole versus isotope temperatures on Greenland: Seasonality does matter, *Geophys. Res. Lett.*, *27*(5), 723–726.

Werner, M., M. Heimann, and G. Hoffmann (2001), Isotopic composition and origin of polar precipitation in present and glacial climate simulations, *Tellus, Ser. B*, *53*, 53–71.

White, J. W. C., L. K. Barlow, D. Fisher, P. Grootes, J. Jouzel, S. J. Johnsen, M. Stuiver, and H. Clausen (1997), The climate signal in the stable isotopes of snow from Summit, Greenland: Results of comparisons with modern climate observations, *J. Geophys. Res.*, *102*(C12), 26,425–26,439.

Williams, D. G., et al. (2004), Evapotranspiration components determined by stable isotope, sap flow and eddy covariance techniques, *Agric. For. Meteorol.*, *125*, 241–258.

Worden, J., D. Noone, and K. Bowman (2007), Importance of rain evaporation and continental convection in the tropical water cycle, *Nature*, *445*, 528–532.

Yepez, E., S. Williams, R. Scott, and G. Lin (2003), Partitioning overstory and understory evapotranspiration in a semiarid savanna woodland from the isotopic composition of water vapor, *Agric. For. Meteorol.*, *119*, 53–68.

Yoshimura, K., T. Oki, N. Ohte, and S. Kanae (2003), A quantitative analysis of short-term ^{18}O variability with a Rayleigh-type isotope circulation model, *J. Geophys. Res.*, *108*(D20), 4647, doi:10.1029/2003JD003477.

Yoshimura, K., S. Miyazaki, S. Kanae, and T. Oki (2006), Iso-MATSIRO, a land surface model that incorporates stable water isotopes, *Global Planet. Change*, *51*, 90–107.

Yoshimura, K., M. Kanamitsu, D. Noone, and T. Oki (2008), Historical isotope simulation using reanalysis atmospheric data, *J. Geophys. Res.*, *113*, D19108, doi:10.1029/2008JD010074.

S. Bony and C. Risi, LMD, IPSL, UPMC, CNRS, 4, Place Jussieu, F-75005 Paris, France. (crlmd@lmd.jussieu.fr)

J. Jouzel, LSCE, IPSL (CEA, CNRS, UVSQ), Bt 701, Orme des Merisiers, F-91191 Gif-sur-Yvette, France.

F. Vimeux, UR Great Ice, IRD, LSCE, IPSL (CEA, CNRS, UVSQ), Bt 701, Orme des Merisiers, F-91191 Gif-sur-Yvette, France.

Process-evaluation of tropospheric humidity simulated by general circulation models using water vapor isotopic observations: 2. Using isotopic diagnostics to understand the mid and upper tropospheric moist bias in the tropics and subtropics

Camille Risi,[1,2] David Noone,[1] John Worden,[3] Christian Frankenberg,[3] Gabriele Stiller,[4] Michael Kiefer,[4] Bernd Funke,[5] Kaley Walker,[6] Peter Bernath,[7] Matthias Schneider,[4,8] Sandrine Bony,[2] Jeonghoon Lee,[3,9] Derek Brown,[1] and Christophe Sturm[10]

Received 26 July 2011; revised 28 December 2011; accepted 30 December 2011; published 6 March 2012.

[1] Evaluating the representation of processes controlling tropical and subtropical tropospheric relative humidity (RH) in atmospheric general circulation models (GCMs) is crucial to assess the credibility of predicted climate changes. GCMs have long exhibited a moist bias in the tropical and subtropical mid and upper troposphere, which could be due to the mis-representation of cloud processes or of the large-scale circulation, or to excessive diffusion during water vapor transport. The goal of this study is to use observations of the water vapor isotopic ratio to understand the cause of this bias. We compare the three-dimensional distribution of the water vapor isotopic ratio measured from space and ground to that simulated by several versions of the isotopic GCM LMDZ. We show that the combined evaluation of RH and of the water vapor isotopic composition makes it possible to discriminate the most likely cause of RH biases. Models characterized either by an excessive vertical diffusion, an excessive convective detrainment or an underestimated in situ cloud condensation will all produce a moist bias in the free troposphere. However, only an excessive vertical diffusion can lead to a reversed seasonality of the free tropospheric isotopic composition in the subtropics compared to observations. Comparing seven isotopic GCMs suggests that the moist bias found in many GCMs in the mid and upper troposphere most frequently results from an excessive diffusion during vertical water vapor transport. This study demonstrates the added value of water vapor isotopic measurements for interpreting shortcomings in the simulation of RH by climate models.

Citation: Risi, C., et al. (2012), Process-evaluation of tropospheric humidity simulated by general circulation models using water vapor isotopic observations: 2. Using isotopic diagnostics to understand the mid and upper tropospheric moist bias in the tropics and subtropics, *J. Geophys. Res.*, *117*, D05304, doi:10.1029/2011JD016623.

1. Introduction

[2] Despite continuous improvements in climate models, uncertainties in the predicted amplitude of climate change and in the magnitude of underlying feedbacks remain high [*Randall et al.*, 2007]. Because the water vapor feedback constitutes one of the largest positive feedbacks in climate models [*Soden and Held*, 2006], assessing the credibility of predicted relative humidity (RH) changes by atmospheric general circulation models (GCMs) is crucial. In addition, RH strongly impacts the formation of cirrus clouds [*Luo and Rossow*, 2004], boundary layer clouds [*Slingo*, 1980; *Wetzel et al.*, 1996; *Betts*, 2000] and deep convective clouds [*Redelsperger et al.*, 2002; *Derbyshire et al.*, 2004]. Predicting the correct regional changes in RH is thus crucial for a correct prediction of cloud feedbacks, which are still among the largest sources of spread in climate change projections [*Bony and Dufresne*, 2005; *Bony et al.*, 2006]. Therefore, the credibility of simulated climate change depends

[1]Department of Atmospheric and Oceanic Sciences, and Cooperative Institute for Research in Environmental Sciences, University of Colorado at Boulder, Boulder, Colorado, USA.
[2]LMD/IPSL, CNRS, Paris, France.
[3]Jet Propulsion Laboratory, California Institute of Technology, Pasadena, California, USA.
[4]Institute for Meteorology and Climate Research, Karlsruhe Institute of Technology, Karlsruhe, Germany.
[5]Instituto de Astrofisica de Andalucía, Granada, Spain.
[6]Department of Physics, University of Toronto, Toronto, Ontario, Canada.
[7]Department of Chemistry, University of York, York, UK.
[8]CIAI, Agencia Estatal de Meteorología, Santa Cruz de Tenerife, Spain.
[9]Korea Polar Research Institute, Incheon, South Korea.
[10]Department of Geology and Geochemistry, Stockholm University, Stockholm, Sweden.

0148-0227/12/2011JD016623

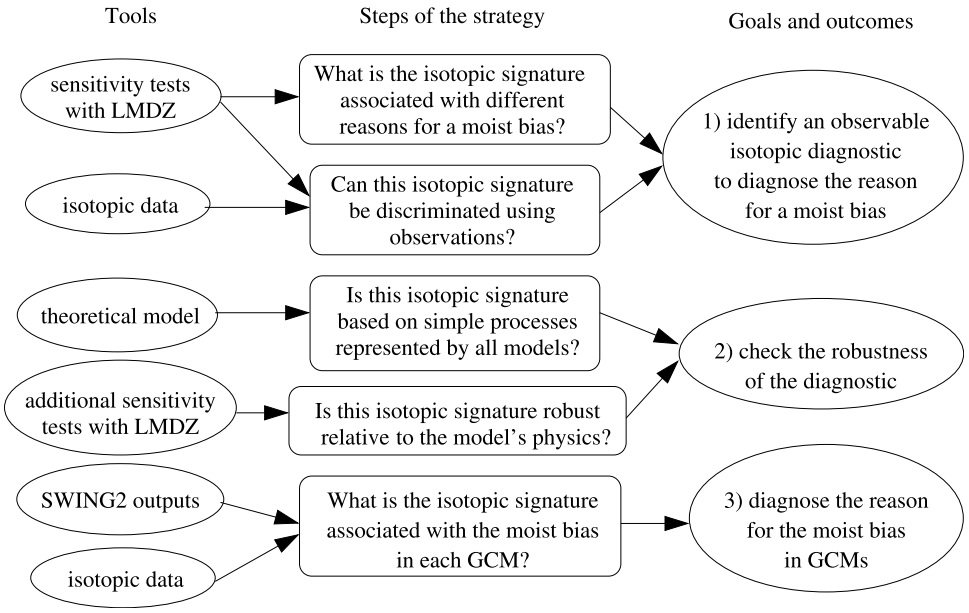

Figure 1. Strategy for developing, testing and applying diagnostics based on the isotopic ratio to identify the cause of the moist bias in models. Rectangles describe the different steps of the strategy used in this paper, and circles explain the tools used at different steps.

on the ability of atmospheric models to correctly simulate the processes that control RH, although no evidence has been shown so far for a systematic relationship between the behavior of models at present and in the future [*John and Soden*, 2007].

[3] Most GCMs exhibit a moist bias in the mid to upper tropical and subtropical troposphere compared to a wide range of data sets [*Soden and Bretherton*, 1994; *Salathe and Chester*, 1995; *Chen et al.*, 1996; *Roca et al.*, 1997; *Chen et al.*, 1998; *Allan et al.*, 2003; *Brogniez et al.*, 2005; *Pierce et al.*, 2006; *John and Soden*, 2007; *Sherwood et al.*, 2010; *Chung et al.*, 2011]. Some of these studies suggest this problem can arise from the parameterization of deep convection [*Chen et al.*, 1996, 1998], others suggest it could be related to an underestimated upper tropospheric large-scale circulation [*Chung et al.*, 2011]. This problem has persisted for more than a decade and questions the capacity of GCMs to accurately represent processes controlling RH. The tropical and subtropical tropospheric RH results from a subtle balance between different processes, among which are large-scale radiative subsidence [e.g., *Sherwood*, 1996; *Schneider et al.*, 2006; *Folkins and Martin*, 2005], detrainment of condensate from convective clouds and its subsequent evaporation [e.g., *Wright et al.*, 2009], evaporation of the falling precipitation [e.g., *Folkins and Martin*, 2005] or lateral mixing [e.g., *Zhang et al.*, 2003]. Therefore, the representation of many processes may potentially contribute to the moist bias. Measurements of humidity alone are not sufficient to diagnose which of this processes are the most likely candidates.

[4] The water vapor stable isotopic composition is affected by fractionation during phase changes. Measurements of water vapor isotopologues therefore provide complementary information on the water budget when combined with humidity because they record the integrated history of phase changes within a given air mass [*Dansgaard*, 1964]. In a companion paper [*Risi et al.*, 2012] (hereafter P1), we have analyzed various data sets (4 satellite, 16 ground-based remote-sensing, 5 surface in situ and 3 aircraft) to document the three-dimensional distribution of the tropospheric water vapor composition and to derive robust characteristics that could be used to evaluate models. For example, we have identified that the δD seasonality in the subtropics and mid latitudes (with higher δD in summer) was a robust characteristic across all data sets and at all tropospheric levels. We have used these data sets to evaluate the isotopic GCM LMDZ and have identified some biases that are robust compared to all data sets, such as the underestimated seasonality in the subtropics. In addition, we have compared 7 GCMs from the SWING2 (Stable Water INtercomparison Group phase) project, and have shown large discrepancies between models regarding important features of the isotopic distribution: meridional gradient, seasonality, and spatial contrasts in the tropics. This suggests that water vapor isotopic measurements could be used to efficiently discriminate models regarding their representation of the processes controlling RH. Further, we have shown that differences in isotopic behavior are not obviously linked to differences in simulated humidity, confirming that water vapor isotopic composition provides additional information compared to humidity measurements. The goal of this paper is thus to exploit the information provided by the combination of water vapor isotopic measurements, to understand the cause of the moist bias in GCMs.

[5] To do so, the approach is illustrated in Figure 1. First, with the isotopic GCM LMDZ, we perform different sensitivity tests that exhibit a moist bias for different causes. From these simulations, we investigate how the different

processes impact the isotopic composition, and how it hurts the agreement with isotopic data sets. This allows us to identify a discriminating diagnostic for the cause of the moist bias that is robust across data sets. Second, we further check the robustness of this diagnostic by creating a theoretical framework to understand the link between the moist bias and isotopic behavior. The framework is used to show that this link can be explained based on simple processes that are represented in all models. We also use additional sensitivity tests to show that the diagnostic does not crucially depend on the model physics. Third, once we have accumulated confidence in the robustness of the diagnostic, we apply it to six other GCMs from the SWING2 project to determine the most frequent cause of the moist bias in models.

[6] We present the LMDZ GCM, the isotopic data sets and the SWING2 database in section 2. We describe the theoretical framework used to interpret the sensitivity tests in section 3. In section 4, we present the sensitivity tests and their impact on RH in section 4. In section 5, we describe the impact of the tests on the water vapor isotopic composition and compare the simulations with the isotopic data. In section 6 we further check its robustness and apply it to SWING2 models. We conclude and propose perspectives for future work in section 7.

2. General Circulation Models and Data Sets

2.1. The LMDZ4 Model and Control Simulation

[7] LMDZ4 (Laboratoire de Météorologie Dynamique-Zoom) [*Hourdin et al.*, 2006] is the atmospheric component of the Institut Pierre-Simon Laplace coupled model: IPSL-CM4 [*Marti et al.*, 2005] used in CMIP3 (Coupled Model Intercomparison Project) [*Meehl et al.*, 2007] and IPSL-CM5A (J.-L. Dufresne et al., Climate change projections using the IPSL-CM5 Earth System Model: from CMIP3 to CMIP5, submitted to *Climate Dynamics*, 2012) used in CMIP5. It is used with a resolution of 2.5° in latitude, 3.75° in longitude and 19 vertical levels. The physical package includes the Emanuel convective scheme [*Emanuel*, 1991; *Emanuel and Zivkovic-Rothman*, 1999], which represents convective systems as an adiabatic updraft, an ensemble of mixed updrafts and downdrafts, and an unsaturated downdraft driven by rain reevaporation. A particular focus had been placed on the parameterization and optimization of microphysical processes, such as the precipitation efficiency ϵ_p representing the proportion of condensate that is converted to precipitation [*Emanuel and Zivkovic-Rothman*, 1999]. Large-scale condensation is represented by a statistical cloud scheme based on the sub-grid-scale distribution of water vapor [*Bony and Emanuel*, 2001]. Water vapor and condensate are advected using a second order monotonic finite volume advection scheme [*Van Leer*, 1977; *Hourdin and Armengaud*, 1999]. The isotopic version of LMDZ is described in detail by *Risi et al.* [2010b].

[8] LMDZ is forced by observed sea surface temperatures (SST) and sea ice following the AMIP (Atmospheric Model Inter-comparison Project) protocol [*Gates*, 1992] from 1978 to 2009. The year 2010 is forced by NCEP (National Center for Environmental Prediction) SSTs [*Kalnay et al.*, 1996] because the AMIP SSTs were not yet available. To facilitate the comparison between simulations and observations on a daily basis, horizontal winds at each vertical level are nudged by ECMWF reanalyses [*Uppala et al.*, 2005] with a relaxation time scale of 1h as in work by *Risi et al.* [2010b]. This nudging procedure has been shown to enable the model to capture the daily weather and isotopic variability well [*Risi et al.*, 2010b; *Vimeux et al.*, 2011; *Gao et al.*, 2010]. For example, in summer 2006 in average over the tropics, the daily correlation at each grid point for the large-scale vertical velocity at 500 hPa is 0.45 between the ECMWF reanalyses and the nudged simulation, compared to only 0.006 between the ECMWF reanalyses and the free-running simulation.

2.2. Data Sets and Comparison Methodology

[9] We focus on evaluating the HDO/H_2O ratio as quantified by the variable δD in ‰: $\delta D = (\frac{R}{R_{SMOW}} - 1) \cdot 1000$, where R is the HDO/H_2O ratio of the water vapor and R_{SMOW} is the Vienna Standard Mean Ocean Water (VSMOW) isotopic ratio [*Craig*, 1961]. To evaluate the simulated three-dimensional water vapor δD distribution from the surface up to the upper-troposphere, we combine various data sets that sample different parts of the atmosphere. We use several satellite data sets, which provide a global coverage: SCIAMACHY (a short-wave infra-red spectrometer) mainly sensitive to the lower troposphere, TES (a nadir-viewing thermal infrared spectrometer) which is mainly sensitive to the mid-troposphere, and ACE-FTS (an infrared solar-occultation instrument) and MIPAS (a limb infrared sounder) which are sensitive in the upper troposphere and above. In addition, we use ground-based remote-sensing (Fourier Transform Infrared) data sets derived from mid-infrared (NDACC, for which water isotopologue retrievals are performed in the framework of the project MUSICA) or near-infrared (TCCON) solar absorption spectra, and in situ measurements made at the surface and by aircraft. These data sets are listed in Table 1 and described in detail in section 3 of P1. Here we use observations made at lower latitudes (45°N–45°S).

[10] The different data sets show significant differences in their absolute δD values, meridional gradients and seasonal amplitudes (section 4.1 of P1), due to the effects of spatio-temporal sampling, instrument sensitivity and measurement errors (section 4.2 of P1). Since remote-sensing data has limited calibration and validation, we will focus the analysis on spatial and temporal variations. It is possible that those variations themselves may be in error, but the use of multiple data sets helps ensure that we draw only conclusions that are robustly supported.

[11] We follow a model-to-satellite approach to estimate what the instruments would observe if operated in the model. First, to take into account the spatiotemporal sampling of the data, we collocate the model output with the data at the daily scale. Second, to take into account the sensitivities of the different remote-sensing instruments to the true state, we apply averaging kernels to model output. Averaging kernels define the sensitivity of the retrieval at each level to the true state at each level. In P1, the model-data comparison methodology for each data set is extensively explained (section 3, Appendix C) and sources of model-data differences are quantified (section 5.1). We will focus the analysis on signals that are larger than these potential

Table 1. The Different Data Sets of Water Vapor Isotopic Composition Used for Model-Data Comparison[a]

Data Set or Network	Reference	Level	Spatial Coverage or Location; Footprint	Period	Precision	Comparison Methodology
			Satellite Measurement			
SCIAMACHY	*Frankenberg et al.* [2009]	total column, mainly sensitive in the boundary layer	global; footprint 120 × 20 km	2003–2005	40‰–100‰, reduced by averaging	collocation
TES	*Worden et al.* [2007]	600 hPa	global; footprint 5.3 × 8.5 km	2004–2008	about 40‰, reduced by averaging	collocation, application of kernels
ACE	*Nassar et al.* [2007]	down to 500 hPa	global, but small number of measurements; limb measurement	2003–2008	about 50‰, reduced by averaging	collocation, smoothing
MIPAS	*Steinwagner et al.* [2010]	down to 300 hPa	global; limb measurement	September 2002–March 2004	about 50‰, reduced by averaging	collocation, application of kernels
			Ground-Based Remote-Sensing			
TCCON network	*Wunch et al.* [2010]	total column	8 stations: Lauder, Wollongong, Darwin, Park Falls, Pasadena, Lamont, Bremen and Ny Alesund	between 1.5 and 6 years	between 5 and 35‰	collocation, application of kernels
NDACC network	*Schneider et al.* [2010]	total column and profiles up to 10 km	8 stations: Arrival Heights, Lauder, Wollongong, Izaña, Jungfraujoch, Karlsruhe, Kiruna and Eureka	between 0.5 and 13 years	5‰ for total column and 10–25‰ for profiles	collocation, application of kernels
			Ground-Based in Situ			
GNIP-vapor network of monthly samples	IAEA web site	surface	3 stations: Vienna, Ankara, Manaus	between 2 and 13 years	undocumented	collocation
Isolated data sets of daily samples	*Angert et al.* [2008]; *Risi et al.* [2010b]	surface	2 stations: Rehovot and Saclay	daily samples during 1 to 2 years	1‰	collocation
Picarro in Hawaii	*Johnson et al.* [2011]	surface at 680 hPa	Hawaii	3 weeks	5 to 10‰	collocation
Southern Ocean surface samples	*Uemura et al.* [2008]	surface	Southern Ocean	1 month	1‰	collocation
			Aircraft			
Flights in the 60s	*Ehhalt et al.* [2005]	profiles between 1.5 km and 9.2 km	3 sites in the United States: Nebraska, Santa Barbara and the Death Valley	a few isolated days	1‰	collocation
CR-AVE and TC4 campaigns	*Sayres et al.* [2010]	profiles between 475 hPa and 64 hPa	near Costa-Rica	1 week in winter 2006, 10 days in summer 2007	17‰ for ICOS and 50‰ for Hoxotope	collocation

[a]We detail the levels at which the measurements are performed or are the most sensitive, the location for ground-based data sets, the footprint for satellite data sets, the period over which we use the measurements, the precision specified in the reference papers or calculated in Appendix B of P1, and the methodology that we use for model-data comparison.

source of errors (i.e. larger than 10 or 20‰) and that are robust across data sets.

2.3. SWING2 Models

[12] We compare seven simulations by six other GCMs participating in the SWING2 inter-comparison project (http://people.su.se/~cstur/SWING2/). Some of them are nudged by reanalyses, some of them are not (i.e. they are free-running) (Table 2). The LMDZ control simulations is one of the SWING2 simulations and has been rigorously compared with each data set through collocation with the data (see P1). Since daily values are not available in the SWING2 archive, it is not possible to collocate other model outputs with the data. Therefore, we use the LMDZ control

Table 2. List of the Different SWING2 Models Used in This Study and Their Respective Simulations[a]

GCM	Reference	Simulations	Horizontal Resolution	λ	Isotopic Processes During Rainfall
GISS	*Schmidt et al.* [2007]	free-running and nudged by NCEP	46 × 72	0.004	*Hoffmann et al.* [1998]
ECHAM4	*Hoffmann et al.* [1998]	nudged by ECMWF	64 × 128	0.003	*Hoffmann et al.* [1998]
LMDZ4	*Risi et al.* [2010b]	free-running and nudged by ECMWF	72 × 96	0.004	*Bony et al.* [2008], *Stewart* [1975] with $h_{eff} = \phi + (1 - \phi) \cdot h$ and $\phi = 0.9$
GSM	*Yoshimura et al.* [2008]	nudged by NCEP	73 × 144	0.003	*Hoffmann et al.* [1998], *Stewart* [1975] with $h_{eff} = \min(1.4 \cdot h, 1)$
CAM2	*Lee et al.* [2007]	free-running	64 × 128	0.004	*Lee and Fung* [2008], *Stewart* [1975] with $h_{eff} = \min(h + 0.5, 1)$
HadAM	*Tindall et al.* [2009]	free-running	73 × 96	0.005	*Hoffmann et al.* [1998], *Stewart* [1975] with $h_{eff} = \phi + (1 - \phi) \cdot h$ and $\phi = 0.7$
MIROC	*Kurita et al.* [2011]	free-running	73 × 96	0.003	*Hoffmann et al.* [1998], *Stewart* [1975]

[a]"Free-running" refers to standard AMIP-style simulations [*Gates*, 1992] forced by observed sea surface temperatures, and whose winds are not nudged. The λ parameter refers to the formulation of supersaturation S_i with respect to ice as a function of temperature T following $S_i = 1 - \lambda \cdot T$, involved in the kinetic fractionation during ice condensation [*Jouzel and Merlivat*, 1984]. The representation of isotopic processes during rainfall for each model is described in the indicated reference, and the calculation of the effective relative humidity around raindrops (h_{eff}) as a function of the relative humidity simulated by the physical package (h) is also given when available in references.

simulation as a reference against which we compare the SWING2 models' monthly outputs.

3. Theoretical Framework to Understand Processes Controlling Humidity and Isotopic Composition

[13] We develop a simple single-column theoretical framework to understand the sensitivity tests with the LMDZ GCM. Given its simplicity, we aim to provide qualitative insights into the main effects on humidity and water vapor isotopic composition of the different micro-physical and macro-physical processes tested in the experiments, rather than to make quantitative predictions.

3.1. Principle

[14] The theoretical framework components and notations are illustrated in Figure 2a. It is inspired by the last saturation theory as explained by *Sherwood* [1996]. *Sherwood* [1996] sets RH to a given value near saturation in convective regions, leading to a fixed profile of specific humidity (q) in convective regions. Specific humidity is then conserved in the air masses that leave the convective regions and slowly subside, leading to a decrease in RH. This framework is also consistent with the simple single-column model of *Folkins and Martin* [2005] in which the tropical mid and upper troposphere is moistened by convective clouds detrainment and dried by radiative subsidence outside the clouds. Here we extend these previous frameworks in two ways. First, we calculate the water vapor isotopic composition in addition to the humidity. Second, we take into account additional processes that are crucial for the water budget of GCMs, such as cloud microphysics, water vapor transport at the large-scale and the associated diffusion.

[15] In the real world in convective regions, ascent is concentrated in convective cores and cloud-free regions are subsident [*Emanuel et al.*, 1994], and this was the basis for frameworks such as that of *Folkins and Martin* [2005]. In GCMs however, water vapor transport by large-scale ascent is resolved by the large-scale advection scheme. The large-scale upward transport of water vapor is partly compensated (and sometimes over-compensated) by the compensating subsidence in the convection scheme [*Arakawa and Shubert*, 1974]. The proportion of the total upward water vapor transport that is treated by the large-scale advection scheme or by the convection scheme are somewhat arbitrary and model-dependent, but it impacts the vertical distribution of chemical tracers [*Lawrence and Salzmann*, 2008]. We thus expect an impact on the isotopic composition as well. Contrary to *Sherwood* [1996] and *Folkins and Martin* [2005], our goal is to interpret biases in GCMs, and therefore we need to take into account the vertical water vapor transport by the large-scale advection.

[16] To illustrate the water budget in the LMDZ GCM, we consider two regions based on monthly mean large-scale

Figure 2. (a) Illustration of the simple single-column model developed to interpret the sensitivity experiments. Characteristic profiles of specific humidity and isotopic composition $q_{t,\,dtr}$ and δD_{dtr} in convective plumes are assumed and depend on the precipitation efficiency ϵ_p in convective clouds and on the humidity and isotopic composition at the lifting condensation level q_{s0} and δD_0. The humidity and δD in the convective region, q_{asc} and δD_{conv}, are controlled by the balance between moistening by convective detrainment of air from convective plumes, moistening by large-scale ascent, and drying by large-scale condensation in anvils and cirrus clouds. In subsidence regions, the humidity and isotopic composition q_{subs} and δD_{subs} are controlled by the balance between moistening by horizontal mixing with convective regions and drying by large-scale subsidence. Vertical diffusion has also a moistening effect in both regions. (b) Major tendencies involved in the water budget of the troposphere in convective regions ($\omega_{500} < -35$ hPa/d), as diagnosed from the control simulation of LMDZ: vertical transport, convective detrainment, large-scale condensation and the residual from these 3 terms. (c) Same as Figure 2b but for subsidence regions ($\omega_{500} > 35$ hPa/d): vertical transport, large-scale condensation, horizontal advection and the residual from these 3 terms. The "vertical transport" tendency includes both the effect of large-scale vertical advection and compensating subsidence in the convective scheme. (d and e) Same as Figures 2b and 2c but as computed from the simple single-column model. The diffusive term was included as part of the vertical transport term, since in LMDZ it is intrinsic to the advection scheme.

vertical velocity at 500 hPa (ω_{500}) [*Bony et al.*, 2004]. Figure 2b shows the major tendencies involved in the water budget as simulated by the control simulation of LMDZ in regions of large-scale ascent ($\omega_{500} < -35$ hPa/day, i.e. convective regions). We combine the tendencies by large-scale vertical advection and by compensating subsidence in the convective scheme into one single tendency representing the total vertical transport in the environment (i.e. outside convective cores). To first order, in the boundary layer of convective regions, moistening by surface evaporation balances drying by downward vertical transport. In the mid and upper troposphere (between 600 hPa and 200h Pa) of convective regions, the air is moistened by convective detrainment (consistent with *Sherwood* [1996] and *Folkins and Martin* [2005] and by upward vertical transport in the environment. This moistening is balanced by drying by large-scale condensation, which represents condensation in anvils or cirrus clouds associated with convection. In the mid and upper troposphere of regions of large-scale descent ($\omega_{500} > 35$ hPa/day), the air is moistened mainly by horizontal advection from convective regions, and dehydrated mainly by downward vertical transport (Figure 2c). We

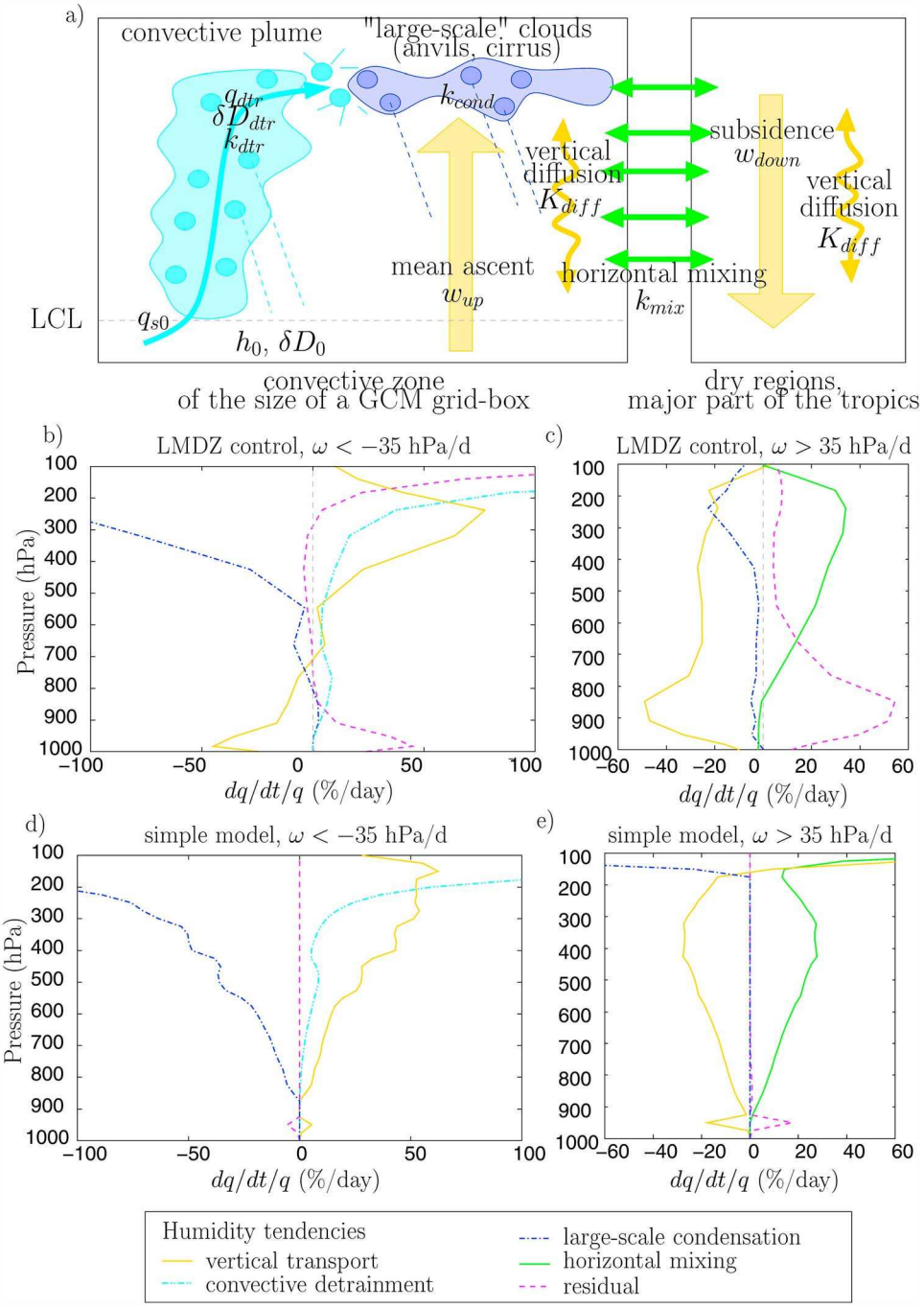

Figure 2

develop a theoretical framework that focuses on the mid and upper troposphere and represents these major tendencies in convective and subsidence regions.

3.2. Water Budget in Convective Regions

[17] In the simple framework, we assume that the temporal evolution of q in regions of large-scale ascent (q_{asc}) is driven by four contributions: (1) convective detrainment, (2) total vertical transport in the environment, (3) diffusion associated with this transport due to intrinsic numerical diffusivity of advection schemes, and (4) large-scale condensation:

$$\frac{dq_{asc}}{dt} = \left(\frac{dq_{asc}}{dt}\right)_{dtr} + \left(\frac{dq_{asc}}{dt}\right)_{env} + \left(\frac{dq_{asc}}{dt}\right)_{diff} + \left(\frac{dq_{asc}}{dt}\right)_{cond} \quad (1)$$

where we express the tendency due to convective detrainment as:

$$\left(\frac{dq_{asc}}{dt}\right)_{dtr} = k_{dtr} \cdot \left(q_{t,dtr} - q_{asc}\right) \quad (2)$$

where k_{dtr} is the rate constant of convective detrainment and $q_{t,dtr}$ is the total cloud water (vapor plus condensate) that is detraining from convective plumes. $q_{t,dtr}$ equals the humidity entrained into the plume minus the precipitation:

$$q_{t,dtr} = q_{s0} - \epsilon_p \cdot (q_{s0} - q_s) \quad (3)$$

where q_s is the humidity at saturation, q_{s0} is the specific humidity entrained into the plume and ϵ_p is the precipitation efficiency in convective updrafts. We neglect the effect of entrainment on $q_{t,dtr}$, as justified by the fact that humidity and isotopic properties of the air detrained from convective plumes is very similar to those in the adiabatic updraft, consistent with the relatively small entrainment in the Emanuel scheme [*Derbyshire et al.*, 2004; *Grandpeix et al.*, 2004]. Therefore, we assume that q_{s0} is the humidity at the lifting condensation level (LCL).

[18] We express the tendency due to vertical transport in the environment as:

$$\left(\frac{dq_{asc}}{dt}\right)_{env} = -w_{env} \cdot \frac{dq_{asc}}{dz} \quad (4)$$

where w_{env} is the vertical wind speed (positive upward) that sums the large-scale ascending speed and the downward compensating subsidence in the convective scheme. In regions of large-scale ascent, w_{env} is always positive.

[19] We express the tendency due to diffusion as:

$$\left(\frac{dq_{asc}}{dt}\right)_{diff} = K_{diff} \cdot \frac{d^2 q_{asc}}{dz^2} \quad (5)$$

where K_{diff} is the diffusivity constant associated with vertical water vapor transport.

[20] For the tendency due to large-scale condensation, as is the case in most GCMs, we assume that RH varies at the sub-grid-scale so that condensation starts for a grid average q_{asc} lower than the saturation specific humidity (q_s). As an example, we assume a uniform distribution of RH with a standard deviation σ_h. We thus get:

$$\left(\frac{dq_{asc}}{dt}\right)_{cond} = -k_{cond} \cdot (q_{asc} - q_s \cdot (1 - \sigma_h)) \quad (6)$$

where k_{cond} is the rate constant of large-scale condensation.

[21] We substitute equations (2), (4), (5), and (6) into equation (1) and solve it numerically as detailed in section 3.5. At steady state, q_{asc} is given by:

$$q_{asc} = \frac{1}{k_{dtr} + k_{cond}} \cdot \left(k_{dtr} \cdot q_{t,dtr} + k_{cond} \cdot q_s \cdot (1 - \sigma_h) - w_{env} \cdot \frac{dq_{asc}}{dz} + K_{diff} \cdot \frac{d^2 q_{asc}}{dz^2}\right). \quad (7)$$

[22] If the detrainment term dominates, then q_{asc} tends toward $q_{t,\ dtr}$. If the condensation term dominates, then q_{asc} tends toward $q_s \cdot (1 - \sigma_h)$, which is smaller. In practice, q_{asc} is bounded between these two extremes, and for reasonable sets of parameters it stays below saturation. q_{asc} increases with ϵ_p, w_{adv} and K_{diff}, and decreases with σ_h.

3.3. Water Budget in Subsidence Regions

[23] We assume that the temporal evolution of q in subsidence regions (q_{subs}) is driven by 4 contributions: (1) horizontal transport from convective regions, (2) downward vertical transport in the environment, (3) diffusion associated with this transport due to intrinsic numerical diffusivity of advection schemes, and (4) large-scale condensation:

$$\frac{dq_{subs}}{dt} = \left(\frac{dq_{subs}}{dt}\right)_{mix} + \left(\frac{dq_{subs}}{dt}\right)_{subs} + \left(\frac{dq_{subs}}{dt}\right)_{diff} + \left(\frac{dq_{subs}}{dt}\right)_{cond} \quad (8)$$

where we express the tendency due to horizontal transport from convective region as:

$$\left(\frac{dq_{subs}}{dt}\right)_{dtr} = k_{mix} \cdot (q_{asc} - q_{subs}) \quad (9)$$

with k_{mix} the rate constant of horizontal mixing. We express the tendency due to downward vertical transport as:

$$\left(\frac{dq_{subs}}{dt}\right)_{subs} = w_{subs} \cdot \frac{dq_{subs}}{dz} \quad (10)$$

where w_{subs} is the vertical wind speed (positive downward) corresponding to the large-scale subsidence. We express the two remaining tendencies in exactly the same way as for convective regions (equations (5) and (6)). We solve equation (8) numerically (section 3.5). In practice, the condensation term is very small due to the dryness of subsidence regions. This term is present only for numerical stability reasons near 100 hPa. Therefore, at steady state, q_{subs} is given approximately by:

$$q_{subs} = q_{asc} + \frac{1}{k_{mix}} \cdot \left(w_{subs} \cdot \frac{dq_{subs}}{dz} + K_{diff} \cdot \frac{d^2 q_{subs}}{dz^2}\right). \quad (11)$$

[24] It follows that all factors controlling q_{asc} also impact q_{subs}. If the mixing term dominates, then q_{subs} tends toward q_{asc}. If the subsidence term dominates, then q_{subs} reflects the value of q_{asc} much higher in altitude. In practice, q_{subs} is bounded between q_{asc} at the same level and q_{asc} higher in altitude. In addition to factors controlling q_{asc}, q_{subs} also increases with k_{mix} and K_{diff}, and decreases with w_{subs}.

3.4. Isotopic Composition

[25] Water vapor isotopic species are treated exactly like normal water during advection, mixing and diffusion, and are assumed to follow Rayleigh distillation during large-scale condensation.

[26] The isotopic ratio in convective plumes is constrained by the mass conservation underlying equation (3):

$$R_0 = f \cdot R_v + (1-f) \cdot R_c \tag{12}$$

where $f = \frac{q_s}{q_{s0}}$ is the fraction of vapor that remains after condensation in the cloud, and R_0, R_v and R_c are respectively the isotope ratio of the vapor at the LCL, the residual vapor and the accumulated condensate. We assume that R_v follows a Rayleigh distillation: $R_v = R_{v0} \cdot f^{\alpha-1}$, where α is the effective fractionation coefficient taking into account both equilibrium and kinetic fractionation consistently with LMDZ simulations [*Merlivat and Nief*, 1967; *Majoube*, 1971a, 1971b; *Jouzel and Merlivat*, 1984]. As a fraction ϵ_p of the condensate precipitates, we obtain the isotope ratio of the total water in convective plumes [*Bony et al.*, 2008]:

$$R_{dtr} = R_0 \cdot \frac{1-\epsilon_p \cdot (1-f^{\alpha})}{1-\epsilon_p \cdot (1-f)}. \tag{13}$$

[27] If the water balance in convective regions is mainly between large-scale advection and condensation, then R_{conv} is predicted by a Rayleigh distillation. In contrast, if the detrainment term dominates, the isotopic ratio R_{conv} tends toward R_{dtr}, which is much higher than predicted by a Rayleigh distillation. This is consistent with the effect of convective detrainment on upper tropospheric δD evidenced by observational studies [e.g., *Webster and Heymsfield*, 2003; *Sayres et al.*, 2010]. In practice, R_{conv} is bounded by these two extreme values. In subsidence regions, the isotopic ratio R_{subs} at a given level will be intermediate between R_{conv} at this level and R_{conv} higher in altitude. In addition, R_{subs} increases with vertical diffusion.

3.5. Numerical Application

[28] Equations (1) and (8) and their isotopic counterparts are discretized on the LMDZ vertical grid and solved numerically. We use the annual mean, tropical average temperature profile simulated by LMDZ to calculate profiles of q_s and α that will be used in all calculations. This is justified by the fact that temperature is relatively uniform in the horizontal in the tropics [*Sobel and Bretherton*, 2000] and are very similar in all our simulations. We assume that in the sub-cloud layer (below the LCL calculated at 925 hPa) RH and δD are constant at 80% and -70‰ respectively, consistent with the annual mean, tropical-average values simulated by LMDZ. These values are kept constant as a boundary condition throughout the numerical resolution, and this allows us to implicitly account for the effect of surface evaporation. The values of q and δD are also relaxed to the value predicted by a Rayleigh distillation above 100 hPa, where almost no convection penetrates. The choice of the upper bound has very little impact. The vertical profile of ϵ_p is exactly the same as in LMDZ: in the control simulation, $\epsilon_p = 0$ up to 150 hPa above LCL, $\epsilon_p = 0.99$ above 500 hPa above LCL, and ϵ_p varies linearly between these two values from 150 hPa to 500 hPa above LCL [*Emanuel and Zivkovic-Rothman*, 1999; *Bony and Emanuel*, 2001]. The vertical profile of σ_h is taken to mimic the behavior of large-scale condensation scheme of LMDZ: σ_h varies linearly from 0 at the surface to 0.4 at 100 hPa.

[29] All other variables were optimized to reproduce the tendencies simulated by LMDZ (Figures 2b and 2c) in the mid and upper troposphere. We calculate w_{up} and w_{down} by assuming that the profiles of vertical velocity in hPa/day follow a cubic shape with a maximum at 500 hPa. We take $\omega_{up} = 40$ hPa/day and $\omega_{down} = 40$ hPa/day at 500 hPa. We assume that the profile of k_{dtr} follows a Gaussian shape with a maximum at 120 hPa, a standard deviation at 300 hPa and a maximum of 0.2 day^{-1}. We assume that k_{cond} equals 0.33 day^{-1}. We assume that k_{mix} varies linearly between 0.05 day^{-1} and 1 day^{-1} from 800 hPa to 100 hPa. Finally, K_{diff} is taken so that the diffusion is equivalent to exchanging a thickness $\omega_{diff} \cdot dt$ of air between each adjacent level at each time step dt, with $\omega_{diff} = 20$ hPa/day. This value was taken as the minimum value to allow numerical stability of the single-column model.

[30] With this set of parameters, the simple single-column model reproduces satisfactorily the vertical profiles of the main tendencies involved in the mid and upper tropospheric water balance simulated by LMDZ, though in a simplified way (Figures 2d and 2e). The model fails near the surface, which is neither surprising nor problematic since we focus on mid and upper tropospheric processes. As the model was tuned to reproduce the humidity tendencies for the control simulation, the capacity of the simple framework to predict the RH and isotopic profiles simulated by LMDZ in the different sensitivity tests can be viewed as an independent check of the simple framework.

4. Sensitivity of RH to the Model Physics, Nudging and Resolution

4.1. Sensitivity to Parameterized Processes

[31] Numerous studies have shown that GCMs suffer from a moist bias compared to various data sets in the tropical upper troposphere and in the subtropical mid-to-upper troposphere, following a horse-shoe pattern [*Soden and Bretherton*, 1994; *Salathe and Chester*, 1995; *Chen et al.*, 1996; *Roca et al.*, 1997; *Chen et al.*, 1998; *Allan et al.*, 2003; *Brogniez et al.*, 2005; *Pierce et al.*, 2006; *John and Soden*, 2007; *Sherwood et al.*, 2010; *Chung et al.*, 2011]. As an illustrative example, Figure 3 compares the simulated RH in the control LMDZ simulation with the AIRS (Atmospheric Infra-Red Sounder data) data [*Aumann et al.*, 2003]. Consistent with previous studies and other GCMs, LMDZ exhibits a moist bias throughout the mid and upper troposphere in tropical average (Figure 3a). Figure 3b shows composites of RH at 350 hPa as a function of monthly mean ω_{500}. Due to a clear-sky sampling bias in AIRS [*Fetzer et al.*, 2006], upper-tropospheric RH in deep convective tropical regions could be underestimated by as much as 10–20% [*Pierce et al.*, 2006]. The moist bias seems to be stronger in regions of large-scale ascent than in regions of large-scale descent in Figure 3b, but this is likely an artifact of the clear-sky bias. This does not contradict the fact that in most GCMs, including LMDZ, the moist bias is most pronounced

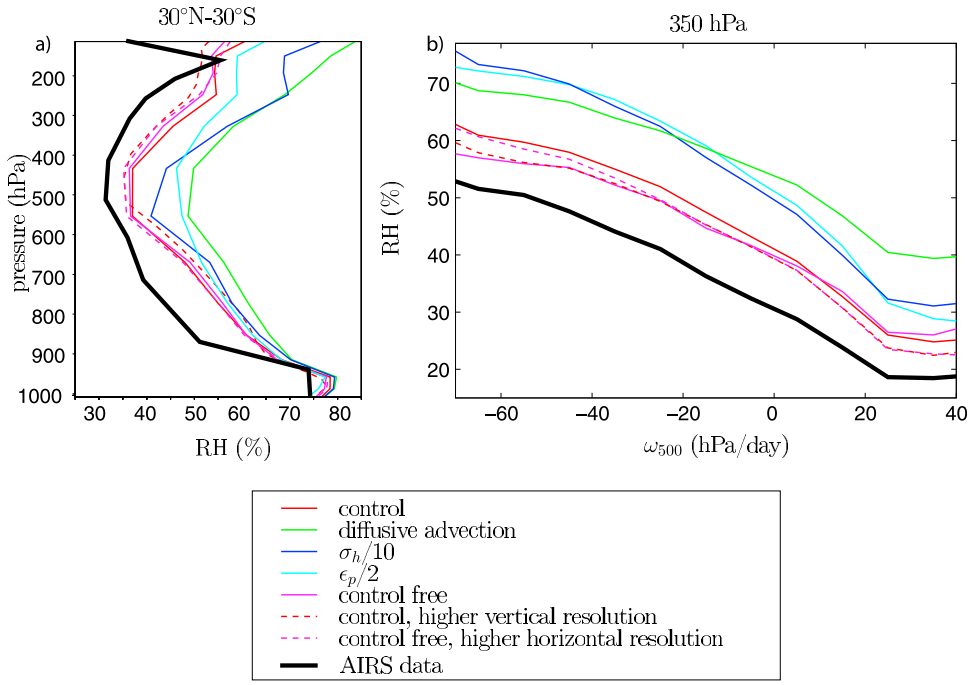

Figure 3. (a) Annual mean relative humidity (RH) profiles averaged over the tropics (30°S–30°N) simulated by the various versions of LMDZ (colors) and observed by AIRS (black). (b) Composites of monthly mean RH at 350 hPa as a function of the large-scale vertical velocity at 500 hPa (ω_{500}) over the tropics simulated by the various versions of LMDZ and observed by AIRS.

in subtropical regions. An accurate comparison of LMDZ with AIRS is beyond the scope of this paper.

[32] To understand the cause of the moist bias, we performed sensitivity tests in which the model physics was degraded in 3 different ways, corresponding to 3 possible causes for a larger moist bias (Table 3). Hereafter, they are referred to as "moist bias" simulations. We conducted tests with a larger rather than smaller moist bias because (1) the goal is to see how isotopic measurements can help understand biases, and (2) since the control simulation is already slightly biased, trying to improve the RH for different causes would lead to error compensations that would make the presentation of the results less straightforward. All these sensitivity tests are nudged by the ECMWF winds, so that the large-scale circulation is similar in all the simulations. This methodology excludes dynamical feedbacks, and thus allows us to focus on differences that are due to physical processes only.

[33] In the "diffusive advection" simulation, we replace *Van Leer*'s [1977] second-order advection scheme by a simple upstream scheme [*Godunov*, 1959]. This is the version described by *Risi et al.* [2010b] and provided to the SWING2 archive. The upstream scheme is intrinsically more diffusive. This leads to a 15% stronger moist bias throughout the tropical troposphere (Figure 3a, green). Additional tests show that most of the moistening in this simulation is due to excessive diffusion in the vertical, rather than the horizontal, advective scheme. In the theoretical framework, this simulation corresponds to an increase in K_{diff}. Vertical diffusion moistens the mid and upper-troposphere due to down gradient moisture flux and to the concavity of q profiles as a function of height. The moist bias is strongest in the subsidence region, because the diffusive moistening accumulates in air parcels as they subside from tropical regions (Figure 3b). In the theoretical framework, this is represented by the diffusion term being present in both convective and subsidence regions (equations (1) and (8)).

[34] In the "$\sigma_h/10$" simulation, the sub-grid-scale variability in water vapor, which is used to predict large-scale condensation in the *Bony and Emanuel* [2001] statistical cloud scheme, is divided by 10 at all levels. This reduces the proportion of air in the grid box exceeding saturation. Therefore, large-scale condensation decreases and contributes less to the dehydration of air masses, leading to a

Table 3. Summary of the Four Main Sensitivity Simulations Performed With the LMDZ GCM

Name	Description
Control	Control simulation described with the actual AR4 version of LMDZ4.
Diffusive advection	Same as control but a simple upstream scheme [*Godunov*, 1959] is used rather than the second order advection scheme [*Van Leer*, 1977; *Hourdin and Armengaud*, 1999]. This is the simulation described by *Risi et al.* [2010b] and provided to SWING2.
$\sigma_h/10$	Same as control but the sub-grid-scale variability in water vapor used to predict large-scale condensation and nebulosity is divided by 10.
$\epsilon_p/2$	Same as control but the precipitation efficiency in both the convective and large-scale precipitation schemes was divided by 2.

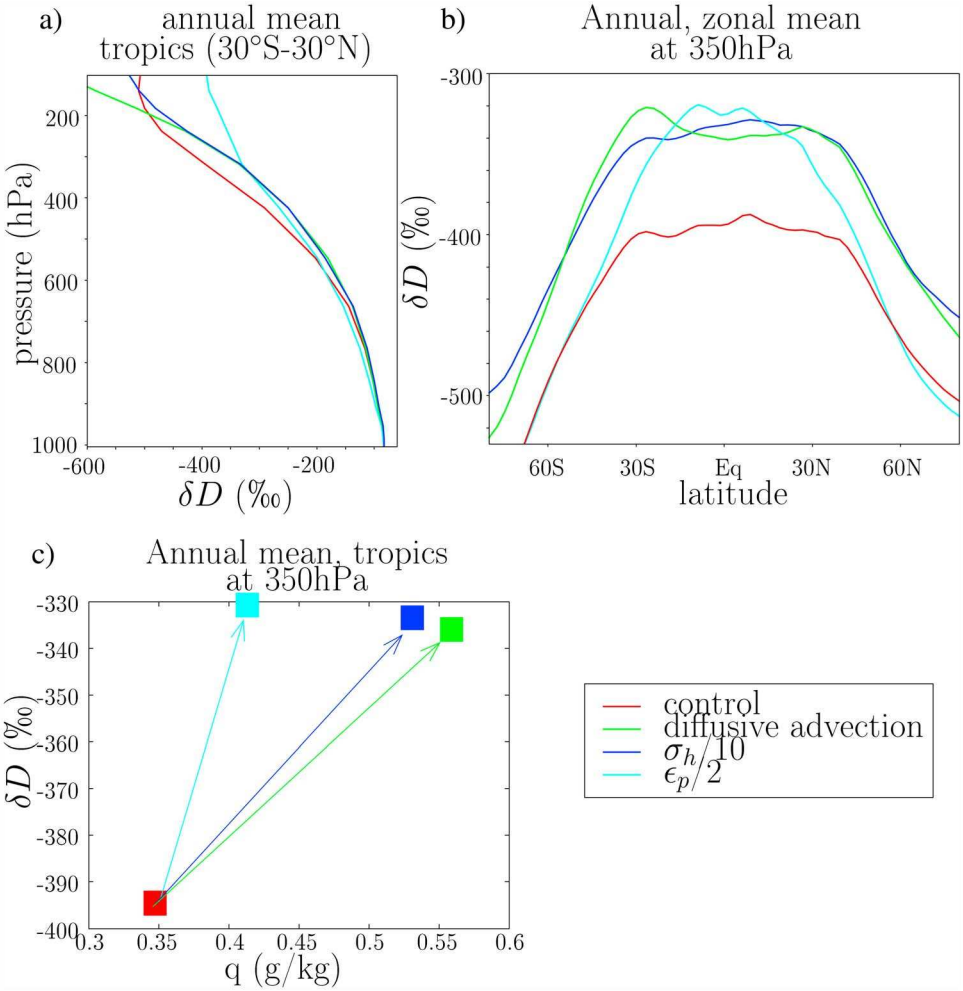

Figure 4. Comparison of annual mean water vapor δD simulated by the control simulation and by the three moist bias simulations. (a) Vertical profiles of tropical (30°S–30°N) average δD. (b) Zonal mean δD at 350 hPa. (c) Tropical average δD at 350 hPa as a function of annual mean, tropical average q at 350 hPa.

stronger moist bias by about 15% in the upper troposphere (Figure 3, blue). This is consistent with the theoretical framework, in which dividing σ_h by 10 leads to an increase in the lower bound for q_{asc} toward saturation. The effect of σ_h is largest in regions of large-scale ascent (Figure 3b), because this is where the large-scale condensation scheme plays a significant role. In subsidence regions, its effect is smaller.

[35] Finally, in the "$\epsilon_p/2$" simulation, the precipitation efficiency ϵ_p in the convective scheme was divided by 2. Therefore, a higher proportion of the condensate evaporates into the environment rather than precipitates, significantly moistening the atmosphere by 5 to 10% (Figure 3a, cyan). This is consistent with the theoretical framework, in which the increase in ϵ_p leads to an increase of $q_{t,dtr}$, which constitutes the upper bound for q_{asc}. Again, the effect is largest in regions of large-scale ascent (Figure 3b), because this is where convective detrainment plays a significant role.

[36] The large sensitivity of RH to micro- and macrophysical cloud processes seems to contradict some earlier studies. *Sherwood* [1996] argued that cloud processes act to bring the convective column close to saturation, and have thus very limited quantitative effect of RH [*Sherwood and Meyer*, 2006]. However, at the scale of a GCM grid box, the atmospheric column is not necessarily close to saturation in convective regions. Therefore, there is room for modulation of the RH by cloud processes. Then, since RH in convective regions serves as an initial condition for the RH in other dynamical regimes through large-scale transport and subsidence, RH modulations in convective regions by cloud processes propagate to other regimes. Using a simple back-trajectory model, *Dessler and Sherwood* [2000] had shown that the large-scale circulation alone could explain to first order the observed RH distribution in the upper troposphere. They showed an influence of both sub-grid-scale heterogeneity and condensate detrainment, consistent with our study, but they discarded these processes on the basis that each of them individually worsen their simulation. In GCMs however, both these processes play a simultaneous role (Figure 2b) and the degree to which they compensate each

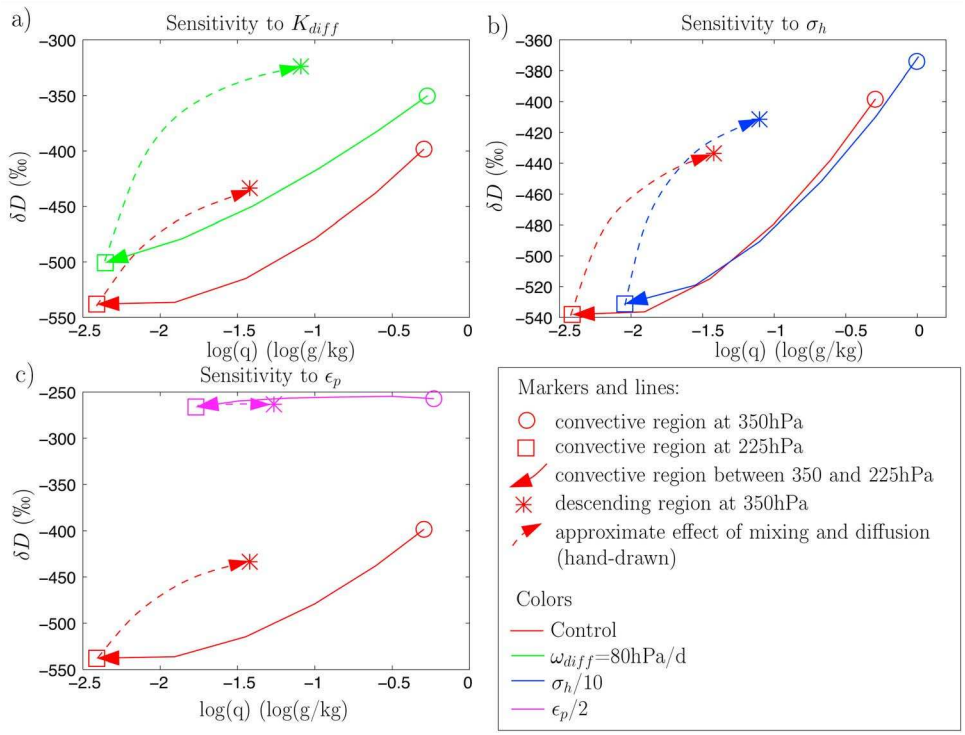

Figure 5. Illustration of how the simple theoretical model captures the behavior of q and δD for the sensitivity simulations, at 350 hPa as an example. Diagrams of δD versus $\log(q)$ are shown so that Rayleigh distillation follows approximately a straight line. On each subplot, the mechanisms for the control simulation is shown in red. The vertical profile in the convective region between 350 hPa (circle) and 225 hPa (square) follows the thick line. In subsidence regions, the humidity and δD (star) reflect a mixture between the air from convective regions at the same level and from levels above, and is further affected by vertical diffusion, following the hand-drown dashed line. These markers and lines are shown also for the three moist bias simulations: diffusive advection (Figure 5a, green), $\sigma_h/10$ (Figure 5b, blue) and $\epsilon_p/2$ (Figure 5c, pink). Note that $\log(q)$ values of -2.5, -2, -1.5, -1, -0.5 and 0 correspond to q values of 0.08, 0.14, 0.22, 0.37, 0.61 and 1 g/kg.

other affects the simulated RH. To summarize, while large-scale circulation is the major control on RH spatial variations in a given model, there is a wide margin for variations in mean RH associated with the representation of cloud processes.

4.2. Sensitivity to the Nudging and Resolution

[37] To assess the relative importance of uncertainties related to large-scale circulation in simulating RH, we compared the control simulation with nudged wind fields to a free-running simulation (i.e. without nudging). The effect on RH is however smaller (<5%) than the effect of the model physics (Figure 3, pink).

[38] Strong gradients of RH arise in the tropics and subtropics because the timescale of mixing processes is longer than that of radiative subsidence [*Pierrehumbert*, 1998; *Zhang et al.*, 2003]. A higher resolution may improve the simulation of RH by GCMs [*Sherwood et al.*, 2010]. We thus performed free-running and nudged simulations at a higher horizontal resolution (1.25° in latitude × 2.5° in longitude). The impact of resolution is slightly stronger for the free-running simulation, because it allows the model to create its own finer scale circulation. The RH is decreased by 2–3% in the subtropics, where the RH gradients are the strongest. This impact is much smaller than that of physical processes (Figure 3).

[39] Therefore, improving the representation of large-scale circulation or improving horizontal resolution has a smaller effect on the RH simulation than changing the model physics. Since the large-scale circulation is relatively well simulated in GCMs, the uncertainties that remain are related to the models physics. Therefore, while the large-scale circulation is the main control on RH, it is not the major source of uncertainty. This is confirmed by the fact that reanalyses models also exhibit the moist bias [*Salathe and Chester*, 1995; *Chen et al.*, 1998].

[40] We thus mainly focus on the sensitivity tests which are designed to test to the model physics.

[41] Coarse vertical resolution has also been suggested to contribute to the moist bias [*Pope et al.*, 2001]. We expect the vertical advection to be less diffusive at finer vertical resolution, with an effect opposite to the "diffusive advection" simulation. The simulation at higher vertical resolution (39 vertical levels rather than 19) indeed leads to a decrease in RH of about 5% (Figure 3a, dashed red). Since this simulation provides redundant information compared to the

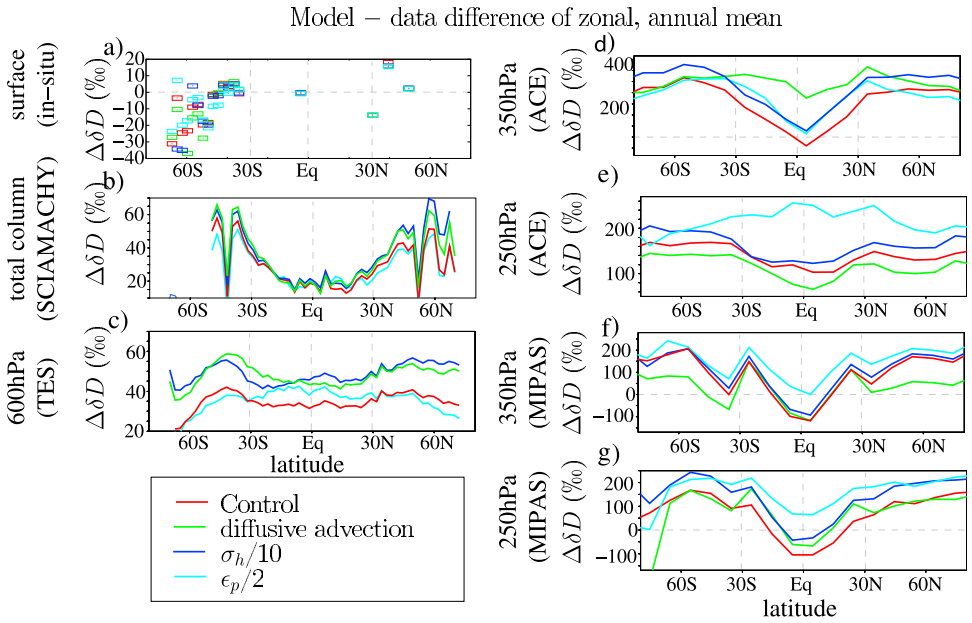

Figure 6. Model-data difference for zonal, annual mean δD at different levels and compared to different data sets: (a) at the surface compared to in situ data, (b) total column compared to SCIAMACHY, (c) at 600 hPa compared to TES, (d) at 350 hPa compared to ACE, (e) at 250 hPa compared to ACE, (f) at 350 hPa compared to MIPAS, and (g) at 250 hPa compared to MIPAS. The model-differences are shown for the control simulation and each of the three moist bias simulations. Model output was collocated and kernel-weighted as explained in section 2.2. Right column. Ground-based remote-sensing and in situ data sets are not shown in the plots for clarity, but their results are summarized in Table 4.

"diffusive advection" simulation, we focus on the latter for the sake of brevity.

5. Isotopic Fingerprint of Different Causes for the Moist Bias

[42] The goal of this section is threefold. First, we compare the isotopic behavior associated with the different causes of a moist bias in our sensitivity tests. If the isotopic behavior is significantly different between the simulations in a way that is complementary to the behavior of RH, then this isotopic behavior could be used as a diagnostic for the moist bias. Second, we interpret the isotopic behavior using the theoretical framework, to check that we understand the processes at play. Third, we compare the simulations to the data, to identify which one most closely matches the observations and to assess to what extent the isotopic measurements can help discriminate between the different simulations.

5.1. Zonal, Annual Means

[43] Figure 4a compares tropical mean profiles of δD for the control and moist bias simulations. In all moist bias simulations δD is higher than in the control between 500 and 200 hPa. The increase in δD is the strongest in "$\epsilon_p/2$" in the upper troposphere. Figure 4b compares the zonal mean δD at 350 hPa. The level 350 hPa is chosen as representative of the upper troposphere where the isotopic differences between the tests are the strongest. Most of our analysis focuses on this level. In the "advective diffusion" and "$\sigma_h/10$" simulations, upper tropospheric δD increases at all latitudes (Figure 4b), whereas in the "$\epsilon_p/2$" simulation, the δD increase is concentrated in the tropics, consistent with the convective detrainment acting mainly in the tropics. The increase in δD does not obviously relate to the increase in q or RH following Rayleigh distillation: the increase in tropical δD is largest in the "$\epsilon_p/2$" simulation, although the increase in q or RH is smallest for this simulation (Figure 4c). This shows that δD is particularly sensitive to convective detrainment and provides additional information compared to traditional humidity variables.

[44] To understand the δD increase in the moist bias simulations, in Figure 5 we illustrate the results of the theoretical framework (section 3) at 350 hPa in a δD versus log (q) diagram, in which Rayleigh distillations are approximately straight lines. The solid red arrow shows the δD profile in convective regions from 350 hPa (red circle) up to 225 hPa (red square) for the control case. In convective regions, δD decreases as q decreases with altitude, but less steeply than predicted by Rayleigh distillation, due to convective detrainment of condensate [e.g., *Moyer et al.*, 1996]. Then, as explained in section 3.3, δD in subsidence regions at 350 hPa is a mixture between δD in convective regions at 350 hPa and δD in convective regions higher up (e.g. 225 hPa). The dashed red arrow shows the effect of mixing the air at 350 hPa and 225 hPa, combined with the effect of vertical diffusion. The red star shows the resulting δD at 350 hPa in subsidence regions. Since mixing lines are curved in a way that leads to higher δD compared to Rayleigh lines [e.g., *Brown et al.*, 2008; *Galewsky and Hurley*, 2010; *Noone et al.*, 2011], δD in subsidence regions is higher for a given q than in convective regions. Vertical

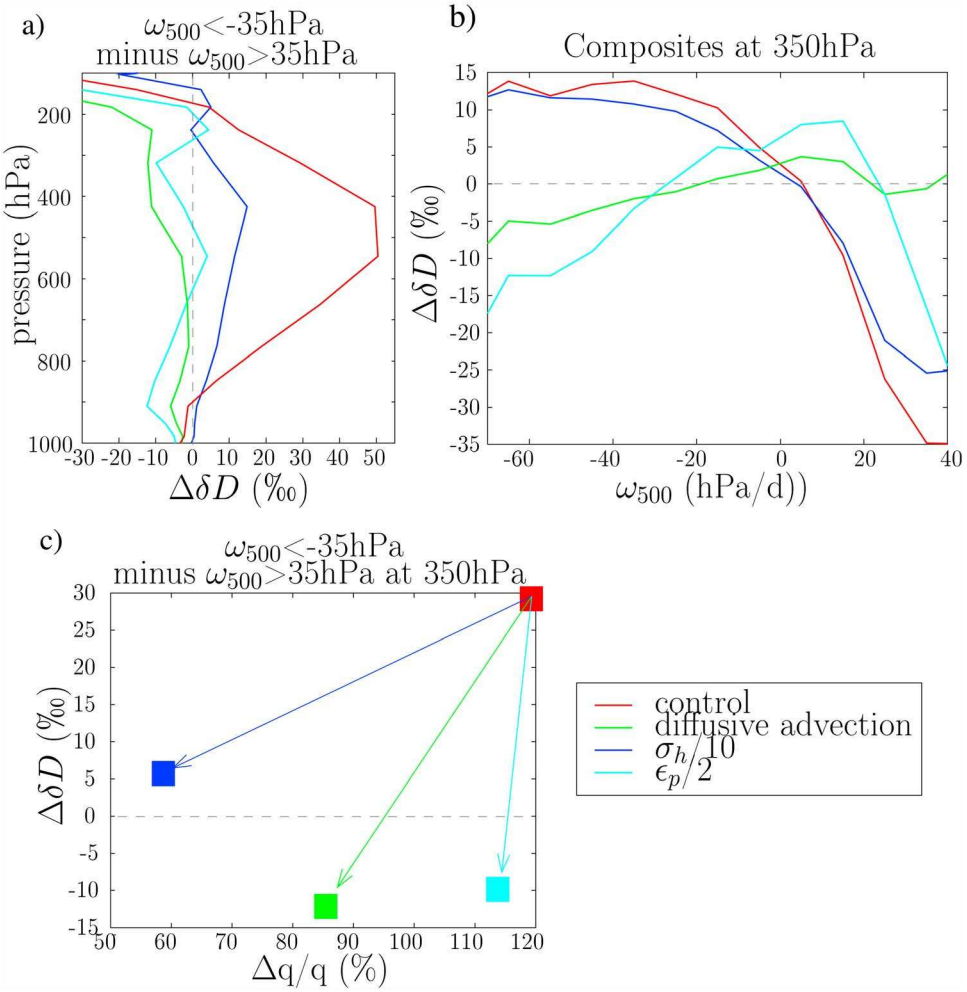

Figure 7. Comparison of water vapor δD simulated by the control simulation and the by three moist bias simulations, binned into dynamical regimes. (a) Vertical profiles of the difference between composite of monthly mean δD in regions of large-scale ascent (tropical grid cells where $\omega_{500} < -35$ hPa/d) and composite of monthly mean δD in subsidence regions (tropical grid cells where $\omega_{500} > 35$ hPa/d). The variable ω_{500} refers to the large-scale vertical velocity at 500 hPa, with negative (positive) values in regions of large-scale ascent (subsidence). (b) Composites of monthly mean δD at 350 hPa as a function of ω_{500} over the tropics. The annual mean, tropical average was subtracted to focus on contrasts between dynamical regimes. (c) Composite of monthly mean δD at 350 hPa in convective regions minus that in subsidence regions, as a function of the same difference for q. The difference in q was normalized and expressed in % as follows: $(q_{asc} - q_{subs})/(q_{asc} + q_{subs}) \cdot 200$.

diffusion also contributes to the δD increase, since diffusion acts like mixing.

[45] We now use the theoretical framework to interpret the δD difference between the sensitivity tests. When vertical diffusion is stronger (here, we take ω_{diff} = 80 hPa/d compared to 20 hPa/d in the control), convective regions are slightly moistened and have a significantly higher δD due to the curvature of mixing lines (Figure 5a, green). In subsidence regions, the δD is even further increased, due to the additional diffusion along the way. In the "σ_h/10" simulation, the distillation curve in convective regions remains approximately the same, but since large-scale condensation is less efficient, the distillation does not go as far as in the control (Figure 5b, blue). q and δD are thus higher in convective regions and this signature is conserved during the subsidence, leading to higher q and δD everywhere. In "ϵ_p/2", more condensate is detrained from convective towers, so that δD in convective regions is much higher, especially in the upper troposphere where detrainment is largest (Figure 5c, cyan). This higher δD is then conserved during subsidence in subsidence regions.

[46] To summarize, the increase in δD associated with the moistening has a very different cause in each of the three sensitivity tests. As a result, for a given increase in q relatively to the control, the δD increase is very different between the tests (Figure 4c). In particular, the theoretical model is able to predict that for "ϵ_p/2", δD is 3–4 times more sensitive to changes in q than for "advective diffusion" or "σ_h/10".

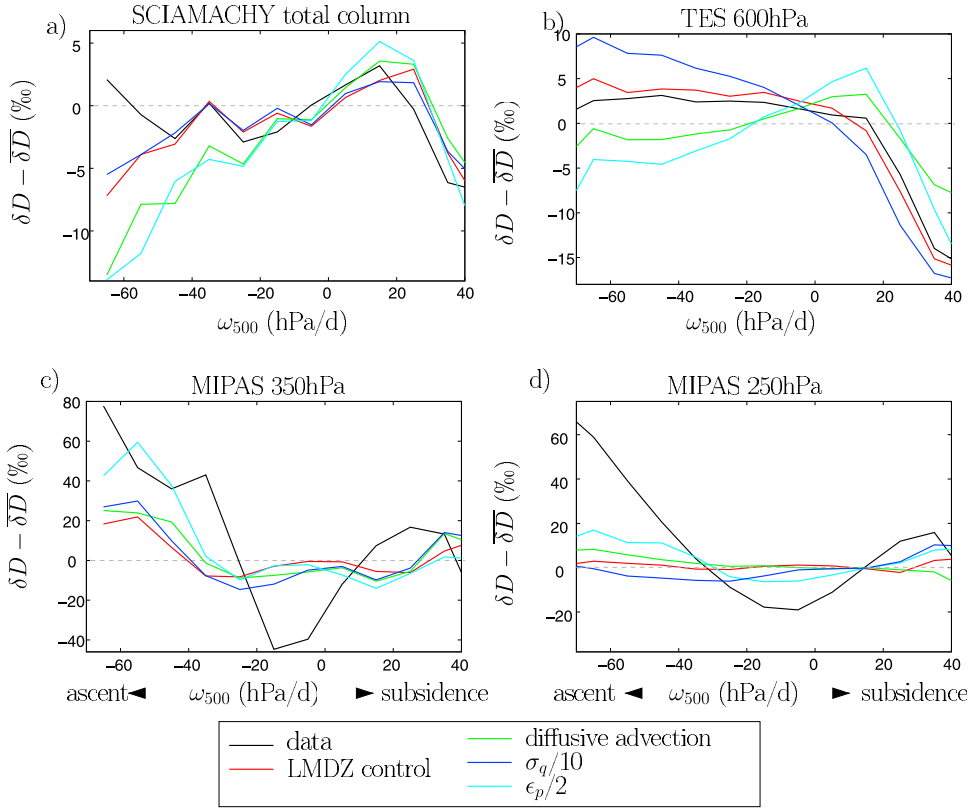

Figure 8. Composites of monthly mean δD as a function of ω_{500} for the control simulation and the three moist bias simulations compared to the data at different levels. (a) Total column δD compared to SCIAMACHY, (b) at 600 hPa compared to TES, (c) at 350 hPa compared to MIPAS, and (d) at 250 hPa compared to MIPAS. Model outputs were collocated and kernel-weighted as explained in section 2.2.

[47] Could isotopic observations help discriminate between the different simulations? Figure 6 shows the model-data differences at different levels and for different data sets. The differences between simulations evidenced previously persist even after taking into account the spatiotemporal sampling and instrument sensitivity effects: for example, "$\epsilon_p/2$" remains more enriched than all other simulations in the tropical upper troposphere by more than 100‰. However, in absence of absolute calibration for upper-tropospheric data sets, it is impossible to identify the most realistic simulation in terms of absolute δD.

5.2. Variations With Dynamical Regime

[48] In the tropics, it is convenient to examine model output as a function of dynamical regime characterized by the monthly mean large-scale vertical velocity ω_{500} [*Bony et al.*, 2004]. Figure 7a shows profiles of δD differences between tropical regions of large-scale ascent and descent, and Figure 7b shows δD at 350 hPa as a function of ω_{500}. The sensitivity tests show very different behaviors, both quantitatively and qualitatively. The only common feature between all simulations is that at the surface, convective regions have a lower δD than subsidence regions (Figure 7a). Strong precipitation events have long been observed to be associated with a lower δD in the precipitation and the surface vapor (i.e. amount effect [*Dansgaard*, 1964]), and this has been shown to involve processes restricted to the lower troposphere such as rain re-evaporation or unsaturated downdrafts [*Lawrence et al.*, 2004; *Risi et al.*, 2008, 2010a; *Field et al.*, 2010]. In contrast, from 900 to 200 hPa in the control simulation, δD is lower in regions of large-scale subsidence than in regions of large-scale ascent, by up to 50‰ around 500 hPa. This is expected from the simple model (Figure 5, stars versus circles), since the low δD values found in the upper troposphere of large-scale ascent regions are largely conserved during subsidence. The decrease of δD as ω_{500} increases is the strongest for $\omega_{500} > 0$ hPa (Figure 7b).

[49] In the "$\sigma_h/10$" simulation, the contrast between convective and subsidence regions is slightly weaker, with higher δD in subsidence regions. In the "$\epsilon_p/2$" simulation, the decrease of δD as ω_{500} increases is similar to the control for $\omega_{500} > 20$ hPa/d. However, for $\omega_{500} < 20$ hPa/d, δD decreases as ω_{500} decreases throughout the entire troposphere. Similarly, in the "diffusive advection" simulation, δD decreases as ω_{500} decreases for $\omega_{500} < 20$ hPa/d. In addition, contrary to all other simulations, δD does not decrease with ω_{500} for $\omega_{500} > 20$ hPa/d. Even in strongly subsiding regions, δD is always higher than in convective regions throughout the free troposphere.

[50] We notice that the spread in our simulations is not obviously linked to the behavior of q: "advective diffusion" exhibits the most negative δD difference between convective and subsidence regions, but not the weakest contrast for q (Figure 9). We also checked that the isotopic behavior is not related to how the precipitation rate varies with ω_{500}. This

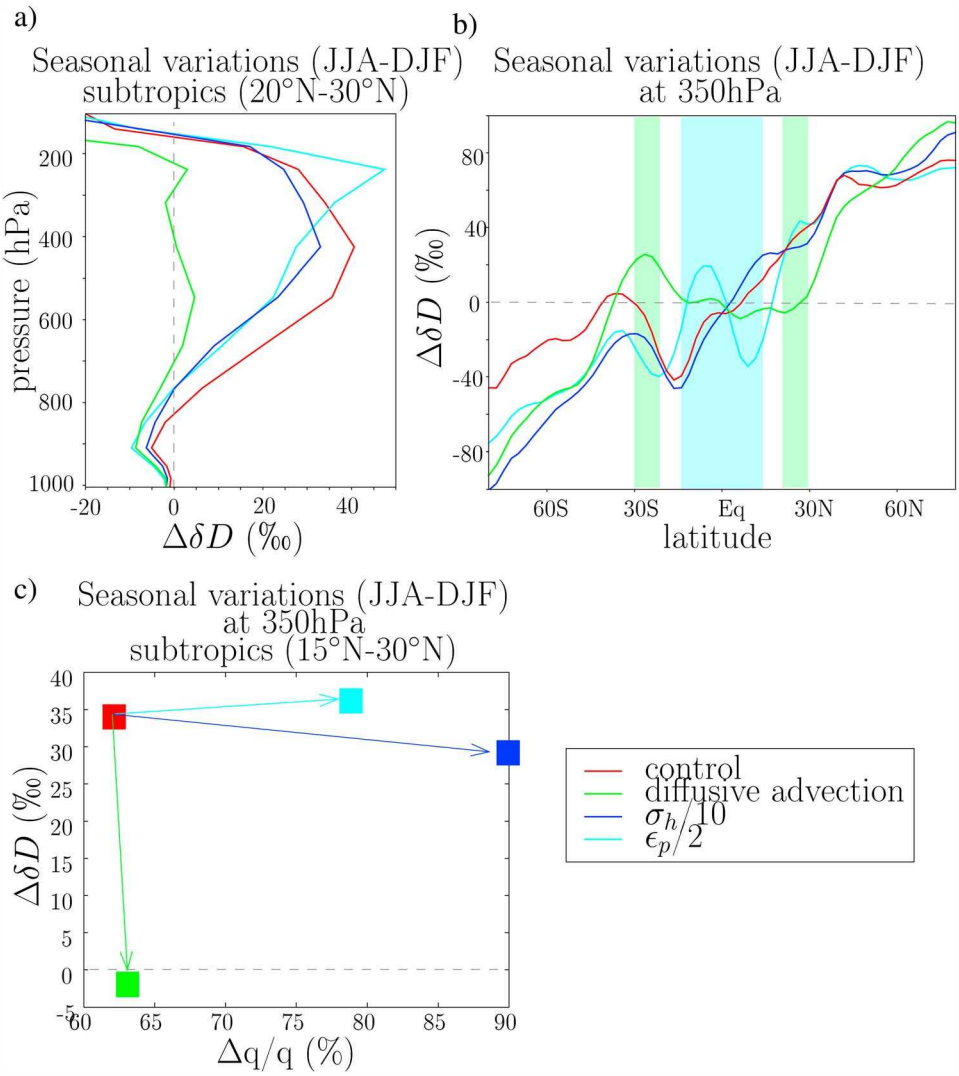

Figure 9. Comparison of seasonal variations of water vapor δD simulated by the control simulation and by the three moist bias simulations. (a) Vertical profiles of seasonal variations (JJA-DJF) in δD in average over the Northern subtropics (20°N–30°N). (b) Seasonal variations at 350hPa as a function of latitude. Cyan and green shadings highlight the deep tropical (15°S–15°N) and subtropical (20°N–30°N) regions where the seasonality is reversed in the "$\epsilon_p/2$" and "diffusive advection" simulations respectively. (c) Seasonal variations of δD at 350hPa in average over the Northern subtropics, as a function of the same seasonal variations for q. The variation in q was normalized by annual mean q and expressed in %.

shows again that δD provides complementary information on the relative magnitude of processes contributing to the moisture balance.

[51] We use the simple theoretical framework to explain the different isotopic behavior. In the "diffusive advection" simulation, the stronger vertical diffusion in subsidence regions leads to a stronger δD increase than in the control. If the diffusion is sufficiently strong, it can overcome the effect of subsidence, leading to higher δD in subsidence regions than in convective regions (Figure 5a). In the "$\sigma_h/10$" simulation, q and δD are higher at all levels in convective regions, so this signal is preserved during subsidence (Figure 5b). Hence, the δD contrast between convective and subsidence regions is similar to that in the control. Finally, in the "$\epsilon_p/2$" simulation, the vertical gradient in δD in the convective region is weaker than in the control, due to the effect of condensate detrainment in the upper troposphere (Figure 5c). Therefore, the effect of subsidence on the δD is weaker, leading to the weaker contrast between subsidence and convective regions. In addition, the very low δD in very convective regions can be due to the much weaker convective mass fluxes in the "$\epsilon_p/2$" simulation than in the control. Indeed, since most of the condensate detrains rather than precipitates, the model has to produce precipitation by an alternative means, i.e. by large-scale condensation. Therefore, in convective regions, large-scale condensation is stronger and convective detrainment fluxes are smaller in the "$\epsilon_p/2$" simulation than in the control, explaining why δD is so low in convective regions in the "$\epsilon_p/2$" simulation.

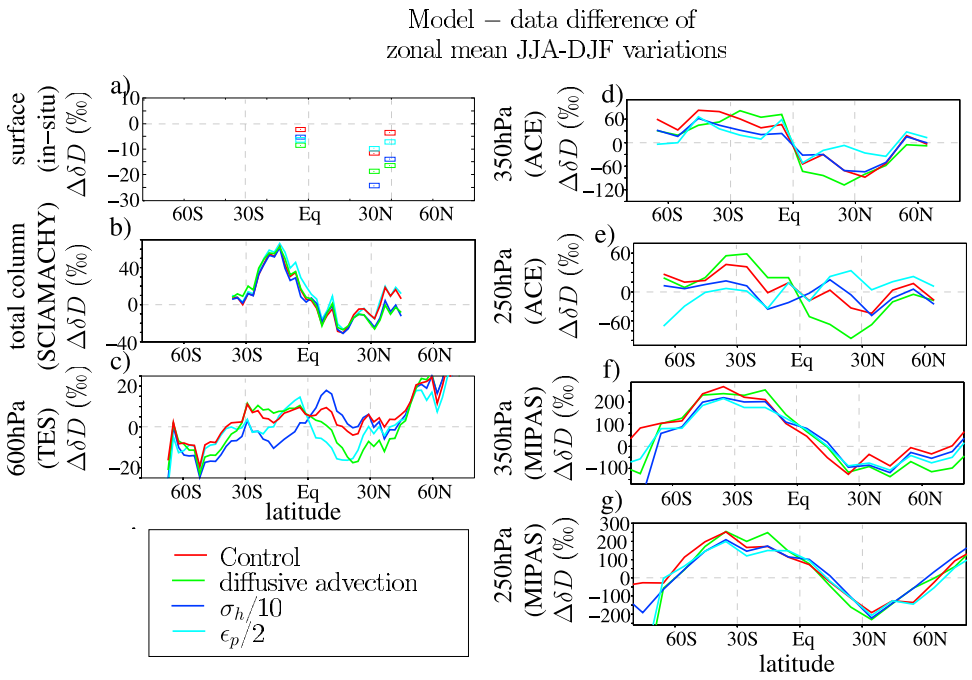

Figure 10. Same as Figure 6 but for model-data differences of zonal mean seasonal variations (JJA-DJF). Note that two kinds of differences (model-data and JJA-DJF) have been compacted into the $\Delta\delta D$ notation.

[52] Figure 8 shows that even after taking into account spatiotemporal sampling and instrument sensitivity corresponding to the different data sets, the main δD characteristics of our simulations remain. The isotopic data could thus help discriminate which of these very distinct behavior better represents the real atmosphere. In the lower and mid troposphere, the control simulation has the best agreement with SCIAMACHY and TES, whereas the "diffusive advection" and "$\epsilon_p/2$" simulations exhibit excessively low δD values in convective regions. (Figures 8a and 8b). In the upper-troposphere however, none of the simulations is able to match the strong increase in δD in regimes of large-scale ascent.

5.3. Seasonal Variations

[53] In the tropics and the subtropics, much of the seasonal variations are associated with seasonal variations in dynamical regimes. When ascending motions are more frequent, δD is expected to be higher as explained in section 5.2. In the control simulation, at all latitudes, upper tropospheric δD is higher in summer than in winter (Figures 9a and 9b). This is consistent with more frequent ascending motions in summer than in winter due to the location of the inter-tropical convergence zone. In the subtropics in both hemispheres, the higher δD in summer holds from 900 hPa to 200 hPa, so it is very robust. The maximum seasonality is around 500 hPa, as was the case for variations with ω_{500}.

[54] As was the case for variations with ω_{500}, the "$\sigma_h/10$" simulation has an isotopic behavior that is quite similar to the control. "$\epsilon_p/2$" also has a similar behavior in the subtropics (where large-scale motions are mostly subsiding), but δD is lower in summer than in winter in deep tropical regions (15°S–15°N) (Figure 9b). This is consistent with the very low δD in convective regions in this simulation (Figure 9). Finally, in the "diffusive advection" simulation, the seasonality is very weak, or even reversed, in the subtropics in both hemispheres (20°S–30°S and 20°N–30°N). This is consistent with the δD being higher in subsidence regions than in convective regions in this simulation.

[55] Therefore, the understanding of isotopic variations across dynamical regimes (section 5.2) allows us to understand the different behaviors of our simulations in terms of isotopic seasonality. Again, the different isotopic behaviors are not obviously related to those in humidity (Figure 9c), showing the added value of isotopic measurements to discriminate between the simulations.

[56] At all levels, the control simulation underestimates the isotopic seasonality in the subtropics (Figure 10). This is robust in the comparisons between the model and all data sets (in situ, ground-based remote-sensing and satellites). The robustness of this result is further discussed in P1. Therefore, the underestimated or even reversed seasonality in the "diffusive advection" simulation worsens the model-data agreement. Compared to ACE for example, the δD seasonality is more underestimated in the "diffusive advection" simulation than in the control by 40–50‰ in the Northern subtropics (Figures 10d and 10e). The magnitude of this difference is unlikely to be affected by absolute calibration problems in the data since we are looking at variations. In addition, it is larger than any additional sources of model-data comparison uncertainties detailed in P1. Therefore, the deterioration of the simulated subtropical seasonality in the "diffusive advection" simulation is robustly constrained by the comparison with the ACE data. It is also observable in the subtropics at 600hPa compared to TES (Figure 10c) and compared to MIPAS at 350 hPa (Figure 10f) and at 250 hPa (Figure 10g), except for MIPAS in the Northern Hemisphere.

[57] To measure the degree to which our simulations capture the δD seasonality in the subtropics and lower

Table 4. Quantitative Metrics to Compare the Model-Data Agreement Between the Different LMDZ Simulations[a]

Feature	Metric	Region	Data Set	Level	Control	Diffusive Advection	$\sigma_h/10$	$\epsilon_p/2$
Zonal mean seasonal variations (JJA-JF)	amplitude ratio	20°N–30°N	SCIAMACHY	total column	*0.67*	**0.40**	0.41	0.60
	amplitude ratio	20°N–30°N	TES	600 hPa	*1.02*	**0.27**	1.14	0.57
	amplitude ratio	20°N–30°N	MIPAS	350 hPa	**−0.06**	0.02	0.21	*0.26*
	amplitude ratio	20°N–30°N	ACE	350 hPa	0.37	**0.07**	*0.39*	0.38
	amplitude ratio	20°N–30°N	MIPAS	250 hPa	0.11	**−0.35**	0.11	*0.92*
	amplitude ratio	20°N–30°N	ACE	250 hPa	0.31	**−0.99**	0.88	*1.92*
	amplitude ratio	20°N–30°N	SCIAMACHY	total column	0.13	**−0.09**	*0.14*	0.02
	amplitude ratio	20°N–30°N	TES	600 hPa	0.35	**0.19**	*1.17*	1.10
	amplitude ratio	20°N–30°N	MIPAS	350 hPa	−0.21	**−0.26**	−0.10	*0.04*
	amplitude ratio	20°N–30°N	ACE	350 hPa	−0.16	**−0.39**	−0.01	*0.16*
	amplitude ratio	20°N–30°N	MIPAS	250 hPa	−0.52	**−1.05**	0.20	*0.51*
	amplitude ratio	20°N–30°N	ACE	250 hPa	−0.14	**−0.72**	0.72	*0.98*
Seasonal variations (JJA-JF) at all subtropical and stations (15°S–45°S and 15°S–45°N)	amplitude ratio	Wollongong (34.41°S)	NDACC	total column	0.72	**0.51**	0.64	*0.74*
	amplitude ratio	Wollongong (34.41°S)	TCCON	total column	0.40	**0.30**	*0.60*	0.32
	amplitude ratio	Wollongong (34.41°S)	NDACC	600 hPa	*2.72*	**1.71**	2.50	2.86
	amplitude ratio	Izaña (28.30°N)	NDACC	600 hPa	*0.37*	**0.21**	0.28	0.30
	amplitude ratio	Pasadena (34.2°N)	TCCON	total column	**−0.79**	−0.64	*0.82*	−0.84
	amplitude ratio	Oklahoma (36.6°N)	TCCON	total column	0.59	**0.35**	0.45	*1.0*
	amplitude ratio	Santa Barbara (34°N)	Ehhalt	350 hPa	0.84	**0.29**	0.80	0.85
	amplitude ratio	Death Valley (36°N)	Ehhalt	350 hPa	0.38	**0.11**	0.39	0.34
	amplitude ratio	Nebraska (41.83°N)	Ehhalt	350 hPa	0.93	**0.69**	0.83	0.89
Spatial variations of annual mean	standard deviation ratio	45°S–45°N	SCIAMACHY	total column	**0.42**	0.48	0.43	*0.59*
	standard deviation ratio	45°S–45°N	TES	600 hPa	0.85	**0.74**	0.80	*1.07*
	standard deviation ratio	45°S–45°N	MIPAS	250 hPa	**0.25**	*0.46*	0.32	0.45
	correlation	45°S–45°N	SCIAMACHY	total column	*0.62*	*0.62*	0.61	**0.59**
	correlation	45°S–45°N	TES	600 hPa	*0.93*	0.91	0.92	**0.86**
	correlation	45°S–45°N	MIPAS	250 hPa	0.54	0.61	**0.51**	*0.73*
Spatial variations of seasonal variations (JJA-JF)	standard deviation ratio	45°S–45°N	SCIAMACHY	total column	**0.31**	0.40	**0.31**	*0.46*
	standard deviation ratio	45°S–45°N	TES	600 hPa	0.96	**0.82**	*0.99*	1.18
	standard deviation ratio	45°S–45°N	MIPAS	250 hPa	**0.33**	0.36	0.37	*0.44*
	correlation	45°S–45°N	SCIAMACHY	total column	0.40	*0.45*	0.44	0.43
	correlation	45°S–45°N	TES	600 hPa	*0.73*	**0.61**	**0.61**	0.63
	correlation	45°S–45°N	MIPAS	250 hPa	0.47	**0.13**	*0.59*	0.53
Daily variability	standard deviation ratio	Izaña (28.30°N)	ground-based remote-sensing	4.2 km	*0.69*	**0.40**	0.51	0.68
	correlation	Izaña (28.30°N)	ground-based remote-sensing	4.2 km	**0.39**	*0.45*	0.42	0.34

[a]For each feature that we try to evaluate, we look at different metrics, regions, data sets and/or levels. To evaluate the seasonality, we calculate the ratio of amplitude as the amplitude of seasonal variations (JJA-DJF) for the simulation divided by that for the data, in average over the specified region or at the specified site. To evaluate spatial variations, we calculate the standard deviation ratio as the standard deviation in the simulation divided by that in the data, and the correlation between the simulation and the data. The same applies to evaluate daily variations at Izaña. For a each metric, the simulation with the lowest (resp. highest) seasonality, standard deviation or correlation is highlighted in bold (resp. in italic).

midlatitudes, we calculate the ratio of the simulated JJA-DJF variations to the observed JJA-DJF variations, at different levels, in different hemispheres and compared to different data sets (Table 4, zonal mean seasonal variations and seasonal variations (JJA-DJF)). Although there is no consensus on which simulation performs the best, the "advective diffusion" simulation has the lowest seasonality in 20 of these metrics, corresponding to the worst model-data agreement in 19 of these metrics. For example, for the average over 20°S–30°S and over 20°N–30°N, the "advective diffusion" simulation has the worst underestimate of the seasonality compared to all satellite data sets except when compared to MIPAS in the Northern Hemisphere. Between 20°S–45°S and 20°N–45°N, this is also the case for all of the aircraft data sets and at all ground-based remote-sensing stations except at Pasadena.

[58] To summarize, in LMDZ, when a moist bias is due to excessively diffusive vertical advection, the isotopic seasonality in the subtropics is distinctively lower. This can be robustly identified by comparison with almost all data sets, especially with ground-based remote-sensing and ACE data sets.

5.4. Spatial Variations

[59] Spatial variations partially reflect variations in dynamical regimes. Spatial variations in the control simulation and in the SCIAMACHY, TES and MIPAS data sets are extensively discussed in P1. To measure the degree to which simulations reproduce spatial patterns of annual mean δD, we calculate the spatial correlations between simulated and observed annual mean δD, and the ratio of the simulated spatial standard deviation to the observed spatial standard deviation of annual mean δD (Table 4, spatial variations of annual mean). To measure the degree to which simulations reproduce spatial patterns of δD seasonality, we calculate the same metrics for JJA-DJF variations (Table 4, spatial variations of seasonal variations (JJA-DJF)). No consensus emerges regarding the best or worst performing simulation. The control simulation is most frequently the best in capturing the spatial patterns (as quantified by correlations). In

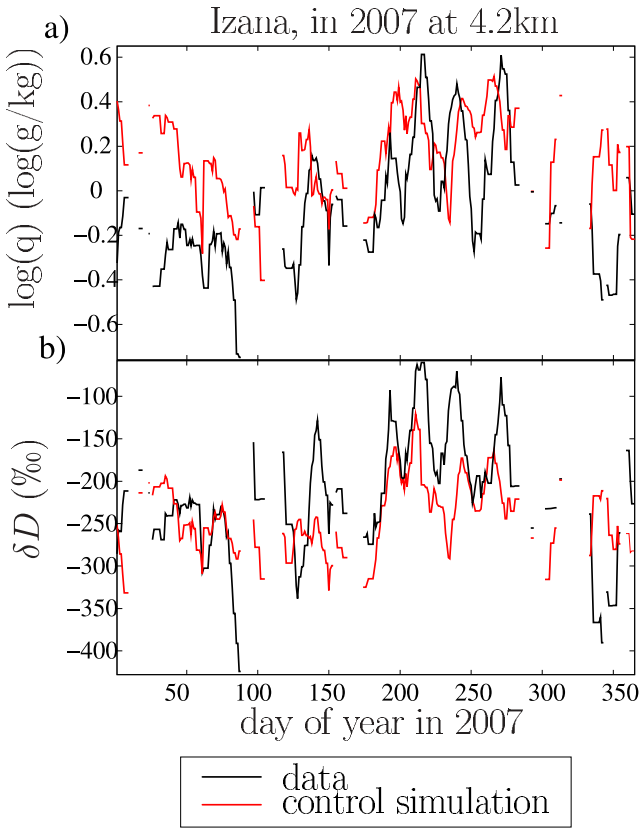

Figure 11. (a) Daily specific humidity q (in logarithmic scale) and (b) vapor δD at 4.2 km retrieved by the ground-based remote-sensing at Izaña (solid black) and simulated by the four versions of LMDZ, during the year 2007. Time series were applied a 5-day running mean, and model outputs were collocated with the data and kernel-weighted with averaging kernels. On the right are shown the average values plus and minus one standard deviation. Note that $\log(q)$ values of -0.6, -0.4, -0.2, 0, 0.2, 0.4 and 0.6 correspond to q values of and 0.25, 0.40, 0.82, 1, 1.22, 1.49 and 1.82 g/kg.

contrast, the "$\epsilon_p/2$" simulation is most frequently the best in capturing the amplitude of spatial variations (as quantified by the ratio of standard deviation), consistent with the strong δD variations with ω_{500} in the latter simulation. Overall, spatial variations of isotopic ratio are less capable at discriminating between the simulations than is the seasonality.

5.5. Intraseasonal Variability in the Subtropics

[60] We have shown that the different sensitivity tests behave differently in subsidence regions (section 5.3). In the subtropics, strong synoptic and intraseasonal variability in RH arise because of strong contrasts between highly dehydrated air and moist plumes from the tropics [*Pierrehumbert*, 1998; *Pierrehumbert and Roca*, 1998; *Zhang et al.*, 2003]. We thus look in more details at the daily ground-based remote-sensing data at the subtropical station Izaña. In the theoretical framework, Izaña can be considered a subsidence region in which the daily data capture variability in the balance of subsidence and horizontal mixing from convective regions nearby.

[61] Despite the nudging, GCMs have difficulties in capturing the timing of the subtropical synoptic and intraseasonal variations. Figure 11a shows the comparison of daily data for the year 2007 at 4.2 km, when LMDZ captures best the timing of humidity modulations. The data features very strong intraseasonal variations, with peak-to-peak variations in q of 4 g/kg and in δD of 150‰ in summer (Figures 11a and 11b). In the control simulation, the q fluctuations are slightly underestimated and the air is on average too moist (consistent with section 5.1). The magnitude of δD fluctuations is also slightly underestimated.

[62] In moist bias simulations, annual mean q and δD are higher (Figure 12, consistent with section 5.1). In the "diffusive advection" simulation, the standard deviations of fluctuations are 25% weaker for q and 45% weaker for δD than in the control. This is associated with an underestimated slope of δD vs q (Figure 11a). This is consistent with the accumulating effect of continuous vertical diffusion during subsident transport from the tropics to Izaña. q and δD thus increase most strongly during the driest periods, when air travels for a longer period. Hence the lower variability in q and δD. In addition, due to the curvature of mixing lines (Figure 5a), diffusion increases δD much more strongly for a given increase in q than predicted by Rayleigh distillation. Hence the lower slope of δD vs q.

[63] In contrast, in the "$\sigma_h/10$" and "$\epsilon_p/2$" simulations, q and δD are mainly affected in convective regions where most of the large-scale condensation and convective detrainment take place. The increases in q and δD in convective regions are preserved to some extent in subsidence regions, but the slopes of δD vs q are not as strongly affected as for the "diffusive advection" simulation (Figures 12b and 12c).

[64] Therefore, the tests exhibit different daily variations in the subtropics, and these are consistent with the predictions from the theoretical framework under different dynamical regimes. The control simulation captures best the timing and amplitude of δD variations, while the "diffusive advection" simulation underestimates δD fluctuations the worst (Table 4, daily variability). Therefore, this remote-sensing data set, combined with all the other data sets documenting isotopic seasonality, can robustly identify the shortcoming in the numerical scheme used to account for vertical transport in models. This results can be obtained from both daily and seasonal mean data.

6. Isotopic Seasonality in the Subtropics as a Diagnostic for the Moist Bias

[65] We have shown that different processes potentially explaining the moist bias commonly seen in GCMs have a different isotopic signature, in the annual mean, seasonal cycle and intraseasonal variability, as summarize in Table 5. We have also shown that this isotopic signature provides complementary information compared to humidity variables. Compared to the data, the most pronounced isotopic bias is the underestimated or reversed δD subtropical seasonality in the "diffusive advection" simulation. This can be seen at all mid and upper tropospheric levels and in most data sets (section 5.3). Therefore, we focus on using the isotopic seasonality as an observable diagnostic to understand the cause of the moist bias in GCMs. In the next section, we

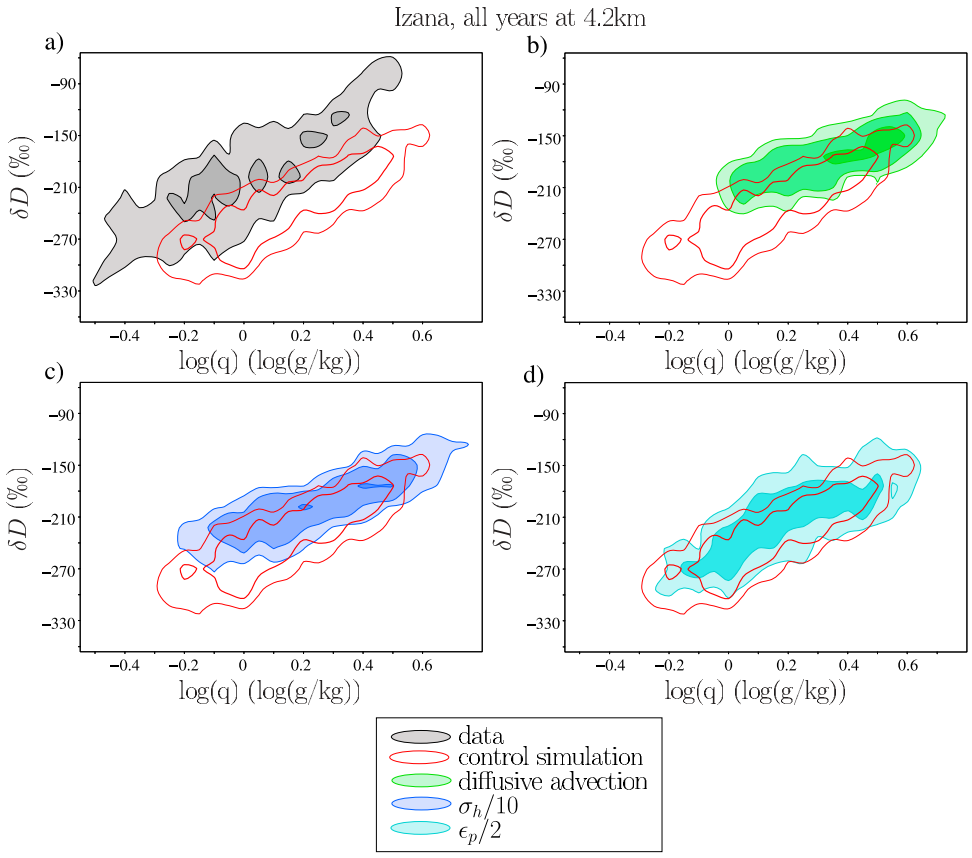

Figure 12. Probability density function (PDF) for the joint $q - \delta D$ distribution at 4.2 km at Izaña. The scale for q is logarithmic: log(q) values of −0.4, −0.2, 0, 0.2, 0.4 and 0.6 correspond to q values of and 0.40, 0.82, 1, 1.22, 1.49 and 1.82 g/kg. The PDFs were calculated from all years of data and binned into bins of 0.05 log(g/kg) and 24‰ and lines correspond to densities of 0.5% (thinnest lines or lightest colors), 1.5% (medium lines and colors) and 4% (thickest lines and darkest colors). For clarity, the PDF for the control simulation (red) is compared to (a) the data (gray), (b) sensitivity tests with diffusive advection (green), (c) $\sigma_h/10$ (blue) and (d) $\epsilon_p/2$ (cyan).

describe the way in which the seasonality diagnostic is used (section 6.1), check its robustness (section 6.2) and then apply it to the SWING2 models (section 6.3).

6.1. The Isotopic Seasonality Diagnostic

[66] Figure 13a shows the subtropical (20°N–30°N) δD seasonality at 350 hPa as a function of tropical (30°S–30°N) annual-mean RH, for the different simulations. As explained earlier, when a moist bias is due to excessively diffusive advection, the seasonality is reversed (green square). This is not the case for the other causes for a moist bias considered in the sensitivity tests (blue and cyan squares). In the δD seasonality versus RH diagram, we will use the slope S between different simulations to diagnose the cause of a moist bias, as illustrated by arrows on Figure 13a. A slope S of the order of −2 to −4‰/% indicates a moist bias that is due to excessively diffusive advection.

[67] We also plot on Figure 13a the approximate position of the data based on AIRS and ACE. The position is subject to large errors for δD because of the sampling mismatch between the observations and monthly mean model outputs. ACE has a much weaker seasonality than MIPAS (P1), so

Table 5. Summary of How Different Causes for a Moist Bias in LMDZ Affects the Isotopic Behavior

	Effect on Isotopic Behavior		
Cause of Moist Bias	Tropical Mean δD	δD Seasonality in the Subtropics	Intraseasonality in the Subtropics
Excessive diffusion during water vapor transport	overestimated in the mid and upper troposphere	underestimated or reversed in the mid and upper troposphere	underestimated variability of δD due to underestimated q-δD slope
Underestimated sub-grid-scale variability of water vapor	overestimated in the mid and upper troposphere	unaffected	overestimated for q but underestimated for δD
Excessive condensate detrainment	overestimated in the upper troposphere with a stronger slope of δD change versus q change.	unaffected	unaffected

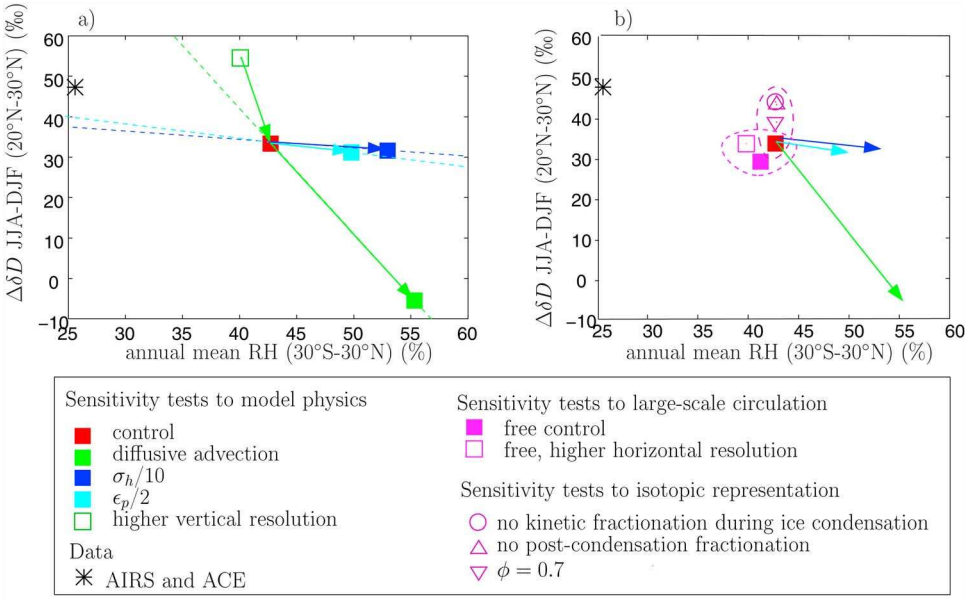

Figure 13. (a) Relationship between annual mean RH at 400 hPa averaged over 30°S–30°N, and seasonal variation (JJA-DJF) of δD at 400 hPa averaged over 20°N–30°N for the different LMDZ simulations (colored squares). The black star indicate corresponding RH and δD values observed by AIRS and ACE-FTS respectively. Note that the comparison with ACE-FTS is qualitative since model outputs cannot be properly collocated with the data on this plot. ACE has a lower δD seasonality than MIPAS, so it likely represent a lower bound. (b) Same as Figure 13a but with some sensitivity tests to the nudging, the horizontal resolution and the isotopic representation. The dashed red and dashed purple circles highlights the proximity to the control of these sensitivity tests.

that ACE likely provides a lower bound for observed δD seasonality. Despite these limitations, based on the consensus that emerged from section 5.3 and Figure 4, the control simulation likely lies between the data and the "diffusive advection" simulation. This suggest that the cause of the moist bias in the control simulation is likely excessively diffusive advection.

[68] The diffusivity of an advection scheme is an intrinsic and unwanted property that cannot be tuned. One way to reduce the diffusion during vertical advection is to increase the vertical resolution. To test whether this solves consistently the moist-bias and the underestimated δD seasonality, we add on Figure 13a the simulation with higher vertical resolution. This simulation is drier and has a stronger seasonality, following a slope similar to that of the "diffusive advection" simulation. This suggests that our δD seasonality diagnostic can detect moist biases that are due to excessive diffusion in a consistent way, be they caused by too diffusive an advection scheme or by to too low a vertical resolution.

6.2. Robustness of the Diagnostic With Respect to Large-Scale Circulation, Isotopic Representation, Diagnostic Definition and Model Physics

[69] Before we apply the slope diagnostic to all GCMs, we check that aspects of the model simulations that are unrelated to the model physics have relatively little impact. First, we recall that sensitivity tests to the nudging and to the horizontal resolution have a comparatively small impact on both RH and δD. On Figure 13b (pink), these tests are very close to the control simulation (dashed red circle). This suggests that differences in RH or in δD seasonality between different models are more likely due the model physics than to differences in the large-scale circulation.

[70] Second, we investigate the impact of differences in the isotopic representation. All SWING2 models use the same equilibrium fractionation coefficients and make similar assumptions during condensation processes (i.e. closed system during liquid condensation and Rayleigh fractionation during ice condensation). Isotopic differences between models can however arise from differences in diffusivity coefficients [*Cappa et al.*, 2003; *Merlivat*, 1978], in kinetic fractionation during ice condensation [*Jouzel and Merlivat*, 1984] or in the representation of isotopic fractionation during rain re-evaporation. Diffusivity coefficients have been shown to affect deuterium excess with very little effect on δD [*Mathieu et al.*, 2002; *Yoshimura et al.*, 2010]. Regarding ice condensation, in all models the supersaturation over ice S_i varies with temperature T following $S_i = 1 - \lambda \cdot T$, where λ is a tunable parameter. Among all SWING2 models, λ varies from 0.003 (e.g. ECHAM, GSM [*Hoffmann et al.*, 1998; *Yoshimura et al.*, 2008]) to 0.005 (HadAM [*Tindall et al.*, 2009]) and is set to 0.004 in LMDZ (Table 2). As an extreme test, we tried $\lambda = 0$ (Figure 13b, purple circle). Although it affects annual mean δD in the upper troposphere, it has a very limited effect on δD seasonality. Regarding isotopic parameterization during rain re-evaporation, there is a wide diversity among models (Table 2). To encompass this diversity, we performed two additional tests with no post-condensation at all [e.g., *Field et al.*, 2010] and with very strong kinetic fractionation respectively (Figure 13b, purple triangles). To represent strong kinetic effects, we change parameter ϕ from 0.9 to 0.7 when calculating the effective

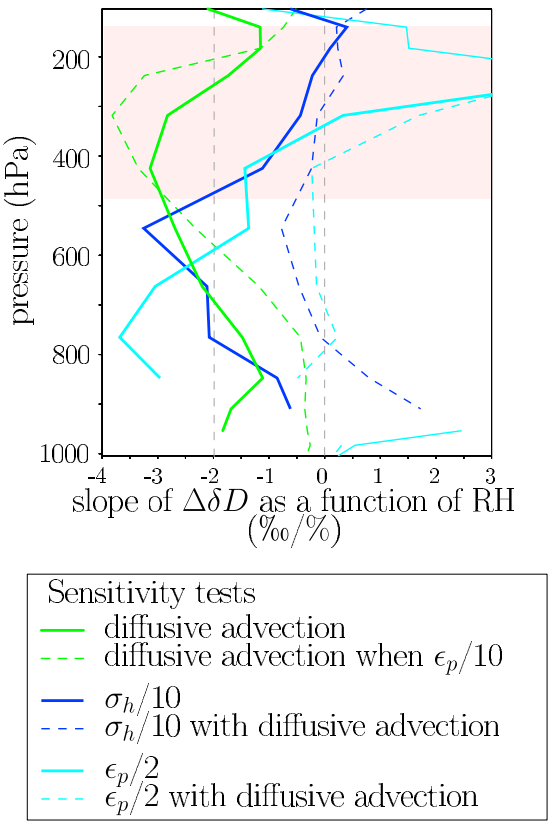

Figure 14. Slope of the seasonal difference in δD versus RH, as in Figure 13, as a function of height for the different sensitivity tests compared to the control. Slopes are shown only where the RH of the two simulations differs by more than 1%. Solid lines: the control simulation and the moist bias simulations are those described in sections 2.1 and 4.1. Dashed lines: same as solid, but both the control and the sensitivity simulations were modified to test the robustness to the model physics. Dashed green: both the control and "diffusive advection" simulations were redone with $\epsilon_p/2$. Dashed blue: both the control and "$\sigma_h/2$" simulations were redone with diffusive advection. Dashed cyan: both the control and "$\epsilon_p/2$" simulations were redone with diffusive advection.

RH around raindrops (h_{eff}) as a function of simulated RH (h) following $h_{eff} = \phi + (1 - \phi) \cdot h$ [*Bony et al.*, 2008; *Risi et al.*, 2010b]. These tests have much smaller impacts than the sensitivity tests to the model physics. Therefore, we conclude that the details of the isotopic implementation is likely not the major factor contributing to the δD seasonality dispersion between models.

[71] We now check the robustness of our diagnostic with respect to altitude. Figure 14 shows the slope S between various pairs of simulations as a function of altitude. The slope between the control and the "diffusive advection" simulation is much more negative than for the other tests from 500 to 150 hPa (solid green). The diagnostic is thus robust with respect to altitude.

[72] We also checked the robustness with respect to the geographical domain. We tested different subtropical domains for δD seasonality (20°N–30°N, 15°N–30°N, 20°N–35°N, 25°N–35°N) and different tropical domains for annual-mean RH (30°S–30°N, 25°S–25°N and 20°S–20°N). The slopes S range within [−3.1, −2.5], [−0.6,0] and [−1.0, −0.3] for the "diffusive advection", "$\sigma_h/10$" and "$\epsilon_p/2$" simulations respectively. Therefore, whatever the choice of the geographical domain, the behavior of the "diffusive advection" can be clearly distinguished from that of the other simulations.

[73] Finally, the robustness of the slope diagnostic with respect to model physics is a necessary condition to apply the diagnostic to all GCMs. The ability to understand the isotopic behavior of the tests with a simple theoretical framework, which involves simple physical processes that are represented in all GCMs, suggests the applicability of these diagnostics to all GCMs. As an additional check, we calculated the slopes S for pairs of simulations with a modified physics. For example, when ϵ_p is divided by two in both the control and "diffusive advection" simulations, the effect of diffusive advection is a deterioration of the seasonality following the same slope S of about −2 to −4‰/% (Figure 14, dashed green). Similarly, when ϵ_p is divided by 2 in both the control and "$\sigma_h/10$" simulations, or when using the diffusive advection scheme in both the control and "$\epsilon_p/2$" simulations, the slopes S characterizing the sensitivity to σ_h and ϵ_p remain much less negative than −2‰/% between 500 and 150 hPa (Figure 14, dashed blue and cyan). Therefore, the isotopic diagnostic is robustly related to the source of the bias and relatively independent of other aspects of model physics.

6.3. Application to SWING2 GCMs

[74] Figure 15b shows the δD seasonality versus RH diagram for the other SWING2 simulations (black markers). As expected, all models are too moist. Models show a very wide spread in δD seasonality, spanning more than 70‰, with variations even in the sign. Isotopic observations can thus discriminate between models despite the large uncertainties in the data sets. The spread in our LMDZ sensitivity tests (about 40‰) is of the same order of magnitude as that in SWING2 models. Most models plot around the line connecting the control and "diffusive advection" simulations (dashed green). Models with the driest troposphere exhibit the strongest (and presumably most realistic: Figure 4) δD seasonality (e.g. Had-AM), while the moistest models exhibit the worst reversed seasonality (e.g. CAM, GSM). This suggests that in many GCMs, excessive diffusion during vertical advection is a likely cause of the moist bias, and the major source of RH dispersion between models.

[75] This result is robust with altitude (Figure 15b): the correlation among models in this diagram is lower than −0.7 from 600 to 250 hPa, and at all these levels the corresponding slope S among models is between than −2 and −4‰/%. This value corresponds to the slope S characterizing the "diffusive advection" simulation at these levels (Figure 15a).

[76] Some GCMs deviate from the "diffusive advection" line (e.g. GISS, MIROC) suggesting that other processes may be responsible for the moist bias in some models. For example, *Wright et al.* [2010] suggest that excessive rainfall evaporation in the GISS model may contribute to its moist bias. However, errors in large-scale circulation are not likely to be the major source of the moist bias and of the spread between models. The small effect of nudging the large-scale circulation in LMDZ is supported by the equally small effect

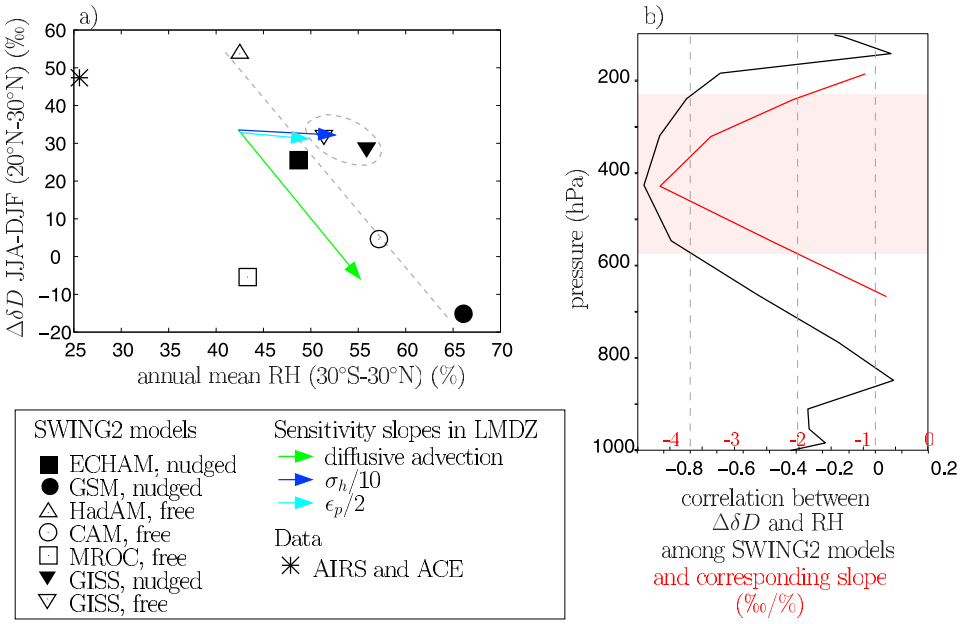

Figure 15. (a) Same as Figure 13 but for the different SWING2 models (black markers), with sensitivity tests to LMDZ physics superimposed as colored arrows. The dashed gray circle highlights the proximity between the free-running and the nudged runs of the GISS model. The dashed gray line visualizes the link between RH and δD seasonality exhibited by most GCMs, following the same slope as for the "diffusive advection" simulation. (b) Correlation (black) and slope (red) of the relationship between subtropical seasonal δD variations and annual mean tropical RH among the SWNG2 models. The slope is plotted only where the correlation is lower than -0.7. The pink shading highlights the range of altitude where the behavior of the "diffusive advection" simulation differs strongly from the other tests (Figure 15a), and where the SWING2 models exhibit a correlation between seasonality and RH lower than -0.7 (Figure 15b).

for the GISS model (dashed gray circle). In addition, the best performing model for RH and δD seasonality is Had-AM, which happens to be run in a free-running mode, while the worst performing model is GSM, which happens to be run in a nudged mode and with the highest horizontal resolution. This further supports the suggestion that the representation of physical processes and advection numerics are larger sources of uncertainties on RH than the large-scale circulation. While it has been shown that nudging might improve the simulation at high latitudes [e.g., *Yoshimura et al.*, 2008; *Risi et al.*, 2010b], a correct large-scale circulation does not guarantee that the tropical and subtropical RH and isotopic distribution are realistic.

7. Conclusion

[77] We show that different processes affecting RH in GCMs impact the water vapor isotopic composition differently. Water vapor isotopic measurements can thus be used as an observational diagnostic to detect and understand causes of RH biases in GCMs. This study proposes an approach to practically do so. The isotopic sensitivity to various physical processes is first understood using sensitivity tests and a simple framework. An isotopic diagnostic based on observations is then designed, and its robustness with respect to the data set used and other aspects of the model physics and isotopic representation is checked. This diagnostic is finally applied to a wider range of models to diagnose the reason for their bias.

[78] As an example, in this study we aim at understanding the reasons for the moist bias in the tropical mid and upper troposphere that has persisted in GCMs for more than a decade. We show that the isotopic seasonality in the subtropics can robustly discriminate simulations in which the moist bias is due to excessively diffusive vertical advection. Applying this isotopic diagnostic to an ensemble of GCMs suggests that excessive diffusion during vertical advection is the most frequent cause of moist bias in GCMs. However, our approach bears some limitations: (1) the lack of validation of upper-tropospheric isotopic data sets, (2) the limited number of our sensitivity tests to the model physics, leaving some other possible sources of moist bias unexplored, (3) the limited subset of GCMs with an isotopic representation and (4) the absence of similar sensitivity tests in the other isotopic GCMs to further check the universality of our diagnostic.

[79] Although it has long been recognized that the large-scale circulation controls the spatial distribution of RH to first order [*Sherwood*, 1996; *Pierrehumbert and Roca*, 1998], our study highlights the importance of uncertainties related to parameterized processes controlling RH and advection numerics. If excessive diffusion during vertical advection is indeed the most frequent cause of moist bias in GCMs, this problem can be solved by improving the advection scheme, or alternatively by increasing the vertical resolution. This is consistent with sensitivity to vertical resolutions in other GCMs [*Pope et al.*, 2001; *Roeckner*

et al., 2006], and supports the importance of vertical resolution [*Tompkins and Emanuel*, 2007]. It would be interesting to apply our isotopic diagnostic to more models, in particular those for which other causes for the moist biases have been hypothesized but which did not participate in SWING2 (e.g. Geophysical Fluid Dynamics Laboratory model [*Chung et al.*, 2011]).

[80] **Acknowledgments.** We thank Debra Wunch, Vanessa Sherlock, Nicholas Deutscher, David Griffith, Paul Wennberg, Kimberly Strong, Sabine Barthlott, Frank Hase, Omaira García, Dan Smale, Emmanuel Mahieu, Justus Notholt, Thorsten Warneke and Geofrey Toon for their roles in acquiring the ground-based remote-sensing data and developing the retrievals, for making the data available, for helping with the data processing and for their useful advice to develop the rigorous model-data comparison methodology used in this paper. We thank David Sayres for providing in situ and aircraft data. We also thank Debra Wunch, Vanessa Sherlock, Nicholas Deutscher, Paul Wennberg and Kimberly Strong for detailed comments on the manuscript. Level-1b data of MIPAS have been provided by ESA. The ACE mission is supported mainly by the Canadian Space Agency. We thank the Anderson Group at Harvard University for providing ICOS and Hoxotope in situ aircraft data. We acknowledge all FTIR activities as in P1. The mid-infrared FTIR retrievals have been performed in the framework of the project MUSICA (http://www.imk-asf.kit.edu/english/musica), which is funded by the European Research Council under the European Community's Seventh Framework Programme (FP7/2007–2013)/ERC grant agreement 256961. We thank Omaira García who was in charge of the FTIR activities at Izaña. We thank all SWING2 members for producing and making available their model outputs. SWING2 was supported by the Isotopic Hydrology Programme at the International Atomic Energy Agency (more information on http://people.su.se/∼cstur/SWING2). We thank Françoise Vimeux for discussions. This work was supported by NASA Energy and Water-cycle Study (07-NEWS07-0020) and NASA Atmospheric Composition program (NNX08AR23G). We thank anonymous reviewers for their constructive comments.

References

Allan, R., M. A. Ringer, and A. Slingo (2003), Evaluation of moisture in the Hadley Centre climate model using simulations of HIRS water-vapour channel radiances, *Q. J. R. Meteorol. Soc.*, *129*(595), 3371–3389.

Angert, A., J.-E. Lee, and D. Yakir (2008), Seasonal variations in the isotopic composition of near-surface water vapour in the eastern Mediterranean, *Tellus, Ser. B*, *60*(4), 674–684.

Arakawa, A., and W. Shubert (1974), Interactions of cumulus cloud ensemble with the large-scale environment. Part I, *J. Atmos. Sci.*, *31*, 671–701.

Aumann, H. H., et al. (2003), AIRS/AMSU/HSB on the Aqua mission: Design, science objectives, data products, and processing systems, *IEEE Trans. Geosci. Remote Sens.*, *41*, 253–264.

Betts, A. K. (2000), Idealized model for equilibrium boundary layer over land, *J. Hydrometeorol.*, *1*, 507–523.

Bony, S., and J. Dufresne (2005), Marine boundary layer clouds at the heart of tropical cloud feedback uncertainties in climate models, *Geophys. Res. Lett.*, *32*, L20806, doi:10.1029/2005GL023851.

Bony, S., and K. A. Emanuel (2001), A parameterization of the cloudiness associated with cumulus convection: Evaluation using TOGA COARE data, *J. Atmos. Sci.*, *58*, 3158–3183.

Bony, S., J.-L. Dufresne, H. Le Treut, J.-J. Morcrette, and C. Senior (2004), On dynamic and thermodynamic components of cloud changes, *Clim. Dyn.*, *22*, 71–86.

Bony, S., et al. (2006), How well do we understand and evaluate climate change feedback processes?, *J. Clim.*, *19*, 3445–3482.

Bony, S., C. Risi, and F. Vimeux (2008), Influence of convective processes on the isotopic composition (δ^{18}O and δD) of precipitation and water vapor in the tropics: 1. Radiative-convective equilibrium and TOGA-COARE simulations, *J. Geophys. Res.*, *113*, D19305, doi:10.1029/2008JD009942.

Brogniez, C., R. Roca, and L. Picon (2005), Evaluation of the distribution of subtropical free tropospheric humidity in AMIP-2 simulations using METEOSAT water vapor channel data, *Geophys. Res. Lett.*, *32*, L19708, doi:10.1029/2005GL024341.

Brown, D., J. Worden, and D. Noone (2008), Comparison of atmospheric hydrology over convective contnental regions using water vapor isotope measurements from space, *J. Geophys. Res.*, *113*, D15124, doi:10.1029/2007JD009676.

Cappa, C., M. Hendricks, D. DePaolo, and R. Cohen (2003), Isotopic fractionation of water during reevaporation, *J. Geophys. Res.*, *108*(D16), 4525, doi:10.1029/2003JD003597.

Chen, C., E. Roeckner, and B. J. Soden (1996), A comparison of satellite observations and model simulations of column-integrated moisture and upper-tropospheric humidity, *J. Clim.*, *9*, 1561–1585.

Chen, M., R. B. Rood, and W. G. Read (1998), Upper tropospheric water vapor from GEOS reanalysis and UARS MLS observation, *J. Geophys. Res.*, *103*(D16), 19,587–19,594.

Chung, E.-S., B. J. Soden, B.-J. Sohn, and J. Schmetz (2011), Model-simulated humidity bias in the upper troposphere and its relation to the large-scale circulation, *J. Geophys. Res.*, *116*, D10110, doi:10.1029/2011JD015609.

Craig, H. (1961), Isotopic variations in meteoric waters, *Science*, *133*, 1702–1703.

Dansgaard, W. (1964), Stable isotopes in precipitation, *Tellus*, *16*, 436–468.

Derbyshire, S. H., I. Beau, P. Bechtold, J.-Y. Grandpeix, J.-M. Piriou, J.-L. Redelsperger, and P. M. M. Soares (2004), Sensitivity of moist convection to environmental humidity, *Q. J. R. Meteorol. Soc.*, *130*(604), 3055–3079.

Dessler, A. E., and S. C. Sherwood (2000), Simulations of tropical upper tropospheric humidity, *J. Geophys. Res.*, *105*(D15), 20,155–20,263.

Ehhalt, D. H., F. Rohrer, and A. Fried (2005), Vertical profiles of HDO/H_2O in the troposphere, *J. Geophys. Res.*, *110*, D13301, doi:10.1029/2004JD005569.

Emanuel, K. A. (1991), A scheme for representing cumulus convection in large-scale models, *J. Atmos. Sci.*, *48*, 2313–2329.

Emanuel, K. A., and M. Zivkovic-Rothman (1999), Development and evaluation of a convection scheme for use in climate models, *J. Atmos. Sci.*, *56*, 1766–1782.

Emanuel, K., D. Neelin, and C. Bretherton (1994), On large-scale circulations in convecting atmospheres, *Q. J. R. Meteorol. Soc.*, *120*, 1111–1143.

Fetzer, E. J., B. H. Lambrigtsen, A. Eldering, H. H. Aumann, and M. T. Chahine (2006), Biases in total precipitable water vapor climatologies from Atmospheric Infrared Sounder and Advanced Microwave Scanning Radiometer, *J. Geophys. Res.*, *111*, D09S16, doi:10.1029/2005JD006598.

Field, R. D., D. B. A. Jones, and D. P. Brown (2010), The effects of post-condensation exchange on the isotopic composition of water in the atmosphere, *J. Geophys. Res.*, *115*, D24305, doi:10.1029/2010JD014334.

Folkins, I., and R. Martin (2005), The vertical structure of tropical convection and its impact on the budgets of water vapor and ozone, *J. Atmos. Sci.*, *62*, 1560–1573.

Frankenberg, C., et al. (2009), Dynamic processes governing lower-tropospheric HDO/H_2O ratios as observed from space and ground, *Science*, *325*, 1374–1377.

Galewsky, J., and J. V. Hurley (2010), An advection-condensation model for subtropical water vapor isotopic ratios, *J. Geophys. Res.*, *115*, D16116, doi:10.1029/2009JD013651.

Gao, J., V. Masson-Delmotte, T. Yao, C. Risi, G. Hoffmann, and L. Tian (2010), Precipitation water stable isotopes in the south Tibetan Plateau: Observations and modelling, *J. Clim.*, *24*, 3161–3178, doi:10.1175/2010JCLI3736.1.

Gates, W. L. (1992), AMIP: The Atmospheric Model Intercomparison Project, *Bull. Am. Meteorol. Soc.*, *73*, 1962–1970.

Godunov, S. K. (1959), Finite-difference methods for the numerical computations of equations of gas dynamics, *Math. Sb.*, *7*, 271–290.

Grandpeix, J. Y., V. Phillips, and R. Tailleux (2004), Improved mixing representation in Emanuel's convection scheme, *Q. J. R. Meteorol. Soc.*, *130*, 3207–3222.

Hoffmann, G., M. Werner, and M. Heimann (1998), Water isotope module of the ECHAM atmospheric general circulation model: A study on timescales from days to several years, *J. Geophys. Res.*, *103*, 16,871–16,896.

Hourdin, F., and A. Armengaud (1999), The use of finite-volume methods for atmospheric advection of trace species. Part I: Test of various formulations in a General Circulation Model, *Mon. Weather Rev.*, *127*, 822–837.

Hourdin, F., et al. (2006), The LMDZ4 general circulation model: Climate performance and sensitivity to parametrized physics with emphasis on tropical convection, *Clim. Dyn.*, *27*, 787–813.

John, V. O., and B. J. Soden (2007), Temperature and humidity biases in global climate models and their impact on climate feedbacks, *Geophys. Res. Lett.*, *34*, L18704, doi:10.1029/2007GL030429.

Johnson, L. R., Z. Sharp, J. Galewsky, M. Strong, P. Gupta, D. Baer, and D. Noone (2011), Hydrogen isotope measurements of water vapor and a correction for laser instrument measurement bias at low water vapor concentrations: Applications to measurements from Mauna Loa Observatory, Hawaii, *Rapid Commun. Mass Spectrom.*, *25*, 608–616.

Jouzel, J., and L. Merlivat (1984), Deuterium and oxygen 18 in precipitation: modeling of the isotopic effects during snow formation, *J. Geophys. Res.*, *89*, 11,749–11,757.

Kalnay, E., et al. (1996), The NCEP/NCAR 40-year reanalysis project, *Bull. Am. Meteorol. Soc.*, *77*, 437–470.

Kurita, N., D. Noone, C. Risi, G. A. Schmidt, H. Yamada, and K. Yoneyama (2011), Intraseasonal isotopic variation associated with the Madden-Julian Oscillation, *J. Geophys. Res.*, *116*, D24101, doi:10.1029/2010JD015209.

Lawrence, J. R., S. D. Gedzelman, D. Dexheimer, H.-K. Cho, G. D. Carrie, R. Gasparini, C. R. Anderson, K. P. Bowman, and M. I. Biggerstaff (2004), Stable isotopic composition of water vapor in the tropics, *J. Geophys. Res.*, *109*, D06115, doi:10.1029/2003JD004046.

Lawrence, M. G., and M. Salzmann (2008), On interpreting studies of tracer transport by deep cumulus convection and its effects on atmospheric chemistry, *Atmos. Chem. Phys.*, *8*(20), 6037–6050.

Lee, J.-E., and I. Fung (2008), "Amount effect" of water isotopes and quantitative analysis of post-condensation processes, *Hydrol. Processes*, *22*(1), 1–8.

Lee, J.-E., I. Fung, D. DePaolo, and C. C. Fennig (2007), Analysis of the global distribution of water isotopes using the NCAR atmospheric general circulation model, *J. Geophys. Res.*, *112*, D16306, doi:10.1029/2006JD007657.

Luo, Z., and W. B. Rossow (2004), Characterizing tropical cirrus life cycle, evolution, and interaction with upper-tropospheric water vapor using Lagrangian trajectory analysis of satellite observations, *J. Clim.*, *17*, 4541–4563.

Majoube, M. (1971a), Fractionnement en O18 entre la glace et la vapeur d'eau, *J. Chim. Phys.*, *68*, 625–636.

Majoube, M. (1971b), Fractionnement en Oxygéne 18 et en Deutérium entre l'eau et sa vapeur, *J. Chim. Phys.*, *10*, 1423–1436.

Marti, O., et al. (2005), The new IPSL climate system model: IPSL-CM4, technical report, IPSL, Paris.

Mathieu, R., D. Pollard, J. Cole, J. W. C. White, R. S. Webb, and S. L. Thompson (2002), Simulation of stable water isotope variations by the GENESIS GCM for modern conditions, *J. Geophys. Res.*, *107*(D4), 4037, doi:10.1029/2001JD900255.

Meehl, G. A., K. Covey, T. Delworth, M. Latif, B. McAvaney, J. F. B. Mitchell, R. J. Stouffer, and K. Taylor (2007), The WCRP CMIP3 multimodel dataset: A new era in climate change research, *Bull. Am. Meteorol. Soc.*, *7*, 1383–1394.

Merlivat, L. (1978), Molecular diffusivities of H2O16, HDO16, and H2O18 in gases, *J. Chem. Phys.*, *69*, 2864–2871.

Merlivat, L., and G. Nief (1967), Fractionnement isotopique lors des changements d'états solide-vapeur et liquide-vapeur de l'eau à des températures inférieures à 0°C, *Tellus*, *19*, 122–127.

Moyer, E. J., F. W. Irion, Y. L. Yung, and M. R. Gunson (1996), ATMOS stratospheric deuterated water and implications for troposphere-stratosphere transport, *Geophys. Res. Lett.*, *23*, 2385–2388.

Nassar, R., P. F. Bernath, C. D. Boone, A. Gettelman, S. D. McLeod, and C. P. Rinsland (2007), Variability in HDO/H_2O abundance ratio in the tropical tropopause layer, *J. Geophys. Res.*, *112*, D21305, doi:10.1029/2007JD008417.

Noone, D., et al. (2011), Properties of air mass mixing and humidity in the subtropics from measurements of the D/H isotope ratio of water vapor at the Mauna Loa Observatory, *J. Geophys. Res.*, *116*, D22113, doi:10.1029/2011JD015773.

Pierce, D. W., T. P. Barnett, E. J. Fetzer, and P. J. Gleckler (2006), Three-dimensional tropospheric water vapor in coupled climate models compared with observations from the AIRS satellite system, *Geophys. Res. Lett.*, *33*, L21701, doi:10.1029/2006GL027060.

Pierrehumbert, R. T. (1998), Lateral mixing as a source of subtropical water vapor, *Geophys. Res. Lett.*, *25*(2), 151–154.

Pierrehumbert, R. T., and R. Roca (1998), Evidence for control of Atlantic subtropical humidity by large scale advection, *Geophys. Res. Lett.*, *25*, 4537–4540.

Pope, V. D., J. A. Pamment, D. R. Jackson, and A. Slingo (2001), The representation of water vapor and its dependence on vertical resolution in the Hadley Centre Climate Model, *J. Clim.*, *14*, 3065–3085.

Randall, D., et al. (2007), Climate models and their evaluation, in *Climate Change 2007: The Physical Science Basis. Contribution of Working Group I to the Fourth Assessment Report of the Intergovernmental Panel on Climate Change*, edited by S. Solomon et al., pp. 591–662, Cambridge Univ. Press, Cambridge, U. K.

Redelsperger, J.-L., D. B. Parsons, and F. Guichard (2002), Recovery processes and factors limiting cloud-top height following the arrival of a dry intrusion observed during TOGA COARE, *J. Atmos. Sci.*, *59*, 2438–2457.

Risi, C., S. Bony, and F. Vimeux (2008), Influence of convective processes on the isotopic composition ($\delta^{18}O$ and δD) of precipitation and water vapor in the tropics: 2. Physical interpretation of the amount effect, *J. Geophys. Res.*, *113*, D19306, doi:10.1029/2008JD009943.

Risi, C., S. Bony, F. Vimeux, M. Chong, and L. Descroix (2010a), Evolution of the water stable isotopic composition of the rain sampled along Sahelian squall lines, *Q. J. R. Meteorol. Soc.*, *136*(S1), 227–242.

Risi, C., S. Bony, F. Vimeux, and J. Jouzel (2010b), Water stable isotopes in the LMDZ4 General Circulation Model: Model evaluation for present day and past climates and applications to climatic interpretation of tropical isotopic records, *J. Geophys. Res.*, *115*, D12118, doi:10.1029/2009JD013255.

Risi, C., et al. (2012), Process-evaluation of tropospheric humidity simulated by general circulation models using water vapor isotopologues: 1. Comparison between models and observations, *J. Geophys. Res.*, *117*, D05303, doi:10.1029/2011JD016621.

Roca, R., L. Picon, M. Desbois, H. Le Treut, and J.-J. Morcrette (1997), Direct comparison of Meteosat water vapor channel data and general circulation model results, *Geophys. Res. Lett.*, *24*(2), 147–150.

Roeckner, E., R. Brokopf, M. Esch, M. Giorgetta, S. Hagemann, L. Kornblueh, E. Manzini, U. Schlese, and U. Schulzweida (2006), Sensitivity of simulated climate to horizontal and vertical resolution in the ECHAM5 atmosphere model, *J. Clim.*, *19*(16), 3771–3791.

Salathe, E. J., and D. Chester (1995), Variability of moisture in the upper troposphere as inferred from TOVS satellite observations in the ECMWF model analyses in 1989, *J. Clim.*, *8*, 120–132.

Sayres, D. S., L. Pfister, T. F. Hanisco, E. J. Moyer, J. B. Smith, J. M. S. Clair, A. S. O'Brien, M. F. Witinski, M. Legg, and J. G. Anderson (2010), Influence of convection on the water isotopic composition of the tropical tropopause layer and tropical stratosphere, *J. Geophys. Res.*, *115*, D00J20, doi:10.1029/2009JD013100.

Schmidt, G., A. LeGrande, and G. Hoffmann (2007), Water isotope expressions of intrinsic and forced variability in a coupled ocean-atmosphere model, *J. Geophys. Res.*, *112*, D10103, doi:10.1029/2006JD007781.

Schneider, M., K. Yoshimura, F. Hase, and T. Blumenstock (2010), The ground-based FTIR network's potential for investigating the atmospheric water cycle, *Atmos. Chem. Phys.*, *10*, 3427–3442.

Schneider, T., K. L. Smith, P. A. O'Gorman, and C. C. Walker (2006), A climatology of tropospheric zonal-mean water vapor fields and fluxes in isentropic coordinates, *J. Clim.*, *19*(22), 5918–5933.

Sherwood, S. C. (1996), Maintenance of the free tropospheric tropical water vapor distribution. Part II: Simulation of large-scale advection, *J. Clim.*, *11*, 2919–2934.

Sherwood, S., and C. Meyer (2006), The general circulation and robust relative humidity, *J. Clim.*, *19*(24), 6278–6290.

Sherwood, S. C., W. Ingram, Y. Tsushima, M. Satoh, M. Roberts, P. L. Vidale, and P. A. O'Gorman (2010), Relative humidity changes in a warmer climate, *J. Geophys. Res.*, *115*, D09104, doi:10.1029/2009JD012585.

Slingo, J. M. (1980), A cloud parametrization scheme derived from GATE data for use with a numerical model, *Q. J. R. Meteorol. Soc.*, *106*(450), 747–770.

Sobel, A. H., and C. S. Bretherton (2000), Modeling tropical precipitation in a single column, *J. Clim.*, *13*, 4378–4392.

Soden, B. J., and C. Bretherton (1994), Evaluation of water vapor distribution in general circulation models using satellite observations, *J. Geophys. Res.*, *99*(D1), 1187–1210, doi:10.1029/93JD02912.

Soden, B. J., and I. M. Held (2006), An assessment of climate feedbacks in coupled ocean?atmosphere models, *J. Clim.*, *19*, 3354–3360, doi:10.1175/JCLI3799.1.

Steinwagner, J., S. Fueglistaler, G. Stiller, T. von Clarmann, M. Kiefer, P.-P. Borsboom, A. van Delden, and T. Röckmann (2010), Tropical dehydration processes constrained by the seasonality of stratospheric deuterated water, *Nat. Geosci.*, *3*, 262–266, doi:10.1038/NGEO822.

Stewart, M. K. (1975), Stable isotope fractionation due to evaporation and isotopic exchange of falling waterdrops: Applications to atmospheric processes and evaporation of lakes, *J. Geophys. Res.*, *80*, 1133–1146.

Tindall, J. C., P. Valdes, and L. C. Sime (2009), Stable water isotopes in HadCM3: Isotopic signature of El Niño–Southern Oscillation and the tropical amount effect, *J. Geophys. Res.*, *114*, D04111, doi:10.1029/2008JD010825.

Tompkins, A. M., and K. Emanuel (2007), The vertical resolution sensitivity of simulated equilibrium temperature and water-vapour profiles, *Q. J. R. Meteorol. Soc.*, *126*(565), 1219–1238.

Uemura, R., Y. Matsui, K. Yoshimura, H. Motoyama, and N. Yoshida (2008), Evidence of deuterium-excess in water vapour as an indicator of ocean surface conditions, *J. Geophys. Res.*, *113*, D19114, doi:10.1029/2008JD010209.

Uppala, S., et al. (2005), The ERA-40 re-analysis, *Q. J. R. Meteorol. Soc.*, *131*, 2961–3012.

Van Leer, B. (1977), Towards the ultimate conservative difference scheme: IV. A new approach to numerical convection, *J. Comput. Phys.*, *23*, 276–299.

Vimeux, F., G. Tremoy, C. Risi, and R. Gallaire (2011), A strong control of the South American SeeSaw on the intraseasonal variability of the isotopic composition of precipitation in the Bolivian Andes, *Earth. Planet. Sci. Lett.*, *307*(1–2), 47–58.

Webster, C. R., and A. J. Heymsfield (2003), Water isotope ratios D/H, $^{18}O/^{16}O$, $^{18}O/^{16}O$ in and out of clouds map dehydration pathways, *Science*, *302*, 1742–1746.

Wetzel, P. J., S. Argentini, and A. Boone (1996), Role of land surface in controlling daytime cloud amount: Two case studies in the GCIP-SW area, *J. Geophys. Res.*, *101*, 7359–7370.

Worden, J., D. Noone, and K. Bowman (2007), Importance of rain evaporation and continental convection in the tropical water cycle, *Nature*, *445*, 528–532.

Wright, J. S., A. H. Sobel, and G. A. Schmidt (2009), The influence of condensate evaporation on water vapor and its stable isotopes in a GCM, *Geophys. Res. Lett.*, *36*, L12804, doi:10.1029/2009GL038091.

Wright, J. S., A. Sobel, and J. Galewsky (2010), Diagnosis of zonal mean relative humidity changes in a warmer climate, *J. Clim.*, *23*, 4556–4569, doi:10.1175/2010JCLI3488.1.

Wunch, D., et al. (2010), Calibration of the total carbon column observing network using aircraft profile data, *Atmos. Meas. Tech.*, *3*, 1351–1362, doi:10.5194/amt-3-1351-2010.

Yoshimura, K., M. Kanamitsu, D. Noone, and T. Oki (2008), Historical isotope simulation using reanalysis atmospheric data, *J. Geophys. Res.*, *113*, D19108, doi:10.1029/2008JD010074.

Yoshimura, K., M. Kanamitsu, and M. Dettinger (2010), Regional downscaling for stable water isotopes: A case study of an atmospheric river event, *J. Geophys. Res.*, *115*, D18114, doi:10.1029/2010JD014032.

Zhang, C., B. Mapes, and B. J. Soden (2003), Bimodality in tropical water vapour, *Q. J. R. Meteorol. Soc.*, *129*(594), 2847–2866.

P. Bernath, Department of Chemistry, University of York, York YO10 5DD, UK.

S. Bony, LMD/IPSL, CNRS, Case Postale 99, 4 Place Jussieu, F-75252 Paris, France.

D. Brown, D. Noone, and C. Risi, Department of Atmospheric and Oceanic Sciences, University of Colorado at Boulder, Bldg. 318, 216 UCB, Main Campus, Boulder, CO 80309, USA. (camille.risi@colorado.edu)

C. Frankenberg and J. Worden, Jet Propulsion Laboratory, California Institute of Technology, 4800 Oak Grove Dr., Pasadena, CA 91109, USA.

B. Funke, Instituto de Astrofísica de Andalucía, Apdo. 3004, E-18008 Granada, Spain.

M. Kiefer, M. Schneider, and G. Stiller, IMK-ASF, Institute for Meteorology and Climate Research, Karlsruhe Institute of Technology, PO Box 3640, D-76021 Karlsruhe, Germany.

J. Lee, Korea Polar Research Institute, Incheon 406-840, South Korea.

C. Sturm, Department of Geology and Geochemistry, Stockholm University, SE-10961 Stockholm, Sweden.

K. Walker, Department of Physics, University of Toronto, 60 St. George St., Toronto, ON M5S 1A7, Canada.

WATER RESOURCES RESEARCH, VOL. 49, 4136–4156, doi:10.1002/wrcr.20312, 2013

Role of continental recycling in intraseasonal variations of continental moisture as deduced from model simulations and water vapor isotopic measurements

Camille Risi,[1] David Noone,[2] Christian Frankenberg,[3] and John Worden[3]

Received 5 November 2012; revised 9 April 2013; accepted 14 May 2013; published 22 July 2013.

[1] Climate models suggest an important role for land-atmosphere feedbacks on climate, but exhibit a large dispersion in the simulation of this role. We focus here on the role of continental recycling in the intraseasonal variability of continental moisture, and we explore the possibility of using water isotopic measurements to observationally constrain this role. Based on water tagging, we design a diagnostic, named D1, to estimate the role of continental recycling on the intraseasonal variability of continental moisture simulated by the general circulation model LMDZ. In coastal regions, the intraseasonal variability of continental moisture is mainly driven by the variability in oceanic moisture convergence. More inland, the role of continental recycling becomes important. The simulation of this role is sensitive to model parameters modulating evapotranspiration. Then we show that δD in the low-level water vapor is a good tracer for continental recycling, due to the enriched signature of transpiration. Over tropical land regions, the intraseasonal relationship between δD and precipitable water, named D1_iso, is a good observational proxy for D1. We test the possibility of using D1_iso for model evaluation using two satellite data sets: GOSAT and TES. LMDZ captures well the spatial patterns of D1_iso, but underestimates its values. However, a more accurate description of how atmospheric processes affect the isotopic composition of water vapor is necessary before concluding with certitude that LMDZ underestimates the role of continental recycling.

Citation: Risi, C., D. Noone, C. Frankenberg, and J. Worden (2013), Role of continental recycling in intraseasonal variations of continental moisture as deduced from model simulations and water vapor isotopic measurements, *Water Resour. Res.*, *49*, 4136–4156, doi:10.1002/wrcr.20312

1. Introduction

1.1. Goals

[2] Many studies have suggested an important role of the land surface on atmospheric conditions at a broad range of time scales [*Rowntree and Bolton*, 1983; *Nicholson*, 2000; *Koster et al*., 2004; *Seneviratne et al*., 2010; *Gimeno et al*., 2012]. Land-atmosphere feedbacks are particularly important for the intraseasonal variability of precipitation [*Beljaars et al*., 1996] and extreme events such as droughts or floods [*Dirmeyer and Brubaker*, 1999; *Pal and Eltahir*, 2001; *Seneviratne et al*., 2006; *Zaitchik et al*., 2006; *Fischer et al*., 2007]. However, climate models exhibit a large dispersion in the simulation of land-atmosphere feedbacks [*Koster et al*., 2002, 2004; *Lawrence and Slingo*, 2005; *Koster et al*., 2006; *Guo et al*., 2006; *Wei and Dirmeyer*, 2010]. It is however difficult to discriminate which model represents land-atmosphere feedbacks in the most realistic way. The motivation underlying this paper is to find observational constraint for land-atmosphere feedbacks. These feedbacks are complex in the sense that precipitation might be either enhanced or decreased when the soil is wetter depending on conditions [*Findell and Eltahir*, 2003a, 2003b; *Ferguson and Wood*, 2011].

[3] Land-atmosphere feedbacks can be either local (sometimes called "direct") or regional (sometimes called "indirect").

[4] Local feedbacks involve the effect of surface fluxes on the local atmospheric conditions. Positive or negative effects of soil moisture on subsequent precipitation are possible depending on large-scale atmospheric conditions [*Betts*, 1992; *de Ridder*, 1997; *Findell and Eltahir*, 2003a, 2003b; *Ek and Holtslag*, 2004; *Santanello et al*., 2009, 2011; *Tuinenburg et al*., 2011; *Ferguson and Wood*, 2011; *Ferguson et al*., 2012], on the spatial scale of soil moisture anomalies [*Taylor et al*., 2011], on the type of convective system [*Taylor et al*., 2009] or on whether the variable of interest is precipitation intensity or frequency [*d'Odorico*

Additional supporting information may be found in the online version of this article.

[1]Laboratoire de Météorologie Dynamique, Institut Pierre Simon Laplace, CNRS, Paris, France.
[2]Department of Atmospheric and Oceanic Sciences, CIRES, University of Colorado, Boulder, Colorado, USA.
[3]Jet Propulsion Laboratory, California Institute of Technology, Pasadena, California, USA.

Corresponding author: C. Risi, LMD/IPSL, CNRS, Paris 75005, France. (camille.risi@lmd.jussieu.fr)

0043-1397/13/10.1002/wrcr.20312

and Porporato, 2004]. On the one hand, if the soil is wetter, evapo-transpiration increases, which moistens the boundary layer, lowers the condensation level and favors convection [e.g., *Betts*, 1992; *Taylor and Lebel*, 1998; *Santanello et al*., 2009; *Lintner et al*., 2012]. On the other hand, if the soil is drier, then latent heat fluxes decrease at the expense of sensible heat flux, which warms the boundary layer, leads to more vigorous thermals and higher boundary layer top, and favors convection triggering [e.g., *Porporato*, 2009; *Santanello et al*., 2009; *Westra et al*., 2012; *Taylor et al*., 2012]. In models, the relative importance of these two effects may additionally depend on the model physics and resolution [*Hohenegger et al*., 2009]. Local feedbacks can also involve small-scale soil moisture gradients and associated mesoscale circulations [*Taylor et al*., 2007, 2009, 2011] and radiative effects of clouds [*Schär et al*., 1999; *Betts*, 2004; *Schlemmer et al*., 2011, 2012].

[5] Regional feedbacks involve the effect of surface fluxes on remote atmospheric conditions and on large-scale circulation. Positive and negative effects are possible depending on conditions. On the one hand, if the soil is wetter, then the evapo-transpiration increases. This moistens the atmosphere and favors convection downstream air mass trajectories [*Eltahir and Bras*, 1994]. For example, this can contribute to lower precipitation downstream of deforested areas [*Spracklen et al*., 2012]. This can also contribute to the persistence of droughts [*Rodriguez-Iturbe et al*., 1991a, 1991b; *Entekhabi et al*., 1992]. On the other hand, if the soil is drier, the surface temperature increases which favors large-scale convergence of tropospheric humidity, and thus favors convection [*Kleidon and Heimann*, 2000; *Cook et al*., 2006; *Goessling and Reick*, 2011]. For example, this may contribute to lower precipitation over irrigated regions [*Lee et al*., 2009a; *Saeed et al*., 2009; *Guimberteau et al*., 2012]. Storms might also become more intense despite a less frequent triggering [*Lee et al*., 2012]. In the case of a positive feedback, continental recycling increases; in the case of a negative feedback, it decreases.

[6] This paper focuses on regional-scale feedbacks. Such feedbacks have been less studied than local feedbacks because it is often thought that the effect of the direct input of water vapor through continental recycling is small, due to the long residence time scale (10 days) of water vapor in the atmosphere [*McDonald*, 1962]. The importance of continental recycling however strongly depends on the region considered [*Koster et al*., 1986], on the spatial scale considered [*Budyko*, 1974; *Burde et al*., 1996; *Trenberth*, 1999] and on the methodology used to quantify continental recycling [*Eltahir and Bras*, 1996]. Progress have been made to more robustly quantify the sources and sinks of precipitation and of water vapor (review by *Gimeno et al*. [2012]) and underline the importance of continental recycling in some continental regions [*Dominguez et al*., 2006; *Gimeno et al*., 2010; *van der Ent et al*., 2010]. Quantifying the role of continental recycling on precipitation usually involves regional atmospheric water budgets based on reanalyses, on a combination of reanalyses and observations [*Eltahir and Bras*, 1996; *Gong and Eltahir*, 1996; *Schär et al*., 1999; *Bosilovich and Schubert*, 2002; *Dirmeyer and Brubaker*, 2007; *Dominguez and Kumar*, 2008; *Dirmeyer et al*., 2008, 2009] or on models [*Brubaker et al*., 1994]. There are, however, two drawbacks to this approach. First, it is difficult for such moisture budgets to accurately take into account the effect of mixing and of subgrid scale water vapor transport, sources, and sinks. Second, reanalyses are model products and their derived budgets are difficult to evaluate observationally. In this paper, to circumvent the first drawback, we use a water tagging approach [e.g., *Joussaume et al*., 1984; *Koster et al*., 1986; *Numaguti et al*., 1999; *Yoshimura et al*., 2004; *Risi et al*., 2010b], which accurately tracks the water vapor through each transport, mixing, and phase change process online in a global model. To deal with the second issue, we explore the possibility of using water isotopic measurements.

[7] The water molecule has several isotopologues. The most common isotopologue is $H_2{}^{16}O$ (hereafter called H_2O), but heavier isotopologues are also found: $HD^{16}O$ (hereafter call HDO, with D standing for deuterium) and $H_2{}^{18}O$. The water vapor isotopic composition (e.g., the concentration in HDO) is sensitive to the evaporative origin. For example, in the tropics, water evaporated from land surface is more enriched in heavy isotopes than water evaporated from the ocean [*Gat*, 1996]. Several studies have tried to exploit this property to infer continental recycling or to partition it into evaporation and transpiration, using isotopic measurements in the precipitation [*Salati et al*., 1979; *Gat and Matsui*, 1991]. However, precipitation is strongly affected by postcondensational processes [*Stewart*, 1975; *Lee and Fung*, 2008; *Risi et al*., 2010a]. The isotopic composition of water vapor more directly reflects the moisture origin. The development of water vapor isotopic measurements from satellite now offers a unique opportunity to exploit the water isotopic composition as an indication for continental recycling [*Risi et al*., 2010b].

[8] The goal of our paper is thus to explore the possibility to use water isotopic measurements from satellites to observationally constrain the role of continental recycling on the intraseasonal variability of precipitation. More specifically, given the close relationship between precipitation and precipitable water (W) in the tropics [*Raymond*, 2000; *Bretherton et al*., 2004], we will focus on evaluating the role of continental recycling on the intraseasonal variability of W in the tropics.

1.2. Overview of the Methodology

[9] To achieve this goal, we use an atmospheric general circulation model (GCM) coupled to a land surface model. Our strategy has three steps. First, we develop a diagnostic for the role of continental recycling variability on the intraseasonal variability of W. This diagnostic is called D1 and is calculated from a GCM simulation in which water vapor from different origins is tagged. We quantify and discuss the role of continental recycling in this simulation. Two sensitivity tests to the land surface physics are also presented in which the role of continental recycling is either larger or weaker than in the control, as quantified by D1.

[10] Second, we try to find an observation-based proxy for D1 to identify the simulation which has the most realistic role of continental recycling. While D1 is not directly observable, our hypothesis is that water vapor isotopic composition measurements may track continental recycling and its intraseasonal variations. In addition to water tagging, our GCM is also equipped with water isotopic diagnostics. We focus on the HDO/H_2O ratio of water vapor,

expressed in ‰ as anomalies relatively to the ocean surface: $\delta D = \left(\frac{HDO/H_2O}{(HDO/H_2O)_{SMOW}} - 1\right) \cdot 1000$, where SMOW is the standard mean ocean water [*Dansgaard*, 1964]. We show a good relationship between continental recycling and lower tropospheric δD at the intraseasonal time scales over several regions. Based on those results, and on the availability of isotopic observations, we propose an isotope-based, observable proxy for D1, named D1_iso.

[11] Third, we compare simulated D1_iso with data, to assess to what extent data can help identify the most realistic simulation in terms of D1. To do so, we use two satellite data sets which are sensitive to the isotopic composition of the boundary layer water vapor and which have a good spatio-temporal coverage: the GOSAT (Greenhouse gases Observing SATellite) satellite data set [*Frankenberg et al*., 2012] and the new version of the TES (Tropospheric Emission Spectrometer) retrievals [*Worden et al*., 2012a].

[12] The paper is organized according to these three steps. After a description of the model simulations, of the data sets and of the methodology (section 2), we quantify the role of continental recycling on intraseasonal variability of *W* in our simulations (section 3). We show the link between continental recycling and water vapor isotopic composition in section 4, and discuss a possible isotopic-based observable constraint to our model simulations in section 5. We conclude in section 6.

2. Material and Methods

2.1. Models

[13] We use the LMDZ4 (Laboratoire de Météorologie Dynamique-Zoom version 4) model, which is the atmospheric component of the IPSL-CM4 and IPSL-CM5A ocean-atmosphere coupled models [*Marti et al*., 2005; *Dufresne et al*., 2012] used in CMIP3 and CMIP5 [*Meehl et al*., 2007]. It is used with a resolution of 2.5° in latitude, 3.75° in longitude and 19 vertical levels. The physical package is comprehensively described in *Hourdin et al*. [2006]. The isotopic version of LMDZ, named LMDZ-iso, is described in detail in *Risi et al*. [2010c]. Isotopic processes are represented in a way similar to other isotopic GCMs [*Jouzel et al*., 1987, 1991; *Hoffmann et al*., 1998; *Noone and Simmonds*, 2002; *Schmidt et al*., 2005; *Lee et al*., 2007a; *Yoshimura et al*., 2008; *Tindall et al*., 2009]. Isotopic processes associated with rain reevaporation, crucial in controlling the precipitation composition [*Lee and Fung*, 2008; *Bony et al*., 2008; *Risi et al*., 2010c] and vapor composition [*Worden et al*., 2007; *Field et al*., 2010] are represented in detail [*Bony et al*., 2008].

[14] The default land surface scheme in LMDZ is a simple bucket in which no distinction is made between bare soil evaporation and transpiration, and no fractionation is considered during evapo-transpiration [*Risi et al*., 2010c]. Since we focus here on land-atmosphere interaction, a more accurate description of isotopic fractionation during land surface evapo-transpiration is necessary. Therefore, LMDZ-iso was coupled with the ORCHIDEE-iso land surface model [*Ducoudré et al*., 1993; *Krinner et al*., 2005]. This model includes a two-layer soil model [*Choisnel et al*., 1995]. The very low vertical resolution of the soil in this model may impact the realism of the simulation [*de Rosnay et al*., 2000]. The model decomposes evapotranspiration through evaporation of canopy-intercepted water, bare soil evaporation, plant transpiration, and snow sublimation. For simplicity and for easier interpretation of the results, we disabled the dynamic vegetation model [*Sitch*, 2003], the carbon allocation model [*Krinner et al*., 2005] and the canopy interception module. Vegetation fractions are prescribed.

[15] The isotopic implementation in ORCHIDEE is described in detail in [*Risi*, 2009]. Water stable isotopes are passively transported between the different water reservoirs by nonfractionating water fluxes. The isotopic composition of soil water is assumed homogeneous vertically and equal to the weighted average of the two soil layers. We assume that surface runoff has the composition of the excess inflow into the soil, that is, precipitation or snow melt, and that drainage has the composition of soil water [*Gat*, 1996]. Isotope fractionation during evaporation of bare soil is modeled using *Craig and Gordon* [1965] equation and the kinetic fractionation formulated by *Mathieu and Bariac* [1996]. Isotope fractionation processes during transpiration [*Washburn and Smith*, 1934; *Barnes and Allison*, 1988] and snow sublimation [*Hoffmann et al*., 1998; *Noone and Simmonds*, 2002] are neglected. ORCHIDEE-iso has been evaluated against measurements of soil, stem, leaf, river, and precipitation water both in stand-alone mode at several instrumented sites and in LMDZ-coupled mode [*Risi*, 2009]. The coupled LMDZ-ORCHIDEE model was also evaluated and used in *Risi et al*. [2010b].

2.2. Simulation Setup

[16] LMDZ is forced by observed sea surface temperatures following the AMIP protocol [*Gates*, 1992]. To ensure a realistic large-scale circulation and daily variability [*Yoshimura et al*., 2008; *Risi et al*., 2010c], horizontal winds at each vertical level are nudged by ECMWF (European Centre for Medium-Range Weather Forecasts) reanalyses [*Uppala et al*., 2005].

[17] Water tagging is available in both LMDZ and ORCHIDEE [*Risi et al*., 2010b]. To track the origin of water vapor and continental recycling, nine tracers were used: H_2O tracer emitted from bare soil or snow evaporation, H_2O tracer emitted from plant transpiration, H_2O tracer emitted from the ocean, and $H_2{}^{18}O$ and HDO emitted from these three sources.

[18] In addition, we perform two sensitivity tests (Table 1) in which the role of continental recycling on *W* variations is different from that in the control simulation. This allows us to assess whether two simulations, in which the role of continental recycling on *W* variations is different, can be discriminated based on their water isotopic composition. First, in the "baresoil" simulation, we modify the calculation of the bare soil fraction as a function of the leaf area index (LAI). In the control simulation, the bare soil fraction decreases linearly with LAI [*Ducoudré et al*., 1993], whereas in the "baresoil" simulation, it decreases exponentially with LAI [*d'Orgeval*, 2006]. As a result, in "baresoil" the bare soil fraction is lower over most regions. Second, in the "rveg" simulation, we reduce the stomatal resistance. In the control simulation, the stomatal resistance is calculated as a function of radiative fluxes and LAI. In the "rveg" simulation, we keep the same calculation but divide the result by a factor of 5.

[19] For computer limitation reasons, simulations were run for 3 years and the last year was analyzed. Simulations

Table 1. Time Period and Characteristics of the LMDZ and LMDZ-ORCHIDEE Simulations Used in This Paper

Name	Year	Coupling With ORCHIDEE	Bare Soil Function	Stomatal Resistance	Water Tagging
Control	2006	Yes	*Ducoudré et al*. [1993]	0.5	Yes
Baresoil	2006	Yes	*d'Orgeval* [2006]	0.5	Yes
rveg	2006	Yes	*Ducoudré et al*. [1993]	0.1	Yes
LMDZ	1997–2012	No	None	None	No

are performed with perpetual 2006 conditions, 2006 being chosen arbitrarily. Simulations are started from a control perpetual-2006 simulation that had the time to equilibrate during 20 years. Despite the shortness of the simulations, the nudging ensures that the difference between the sensitivity tests is due to differences in the physical content of the model rather than to internal variability.

2.3. GOSAT Data

[20] Similar to SCIAMACHY [*Frankenberg et al*., 2009], GOSAT measurements enable to retrieve the total-column water vapor content in both H_2O (i.e., precipitable water W) and HDO [*Frankenberg et al*., 2012]. From these retrievals, column-integrated δD is calculated. Since most of the total-column vapor is in the lower troposphere, column-integrated δD is strongly weighted toward the δD of the boundary layer [*Frankenberg et al*., 2009]. We use measurements from April 2009 to June 2011. The precision of each measurement is 20–40‰, but it can be refined by averaging several measurements. For a first brief study of GOSAT δD data uncertainty, please refer to *Boesch et al*. [2012]. Observed column-integrated H_2O and HDO have been corrected following *Frankenberg et al*. [2012]. No absolute calibration exists for column-integrated δD and we thus focus on spatiotemporal variations only.

[21] We select only GOSAT measurements that met several quality criteria. Cloud scenes are screened out. Retrieved W must agree within 30% with ECMWF reanalyses. Errors on retrieved W and column-integrated HDO must be lower than 15%. Retrieval χ^2 [*Frankenberg et al*., 2012] must be lower than 0.3. Retrieved δD must be within −900‰ and 1000‰ to exclude a few obviously anomalous values.

[22] To compare rigorously LMDZ with GOSAT, we take into account spatiotemporal sampling. This is possible only if LMDZ is nudged toward reanalysis for the GOSAT observation period. Therefore, we use an additional nudged LMDZ simulation covering 1997–2012 (Table 1). Contrary to SCIAMACHY but similar to TES [*Worden et al*., 2006], the retrieval method for GOSAT yields averaging kernels that describe the sensitivity of the retrieved W and column-integrated δD to the different atmospheric levels. For a rigorous model-data comparison, we apply averaging kernels to the model outputs [*Risi et al*., 2012a].

[23] When interpreting HDO$/H_2O$ remote sensing data, several limitations must be taken into account. First, HDO$/H_2O$ retrievals depend on spectroscopic parameters that are typically determined by laboratory measurements. These measurements are difficult especially for the relatively weak lines in the near infrared [*Scheepmaker et al*., 2012]. Spectroscopic biases could further depend on humidity content. Second, the sensitivity of the measurements needs to be considered, and a priori constrains can significantly affect the retrievals [*Boesch et al*., 2012]. The HDO sensitivity depends on the H_2O content of the atmosphere. To quantify this effect, we calculated the difference between convolved total-column δD and raw total-column δD in the LMDZ model, and analyzed the link with precipitable water. We find that in some regions, when the atmosphere is drier, the sensitivity of the instrument is such that retrieved δD is artificially reduced compared to real δD (supporting information). As a consequence, relationships between δD and W may be distorted (supporting information). When convolving LMDZ outputs with averaging kernels, this effect is taken into account so that convolved outputs, and GOSAT retrievals are comparable.

2.4. TES Data

[24] TES measurements enable to retrieve some information on the vertical distribution of specific humidity (q) and δD in the troposphere. While a first processing of the data had led to δD retrievals being mainly sensitive around 600 hPa [*Worden et al*., 2006], a new processing leads to enhanced vertical sensitivity from 900 to 400 hPa [*Worden et al*., 2012a]. We use measurements from 2004 to 2008 compiled into the so-called "lite product" available on http://tes.jpl.nasa.gov/data/. The precision of each measurement is about 30‰ at low levels, but as for GOSAT, it can be refined by averaging several measurements. We select only TES measurements with a valid quality flag and a degree of freedom of the signal (DOFS) greater than 0.5. On average over the tropics, the DOFS of the retrievals that we use is 1.8. Therefore, TES has a larger DOFS than GOSAT, whose DOFS is one since it retrieves column abundances.

[25] A correction was applied on observed δD following the calibration study of *Worden et al*. [2010]. However, since absolute calibration remains uncertain, as for GOSAT we will focus on spatio-temporal variations only.

[26] To compare directly the TES data with the GOSAT data, we calculate W and column-integrated δD from the TES profiles. Column-integrated δD is consistent (spatial correlation greater than 0.5) with δD retrieved at any single level between about 900 and 700 hPa.

[27] As for GOSAT, to compare LMDZ to TES, we take into account spatio-temporal sampling and instrument sensitivity through collocation and convolution with TES averaging kernels [*Risi et al*., 2012a] using the nudged 1997–2012 LMDZ simulation. Model-prior differences in humidity in the upper troposphere may distort convolved δD profiles, as was the case for CH_4 in *Worden et al*. [2012b], but this effect is masked when considering total-column δD.

[28] As for GOSAT, limitations of the remote sensing data should be taken into account [*Worden et al*., 2006;

Schneider and Hase, 2011]. Spectroscopic biases are possible. The bias in δD depends on the sensitivity of the measurement [*Worden et al*., 2010], which may depend on the H_2O and HDO /H_2O content. Direct dependence of the δD bias on atmospheric conditions were not considered [*Worden et al*., 2010], but they might exist. In addition, the sensitivity of the measurement, including limited vertical resolution and effect of a priori constraint, needs to be considered. The HDO sensitivity depends, among many other factors, on the H_2O content of the atmosphere. As a consequence, relationships between δD and W may be distorted. The effect of instrument sensitivity is to slightly enrich or deplete column-integrated δD on days when the atmosphere is drier, depending on regions (supporting information).

2.5. Water Tagging Approach to Quantify the Role of Continental Recycling on Intraseasonal Moisture Variability

[29] As introduced in section 1.2, we use the water tagging approach to quantify the role of continental recycling in intraseasonal variations of precipitable water. By intraseasonal, we mean the daily variability within a given season. Therefore, hereafter, we use daily outputs and data and we focus on the June-July-August (JJA) and December-January-February (DJF) seasons. This limits contamination by seasonal variations that occur mainly during the transition seasons.

[30] First, we quantify the continental recycling by the fraction of the vapor originating from continental evaporation in the lowest-level vapor, noted r_{con}. We define continental evaporation as the sum of the bare-soil evaporation, snow sublimation, and transpiration. We choose to estimate r_{con} from the lowest-level vapor of the model because (1) this vapor is the most representative of the moisture convergence and (2) this vapor is the most directly affected by continental evaporation. In the tropics, the fraction of the vapor originating from continental evaporation increases with altitude and reaches a maximum in the upper troposphere, which is due to fast injection of continental-evaporated water vapor by deep convection over land regions. This water vapor accumulates in the tropical upper troposphere and subsides slowly in the Hadley-Walker cell. We are not interested in this effect, hence our choice to quantify r_{con} in the lowest-level vapor.

[31] The role of continental recycling in intraseasonal variations of precipitable water (W) can be either positive or negative. If the role of continental recycling is positive, then an increase in W is associated with an increase in r_{con}. In contrast, if the increase in W is associated with an increase in moisture convergence, then this moisture convergence will bring moisture from further away and with a larger proportion of oceanic moisture. In this case, the increase in W is associated with a decrease in r_{con}. More quantitatively, we decompose the moisture W into oceanic moisture ($W_{oce} = (1 - r_{con}) \cdot W$) and continental moisture ($W_{con} = r_{con} \cdot W$). Therefore, W variations (dW) can be decomposed into:

$$\mathrm{d}W = \mathrm{d}W_{oce} + \mathrm{d}W_{con} = \mathrm{d}W_{oce} + \mathrm{d}r_{con} \cdot W + \mathrm{d}W \cdot r_{con} \quad (1)$$

rearranging this equations yields:

$$\mathrm{dln}\,(W) = \mathrm{dln}\,(W_{oce}) + \mathrm{dln}\left(\frac{1}{1 - r_{con}}\right) \quad (2)$$

[32] Atmospheric moisture variations can thus be decomposed into two terms: variations in oceanic moisture advection and variations in continental recycling (respectively first and second term on the right-hand side). When $\mathrm{dln}\left(\frac{1}{1-r_{con}}\right)$ is positively correlated with $\mathrm{dln}\,(W)$, then continental recycling contributes positively to W variations. In this case, continental recycling contributes all the more as $\frac{\mathrm{dln}\left(\frac{1}{1-r_{con}}\right)}{\mathrm{dln}\,(W)}$ is large. For example, when $\frac{\mathrm{dln}\left(\frac{1}{1-r_{con}}\right)}{\mathrm{dln}\,(W)} = 1$, then r_{con} variations are responsible for 100% of W variations. In contrast, when $\mathrm{dln}\left(\frac{1}{1-r_{con}}\right)$ is negatively correlated with $\mathrm{dln}\,(W)$, then continental recycling contributes negatively to W variations. In this case, oceanic moisture convergence contributes positively. The role of moisture convergence is all the larger as $\frac{\mathrm{dln}\left(\frac{1}{1-r_{con}}\right)}{\mathrm{dln}\,(W)}$ is largely negative. Hereafter, we quantify the role of continental recycling on moisture variations by the diagnostic D1:

$$D1 = \frac{\mathrm{dln}\left(\frac{1}{1-r_{con}}\right)}{\mathrm{dln}\,(W)} \cdot 100 \quad (3)$$

expressed in percentage.

3. Simulated Role of Continental Recycling on Intraseasonal Moisture Variability

3.1. Simulated Continental Recycling

[33] Figure 1 shows that r_{con} values range from <5% over most of the oceans up to 85% in Siberia in summer. These values are very consistent with previous estimates using water tagging [*Koster et al*., 1986; *Yoshimura et al*., 2004] or moisture budgets at the global scale [*van der Ent et al*., 2010; *Goessling and Reick*, 2011], both in magnitude and in spatial and seasonal patterns. They are however much larger than estimates of recycling rates based on regional water budgets [*Budyko*, 1974; *Brubaker et al*., 1993; *Trenberth*, 1999; *Schär et al*., 1999]. Those recycling rates estimates are not directly comparable to r_{con} because they represent the fraction of the precipitation or of the vapor originating from evapo-transpiration within a domain of interest, and results depend on the size [*Trenberth*, 1999] and shape of the domain [*van der Ent and Savenije*, 2011].

3.2. Role of Continental Recycling on Intraseasonal Moisture Variability for the Control Simulation

[34] Figures 2a–2d show the daily correlation and slope (D1) of $\ln\left(\frac{1}{1-r_{con}}\right)$ as a function of ln(W) for JJA and DJF. In coastal regions where the influence of moisture advection from the ocean is strong, the correlation and D1 are negative (coastal United States, Europe, coastal northeastern South America, India during the monsoon season, coastal western Africa during the monsoon season). In high latitudes where most of the vapor originates from continental recycling, D1 reaches the highest positive values. In South America, during both seasons, there is a gradient toward the interior following air mass trajectories: intraseasonal variations of W are driven mainly by large-scale convergence of oceanic moisture near the coast, but

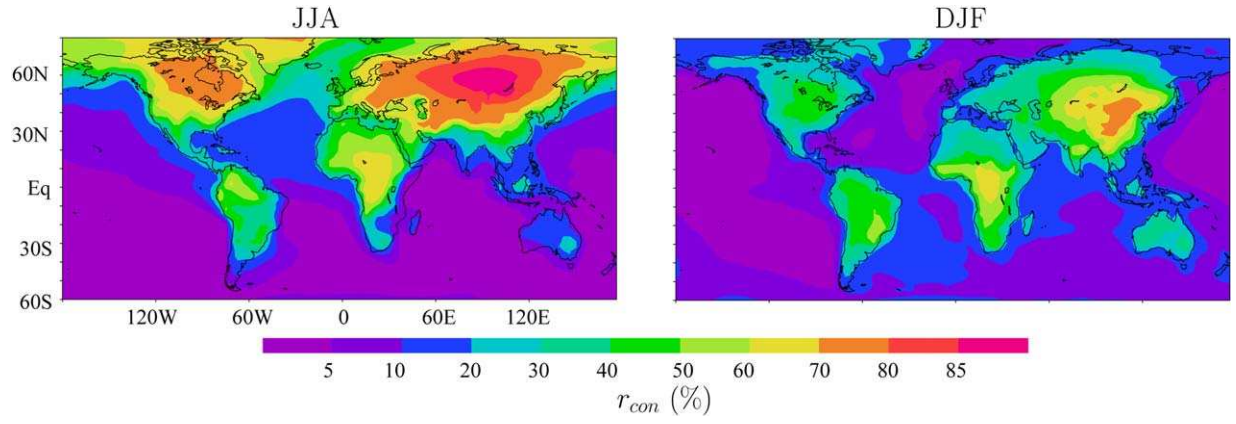

Figure 1. Proportion of the low-level vapor originating form continental recycling (r_{con}) in (a) JJA and (b) DJF as diagnosed from water tagging.

become more and more driven by changes in continental recycling toward the interior. The same effect can be seen in the Sahel during summer.

[35] Quantitatively, in South America for example, D1 goes from about −100% near the coast to about 100% in the Amazon interior. This means that near the coast, when W doubles, it is associated with a tripling of the oceanic contribution and it is attenuated by a reduction of r_{con} (i.e., according to equation (2), $\mathrm{dln}(W) = +100\%$, $\mathrm{dln}\,(W_{oce}) = +200\%$ and $\mathrm{dln}\left(\frac{1}{1-r_{conv}}\right) = -100\%$). In the Amazon interior, when W doubles, it is fully explained by the increase in r_{con} (i.e., $\mathrm{dln}(W)=+100\%$, $\mathrm{dln}\,(W_{oce}) = 0\%$ and $\mathrm{dln}\left(\frac{1}{1-r_{conv}}\right) = +100\%$).

[36] Our maps of the role of continental recycling on W variability are not directly comparable to the maps of the magnitude of land-atmosphere feedbacks by *Koster et al.* [2004], who quantified the sum of all local and regional

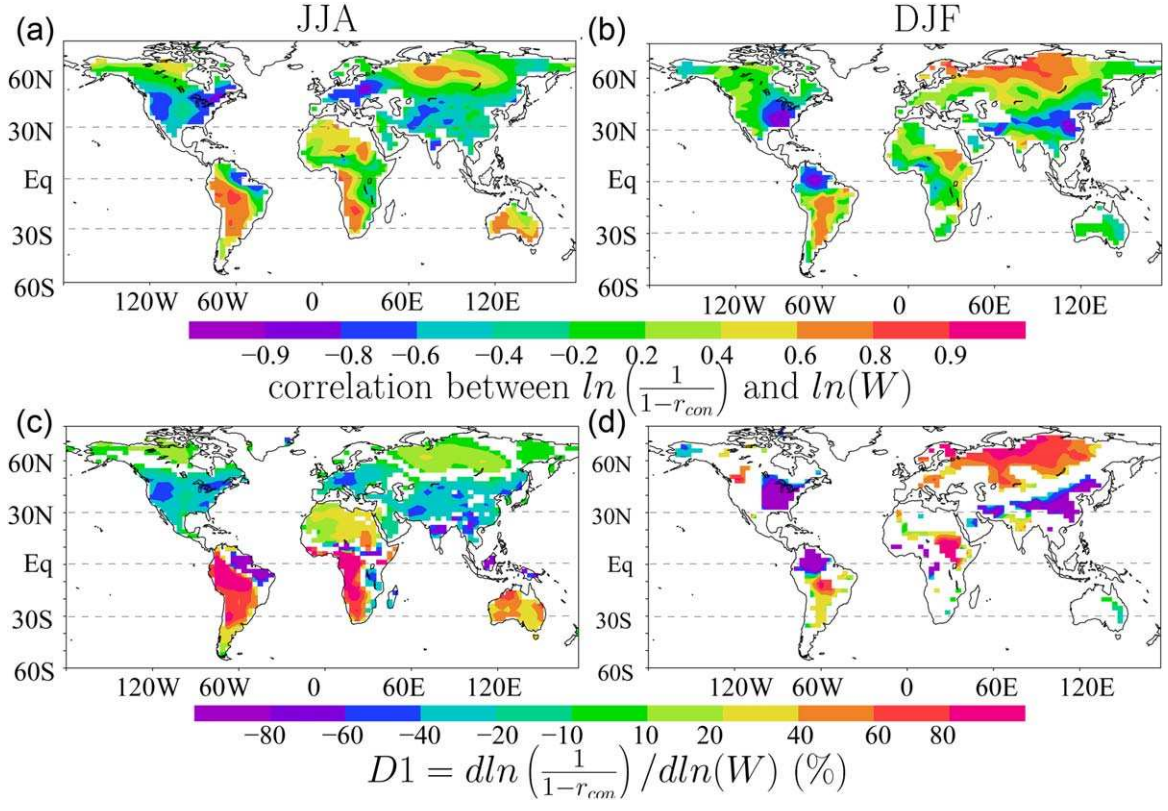

Figure 2. (a) Daily correlation coefficient (r) of the linear regression between $\ln(W)$ and $\ln\left(\frac{1}{1-r_{con}}\right)$ in JJA. (c) Slope of this linear regression, where the correlation coefficient is greater than 0.2 (Figures 2b and 2d). Same as Figures 2a and 2c but in DJF.

effects of land moisture, while we quantify just the regional effect through continental recycling. For example, the thermodynamical role of surface fluxes on atmospheric instability and on the boundary layer activity [e.g., *Findell and Eltahir*, 2003a] is implicitly included in *Koster et al*. [2006] but not in our study.

[37] Still we can compare our maps with some previous studies. Most previous studies have focused on linking moisture origin to precipitation variability rather than to W as we do here. Therefore, their results and ours are not directly comparable, though precipitation and W are significantly correlated over most of the globe. Most of these studies have so far focused on Europe and on the United States. In Europe, our negative sign is consistent with *Schär et al*. [1999], who found that the moisture convergence effect dominates over the continental recycling effect for summer precipitation. It is also consistent with *Dufourg and Ducrocq* [2011], who found an oceanic origin for extreme precipitation events and floods in southern France. In the central plains of the United States, our negative sign is consistent with *Zangvil et al*. [2004] and *Dominguez and Kumar* [2008], who found anticorrelation between precipitation and recycling rates at intraseasonal time scales. *Dominguez et al*. [2008] however found a positive correlation of continental recycling with summer precipitation variability in southwestern United States at the interannual scale, while we find a negative correlation there at the intraseasonal scale.

3.3. Sensitivity to Land Surface Model Representation

[38] The goal of our sensitivity tests is to compare simulations in which the role for continental recycling on intraseasonal variations of W is different. We check that this difference is reflected by our D1 diagnostic (Figure 3).

[39] When the bare soil fraction is reduced, D1 decreases over most of the tropics: South America, Southeast Asia, and Australia in both seasons, in western Africa in winter and in southwestern United States in winter (Figures 3a and 3b). Some regions behave differently due to different atmospheric contexts, but here we focus on the broad patterns. On average over the tropics, D1 values are about half in "baresoil" compared to that in the control.

[40] In contrast, when the stomatal resistance is reduced, D1 increases over most of the tropics: South America and the Congo basin in both seasons, southern Africa in summer (Figures 3c and 3d). On average over the tropics, D1 values are about 50% larger in "rveg" compared to the control.

[41] The decrease of D1 as the bare soil fraction decreases can be explained as follows: bare soil areas are more sensitive than vegetated areas to changes in the soil water content. Over bare soil, a small change in soil water content will lead to stronger changes in evaporation, thus leading to stronger changes in continental recycling. Over vegetated areas, plants can transpire water with a similar rate over a broader range of soil water content. Therefore, as the bare-soil fraction decreases, the r_{con} variations at intraseasonal variations are smaller. This interpretation is confirmed by the fact that on average over the tropics, the correlation between soil water content and evapo-transpiration ratio to potential evapotranspiration [*Milly*, 1992] is lower in "baresoil" than in the control simulation (Figure 3e). In contrast, the increase of D1 as the stomatal resistance decreases can be explained as follows: reduced stomatal resistance leads to stronger transpiration, which dehydrates the soil. At lower soil water contents, evapo-transpiration becomes more sensitive to soil water content. This interpretation is also confirmed by the fact that on average over the tropics, the correlation between soil water content and evapo-transpiration ratio to potential evapo-transpiration is higher in "rveg" than in the control simulation (Figure 3e). The important role of the coupling between soil water and evapo-transpiration in determining the intensity of land-atmosphere feedbacks was already pointed out by *Guo et al*. [2006].

[42] In the following, we will explore whether isotopic observations can help us assess which simulation has the most realistic role of continental recycling in intraseasonal variation of W.

4. Isotopic Signature of Continental Recycling and of its Variability

4.1. Isotopic Signature of Evaporative Sources

[43] First, water tagging allows us to document the different isotopic signatures of each evaporative source. For comprehensiveness, we will document both the isotopic composition in terms of enrichment in heavy isotopes (quantified by δD or δ^{18}O) and in terms of the relative enrichment in HDO compared to that in $H_2{}^{18}O$ (quantified by d-excess $= \delta D - 8 \cdot \delta^{18}O$, *Dansgaard* [1964]. We show that in the tropical low-level vapor, each evaporative origin has a distinct isotopic signature (Figure 4).

[44] Water vapor from vegetation transpiration is much more enriched than oceanic evaporation. This property may contribute to the maximum enrichment that is observed by satellites over tropical land masses [*Worden et al*., 2007; *Brown et al*., 2008; *Frankenberg et al*., 2009]. This is because lighter isotopes evaporate more easily from free liquid surfaces. With typical tropical oceanic conditions (25°C surface temperature, 75% humidity, $\delta^{18}O \simeq -12‰$, and $\delta D \simeq -83‰ \delta D \simeq -83‰$ in ambient vapor), ocean evaporation is $\simeq 5‰ \simeq 5‰$ more enriched in $H_2{}^{18}O$ and $\simeq 5‰ \simeq 5‰$ more enriched in HDO than the ambient vapor. In contrast, transpiration is not associated with fractionation relatively to soil water, because there is no fractionation during root extraction [*Washburn and Smith*, 1934; *Barnes and Allison*, 1988; *Flanagan and Ehleringer*, 1991] and all water extracted by the root needs to be transpired shortly after. Soil water originates from precipitation, which is to first order at equilibrium with the ambient vapor [*Field et al*., 2010]. For typical tropical conditions (25°C), precipitation is $\simeq 10‰ \simeq 10‰$ more enriched in $H_2{}^{18}O$ and $\simeq 80‰ \simeq 80‰$ more enriched in HDO than the ambient vapor. Note that this reasoning holds in the tropics only. In the extra-tropics, under depleted water vapor the oceanic evaporation becomes more enriched than the transpiration of precipitation (e.g., for typical North Atlantic conditions, with 5°C surface temperature, 75% humidity, $\delta^{18}O \simeq -17‰$, and $\delta D \simeq -130‰ \delta D \simeq -130‰$ in ambient vapor, ocean evaporation is $\simeq 18‰ \simeq 18‰$ and $\simeq 130‰ \simeq 130‰$ more enriched in $H_2{}^{18}O$ and HDO than the ambient vapor, while transpiration of precipitation at equilibrium with the ambient vapor at 5°C is $\simeq 11‰ \simeq 11‰$ and $\simeq 100‰ \simeq 100‰$ more enriched in

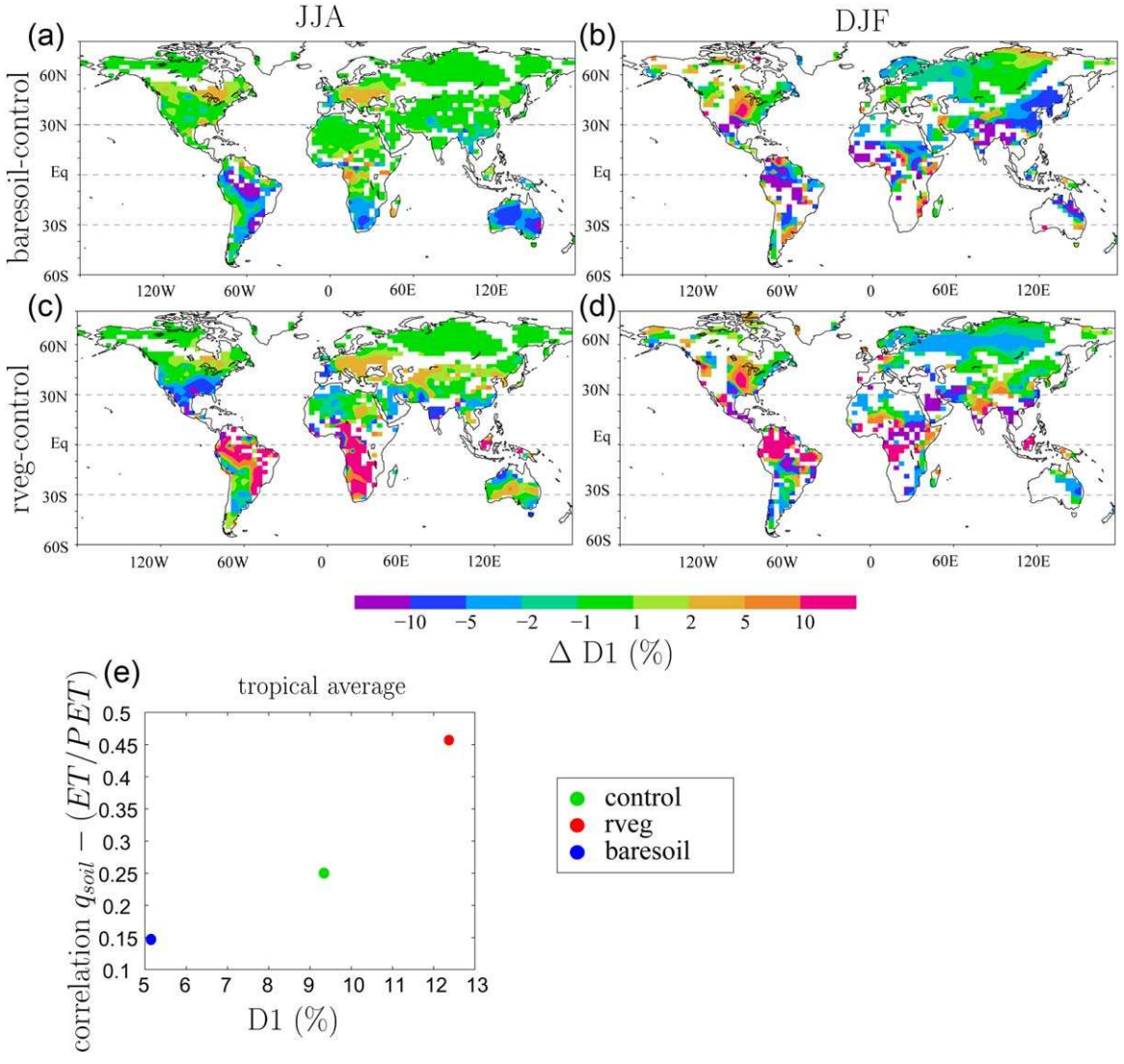

Figure 3. Difference in the D1 diagnostic between sensitivity tests and control simulation. The sensitivity tests are (a, b) "baresoil" (less bare soil fraction) and (c, d) "rveg" (reduced stomatal resistance) described in the section 2.2. Linear regression is calculated on daily time series for JJA (Figures 3a and 3c) and DJF and results are shown only when the correlation coefficient is greater than 0.2. These figures are the same as Figures 2b and 2d but for differences between simulations. (d) Mean correlation coefficient between soil water content and the ratio of evapo-transpiration to potential evapo-transpiration, as a function of mean slope of the linear regression between ln(W) and r_{con}. Means are calculated over the tropics (30°S−30°N) and over JJA and DJF, at all locations and seasons where the correlation coefficient is greater than 0.2 for all three simulations, to represent average over the same spatial domain for all three simulations.

$H_2{}^{18}O$ and HDO than the ambient vapor). What remains always true, however, is that transpiration acts to enrich the overlying water vapor.

[45] Evaporation from bare soil is characterized by a stronger d-excess. This is because kinetic fractionation during the evaporation of soil water is very strong [*Mathieu and Bariac*, 1996; *Braud et al*., 2009a, 2009b]. As kinetic fractionation increases, the diffusivity coefficients become important and the evaporation of HDO is favored by its high diffusivity. This property was the basis of studies trying to partition continental recycling into its transpiration and evaporation components [*Gat and Matsui*, 1991].

[46] These two properties could in theory be exploited to quantify both the continental recycling (with $\delta^{18}O$ or δD) and its components (with d-excess). In practice, there are observational limitations. D-excess is difficult to measure by satellite. Water vapor in situ measurements with sufficient precision are developing [e.g., *Noone et al*., 2012; *Tremoy et al*., 2012] but are still very scarce. Satellites can measure δD from space with reasonable precision and spatio-temporal coverage, but lack absolute calibration. Placing satellite measurements on Figure 4 in an attempt to quantify continental recycling is thus not applicable. This is why in this paper, we focus on

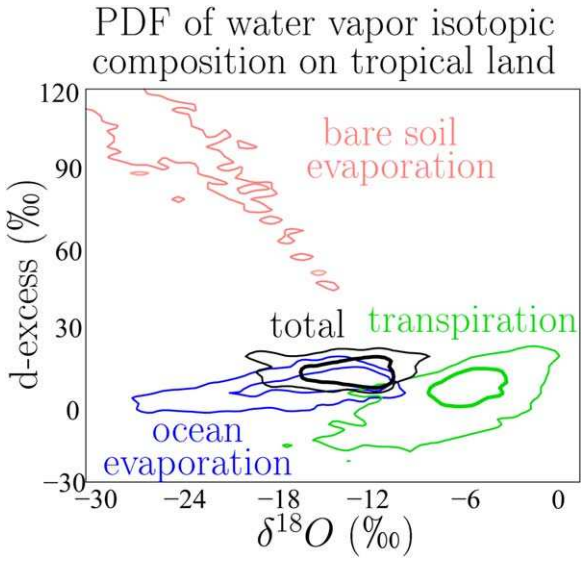

Figure 4. Probability density function of the isotopic composition (δ^{18}O and d-excess) of water vapor at the lowest model level for all tropical land locations and for all days in 2006, for total vapor (black) and vapor originating from ocean evaporation (blue), land surface transpiration (green), and bare soil evaporation (pink).

exploiting the column-integrated δD variability at the intraseasonal scale.

4.2. Intraseasonal Link

[47] To assess to what extent water isotopic measurements can be useful to estimate the role of continental recycling in intraseasonal variations of moisture, we calculate the daily correlation between r_{con} and column-integrated δD (Figures 5a and 5b). Since evapo-transpiration is dominated by isotopically enriched transpiration, we expect positive correlations. We can see strong positive correlations in regions of strong r_{con} (Siberia, northern America) and in tropical regions where the role of continental recycling at intraseasonal scale is strong (South America, Sahel, Congo basin, southern Africa in DJF). Overall, we find similar patterns as for D1 (2): δD is most sensitive to r_{con} where r_{con} has the most positive role in intraseasonal variability of moisture.

[48] Correlations would be even better if we had used δD in the lowest level rather than column-integrated values. Over almost all regions of the globe, the correlation between vapor δD at a given layer and r_{con} decreases with height (Figures 5c–5e). This is why we need δD measurements at the surface, in the lower troposphere or in the total column, if we want to extract information about r_{con} from such measurements.

[49] A good correlation does not necessarily imply a causal relationship, that is, that r_{con} is the main factor controlling δD. First, the good correlation may just be a artifact due to δD being controlled by other factors that correlate with r_{con} by chance. To discard this possibility, we checked that correlations between δD and r_{con} over land are overall preserved even if we calculate partial correlations from multiple-linear regressions of δD as a function of r_{con}, temperature, and precipitation (not shown). Second, there could be a good correlation even though the contribution of r_{con} variations to δD variations are quantitatively small. To quantify the contribution of r_{con} variations to δD variations, we use a water-tagging-based decomposition of δD variations following [*Risi et al.*, 2010b]. This decomposition is based on the fact that $\delta D = r_{con} \cdot \delta D_{con} + (1 - r_{con}) \cdot \delta D_{oce}$, where δD_{con} and δD_{oce} are the compositions of the vapor originating from continental recycling and oceanic evaporation, respectively. Therefore, to first order,

$$d\delta D \simeq dr_{con} \cdot \left(\overline{\delta D_{con} - \delta D_{oce}}\right) + (1 - \overline{r_{con}}) \cdot d\delta D_{oce} + \overline{r_{con}} \cdot d\delta D_{con} \quad (4)$$

[50] The overbar denotes temporal average. The first term on the right-hand side represents the impact of r_{con} variations, that is, the impact of changing origins of moisture. The second and third terms on the right-hand side quantify the impact of surface conditions during oceanic evaporation (impacting δD_{oce}), the impact of surface conditions during land surface evapo-transpiration (impacting δD_{con}) and the impact of all atmospheric processes along air-mass trajectories (impacting both δD_{oce} and δD_{con}).

[51] The contribution of r_{con} variations to δD variations can thus be quantified in % as $\frac{dr_{con}}{d\delta D} \cdot \left(\overline{\delta D_{con} - \delta D_{oce}}\right) \cdot 100$, where $\frac{dr_{con}}{d\delta D}$ is the slope of r_{con} as a function of δD. When this quantity is 100%, variations in r_{con} totally account for δD variations. When it is near 0%, other processes (i.e., second and third terms on the right-hand side of equation (4)) contribute to δD variations. When it exceeds 100%, other processes counterbalance the effect of r_{con}. In most regions where correlation between r_{con} and δD is greater than 0.4, r_{con} variations contribute for more than 40% of δD variations (Figure 6). On average, over all tropical regions where the correlation between r_{con} and δD is greater than 0.4, r_{con} variations contribute for 87% of δD variations. In particular, in western Africa in both seasons, in the Congo basin in DJF and in South America in JJA, δD variations are mainly caused by r_{con} variations. In the Sahel in JJA, this is consistent with *Risi et al.* [2010b]. In the Amazon in DJF, r_{con} contributes a bit less to δD variations. The δD variations in this region and season might be partly associated with convective activity [e.g., *Vimeux et al.*, 2005, 2011]. Similarly in high latitudes (e.g., Siberia), r_{con} variations contribute less to δD variations. The δD variations in these regions are also probably controlled by temperature [e.g., *Kurita et al.*, 2004].

4.3. Isotopic Proxy for the Water-Tagging-Based Diagnostic

[52] Based on these encouraging results, we propose an observable proxy for D1, named D1_iso, calculated as the slope of column-integrated δD as a function of $\ln(W)$:

$$\text{D1\_iso} = \frac{d\delta D}{d\ln(W)}$$

[53] We use $\ln(W)$ because the relationship of δD as a function of W is nonlinear [e.g., *Frankenberg et al.*, 2009; *Galewsky and Hurley*, 2010] and because the Rayleigh

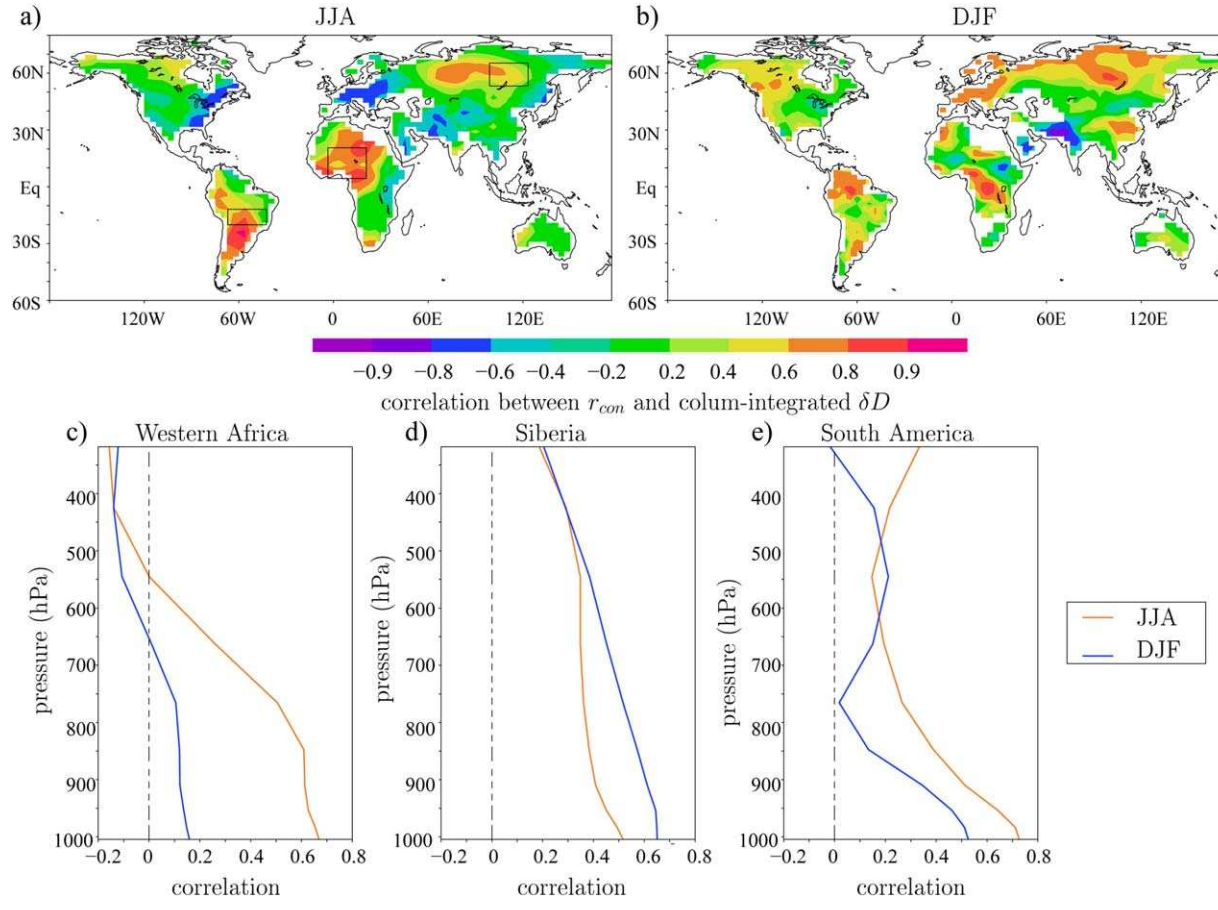

Figure 5. Daily correlation coefficient between r_{con} of the low-level vapor and column-integrated δD in (a) JJA and (b) DJF. Vertical profiles of the daily correlation coefficient between r_{con} and δD of the vapor at each vertical level, on average over different regions: (c) western Africa (10°N–20°N–0°E–20°E), (d) Siberia (55°N–65°N–110°E–120°E), and (e) South America (20°S–10°S–70°W–50°W), for different seasons JJA (orange) and DJF (blue).

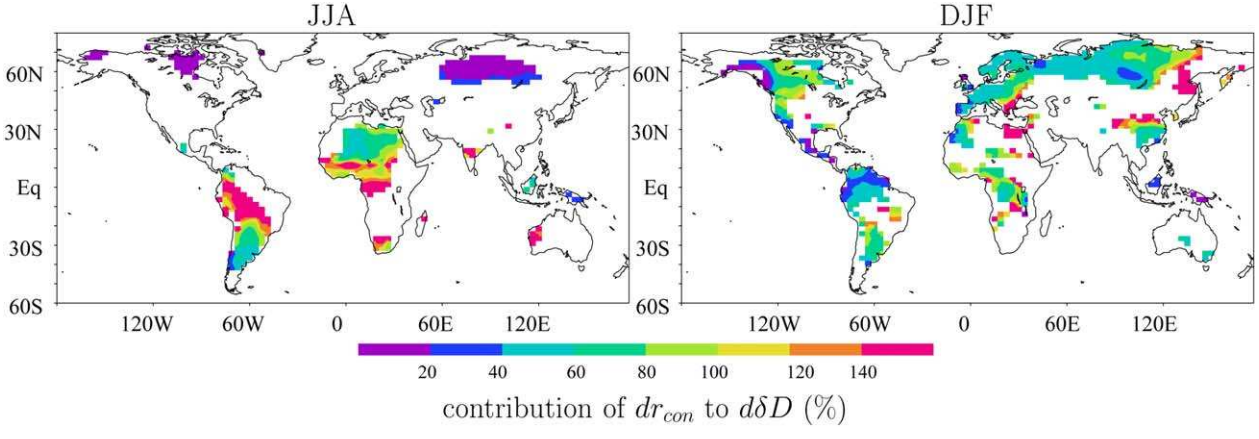

Figure 6. Quantitative contribution of r_{con} variations to column-integrated δD daily variations in (a) JJA and (b) DJF, as quantified by $\frac{\mathrm{d}r_{con}}{\mathrm{d}\delta\mathrm{D}} \cdot \left(\overline{\delta\mathrm{D}_{con} - \delta\mathrm{D}_{oce}}\right) \cdot 100$ (see text for variable definitions) The slope $\frac{\mathrm{d}r_{con}}{\mathrm{d}\delta\mathrm{D}}$ is calculated where the correlation coefficient between r_{con} and column-integrated δD is greater than 0.4.

distillation predicts a linear relationship between δD and ln(W). D1_iso shares similar spatial and seasonal patterns with D1 (Figure 7). For example, in South America and in western Africa, patterns are very similar in D1 and in D1_iso. In these regions, as we go inland, D1 and D1_iso both increase. This is confirmed by correlations of 0.86 and 0.97 between D1 and D1_iso in these regions (Figures 7e and 7f).

[54] The maps in Figure 7 could be interpreted independently of continental recycling, by the combination of two effects: the distillation effect and the amount effect [*Risi et al.*, 2010b]. When the distillation effect dominates, the drier the air in terms of W, the more depleted the vapor. This dryness could come either from cooling as air goes poleward (i.e., temperature effect, *Dansgaard* [1964]), or from large-scale subsidence from higher in the troposphere [*Galewsky and Hurley*, 2010]. This explains at least partially the positive correlations in high latitudes and dry subtropical regions. When the amount effect dominates, the more intense the convection, the more depleted the vapor, due to the depleting effect of unsaturated downdrafts, rainfall reevaporation in a moist environment and rain-vapor

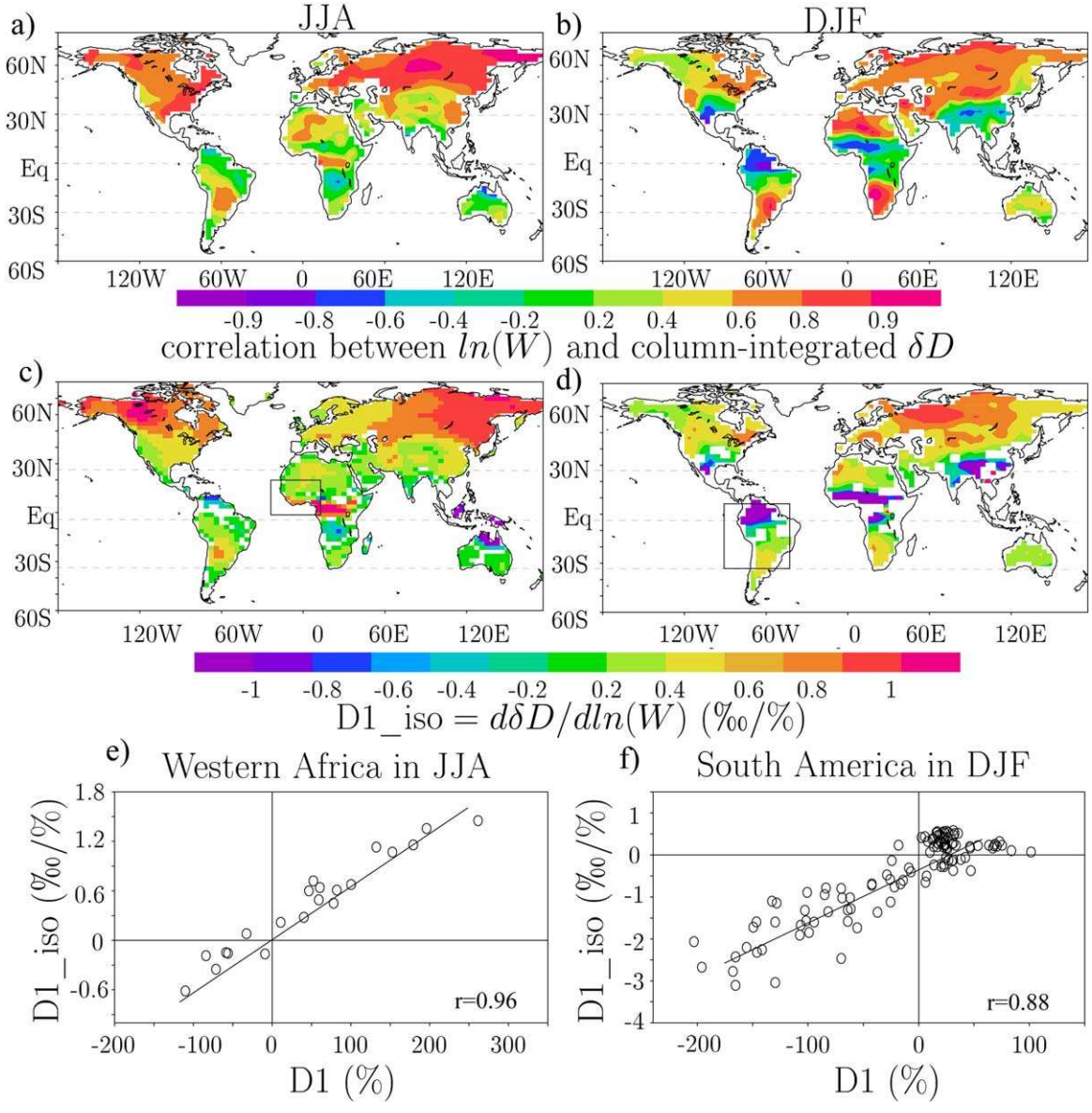

Figure 7. (a) Daily correlation coefficient (r) of the linear regression between precipitable water and δD of total column water vapor in JJA. (b) Slope of this linear regression, where the correlation coefficient is greater than 0.2. (c and d) Same as Figures 7a and 7b but in DJF. This figure can be compared with Figure 2. Such comparison is shown as scatterplots with this example of western Africa in (e) JJA and South America in (f) DJF. These scatterplots show the slope of the linear regression between precipitable water and δD of total column water vapor, as a function of the slope of the linear regression between precipitable water and r_{con}, for each location in the black rectangle of the above map (20°W–15°E–5°N–20°N for western Africa and 90°W–30°W–30°S–10°N for South America).

diffusive exchanges [*Lawrence et al*., 2004; *Risi et al*., 2008; *Worden et al*., 2007; *Field et al*., 2010]. This explains at least partially the negative correlations in convective regions.

[55] However, the resemblance between Figures 2 and 7 in many parts of the tropics suggest that over tropical land and at the intraseasonal scale, continental recycling may play a role in controlling δD that has been so far underestimated. Furthermore, we have shown in section 4.2 that r_{con} variations contribute quantitatively to δD variations. The pure distillation and amount effects can be estimated in places where D1 is zero, corresponding to the intercepts in Figures 7e and 7f. As expected, in the dry Sahel, the distillation effect leads to very slightly positive $d\delta D/d\ln(W)$ and in the moist Amazon, the amount effect leads to negative $d\delta D/d\ln(W)$.

4.4. Potential to Discriminate Between Sensitivity Tests

[56] In the previous section, we have shown a spatial link between D1 and D1_iso. Now we check whether D1_iso can discriminate between simulations differing by D1. Figure 8 shows the maps of the D1_iso differences between the sensitivity tests and the control simulation. These maps share similar patterns with the corresponding maps for D1 (Figure 3). For example D1 is lower in "baresoil" than in the control simulation, and so is D1_iso, in South America in JJA and DJF, in western Africa in DJF and in southeastern Asia in DJF. D1 is higher in the "rveg" than in the control simulation, and so is D1_iso, in most of South America in JJA and DJF and in most of Africa in JJA. In South America in particular, where D1 is the largest in "baresoil" compared to the control, D1_iso is also the largest in "baresoil" compared to the control. The reverse holds for "rveg" (Figure 8e). This can be seen also in tropical average (Figure 8f).

[57] Figure 8f plots an observable diagnostic (D1_iso) as a function of a nonobservable diagnostic (D1) which is of interest to evaluate the simulation of land-atmosphere coupling in climate models. The ultimate goal would thus be to add on this plot real observations for D1_iso. This would help us constrain D1: for example, if average observed D1_iso is positive, this would suggest that the "rveg" simulation, with a relatively high D1, is more realistic. *Hall and Qu* [2006] applied a similar approach to constrain the snow albedo feedback. However, using D1_iso to constrain D1 is possible only if the observational uncertainty on D1_iso is small enough compared to the simulation spread. In the next section, we check this condition.

5. Comparison With Data

5.1. Basic Annual Mean Comparison

[58] Figure 9 compares annual-mean column-integrated δD observed by GOSAT and TES and simulated by LMDZ after collocation and convolution by the kernels corresponding to each data set. The spatial patterns of δD retrieved by GOSAT and TES are very consistent with each other (Figures 9a and 9d). They both capture the decrease of δD with latitude and with altitude (e.g., Tibet), lower values in dry oceanic (e.g., off Peru) and continental (e.g., Sahara) regions and a local minimum over the southeastern Asia. The spatial correlations between the two fields are 0.81 at the global scale and 0.56 in the tropics. Overall, spatial variations are smoother in TES than in GOSAT (Figures 9b and 9e): the global spatial standard deviation is 58% smaller in TES than in GOSAT (Table 3). This is partly due to the smoothing effect of TES kernels (Figures 9e and 9f), which decreases the global spatial standard deviation by 36% (Table 2).

[59] To first order, LMDZ captures well the spatial patterns for both GOSAT and TES. When collocation and convolution are applied, the correlations between simulated and observed δD are 0.98 globally and 0.92 in the tropics for GOSAT, and 0.95 globally and 0.90 in the tropics for TES. In all cases, the convolution with the kernels improves the correlation coefficients by 0.06 up to 0.23. Compared to both data sets, LMDZ underestimates the equatorpole gradient, consistent with the results from other data sets [*Risi et al*., 2012a] and models [*Yoshimura et al*., 2001; *Werner et al*., 2011]. In addition, when compared to GOSAT, LMDZ simulates maxima over the ocean east of South America and Africa, rather than over land masses as in the data. This appears to be an artifact of the convolution, because model outputs without convolution show maxima over land masses (Figures 9b and 9c).

5.2. Comparison of Intraseasonal Relationships

[60] Figure 10 compares the observed and simulated daily correlations between $\ln(W)$ and column-integrated δD. The main spatial patterns described in section 4.3 are found in GOSAT observations (Figures 9a and 9b), with maximum positive correlations over the dry Sahara, the southern half of South America, southern Africa, and Australia and high boreal latitudes in summer.

[61] LMDZ captures well the correlation patterns and magnitudes observed by both GOSAT and TES. Compared to GOSAT observations, LMDZ underestimates the correlation over the Sahara (consistent with *Risi et al*. [2010b]). But this underestimate is not noticeable compared to TES. Compared to both GOSAT and TES, LMDZ overestimates the negative correlations over convective regions (northern South America in DJF, Central America in JJA, and southeastern Asia in both seasons). An overestimated amount effect was also found for other models [*Lee et al*., 2009b]. In addition, humidity biases in LMDZ lead convolved outputs to artificially feature larger negative correlations in these regions than initially simulated (supporting information).

[62] The slopes of column-integrated δD as a function of $\ln(W)$ (i.e., D1_iso) are compared in Figure 11, for locations where correlations are greater than 0.2 for GOSAT and than 0.1 for TES. This figure mirrors the D1_iso maps of Figures 7b and 7d, in the sense that it represents the same maps but after accounting for GOSAT and TES spatio-temporal sampling and instrument sensitivity. Qualitatively, the main spatial features described in section 4.3 are captured by GOSAT and TES. Quantitatively, GOSAT exhibits larger slopes (Figures 11a–11d), about twice larger in tropical average (Table 3). Some of these differences can be attributed to different instrument sensitivities. In GOSAT, the effect of instrument sensitivity is to systematically attenuate negative slopes (supporting information). Apart from this effect, instrument sensitivity as reflected by averaging kernels are not expected to systematically distort

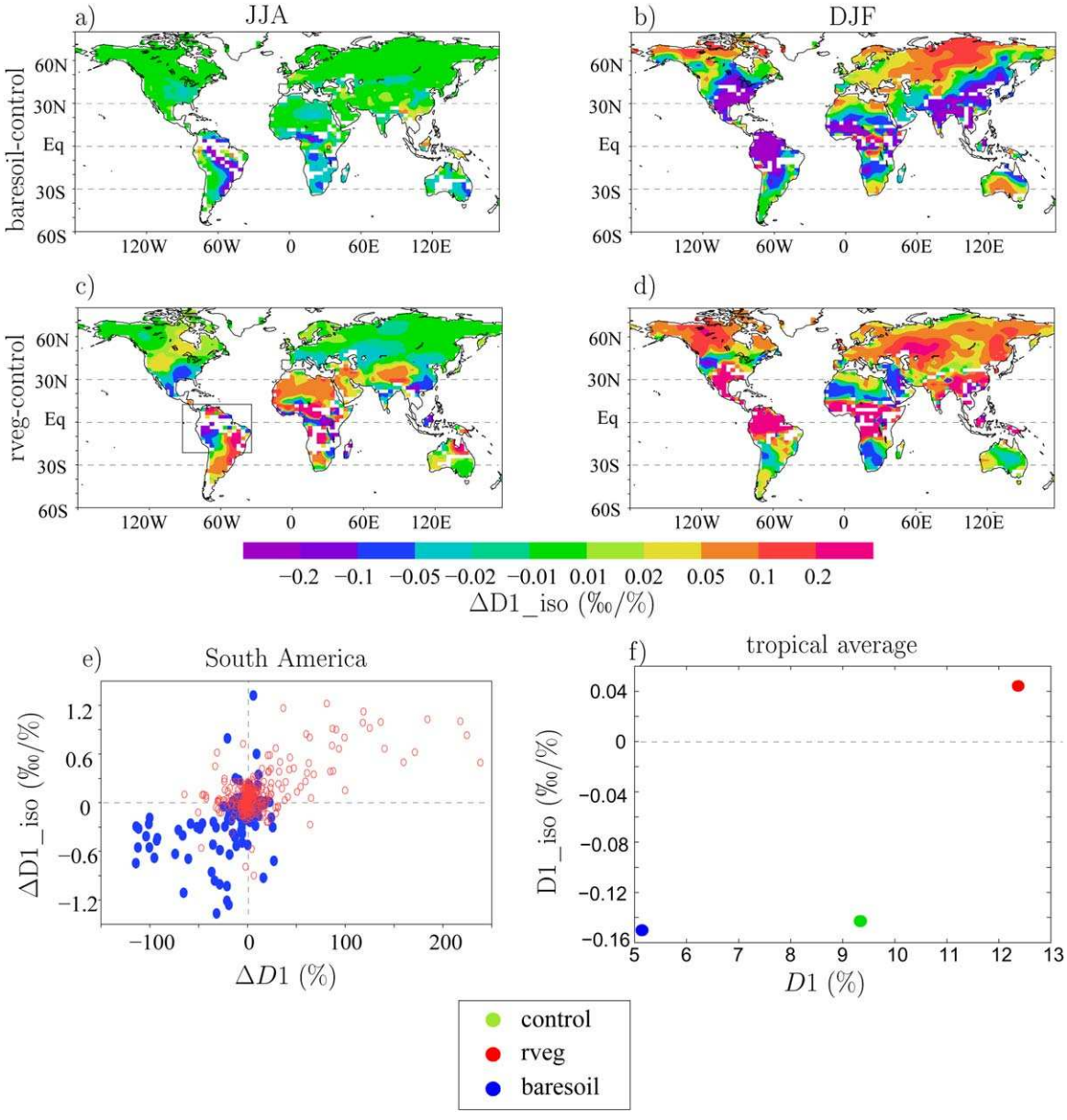

Figure 8. Difference between sensitivity tests and control simulation in D1_iso (the slope of the linear regression between ln(W) and column-integrated δD). The sensitivity tests are (a, b)"baresoil" (less bare soil fraction) and (c, d) "rveg" (reduced stomatal resistance). Linear regression is calculated on daily time series for JJA (Figure 8a and 8c) and DJF and results are shown only when the correlation coefficient is greater than 0.2. This figure is like Figures 7b and 7e but for differences between simulations. It can be compared with Figure 3. (e) Difference between sensitivity tests and control simulation in the slope of the linear regression between ln(W) and column-integrated δD (D1_iso), as a function of the difference between sensitivity tests and control simulation in the slope of the linear regression between ln(W) and $\ln(1 - r_{con})$ (D1), at all locations in South America (20°S−15°N−90°W−30°W) black rectangle on c in DJF. (f) Same as Figure 8e but tropical mean (30°S−30°N) and average over JJA and DJF. Means are calculated over all locations and seasons where correlation coefficients are greater than 0.2 for all three simulations, to represent average over the same spatial domain for all three simulations.

δD versus ln(W) slopes (supporting information). Differences between TES and GOSAT in the regions of positive slopes could thus be attributed to observation biases that depend differently on W in TES and in GOSAT.

[63] When collocated and convolved with the appropriate averaging kernels, LMDZ simulates qualitatively well the spatial patterns of D1_iso (Figure 11). Quantitatively, however, LMDZ, underestimates D1_iso compared to

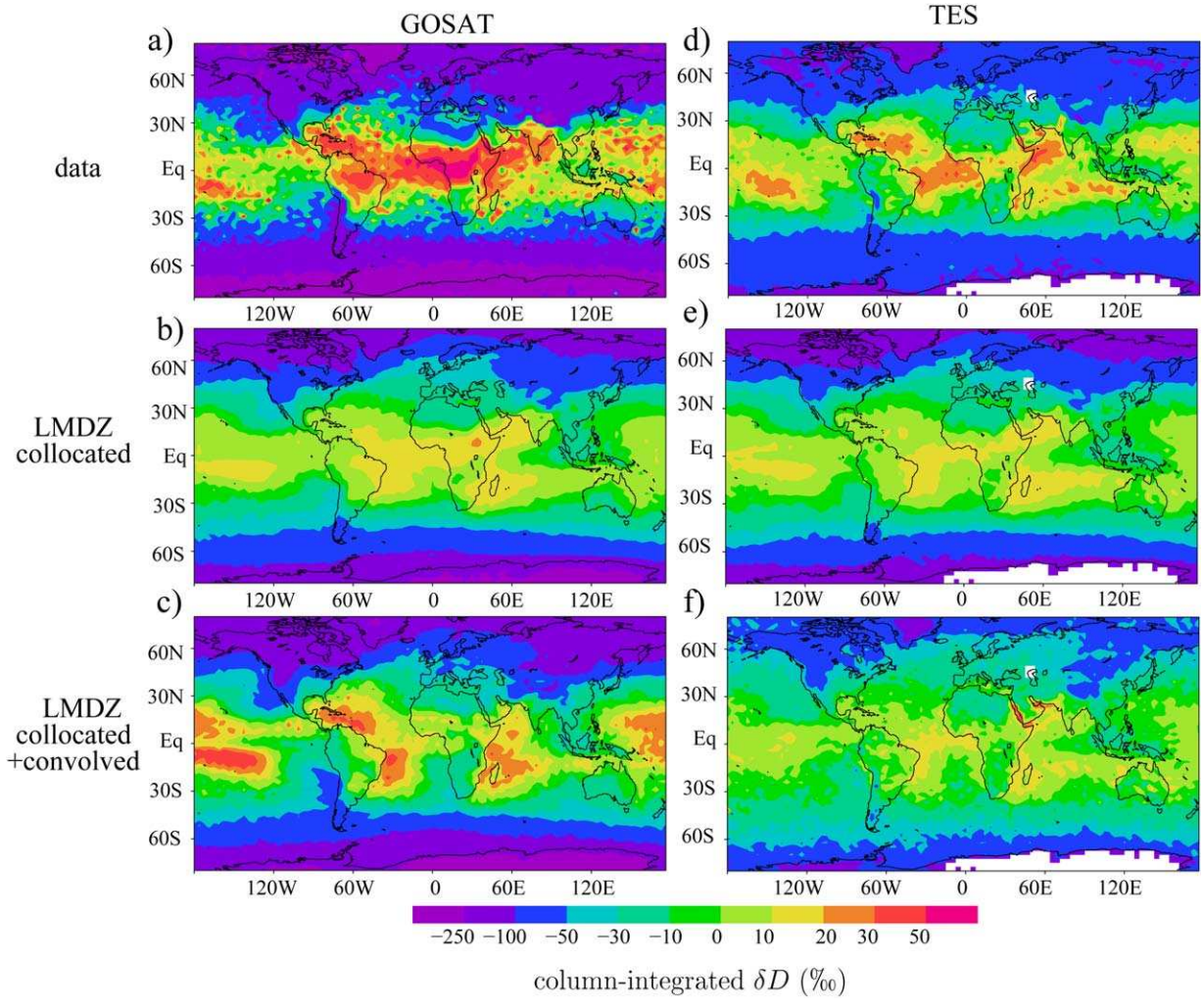

Figure 9. Comparison of column-integrated δD between (a) GOSAT observations, (b) collocated LMDZ outputs,and (c) collocated LMDZ outputs convolved with GOSAT averaging kernels. (d–f) Same as Figures 9a–9c but for comparison of column-integrated δD between TES and LMDZ. To focus on spatial variations in absence of absolute calibration, we subtract the mean δD over 40°S−40°N for each δD map. The spatial standard deviation at the global scale of these maps is indicated in Table 2.

both GOSAT and TES. In tropical average where observed slopes are positive, LMDZ underestimates slopes by a factor of about 2 compared to GOSAT and about 4 compared to TES (Table 3). This is due to an underestimate of both negative and positive slopes. First, LMDZ simulates negative slopes in moist tropical regions that have a greater extent than observed. In regions where observed slopes are negative, simulated slopes are also too negative. This is consistent with an overestimate of the amount effect [*Lee et al*., 2009b]. But this could also be attributed to the effect of humidity biases: even if simulated δD is correct, humidity biases in LMDZ lead convolved outputs to systematically decrease negative slopes (supporting information). Second, LMDZ underestimates positive slopes in the driest regions, such as the Sahara in winter, especially compared to GOSAT. This cannot be explained by humidity biases, since humidity biases in LMDZ lead convolved outputs to systematically increase positive slopes compared to GOSAT. Therefore, although GOSAT and TES have different sensitivities to δD, both data sets suggest that LMDZ underestimates D1_iso.

Table 2. Spatial Standard Deviation at the Global Scale of Column-Integrated δD for GOSAT and TES Observations, Collocated LMDZ Outputs, and Collocated and Convolved LMDZ Outputs[a]

Data Set	GOSAT	TES
Observations	114	49
Collocated LMDZ outputs	54	53
Collocated and Convolved LMDZ outputs	69	35

[a]LMDZ outputs are collocated and convolved to compare either with GOSAT or TES observations. All values are expressed in ‰.

Table 3. Comparison of the Slopes (Columns 2 and 3) of Column-Integrated δD as a Function ln(W), on Average Over JJA and DJF and Over All Tropical Land Locations, for GOSAT and TES Observations, Raw LMDZ Outputs, Collocated LMDZ Outputs, Collocated and Convolved LMDZ Outputs, and for Our Three LMDZ-ORCHIDEE Simulations[a]

Data Set	GOSAT	TES	GOSAT Where Observed Slopes Are Positive	TES Where Observed Slopes Are Positive	GOSAT in Western Africa in JJA	TES in Western Africa in JJA
Data	0.50	0.26	0.99	0.30	1.42	0.26
Raw LMDZ outputs	−0.24	−0.18	−0.02	−0.17	0.01	−0.04
Collocated LMDZ outputs	0.07	0.10	0.10	0.12	0.24	−0.20
Collocated and convolved LMDZ outputs	−0.05	0.04	0.43	0.07	0.76	−0.70
Raw LMDZ-ORCHIDEE control	−0.39	−0.27	−0.19	−0.24	−0.15	−0.46
Raw LMDZ-ORCHIDEE baresoil	−0.47	−0.33	−0.26	−0.30	−0.20	−0.56
Raw LMDZ-ORCHIDEE rveg	−0.33	−0.15	−0.13	−0.14	−0.23	−0.03

[a]Values are in ‰/%. Tropical land averages are calculated where the correlation coefficients for all the simulations and observations are greater than 0.1, to ensure that averages are done over the same spatial domain for all quantities that we compare. Columns 4 and 5: same as columns 2 and 3 but over tropical land points were observed slopes are positive. Columns 6 and 7: same as columns 2 and 3 but over western Africa (defined as 20°W–15°E–5°N–20°N as in Figure 5) in JJA.

[64] The suggestion that LMDZ underestimates D1_iso is further supported by comparison with ground-based remote-sensing measurements of column-integrated δD (not shown). We selected four TCCON sites [*Wunch et al*., 2011] and two MUSICA sites [*Schneider et al*., 2010a, 2010b] that lie over land and with a significant continental influence: Park Falls, Lamont and Pasadena (United States), Bremen (Germany) for TCCON and Jungfraujoch (Switzerland), Karlsruhe (Germany) for MUSICA. After convolution with appropriate averaging kernels [*Risi et al*., 2012a], LMDZ underestimate D1_iso at all sites and for both JJA and DJF, except at Karlsruhe in JJA. Therefore, almost all available data sets suggest that LMDZ underestimates D1_iso.

5.3. Implications for Model Evaluation of the Role of Continental Recycling

[65] The fact that LMDZ underestimates D1_iso compared to both GOSAT and TES suggests that LMDZ underestimates the role of continental recycling in intraseasonal variations of continental moisture. On average over tropical land points, LMDZ-ORCHIDEE simulates D1_iso values that are even lower than in stand-alone LMDZ (Table 3). This suggests that the coupling with ORCHIDEE weakens the role of continental recycling on the intraseasonal variability of continental moisture. This can be explained by the fact that in ORCHIDEE, transpiration has access to a deeper reservoir of soil moisture that fluctuates at a lower frequency. Therefore, the presence of vegetation in ORCHIDEE smoothes the evapo-transpiration variations. In ORCHIDEE, increasing the sensitivity of evapo-transpiration to soil moisture may improve the model-data agreement (section 3.3).

[66] An important caveat of our approach is that D1_iso may not only reflect the role of continental recycling. As discussed in section 4.3, the distillation and amount effects may also play a role. If we find that in a model simulation, the slope is too low, how can we ensure that this is only due to the underestimated role of continental recycling? It may also be due to the distillation effect which is not efficient enough (e.g., excessive diffusion: *Risi et al*. [2012b], or because the depleting effect of convection is too strong (e.g., excessively strong unsaturated downdrafts). An idea could be to compare D1_iso over land versus ocean, assuming that the distillation and convection effects over land and ocean would be the same. But it would not be conclusive either because convection over land and ocean has a different character [*Zipser and LeMone*, 1980; *Nesbitt and Zipser*, 2003; *Liu and Zipser,* 2005].

[67] In section 4.2, we showed that in western Africa in both seasons, in the Congo basin in DJF and in South America in JJA, simulated δD variations were mainly caused by r_{con} variations. This suggests that in this regions we may have more confidence that the underestimate of D1_iso (Table 3) can be interpreted as an underestimate of the role of continental recycling.

6. Conclusions

[68] In this paper, we design a water-tagging-based diagnostic, named D1, to estimate the role of continental recycling on the intraseasonal variability of continental moisture and precipitation. Consistent with previous studies [e.g., *Schär et al*., 1999], we show that this role is limited in coastal regions, in Europe and in the United States, where the intraseasonal variability of continental moisture is mainly driven by variability in moisture convergence bringing mainly oceanic precipitation. However, on deeper continental interiors (e.g., Siberia) and in tropical land regions where the continental recycling is strong (e.g., southern America, Congo basin), the role of continental recycling on the intraseasonal variability of continental moisture becomes important. We show that this role is sensitive to model parameter choice, for example, those modulating the relationship between soil-water content and evapo-transpiration. We aim at proposing an observational constrain for the simulation of this role.

[69] We show that low-level δD is a good tracer for variability in continental recycling at the intraseasonal scale, due to the enriched signature of transpiration. We show that over land regions, the relationship between column-integrated δD and the logarithm of precipitable water, named D1_iso, is a good observable proxy for D1 in several regions, in particular in western Africa, in the Congo basin and in South America. This proxy could help

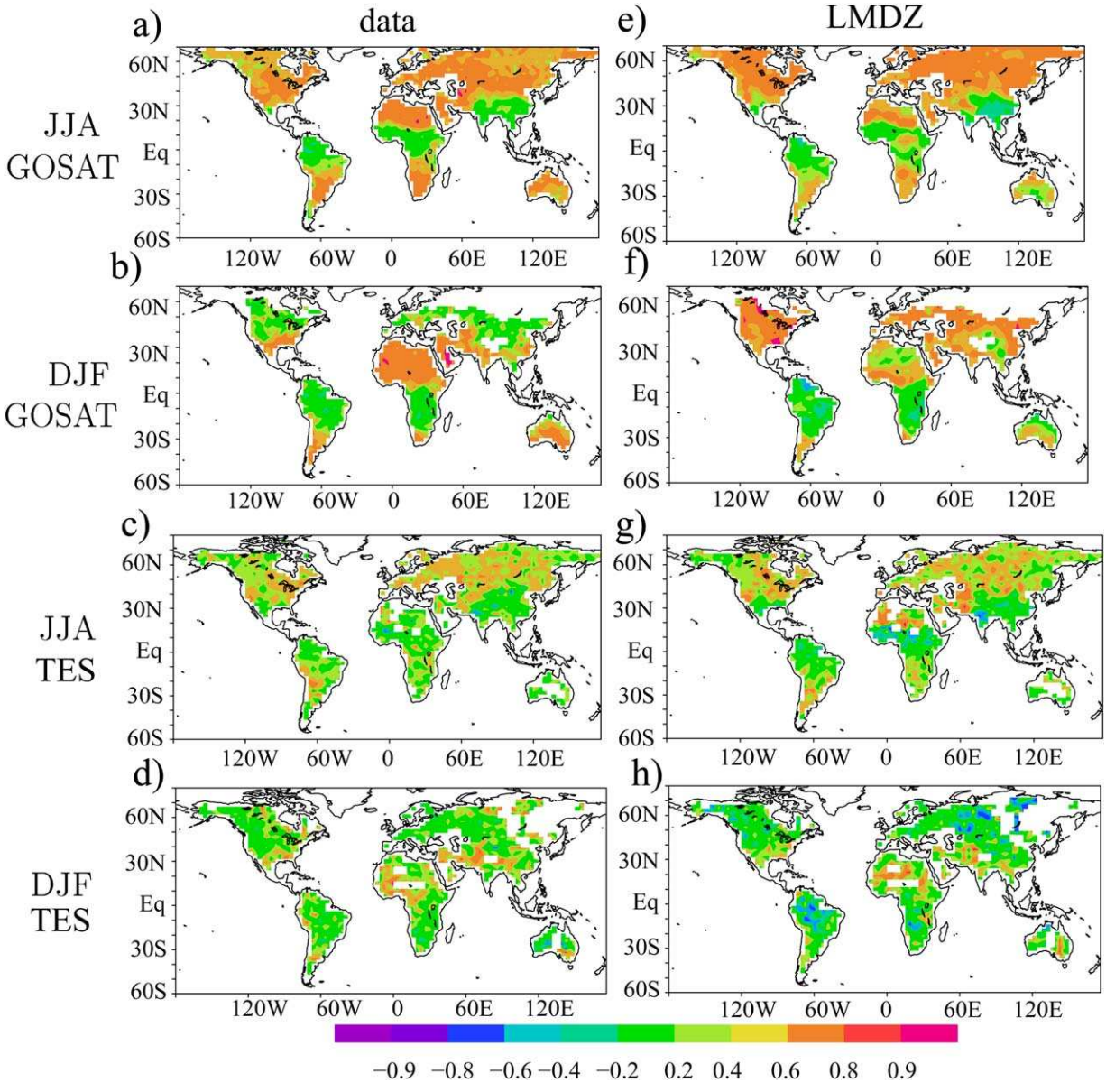

Figure 10. Correlation coefficient for the relationship of column-integrated δD as a function of ln(W), for (a, b) GOSAT observations, for the (c, d) TES data, for (e, f) LMDZ outputs after collocation and convolution by GOSAT kernels, and for (g, h) LMDZ outputs after collocation and convolution by TES kernels. Results are shown for both JJA and DJF.

discriminate between different simulations to select the one with the most realistic role of continental recycling on the intraseasonal variability of continental moisture.

[70] We test this possibility with two satellite data sets: GOSAT and TES. Compared to both data sets, LMDZ underestimates D1_iso. This suggests that LMDZ underestimates the role of continental recycling on the intraseasonal variability of continental moisture. However, a doubt subsists whether other misrepresentation of atmospheric processes independent of continental recycling (e.g., convection, large-scale circulation) may also contribute to this underestimate. The respective role of continental recycling and atmospheric processes on water vapor isotopic composition need to be more accurately quantified and understood, before we can practically use isotopic data to evaluate models in terms of continental recycling. This requires a more detailed model analysis and a more careful evaluation against isotopic measurements.

[71] Finally, the different sensitivity between GOSAT and TES calls for more calibration and cross-validation studies which would not only focus on mean δD [e.g., *Worden et al*., 2010] but also on δD variations. The development of in situ measurements [e.g., *Gupta et al*., 2009; *Lee et al*., 2007b; *Welp et al*., 2012], on the ground or onboard

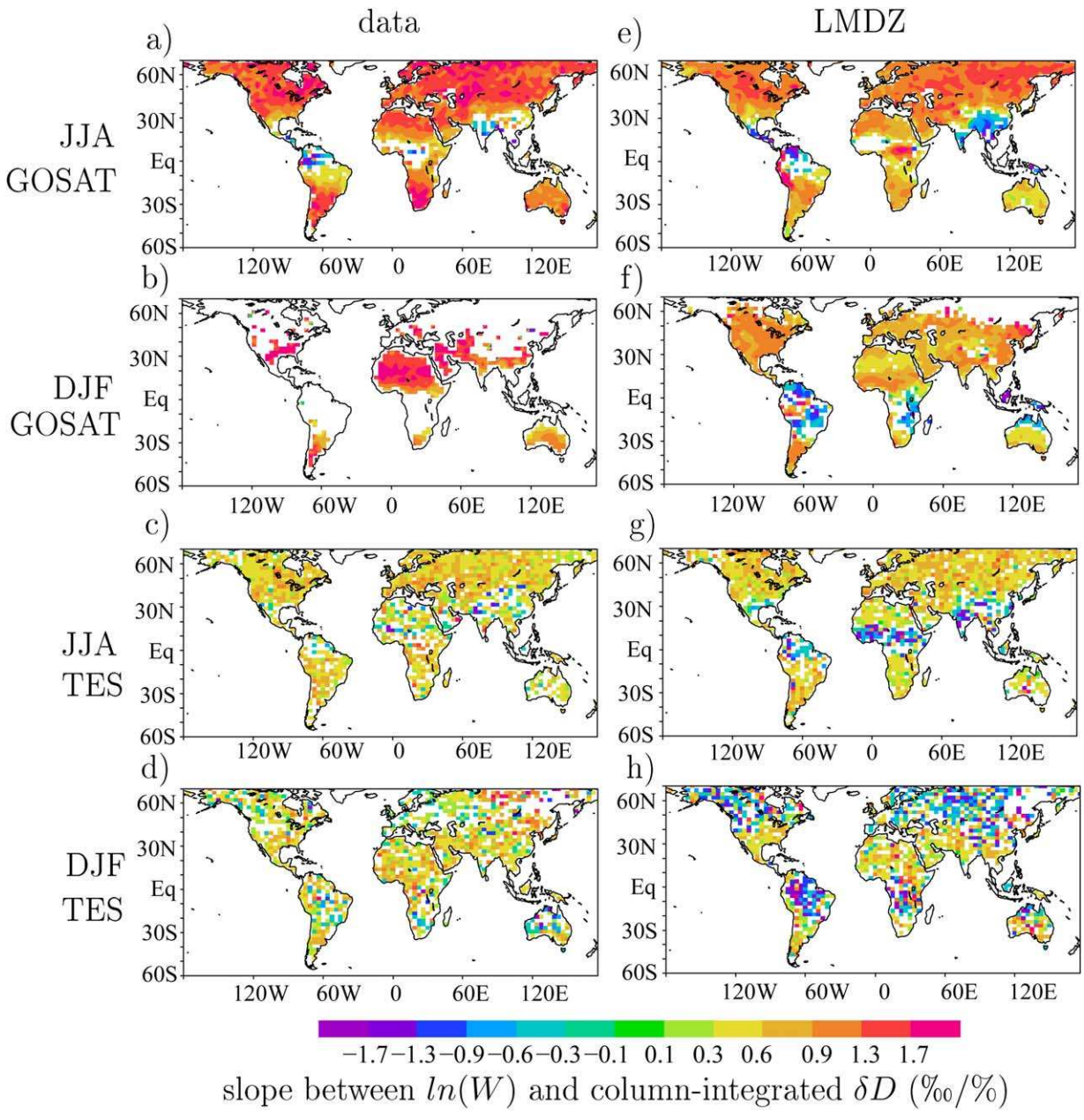

Figure 11. Same as Figure 10 but for slopes (i.e., D1_iso) instead of correlation coefficients. Slopes are plotted where correlation coefficients are greater than 0.2. The average over all tropical land points of these slopes are indicated in Table 3.

aircrafts, will offer more validation opportunities for satellite data sets and models.

[72] **Acknowledgments.** LMDZ and LMDZ-ORCHIDEE simulations were performed on the NEC supercomputer of the IDRIS computing center. We thank Matthias Schneider and two anonymous reviewers for their constructive comments during the review process.

References

Barnes, C., and G. Allison (1988), Tracing of water movement in the unsaturated zone using stable isotopes of hydrogen and oxygen, *J. Hydrol.*, *100*, 143–176.

Beljaars, A., P. Viterbo, M. J. Miller, and A. K. Betts (1996), The anomalous rainfall over the united states during July 1993: Sensitivity to land surface parameterization and soil moisture anomalies, *Mon. Weather Rev*, *124*, 362–383.

Betts, A. K. (1992), Fife atmospheric boundary layer budget methods, *J. Geophys. Res*, *97*, D18, 18,523–18,532.

Betts, A. K. (2004), Understanding hydrometeorology using global models, *Bull. Am. Meteorol. Soc.*, *85*(11), 1673–1688, doi:10.1175/BAMS-85-11.

Boesch, H., N. M. Deutscher, T. Warneke, K. Byckling, A. J. Cogan, D. W. T. Griffith, J. Notholt, R. J. Parker, and Z. Wang, (2012), HDO/H_2O ratio retrievals from GOSAT, *Atmos. Meas. Tech. Discuss.*, *5*, 5, 6643–6677, doi:10.5194/amtd-5–6643-2012.

Bony, S., C. Risi, and F. Vimeux (2008), Influence of convective processes on the isotopic composition (deltaO18 and deltaD) of precipitation and water vapor in the Tropics. Part 1: Radiative-convective equilibrium and TOGA-COARE simulations, *J. Geophys. Res.*, *113*, D19305, doi:10.1029/2008JD009942.

Bosilovich, M. G., and S. D. Schubert (2002), Water vapor tracers as diagnostics of the regional hydrologic cycle, *J. Hydrometeorol*, *3*, 149–165.

Braud, I., T. Bariac, P. Biron, and M. Vauclin (2009a), Isotopic composition of bare soil evaporated water vapor, Part II: Modeling of RUBIC IV experimental results, *J. Hydrol.*, *369*, 17–29.

Braud, I., P. Biron, T. Bariac, P. Richard, L. Canale, J. Gaudet, and M. Vauclin (2009b), Isotopic composition of bare soil evaporated water vapor. Part I: RUBIC IV experimental setup and results, *J. Hydrol.*, *369*, 1–16.

Bretherton, C. S., M. E. Peters, and L. E. Back (2004), Relationships between water vapor path and precipitation over the tropical oceans, *J. Clim*, *17*, 1517–1528.

Brown, D., J. Worden, and D. Noone (2008), Comparison of atmospheric hydrology over convective continental regions using water vapor isotope measurements from space, *J. Geophys. Res.*, *113*, D15124, doi:10.1029/2007JD009676.

Brubaker, K. L., D. Entekhabi, and P. Eagleson (1993), Estimation of continental precipitation recycling, *J. Clim.*, *6*, 1077–1099.

Brubaker, K., D. Entekhabi, and P. Eagleson (1994), Atmospheric water-vapor transport and continental hydrology over the America, *J. Hydrol.*, *155*, 407–428.

Budyko (1974), *Climate and Life*, Elsevier, New York.

Burde, G. I., A. Zangvil, and P. J. Lamb (1996), Estimating the role of local evaporation in precipitation for a two-dimensional region, *J. Clim.*, *9*, 1328–1338.

Choisnel, E., S. V. Jourdain, and C. J. Jaquart (1995), Climatological evaluation of some fluxes of the surface energy and soil water balances over France, *Ann. Geophys.*, *13*, 666–674.

Cook, B. I., B. B. Gordon, and S. Levis (2006), Soil moisture feedbacks to precipitation in southern Africa, *J. Clim.*, *19*, 4198–4206.

Craig, H., and L. I. Gordon (1965), Deuterium and oxygen-18 variations in the ocean and marine atmosphere, in Stable Isotopes in Oceanographic Studies and Paleotemperatures, pp. 9–130, Laboratorio di Geologia Nucleate, Pisa, Italy.

Dansgaard (1964), Stable isotopes in precipitation, *Tellus*, *16*, 436–468.

de Ridder, K. (1997), Land surface processes and the potential for convective precipitation, *J. Geophys. Res.*, *102*, D25, 30,085–30,090.

de Rosnay, P., M. Bruen, and J. Polcher (2000), Sensitivity of the surface fluxes to the number of layers in the soil model used in GCMs, *Geophys. Res. Lett.*, *27*(20), 3329–3332.

Dirmeyer, P. A., and K. L. Brubaker (1999), Contrasting evaporative moisture sources during the drought of 1988 and the flood of 1993, *J. Geophys. Res.*, *104*(D16), 19,383–19,397.

Dirmeyer, P. A., and K. L. Brubaker (2007), Characterization of the global hydrologic cycle from a back-trajectory analysis of atmospheric water vapor, *J. Hydrometeorol.*, *8*(1), 20–37, doi:10.1175/JHM557.1.

Dirmeyer, P. A., C. A. Schlosser, and K. L. Brubaker (2008), Precipitation, recycling, and land memory: An integrated analysis, *J. Hydrometeorol.*, *10*, 278–288.

Dirmeyer, P. A., K. L. Brubaker, and T. DelSole (2009), Import and export of atmospheric water vapor between nations, *J. Hydrol.*, *365*(1–2), 12–12, doi:10.1016/j.jhydrol.2008.11.016.

d'Odorico, P., and A. Porporato (2004), Preferential states in soil moisture and climate dynamics, *Proc. Natl. Acad. Sci.*, *101*(24), 8848–8851, doi:10.1073/pnas.0401428101.

Dominguez, F., and P. Kumar (2008), Precipitation recycling variability and ecoclimatological stability – A study using NARR data. Part I: Central U.S. Plains ecoregion, *J. Clim.*, *21*:5165–5186, http://dx.doi.org/10.1175/2008JCLI1756.1.

Dominguez, F., P. Kumar, X. Liang, and M. Ting (2006), Impact of atmospheric moisture storage on precipitation recycling, *J. Clim.*, *19*(8), 1513–1530, doi:10.1175/JCLI3691.1.

Dominguez, F., P. Kumar, and E. R. Vivoni (2008), Precipitation recycling variability and ecoclimatological stability? A study using NARR data. Part II: North American Monsoon Region, *J. Clim.*, *21*, 5187–5203.

d'Orgeval, T. (2006), Impact du changement climatique sur le cycle de l'eau en Afrique de l'Ouest: Modélisation et incertitudes. PhD thesis, Univ. Paris 6.

Ducoudré, N., K. Laval, and A. Perrier (1993), SECHIBA, a new set of parametrizations of the hydrological exchanges at the land-atmosphere interface within the LMD atmospheric general circulation model, *J. Clim.*, *6*, 248–273.

Duffourg, F., and V. Ducrocq (2011), Origin of the moisture feeding the heavy precipitating systems over southeastern France, *Nat. Hazards Earth Syst. Sci.*, *11*(4), 1163–1178.

Dufresne, J.-L., et al. (2012), Climate change projections using the IPSL-CM5 earth system model: From CMIP3 to CMIP5, *Clim. Dyn.*, *40*(9–10), 1–43, doi:10.1007/s00382-012-1636-1.

Ek, M. B., and A. A. M. Holtslag (2004), Influence of soil moisture on boundary layer cloud development, *J. Hydrometeorol.*, *5*, 86–99.

Eltahir, E. A. B., and R. L. Bras (1994), Precipitation recycling in the Amazon basin, *Q. J. R. Meteorol. Soc.*, *120*(518), 861–880, doi:10.1002/qj.49712051806.

Eltahir, E. A. B., and R. L. Bras (1996), Precipitation recycling, *Rev. Geophys.*, *34*(3), 367–378.

Entekhabi, D., I. Rodriguez-Iturbe, and R. L. Bras (1992), Variability in large-scale water balance with land surface-atmosphere interaction, *J. Clim.*, *5*, 798–813.

Ferguson, C. R., and E. F. Wood (2011), Observed land-atmosphere coupling from satellite remote-sensing and re-analysis, *J. Hydrometeorol.*, *12*, 1221–1254, http://dx.doi.org/10.1175/2011JHM1380.1.

Ferguson, C. R., E. F. Wood, and R. K. Vinukollu (2012), A global intercomparison of modeled and observed land-atmosphere coupling, *J. Hydrometeorol.*, *13*, 749–784, http://dx.doi.org/10.1175/JHM-D-11–0119.1.

Field, R. D., D. B. A. Jones, and D. P. Brown (2010), The effects of post-condensation exchange on the isotopic composition of water in the atmosphere, *J. Geophys. Res.*, *115*, D24305, doi:10.1029/2010JD014334.

Findell, K. L., and E. A. B. Eltahir (2003a), Atmospheric controls on soil moisture-boundary layer interactions. Part I: Framework development, *J. Hydrometeorol.*, *4*, 552–569.

Findell, K. L., and E. A. B. Eltahir (2003b), Atmospheric controls on soil moisture? Boundary layer interactions. Part II: Feedbacks within the continental United States, *J. Hydrometeorol.*, *4*, 570–583.

Fischer, E. M., S. I. Seneviratne, D. Lüthi, and C. Schär (2007), Contribution of land-atmosphere coupling to recent European summer heat waves, *Geophys. Res. Lett.*, *34*, L06707, doi:10.1029/2006GL029068.

Flanagan, L. B., and J. R. Ehleringer (1991), Stable isotope composition of stem and leaf water: Applications to the study of plant use, *Funct. Ecol.*, *5*(2), 270–277.

Frankenberg, C., et al. (2009), Dynamic processes governing lower-tropospheric HDO/H_2O ratios as observed from space and ground, *Science*, *325*, 1374–1377.

Frankenberg, C., D. Wunch, G. Toon, C. Risi, R. Scheepmaker, Lee, J.-E, and J. Worden (2012), Water vapor isotopologues retrievals from high resolution GOSAT short-wave infrared spectra, *Atmos. Chem. Phys. Discuss.*, *5*, 6357–6386, doi:10.5194/amtd-5–6357-2012.

Galewsky, J., and J. V. Hurley (2010), An advection-condensation model for subtropical water vapor isotopic ratios, *J. Geophys. Res.*, *115* (D16), D16115, doi:10.1029/2009JD013651.

Gat, J. R. (1996), Oxygen and hydrogen isotopes in the hydrologic cycle, *Annu. Rev. Earth Planet. Sci.*, *24*, 225–262.

Gat, J. R., and E. Matsui (1991), Atmospheric water balance in the Amazon basin: An isotopic evapotranspiration model, *J. Geophys. Res.*, *96*, 13,179–13,188.

Gates, W. L. (1992), AMIP: The atmospheric model intercomparison project, *Bull. Am. Meteorol. Soc.*, *73*, 1962–1970.

Gimeno, L., A. Drumond, R. Nieto, R. M. Trigo, and A. Stohl (2010), On the origin of continental precipitation, *Geophys. Res. Lett.*, *37*, L13804, doi:10.1029/2010GL043712.

Gimeno, L., A. Stohl, R. M. Trigo, F. Dominguez, K. Yoshimura, L. Yu, A. Drumond, A. M. Duran-Quesada, and R. Nieto (2012), Oceanic and terrestrial sources of continental precipitation, *Rev. Geophys.*, *50*, RG4003, doi:10.1029/2012RG000389.

Goessling, H. F., and C. H. Reick (2011), What do moisture recycling estimates tell us? Exploring the extreme case of non-evaporating continents, *Hydrol. Earth Syst. Sci.*, *15*, 3217–3225.

Gong, C., and E. Eltahir (1996), Sources of moisture for rainfall in West Africa, *Water Resour. Res.*, *10*, 3115–3121.

Guimberteau, M., K. Laval, A. Perrier, and J. Polcher (2012), Global effect of irrigation and its impact on the onset of the Indian summer monsoon, *Clim. Dyn*, *39*(6), 1329–1348, doi:10.1007/s00382-011-1252-5.

Guo, Z., et al. (2006), GLACE: The global land–atmosphere coupling experiment. Part II: Analysis, *J. Hydrometeorol.*, *7*(4), 611–625, doi:10.1175/JHM511.1.

Gupta, P., D. Noone, J. Galewsky, C. Sweeney, and B. H. Vaughn (2009), Demonstration of high-precision continuous measurements of water vapor isotopologues in laboratory and remote field deployments using wavelength-scanned cavity ring-down spectroscopy (WS-CRDS) technology, *Rapid Commun. Mass Spectrom.*, *23*, 2534–2542.

Hall, A., and X. Qu (2006), Using the current seasonal cycle to constrain snow albedo feedback in future climate change, *Geophys. Res. Lett.*, *33*, L03502, doi:10.1029/2005GL025127.

Hoffmann, G., M. Werner, and M. Heimann (1998), Water isotope module of the ECHAM atmospheric general circulation model: A study on timescales from days to several years, *J. Geophys. Res.*, *103*, 16,871–16,896.

Hohenegger, C., P. Brockhaus, C. Bretherton, and C. Schär (2009), The soil moisture-precipitation feedback in simulations with explicit and parameterized convection, *J. Clim.*, *22*, 5003–5020.

Hourdin, F., et al. (2006), The LMDZ4 general circulation model: Climate performance and sensitivity to parameterized physics with emphasis on tropical convection, *Clim. Dyn.*, *27*, 787–813.

Joussaume, S., J. Jouzel, and R. Sadourny (1984), A general circulation model of water isotope cycles in the atmosphere, *Nature*, *311*, 24–29.

Jouzel, J., R. D. Koster, R. J. Suozzo, G. L. Russel, J. W. C. White, and W. S. Broecker (1987), Simulations of the HDO and H_2O18 atmospheric cycles using the NASA GISS General Circulation Model: The seasonal cycle for present day conditions, *J. Geophys. Res.*, *92*, 14,739–14,760.

Jouzel, J., R. Koster, R. Suozzo, G. Russell, J. White, and W. Broecker (1991), Simulations of the HDO and H2O-18 atmospheric cycles using the NASA GISS general circulation model: Sensitivity experiments for present-day conditions, *J. Geophys. Res.*, *96*, 7495–7507.

Kleidon, A., and M. Heimann (2000), Assessing the role of deep rooted vegetation in the climate system with model simulations: Mechanism, comparison to observations and implications for Amazonian deforestation, *Clim. Dyn.*, *16*, 183–199.

Koster, R., J. Jouzel, R. Suozzo, G. Russell, W. Broecker, D. Rind, and P. Eagleson (1986), Global sources of local precipitation as determined by the NASA/GISS GCM, *Geophys. Res. Lett.*, *13*(2), 121–124, doi:10.1029/GL013i002p00121.

Koster, R. D, P. A. Dirmeyer, A. N. Hahmann, R. Ijpelaar, L. Tyahla, P. Cox, and M. J. Suarez (2002), Comparing the degree of land-atmosphere interaction in four atmospheric general circulation models, *J. Hydrometeorol.*, *3*, 363–375.

Koster, R. D, et al. (2004), Regions of strong coupling between soil moisture and precipitation, *Science*, *305*, 1138–1140, doi:10.1126/science.1100217.

Koster, R. D., et al. (2006), GLACE: The global land-atmosphere coupling experiment. Part I: Overview, *J. Hydrometeorol.*, *7*, 590–610.

Krinner, G., N. Viovy, de Noblet-Ducoudré, N., J. Ogée, J. Polcher, P. Friedlingstein, P. Ciais, S. Sitch, and I. C. Prentice (2005), A dynamic global vegetation model for studies of the coupled atmosphere-biosphere system, *Global Biogeochem. Cycles*, *19*, GB1015, doi:10.1029/2003GB002199.

Kurita, N., N. Yoshida, G. Inoue, and E. A. Chayanova (2004), Modern isotope climatology of Russia: A first assessment, *J. Geophys. Res.*, *109*, D03102, doi:10.1029/2003jd004046.

Lawrence, D. M., and J. Slingo (2005), Weak land-atmosphere coupling strength in hadAM3: The role of soil moisture variability, *J. Hydrometeorol.*, *6*(5), 670–680.

Lawrence, J. R., S. D. Gedzelman, D. Dexheimer, H.-K. Cho, G. D. Carrie, R. Gasparini, C. R. Anderson, K. P. Bowman, and M. I. Biggerstaff (2004), Stable isotopic composition of water vapor in the tropics, *J. Geophys. Res.*, *109*:D06115, doi:10.1029/2003JD004046.

Lee, E., T. N. Chase, R. Balaji, R. G. Barry, T. W. Biggs, and P. J. Lawrence (2009a), Effects of irrigation and vegetation activity on early Indian summer monsoon variability, *Int. J. Climatol.*, *29*(4), 573–581.

Lee, J.-E., and I. Fung (2008), ''Amount effect'' of water isotopes and quantitative analysis of post-condensation processes, *Hydrol. Process.*, *22*(1), 1–8.

Lee, J.-E., I. Fung, DePaolo, D, and C. C. Fennig (2007a), Analysis of the global distribution of water isotopes using the NCAR atmospheric general circulation model, *J. Geophys. Res.*, *112*, D16306, doi:10.1029/2006JD007657.

Lee, J.-E., B. R. Lintner, J. D. Neelin, X. Jiang, P. Gentine, C. K. Boyce, B. F. Joshua, J. T. Perron, T. L. Kubar, J. Lee, and J. Worden (2012), Reduction of tropical land region precipitation variability via transpiration, *Geophys. Res. Lett*, *39*, L19704, doi:10.1029/2012GL053417.

Lee, J.-E., R. Pierrehumbert, A. Swann, and B. R. Lintner (2009b), Sensitivity of stable water isotopic values to convective parameterization schemes, *Geophys. Res. Lett.*, *36*, L23801, doi:10.1029/2009GL040880.

Lee, X., K. Kim, and R. Smith (2007b), Temporal variations of the 18O/16O signal of the whole-canopy transpiration in a temperate forest, *Global Biogeochem. Cycles*, *21*, GB3013, doi:10.1029/2006GB002871.

Lintner, B. R., P. Gentine, K. L. Findell, F. D'Andrea, A. H. Sobel, and G. D. Salvucci (2012), An idealized prototype for large-scale land atmosphere coupling, *J. Clim.*, *26*, 2379–2389, http://dx.doi.org/10.1175/JCLI-D-11–00561.1.

Liu, C., and E. J. Zipser (2005), Global distribution of convection penetrating the tropical tropopause, *J. Geophys. Res.*, *110*, D23104, doi:10.1029/2005JD006063.

Marti, O., et al. (2005), The new IPSL climate system model: IPSL-CM4. Tech. Rep., Note of the Modeling Pole of IPSL, 26: 1–86.

Mathieu, R., and T. Bariac (1996), A numerical model for the simulation of stable isotope profiles in drying soils, *J. Geophys. Res.*, *101*(D7), 12,685–12,696.

McDonald, J. E. (1962), The evaporation-precipitation fallacy, *Weather*, *17*(5), 168–177.

Meehl, G. A., K. Covey, T. Delworth, M. Latif, B. McAvaney, J. F. B. Mitchell, R. J. Stouffer, and K. Taylor (2007), The WCRP CMIP3 multimodel dataset: A new era in climate change research, *Bull. Am. Meteorol. Soc.*, *7*, 1383–1394.

Milly, P. C. D. (1992), Potential evaporation and soil moisture in general circulation models, *J. Clim.*, *5*, 209–226, http://dx.doi.org/10.1175/1520−0442.

Nesbitt, S. W., and E. J. Zipser (2003), The diurnal cycle of rainfall and convective intensity according to three years of TRMM measurements, *J. Clim.*, *16*(10), 1456–1475.

Nicholson, S. E. (2000), Land surface processes and Sahel climate, *Rev. Geophys.*, *38*, 117–139.

Noone, D., and I. Simmonds (2002), Associations between delta18O of water and climate parameters in a simulation of atmospheric circulation for 1979–95, *J. Clim.*, *15*, 3150–3169.

Noone, D., et al. (2012), Factors controlling moisture in the boundary layer derived from tall tower profiles of water vapor isotopic composition following a snowstorm in Colorado, *Atmos. Chem. Phys. Discuss.*, *12*, 16,327–16,375, doi:10.5194/acpd-12–16327-2012.

Numaguti, A. (1999), Origin and recycling processes of precipitating water over the Eurasian continent: Experiments using an atmospheric general circulation model, *J. Geophys. Res*, *104*, 1957–1972, doi:10.1029/1998JD200026.

Pal, J. S., and E. A. B. Eltahir (2001), Pathways relating soil moisture conditions to future summer rainfall within a model of the land-atmosphere system, *J. Clim.*, *14*, 1227–1242.

Porporato, A. (2009), Atmospheric boundary-layer dynamics with constant bowen ratio, *Boundary Layer Meteorol.*, *132*(2), 227–240, doi:10.1007/s10546-009-9400-8.

Raymond, D. J. (2000), Thermodynamic control of tropical rainfall, *J. R. Meteorol. Soc.*, *126*, 889–898.

Risi, C. (2009), Les isotopes stables de l'eau: Applications l'étude du cycle de l'eau et des variations du climat, PhD thesis, Univ. Pierre Marie Curie.

Risi, C., S. Bony, and F. Vimeux (2008), Influence of convective processes on the isotopic composition (O18 and D) of precipitation and water vapor in the tropics: Part 2: Physical interpretation of the amount effect, *J. Geophys. Res.*, *113*, D19306, doi:10.1029/2008JD009943.

Risi, C., S. Bony, F. Vimeux, M. Chong, and L. Descroix (2010a), Evolution of the water stable isotopic composition of the rain sampled along Sahelian squall lines, *Q. J. R. Meteorol. Soc.*, *136*(S1), 227–242.

Risi, C., S. Bony, F. Vimeux, C. Frankenberg, and D. Noone (2010b), Understanding the Sahelian water budget through the isotopic composition of water vapor and precipitation, *J. Geophys. Res.*, *115*, D24110, doi:10.1029/2010JD014690.

Risi, C., S. Bony, F. Vimeux, and J. Jouzel (2010c), Water stable isotopes in the LMDZ4 general circulation model: Model evaluation for present day and past climates and applications to climatic interpretation of tropical isotopic records, *J. Geophys. Res.*, *115*, D12118, doi:10.1029/2009JD013255.

Risi, C., et al. (2012a), Process-evaluation of tropical and subtropical tropospheric humidity simulated by general circulation models using water vapor isotopic observations. Part 1: Model-data intercomparison, *J. Geophys. Res.*, *117*, D05303, doi:10.1029/2011JD016621.

Risi, C., et al. (2012b), Process-evaluation of tropical and subtropical tropospheric humidity simulated by general circulation models using water vapor isotopic observations. Part 2: An isotopic diagnostic of the mid and upper tropospheric moist bias, *J. Geophys. Res.*, *117*, D05304, doi:10.1029/2011JD016623.

Rodriguez-Iturbe, I., D. Entekhabi, and R. L. Bras (1991a), Nonlinear dynamics of soil-moisture at climate scales:1. Stochastic-analysis, *Water Resour. Res.*, *27*(8), 1899–1906.

Rodriguez-Iturbe, I., D. Entekhabi, Lee, J.-S., and R. L. Bras (1991b), Nonlinear dynamics of soil moisture at climate scales: 2. Chaotic analysis, *Water Resour. Res.*, *27*(8), 1907–1915.

Rowntree, P. R., and J. A. Bolton (1983), Simulation of the atmospheric response to soil moisture anomalies over Europe, *Q. J. R. Meteorol. Soc.*, *109*(461), 501–526.

Saeed, F., S. Hagemann, and D. Jacob (2009), Impact of irrigation on the south Asian monsoon, *Geophys. Res. Lett.*, *36*, L20711, doi:10.1029/2009GL040625.

Salati, E., A. Dall'Olio, E. Matsui, and J. Gat (1979), Recycling of water in the Amazon basin: An isotopic study, *Water Resour. Res.*, *15*, 1250–1258.

Santanello, J. A., C. D. Peters-Lidard, S. V. Kumar, C. Alonge, and W.-K. Tao (2009), A modeling and observational framework for diagnosing local land–atmosphere coupling on diurnal time scales, *J. Hydrometeorol.*, *10*, 577–599, doi:10.1175/2009JHM1066.1.

Santanello, J. A., C. D. Peters-Lidard, and S. V. Kumar (2011), Diagnosing the sensitivity of local land? Atmosphere coupling via the soil moisture-boundary layer interaction, *J. Hydrometeorol.*, *12*, 766–786.

Scheepmaker, R. A., C. Frankenberg, A. Galli, A. Butz, H. Schrijver, N. M. Deutscher, D. Wunch, T. Warneke, S. Fally, and I. Aben (2012), Improved water vapour spectroscopy in the 4174–4300cm-1 region and its impact on sciamachy HDO/H_2O measurements, *Atmos. Meas. Tech. Discuss.*, *5*, 8539–8578, doi:10.5194/amtd-5–8539-2012.

Schlemmer, L., C. Hohenegger, J. Schmidli, C. Bretherton, and C. Schär (2011), An idealized cloud-resolving framework for the study of midlatitude diurnal convection over land, *J. Atmos. Sci*, *68*, 1041–1057.

Schlemmer, L., C. Hohenegger, J. Schmidli, and C. Schär (2012), Diurnal equilibrium convection and land surface-atmosphere interactions in an idealized cloud-resolving model, *Q. J. R. Meteorol. Soc.*, *138*(667), 1526–1539.

Schmidt, G., G. Hoffmann, D. Shindell, and Y. Hu (2005), Modelling atmospheric stable water isotopes and the potential for constraining cloud processes and stratosphere-troposphere water exchange, *J. Geophys. Res.*, *110*, D21314, doi:10.1029/2005JD005790.

Schneider, M., and F. Hase (2011), Optimal estimation of tropospheric H_2O and deltaD with IASI/METOP, *Atmos. Chem. Phys.*, *11*, 11207–11220, doi:10.5194/acp-11–11207-2011.

Schneider, M., G. Toon, J.-F. Blavier, F. Hase, and T. Leblanc (2010a), H_2O and deltaD profiles remotely-sensed from ground in different spectral infrared regions, *Atmos. Meas. Tech.*, *3*, 1599–1613.

Schneider, M., K. Yoshimura, F. Hase, and T. Blumenstock (2010b), The ground-based FTIR network's potential for investigating the atmospheric water cycle, *Atmos. Chem. Phys.*, *10*, 3427–3442.

Schär, C., D. Lüthi, and U. Beyerle (1999), The soil-precipitation feedback: A process study with a regional climate model, *J. Clim.*, *12*, 722–741.

Seneviratne, S. I., D. Lüthi, M. Litschi, and C. Schär (2006), Land-atmosphere coupling and climate change in Europe, *Nature*, *443*(14), 205–209, doi:10.1038/nature05095.

Seneviratne, S. I., T. Corti, E. L. Davin, M. Hirschi, E. B. Jaeger, I. Lehner, B. Orlowsky, and A. J. Teuling (2010), Investigating soil moisture-climate interactions in a changing climate: A review, *Earth-Sci Rev.*, *99*(3–4), 125–161, http://dx.doi.org/10.1016/j.earscirev.2010.02.004.

Sitch, S. et al. (2003), Evaluation of ecosystem dynamics, plant geography and terrestrial carbon cycling in the LPJ dynamic vegetation model, *Global Change Biol.*, *9*, 161–185.

Spracklen, D. V., S. R. Arnold, and C. M. Taylor (2012), Observations of increased tropical rainfall preceded by air passage over forests, *Nature*, *489*, 282–285, doi:10.1038/nature11390.

Stewart, M. K. (1975), Stable isotope fractionation due to evaporation and isotopic exchange of falling waterdrops: Applications to atmospheric processes and evaporation of lakes, *J. Geophys. Res.*, *80*, 1133–1146.

Taylor, C. M., and T. Lebel (1998), Observational evidence of persistent convective-scale rainfall patterns, *Mon. Weather Rev.*, *126*, 1597–1607, http://dx.doi.org/10.1175/1520−0493.

Taylor, C. M., D. J. Parker, and P. P. Harris (2007), An observational case study of mesoscale atmospheric circulations induced by soil moisture, *Geophys. Res. Lett*, *34*, L15801, doi: 10.1029/2007GL030572.

Taylor, C. M., P. P. Harris, and D. J. Parker (2009), Impact of soil moisture on the development of a Sahelian mesoscale convective system: a case-study from the AMMA special observing period, *Q. J. R. Meteorol. Soc.*, *136*, 456–470, doi:10.1002/qj.465.

Taylor, C. M., A. Gounou, F. Guichard, P. P. Harris, R. J. Ellis, F. Couvreux, and M. De Kauwe (2011), Frequency of Sahelian storm initiation enhanced over mesoscale soil-moisture patterns, *Nat. Geosci.*, *4*, 430–433.

Taylor, C. M., R. A. M. de Jeu, F. Guichard, P. P. Harris, and W. A. Dorigo (2012), Afternoon rain more likely over drier soils, *Nature*, *489*, 423–426, doi:10.1038/nature11377.

Tindall, J. C., P. Valdes, and L. C. Sime (2009), Stable water isotopes in HadCM3: Isotopic signature of El Nino-Southern Oscillation and the tropical amount effect, *J. Geophys. Res.*, *114*, D04111, doi:10.1029/2008JD010825.

Tremoy, G., F. Vimeux, S. Mayaki, I. Souley, O. Cattani, G. Favreau, and M. Oi (2012), A 1-year long delta18O record of water vapor in Niamey (Niger) reveals insightful atmospheric processes at different timescales, *Geophys. Res. Lett.*,*39*, L08805, doi:10.1029/2012GL051298.

Trenberth, K. (1999), Atmospheric moisture recycling: Role of advection and local evaporation, *J. Clim.*, *12*, 1368–1381.

Tuinenburg, O. A., R. W. A. Hutjes, C. M. J. Jacobs, and P. Kabat, (2011), Diagnosis of local land–atmosphere feedbacks in India, *J. Clim.*, *24*, 251–266, doi:10.1175/2010JCLI3779.1.

Uppala, S.,, et al. (2005), The ERA-40 re-analysis, *Q. J. R. Meteorol. Soc.*, *131*, 2961–3012.

van der Ent, R. J., H. H. G. Savenje, B. Schaefli, and S. C. Steele-Dunne (2010), Origin and fate of atmospheric moisture over continents, *Water Resour. Res.*, *46*, 1853–1863, doi:10.5194/acp-11-1853-2011.

van der Ent, R. J., and H. H. G. Savenje (2011), Length and time scales of atmospheric moisture recycling, *Atmos. Chem. Phys.*, *11*, 1853–1863, doi:10.5194/acp-11-1853-2011.

Vimeux, F., R. Gallaire, S. Bony, G. Hoffmann, and J. C. H. Chiang (2005), What are the climate controls on deltaD in precipitation in the Zongo Valley (Bolivia)? Implications for the Illimani ice core interpretation, *Earth Planet. Sci. Lett.*, *240*, 205–220.

Vimeux, F., G. Tremoy, C. Risi, and R. Gallaire (2011), A strong control of the South American SeeSaw on the intraseasonal variability of the isotopic composition of precipitation in the Bolivian Andes, *Earth Planet. Sci. Lett.*, *307*(1–2), 47–58.

Washburn, E., and E. Smith (1934), The isotopic fractionation of water by physiological processes, *Science*, *79*, 188–189.

Wei, J., and P. A. Dirmeyer (2010), Toward understanding the large-scale land-atmosphere coupling in the models: roles of different processes, *Geophys. Res. Lett.*, *37*, L19797, doi:10.1029/2010GL044769.

Welp, L., W. Lee, T. J. Griffis, X.-F. Wen, W. Xiao, S. Li, X. Sun, Z. Hu, M. Val Martin, and J. Huang (2012), A meta-analysis of water vapor deuterium-excess in the midlatitude atmospheric surface layer, *Global Biogeochem. Cycles*, *26*, GB3021, doi:10.1029/2011GB004246.

Werner, M., P. M. Langebroek, T. Carlsen, M. Herold, and G. Lohmann (2011), Stable water isotopes in the ECHAM5 general circulation model: Toward high-resolution isotope modeling on a global scale, *J. Geophys. Res.*, *116*, D15109, doi:10.1029/2011JD015681.

Westra, D., G. J. Steeneveld, and A. A. M. Holtslag (2012), Some observational evidence for dry soils supporting enhanced high relative humidity at the convective boundary layer top, *J. Hydrometeorol.*, *13*, 1347–1358.

Worden, J., et al. (2006), Tropospheric emission spectrometer observations of the tropospheric HDO/H_2O ratio: Estimation approach and characterization, *J. Geophys. Res.*, *111*, D16309, doi:10.1029/2005JD006606.

Worden, J., D. Noone, and K. Bowman (2007), Importance of rain evaporation and continental convection in the tropical water cycle, *Nature*, *445*, 528–532.

Worden, J., D. Noone, J. Galewsky, A. Bailey, K. Bowman, D. Brown, J. Hurley, S. Kulawik, J. Lee, and M. Strong (2010), Estimate of bias in Aura TES HDO/H_2O profiles from comparison of TES and in situ HDO/H_2O measurements at the Mauna Loa Observatory, *Atmos. Chem. Phys. Discuss*, *10*, 25,355–25,388, doi:10.5194/acpd-10–25355-2010.

Worden, J., S. Kulawik, C. Frankenberg, K. Bowman, V. Payne, K. Cady-Peirara, K. Wecht, J.-E. Lee, and D. Noone (2012a), Profiles of CH_4, HDO, H2O, and N_2O with improved lower tropospheric vertical resolution from Aura TES radiances, *Atmos. Meas. Tech. Discuss*, *5*, 397–411, doi:10.5194/amt-5–397-2012.

Worden, J., K. Wecht, C. Frankenberg, M. Alvarado, K. Bowman, E. Kort, S. Kulawik, M. Lee, V. Payne, and H. Worden (2012b), CH_4 and CO distributions over tropical fires as observed by the Aura TES satellite instrument and modeled by GEOS-Chem, *Atmos. Chem. Phys. Discuss.*, *12*, 26,207–26,243.

Wunch, D., G. C. Toon, J.-F. L. Blavier, R. A. Washenfelder, J. Notholt, B. J. Connor, D. W. T. Griffith, V. Sherlock, and P. O. Wennberg (2011), The total carbon column observing network, *Phil. Trans. R. Soc. A*, *369*(1943), 2087–2112, doi:10.1098/rsta.2010.0240.

Yoshimura, K., C. Frankenberg, J. Lee, M. Kanimatsu, J. Worden, and T. Rockmann (2001), Comparison of an isotopic atmospheric general circulation model with new quasi-global satellite measurements of water vapor isotopologues, *J. Geophys. Res.*, *116*:D19118, doi:10.1029/2011JD016035.

Yoshimura, K., T. Oki, N. Ohte, and S. Kanae (2004), Colored moisture analysis estimates of variations in 1998 Asian monsoon water sources, *J. Meteorol. Soc. Japan*, *82*, 1315–1329.

Yoshimura, K., M. Kanamitsu, D. Noone, and T. Oki (2008), Historical isotope simulation using reanalysis atmospheric data, *J. Geophys. Res.*, *113*, D19108, doi:10.1029/2008JD010074.

Zaitchik, B. F., A. K. Macalady, L. R. Bonneau, and R. B. Smith (2006), Europe's 2003 heat wave: A satellite view of impacts and land-atmosphere feedbacks, *Int. J. Climatol.*, *26*(6), 743–769.

Zangvil, A., D. H. Portis, and P. J. Lamb (2004), Investigation of the large-scale atmospheric moisture field over the midwestern United States in relation to summer precipitation. Part II: Recycling of local evapotranspiration and association with soil moisture and crop yields, *J. Clim.*, *17*, 3283–3301.

Zipser, E., and M. A. LeMone (1980), Cumulonimbus vertical velocity events in gate. Part II: Synthesis and model core structure, *J. Atmos. Sci.*, *37*, 2458–2469.